ASTES

Advances in Science, Technology & Engineering Systems Journal

Special Issue

Innovative Research in Applied Science, Engineering and Technology

2020

www.astesj.com
ISSN: 2415-6698

EDITORIAL BOARD
(Special Issue)

Editor-in-Chief

Prof. Passerini Kazmerski
Pritzker School of Molecular Engineering, University of Chicago, USA

Guest Editors

Prof. Bachir BENHALA
Department of Physics, Faculty of Sciences, Meknes, Moulay Ismail University, Morocco

Prof. Amin SALLEM
Electronic and Information Technology Laboratory LETI, Higher Institute of Industrial Management of Sfax ISGIS, University of Sfax, Tunisia

Prof. Pedro Miguel Ribeiro Pereira
Department of Electrical and Computer Engineering DEE/DEEC, NOVA School of Science and Technology FCT NOVA, NOVA University Lisbon, Portugal

Prof. Khalifa MANSOURI
Department of Mathematics and Computer Science, ENSET Mohammedia, Hassan II University of Casablanca, Morocco

Prof. Noureddine EL MAKHFI
Department of Mathematics and Computer Science PMIC related lab, Faculty of Science and Technology Al Hoceima, Abdelmalek Essaadi University, Morocco

Prof. Mohammed QBADOU
Department of Mathematics and Computer Science SSDIA/M2S2I labs, ENSET Mohammedia, Hassan II University of Casablanca, Morocco

Prof. Abdelhadi RAIHANI
Electrical Engineering Department, ENSET Mohammedia, Hassan II University of Casablanca, Morocco

Editorial

The Special Issue on *Innovative Research in Applied Science, Engineering and Technology (2020)* in the *Advances in Science, Technology and Engineering Systems Journal (ASTES Journal)* presents a diverse and forward-looking compilation of research that reflects the critical role of applied innovation in addressing contemporary scientific and engineering challenges. The year 2020 marked a period of intensified focus on translating theoretical knowledge into practical solutions, as global demands required rapid, efficient, and impactful technological responses. This special issue brings together contributions that exemplify the integration of applied science with engineering practices and technological development, highlighting the importance of innovation in real-world problem-solving.

A central theme of this issue is the application of scientific principles to develop engineering solutions that are both effective and scalable. The included studies demonstrate how advancements in applied sciences—ranging from physics and chemistry to computational and environmental sciences—are being utilized to enhance engineering processes and system performance. Through the use of experimental investigations, analytical modeling, and simulation-based approaches, researchers have developed solutions that address practical challenges in areas such as materials engineering, energy systems, and industrial processes.

The role of emerging technologies is also prominently emphasized throughout this collection. Advances in artificial intelligence, machine learning, and data analytics have significantly influenced the way applied research is conducted and implemented. These technologies enable more accurate predictions, optimized designs, and intelligent control systems, thereby improving efficiency and reliability across various applications. The contributions in this issue illustrate how digital tools and computational techniques are being leveraged to drive innovation in fields such as smart systems, automation, and advanced manufacturing.

Another important aspect highlighted in this special issue is the focus on sustainability and resource efficiency. As global concerns regarding environmental impact and resource depletion continue to grow, applied research has increasingly aimed to develop solutions that are environmentally responsible and economically viable. The studies presented explore innovative approaches to renewable energy integration, waste reduction, and sustainable material development, demonstrating how applied science and engineering can contribute to long-term environmental stewardship.

Interdisciplinary collaboration emerges as a key driver of innovation within this issue. The complexity of modern challenges necessitates the integration of knowledge from multiple disciplines, enabling researchers to develop more comprehensive and effective solutions. The works featured highlight how collaboration between scientists, engineers, and technologists leads to the creation of systems that are not only technically advanced but also adaptable to diverse applications and conditions.

The editorial team extends its sincere appreciation to all authors, reviewers, and contributors for their valuable efforts in making this special issue possible. Their dedication has ensured the publication of high-quality research that advances applied science, engineering, and technology. The collection presented in this issue reflects a continued emphasis on innovation, practicality, and interdisciplinary engagement, offering meaningful insights and a strong foundation for future advancements in applied research and technological development.

Guest Editor

Prof. Bachir Benhala

ADVANCES IN SCIENCE, TECHNOLOGY AND ENGINEERING SYSTEMS JOURNAL

Special Issue **June 2020**

Quantitative Approach in Enhancing Decision Making Through Big Data as An Advanced Technology
Hana Yousuf, Asma Yousuf Zainal

Convolutional Neural Network Based Classification of Patients with Pneumonia using X-ray
Hicham Moujahid, Bouchaib Cherradi, Oussama El Gannour, Lhoussain Bahatti, Oumaima Terrada, Soufiane Hamida

Thermal Performance Analysis of Parabolic Trough Solar Collector System in Climatic Conditions of Errachidia City, Morocco
Mohamed Hajjaj, Amine Tilioua, Abdellah Mellaikhafi, Abella Bouaaddi
The Role of Promotion in Mobile Wallet Adoption – A Research in Vietnam
Ha Hoang, Tan Trinh Le

Survey Analysis: Enhancing the Security of Vectorization by Using word2vec and CryptDB
Hana Yousuf, Said Salloum

Development of Soil Moisture Monitoring by using IoT and UAV-SC for Smart Farming Application
Sarun Duangsuwan, Chakree Teekapakvisit, Myo Myint Maw

The Role of KM in Enhancing AI Algorithms and Systems
Hani AlGhanem, Mohammad Shanaa, Said Salloum, Khaled Shaalan

The Probe Mark Discoloration on Bond Pad and Wafer Storage
Wen-Fei Hsieh, Henry Lin, Vincent Chen, Irene Ou, Yung-Song Lou

Shape Optimization of Planar Inductors for RF Circuits using a Metaheuristic Technique based Evolutionary Approach
Imad El Hajjami, Bachir Benhala, Hamid Bouyghf

New Algorithm for the Development of a Musical Words Descriptor for the Artificial Composition of Music
Mehdi Zhar, Omar Bouattane, Lhoussain Bahatti

Study of the Effect of Abnormalities in the External Ear Inducing Hearing Problems
Jihane Melloui, Jamila Bakkoury, Omar Bouattane

Contextual Word Representation and Deep Neural Networks-based Method for Arabic Question Classification
Alami Hamza, Noureddine En-Nahnahi, Said El Alaoui Ouatik

Monte Carlo Estimation of Dose in Heterogeneous Phantom Around 6MV Medical Linear Accelerator
Zakaria Aitelcadi, Mohamed Reda Mesradi, Redouane El Baydaoui, Ahmed Bannan, Abdennacer Ait Ayoub, Kamal Saidi, Saad Elm

5G mm-wave Band pHEMT VCO with Ultralow PN
Abdelhafid Es-Saqy, Maryam Abata, Mohammed Fattah, Said Mazer, Mahmoud Mehdi, Moulhime El Bekkali, Catherine Algani

An Adaptive Nonlinear Sensorless Controller of Doubly Fed Induction Generator Driven By Wind Turbine
Radouane Ourhdir, Mohammed Rachidi

Damage Accumulation Model for Cracked Pipes Subjected to Water Hammer
Zakaria Mighouar, Laidi Zahiri, Hamza Khatib, Khalifa Mansouri

Multi Closed-loop Adaptive Neuro-Fuzzy Inference System for Quadrotor Position Control
Halima Housny, El Ayachi Chater, Hassan El Fadil

Development of an Adaptive HVAC Fuzzy Logic Controller for Commercial Facilities: A Case Study
Hamidi Meryem, Bouattane Omar, Raihani Abdelhadi, Khalili Tajeddine

Human-Robot Multilingual Verbal Communication – The Ontological Knowledge and Learning Models
Mohammed Qbadou, Intissar Salhi, Hanaâ El Fazazi, Khalifa Mansouri, Michail Manios, Vassilis Kaburlasos

Numerical Study of Gas Microflow within a Triangular Lid-driven CavityYoussef Elguennouni, Mohamed Hssikou, Jamal Baliti, Mohammed Alaoui

Fast and Efficient Maximum Power Point Tracking Controller for Photovoltaic Modules
Khalid Chennoufi, Mohammed Ferfra

Experimental and Numerical Study of the Mechanical Behavior of Bio-Loaded PVC Subjected to Aging
Abdelghani Lakhdar, Aziz Moumen, Laidi Zahiri, Mustapha Jammoukh, Khalifa Mansouri

Sustainable Development Practices in the Moroccan Small and Medium Enterprise: by What Purpose?
Keltoum Rahali, Abdelaziz Chaouch, Elmahjoub Aouane, Sami Chbika, Abderrazzak Khohmimidi, Mustapha Kouzer, Abdellatif Elouadi

Earthquake Response of Multi-Storey Infilled Reinforced Concrete Buildings
Miloud Mouzzoun, Abdelkader Cherrabi

Machine Learning for Network Intrusion Detection Based on SVM Binary Classification Model
Anouar Bachar, Noureddine El Makhfi, Omar EL Bannay

Investment of Classic Deep CNNs and SVM for Classifying Remote Sensing Images
Khalid A. AlAfandy, Hicham, Mohamed Lazaar, Mohammed Al Achhab

The Effects of Transmission Power and Modulation Schemes on the Performance of WBANs in Medical Applications
Marwa Boumaiz, Mohammed El Ghazi, Mohammed Fattah, Anas Bouayad, Moulhime El Bekkali

A Study on Methodology of Improvement the Hydraulic System for Cometto Self-Propelled Trailer
Hai Minh Nguyen-Tran, Quang Minh Pham, Hoa Binh Le-Nguyen, Cao Tri Nguyen, Tri Nhut Do

Advanced Design of Current-mode Pass-band Filter using Ant Colony Optimization Technique
Kritele Loubna, Benhala Bachir, Zorkani Izeddine

Fabrication and Properties of Hybrid Membranes Based on Poly (Vinyl Alcohol), Sulfosuccinic Acid of Heteropolyacid with or without Silica for Fuel Cells Applications
Said Maarouf, Zouhair Alouane, Bouchra Tazi, Farhate Guenoun, Khalil Fouad

Understanding Risk Assessment in the Context of Fractional Ownership using Ethereum Smart Contracts
Mohamed Laarabi, Abdelilah Maach

Comparison by Correlation Metric the TOPSIS and ELECTRE II Multi-Criteria Decision Aid Methods: Application to the Environmental Preservation in the European Union Countries
Mohammed Chaouki Abounaima, Loubna Lamrini, Noureddine EL Makhfi and Mohamed Ouzarf

ASTES

Advances in Science, Technology and Engineering Systems Journal Vol. 5, No. 5, 109-116 (2020)

www.astesj.com

Special Issue on Innovative Research in Applied Science, Engineering and Technology

ASTESJ

ISSN: 2415-6698

Quantitative Approach in Enhancing Decision Making Through Big Data as An Advanced Technology

Hana Yousuf[1,*], Asma Yousuf Zainal[2]

[1]*Faculty of Engineering & IT, The British University in Dubai, 345015, United Arab Emirates*

[2]*Faculty of Business Management, The British University in Dubai, 345015, United Arab Emirates*

ARTICLE INFO

Article history:
Received: 23 July, 2020
Accepted: 23 August, 2020
Online: 09 September, 2020

Keywords:
Big Data
Discussion Making
Quantitative Method
Percentage Analysis
Chi-Square
Correlation Analysis
Regression Analysis

ABSTRACT

The technology of Big Data got the capability to process large amounts of data, manage them effectively and make retrieval whenever it is required. Decision making in any organisation is a challenging task since decisions need to be made based on the accessibility of data and its status, this becomes more challenging especially in large organisations that generate massive amount of information and data every single day.
Implementation of latest advanced technologies like Big Data is imperative for any organization to make decisions which reduces time and pave the fourth industrial revolution. Even though this is vital in today's business world, there are still few organizations that are hesitant to adopt it.
This paper illustrates the relation between Big Data and effective decision making by implementing a quantitative analysis through questionnaire. The conducted analysis is implemented using SPSS through correlational perspective, where percentage analysis, Chi-Square, correlation, and regression analyses are performed to obtain results.
It is clearly depicted that large organizations transition to adopt Big Data to aid their decision making, where medium and smaller organizations were slowly transitioning the adoption. In spite of this, most of employees, irrespective of the type of organization agree that Big Data is indeed a powerful advanced technology as they were satisfied by the organizational direction they have taken.

1. Introduction

1.1. Background

Digital technologies are transforming the way organizations function sparking the necessity for creative approaches and a wide range of highly functional presentations [1]. Facilities of storing have grown drastically in the past years along with data collection approaches where large amounts of data are also becoming readily accessible. In every moment, new set of data are being generated by various sources, these data need to be processed and evaluated in new forms to derive value. In addition, organizations should get as much value as possible from enormous sources & amounts of data stored [2]. Further technologies and devices are available now to corporations and people to generate and collect more data from various groups. These days, an individual entity can own multiple devices, where each device carries extremely large amount of vital information. These types of information are described as Big Data, or data with a volume, velocity, variety and depth that standard techniques make it difficult to handle [3].

Big Data can contain various combinations of data including texts with social emotions, news feeds, site logfiles for audio / video, as well as geographical and location data, Multimedia, xml data, etc [4]. Due to the size, wide range, dramatic changes, different types of storage and analytical techniques, such these information needs fresh type of Big Data analytics. The rising of these kinds of information need to utilize a Big Data and take advantage of its capability in the organizations who have already a clear, simple roadmap and guidelines for managing Big Data in their departments.

Organizations today are enabled to achieve their target and exceed it if they were able to adopt new technologies which consequently leads to generating profit from Big Data analysis. In other sectors, the capability to create transition would distinguish those who are going to lead and those who are going to left behind. Nevertheless, conducting data analysis only is not enough, it must

*Corresponding Author: Hana Yousuf, The British University in Dubai, Tel: +971501010008, Email: hana.yousuf@gmail.com.

be circulated effectively to the employees within the organization in attempt to influence decisions and therefore obtain specific role at the heart of decision-making processes instead of intuition [5]. In order to make smart choices, organizations should be sharing right information to the right individuals at the right time [6]. As such, Big Data attains great expectations, and the effect on enhancing the decision has been explored by various researchers, with McAfee & Brynjolfsson as the strategic front-runners. However, since it is a relatively new area of concept and research, it is essential to have more empirical studies in specific sectors to the research of what impacts Big Data analytics will have on decision-making.

Organizations need contract terms and interpersonal governance, Big Data analytics competences, information sharing, coordination, process integration, flexible infrastructure, quality data sources and decision making qualities to effectively manage a large data chain and make quality decisions [7,8]. Contract compliance relates to the formalization of arrangements with Big Data vendors to increase the consistency of the results. Relational governance that involves collaboration and information sharing for data interpretation and processing maintains trust between organizational entities. To design a Big Data network and overcome the smaller data groups, various participants of the organisation who are part of the Big Data based decision-making environment require collaboration. It is also necessary to connect operations and procedures to cut the price of Big Data and its related analytics. Big Data networks and its operations must be part of the organizational routine, since this will enhance information speed. The flexibility of the network often allows data collection and retrieval. Information accuracy, with respect to the data provider's interest, is also necessary to avoid making mistake decisions that may prove to be quite expensive. In fact, decision-makers will have the capacity to analyse the findings of Big Data analyses and consider their consequences in order to strengthen evidence-driven decision-making capabilities and increase consistency [7].

1.2. Problem Statement

Existing literature on the use of Big Data for decision making system focuses primarily on the issues and advantages of business intelligence and Big Data[8], whereas the practical effects of Big Data analysis to improve business intelligence are still relatively under-researched[9][10][11]. Some research is usually focused on methods, technical issues and their possible solutions in using Big Data analytics for business intelligence, but there is a shortage of literature on the practical implications of using Big Data analytics in general for decision making.

1.3. Research Questions

This research aims to understand employee's perception of Big Data among in enhancing decision making systems. Therefore, the research questions are:

- How relevant is Big Data for decision making in an organization?
- What percentage of the organizations are currently using Big Data?
- Do the employees feel that Big Data is relevant in the current scenarios?

1.4. Literature Review

Big Data is increasingly transforming the way businesses make choices, because new decision-making skills are required in the Big Data era in order to make better judgments [7]. In the available research the dynamic capabilities are often used to address the strengths of Big Data analytics [12].

This research explores the antecedents of large data decision taking capability. Even though its potential effect has been described with respect to the dynamic capabilities [13,14], many elements of the organizations that affect the Big Data sustaining value of a firm remain unexplored.

The capacity of Big Data has defined by [7] as the capacity of a business to start making high-quality Big Data based decisions by handling a Big Data network effectively. [15] have also presented crucial and in-depth insights into diverse Big Data functionalities; however, the study is much more applicable to Big Data value creation. Conversely, the factors that affect the quality of Big Data decision making has discussed by [7]. Effective management of a Big Data networks requires organizations to build up their capacity and capabilities for Big Data management and analytics. The related literature also demonstrates the ability of a organization to interpret data can affect its efficiency and that the ability of the Big Data processing and analytics organizations to make strategic decision is likely to impact.

Leadership plays a vital role in the development and reconfiguration of dynamic capabilities as an effective way of providing direction to organizational members [6]. The leadership contingency principle often implies members will produce the required results by choosing their leadership style appropriately [16]. The existing literature also recognizes the effect of leadership style on various organizational and the behavioural outcomes for example, a leadership focus on knowledge management influences it positively within an organization [17], [18]. Leaders can also influence the information analysis trend by adopting appropriate leadership behaviours [19].

Leadership is an essential impactor of Big Data development, which is generally done through procedure, social and systemic interactions and complementarities [20]. It is further agreed by [21] that leadership is essential to a firm's development of using technology. Specifically, it is correlated with leadership propensity to adapt, understanding of incentives to improve current practices and services in a constructive way, and desire and capacity to incorporate these improvements. Managerial leadership cognition is critical to the improvement of Diagnostic Control Systems (DCS) that are used to manage the environment change [22].

In a wide spectrum of firms, talent management, which is emerging as a key organizational challenge, is considered very important [23]. Researchers have concluded that, despite the limited consequences of current talent management for implementing Big Data, its role in various situations and environments needs to be analysed [24]. Considering the essential function of the talent harnessing, indicated that the application of Big Data may be improved by effective talent management. As information is now more cost effective for organizations, the data analysis components have become more valuable, which means it is easier to hire data scientists.

The growing worth of Big Data specialists makes retaining them valuable to the organizations. While the expertise of statistics is essential, the use of Big Data demands more than conventional statistical abilities. Big Data management requires specific techniques and abilities that might not be easily available at certain locations [25], but are commonly held by the current generation of informatics scientists. Big Data use also requires skills involved in data cleaning and visualization, which suggests that organizations need to nurture key talents The acknowledgment by [26] that HR experts and expertise play in a Big Data setting, who are able to speak the market language and therefore make it easy for leaders to devise strategies to tackle Big Data.

According to the existing literature, efficient talent management practices improve organizational decision-making capabilities [27]. The resource-based perspective suggests organizations should use their strategic resources to achieve sustained competitive advantages [28]. The knowledge-based view argues that knowledge which is connected to its staff is the most essential strategic asset of a firm [18]. Using employee knowledge and skills to reap the maximum benefit., for instance, as long as success is concerned, organizations will incorporate acceptable talent acquisition practices, as indicated in the literature on the usage of Big Data [15].

The decision-making on data analytics requires quality decision-makers and Big Data analysts experts, asserted done by [7] . In addition to performing data analysis, the latter will also deal with contract terms and interpersonal leadership to improve information cooperation and information sharing across organization boundaries, which can affect the quality of Big Data decision. A lack of dedicated talent has been perceived as the major barrier to capturing value from Big Data [25]. Even though there are currently lots of professionals working with Big Data, there is a great amount of talent shortage for the next three to five years [28].

Many developing countries are in the race to utilize AI capabilities linked to Big Data; therefore, effective talent management is essential for businesses to reap the benefits of Big Data and digital technology[29]. As data gets cheaper, the domain's scientists become much more valuable, that further rises the need for integrated talent management procedures to hire, retain and recruit employees required at all levels to fulfil the standards of data analytics aimed at quality decision making. As such, effective talent management plays a significant role in building capacity for organizations [30]-[31].

2. Methodology

2.1. Research Design

Quantitative methodology is used in this work to gather data and conduct the necessary analysis. It is a type of research method that performs mathematical, computational, and statistical approaches using quantifiable data. To carry out the study, the data must be gathered entirely first. Until obtaining the results, the appropriate sample population must be defined depending upon the necessity. Here the target group is the employees of corporate organizations, about the use of Big Data for decision making. The research design will be as correlational research, where percentage analysis, Chi-Square analysis, correlation analysis and regression analysis will be applied.

It is necessary to identify the respondent population to compile the data and to build the questionnaire. Since the work deals with usage of Big Data in different organisations, employees of these organisations must be considered as community sample. Other related technologies like working of Big Data and its advantages which are related to the principles of Big Data and decision making have been extensively discussed in the literature review section.

The data are gathered in the form of questionnaires from specified respondents. The questions are posed to the respondents in the questionnaire, esponses are compiled. The questionnaire are posted directly in the form of (google forms) and sent via email. The answers must be translated into the graphical format for quantitative methods, so that they are appropriate for study. Any variables are established during the study for grouping the questions and answers into categories. There are numerous factors that rely heavily on this to be considered. In this work, it is identified whether the organisations are willing to use Big Data for decision making, and whether they have trust in them. The employees of certain organisations are taken into account for collecting the data for this study.

2.2. Scaling

Scaling is done to simplify data analysis and enable the researchers to better understand the data. Likert scaling is used in this work. Likert scale suggests that an ability / magnitude of attitude is linear, i.e. on a scale from strongly agreeing to disagreeing, and appears to conclude that attitudes will be calculated. There are various types of Likert scale depending on the number of opinions that are captured for each question [32]. A 4-point Likert scale is used in this research which contains 4 options, which are: Strongly Agree, Agree, Disagree and Strongly Disagree.

2.3. Questionnaire Development

The survey questions are deemed more accurate for gathering answers, they are used to gather answers in this research. The biggest drawback in utilizing questionnaires is that the queries tend to be determined at the outset and the subsequent questions cannot be changed on the basis of the first query. In this work, though, only a few questions will be asked, questionnaires are enough. A questionnaire that contains various questions related to the use of bigdata for decision making, and its effectiveness in enhancing the decision-making process is used. The questionnaire consists of a total of ten questions and it is attached in the appendix. Questions 2 and 3 can be considered as independent responses, while the other questions are dependent on these two questions.

2.4. Sampling Technique

When survey is conducted, there are different ways the population sample must be identified. This is because, it won't be feasible to conduct analysis with the entire population. In this case, we must conduct the study on the employees working small, medium and large organizations, where there would be millions of employees around the world. Hence, certain mixture of small- and large-scale organizations are identified randomly. The research paper will adopt Random Sampling technique.

2.5. Field Work

The respondents are randomly chosen and the questionnaires built using Google forms. The employees working in the same research field of different organisations are identified and the form sent to them by emails. Even though the forms are shared with many employees, only some of them had responded, out of which we round the number of respondents to 50 response. The answers are collected in a single dataset, and then SPSS tools used to perform different statistical approaches for quantitative research.

3. Data Analysis

3.1. Methodology

The responses are obtained from the respondents and then analysed through SPSS tool. The methodology used here are the percentage analysis, Chi-square test, correlation analysis, and regression analysis. The collected data analysed in form of statistical analysis as part of quantitative methodology.

Percentage analysis is among the simple mathematical methods that is commonly utilized in primary data processing and understanding. This deals with the number of respondents to a specific query is the proportion arrived from the overall chosen population for the analysis. A Chi-square test is a mathematical hypothesis check that is true while the Chi-square function is applied under the null hypothesis, called the Chi-square test of Pearson and its variants. Correlation coefficient is a statistical calculation of any form of correlation which implies a statistical association between two variables. The variables may be two columns of a specified series of results, also referred to as a survey, or major aspects of a random multivariate vector with a defined distribution. Regression analysis is an effective mathematical tool that analyses the association between two or more relevant variables. While there are several forms of regression analysis, they all analyse at the heart the effect of one or more independent variables on a dependent variable

4. Result

4.1. Percentage Analysis

Out of the four techniques, percentage analysis first analysed as given below. Out of the 50 respondents, 25 respondents, which considered as 50% of the respondents worked in a medium scale organization that had between 100 and 500 as shown in Table 1. The rest of the respondents were range between small and large organizations where 24% employed in small organizations less than 100 employees, and 26% employed in organizations more than 500 employees.

Table 1: Employees contribution based on the organization size

Organization Size	Frequency	Percent
1-100 employees	12	24.0
100-500 employees	25	50.0
More than 500 employees	13	26.0
Total	50	100

The number of respondents whose organization work with Big Data is shown in table 2. Most of the respondents are using Big Data in their organisation systems which is around 72% in, whereas 20% of the respondents' organizations did not use Big Data and 8% said that their organization is studying the implementation of Big Data in near future as shown in Table 2.

Table 2: Organization working with Big Data

Response	Frequency	Percentage
Yes	36	72.0
No	10	20.0
In future	4	8.0
Total	50	100.0

Out of the smaller organizations below 100 employees, around 67% of them are using Big Data in decision making, while 25% of them are not using it and 8% will implement it soon. Among the medium scale organization with employees between 100 and 500, 60% of them are using Big Data in making decision, while 28% of them are not using it and 12% will implement it soon. Among the large organizations with more than 500 employees, all of them use Big Data for decision making systems. The result is shown in Table 3

Table 3: employees' implantation and preference in using Big Data

Employee Size	Frequency	Implementation	Working with Big Data	Percentage
1 – 100 Employees	12	Implemented	8	66.67 %
		Not implemented	3	25.00 %
		Soon will be implemented	1	8.33 %
100-500 employees	25	Implemented	15	60%
		Not implemented	7	28%
		Soon will be implemented	3	12%
> 500 Employees	13	Implemented	13	100%
		Not implemented	0	0%
		Soon will be implemented	0	0%

The importance of the Big Data as recorded from the employee working in different organization size is shown in Table 4. 68% of the respondents said that it is very necessary for making decisions in the organization, while 24% slightly agreed and thought it is might be necessary to be implemented in some

departments and only 8 % of the respondents felt that it is not necessary at all.

Table 4: Importance of Big Data in decision making

Response	Frequency	Percentage
Not Necessary	4	8.0
Slightly necessary	12	24.0
Very necessary	34	68.0
Total	50	100.0

The availability of some form of strategy for Big Data is shown in Table 5. While 32% of the respondents confirmed that there is some form of strategy being used by the company for decision making analysis, 34% of them said that there is no strategy for this, while another 34% of them were not sure of this.

Table 1: Availability of Big Data strategies

Response	Frequency	Percentage
There is a strategy for Big Data	16	32.0
There isn't a strategy for Big Data	17	34.0
Not sure of the availability of a strategy for Big Data	17	34.0
Total	50	100.0

4.2. Chi- Square Test

Chi-square test is used which checks the null hypothesis between different questions. Since the second question influences the other questions, its relationship and hypothesis with other questions are tabulated in tables 6 to 8. The Chi-square value for having a strategy for Big Data, and those working with Big Data is shown in table 6. There are 16 respondents that use Big Data in the organization besides a strategy for usage and implementation, which accounts to 32% of the overall respondents. 20% of the respondents neither use Big Data nor have any strategy for Big Data in the organization. Around 26% of the respondents use Big Data but are not sure whether the organization have any kind of strategy adopts the Big Data implementation or not. A Chi-square of 31.2 is obtained for the relation, and p-value is 0, which shows that this is significant.

Table 2: Association between organisation work with Big Data and organization has any strategy for Big Data

Organization work with Big Data	Organization have any strategy for Big Data			Total	*P*-value
	Yes	No	Not sure		
	n(%)				
Yes	16 (100.0)	7 (41.2)	13 (76.5)	36 (72.0)	0.000**
No	0 (0.0)	10 (58.8)	0 (0.0)	10 (20.0)	
In future	0 (0.0)	0 (0.0)	4 (23.5)	4 (8.0)	
Total	16 (100.0)	17 (100.0)	17 (100.0)	50 (100.0)	

Chi-Square: 31.209, **P<0.001

Similar analysis is done for those working with Big Data and for those organisations that have qualified experts in Big Data. Most of the experts, 72% agree that they have a qualified expert, since their organization works with Big Data. 20% of the respondents do not work with Big Data and claim that they do not have any qualified Big Data experts. It has a very high Chi-square value of 50, and p-value of 0, showing that the result is significant as shown in table 7.

Table 7: Association between organization work with Big Data and organization with qualified Big Data experts

Importance of using Big Data for decision making	Organization with qualified Big Data experts				Total	*P* value
	Strongly Disagree	Disagree	Agree	Strongly agree		
	n(%)		n(%)			
Not Necessary	4 (100.0)	0 (0.0)	0 (0.0)	0 (0.0)	4 (8.0)	0.00**
Slightly necessary	0 (0.0)	0 (0.0)	3 (20.0)	9 (31.0)	12 (24.0)	
Very necessary	0 (0.0)	2 (100.0)	12 (80.0)	20 (69.0)	34 (68.0)	
Total	4 (100.0)	2 (100.0)	15 (100.0)	29 (100.0)	50 (100.0)	

Chi-Square: 50.000, **P<0.001

Similar Chi-square analysis is done for the opinion of importance of working with Big Data and whether the organization has qualified experts. 64% of the respondents feel that using Big Data is necessary and have qualified experts. Out of this 40% strongly agree, and 24% generally agree. Among those who feel Big Data is necessary, only 4% think that they do not have a qualified expert. With correlation too, a high Chi-square value of 51.48 is obtained along with significant results as shown in Table 8.

4.3. Correlation Analysis

Correlation analysis is performed to identify the correlation between two questions. The correlation coefficient implies the statistical association between two variables. Here, the variables are the two columns of the results. The correlation between the questions 2, 6, 7 and 10 are given in table 14. The questions 6,7, and 10 depend on question 2, they have high amount of correlation

with one another. All the coefficients have a value about 0.6, with some even exceeding 0.87 as shown in Table 9.

Table 3: Association between qualified experts and importance of working with Big Data

Importance of using Big Data for decision making	Organization with qualified Big Data experts				Total	*P* value
	Strongly Disagree	Disagree	Agree	Strongly agree		
	n(%)		n(%)			
Not Necessary	4 (100.0)	0 (0.0)	0 (0.0)	0 (0.0)	4 (8.0)	
Slightly necessary	0 (0.0)	0 (0.0)	3 (20.0)	9 (31.0)	12 (24.0)	0.00
Very necessary	0 (0.0)	2 (100.0)	12 (80.0)	20 (69.0)	34 (68.0)	**
Total	4 (100.0)	2 (100.0)	15 (100.0)	29 (100.0)	50 (100.0)	

Chi-Square: 51.481, **P<0.001

Table 9: Correlations analysis organization with Big Data

Questions	Organization working with Big Data	Organization with qualified Big Data experts	Satisfied with the organization in the integration of Big Data tools in the	Organization uses other tools in besides Big Data for decision making.
Organization work with Big Data	1			
Organization contains qualified Big Data experts.	.874**	1		
Satisfied with the organization in the integration of Big Data tools in the	.659**	.661**	1	
Organization uses other tools in besides Big Data for decision making	.659**	.661**	.870**	1

**p<0.001

The correlation between the questions 3, 5, 8 and 9 are given in table 10. The questions 5,8, and 9 depend on question 2, they have high amount of correlation with one another. While compared to the previous table, the correlation coefficient is slightly lesser. All the coefficients have a value about 0.35, with some even exceeding 0.5 as shown.

4.4. Regression Analysis

Regression analysis analyses the association between two or more relevant variables. Here, the correlation between the dependent and the independent variables are assigned. The regression between the 3impact of decision making and the importance of Big Data for decision making is shown in table 11. The Beta represents the slope of the line which shows that the line is very much dependent on the former variable. The standard error is low at 0.185. Hence, the points are not very much spread out from the main line. From the test value of 3.993, the probability variable is calculated, which comes at 0, showing that result is significant.

Table 4: Correlations analysis

Question	Important of Big Data in decision making	Organizations impact of the decision it makes.	Reduces uncertainty in making decisions	Improve decision making process in an organization
Important of Big Data in decision making	1			
Organizations impact of the decision it makes.	.499**	1		
Reduces uncertainty in making decisions	.518**	.389**	1	
Improve decision making process in an organization	.518**	.389**	.560**	1

**p<0.001

H11: There is a significant impact of the importance of Big Data in decision making on the organisations impact for decision making, which is the dependent variable. Hence, there is no null hypothesis here, and there is an alternate hypothesis. The probabilistic values must be less than 0.001, hence ours shows significant results.

Table 5: Association between important Big Data for decision making and organizations' impact for decision making

	Unstandardized Coefficients		R-Square	t value	*P* value
	Beta	SE			
(Constant)	1.116	0.496	0.249	2.251	0.029
Importance of Big Data for decision making	0.740	0.185		3.993	**0.000****

Dependent Variable: Organizations' impact for decision making, **p<0.001
SE: Standard Error

The regression for the association between the organisations working with Big Data and the availability of strategies of Big Data for decision making is shown in table 12. The Beta represents the slope of the line at 0.391which shows that the line is very much dependent on the former variable. The standard error is low at 0.179. Hence, the points are not very much spread out from the main line. From the test value of 2.1888, the probability

variable is calculated, which comes at 0, showing that result is significant.

H11: There is a significant impact of the organisations working with bigdata on the strategies used for Big Data in the organization, which is the dependent variable. Hence, there is no null hypothesis here, and there is an alternate hypothesis. The probabilistic values must be less than 0.001, hence ours shows significant results.

Table 6: Association between Organization work with Big Data and Strategies for Big Data for analytics

	Unstandardized Coefficients		R-Square	t value	*P* value
	Beta	SE			
(Constant)	1.488	0.268	0.191	5.556	0.000
Organization work with Big Data	0.391	0.179		2.188	0.000**

Dependent Variable: Strategies for Big Data for analytics, **p<0.001
SE: Standard Error

The regression for the association between the organisations working with Big Data and the satisfaction of using Big Data is shown in table 13. The Beta represents the slope of the line at 1.193. The standard error is low at 0.179. Hence, the points are not very much spread out from the main line. From the test value of 6.071, the probability variable is calculated, which comes at 0, showing that result is significant.

H11: There is a significant impact of the organisations working with bigdata on the satisfaction of using Big Data in the organization, which is the dependent variable. Hence, there is no null hypothesis here, and there is an alternate hypothesis. The probabilistic values must be less than 0.001, hence ours shows significant results.

Table 7: Association between Organization work with Big Data and Satisfaction

	Unstandardized Coefficients		R-Square	t value	*P* value
	Beta	SE			
(Constant)	4.582	0.294	0.434	15.585	0.000
Organization work with Big Data	1.193	0.196		6.071	**0.000****

Dependent Variable: Satisfaction, **p<0.001
SE: Standard Error

5. Conclusions and Recommendations

From the above analysis, it is depicted that most of the large organizations have already transitioned to using Big Data for decision making in their companies, where medium scale and smaller scale organizations are slowly transitioning. In spite of that, most employees regardless of the type of their organizations agree that Big Data technology is useful, and they are also satisfied by the organization on the direction they have taken. This work has presented a quantitative methodology for understanding the perception of Big Data used in their company. Initially, a brief introduction on decision making and Big Data systems were studied, followed by relevant literature were illustrated in the literature review section. A questionnaire was initiated to perform interview on the public to understand their perception Big Data. Data is collected in through online forms and then analysed through SPSS. The results illustrate that Big Data is very much relevant in the current scenario in corporate organizations. Most of the organizations seem to have already implemented Big Data for decision making purposes and others are rapidly following their footsteps. The same perception was accepted by employees too, where they showcased that using Big Data is indeed useful and most of the employees are satisfied with the way their company is using Big Data.

6. Limitation and Caveats

The Big Data technology can be used to improve effectiveness of decision-making systems. This work used SPSS as a tool to perform percentage analysis, Chi-square, correlation analysis, and regression analysis. The main limitations that hinders the adoption of Big Data is its awareness and knowledge. Many managers are still struggling with older technologies and are not ready to adopt them soon due to fear of change and its related challenges. Upgrading and seeking expert advice can be a good approach to convince them to adopt Big Data. In the future, the same analysis can be performed with more in-depth questions based on different organizational sectors. This work has only used quantitative methodology. In the future, both quantitative and qualitative methodology can be implemented to explore further. There are no caveats to consider in this work.

Acknowledgment

This work is a part of a project undertaken at the British University in Dubai.

References

[1] S. Brunswicker, E. Bertino, S. Matei, "Big Data for Open Digital Innovation - A Research Roadmap," Big Data Research, **2**(2), 53–58, 2015, doi:10.1016/j.bdr.2015.01.008.

[2] M.C.M. Oo, T. Thein, An efficient predictive analytics system for high dimensional big data, Journal of King Saud University - Computer and Information Sciences, 2019, doi:10.1016/j.jksuci.2019.09.001.

[3] S. Fan, R.Y.K. Lau, J.L. Zhao, Demystifying Big Data Analytics for Business Intelligence Through the Lens of Marketing Mix, Big Data Research, **2**(1), 28–32, 2015, doi:10.1016/j.bdr.2015.02.006.

[4] P. Törnberg, A. Törnberg, "The limits of computation: A philosophical critique of contemporary Big Data research," Big Data and Society, **5**(2), 2018, doi:10.1177/2053951718811843.

[5] M. Muniswamaiah, T. Agerwala, C. Tappert, "Big Data in Cloud Computing Review and Opportunities," International Journal of Computer Science and Information Technology, **11**(4), 43–57, 2019, doi:10.5121/ijcsit.2019.11404.

[6] P.J.H. Schoemaker, S. Heaton, D. Teece, "Innovation, Dynamic Capabilities, and Leadership," California Management Review, **61**(1), 15–42, 2018, doi:10.1177/0008125618790246.

[7] M. Janssen, H. van der Voort, A. Wahyudi, "Factors influencing big data decision-making quality," Journal of Business Research, **70**, 338–345, 2017, doi:10.1016/j.jbusres.2016.08.007.

[8] A.Y. Zainal, H. Yousuf, S.A. Salloum, "Dimensions of Agility Capabilities Organizational Competitiveness in Sustaining," in Joint European-US

Workshop on Applications of Invariance in Computer Vision, Springer: 762–772, 2020.
[9] H. Yousuf, M. Lahzi, S.A. Salloum, K. Shaalan, Systematic Review on Fully Homomorphic Encryption Scheme and Its Application, Springer: 537–551, 2021, doi:10.1007/978-3-030-47411-9_29.
[10] S.A. Salloum, M. Al-Emran, K. Shaalan, "Mining Social Media Text: Extracting Knowledge from Facebook," International Journal of Computing and Digital Systems, **6**(2), 2210–142, 2017, doi:10.12785/ijcds/060203.
[11] S.A. Salloum, M. Al-Emran, K. Shaalan, A. Tarhini, "Factors affecting the E-learning acceptance: A case study from UAE," Education and Information Technologies, **24**(1), 509–530, 2019, doi:10.1007/s10639-018-9786-3.
[12] S.F. Wamba, A. Gunasekaran, S. Akter, S.J. fan Ren, R. Dubey, S.J. Childe, "Big data analytics and firm performance: Effects of dynamic capabilities," Journal of Business Research, **70**, 356–365, 2017, doi:10.1016/j.jbusres.2016.08.009.
[13] S. Erevelles, N. Fukawa, L. Swayne, "Big Data consumer analytics and the transformation of marketing," Journal of Business Research, **69**(2), 897–904, 2016, doi:10.1016/j.jbusres.2015.07.001.
[14] R. Dubey, A. Gunasekaran, S.J. Childe, Z. Luo, S.F. Wamba, D. Roubaud, C. Foropon, "Examining the role of big data and predictive analytics on collaborative performance in context to sustainable consumption and production behaviour," Journal of Cleaner Production, **196**, 1508–1521, 2018, doi:10.1016/j.jclepro.2018.06.097.
[15] J. Zeng, K.W. Glaister, "Value creation from big data: Looking inside the black box," Strategic Organization, **16**(2), 105–140, 2018, doi:10.1177/1476127017697510.
[16] Organisational Behaviour - Stephen Robbins, Timothy A. Judge, Bruce Millett, Maree Boyle - Google Books.
[17] M.J. Donate, J.D. Sánchez de Pablo, "The role of knowledge-oriented leadership in knowledge management practices and innovation," Journal of Business Research, **68**(2), 360–370, 2015, doi:10.1016/j.jbusres.2014.06.022.
[18] S. Shamim, S. Cang, H. Yu, "Impact of knowledge oriented leadership on knowledge management behaviour through employee work attitudes," International Journal of Human Resource Management, **30**(16), 2387–2417, 2019, doi:10.1080/09585192.2017.1323772.
[19] S. Shamim, S. Gang, H. Yu, "Influencers of information system usage among employees for knowledge creation. A future research agenda," in SKIMA 2016 - 2016 10th International Conference on Software, Knowledge, Information Management and Applications, Institute of Electrical and Electronics Engineers Inc.: 134–141, 2017, doi:10.1109/SKIMA.2016.7916210.
[20] T. Felin, N.J. Foss, K.H. Heimeriks, T.L. Madsen, "Microfoundations of Routines and Capabilities: Individuals, Processes, and Structure," Journal of Management Studies, **49**(8), 1351–1374, 2012, doi:10.1111/j.1467-6486.2012.01052.x.
[21] O. Koryak, K.F. Mole, A. Lockett, J.C. Hayton, D. Ucbasaran, G.P. Hodgkinson, "Entrepreneurial leadership, capabilities and firm growth," International Small Business Journal: Researching Entrepreneurship, **33**(1), 89–105, 2015, doi:10.1177/0266242614558315.
[22] M. Waleed Fakhr, M. Lahzi Gaid, G. Ibrahim Selim, Secure Translation Using Fully Homomorphic Encryption and Sequence-to-Sequence Neural Networks, 2018.
[23] D.G. Collings, K. Mellahi, W.F. Cascio, "Global Talent Management and Performance in Multinational Enterprises: A Multilevel Perspective," Journal of Management, **45**(2), 540–566, 2019, doi:10.1177/0149206318757018.
[24] T.N. Krishnan, H. Scullion, "Talent management and dynamic view of talent in small and medium enterprises," Human Resource Management Review, **27**(3), 431–441, 2017, doi:10.1016/j.hrmr.2016.10.003.
[25] P. Tambe, "Big data investment, skills, and firm value," Management Science, **60**(6), 1452–1469, 2014, doi:10.1287/mnsc.2014.1899.
[26] D. Angrave, A. Charlwood, I. Kirkpatrick, M. Lawrence, M. Stuart, "HR and analytics: why HR is set to fail the big data challenge," Human Resource Management Journal, **26**(1), 1–11, 2016, doi:10.1111/1748-8583.12090.
[27] L.J. Gutierrez-Gutierrez, V. Barrales-Molina, H. Kaynak, "The role of human resource-related quality management practices in new product development: A dynamic capability perspective," International Journal of Operations and Production Management, **38**(1), 43–66, 2018, doi:10.1108/IJOPM-07-2016-0387.
[28] J.B. Barney, D.J. Ketchen, M. Wright, "The Future of Resource-Based Theory," Journal of Management, **37**(5), 1299–1315, 2011, doi:10.1177/0149206310391805.
[29] H. Yousuf, A.Y. Zainal, M. Alshurideh, S.A. Salloum, Artificial Intelligence Models in Power System Analysis, Springer: 231–242.
[30] W.F. Joyce, J.W. Slocum, "Top management talent, strategic capabilities, and firm performance," Organizational Dynamics, **41**(3), 183–193, 2012, doi:10.1016/j.orgdyn.2012.03.001.
[31] A. Almansoori, M. AlShamsi, S.A. Salloum, K. Shaalan, Critical Review of Knowledge Management in Healthcare, Springer: 99–119, 2021, doi:10.1007/978-3-030-47411-9_6.
[32] D. Kriksciuniene, V. Sakalauskas, R. Lewandowski, "Evaluating the Interdependent Effect for Likert Scale Items," in Lecture Notes in Business Information Processing, Springer: 26–38, 2019, doi:10.1007/978-3-030-36691-9_3.

ASTES

Advances in Science, Technology and Engineering Systems Journal Vol. 5, No. 5, 167-175 (2020)

www.astesj.com

Special Issue on Innovative Research in Applied Science, Engineering and Technology

ASTESJ

ISSN: 2415-6698

Convolutional Neural Network Based Classification of Patients with Pneumonia using X-ray Lung Images

Hicham Moujahid[1], Bouchaib Cherradi[1, 2,*], Oussama El Gannour[1], Lhoussain Bahatti[1], Oumaima Terrada[1], Soufiane Hamida[1]

[1]*SSDIA Laboratory, ENSET Mohammedia, Hassan II University of Casablanca, 28820, Mohammedia, Morocco.*

[2]*STIE Team, CRMEF Casablanca-Settat, provincial section of El Jadida, 24000, El Jadida, Morocco.*

ARTICLE INFO

Article history:
Received: 29 July, 2020
Accepted: 18 August, 2020
Online: 10 September, 2020

Keywords:
Convolutional neural network
Machine learning
Deep learning
Pneumonia detection
Chest x-ray images
COVID-19

ABSTRACT

Analysis and classification of lung diseases using X-ray images is a primary step in the procedure of pneumonia diagnosis, especially in a critical period as pandemic of COVID-19 that is type of pneumonia. Therefore, an automatic method with high accuracy of classification is needed to perform classification of lung diseases due to the increasing number of cases. Convolutional Neural Networks (CNN) based classification has gained a big popularity over the last few years because of its speed and level of accuracy on the image's classification tasks. Through this article, we propose an implementation a CNN-based classification models using transfer learning technique to perform pneumonia detection and compare the results in order to detect the best model for the task according to certain parameters. As this has become a fast expanding field, there are several models but we will focus on the best outperforming algorithms according to their architecture, length and type of layers and evaluation parameters for the classification tasks. Firstly, we review the existing conventional methods and deep learning architectures used for segmentation in general. Next, we perform a deep performance and analysis based on accuracy and loss function of implemented models. A critical analysis of the results is made to highlight all important issues to improve.

1. Introduction

Pneumonia is an infection inflaming air sacs in the lungs, it can be bacterial or viral including covid-19 virus, but symptoms are often similar independently of the factors causing the disease [1]. Doctors need additional analysis or X-ray imaging to identify the cause of the pneumonia. The X-ray imaging of the lungs allows them to identify only if a lung has pneumonia or not [2].

Many germs can cause pneumonia including viruses, bacteria, and fungi commonly collected from the air and can overpower the immune system which leads to critical health situations. Therefore, early diagnosis [3] based on X-ray image classification is very important at first in order to prevent complications and make treatment efficient. Then advanced diagnosis is needed to determine the type and the cause of the pneumonia using medical tests and X-Ray scans.

Manual classification of pneumonia disease still the most efficient way, usually used by radiologists. The principle inconvenient of this method is about the time-consuming, which is a very important factor in the case of a pandemic.

Nowadays, many researchers become very interested in applications of artificial neural networks (ANN), especially convolutional neural networks (CNN). This method is efficient for medical image classification tasks. It makes computers capable of solving many pattern recognition and object extraction problems using datasets of 2D or 3D images. In case of 3D MRI images classification task it requires a huge processing capacity which can be bypassed by adopting a parallel algorithms [4], [5]. In [6], an example of the above parallel approach where the authors propose a parallel c-mean algorithm applied to MRI images classification showing good time complexity on its results.

To overcome the constrain of execution time, using Graphical Processing Units (GPU) become crucial today in medical image processing applications, especially in a context of machine and deep learning algorithms. They can significantly accelerate parallel processing, therefore almost all works related to medical image processing in medical field uses GPUs as accelerators to achieve better and fast results [7], [8].

*B. CHERRADI, CRMEF Casablanca-Settat, provincial section of El Jadida, 24000, Email: bouchaib.cherradi@gmail.com

However, machine learning algorithms and convolutional neural networks (CNNs) models have gained a lot of attention for almost all diseases classification and prediction problematic including breast cancer detection [9], cardio vascular prediction and diagnosis [10], [11], diabetes mellitus prediction [12], [13], etc.

In this work, we make an implementation of some CNN models using transfer learning technique. We used these models to perform pneumonia detection. Results evaluation and comparison is made in order to adapt and select the best model for the task according to certain parameters.

The rest of this paper is organized as follows: In section 2, we present a brief overview of some different classification techniques on relevant related work used for the prediction of various human diseases, and we focused on studies conducted on the prediction of pneumonia disease from lung X-ray images. Section 3 present the used dataset and CNN models. In section 4, we present the models experimental results and discuss the performance evaluation measures. Section 5 concludes this article and presents some perspectives at this work.

2. Related work

In this section, we review some related and similar works that matches classification task for pneumonia diseases using different machine and deep learning models. These models are evaluated within different metrics and reached less or more important performances, depending on their architecture and conception.

Recently many researches published about the pneumonia disease detection, especially ANN based models achieving great results which are very suitable for this type of disease. Note that COVID-19 virus causes severe pneumonia disease.

In 2019, the authors in [14] published a work concerning pneumonia detection applying a combination of mRMR feature selection and machine learning models on the Chest X-ray images. Features extraction is performed using existing CNN models: AlexNet, VGG16 and VGG19 and then combining the results as an input features set to feed and train five different machine learning models: decision tree, k-nearest neighbors, linear discriminant analysis, linear regression, and support vector. The experiment shows the best results for linear discriminant analysis obtaining 99.41% accuracy.

In January of 2020, the authors published in [15] a model based on transfer learning technique for Chest X-ray images of pneumonia disease. This model consists of combining AlexNet, DenseNet121, InceptionV3, resNet18 and GoogleNet generating a new architecture and reaching 96.39% accuracy on test images. The dataset used in this work is from Guangzhou-women-and-Children's Medical Center dataset [16].

Lately, the authors in [17] published a work about another method of automatic pneumonia detection based also on chest X-ray images focusing this time on specific region of interest (ROI) to classify and segment images. The method was compared in this study with five different classifiers: Multilayer perceptron, sequential minimal optimization (SMO), random forest, Classification via regression and classification via logistic regression. The proposed study shows a higher accuracy on logistic regression classifier with accuracy of 95.63% on test dataset.

In [18], another work published about a machine learning algorithm for pneumonia classification. In this work, the authors built a CNN model from scratch in order to classify images of pneumonia disease based on X-ray chest images obtaining a validation accuracy of 93.7%; where an augmentation method was adopted to increase the dataset size. In table 1, we summarize main information's about these works.

Based on these works and others, we develop and compare in this paper some convolutional neural networks in the goal to enhance the test accuracy on pneumonia disease detection from Lung X-ray images. In fact, we will introduce only automatic methods related to deep learning techniques which are the most adapted for the task of classifying 2D images based of lung X-ray datasets.

3. Materials and methods

3.1. Dataset description

The original dataset used in this work is called "Labeled Optical Coherence Tomography (OCT) and Chest X-Ray images for Classification" version 3 [19]. Only Chest X-Ray part is used in experiments. All models developed in this paper are trained and tested on this part of dataset. The concerned lung X-ray database

Table 1: Summary of related works methods and results.

Reference	Year	Method	Number of tested models	Best model or classifier	Dataset	Number of classes	Best accuracy
[14]	2019	Complex of mRMR feature selection and machine learning models	5	Linear Discriminant Analysis	Guangzhou-women-and-Children's Medical Center dataset	2	99.41%
[15]	2020	Transfer learning-based approach	5	Ensemble transfer learning based	Guangzhou-women-and-Children's Medical Center dataset	2	96.39%
[17]	2020	Automatic pneumonia detection based on ROI for classification	5	Logistic Regression	NIH ChestX-ray14 dataset	2	95.63%
[18]	2019	CNN based model for pneumonia disease classification	1	-	Guangzhou-women-and-Children's Medical Center dataset	2	93.7%

Table 2: Dataset distribution over training, validation and testing sub sets.

Dataset	NORMAL	PNEUMONIA
Training subset	1108	2991
Validation subset	238	641
Testing subset	237	641
Total dataset	1583	4273

is composed of 2 types of images: Images for normal patients (NORMAL) and images for patients with pneumonia disease (PNEUMONIA). In table 2, we summarize the structure of the dataset (Training, validation and Testing).

Figure 1 present some samples of normal and pneumonia lung x-ray images.

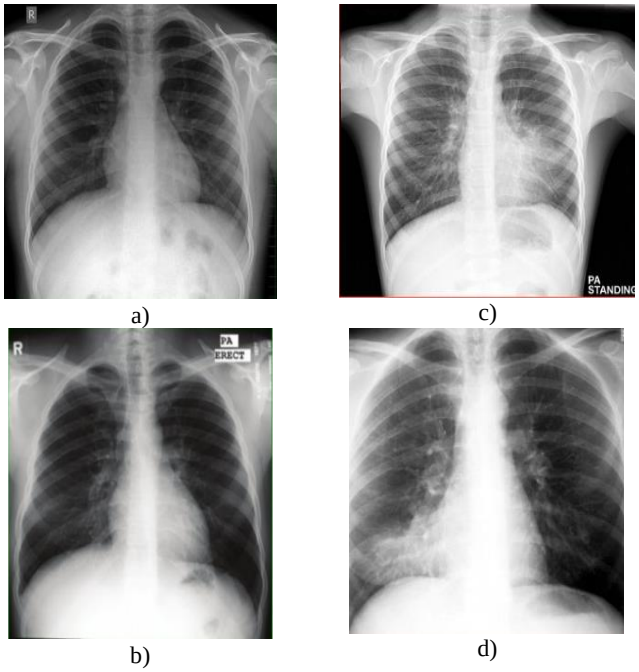

Figure 1: Example of Normal (a & b) and pneumonia (c & d) X-ray samples from the dataset.

3.2. Artificial Neural Network (ANN)

Artificial neural network (ANN) concept is inspired from the human brain being the smarter system that can process real data. The treatment ability came from connections between neurons of the brain. This structure forms a huge natural neural network able to resolve complicated operations in the real world. ANN is about superposing a lot of artificial neurons just like the natural neural network [20]. The elementary ANN (perceptron) is the simplest architecture of an artificial neural network, illustrated in figure 2.

The perceptron composed from input layer having a vector {xi} as inputs, sharable weights in the form of a vector $\{w_i\}$ too and a bias. $\{y_i\}$ presents the output of the perceptron in the form of a vector of probabilities of predictions.

3.3. Convolutional Neural Network (CNN)

Convolutional Neural Network (CNN) is an ANN network but the inverse is not true. CNN are most commonly applied to automatically process visual images. A CNN contains one or more convolution layer.

$$y_i = bias + \sum_{i=1}^{i=n} w_i . x_i = w_1 . x_1 + w_2 . x_2 + \cdots + w_n . x_n \quad (1)$$

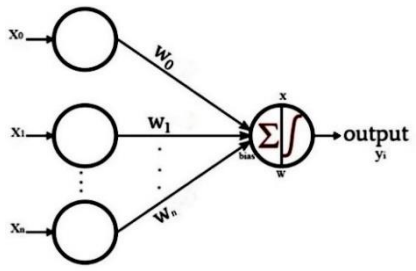

Figure 2: Architecture for a single layer perceptron.

The notion of CNN is old. This abstraction had been verified to work more accurately for recognition of hand written characters [21]. However, this type of networks loses the challenge to process large and heavy images. Therefore, this method was impractical because of the constraints of processing power, lack of memory and datasets availability. Nowadays, these limitations are relatively passed out, because of the technological evolution of storage, memory and methods optimization.

3.4. CNN Architecture

CNNs architecture consists of concatenating multiple types of layers successively which are input layers, convolutional layers and dense layers. In general, convolutional neural networks are based on its process on two principle factors: sharing weights and connectivity between neurons of each convolutional layer.

- Sharing weights: At each convolutional layer, every neuron has its weights that need to be shared to all neurons of the next layer. Those weights need also to be shared to all neurons in the previous layer in order to achieve back propagation process.
- Connectivity: All neurons of each layer are locally connected only to all neurons in the next layer. This connectivity conception reduces the complexity of the network.

Generally, to build a CNN network, an input layer is required with specific configuration including image shapes and patch. Then a convolutional layer's type must follow, also configured with specific number of neurons and specific function of optimization and activation. Each convolutional layer needs a pooling layer to follow with a specific filter of pooling. After that a number of Dense layers must be created before the output layer that requires a loss function to be configured [22].

3.5. Proposed methodology for lung pneumonia classification using CNN

The main steps for any image classification system are: image preprocessing, feature processing included in the convolution process, training the network and validating the resulted model. At the end testing the final CNN model.

Figure 3 shows the general architecture of a CNN model used to detect lung pneumonia containing input layer, convolution layers with *ReLU* activation function, pooling layers and fully connected layers.

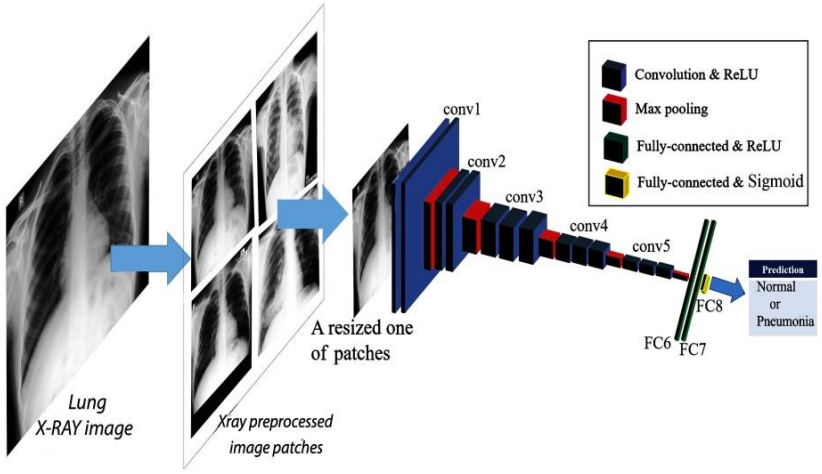

Figure 3: *Illustration of CNN architecture used for pneumonia detection on lung X-ray images.*

- **Dataset preprocessing:** it consists of preparing data to feed the network, this preparation is about reshaping and resizing images, dropping out unusable images and adapting contrast. Also converting raw data to victors and normalizing it [21]. The output of this process feeds a CNN network for training in order to become a pre-trained model, ready for the testing phase [23].

- **Features selection and extraction:** This step is included in the convolution layers, and consists of extracting useful features only, then converted to the adequate format.

  The selection part consists of selecting the most useful features to achieve the classification case of study [24].

- **Training:** At this phase the network is trained by updating weights of neurons across layers, it's called the learning process. This is done by minimizing the loss function and maximizing the accuracy rate of the validation part. If there is only two classes to predict, a sigmoid function is used for the loss optimization [24].

  The learning goal of the model is achieved using an optimizer from a huge scale of optimizers existing in the literature but the back-propagation algorithms are the most used in classification case [21].

- **Classification evaluation metrics**

  Almost all metrics to process the performance of a model are based on some primordial parameters to be calculated:

  True positive abbreviated by TP: Number of images accurately classified as pneumonia matching the ground truth.

  True negative abbreviated by TN: Number of images accurately classified as normal matching the true labels.

  False positive abbreviated by FP: CNN classifies images as containing pneumonia but that it's actually normal according to the ground truth.

  False negative abbreviated by FN: Number of images which the CNN classifies as not containing pneumonia but are actually containing pneumonia according to the ground truth labels [25].

  Based on those calculated parameters, we can compute the precision abbreviated as *P*, recall abbreviated as *R*, the F1 score and the accuracy as:

$$P = TP * \frac{1}{TP+FP} \quad (2)$$

$$R = TP * \frac{1}{TP+FN} \quad (3)$$

$$F1 = 2 * \frac{R*P}{R+P} \quad (4)$$

$$Accuracy = (TP + TN) * \frac{1}{TP+TN+FP+FN} \quad (5)$$

  F1 result is obtained by processing parameters in (Eq.2) and (Eq.3). The formula of this parameter is in (Eq.4).

- **Testing:** On this step we use test set as a different dataset and new one for the model. In order to well testing the model, the ground truth of the test set must be similar to the training set but not correlated. This makes the test more valid and accurate [26].

- **Classification:** This is the last step on the CNN model, it consists of affecting a label to each image from the input features with a specific confidence of decision:

  Initialization: Before to start the learning stage where the weights are updated over epochs. Those weights must have initiated by the initial values, in some cases those values are random. Otherwise those values are generated by a predefined function. The Xavier initialization is the usually used method of initialization [21].

  Activation function: This is the function representing the processing part of a neuron. It depends on the type a layer of the neural network. Most used activation function for layers in CNN network is *ReLU* function [27].

  Pooling: This phase consists of reducing the size of features by applying a filter and keeping only the most important elements. The most popular pooling method in CNN models is max pooling and average pooling. The max pooling consists of selecting only the maximum element in the filter and the average pooling consists of averaging all elements inside the filter [21].

  Regularization: This technic is about reducing over fitting problems and improving performance of the model. There are many methods to ensure regularization, and the most

popular method is dropout. The dropout method is based on eliminating the less important features on each iteration [27].

Loss Function: This hyper parameter defines the function that evaluates how much the trained model can fail predicting the affected task. Its value is reverse to the accuracy value. More the loss is minimal the more the accuracy must be maximal. The quadratic error is the most used for loss function in CNNs [28].

4. Results and discussion

CNNs models have proven interesting results in many applications lately. These models existed in literature differ in the network size, defined optimizers and the type of layers used.

Training task require a big processing capacity which leads us to choose a parallel architecture of processing, by adopting graphical processing unit (GPU), in the virtual environment to accelerate the training step offered by *KAAGLE* platform. In our experiment we used dual cores of CPU with 13 GB of RAM memory equipped with a GPU of 16 GB of RAM memory.

4.1. Building proposed CNN models using transfer learning approach

In our experiment, we build and compile five different models based on existing models in the literature using transfer learning technique.

Depending on the case, each model can succeed or fail the classification task. For our case of pneumonia detection problematic and after running many algorithms many times by trying at each different configuration, we select those architectures in figure 4. With given configurations relatively presenting better results in term of accuracy and loss taking in consideration the over-fitting and the under-fitting problems.

4.2. Compiling and training CNN models

In all models experimented in this work, we add two dropout layers and one dense layer with SOFTMAX activation at the output layer as a classifier. We used a logistic regression algorithm called "RMSProp" optimizer and categorical cross entropy accuracy as a metric during the model compilation.

Weights are initialized using image-net. We decide to not freeze any layer of the original model, because of the nature of pneumonia detection problematic compared to the originally trained dataset.

In order to reduce over fitting on training layers, we used a callback parameter specifying to stop training when no accuracy improvement happened within three successive iterations. That obliges the training process to stop at the epoch where no accuracy improvement happened.

4.3. Validation and testing the given CNN models

While training our proposed models, the validation process goal consists of checking the accuracy of the model in each epoch. Then update weights on the back-propagation process to use in the next epoch for learning. For this task, we used validation dataset as described in figure 1.

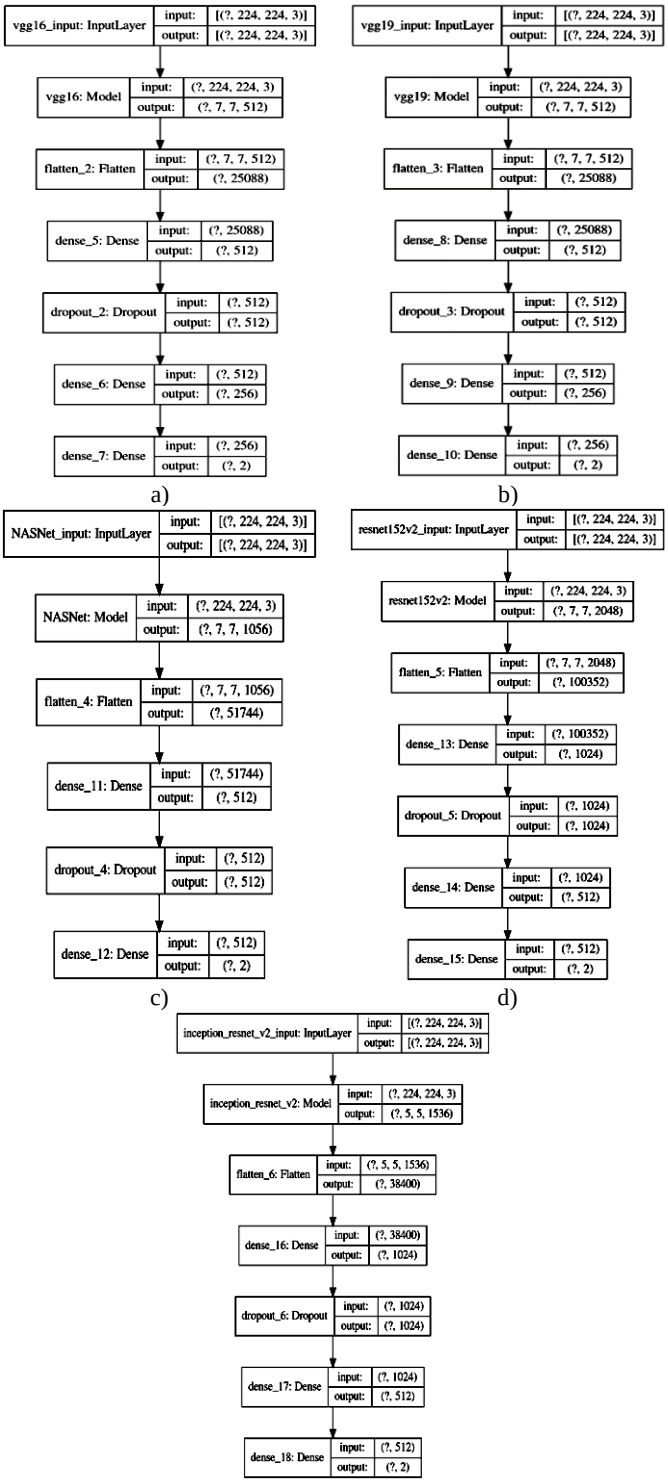

Figure 4: Architecture of proposed transfer learning-based models: (a) VGG16, (b) VGG19, (c) NasNetMobile, (d), ResNet152V2 (e) Inception-Resnet-v2.

In this step, we can get the performance and evaluation metrics for our models before trust them for real case classification.

In general VGG16 gets good results in many cases for fine-tuning task [29], this is the mean reason of choosing this model at first for transfer learning to process pneumonia classification.

As shown in figure 5, for the VGG16 based transfer learning model we get the best accuracy and very interesting accuracy

evolution over iterations compared to other tested models. The accuracy continues improving until the 30th epoch and the convergence between the validation and the training accuracy is very good, which makes this model the most adapted for our task. The first 10 epochs show a fast improvements and convergence of the accuracy then the next epochs converge very well but improves slowly without losing convergence aspect.

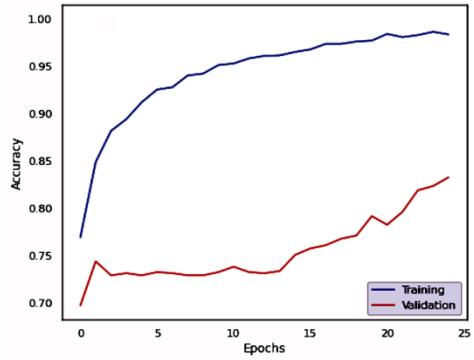

a)

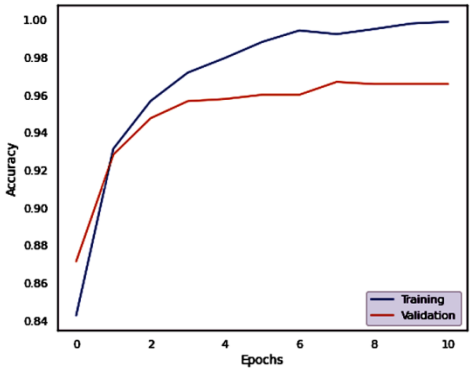

b)

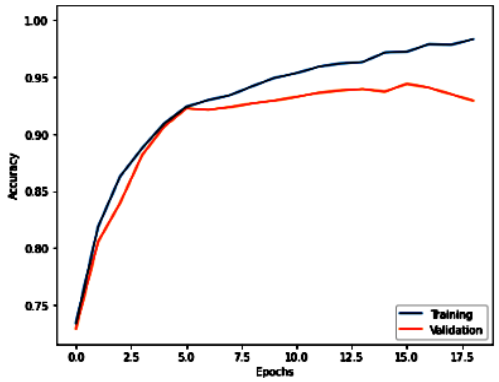

c)

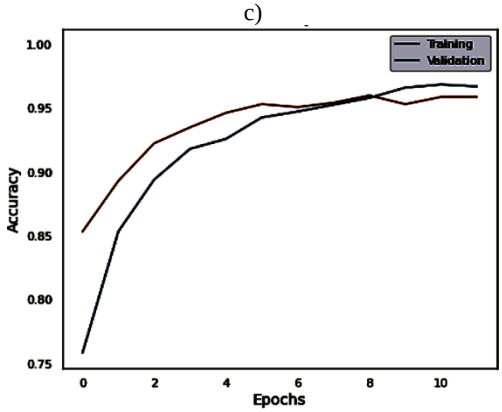

(d)

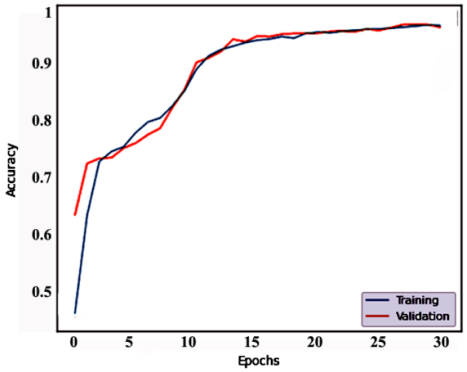

(e)

Figure 5: Evolution of training and validation accuracy over epochs for different models: a) NasNetMobile based model, b) ResNet152V2, c) Inception-Resnet-v2 based model, d) VGG19 based model, e) VGG16 based model.

From figure 6, it's clear that all well predicted features show probability over 80% (green aspect), and the only miss predicted feature (red aspect) here shows a 68% probability of confidence which is also a clear indication for experts to give more interest of verification and correction for non-confident classifications. Therefore, the model can be a good tool to help for pneumonia disease diagnosis. Time and effort for medical experts in diagnosing pneumonia cases specially in the case of COVID-19 can be saved. In fact, human visual system has many limitations about detecting the gray-scale resolutions even with high brightness and contrast, X-Ray images can present a large scale of gray-scale shades than the human eye could detect. This is another reason why the automatic diagnosis is primordial for improving the disease detection.

VGG19 based transfer learning model shows also good accuracy convergence, where the maximum value is achieved on the 10th epoch and relatively starts to stabilize for the next epochs, therefore the algorithm ends to avoid over-fitting.

Models: Inception-Resnet-v2 based model and ResNet152V2 based shows similar accuracy evolution results. Speed of convergence for the first one is performed after 18 epochs but for the second in just 10 epochs. That gives an advantage for the second one. The NasNetMobile based model shows a very bad accuracy results in term of convergence or accuracy values, which makes this model badly ranked for this task.

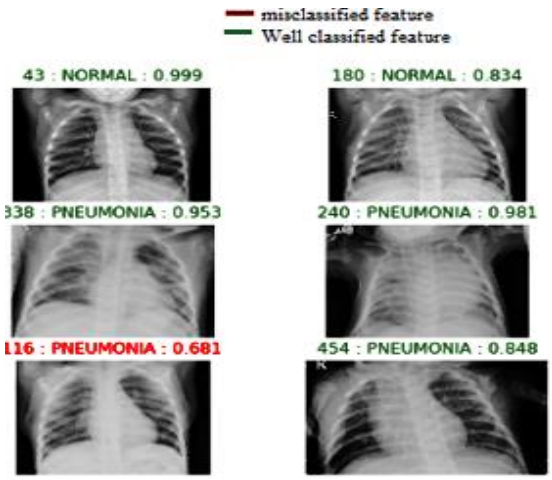

Figure 6: Example of predicted features using a VGG 16 based transfer learning model showing in the left the id number of the feature in the testing dataset and the probability of prediction in the right.

Loss curve is also an important tool to evaluate models just like the accuracy curve. In our experiment, results of loss functions are illustrated in figure 7.

Similarly, to accuracy curve analysis, this tool confirms that VGG16 based model is the best model achieving pneumonia detection task. NasNetMobile based model shows again the worst results for this task. Regarding confusion matrix tool, our models shows the following results:

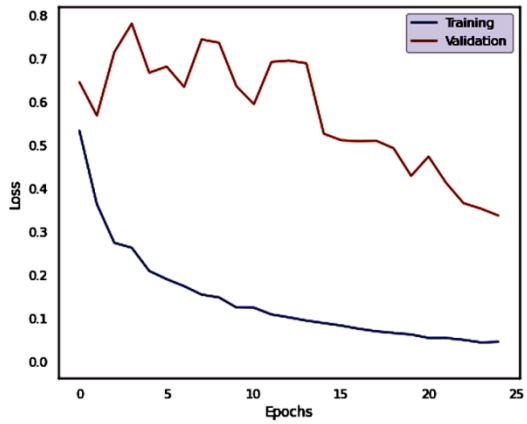

a) NasNetMobile based model

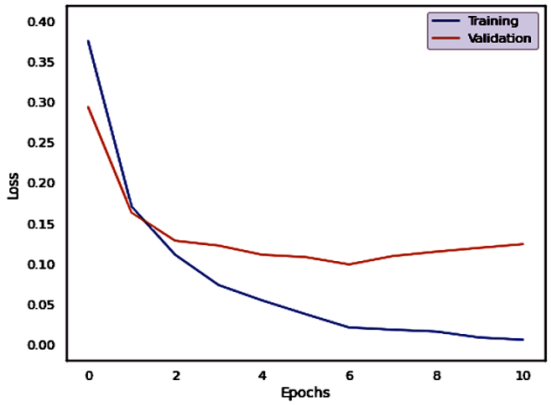

b) ResNet152V2

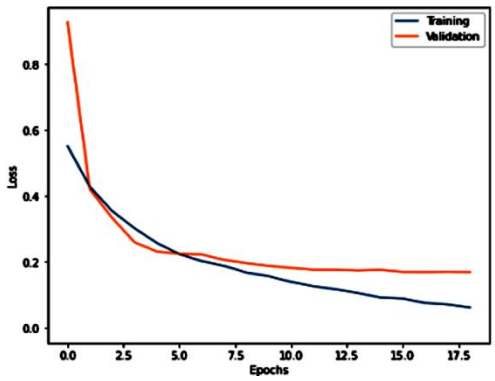

c) Inception-Resnet-v2 based model

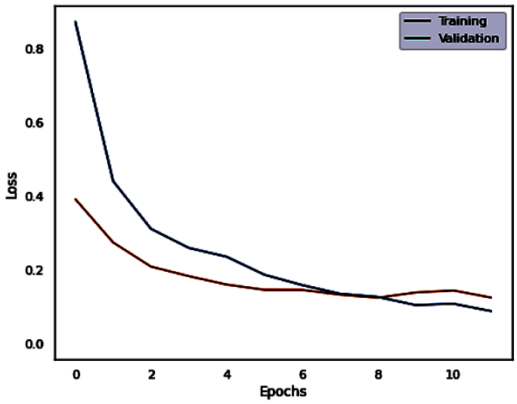

d) VGG19 based model

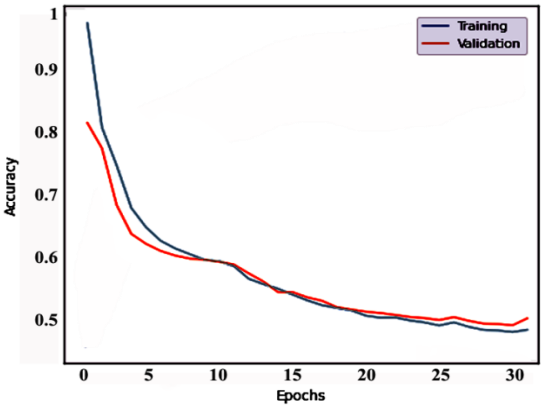

e) VGG 16 based model

Figure 7: Evolution of training and validation loss over epochs for different models: a) NasNetMobile based model, b) ResNet152V2, c) Inception-Resnet-v2 based model, d) VGG19 based model, e) VGG16 based model.

VGG19 based model failed on predicting the 26 case of pneumonia but succeed on predicting 615 of 641 features. The model also failed to predict normal for only 4 cases. In general, this is a good result regarding the total number of cases.

VGG16 based model fails detecting 21 pneumonia cases which make it better than VGG19 based model. But not efficient on detecting pneumonia cases compared to Resnet152V2 based.

However, ResNet152V2 based total fails of 32 predictions including normal and pneumonia cases. Which is more than VGG16 based model. Therefore VGG 16 based model presents the best confusion matrix results in this experiment. The other models in this experiment show fewer interesting results on their confusion matrix. Classification based on CNN methods for Medical images gets the better performance (accuracy) on fine-tuning the model VGG16 modeled by Google Company, showing the results of almost: 97% for pneumonia detection, 11.51% loss. It is clear that

Table 3: Comparison of different implemented CNN models.

Method	Epochs	Learning rate	Optimizer	Activation	Loss function	Accuracy	Loss	Precision	Recall	F1-score
VGG16 based	33	10^{-5}	RMSProp	Softmax	Categorical cross entropy	**96.81%**	**11.51%**	91%	97%	94%
VGG19 based	12	10^{-5}	RMSProp	Softmax	Categorical cross entropy	96.58%	14.43%	**96%**	**99%**	**98%**
NasNetMobile based	25	10^{-5}	RMSProp	Softmax	Categorical cross entropy	83.37%	36.13%	43%	91%	58%
ResNet152V2 based	11	10^{-5}	RMSProp	Softmax	Categorical cross entropy	96.35%	16.27%	93%	94%	93%
InceptionResNetV2 based	18	10^{-5}	RMSProp	Softmax	Categorical cross entropy	94.87%	17.18%	89%	90%	89%

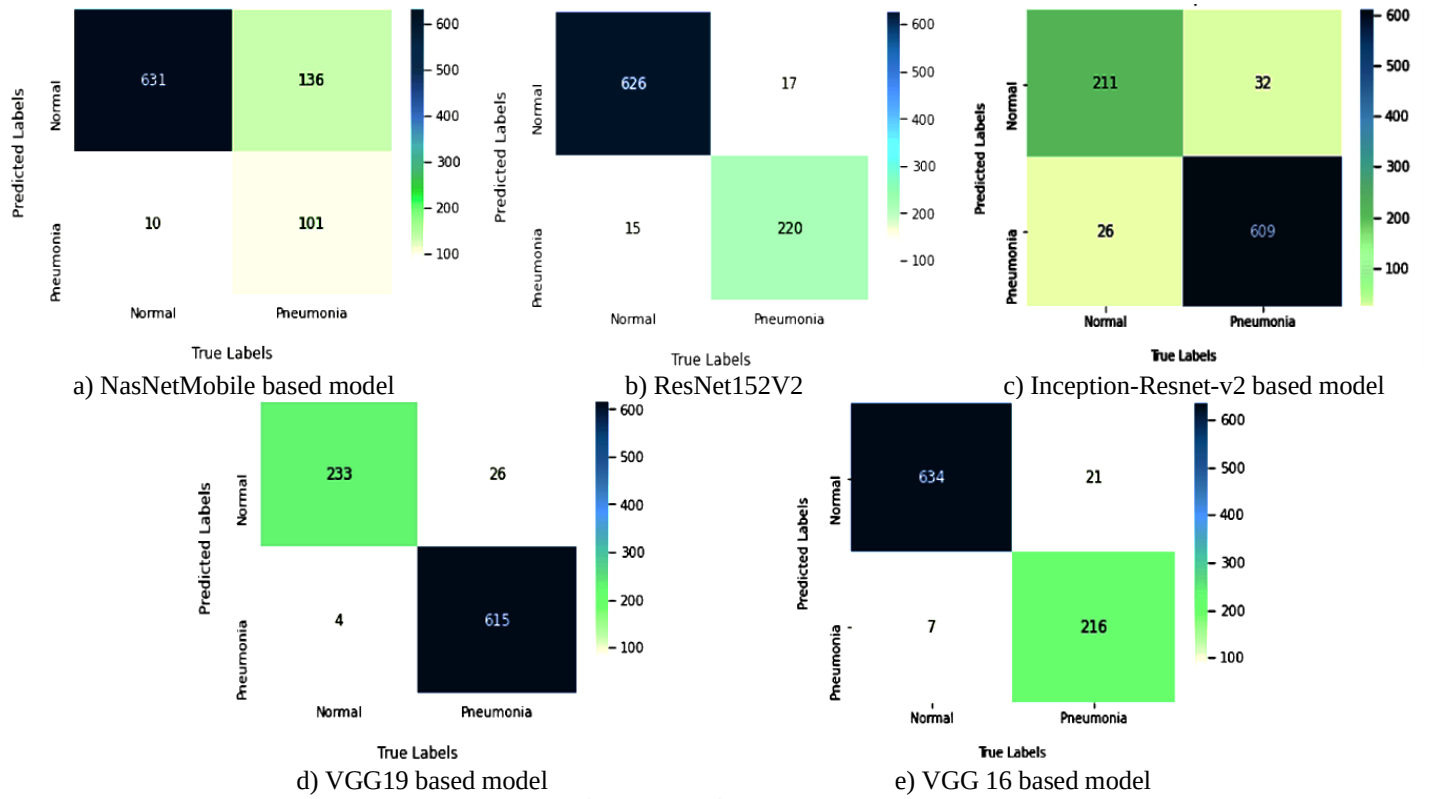

a) NasNetMobile based model b) ResNet152V2 c) Inception-Resnet-v2 based model

d) VGG19 based model e) VGG 16 based model

Figure 1: Confusion matrix of all trained and tested models.

loss function of the model VGG16 based model is minimal; also, its accuracy presents the maximum of all trained models. VGG16 based model get into its maximum value of accuracy on epoch 33 with loss value of 11.51% and precision of 91%. VGG19 based model is very close to the VGG16 based one in term of accuracy, but the rest of the models as showed in table 3 presents relatively bad accuracy results to trust for our task.

ROC curve is a fundamental tool for model performance evaluation based on sensitivity/specificity reports or true positive rate and false positive rate, in this ROC graph each curve the sensitivity (true positive rate) is plotted as a function of a specificity value (false positive rate). Area under the curve (AUC) represents how well the model can distinguish between a normal and pneumonia image called.

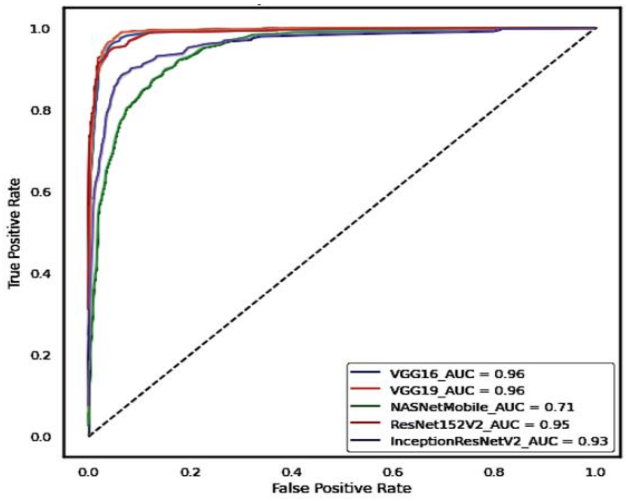

Figure 2: ROC curve comparison for all implemented models.

In general, more the area is big, more the curve is near to the left corner of the graph and more the represented model is better in terms of performance.

5. Conclusion and perspectives

Pneumonia disease classification is a primordial step for diagnosing lung infections which can be caused by several factors including covid-19.

Machine learning methodology especially convolutional neural networks are a very interesting techniques to automatically, efficiently and rapidly output results.

This method faces sense the beginning many problems like the leak of datasets in the world and algorithms complexities in time and processing.

To improve prediction accuracy more and more some extensions must be done, like increasing the dataset by combining multiple independent datasets to set a bigger database of samples that conduct us to use higher processing performances in order to train all the given dataset in a reasonable time and epochs, we need also to preprocess differently the input images by cropping and correcting contrast on X-Ray images based on processing concentration while training, and also proposing the best adapted optimizer on training.

Also, we plan in the future to make our conception of optimized novel model adapted specially for chest X-Ray images. Training stage takes relatively a lot of time depending on the complexity of the algorithm that must be optimized as much as possible and the capacity of available resources. Therefore, there is a lot of required work to achieve by researchers' efforts to take benefits of this magic field in our world.

Conflict of Interest

The authors declare no conflict of interest.

Acknowledgment

This work is a part of a project supported by co-financing from the CNRST (Centre National pour la Recherche Scientifique et Technique) and the Hassan II University of Casablanca, Morocco. The project is selected in the context of a call for projects entitled "Scientific and Technological Research Support Program in Link with COVID-19" launched in April 2020 (Reference: Letter to the Director of "Ecole Normale Supérieure de l'Enseignement Technique de Mohammedia" dated the 10th June 2020).

References

[1] S. Kang, W. Peng, Y. Zhu, S. Lu, M. Zhou, W. Lin, W. Wu, S. Huang, L. Jiang, X. Luo, M. Deng, "Recent progress in understanding 2019 novel coronavirus (SARS-CoV-2) associated with human respiratory disease: detection, mechanisms and treatment," International Journal of Antimicrobial Agents, 105950, 2020, doi:10.1016/j.ijantimicag.2020.105950.

[2] A. Jacobi, M. Chung, A. Bernheim, C. Eber, "Portable chest X-ray in coronavirus disease-19 (COVID-19): A pictorial review," Clinical Imaging, **64**, 35–42, 2020, doi:10.1016/j.clinimag.2020.04.001.

[3] J. Gong, J. Ou, X. Qiu, Y. Jie, Y. Chen, L. Yuan, J. Cao, M. Tan, W. Xu, F. Zheng, Y. Shi, B. Hu, "A Tool to Early Predict Severe Corona Virus Disease 2019 (COVID-19) : A Multicenter Study using the Risk Nomogram in Wuhan and Guangdong, China," Clinical Infectious Diseases, ciaa443, 2020, doi:10.1093/cid/ciaa443.

[4] H. Moujahid, B. Cherradi, L. Bahatti, Convolutional Neural Networks for Multimodal Brain MRI Images Segmentation: A Comparative Study, Springer International Publishing, Cham: 329–338, 2020.

[5] N.A. Ali, B. Cherradi, A. El Abbassi, O. Bouattane, M. Youssfi, "Parallel Implementation and Performance Evaluation of some Supervised Clustering Algorithms for MRI Images Segmentation," in Proceedings of the 4th International Conference on Big Data and Internet of Things, ACM, Rabat Morocco: 1–7, 2019, doi:10.1145/3372938.3373007.

[6] O. Bouattane, B. Cherradi, M. Youssfi, M.O. Bensalah, "Parallel c-means algorithm for image segmentation on a reconfigurable mesh computer," Parallel Computing, **37**(4), 230–243, 2011, doi:10.1016/j.parco.2011.03.001.

[7] N. Ait Ali, B. Cherradi, A. El Abbassi, O. Bouattane, M. Youssfi, "GPU fuzzy c-means algorithm implementations: performance analysis on medical image segmentation," Multimedia Tools and Applications, **77**(16), 21221–21243, 2018, doi:10.1007/s11042-017-5589-6.

[8] N.A. Ali, B. Cherradi, A. El Abbassi, O. Bouattane, M. Youssfi, "Modelling the behavior of the CPU and the GPU versus the clusters number variation for sequential and parallel implementations of BCFCM algorithm," ARPN Journal of Engineering and Applied Sciences, **12**(21), 6030–6038, 2017.

[9] S. Laghmati, A. Tmiri, B. Cherradi, "Machine Learning based System for Prediction of Breast Cancer Severity," in 2019 International Conference on Wireless Networks and Mobile Communications (WINCOM), IEEE, Fez, Morocco: 1–5, 2019, doi:10.1109/WINCOM47513.2019.8942575.

[10] O. Terrada, A. Raihani, O. Bouattane, B. Cherradi, "Fuzzy cardiovascular diagnosis system using clinical data," in 2018 4th International Conference on Optimization and Applications (ICOA), IEEE: 1–4, 2018.

[11] O. Terrada, B. Cherradi, A. Raihani, O. Bouattane, "Atherosclerosis disease prediction using Supervised Machine Learning Techniques," in 2020 1st International Conference on Innovative Research in Applied Science, Engineering and Technology (IRASET), IEEE, Meknes, Morocco: 1–5, 2020, doi:10.1109/IRASET48871.2020.9092082.

[12] O. Daanouni, B. Cherradi, A. Tmiri, "Predicting diabetes diseases using mixed data and supervised machine learning algorithms," in Proceedings of the 4th International Conference on Smart City Applications - SCA '19, ACM Press, Casablanca, Morocco: 1–6, 2019, doi:10.1145/3368756.3369072.

[13] O. Daanouni, B. Cherradi, A. Tmiri, "Diabetes Diseases Prediction Using Supervised Machine Learning and Neighbourhood Components Analysis," in Proceedings of the 3rd International Conference on Networking, Information Systems & Security, ACM, Marrakech Morocco: 1–5, 2020, doi:10.1145/3386723.3387887.

[14] M. Toğaçar, B. Ergen, Z. Cömert, F. Özyurt, "A Deep Feature Learning Model for Pneumonia Detection Applying a Combination of mRMR Feature Selection and Machine Learning Models," IRBM, S1959031819301174, 2019, doi:10.1016/j.irbm.2019.10.006.

[15] V. Chouhan, S. Singh, A. Khamparia, D. Gupta, P. Tiwari, C. Moreira, R. Damasevicius, V. Albuquerque, "A Novel Transfer Learning Based Approach for Pneumonia Detection in Chest X-ray Images," Applied Sciences, **10**, 559, 2020, doi:10.3390/app10020559.

[16] D.S. Kermany, M. Goldbaum, W. Cai, C.C.S. Valentim, H. Liang, S.L. Baxter, A. McKeown, G. Yang, X. Wu, F. Yan, J. Dong, M.K. Prasadha, J. Pei, M.Y.L. Ting, J. Zhu, C. Li, S. Hewett, J. Dong, I. Ziyar, A. Shi, R. Zhang, L. Zheng, R. Hou, W. Shi, X. Fu, Y. Duan, V.A.N. Huu, C. Wen, E.D. Zhang, et al., "Identifying Medical Diagnoses and Treatable Diseases by Image-Based Deep Learning," Cell, **172**(5), 1122–1131.e9, 2018, doi:10.1016/j.cell.2018.02.010.

[17] B.B. Chaudhuri, M. Nakagawa, P. Khanna, S. Kumar, Proceedings of 3rd International Conference on Computer Vision and Image Processing: CVIP 2018, Volume 1, Springer Nature, 2019.

[18] O. Stephen, M. Sain, U.J. Maduh, D.-U. Jeong, "An Efficient Deep Learning Approach to Pneumonia Classification in Healthcare," Journal of Healthcare Engineering, **2019**, 1–7, 2019, doi:10.1155/2019/4180949.

[19] D. Kermany, K. Zhang, M. Goldbaum, "Large Dataset of Labeled Optical Coherence Tomography (OCT) and Chest X-Ray Images," **3**, 2018, doi:10.17632/rscbjbr9sj.3.

[20] C. Senaras, M.N. Gurcan, "Deep learning for medical image analysis," Journal of Pathology Informatics, **9**(1), 25, 2018, doi:10.4103/jpi.jpi_27_18.

[21] Y. Lecun, L. Bottou, Y. Bengio, P. Haffner, "Gradient-based learning applied to document recognition," Proceedings of the IEEE, **86**(11), 2278–2324, 1998, doi:10.1109/5.726791.

[22] S. Srinivas, R.K. Sarvadevabhatla, K.R. Mopuri, N. Prabhu, S.S.S. Kruthiventi, R.V. Babu, An Introduction to Deep Convolutional Neural Nets for Computer Vision, Elsevier: 25–52, 2017.

[23] N. Tajbakhsh, J.Y. Shin, R.T. Hurst, C.B. Kendall, J. Liang, Automatic Interpretation of Carotid Intima–Media Thickness Videos Using Convolutional Neural Networks, Elsevier: 105–131, 2017.

[24] S. Miao, J.Z. Wang, R. Liao, Convolutional Neural Networks for Robust and Real-Time 2-D/3-D Registration, Elsevier: 271–296, 2017.

[25] H. Chen, Q. Dou, L. Yu, J. Qin, L. Zhao, V.C.T. Mok, D. Wang, L. Shi, P.-A. Heng, Deep Cascaded Networks for Sparsely Distributed Object Detection from Medical Images, Elsevier: 133–154, 2017.

[26] N. Srivastava, G. Hinton, A. Krizhevsky, I. Sutskever, R. Salakhutdinov, "Dropout: A Simple Way to Prevent Neural Networks from Overfitting," Journal of Machine Learning Research, **15**(56), 1929–1958, 2014.

[27] H.-I. Suk, An Introduction to Neural Networks and Deep Learning, Elsevier: 3–24, 2017.

[28] F.C. Ghesu, B. Georgescu, J. Hornegger, Efficient Medical Image Parsing, Elsevier: 55–81, 2017.

[29] S.S. Yadav, S.M. Jadhav, "Deep convolutional neural network based medical image classification for disease diagnosis," Journal of Big Data, **6**(1), 113, 2019, doi:10.1186/s40537-019-0276-2.

ASTES

Advances in Science, Technology and Engineering Systems Journal
Vol. 5, No. 5, 217-223 (2020)
www.astesj.com
Special Issue on Innovative Research in Applied Science, Engineering and Technology

ASTES Journal
ISSN: 2415-6698

Thermal Performance Analysis of Parabolic Trough Solar Collector System in Climatic Conditions of Errachidia city, Morocco

Mohamed Hajjaj[*,1], Amine Tilioua[2], Abdellah Mellaikhafi[2], Abella Bouaaddi[1]

[1]*Laboratory Engineering Energy, Materials and Systems, Department of Physics, National School of Applied Sciences, Ibn Zohr University Agadir, 80000, Morocco*

[2]*Thermal and Applied Thermodynamics, Mechanics Energy Efficiency and Renewable Energies Laboratory, Department of Physics, Faculty of Sciences and Techniques Errachidia, Moulay Ismaïl University of Meknès, B.P. 509 Boutalamine Errachidia, Meknes, 50050, Morocco*

ARTICLE INFO

Article history:
Received: 03 July, 2020
Accepted: 19 July, 2020
Online: 14 September, 2020

Keywords:
Parabolic Trough Collector
Absober tube
Solar Domestic Heating Water
Direct Normal Irradiation
Temperature
Modelling

ABSTRACT

The water heating with parabolic trough solar collectors (PTC) is a very widespread and at the same time quite promising solar technology. However, PTC presents several problems in terms of the profitability of water heating. For this reason, our study of water heating with PTC collectors consists of two main parts. In the first part, we investigate the effect of direct normal irradiation in the absorber tube using the TRNSYS software of the Errachidia city. In the second part, the study is entirely focused on the heat balance of the absorber tube in order to estimate the fluid outlet temperature. Besides, a mathematical model is developed to simulate and control the fluid outlet temperature circulating through the absorber tube of the collector. The water outlet temperature prediction was carried out by a thermal performance study of the PTC in weather conditions of Errachidia city (Morocco) using TRNSYS software and Matlab Code in the year's typical days.

1 Introduction

A great deal of effort has been made, especially in the last decade to improve systems for converting solar energy into heat and particularly for electricity production. Parabolic trough reflector technology is the most common and is currently used by the most powerful solar power plants in the world and improving the efficiency of these concentrators is the concern of several researchers. The PTC offers the possibility to produce electricity and hot water from solar energy. The temperature of the fluid can be raised up to 500 ° C. The operating principle of this technology is based on the concentration of the sun's rays on a horizontal tube, where a heat transfer fluid circulates that will be used to transport the heat to the power plant itself. The parabolic-cylindrical collector is composed of a long mirror (usually with silver or polished aluminum plating), rectangular, parabolic cylinder shape and completed by a tube with a double vacuum envelope that runs along the entire length of the focal length line. The sun's rays are reflected by the mirror to converge on the tube. The absorber tube is the essential part of the concentrator, it is often made of copper covered with a selective layer, and it is surrounded by a transparent glass envelope. The parabolic shape of the mirrors allows the sun's rays to be concentrated throughout the tube. By circulating the heat-transfer fluid in the center of this tube, the fluid is heated and conducts the heat to the container with a determined flow rate. As with any concentrating collector, parabolic troughs need to follow the sun in order to concentrate direct solar radiation. As a line concentration collector, the parabolic cylinder has a single axis tracking system. Schematic of the solar PTC system with receiver is presented in Figure 1. Several studies have been conducted by researchers to improve the energy efficiency of parabolic trough systems. Cheng et al [1] examined the temperature distribution at the outer surface of the absorber tube of a CCP as a function of the surface radiation flux distribution using the Monte Carlo MCRT method. The authors have combined the MCRT method and the finite volume method via the Fluent ANSYS calculation code, elaborating a multitude of simulations and taking into account the dependence of the physical properties of the heat transfer fluid (Sylitherm 800 oil) with temperature. The results obtained were compared with previous experimental data [2] and it was noticed that there was a 2% difference in the temperature

[*]Corresponding Author: Mohamed Hajjaj, BP 607 Boutalamine, Errachidia 52000, Morocco. Email: med.hajjaj85@gmail.com

of the heat transfer fluid (HTF) at the absorber outlet. In addition, Kaloudiset al [3] performed a numerical study on the collector of a parabolic-cylinder concentrator system with nano heat transfer fluid, in order to simulate the SEGS LS2 type collector. The authors used four cases of boundary conditions for numerical simulation involving all heat transfer modes at the different tube interfaces.

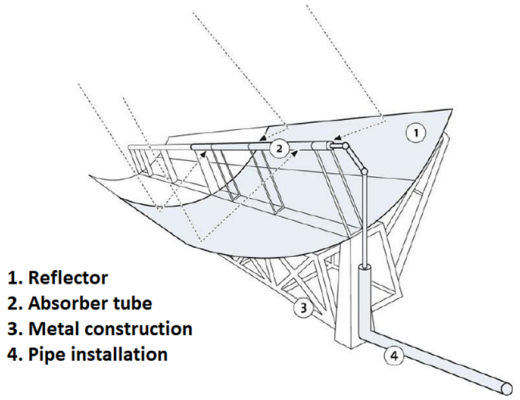

Figure 1: Schematic of the PTC system with receiver [4]

Besides, In [5], the authors have investigated the energy performance of a PTC solar in the climatic conditions of the Algerian Sahara. The authors performed a simple numerical simulation of the one-dimensional implicit finite difference method applied to the energy balance of solar collectors by dividing the absorber tube, the glass cover and the fluid in many segments. Both fluids were used, water and synthetic oil TherminolVP-1 in the simulation. However, simulation results showed that the thermal efficiency is approximately 69.73 and 72.24%, which decreases at higher temperatures of synthetic oil-based fluids but increases by 2% at lower water temperatures. Bellos et al [6] have studied three different types of parabolic cylindrical collectors (vacuum tube receptor, non-vacuum tube receptor and bare tube without cover) to improve the thermal margin with the implementation (Syltherm 800/Cu) in a systematic manner. The use of nanofluids improved performance in the bare tube with 7.16%, 4.87% for the non-evacuated receptor and 4.06% for the evacuated receptor at a flow-rate of 25 L/min. Zhao et al [7] have examinated the global performance of the PTC solar using three different tubes (one smooth and two internally finned tubes), the authors characterized the solar collector performance by energy efficiency, exergy efficiency and thermo-hydraulic efficiency. The results obtained showed that the output temperature of the solar air collectors depends on the solar irradiation, the air flow rate and the geometry parameters of the spindle fin. IPF#2 tubes have the highest collector efficiency and air temperature, while the STube without using pin fins has the lowest values.

In Morocco, the solar plan is part of the national energy strategy which aims at quantitatively assessing the level of security of a secure and sustainable, clean, green and accessible energy provision [8]. The idea is, therefore, to study the energy efficiency of a parabolic trough solar collector and the thermal behavior of an absorber tube to improve their efficiency. The simulation is divided into two steps, the first part includes the simulation using the TRNSYS software [9], on the entire cylindro-parabolic system whose aim is to control this system and especially its operation in Saharan environment, in order to provide hot water in collective buildings [10], and taking into account the specific climatic effects in the Errachidia city (South of Morocco). In the second part, we numerically investigate using a developed Matlab code the geometrical effect of absorber tubes in order to improve the energy efficiency of a parabolic trough solar collector.

2 Theoretical study

2.1 Optical performance of PTC

2.1.1 Concentration rate

The concentration rate is defined as the ratio of the opening surface to the receiver surface[11, 12].

$$C = \frac{S_O}{S_r} \tag{1}$$

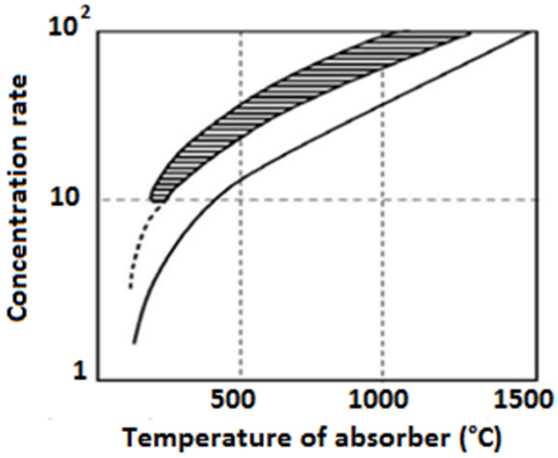

Figure 2: Concentration rate as function of the receiver temperature[11]

Figure 2 shows the variation in concentration rate as a function of absorber temperature.

- Low concentration:

  $1 < C < 10$ involved $T_C \approx 150$ °C

- Average concentration:

  $10 < C < 100$ involved $T_C \approx 1000$ °C

- High concentration:

  $C \geqslant 100$ involved $T_C \geqslant 1000$ °C

2.1.2 Radiation absorption

The radiation absorption is defined as follows [12]:

$$E = E_b.\rho.(\gamma.\tau).C \tag{2}$$

2.2 Thermal performance study of PTC

The thermal performance of PTC can be determined from different methods. The power received of PTC (Q_u) is determined from the quantities (F_R) and (U_L)[12].

2.2.1 Overall heat loss factor U_L (covered tube)

In the event that the tube receiver is covered by a glass selective surface (S_C), the irradiation coefficient in the glass to absorber region is dissimilar from the irradiation coefficient in the absorber to glass region, this coefficient is usually negligible [10]. The coefficient of heat loss is expressed by relationship:

$$F' = \frac{\frac{1}{U_L}}{\frac{1}{U_L} + \frac{D_e}{h_{fi} D_i (\frac{D_e}{2\lambda} \ln \frac{D_e}{D_i})} + \frac{1}{U_L}} \quad (3)$$

$$F_R = \frac{m_f . C_p}{S_r . U_L} . \left[1 - e^{\left(\frac{S_r . U_L . F'}{m_f . C_p}\right)}\right] \quad (4)$$

$$U_L = \left[\frac{S_r}{(h_v + h_{r,c-a}).S_r} + \frac{1}{h_{r,a-c}}\right] \quad (5)$$

$$h_{r,c-a} = \frac{\sigma(T_r^2 - T_c^2).(T_r - T_c)}{\frac{1-\varepsilon_r}{\varepsilon_r} + \frac{1}{F_{rc}} + \frac{(1-\varepsilon_c).S_r}{\varepsilon_c . S_c}} \quad (6)$$

$$h_{r,a-c} = 4.\sigma.\varepsilon.\bar{T}^3 \quad (7)$$

2.2.2 Useful heat (Q_u)

The useful heat is determined from the power recovered by the PTC at the focal line and it is expressed by the following relationship:

$$Q_U = F_R.[E.\rho.\tau.\alpha.\gamma.S_o - U_L.S_r(T_{out} - T_{inl})] \quad (8)$$

2.2.3 The outlet temperature T_{out} of HTF

The output temperature of HTF is determined from the following equation [13]:

$$T_{out} = T_{inl} + \frac{Q_U}{m_f . C_p} \quad (9)$$

2.2.4 Solar concentrator efficiency η

The efficiency of the PTC is given by the following relationship [14].

$$\eta = \frac{Q_U}{E.\gamma.S_o} \quad (10)$$

3 Numerical simulation

3.1 TRNSYS model

To evaluate the thermal efficiency of a solar PTC, we used the TRNSYS software. It allows users to specify the system components and to connect these components together. Each component (type) contains input and output parameters.

In the present study, a new numerical model is developed using the Matlab language to simulate the temperature evolution in the fluid, absorber and glass cover. Concerning the simulation by TRNSYS software, we used the different components such as a parabolic cylindrical collector (type 536) and a pump (type 3d). Other components used: weather (type 109), regulation (type 2b) ON/OFF differential controller, storage tank (type 4c) and online plotter (type 65a). The schematic of the TRNSYS model of the PTC system takes into account water as HTF in the weather conditions of Errachidia city, it is presented in Figure 3.

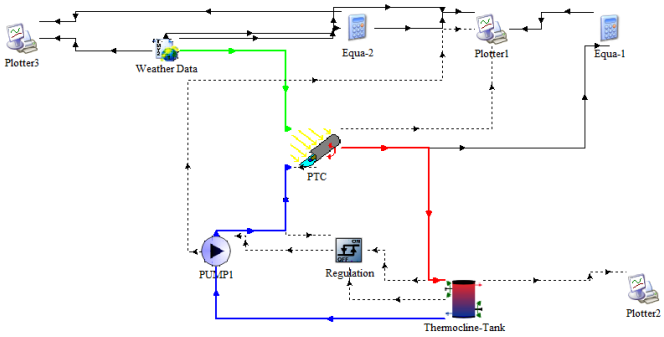

Figure 3: TRNSYS model of a solar PTC with Thermocline- Tank

3.2 Weather data of Errachidia city

Morocco's energy efficiency agency has proposed a new classification of climatic zones, each having different meteorological properties. In addition, the wind speed, ambient temperature, and total radiation on the inclined surface of the city under study are generated by the METEONORM software. According to this study's aims, which focuses on the thermal efficiency of a PTC tube for the Errachidia site. Geographical localization of Errachidia city (semi-arid climate) offers the ideal climatic conditions such as intense sunshine all year round, low humidity and precipitation. The ambient temperature variation all year round in the selected zone is shown in Figure 4. Besides, the estimation of the direct normal irradiation (DNI) throughout the year is shown in Figure 5. The evolution of the annual inlet and outlet temperature of the water is illustrated in Figure 6.

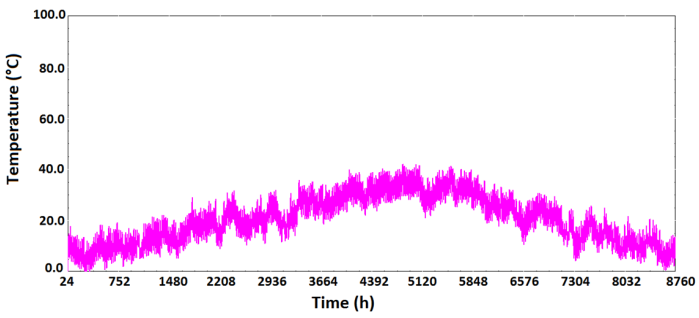

Figure 4: Ambient temperature evolution during one year at the Errachidia site

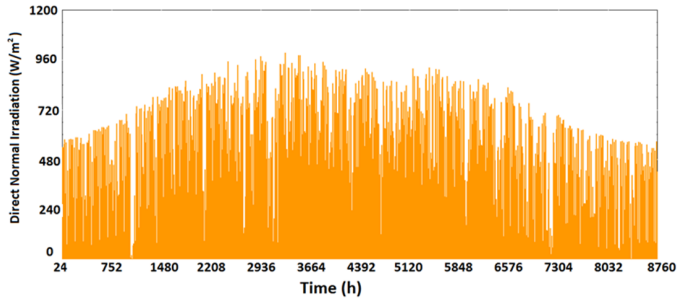

Figure 5: Annual direct normal irradiation in Errachidia city

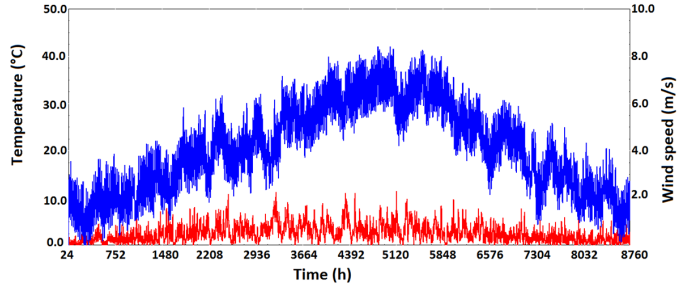

Figure 6: Variation of water inlet and outlet temperature for one year at Errachidia city

4 Results and discussion

The estimation of the amount solar radiation captured by the PTC is based on the method employed by [15]. For modelling the thermal behavior of PTC components in transient regime, we have taken into account the following assumptions :

- The sky is assumed to be a blackbody;
- Under climatic conditions, the physical properties of the glass and the absorber are supposed constant;
- Fluid velocity is supposed to be constant;
- The wind speed is 3.75 m/s;
- The physical properties of the fluid in the absorber are assumed to be temperature dependent;
- The air enclosed between the absorber and the glass is stagnant and transparent.

4.1 Geometrical and optical parameters of PTC

The main element of PTC system which allows receiving incident solar radiation is the absorber, also it allows to convert radiation in the form of heat and transmit it to the HTF. The incident solar radiation is not entirely absorbed and transmitted to the HTF, but part is dissipated as heat loss between the absorber and the cover glass. Figure 7 illustrates heat transfer of the absorber used, taking into consideration the different shares of energy, which were collected by the fluid and lost to the environment.

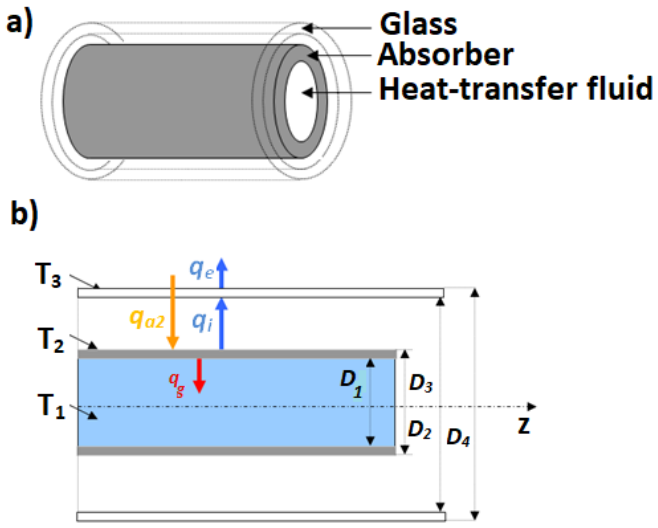

Figure 7: Thermal exchanges between the absorber tube and the other components of PTC

Tables 1 and 2 present the geometric and optical properties of the components of our PTC system. The physical properties of HTF (water) are shown in Table 3. The water temperature and the PTC components calculated from the energy balance [16], for the typical days of the year and for a HTF mass flow rate value of 0.0083 kg/s.

Table 1: Geometrical characteristics of the PTC elements

Geometric characteristics	**Value**
External diameter of the absorber, D_e	1.4 cm
Internal diameter of the glass cover, $D_{(c,i)}$	4.2 cm
External diameter of the glass cover, $D_{(c,e)}$	4.35 cm
Effective width of the mirror, W_{eff}	1 m
Element length, Δz	0.1 m
Collector absorber tube length, L_{tube}	2 m
Focal distance	0.235m

Table 2: Optical properties of materials used

Properties	**Value**
Absorption coefficient of the absorber tube, α	0.8
Glass transmission coefficient, τ	0.8
Reflectance of the mirror surface, ρ_m	0.85
Emissivity of the absorber tube, ε_r	0.12
Emissivity of the glass cover tube , ε_c	0.9

The thermal modelling of the absorber receiver of PTC is done by a calculation and programming procedure under Matlab by solving the energy balance equation. For this purpose, we have developed a calculation program to simulate the fluid temperature at the absorber outlet. The thermal model takes into account all heat transfers: convection in the receiver pipe, in the gap between the absorber and the glass cover, on the one hand, and between the glass cover and the ambient air, on the other hand. The thermal balance equation between the absorber and the HTF can be written :

$$\pi\rho_1 C_1 D_1 \frac{\partial T_1}{\partial t}(z,t) = -\rho_1 C_1 \phi \frac{\partial T_1}{\partial z}(z,t) + q_g(z,t) \quad (11)$$

The initial conditions and limits are given by following relationships:

$$T_1(z,0) = T_{amb}(0) \quad (12)$$

$$T_1(0,t) = T_e(t) \quad (13)$$

where T_e is the inlet temperature and T_{amb} is the ambient temperature.

Table 3: Properties of heat fluid (water)

Properties	Value
Heat capacity, C_f	4180 kJ.kg^{-1}.K^{-1}
Volume flow rate, D_f	30 l/h

Table 4: Comparison of parameter effects on PTC in the present study with other similar works.

Dimension of PTC	Mass flow rate Kg/s	Temperature of water	References
1 m x 2 m	0.0083	149 °C	Present study
1.25 m x 0.8 m	0.0117 - 0.0167	36.5 °C	[16]
1.49 m x 1.49 m	0.00111	104 °C	[17]
1.2 m x 1.5 m	0.0017	65 °C	[18]
1.82 m x 1.03 m	0.00111	50 °C	[19]
6 m x 2.3 m	0.55	165 °C	[20]
7.8 m x 5 m	0.345	47.24 °C	[21]

In order to produce hot water 90°C, for domestic and industrial applications. We have choose the right mass flow and the good PTC dimensions. Table 4 presents a comparison of parameter effects on PTC in the present study with other similar works. We noticed that when the mass flow rate and the opening radius of the collector increases the outlet temperature of the hot water rises. To produce a sufficient quantity of hot water, it is necessary to select parabolic cylindrical collector dimensions in relation to the outlet temperature of the water and the mass flow rate (Table 5).

Table 5: Hot water production in 90°C for different theoretical cases [22]

Dimension of PTC	Mass flow rate Kg/s	Quantity of hot water (L/day)
1.6 m x 1.8 m	0.0074	133.2
1.6 m x 3 m	0.0123	221.4
1.6 m x 6 m	0.0250	450.0
1.6 m x 10 m	0.0411	739.8
1.6 m x 15 m	0.0633	1139.4

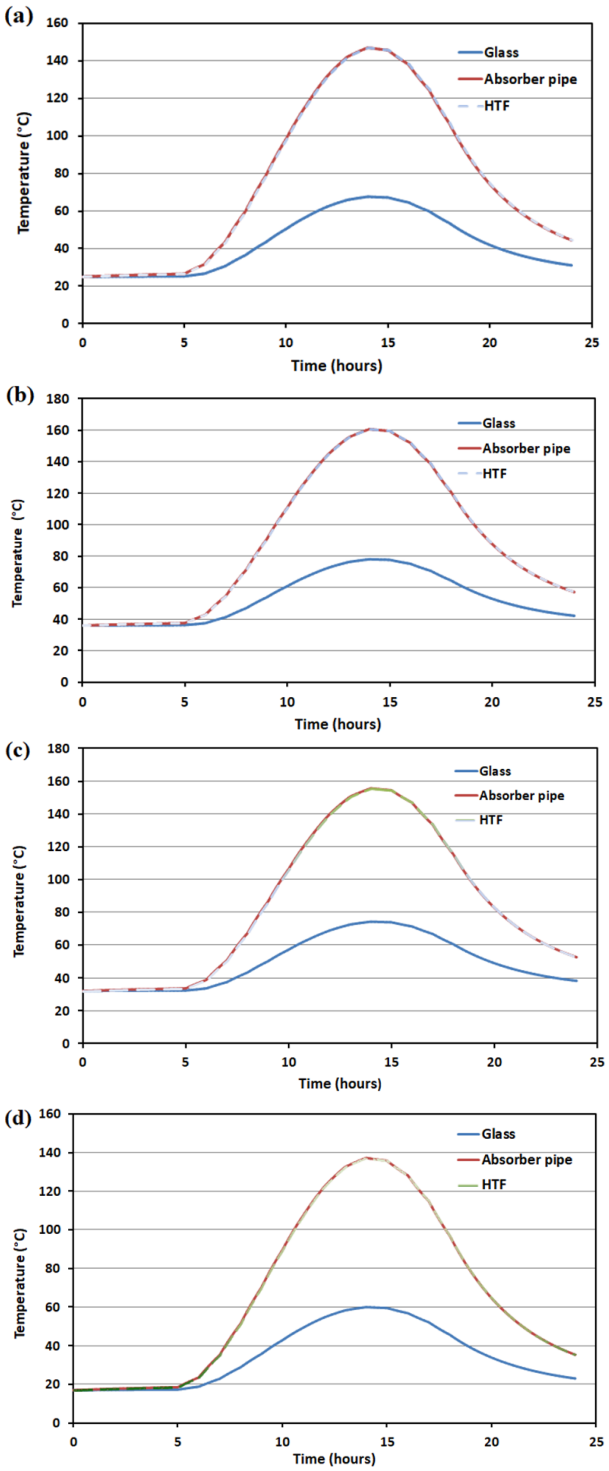

Figure 8: Outlet temperature evolution of fluid, absorber and glass for; (a) March 21, (b) June 21, (c) September 21 and (d) December 21

4.2 Temperature outlet evolution in typical days of year

Figure 8 shows the temperature evolution of the fluid, the absorber and the glass cover versus the time from March 21, June 21, September 21 and December 21, 2019 for the concentrator whose geometric properties are given in Table 1. We observed that the temperature variation depends on the climatic conditions of Errachidia, particu-

larly on the incident solar energy.

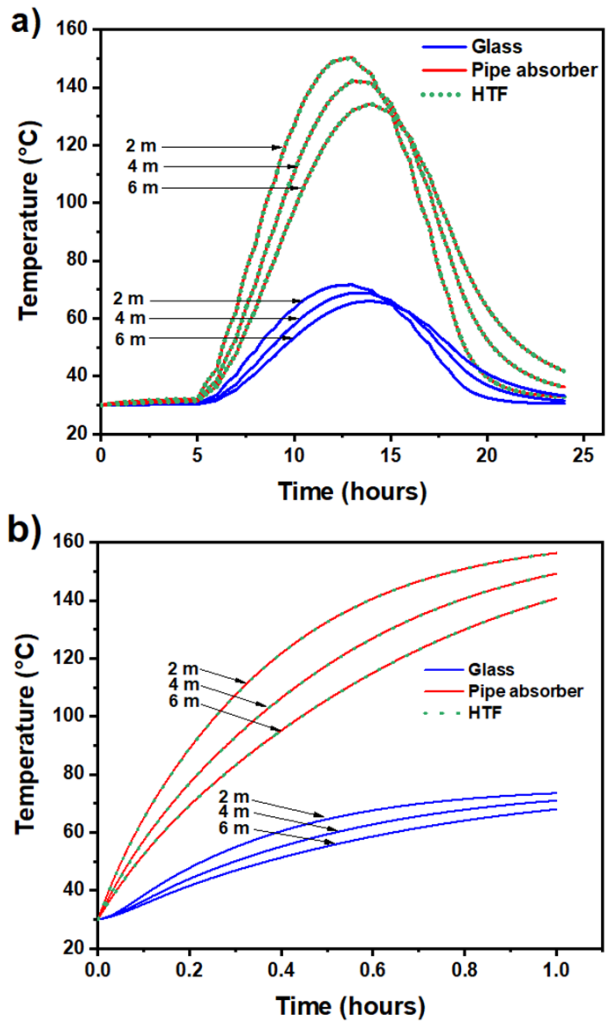

Figure 9: (a) Outlet temperature evolution of the glass, absorber and HTF for; 2 m, 4 m and 6 m of the length tube, (b) PTC temperature - stagnation conditions.

4.3 Absorber tube length effect

The thermal performance of PTC and the water heating requirements depend on the geometric properties of PTC solar. In the modeling we have chosen 3 different absorber lengths 2m, 4m and 6m, respectively. Excluding stagnation, we observe that the risk of overheating at the PTC level does not exist, the temperature of the absorber tube stays below 70°C using water as HTF. The daily variation of the fluid temperature, the absorber tube and the glass cover as a function of time is illustrated in Figure 9a. We noticed that when the receiver pipe length is small the efficiency of the system increases and the temperature of the absorber also increase. We observed that, in theory, the stagnation of the temperature of the absorber and fluid exceeds 158°C of water as HTF. The risk of deterioration of the system in the case of water HTF is important. We also observed that when the absorber tube length is small the temperature of the absorber also increases (Figure 9b).

4.4 Absorber tube thickness effect

Figure 10 shows the thickness effect of the receiver pipe on the fluid daily temperature, the receiver pipe and the glass cover versus of time for 1.5 mm, 2.5 mm and 3.5 mm respectively, for the concentrator whose geometric properties are given in Table 1. We observe that the thickness of the absorber has a small impact on the fluid temperature evolution and stagnation of the temperature compared to the tube length.

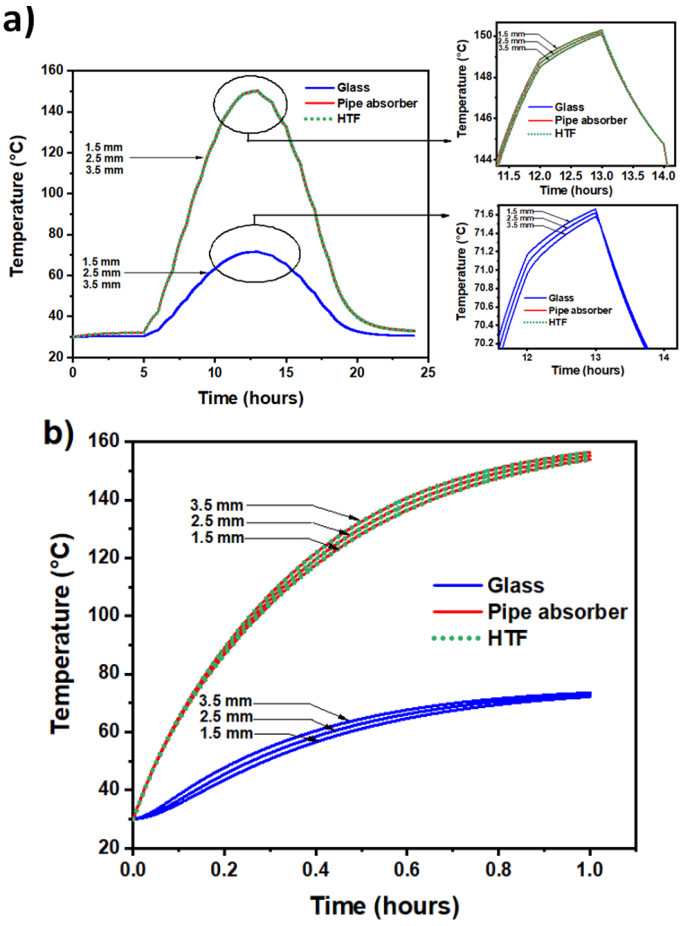

Figure 10: (a) Outlet temperature evolution of HTF, absorber and glass cover for different absorber tube thickness 1.5 mm, 2.5 mm and 3.5 mm; (b) PTC temperature stagnation conditions.

5 Conclusions

In this paper, the study of the water heating circulating in an absorber tube of a solar PTC is investigated. The heating process modeling of the fluid is performed. To verify the temperature of fluid, absorber and glass cover, a mathematical model is elaborated from the heat exchanges of the glass tube with the environment. The geometrical dimensions of the parabolic-cylindrical collector have been taken into account in the modeling. The results obtained in this study showed that there was a significant temperature difference between the inlet and the outlet of PTC for the test days considered. Excluding stagnation, the absorber tube length effect on the fluid temperature evolution was observed. However, the absorber tube thickness effect is very small on the temperature evolution. This

investigation offers multiple perspectives on the use and analysis of parabolic-cylindrical collector behavior such as the optical performance evaluation of the system or to test other heat transfer fluids. Finally, an economic study can be envisaged to evaluate the cost-effectiveness of the system.

Nomenclature

T_a	Ambient temperature (°C)
T_r	Absorber temperature
$\bar{T}$	Average irradiation temperature
T_C	Concentration temperature
T_c	Cover temperature (glass tube)
T_1	Heat transfer fluid temperature
C_p	Calorific power
C_1	Heat-transfer fluid specific heat
D_1	Internal diameter of the absorber
E_p	Incident radiation on the map opening
E	Incident solar radiation (W/m^2)
T_{inl}	Fluid inlet temperature
T_{out}	Fluid outlet temperature
F_{rc}	Form factor between the receiver and the cover, which is equal to 1
h_{fi}	Heat transfer coefficient at inside the absorber (W/(m^2.°C)
m_f	Mass flow
S_o	PTC opening area
S_r	Receiver surface (m^2)
D_e,D_i	Outside and inside diameter of the absorber
q_g	Amount of the energy gained by the heat transfer fluid

Greek Symbols

γ	Optical collector factor
ε_r	Emissivity of the surface of the absorber
λ	Thermal conductivity (W/(m.°C))
τ	Transmission factor
ρ	Reflection factor of the concentrator mirror
ϕ	Heat transfer fluid mass flow rate
ρ_1	Heat transfer fluid density
ε_c	Glass emissivity of the cover
$\tau\alpha$	Transmission-absorption coefficient

Physical constants

σ	Stefan-Boltzmann Constant ($5.667.10^{-8}$W/m^{2}K^4)

Conflict of Interest The authors declare no conflict of interest.

References

[1] Z.D. Cheng, Y.L. He, J. Xiao, Y.B. Tao, R.J. Xu, "Three-dimensional numerical study of heat transfer characteristics in the receiver tube of parabolic trough solar collector", International Communications in Heat and Mass Transfer **37**, 782–787, 2010.

[2] V.E. Dudley, G.J. Kolb, A.R. Mahoney, T.R. Mancini, C.W. Matthews, M. Sloan, D. Kearney, " Test results: SEGS LS-2 solar collector", Sandia National Laboratories, Albuquerque, 1994.DOI: 10.2172/70756

[3] E. Kaloudis, E. Papanicolaou, V. Belessiotis, "Numerical simulations of a parabolic trough solar collector with nanofluid using a two-phase model." Renewable Energy **97**, 218–229, 2016.https://doi.org/10.1016/j.renene.2016.05.046

[4] P. Hubert Wagner, "Thermodynamic simulation of solar thermal power stations with liquid salt as heat transfer fluid", Ph.D Thesis Technical University of Munich, 2012.

[5] Y. Marif, H. Benmoussa, H. Bouguettaia, M. M. Belhadj, M. Zerrouki, "Numerical simulation of solar parabolic trough collector performance in the Algeria Saharan region", Energy Convers. Manage. **85**, 521–529, 2014. https://doi.org/10.1016/j.enconman.2014.06.002.

[6] E. Bellos, C. Tzivanidis, Z. Said, "A systematic parametric thermal analysis of nanofluid-based parabolic trough solar collectors", Sustainable Energy Technologies and Assessments, **39**, 100714, 2020. https://doi.org/10.1016/j.seta.2020.100714

[7] Z. Zhao, F. Bai, X. Zhang, Z. Wang, "Experimental study of pin finned receiver tubes for a parabolic trough solar air collector ", Solar Energy, **207**, 91–102, 2020.

[8] S. Zafar, Africa, Renewable Energy, Solar Energy, Wind Energy, 2019. https://www.ecomena.org/

[9] M. Hajjaj, A. Mellaikhafi, A. Tilioua, C. Messaoudi, A. Bouaaddi, Numerical Investigation and Control The Thermal Storage System in A Single-Tank for CSP Plants,International Journal of Advance Science and Technology, **29**, 10s, 8378–8389, 2020.
http://sersc.org/journals/index.php/IJAST/article/view/24294

[10] Z. D. Cheng, Y. L. He, J. Xiao, Y. B. Tao, and R. J. Xu, "Three-dimensional numerical study of heat transfer characteristics in the receiver tube of parabolic trough solar collector." Int. Commun. Heat Mass Transf., **39**(7), 782–787, 2010. https://doi.org/10.1016/j.icheatmasstransfer.2010.05.002

[11] M. Hajjaj, A. Bouaaddi, A. Mellaikhafi, A. Tilioua, C. Messaoudi, "Simulation of the water outlet temperature in a solar Parabolic Trough Collector in the Errachidia site " in 2020IEEE 1st International Conference (IRASET), Meknes, Morocco, 2020. DOI: 10.1109/IRASET48871.2020.9092323.

[12] J.A. Duffie and W.A. Beckman, Solar Engineering of Thermal Processes, 2nd Edition, John Wiley & Sons Inc, 1991.

[13] W. Chekirou, N. Boukheit, T. Kerbache, "Analyse Thermique pour l'Absorbeur d'un Concentrateur Solaire Cylindro Parabolique", 12ème Journées Internationales de Thermique, 61–64, Morocco, 2005.

[14] M. Li and L.L. Wang, "Investigation of Evacuated Tube Heated by Solar Trough Concentrating System", Energy Convers. Manage., **47**, 3591–3601, 2006. https://doi.org/10.1016/j.enconman.2006.03.003

[15] ASHRAE Handbook, Fenestration Fundamentals, USA, 2001.

[16] A. Valan Arasu and T. Sornakumar, "Performance characteristics of Parabolic Trough Solar Collector system for hot water generation", International Energy Journal, **7**, 137–145, 2006. DOI: 10.2298/TSCI0602167V

[17] M. Rizwan, Md. A. R. Junaidi, M. Suleman and M. A. Hussain, "Experimental verification and analysis of Solar Parabolic Collector for water distillation", International Journal of Engineering Research, **3**, 588–593, 2014. DOI: 10.17950/ijer/v3s10/1008

[18] M. G. Tayade, R. E. Thombre and S. Dutt, "Performance evaluation of Solar Parabolic Trough", International Journal of Scientific and Research Publications, **5**, 1–5, 2015.

[19] K. H. Bhujangrao, "Design and development of prototype cylindrical parabolic solar collector for water heating application", Journal of Renewable Energy Development, **5**, 49–55, 2016. DOI: 10.14710/ijred.5.1.49-55

[20] M. Qu, D. H. Archer and S. V. Masson, "A linear parabolic trough solar collector performance model", Renewable Energy Resources and a Greener Future, VIII-3-3, 2006. DOI: 10.1115/ES2007-36052

[21] D. Sauceda, N. Velazquez, O. Garcia-Valladares and R. Beltran, "Numerical simulation and design of a parabolic trough solar collector used as a direct generator in a solarGAX cooling cycle", J. Mech. Sci. Technol., **25**, 1399–1408, 2011. https://doi.org/10.1007/s12206-011-0326-y

[22] M. E. Soudani, K. E. Aiadi, D. Bechki, "Water heating by Parabolic Trough Collector with storage in the Ouargla region of Algerian Sahara", Materials Today: Proceedings, **24**, 137–139, 2020. https://doi.org/10.1016/j.matpr.2019.07.707

ASTES

Advances in Science, Technology and Engineering Systems Journal Vol. 5, No. 6, 290-298 (2020)

www.astesj.com

Special Issue on Innovative Research in Applied Science, Engineering and Technology

ASTESJ

ISSN: 2415-6698

The Role of Promotion in Mobile Wallet Adoption – A Research in Vietnam

Ha Hoang[1,*], Tan Trinh Le[2]

[1]*University of Economics, The University of Danang, Da Nang 550000, Vietnam*

[2]*Business department, FPT University, Da Nang 550000, Vietnam*

ARTICLE INFO

Article history:
Received: 31 August, 2020
Accepted: 16 October, 2020
Online: 10 November, 2020

Keywords:
Mobile wallet
Mobile payment
Digital economy

ABSTRACT

Mobile wallet is an application that allows users to make online payments using their mobile phones. In the context of an outbreak of COVID-19 epidemic in Vietnam and the world, mobile wallets are considered having many opportunities to change people's cash spending habits. The current study assesses the factors impact on the intention to use the mobile wallet, focusing on understanding the relationship of promotion with common factors in technology adoption research such as perceived risk, perceived usefulness, habits, social influences. The research results also show the direct and indirect effects of promotion on intent to use. From this result, 7 of 9 research hypotheses were accepted. Promotion, often overlooked by researchers, has been proven to be a critical factor when researching technology adoption because it significantly improves the level of intentional interpretation of the research model. This study will be the premise for future researches when studying adoption technology, researchers could integrate promotion to the model to achieve a significant improvement in the level of interpretation as showed in this study.

1. Introduction

PricewaterhouseCoopers (PwC) survey in 27 countries recorded Vietnam as the fastest growing mobile payments market in 2018, with the percentage of users increasing from 37% to 61% [1]. Facing increasingly complicated developments of the COVID-19 epidemic, the Vietnam's Government has also recommended people to limit cash payment and increase the use of online payment services to decrease the risk of infection. As a result, cashless payment methods, including mobile wallets, have a great opportunity to become more and more popular. In Vietnam, the ratio of non-cash payments to the total means of payment is only 14%, so the scope for growth of mobile wallets is huge. This context has created many favorable conditions to help mobile wallets develop and increasingly change the cash using habits of most Vietnamese people, actively contributing to bringing Vietnam towards the cashless economy [2].

Mobile payment means all payment services are made through mobile devices such as laptops, tablets or smartphones. Among them, mobile wallets are the latest e-commerce method that helps customers to make payment, shopping online, booking and share services. In terms of technology, a mobile wallet is an application installed in a smartphone or a tablet which allows consumers to input money and make online payments directly with the mobile wallet [3]. Mobile wallets can also be recognized as the revolution derived from e-wallets. Owning a wide ecosystem is a way of integrating into the digital transformation stream of users, especially young people who love technology. Because of the nature of mobile wallets, it is convenient, fast and secure in payment for daily activities, reducing the risks associated with spending and managing cash.

Although the application of technology has received long-standing attention from the government, it has not developed to achieve the desired scale, required for application in the entire systems payments in Vietnam. Vietnamese clients still prefer to use cash, reflected in the fact that there are still nearly 90% of transactions are paid by cash. Until now, almost no scholars doing research on mobile wallet in Vietnam whereas Vietnam is one of fastest growth in Asia area and is considered as a very attractive market for investors in all fields, especially technological payment. This study was carried out to fill the research gap in Vietnam related to mobile wallet.

This research aims to explore the factors affecting the intention to use of mobile wallet in Vietnam. The results are expected to provide the suggestions for mobile wallet suppliers to reach customers more effectively, and policymakers to drive a cashless economy in Viet Nam. In addition, the role of promotion demonstrated in this study will be the premise for future researches

*Corresponding Author: Ha Hoang, hahoang@due.edu.vn

when studying the adoption of technology, researchers could integrate promotion to the model to achieve a significant improvement in the level of interpretation as showed in this study.

We divided the content of this paper into five parts: The first part focuses on statement problem and meaning of this study comparing previous researches. Part two presents theories related study topic and constructing framework model. Besides that, authors have description research method and sampling characteristic in part three. To test the relationship between factors in the proposed model, we have showed analysis and results in part four and the last part is summary research results and implications.

2. Theoretical background and research framework

2.1. Theoretical background

Vietnam belongs to the group of countries with a high percentage of internet users (70.3%), equivalent to 68.5 million Internet users in 2019. With 43.7 million smartphone users (accounting for 45% of the population in 2019), Vietnam are at the regional average, higher than India, the Philippines, Indonesia and Thailand. Many advanced technologies are being applied such as biometric authentication such as fingerprint, face; quick response code (QR Code); Tokenization of information[4].

The development of technology, the popularity of the internet and smartphones has progressively increased the demand for cashless and digital transactions around the world. Customer attitudes and acceptance regarding mobile payments have also experienced a drastic change [5]. Many studies around the world have also confirmed that customers like technologies that can provide fast, useful services on a mobile platform. Mobile payment services, in which mobile wallets are one of the latest advances in the digital economy, have integrated these features [6, 7, 8].

Mobile wallet is one technology that have many growth opportunities in this condition [9]. Mobile wallets could replace physical wallets and even debit or credit cards in online and direct purchases. We see this technology as a major revolution in the digital economy because in the era of technological revolution, the issues of speed, interoperability, security and privacy of mobile technology have been resolved. In our study, we proposed and tested a research framework model which combined constructs in the TAM and UTAUT models, expanding with new variables for a transitional country like Vietnam such as promotion, a construct built from practice.

Promotion

Promotion is considered as a short-term marketing strategy and used to create awareness and interest in products or services. It helps the companies to attain sales and marketing goals [10]. Moreover, promotion could affect to the consumer's mind like a benefit to him/her, then creating the changes in consumer behavior [11]. Many studies have also confirmed the effect of sales promotions on consumer attitudes and consumer behavior [12, 13, 14]. As a result, promotion is a very useful strategic mean to improve profitability. Sellers are using various promotion strategies, for example coupons, product upgrades, price reduction, free samples and free gifts to increase intention to buy of customers. Promotion can be separated into non-financial and financial promotions [15]. The examples of financial promotions are discount of prices, coupons and vouchers while promotions related non-monetary include bonus products and gifts. The value of the promotion is also perceived relatively [16]. Customers could recognize a monetary promotion as a decline in losses because of this kind of promotion brings a reduction in the purchase cost that consumers have to pay. In contrast, promotion of non-monetary sales could be considered as a profit from the deal [17].

Related to the financial and payment sector, [18] showed the influence of sales promotion to persuade customers to open a bank account [18]. The results of this research showed that 50% of the increase accounts of a bank is the result followed a promotional campaign. Other researches showed the efficiency of promotion to influence the computer purchase and confirmed the positive linkages, promoting the behavior of purchase of financial services [19, 20].

Recent research on omnichannel shopping based on IT has included the promotion in the research model but has not found a meaningful impact of the promotion on intention to use [21].

In Vietnam, a recent study on the determinants of the choice of the customer mobile wallet, promotion in second place in the six elements outlined in the survey. As emphasized by several authors, there are academic and managerial deficiencies in the profound understanding of the relationship between promotion and consumer behavior [22, 23]. Especially in technology adoption, sales promotion still receives very little attention from researchers. That is why the construct of promotion is added to this study.

H1: The promotion of mobile wallet will positively affect the customers' perceived usefulness of this technology.

H2: The promotion of mobile wallet will negatively affect the customers' perceived risk of this technology.

H3: The promotion of mobile wallet will positively affect the social influences of this technology.

H4: The promotion of mobile wallet will positively affect the habit of customers for this technology.

Perceived usefulness

Perceived usefulness was mentioned for the first time by Davis in Technology Acceptance Model (TAM). This term refers to the ability of customers to improve performance by fully using the improved system, reflecting users' willingness to accept [24].

In technology adoption research, performance expectancy refers to an individual's perception that using a technology could provide benefits to customers in performing certain activities [25]. Reflecting a range of attributes that a technology could give benefits to clients, performance has been conceptualized by using system features that could enhance speed, productivity, and chances of task accomplishment and perceived usefulness [25, 26]. Unambiguously, in diverse task settings, performance expectancy was affirmed to affect intentions to use technological systems [27]. Consumers' perception that using mobile wallet would support them to achieve benefits in doing payment tasks could influence the behavioral intention of mobile wallet adoption. The following hypothesis was formulated:

H5: Perceived usefulness will positively affect the user's intention to use mobile wallet.

Perceived risk

Perceived risk was a popular construct used in extended models of UTAUT2 by several researchers. Perceived risk is considered negatively affect on intention to use [8]. Featherman and Pavlou also posited that individual's perceived risk of using a technology has negative influence on perceived usefulness (equivalent to performance expectancy) and behavioral intention toward that technology while his or her perceived ease of use (equivalent to effort expectancy) also has an adverse impact on the perceived risk [28]. Since mobile wallet is a new technology and includes complex and sensitive private information, perceived risks could be a difficulty in adopting this technology. Consumers could face monetary loss because of their improper operating system inaccuracy or potential fraud. As a result, their non-refundable paying money would be sent to wrong receivers or scammers or just be disappeared.

Perceived risk diminishes user's readiness and acceptance of new technology to more security dangers of technology like mobile wallets [7]. Perceived risk could make customers underestimate about the perceived usefulness of a technology and deny accepting it [29]. Some researches showed that perceived risk positively affect on user's intention ([30]; [31]). Two studies in 2015 further explored factors such as social influence, perceived risk and stressed their important role in mobile payment adoption [32, 33]. The following hypotheses were developed:

H6: Perceived risk will negatively affect the intention to use mobile wallet.

Social influence

Social influence is defined as the degree to which an individual perceives that essential referents such as family and friends believe he or she should adopt a specific technology [25].

Recently, in mobile payment adoption, many researches integrated social influences into their research frameworks and obtained some empirical support [34, 35, 36]. A study of Chong et al. (2010) showed that a customer considers the thoughts of their friends and their family before choosing a new technology [37]. If views of others are not favourable, they will resist adopting that technology. Social influence is also found as the most dominant on user's behavioural intention in mobile payments [38]. Based on the arguments above, the following hypothesis was developed:

H7: Social influences will positively affect the intention to use mobile wallet.

Habit

Habit is defined as the degree to which an individual performs behaviors automatically because of learning from prior experiences [25, 39]. The effects of habit on both behavioral intention and actual usage behavior have been proposed and validated by researchers [40, 41].

With the current development of mobile commerce, consumers are using mobile devices like smartphones for almost daily tasks such as internet surfing, social connecting, text and voice chatting, video calling, gaming, shopping, bill paying. Therefore, that development could make mobile-related habits relatively more relevant than before toward the influence on both behavioral intention and actual usage behavior of mobile payment. According to Venkatesh et al. (2012) the role of habits in technology use describes the various fundamental processes that affect technology use. In this study, habit is considered being a familiar behavior or an automatic behavior in using mobile wallets. The following proposition was developed:

H8: Habit will positively affect the user's intention to use mobile wallet.

Intention to use

According to Davis, behavioral intention is considered as the degree to which an individual believes that they will implement a particular behavior [42]. In technology adoption theories, the relationship between behavioral intention and usage behavior has been consistently confirmed [25, 26, 27, 43, 44]. In mobile payment context, there is still a gap between intention and actual use toward the technology. Although the development of mobile commerce has led consumers to use mobile devices in various aspects of their daily lives, the actual amount of mobile payment is still small compared to other forms of payment. Under the technological adoption literature, it can be hypothesized that:

H9: Promotion will positively affect the user's intention to use mobile wallet.

2.2. Research framework

Considered the relationships extracted by hypotheses from previous studies, Figure 1 shows the proposed research model. We included perceived usefulness, social norms, habit; integrated them with perceived risk and a novel construct named promotion. Intention to use and frequency of use applied to measure using behavior.

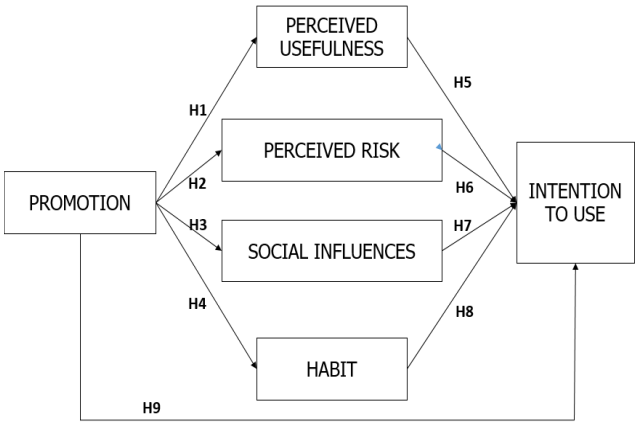

Figure 1: Conceptual framework (Source: own elaboration)

We proposed this research framework because predicting consumer's behavioural adoption and usage should be evaluated from a variety of perspectives. This integrated model can help us have a better recognition of the relationships between these research constructs. These relations are already confirmed in the literature review of previous researches, and the validity of model is confirmed in similar studies except the promotion factor that we added in this study [45, 46, 47]. This proposed model has showed relationship among factors affecting using mobile wallet in Vietnam so that previous studies have not focused on evaluating it.

3. Materials and Methods

Authors have used secondary data from previous studies to construct the proposed research model. We used a survey method with a questionnaire based on the 5-Point Likert Scale to test our research model and developed hypotheses. The potential participants of this research were chosen in convenience sampling method from Da Nang City. 400 young people in Da Nang were contacted by e-mail and social network during the period from January 2020 to April 2020. A link to the survey was included in the messages. 315 valid responses were received. The overall response rate was 78.75%.

3.1. Measurement instrument

The research had seven constructs: perceived risk, social influence, perceived usefulness, habit, promotion, intention to use. Constructs and measurement items in this research were modified from previous works on technology acceptance. Measurement items for constructs of perceived usefulness, social influence, perceived risk, habit were altered from Venkatesh et al. (2012). The scale of intention to use was employed from Davis (1989). All measurement items were measured on a five-point Likert scale, ranging from totally disagree (1) to totally agree (5). The frequency of use measurement was operationalized by one item that measure consumers' actual frequencies of mobile wallet usage.

3.2. Analytical procedures

First, we tested the scales by the Cronbach's alpha, the exploratory factor analysis (EFA) and the confirmatory factor analysis (CFA). In the next stage, we used the Structural Equation Modeling (SEM) method to evaluate the structural relationships between constructs in the theoretical model.

4. Results and Discussion

4.1. Reliability and validity

The reliability and validity of the constructs in the research were evaluated with SPSS 23. We use Cronbach's Alpha reliability test because it is a widely used measure that examines the scale reliability [48]. By measuring the reliability coefficient, the reliability test could assess the consistency of the entire scale. Baron & Kenny (1986) suggested that a scale would be high reliable level if the coefficient alpha is greater than 0.7 while the coefficient alpha is higher than 0.6 means the scale is reliable [49]. Table 2 showed that Cronbach's Alpha of all constructs are above the threshold of 0.7, satisfied internal consistency. All items kept will be included in the analysis Exploratory Factor Analysis (EFA). We used this technique to minimize and summarize data and it is very useful for identifying groups of variables. The relationship of mutually correlated groups of variables consider as several basic factors. Each observed variable will be calculated with a Factor Loading factor, which shows which factor each measurement variable belongs to. The KMO (Kaiser-Meyer-Olkin) coefficient must reach 0.5 or higher, showing that factor analysis is appropriate ($0.5 \leq KMO \leq 1$) [48]. The result of KMO coefficient of the study = 0.889 satisfied the requirements. In addition, Barlett's test is statistically significant (sig = 0.000 < 0.05) proving that the observed variables correlate with each other in the whole [50]. The results of the EFA analysis yielded results consistent with the structure of the six construct. Therefore, all constructs of this model ensure reliability and convergent validity. These constructs would be used in further analysis to test the proposed hypotheses.

In [51], the author recommended that CFA is rigorous to test the overall measurement model and to assess the reliability and validity of the constructs. We measure convergent validity by using composite reliability (CR) and average variance explained (AVE). By the rule of thumb, CR should be above 0.6 and AVE should be above 0.5 for all constructs. As the results shown in Table 1, CRs of all constructs ranges from 0.723 to 0.898 while the AVEs vary from 0.573 to 0.746. These results confirm that our model meets the requirement for convergent validity.

We used the procedure suggested by [52] to check discriminant validity. From this perspective, the AVE for each of the research constructs should be greater than the squared correlation between the construct and other construct. The Table 2 showed the measurement model satisfy the requirement for discriminant validity. The results indicated that the various AVE are lower than the diagonal variables suggesting all the constructs in this study have satisfactory discriminant validity.

Table 3 showed that the CFA model with six concepts also shows a good fit with the data. All the indices satisfied the recommended cut-off point. We conclude that the model fits data well, so this model can be used to test the research hypotheses.

Table 1: Reliability and validity of the tested model

Latent constructs	Cronbach's alpha	CR	AVE	MSV	FL range
SI	0.755	0.723	0.573	0.234	0.503-0.910
PR	0.897	0.898	0.746	0.021	0.810-0.905
PU	0.875	0.883	0.716	0.413	0.775-0.874
HB	0.866	0.870	0.771	0.196	0.836-0.909
PM	0.857	0.856	0.664	0.473	0.743-0.850
IU	0.891	0.892	0.674	0.473	0.692-0.917

Table 2: Factor correlation coefficients

	AVE	IU	PR	PU	PM	SI	HB
IU	0.573	**0.821**					
PR	0.746	-0.143*	**0.864**				
PU	0.716	0.642***	-0.086	**0.846**			
PM	0.771	0.688***	0.005	0.589***	**0.815**		
SI	0.664	0.484***	-0.019	0.422***	0.472***	**0.757**	
HB	0.674	0.443***	-0.116†	0.280***	0.312***	0.396***	**0.878**

Significance of Correlations: (The square root of AVE shown as bold at diagonal)
† $p < 0.100$, * $p < 0.050$, ** $p < 0.010$, *** $p < 0.001$

Table 3: Indices fit criteria

Fit indices	Measurement Model	Structural Model	Threshold limit value	Sources
CMIN/df	1.749	2.221	< 5	[53]
CFI	0.975	0.953	> .90	
GFI	0.937	0.912	> .90	[48]
AGFI	0.907	0.877	> .80	[54]
RMSEA	0.049	0.062	< .08	

Table 4: Results of the hypothesis testing from the structural model

H#	Paths			β	S.E.	C.R.	P-value	Conclusion
H1	PM	→	PU	.722	.075	9.635	***	Supported
H2	PM	→	PR	-.016	.086	-.186	.853	Rejected
H3	PM	→	SI	.387	.081	4.800	***	Supported
H4	PM	→	HB	.380	.084	4.534	***	Supported
H5	PU	→	IU	.282	.055	5.124	***	Supported
H6	PR	→	IU	-.079	.035	-2.255	.024	Supported
H7	SI	→	IU	.097	.071	1.361	.174	Rejected
H8	HB	→	IU	.153	.042	3.602	***	Supported
H9	PM	→	IU	.447	.080	5.556	***	Supported

Table 5: Results of evaluation of indirect effects

Indirect effects	Estimate	Lower	Upper	P	Conclusion
PM to PU to IU	.204	.119	.325	.000	Supported
PM to SI to IU	.038	-.010	.113	.194	Rejected
PM to PR to IU	.001	-.014	.023	.866	Rejected
PM to HB to IU	.058	.026	.106	.002	Supported

Evaluation of direct effects

After assessing reliability and validity of the measurement constructs, in this section we will test the research hypotheses based on review of literature and the framework of research model. To conclude, the significance of each hypothesis, S.E (standardized estimates) and p-value was assessed using SEM (structural equation modelling). As showed in the Table 4, seven of nine hypotheses were accepted.

The results in Table 5 showed that the direct path from PM to IU was significantly mediated by PU and HB. As discussed above, as PU and HB were found to have significant direct effects on intention to use the mobile wallet, the mediating effects of SI and PR in the relationship between PM and IU were partial in this study.

Evaluation of predictive capability

In the current study, 60% of the variance in intention to use mobile wallet was explained by five factors: PM, PU, SI, PR and HB. The R^2 values of intention to use in this attain a moderate level of predictive accuracy [55]. Hence, the predictive accuracy of the research model was satisfied. Comparing with the model not integrated the construct promotion, we found the R^2 value was only 51%. This result showed that promotion is an important factor when researching technology adoption significantly because it improves the level of intentional interpretation of the research model.

4.2. Discussion

In this study, we integrated and explored the promotional factor on users' intentions of mobile wallet. This is an extra factor and thus we have built 3 items to measure the effect of this factor. We combined with other constructs: social influence, perceived risk, perceived usefulness, habit and promotion to measure consumer's perception. The research model was successfully predicting a large variance in intention to use mobile wallet (60%). These results indicate the effectiveness of various constructs of this research model.

Taken as a whole, results show that promotion may affect intention to use and suitable for the study hypothesis. Seven hypotheses were accepted and two hypotheses were rejected (H2 and H7).

PM impact positively to PU

This is the first study to confirm the direct impact of PM on PU. This result also confirms the separation of PM and PU when in many studies that PU also implies the benefits from service use. Indeed, in the current fierce competition context, the perceived benefits measured by traditional items have become almost inevitable. PU-free technologies from customers will almost certainly be rejected. Therefore, PU is almost a must for all companies who want to enter the market need to prove the advantages of their products. However, in order for customers to choose their products, companies need to have appropriate PM strategies, ensuring long-term maintenance, avoiding batches, and ensuring financial efficiency. Implementing the above will ensure mobile wallet providers a long-term competitive advantage in an extremely fierce market with more than 30 mobile wallet providers like in Vietnam.

PM impact positively to SI

This result is also the first time that PM has been shown to have a direct effect on SI. Indeed, when there are attractive promotions, customers will recommend more mobile wallets to acquaintances because they believe that acquaintances will need to use and will bring similar positive experiences. as they experienced. PM has a strong impact on SI and thus mobile wallet providers can take advantage of this factor to offer promotions that can take advantage of even social influences such as referrals to acquaintances who will receive. attractive promotions, for example vouchers, gifts ... Thus, the effectiveness of the promotions in influencing customer behavior in using the mobile wallet will be improved.

PM impact positively to HB

As expected, more promotions will be an important factor in creating habits among users. Therefore, companies need to offer relevant and lasting promotions, striving to maintain the user's habit as a must-have routine. To do this, providers need to develop and integrate more features into the mobile wallet. Just using the mobile wallet can help users solve many problems in life. All of these will form the usage habits for customers, creating customer loyalty for the mobile wallet. The development of a payment ecosystem to provide a convenient and seamless payment experience for users is seen as a key factor for wallets to retain customers in the long run.

PM don't have a significant effect on PR

Usually, when faced with a decision like whether or not to use a mobile wallet, customers often compare gains and losses, risks and opportunities.

However, this result contradicts the original assumption that PM will negatively affect perceptions of risk. The promotions also do not reduce the risk perception of customers because in recent times in Vietnam, many new technology applications have relied on customers' trust and subjectivity to implement the fraudulent behavior like P2P lending applications. Despite being warned, many customers still have serious problems because of the use of these new technologies [56]. Hence the vigilance and precaution of the customer is very high.

PU have a significant and positive impact on IU.

Perceived usefulness in this research has a positive and significant impact on intention to use mobile wallet ($\beta = 0.274$; p-value < 0.001). This result is similar with many previous studies which found that perceived usefulness was one of the most important factors to determine intention to use [3, 57, 58]. Usefulness of a new technology is essential to increase intention to use. These studies also used UTAUT2 as their basis model and reinforced the impact of perceived usefulness on using behaviour [5, 8]. However, we found others study in which perceived usefulness is insignificant in the prediction of the user's intention of mobile wallet services [32].

PR have significant and negative impact on IU

PR has negative and significant effects on IU. In fact, security is always a major worry for the customer while performing payments via mobile wallet [3]. Public sharing of personal information, private information leaks while doing transactions

with mobile wallet are the most common concerns [59]. In contrast, we have several studies in literature revealed the positive relationship between perceived risk and intention to use [31, 60]. Marketing strategies that reach target customers must show customers that there are no risks involved in using mobile wallet. This would lessen perceived risk of customers and therefore improve their intention to use mobile wallet. A risk-free environment once created would result in a greater intention to use a mobile wallet app.

SI don't have a significant effect on IU

SI in the current research does not show a significant impact on IU. It is contrast with results of previous studies which confirmed that friends, family and relatives significantly influence the user's intention [8, 25, 33].

HB have a significant and positive impact on IU

HB was accepted in this research as a significant factor influencing intention to use mobile wallet. This result supports the perspective of Venkatesh et al (2012) who confirmed HB as a critical predictor of customer intention. Take into consideration, the mobile wallet providers need to make an effort in creating the condition where mobile wallet becomes a habit with consumers. For example, they can integrate the e-commerce ecosystem in using the mobile wallet as a payment method or think about give cashback promotion for payment in the retail market. This effort would generate a habit for the consumer to use a mobile wallet more frequent for daily life.

PM have significant and positive impact on IU

Among the constructs in the model which have a direct relationship with IU, PM was shown to have the strongest impact to IU ($\beta = 0.439$; p-value < 0.001). In a survey conducted in major cities in Vietnam about the key factors influencing consumers' choice of mobile wallets, diverse and regular promotions were assessed as one of the deciding factors to choose a mobile wallet. In fact, many people used a technology for the first time because of attractive promotions. As mentioned in the first part of this paper, this is a factor that has received little attention from academics when studying the consumer adoption of new technology. However, as showed in the results, mobile wallets' suppliers need to have many attractive promotions to gain consumer acceptance. Compared to other platforms, mobile wallets do not have many attractive promotions and that may be the reason that mobile wallets are still not popular in the Vietnamese market.

From practical perspectives, the results of this study provide empirical evidence on critical factors to be considered by not only suppliers but also marketers of the mobile wallet. It reveals that promotion and usefulness of use of mobile wallets are the most important factors in user adoption. These factors will improve intention of use of a mobile wallet. To get users to use a mobile wallet, application developers must emphasize the benefits of usefulness and attractive promotion related with this new financial service.

5. Conclusions and limitations

This study is successful in providing an integrated research model for academics to test the impact of social, psychological, and risk factors on technology adoption. In addition, it also helps companies providing mobile wallet services by identifying key factors that influence users' decisions and helping them to have the most comprehensive view of customers. Using SEM analysis, 7 of 9 hypothesis research were accepted. Results of this research are found significant and coherent with previous works on mobile payment and mobile wallet.

This research model explains 60% of intention to use mobile wallet in Vietnam, whereas the same model but without construct promotion explained only 50% in the variation in intention to use mobile wallet. This result demonstrated that putting the new promotion variable to the research model of the adoption and use of technology is necessary and that makes the theoretical contribution of the current study. This is also the premise for future researches when studying the adoption of technology, researchers could integrate promotion to the model to achieve a significant improvement in the level of interpretation as showed in this study.

Last but not least, in this study, we proposed the scale used to measure promotion based on the literature, expert panel and interviews with focus group. The items in this scale will provide the foundation for further research concerning technology adoption such as mobile wallet.

Beside of our study's major contribution that adds into the existing body of knowledge, we also recognize its limitations, mostly regarding the sampling with typically young, highly educated people as responders. In addition, our results have limitation regarding the specific context of Danang city. Danang is an average city with a relatively limited market as its population is approximately one million people. This sample only covers with young people in this city. In order to further enhance its generality, future research could extend the study to more cities or conduct in more countries in Southeast Asia to improve the generalization of the study. Although this research contributes more empirical results in this area, it also has some limitations and therefore further studies in this area will be needed.

Conflict of Interest

There is no conflict of interest regarding this study.

Acknowledgment

This study involves no supporting grants.

References

[1] PricewaterhouseCoopers, Mobile payments in Vietnam fastest growing globally, Thailand emerges second in Southeast Asia, PwC, Nov. 2020.

[2] H. Ha, "The Cashless Economy in Vietnam-The Situation and Policy Implications," Journal of Reviews on Global Economics, **9**, 216-223, 2020. doi: 10.6000/1929-7092.2020.09.20.

[3] K. Madan, R. Yadav, "Behavioural intention to adopt mobile wallet: a developing country perspective," Journal of Indian Business Research, 2016, doi: 10.1108/JIBR-10-2015-0112.

[4] B. An, (2020). The ecosystem makes a breakthrough for electronic wallets [Press release]

[5] A.A. Alalwan, Y.K. Dwivedi, N.P. Rana, "Factors influencing adoption of mobile banking by Jordanian bank customers: Extending UTAUT2 with trust," International Journal of Information Management, **37**(3), 99–110, 2017, doi: 10.1016/j.ijinfomgt.2017.01.002

[6] D.-H. Shin, "Towards an understanding of the consumer acceptance of mobile wallet," Computers in Human Behavior, **25**(6), 1343-1354, 2009, doi:10.1016/j.chb.2009.06.001.

[7] P.G. Schierz, O. Schilke, B.W. Wirtz, "Understanding consumer acceptance of mobile payment services: An empirical analysis," Electronic Commerce

Research and Applications, **9**(3), 209–216, 2010, doi: 10.1016/j.elerap.2009.07.005.
[8] R. Thakur, M. Srivastava, "Adoption readiness, personal innovativeness, perceived risk and usage intention across customer groups for mobile payment services in India," Internet Research, 2014, doi:10.1108/IntR-12-2012-0244.
[9] Kapoor, K. K., Dwivedi, Y. K., & Williams, M. D., "Examining the role of three sets of innovation attributes for determining adoption of the interbank mobile payment service," Information Systems Frontiers, **17**(5), 1039-1056, 2015, doi: 10.1007/s10796-014-9484-7.
[10] J. Dubey, "Personal care products: Sales promotion and brand loyalty," Journal Of Contemporary Management Research, **8**(1), 52, 2014.
[11] J.B. Yusuf, "Ethical implications of sales promotion in Ghana: Islamic perspective," Journal of Islamic Marketing, 2010, doi:10.1108/17590831011082400.
[12] F. de O. Santini, C.H. Sampaio, M.G. Perin, V.A. Vieira, "An analysis of the influence of discount sales promotion in consumer buying intent and the moderating effects of attractiveness," Revista de Administração (São Paulo), **50**(4), 416–431, 2015, doi:10.5700/rausp1210.
[13] S. Mussol, P. Aurier, G.S. de Lanauze, "Developing in-store brand strategies and relational expression through sales promotions," Journal of Retailing and Consumer Services, **47**, 241–250, 2019, doi: 10.1016/j.jretconser.2018.11.020.
[14] A. Mughal, A. Mehmood, A. Mohiuddeen, B. Ahmad, "The impact of promotional tools on consumer buying behavior: a study from Pakistan," Journal of Public Administration and Governance, **4**(3), 402–414, 2014, doi: 10.5296/jpag.v4i3.6680.
[15] P. Chandon, B. Wansink, G. Laurent, "A benefit congruency framework of sales promotion effectiveness," Journal of Marketing, **64**(4), 65–81, 2000, doi: 10.1509/jmkg.64.4.65.18071.
[16] J.Y. Kim, B.P. Min, "Comparison of effectiveness between various sales promotions," Korean Management Review, **34**(2), 445–469, 2005.
[17] M. Palazon, E. Delgado-Ballester, "Effectiveness of price discounts and premium promotions," Psychology & Marketing, **26**(12), 1108–1129, 2009, doi: 10.1002/mar.20315.
[18] R.H. Preston, F.R. Dwyer, W. Rudelius, "The Effectiveness of Bank Premiums: Stoneware… calculators… and Mercedes Sport Coupes–do they pay their way?," Journal of Marketing, **42**(3), 96–101, 1978, doi: 10.1177/002224297804200317.
[19] A. d'Astous, I. Jacob, "Understanding consumer reactions to premium-based promotional offers," European Journal of Marketing, 2002, doi: 10.1108/03090560210445173.
[20] R.B. Boschetti, Promoção de vendas não monetária e seus efeitos na intenção de compra e na escolha da marca de serviços financeiros, Pontifícia Universidade Católica do Rio Grande do Sul, 2012.
[21] Y. Lee, H. Cheon, "A Study on the Factors Affecting the User Intention of Omnichannel Shopping Based on Information Technology," in Proceedings of the 2019 5th International Conference on E-Business and Applications, 20–24, 2019, doi: 10.1145/3317614.3317623.
[22] A. d'Astous, V. Landreville, "An experimental investigation of factors affecting consumers' perceptions of sales promotions," European Journal of Marketing, 2003, doi: 10.1108/03090560310495447.
[23] H. Haans, E. Gijsbrechts, "'One-deal-fits-all?' On category sales promotion effectiveness in smaller versus larger supermarkets," Journal of Retailing, **87**(4), 427–443, 2011, doi: 10.1016/j.jretai.2011.05.001.
[24] F.D. Davis, R.P. Bagozzi, P.R. Warshaw, "User Acceptance of Computer Technology: A Comparison of Two Theoretical Models," Management Science, **35**(8), 982–1003, 1989, doi:10.1287/mnsc.35.8.982.
[25] Venkatesh, Thong, Xu, "Consumer Acceptance and Use of Information Technology: Extending the Unified Theory of Acceptance and Use of Technology," MIS Quarterly, **36**(1), 157, 2012, doi:10.2307/41410412.
[26] Venkatesh, Morris, Davis, Davis, "User Acceptance of Information Technology: Toward a Unified View," MIS Quarterly, **27**(3), 425, 2003, doi:10.2307/30036540.
[27] G. Baptista, T. Oliveira, "Understanding mobile banking: The unified theory of acceptance and use of technology combined with cultural moderators," Computers in Human Behavior, **50**, 418–430, 2015, doi:10.1016/j.chb.2015.04.024.
[28] M.S. Featherman, P.A. Pavlou, "Predicting e-services adoption: a perceived risk facets perspective," International Journal of Human-Computer Studies, **59**(4), 451–474, 2003, doi: 10.1016/S1071-5819(03)00111-3.
[29] E. Swilley, "Technology rejection: the case of the wallet phone," Journal of Consumer Marketing, **27**(4), 304–312, 2010, doi:10.1108/07363761011052341.
[30] H. Lee, Y. Lee, D. Yoo, "The determinants of perceived service quality and its relationship with satisfaction," Journal of Services Marketing, 2000, doi: 10.1108/08876040010327220.
[31] J.-H. Wu, S.-C. Wang, "What drives mobile commerce?," Information & Management, **42**(5), 719–729, 2005, doi:10.1016/j.im.2004.07.001.
[32] E.L. Slade, Y.K. Dwivedi, N.C. Piercy, M.D. Williams, "Modeling consumers' adoption intentions of remote mobile payments in the United Kingdom: extending UTAUT with innovativeness, risk, and trust, " Psychology & Marketing, **32**(8), 860-873, 2015, doi:10.1002/mar.20823.
[33] Y. Yang, Y. Liu, H. Li, B. Yu, "Understanding perceived risks in mobile payment acceptance," Industrial Management & Data Systems, 2015, doi:10.1108/IMDS-08-2014-0243.
[34] J.-C. Gu, S.-C. Lee, Y.-H. Suh, "Determinants of behavioral intention to mobile banking," Expert Systems with Applications, **36**(9), 11605–11616, 2009, doi:10.1016/j.eswa.2009.03.024.
[35] U. Tandon, R. Kiran, A.N. Sah, "Understanding Online Shopping Adoption in India: Unified Theory of Acceptance and Use of Technology 2 (UTAUT2) With Perceived Risk Application," Service Science, **8**(4), 420–437, 2016, doi:10.1287/serv.2016.0154.
[36] P. Duarte, S. Costa e Silva, M.B. Ferreira, "How convenient is it? Delivering online shopping convenience to enhance customer satisfaction and encourage e-WOM," Journal of Retailing and Consumer Services, **44**, 161–169, 2018, doi:10.1016/j.jretconser.2018.06.007.
[37] A.Y.L. Chong, N. Darmawan, K.B. Ooi, B. Lin, "Adoption of 3G services among Malaysian consumers: an empirical analysis," International Journal of Mobile Communications, **8**(2), 129, 2010, doi:10.1504/IJMC.2010.031444.
[38] G.W.-H. Tan, K.-B. Ooi, "Gender and age: Do they really moderate mobile tourism shopping behavior?," Telematics and Informatics, **35**(6), 1617–1642, 2018, doi:10.1016/j.tele.2018.04.009.
[39] Limayem, Hirt, Cheung, "How Habit Limits the Predictive Power of Intention: The Case of Information Systems Continuance," MIS Quarterly, **31**(4), 705, 2007, doi:10.2307/25148817.
[40] Pavlou, Fygenson, "Understanding and Predicting Electronic Commerce Adoption: An Extension of the Theory of Planned Behavior," MIS Quarterly, **30**(1), 115, 2006, doi:10.2307/25148720.
[41] N.K. Lankton, E.V. Wilson, E. Mao, "Antecedents and determinants of information technology habit," Information & Management, **47**(5), 300–307, 2010, doi:10.1016/j.im.2010.06.004.
[42]. F. D. Davis, A technology acceptance model for empirically testing new end-user information systems: Theory and results, Ph. D Thesis, Massachusetts Institute of Technology, 1985.
[43] F.D. Davis, R.P. Bagozzi, P.R. Warshaw, "User Acceptance of Computer Technology: A Comparison of Two Theoretical Models," Management Science, **35**(8), 982–1003, 1989, doi:10.1287/mnsc.35.8.982.
[44] V. Venkatesh, F.D. Davis, "A Theoretical Extension of the Technology Acceptance Model: Four Longitudinal Field Studies," Management Science, **46**(2), 186–204, 2000, doi:10.1287/mnsc.46.2.186.11926.
[45] C. Kim, M. Mirusmonov, I. Lee, "An empirical examination of factors influencing the intention to use mobile payment," Computers in Human Behavior, **26**(3), 310–322, 2010, doi: 10.1016/j.chb.2009.10.013.
[46] F. Liébana-Cabanillas, V. Marinković, Z. Kalinić, "A SEM-neural network approach for predicting antecedents of m-commerce acceptance," International Journal of Information Management, **37**(2), 14–24, 2017, doi:10.1016/j.ijinfomgt.2016.10.008.
[47] N. Shaw, "The mediating influence of trust in the adoption of the mobile wallet," Journal of Retailing and Consumer Services, **21**(4), 449–459, 2014, doi:10.1016/j.jretconser.2014.03.008.
[48] J.F. Hair, W.C. Black, B.J. Babin, R.E. Anderson, R.L. Tatham, Multivariate data analysis, Prentice hall Upper Saddle River, NJ, 2006.
[49] R.M. Baron, D.A. Kenny, "The moderator–mediator variable distinction in social psychological research: Conceptual, strategic, and statistical considerations.," Journal of Personality and Social Psychology, **51**(6), 1173–1182, 1986, doi:10.1037/0022-3514.51.6.1173.
[50] M.S. Bartlett, "A Note on the Multiplying Factors for Various χ^2 Approximations," Journal of the Royal Statistical Society: Series B (Methodological), **16**(2), 296–298, 1954, doi:10.1111/j.2517-6161.1954.tb00174.x.
[51] M.S. Garver, J.T. Mentzer, "Logistics research methods: employing structural equation modeling to test for construct validity," Journal of Business Logistics, **20**(1), 33, 1999.
[52] C. Fornell, D.F. Larcker, "Evaluating structural equation models with unobservable variables and measurement error," Journal of Marketing Research, **18**(1), 39–50, 1981, doi: 10.2307/3151312.

[53] P.M. Bentler, P. Dudgeon, "COVARIANCE STRUCTURE ANALYSIS: Statistical Practice, Theory, and Directions," Annual Review of Psychology, **47**(1), 563–592, 1996, doi:10.1146/annurev.psych.47.1.563.

[54] L. Hu, P.M. Bentler, "Cutoff criteria for fit indexes in covariance structure analysis: Conventional criteria versus new alternatives," Structural Equation Modeling: A Multidisciplinary Journal, **6**(1), 1–55, 1999, doi:10.1080/10705519909540118.

[55] J. Henseler, C.M. Ringle, R.R. Sinkovics, The use of partial least squares path modeling in international marketing, Emerald Group Publishing Limited, 2009.

[56] T.D. Uyen, H. Ha, "The sharing economy and collaborative finance: The case of P2P lending in Vietnam," Jurnal Ilmiah Ekonomi Bisnis, **22**(2), 2017.

[57] F. Liébana-Cabanillas, J. Sánchez-Fernández, F. Muñoz-Leiva, "Antecedents of the adoption of the new mobile payment systems: The moderating effect of age," Computers in Human Behavior, **35**, 464–478, 2014, doi:10.1016/j.chb.2014.03.022.

[58] I.R. de Luna, F. Liébana-Cabanillas, J. Sánchez-Fernández, F. Muñoz-Leiva, "Mobile payment is not all the same: The adoption of mobile payment systems depending on the technology applied," Technological Forecasting and Social Change, **146**, 931–944, 2019, doi:10.1016/j.techfore.2018.09.018.

[59] A. Hossain, R. Quaresma, H. Rahman, "Investigating factors influencing the physicians' adoption of electronic health record (EHR) in healthcare system of Bangladesh: An empirical study," International Journal of Information Management, **44**, 76–87, 2019, doi:10.1016/j.ijinfomgt.2018.09.016.

[60] Y.-Y. Wang, Y.-S. Wang, T.-C. Lin, "Developing and validating a technology upgrade model," International Journal of Information Management, **38**(1), 7–26, 2018, doi:10.1016/j.ijinfomgt.2017.07.003.

ASTES

Advances in Science, Technology and Engineering Systems Journal Vol. 5, No. 4, 374-380 (2020)

www.astesj.com

Special Issue on Innovative Research in Applied Science, Engineering and Technology

ASTESJ

ISSN: 2415-6698

Survey Analysis: Enhancing the Security of Vectorization by Using word2vec and CryptDB

Hana Yousuf[1], Said Salloum[1,2,*]

[1]*Faculty of Engineering &IT, The British University in Dubai, 345015, United Arab Emirates*

[2]*Research Institute of Sciences & Engineering, University of Sharjah, 27272, United Arab Emirates*

ARTICLE INFO

Article history:
Received: 24 June, 2020
Accepted: 17 July, 2020
Online: 28 July, 2020

Keywords:
Natural Language Processing
Vectorisation
Word2vec
CryptDB

ABSTRACT

Vectorization is extracting data from strings through Natural Language Processing by using different approaches; one of the best approaches used in vectorization is word2vec. To make the vectorized data secure, we must apply a security method, which will be CryptDB. The paper is analyzing the survey, which is created to interview security engineers through the SPSS tool. By analyzing the responses from software security engineers, it is seen that both word2vec and CryptDB works significantly. Word2vec is an effective vectorization approach, while CryptDB is an effective, secure database. In future work, we will be developing a secure vectorization using both approaches.

1. Introduction

A vector is a set of real numbers that is converted from a string. This is performed to extract useful data from a specific work using Natural Language Processing (NLP) techniques through deep learning and machine learning techniques [1]–[6]. This conversion is known as vectorization or word embedding. It converts multiple words or an entire phrase to the corresponding vector format of real numbers that are utilized to predict the words and similarities. This would be helpful for classifying texts, identifying similar words, clustering the documents, or extracting the features [7]. On the whole, vectorization is a term referring to the conversion of scalar instructions to vector instructions. The data is stored in vector format, where the loop is reconfigured in such a way that multiple elements can be processed in place of a single array. Vectorisation is used for executing systematic computation where large amounts of data must be processed effectively. Since the size of the code is reduced, the number of bugs is also reduced. It is also easier to substitute the values in mathematical expressions, thereby making the calculation easier and also easier to read and the data can be stored in compact manner.

Technically speaking, in word embeddings, the individual words are characterized as vectors with real value in a predefined cell [8]. The individual words are mapped to their respective vectors. The values of these vectors are trained similarly to neural networks; hence they are often grouped under deep learning techniques. Representations are provided based on the similarities between the words, thereby understanding their meanings. An embedding layer is a part of the work embedding which is trained jointly with neural network models on specific NLP like classifying the documents or language modelling [9]. The document containing the lexical data must be cleaned so that the individual words are hot encoded. They are initially initialized with smaller random numbers. The method of training embedding layers needs a large amount of training data. This approach of learning an embedding layer requires a lot of training data and can be slow, but will learn an embedding both targeted to the specific text data and the NLP task.

There are many word embedding approaches where the modes have been pre-trained. Some of them are word2vec, Glove, and Fast text from Google, Stanford, and Facebook, respectively [10]. Word2vec was developed by Toma Mikolov and other researchers from Google in 2013 [11]. It is necessary to understand why word2vec was created. The other NLP systems at that period used to consider the words as individual atomic units. There were no similarities between the words, and the models were no effective for smaller datasets. Hence, larger datasets with complicated models have used neural network approaches for training complicated data models and works better for larger datasets with lots of vocabulary. Therefore, since the neural network is used in word2vec, it works effectively in measuring the quality of the resulting vectorized contents. Hence, the degree of similarity is considered for identifying similar words and grouping them.

*Corresponding Author: Said Salloum, University of Sharjah, UAE. Tel: +971507679647 Email: ssalloum@sharjah.ac.ae

In order to improve the architecture for the word representations, the accuracy must be improved, and the computational complexity must be minimized. Hence, neural network models like Recurrent and Feedforward neural networks are linked to Net Language Model (NLM) [12]. They can be trained through Backpropagation or Stochastic gradient descent. In FFNNLM, it contains the layers like input, hidden, and output layers like any other work. In addition, it also contains the projection layer. Since the computation between hidden layers and projection layers are complicated, the data in the projection layer becomes denser [13]. In RNNLM, the model has more complicated patterns and layers; hence projection layer is not required in this model. Only the three basic layers of the deep network are sufficient.

There are two different models for learning that can be part of the word2vec technique for learning the word embeddings. They are:

- Continuous Bag-of-Words (CBOW)
- Continuous Skip-Gram

The former gets trained based on the prediction of the present word based on its context, while the latter gets trained by learning the surrounding words, which will lead to the present word. Both of them focus on learning the words concerning their context and usage and also the configurable parameters of the models. The major benefit of the technique is that higher-quality word embeddings may be trained effectively with reduced space and time requirements. This allows bigger embeddings to get trained with higher magnitudes and more lexical data. The architecture of the word2vec algorithm is given in Figure 1.

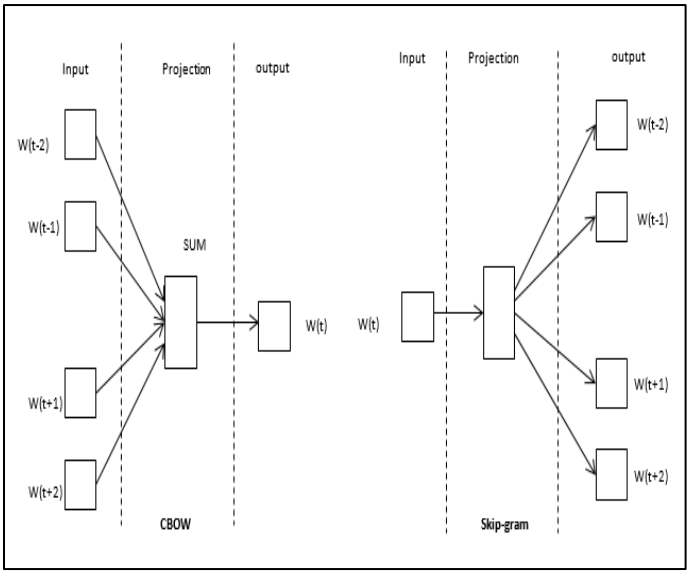

Figure 1: Architecture of word2vec

Network Functions Virtualisation (NFV) is a network architecture that utilizes IT virtualization to virtualize the entire classes of network node functions into structural blocks [14], [15]. Firewalls and network intrusions detections are necessary to provide security to the hardware. Hence these must be utilized in the application layer of the system [16]. Vectorisation is gradually taking center stage, which is being utilized in hardware equipment [17]. Newer processors are altering their architectures to improve the security for vectorization [18]. In these CPUs, it is obligatory to achieve vectorization for attaining higher performance [19]. When vectorized query execution is utilized, the processes are streamlined by processing multiple blocks at the same time. This may usually be 1024 blocks. Within the block, every column is saved as a single array, i.e., vector. Simple arithmetic operations and comparisons are performed by rapid iterations of vectors in a tight loop with very few function calls or conditional branches in the loop. These loops compile in a streamlined manner with fewer instructions and complete the instructions with a reduced clock cycle by utilizing the processors and cache memory.

The databases may be vulnerable to sensitive information or theft and can be attacked since the attackers can take advantage of the bugs in order to gain access to private information. Also, the attackers may seize and leak the data to those who require them. Hence, the confidentiality and piracy of the database must be safeguarded. CryptDB provides confidentiality against the attackers through SQL databases [20]. The query processes in the SQL are encrypted by collecting effective SQL aware encryption schemes. The process can also be used for encrypting the credential keys so that an item can be decrypted with merely a password. Since the processes and data are encrypted, the database administrator will not be able to view the data. In case of an attack on the server, the invader would not be able to gain access to the decrypted data. The database is capable of handling multiple queries simultaneously with fewer maintenance costs.

2. Literature Review

A study by [21] has assessed security risks through both quantitative and qualitative analysis. A critical review of the existing standards has been performed [22], [23], and then the results of the quantitative data are compared to qualitative data. From the analysis, it has been identified that long term security was preferred by the security engineers, and the financial impact of the information security is difficult to calculate quantitatively. A similar analysis has been performed by [24] on the performance of information security and security awareness of the engineers. Interviews have been performed in an IT company for exploring the personal role of information security workers. It was learned that most of the workers did not have any individual security responsibilities; higher workload increases the conflict between security and performance. They must be involved more into the processes to have a better-balanced improvement in security and performance.

The different types of databases have been discussed in [25] and have focussed on the CryptDB database. The type that provides the most secure among the different types of CryptDB database is Random (RND). This type is attributed to providing security against under a probabilistic adaptive plain text attack. The available data has been split and then mapped into the respective ciphertexts using the vectorized process. Ransom makes sure that the calculations are conducted directly on the ciphertexts. Encryption approaches like AES and Blowfish are performed simultaneously in RND with a random initialization vector. AES is used more than Blowfish for 64-bit block sizes since AES has 128-bit blocks that cause the ciphertexts to be very long.

Researchers of [26] has proposed the vectorization in the form of cryptographic security and digital map in this implementation.

Data encryption has been used to provide security to the network in this work. An iterative encryption organization has been proposed for compressing the vector domain in copy protection and retrieving the control of vector data. The cipher size is reduced by encrypting the various processes through Minimum Coding Object (MCO). The mean points of the data are permutated with position-based encryption, and then the secondary data is fit inside.

A Ciphertext policy with consistent size has been introduced by [27] known as Cipher-text Policy Hidden Vector Encryption (CP-HVE). This type of encryption is unique, where the IBE gets anonymous and utilizes the identity as the main parameters where the attributes linked with the ciphertext or secret keys contain wild-cards. Different arrangements have been utilized, one with a composite ordered bi-linear group while it is a prime ordered bilinear group. These schemes offer higher security by distinguishing the plaintext and ciphertext. This vectorized encryption can have a uniform size than the other HVE methods.

Scholars of [28] has performed quantitative analysis using word2vec to form semantic forms of Naturalistic Driving Data (NDD). Since large amounts of data must be compressed and create compact versions without any loss, the performance has been carried out. Quantitative analysis has been performed to identify the semantic link between the sequences in words. [29] has proposed an automatic intrusion detection system known as MalDozer for the Android operating system. It uses deep learning techniques for classifying the sequences and then word2vec has been used for API for detecting the patterns and malware in the system. The proposed approach has been implemented on servers and evaluated on multiple devices. The result shows the proposed approach and showed high accuracy

According to a study by [30] has also performed quantitative analysis for sentiment analysis. Word2vec method has been used for extracting the features, and then Principal Component Analysis (PCA) was used to identify the important elements and structure. Various classifiers have been compared for performing the work and evaluating the results. In [31] has conducted research for the holistic management of cybersecurity by both quantitative and qualitative methodologies. From the analysis, it was concluded that small and medium-sized businesses had no structural mechanisms to reduce security risks. Instead, they applied the solutions after the breach takes place. Hence, there are not equipped to handle the risks and threats beforehand. The main elements of the framework are identified as external factors, assessing the risks and organizational behaviors.

A study by [32] has proposed a one-shot learning approach for the rapid detection of the attacks. The implementation has been performed for computer vision for recognizing images and texts. Memory Augmented Neural Network has been used in this work, combined with malware detection. Word2vec was used for converting the Application Programming Interface (API) sequences into numeric vectors before getting fed into the one-shot learning network. High accuracy was obtained due to the vectorization using word2vec.

In [33] has proposed a malware detection approach, namely DroidVecDeep, that uses a deep learning approach. Different features are extracted and then ranked by utilizing the Mean Decrease Impurity approach. The features are then transformed into compact vectors on the basis of word2vec. A deep learning model is used to train the classifier, and various malware detection methods are compared. From the results, it is seen that the proposed approach works better than other detection techniques. Hence, vectorization using word2vec is an effective algorithm with deep learning.

A study by [34] has performed group encryption with lattice assumptions through the relation between the matrix vectors. The implementation has been performed through the proposed model, and it was seen that the proposed model provided higher security with certain assumptions. Public key encryption has been used to demonstrate the processes of the novel methodology. However, only generic data has been vectorized rather than the processes.

In [35] has also utilized word2vec for constructing vectors with context sentences and sense the definition vectors giving scores to individual words. WordNet database has been used for retrieving the words and structure and get trained. Scores are based on specific thresholds, and they will be combined with the probability of SEMCOR, which is a sense tagged corpus. It is seen from the results that the performance is better without the probability of distribution. A study by [36] has developed a framework for improving network security. The related studies that focus on network security have been studied with respect to changes to ensure security, passive defenses, the formation of strategy, and overall trend prediction. A detailed critical analysis has been performed by comparing the related articles. The process has included representations, analysis of the solution, predicting the situation, and acquiring the factors.

Encryption is usually performed in such a way that there is very little loss in the vectorized data. A study by [37] has implemented word2vec with Long Short-Term Memory (LSTM) approach for provided security from the attacks. The opcodes have been analyzed in the executable files and maybe clustered using the LSTM network. Word2vec was used for converting the names of the API through one hot encoding results in higher dimensional vectors since the individual cases are represented using the individual dimensions. The proposed approach had better performance than a one-hot encoding-based approach. The issues with data encryption and decryption have been analyzed by [38] through a questionnaire-based methodology. An overview of different schemes for single and multiple secrets of image data has been performed. The different factors that are taken into consideration for the encryption are contrast, capacity, number of shares, type of shares, accuracy, security, and the image format. From these factors, the issues have been identified and have been suggested to address them through novel methods.

Authors of [39] has analyzed the trends in blockchain technology by using word2vec in combination with Latent Semantic Analysis (LSA). Most existing research work has used effort demanding a complete textual investigation and traditional bibliometric approaches. Hence, k means clustering approach has been used for capturing the lexical context. Annual trend analysis has been used for various chains of blockchain. It is seen that the proposed approach has higher accuracy with respect to quantitative methodology. A qualitative approach has also been performed.

From the above review of literature, it can be seen that there are not many studies performing quantitative analysis through

interviews and questionnaires. Most of the studies have directly improved the work by trying to implement the algorithms; however, there are hardly any studies that analyze the management problem by interviewing the public on this. Hence, a comprehensive methodology is required to directly interview the concerned people and collect the data to understand the problem faced and create an effective solution.

3. Methodology

In this work, the quantitative methodology is used to collect the data and analyze the problem. The quantitative methodology can be defined as a type of analysis that uses data that can be easily quantifiable to perform mathematical, computational, and statistical approaches [40]–[52]. Data is collected from the potential sample population through any of the sampling methods in the form of questionnaires [53]. These sets of questions may be asked directly or through the internet in the form of polls or mails. The responses are always converted to the numerical form in such a way that they are quantifiable. The implementation uses interpretivism to understand the problem and gain solutions. Interpretivism is a type of methodology that the researcher implements for synthesizing the facts that are derived from the sources. These facts depend on lots of factors that cannot be measured physically, or they are difficult to measure. The factors may fall under social, cultural, or economic categories. This is analyzed to realize whether the database or security engineers know how to provide security to the database that is vectorized.

The quantitative strategy is applicable for this research since the link between the various variables can be set by interpreting them [54]. This requires interviews to be conducted through questionnaires. The questionnaire addressed the software engineer, who is the most suitable discipline to responded and address the issues in dealing with wrd2vec and CryptDB. Questionnaires are selected for this analysis since they are more reliable and can collect data from lots of respondents quickly and effectively. This is essentially true for larger projects with thousands of respondents. The major disadvantage, however, is that the format is fixed for the entire population and cannot be customized depending on the respondent and this removes the likelihood of in-depth analysis. However, this work does not require variable responses, and hence questionnaires are sufficient. A survey contains various questions relating to the knowledge of vectorization, and security is distributed to the engineers of different companies. They are selected based on the different available companies identified online and their engineers are contacted through email. The responses are captured through online forms and surveys and then compiled together. A total of 30 responses are captured in this way. No sampling strategy was followed here, and only one group of respondents is identified. The questionnaire consists of eleven questions divided into three groups. The groups are dedicated to experience, security, and time. The experience gets from the data related to the educational background and work experience of the respondents. Security aspect relates to the knowledge of the correspondence on security of word2vec and vectorization. Time measures the ability of the security engineers to manage time in performing any changes to the design of the database. The results from the questionnaire are compiled into a single file. Since the number of respondents is very small, detailed analysis is not required. In this work, SPSS software is used for the quantitative analysis.

4. Data Analysis

From the collected results, the analysis performed through SPSS tool is discussed in this section. Table 1 gives details of the qualification of the respondents. A major portion of them is undergraduates at 53.5%, followed by postgraduates at 30%, doctorates at 10%, and certification courses at 6.7%. Table 2 explains the work experience of the respondents. Most of the respondents have experienced between 4 and 8 years, while only 2 respondents had experienced less than four years, suggesting that most of the respondents are well experienced. This is because they are in a senior position. Around 30% of the respondent had more than nine years' experience, out of which 10% had more than 15 years of experience. The respondents who have completed certificate courses have a very high experience, which conveys that only graduates are allowed to become security engineers in the recent decade.

Table 1: Frequency of Qualification

Qualification	Number of respondents	Percent
Computer certification course	2	6.7
Undergraduate	16	53.3
Postgraduate	9	30.0
Doctorate	3	10.0
Total	30	100.0

Table 2: Frequency of Experience

Experience	Number of respondents	Percent
0-3 years	2	6.7
4-8 years	19	63.3
9-15 years	6	20.0
More than 15 years	3	10.0
Total	30	100.0

The ability to solve the security problems in vectorization is given in Table 3. It is seen that most of the respondents are able to solve security issues, with 60% of them pertaining to certain problems, while 33.3% were confident of solving all the problems. Two of the respondents said that they are unable to solve security issues. While more than 90% of the respondents are able to solve security problems, only 66.7% of them have used the CryptDB database for security, as shown in Table 4. The data is also visualized in Figure 2.

Table 3: Ability to solve the security issues during vectorization

Ability to solve the security issues during vectorization	Number of respondents	Percent
Unable to solve the problems	2	6.7
Can solve certain problems	18	60.0
Can effectively solve all the problems	10	33.3
Total	30	100.0

Table 4: Frequency of use of CryptDB database

Use CryptDB database	Number of respondents	Percent
Yes	20	66.7
No	10	33.3
Total	30	100.0

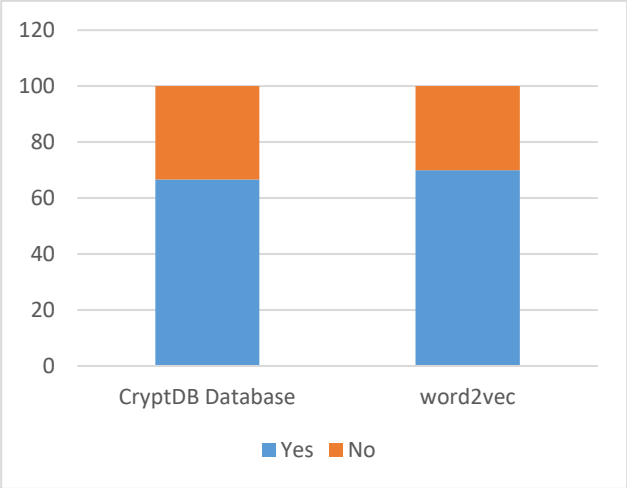

Figure 2: Use of CryptDB and word2vec

A large portion of the respondents has used word2vec embedding for vectorization. Around 70% of them have used them, while the other 30% have either used other types of embedding techniques or never used vectorization as shown in Table 5.

Table 5: Frequency of use of Word2ved embedding

Do you use Word2vec embedding?	Number of respondents	Percent
Yes	21	70.0
No	9	30.0
Total	30	100.0

Since word2vec can be performed easily, it is implemented; however it takes time for embedding them along with the secure database. Only a few of the respondents could complete the implementation within a day, while almost three quarters of the respondents will take from 2 to 7 days. 13.3% of the respondents will take more than a week to complete as shown in Table 6.

Table 6: Time taken for Word2ved embedding

Time is taken for Word2ved embedding	Number of respondents	Percent
Within a day	4	13.3
Takes about a week	22	73.3
Takes more than a week	4	13.3

Once the database is secured, then there might be possibilities of making changes to the design or contents in the work. This might be easy for some minor modifications, where the contents can be modified easily. However, for adding a new component or embed a new element, the design has to be modified, which would take some time. Most of the respondents at around 86.7% of them responded that it would take a long time for them to make changes in the design, only 13.3% of them said it could be done quickly as shown in Table 7.

Table 7: Frequency of changes be made in the design quickly if required

Can any changes be made in the design quickly if required	Number of respondents	Percent
Yes, design can be changed quickly	4	13.3
It takes a long time to make design changes	26	86.7
Total	30	100.0

Even though most respondents have used CryptDB and word2vec, they do not use it in their everyday results. Table 8 shows whether the respondents use CryptDB and word2vec regularly.

Table 8: Frequency of the usage of the concepts

Which one do you use regularly?	Number of respondents	Percent
CryptDB	10	33.3
Word2vec	9	30.0
Both	11	36.7

The mean and the standard deviation for the security is also given in Table 9 for the CryptDB database and word2vec embedding. The p values are seen to be at 0.002, which is considered to be a significant value.

Table 9: Difference in mean security between types of database

	CryptDB database	Word2vec	Both	p-value
	Mean ± SD			
Security	2.73±0.90	2.63±0.51	3.64±0.35	**0.002****

Table 10 gives the opinion of the engineers related to database security. Most of the engineers strongly agree that their database is secure. 40% of the respondents strongly agree, followed by 26.7% agreeing that their database is secure. On the other hand, 32% of the respondents do not agree to this and feel that security must be improved. The majority of the respondents also feel that CryptDB would improve security in the database. 66.7% of the respondents agree, while the other 33.3% disagree that CryptDB improves the security features. While 40% of the respondents strongly agree, only 3.3% of them strongly disagree with CryptDB. Most of the respondents also agree that a secure database must be used for secure vectorizations. 86.7% of the respondents agree that a secure database must be used, while 13.3% of them disagree that security is not required.

The descriptive statistics for the database security are shown in Table 11. Out of the 4-point scale from strongly disagree to strongly agree, a mean of 3.3 is seen along with a standard deviation of 0.76 for the 30 respondents. This is more inclined towards the right with more people agreeing to the conditions in table 10. Since the mean is near 3, more people just agree to the

points while some of them strongly agree. The frequency of disagreeing and strongly disagree is also less.

Table 10: Database security

		N	%
My database is secure	Strongly Disagree	5	16.7
	Disagree	5	16.7
	Agree	8	26.7
	Strongly Agree	12	40.0
CryptDB database improve the security features	Strongly Disagree	1	3.3
	Disagree	9	30.0
	Agree	8	26.7
	Strongly Agree	12	40.0
Secure database must be used for vectorization?	Strongly Disagree	1	3.3
	Disagree	3	10.0
	Agree	16	53.3
	Strongly Agree	10	33.3

Table 11: Descriptive statistics for security

	N	Minimum	Maximum	Mean	SD
Security	30	1.33	4.00	3.03	0.76

5. Conclusions and Recommendations

From the above analysis, it is identified that most of the scientists think that security is necessary for the databases. Even though there are a lot of secure databases and word embedding options, however, around 63% of the interviewed engineers use CryptDB for security purposes, and around 66% use word2vec for embedding options. While many scientists agree that security must be improved in the databases, most scientists completely agree that CryptDB can definitely improve security. Also, most of the engineers accept that word2vec is an effective way to completely improve the vectorization. This work has presented a quantitative methodology for understanding the link between the word vectorization approach word2vec and providing security to the database by using CryptDB. Initially, a brief introduction to both these terminologies concerning vectorization was studied, and then related studies have been studied in the literature review. A questionnaire was created to perform interviews on security engineers. Data is collected in the form of online forms, and then, the data is analyzed through SPSS tool. From the data, it is identified that both word2vec and CryptDB is recommended for embedding the words and security, respectively. The simultaneous use of both of them is suggested as an effective combination for secure vectorization. Hence, the implementation of both of them together is considered as future scope of this work.

6. Limitation and Caveats

The gap identified is that even though many researchers have individually implemented them both. They haven't been implemented together. Also, most of the studies have implemented them technically, but haven't performed interview-based analysis. The limitation of this work was due to the lockdown that happened in March due to COVID-19, and the analysis was conducted on a small scale group of security engineers, the number of correspondents considered in the study was little. In future work, the study will consider both quantitative and qualitative methods. In this study, there are no caveats discussed in this paper.

References

[1] H. Zamani and W. B. Croft, "Relevance-based word embedding," in *Proceedings of the 40th International ACM SIGIR Conference on Research and Development in Information Retrieval*, 2017, 505–514. https://doi.org/10.1145/3077136.3080831

[2] S. A. Salloum, M. Alshurideh, A. Elnagar, and K. Shaalan, "Mining in Educational Data: Review and Future Directions," in *Joint European-US Workshop on Applications of Invariance in Computer Vision*, 2020, 92–102. https://doi.org/10.1007/978-3-030-44289-7_9

[3] S. A. Salloum, R. Khan, and K. Shaalan, "A Survey of Semantic Analysis Approaches," in *Joint European-US Workshop on Applications of Invariance in Computer Vision*, 2020, 61–70. https://doi.org/10.1007/978-3-030-44289-7_6

[4] M. Al-Emran, S. Zaza, and K. Shaalan, "Parsing modern standard Arabic using Treebank resources," in *2015 International Conference on Information and Communication Technology Research, ICTRC 2015*, 2015. 10.1109/ICTRC.2015.7156426

[5] C. Mhamdi, M. Al-Emran, and S. A. Salloum, *Text mining and analytics: A case study from news channels posts on Facebook*, vol. 740. 2018. https://doi.org/10.1007/978-3-319-67056-0_19

[6] M. Al-Emran, "Hierarchical Reinforcement Learning: A Survey," *Int. J. Comput. Digit. Syst.*, 4(2), 137–143, 2015. http://dx.doi.org/10.12785/IJCDS/040207

[7] H. Zamani and W. B. Croft, "Estimating embedding vectors for queries," in *Proceedings of the 2016 ACM International Conference on the Theory of Information Retrieval*, 2016, 123–132. https://doi.org/10.1145/2970398.2970403

[8] O. Press and L. Wolf, "Using the output embedding to improve language models," *arXiv Prepr. arXiv1608.05859*, 2016. https://arxiv.org/abs/1608.05859

[9] K. Hashimoto, C. Xiong, Y. Tsuruoka, and R. Socher, "A joint many-task model: Growing a neural network for multiple nlp tasks," *arXiv Prepr. arXiv1611.01587*, 2016. https://arxiv.org/abs/1611.01587

[10] D. Sarkar, "The Promise of Deep Learning," in *Text Analytics with Python*, Springer, 2019, 631–659. https://doi.org/10.1007/978-1-4842-4354-1_10

[11] T. Mikolov, K. Chen, G. Corrado, and J. Dean, "Efficient estimation of word representations in vector space," *arXiv Prepr. arXiv1301.3781*, 2013. https://arxiv.org/abs/1301.3781

[12] S. Ghosh, M. Chollet, E. Laksana, L.-P. Morency, and S. Scherer, "Affect-lm: A neural language model for customizable affective text generation," *arXiv Prepr. arXiv1704.06851*, 2017. https://arxiv.org/abs/1704.06851

[13] T.-H. Yang, T.-H. Tseng, and C.-P. Chen, "Recurrent neural network-based language models with variation in net topology, language, and granularity," in *2016 International Conference on Asian Language Processing (IALP)*, 2016, 71–74. 10.1109/IALP.2016.7875937

[14] Y. Li and M. Chen, "Software-defined network function virtualization: A survey," *IEEE Access*, 3, 2542–2553, 2015. 10.1109/ACCESS.2015.2499271

[15] R. Mijumbi, J. Serrat, J.-L. Gorricho, N. Bouten, F. De Turck, and R. Boutaba, "Network function virtualization: State-of-the-art and research challenges," *IEEE Commun. Surv. tutorials*, 18(1), 236–262, 2015. 10.1109/COMST.2015.2477041

[16] J. F. Kurose, *Computer networking: A top-down approach featuring the internet, 3/E*. Pearson Education India, 2005.

[17] "Intel Corporation (2015). Intel Vectorization Tools. [Online].," 2015.

[18] "Intel (2013). Intel® Xeon PhiTM Processors. [Online]," 2013.

[19] C. Stylianopoulos, L. Johansson, O. Olsson, and M. Almgren, "CLort: High Throughput and Low Energy Network Intrusion Detection on IoT Devices with Embedded GPUs," in *Nordic Conference on Secure IT Systems*, 2018, 187–202. https://doi.org/10.1007/978-3-030-03638-6_12

[20] R. A. Popa, C. M. S. Redfield, N. Zeldovich, and H. Balakrishnan, "CryptDB: processing queries on an encrypted database," *Commun. ACM*, vol. 55, no.

9, 103–111, 2012.
[21] A. Munteanu, "Information security risk assessment: The qualitative versus quantitative dilemma," in *Managing Information in the Digital Economy: Issues & Solutions-Proceedings of the 6th International Business Information Management Association (IBIMA) Conference*, 2006, 227–232. https://papers.ssrn.com/sol3/papers.cfm?abstract_id=917767
[22] S. A. Salloum, M. Alshurideh, A. Elnagar, and K. Shaalan, "Machine Learning and Deep Learning Techniques for Cybersecurity: A Review," in *Joint European-US Workshop on Applications of Invariance in Computer Vision*, 2020, 50–57. https://doi.org/10.1007/978-3-030-44289-7_5
[23] S. K. Yousuf H., Lahzi M., Salloum S.A., "Systematic Review on Fully Homomorphic Encryption Scheme and Its Application.," *Al-Emran M., Shaalan K., Hassanien A. Recent Adv. Intell. Syst. Smart Appl. Stud. Syst. Decis. Control. vol 295. Springer, Cham*, 2021. https://doi.org/10.1007/978-3-030-47411-9_29
[24] E. Albrechtsen, "A qualitative study of users' view on information security," *Comput. Secur.*, 26(4), 276–289, 2007. https://doi.org/10.1016/j.cose.2006.11.004
[25] R. A. Popa, C. M. S. Redfield, N. Zeldovich, and H. Balakrishnan, "CryptDB: protecting confidentiality with encrypted query processing," in *Proceedings of the Twenty-Third ACM Symposium on Operating Systems Principles*, 2011, 85–100. https://doi.org/10.1145/2043556.2043566
[26] B.-J. Jang, S.-H. Lee, and K.-R. Kwon, "Perceptual encryption with compression for secure vector map data processing," *Digit. Signal Process.*, vol. 25, 224–243, 2014. https://doi.org/10.1016/j.dsp.2013.09.013
[27] T. V. X. Phuong, G. Yang, and W. Susilo, "Efficient hidden vector encryption with constant-size ciphertext," in *European Symposium on Research in Computer Security*, 2014, 472–487. https://doi.org/10.1007/978-3-319-11203-9_27
[28] Y. Fuchida, T. Taniguchi, T. Takano, T. Mori, K. Takenaka, and T. Bando, "Driving word2vec: Distributed semantic vector representation for symbolized naturalistic driving data," in *2016 IEEE Intelligent Vehicles Symposium (IV)*, 2016, 1313–1320. 10.1109/IVS.2016.7535560
[29] E. B. Karbab, M. Debbabi, A. Derhab, and D. Mouheb, "Android malware detection using deep learning on API method sequences," *arXiv Prepr. arXiv1712.08996*, 2017. https://arxiv.org/abs/1712.08996
[30] X. Ge, X. Jin, and Y. Xu, "Research on sentiment analysis of multiple classifiers based on word2vec," in *2018 10th International Conference on Intelligent Human-Machine Systems and Cybernetics (IHMSC)*, 2018, vol. 2, 230–234. 10.1109/IHMSC.2018.10159
[31] J. Jung, "A Study of Cyber Security Management within." University of Portsmouth, 2018.
[32] T. K. Tran, H. Sato, and M. Kubo, "One-shot Learning Approach for Unknown Malware Classification," in *2018 5th Asian Conference on Defense Technology (ACDT)*, 2018, 8–13. 10.1109/ACDT.2018.8593203
[33] T. Chen, Q. Mao, M. Lv, H. Cheng, and Y. Li, "DroidVecDeep: Android Malware Detection Based on Word2Vec and Deep Belief Network.," *TIIS*, 13(4), 2180–2197, 2019.
[34] B. Libert, S. Ling, F. Mouhartem, K. Nguyen, and H. Wang, "Zero-knowledge arguments for matrix–vector relations and lattice-based group encryption," *Theor. Comput. Sci.*, 759, 72–97, 2019. https://doi.org/10.1007/978-3-662-53890-6_4
[35] K. Orkphol and W. Yang, "Word sense disambiguation using cosine similarity collaborates with Word2vec and WordNet," *Futur. Internet*, vol. 11, no. 5, p. 114, 2019. https://doi.org/10.3390/fi11050114
[36] Y. Li, G. Huang, C. Wang, and Y. Li, "Analysis framework of network security situational awareness and comparison of implementation methods," *EURASIP J. Wirel. Commun. Netw.*, 2019(1), 205, 2019. https://doi.org/10.1186/s13638-019-1506-1
[37] J. Kang, S. Jang, S. Li, Y.-S. Jeong, and Y. Sung, "Long short-term memory-based malware classification method for information security," *Comput. Electr. Eng.*, 77, 366–375, 2019. https://doi.org/10.1016/j.compeleceng.2019.06.014
[38] L. R. Logeshwari, R. & Parvathy, "A Quantitative and Qualitative Reasoning of Various Visual Cryptographic Schemes to Uphold Secrecy. International Journal of Innovative Technology and Exploring Engineering. [Online]. 8 (11). 1148–1151.," 2019.
[39] S. Kim, H. Park, and J. Lee, "Word2vec-based latent semantic analysis (W2V-LSA) for topic modeling: a study on blockchain technology trend analysis," *Expert Syst. Appl.*, 113401, 2020. https://doi.org/10.1016/j.eswa.2020.113401
[40] C. Q. (2019). Dhir, R.K., de Brito, J., Silva, R. V. & Lye, "Methodology. In: Sustainable Construction Materials.," *[Online]. Elsevier*, 15–34, 2019.
[41] S. A. S. Salloum and K. Shaalan, "Investigating students' acceptance of E-learning system in Higher Educational Environments in the UAE: Applying the Extended Technology Acceptance Model (TAM)." The British University in Dubai, 2018.
[42] M. Habes, M. Alghizzawi, S. Ali, A. SalihAlnaser, and S. A. Salloum, "The Relation among Marketing ads, via Digital Media and mitigate (COVID-19) pandemic in Jordan," *Int. J. Adv. Sci.*, 29(7), 2326–12348, 2020.
[43] M. Habes, M. Alghizzawi, S. A. Salloum, and C. Mhamdi, "Effects of Facebook Personal News Sharing on Building Social Capital in Jordanian Universities," in *Recent Advances in Intelligent Systems and Smart Applications*, Springer, 2020, 653–670. https://doi.org/10.1007/978-3-030-47411-9_35
[44] S. S. A. Al-Maroof R.S., "An Integrated Model of Continuous Intention to Use of Google Classroom.," *Al-Emran M., Shaalan K., Hassanien A. Recent Adv. Intell. Syst. Smart Appl. Stud. Syst. Decis. Control. vol 295. Springer, Cham*, 2021. https://doi.org/10.1007/978-3-030-47411-9_18
[45] S. A. Salloum, A. Q. M. Alhamad, M. Al-Emran, A. A. Monem, and K. Shaalan, "Exploring Students' Acceptance of E-Learning Through the Development of a Comprehensive Technology Acceptance Model," *IEEE Access*, vol. 7, 128445–128462, 2019. 10.1109/ACCESS.2019.2939467
[46] S. A. Salloum and M. Al-Emran, "Factors affecting the adoption of E-payment systems by university students: Extending the TAM with trust," *Int. J. Electron. Bus.*, 14(4), 371–390, 2018. https://doi.org/10.1504/IJEB.2018.098130
[47] S. A. Salloum and K. Shaalan, "Factors affecting students' acceptance of e-learning system in higher education using UTAUT and structural equation modeling approaches," in *International Conference on Advanced Intelligent Systems and Informatics*, 2018, 469–480. https://doi.org/10.1007/978-3-319-99010-1_43
[48] S. A. Salloum and K. Shaalan, "Adoption of e-book for university students," in *International Conference on Advanced Intelligent Systems and Informatics*, 2018, 481–494. https://doi.org/10.1007/978-3-319-99010-1_44
[49] M. Al-Emran, I. Arpaci, and S. A. Salloum, "An empirical examination of continuous intention to use m-learning: An integrated model," *Educ. Inf. Technol.*, 2020. https://doi.org/10.1007/s10639-019-10094-2
[50] S. A. Salloum, M. Al-Emran, R. Khalaf, M. Habes, and K. Shaalan, "An Innovative Study of E-Payment Systems Adoption in Higher Education: Theoretical Constructs and Empirical Analysis," *Int. J. Interact. Mob. Technol.*, 13(6), 2019. https://onlinejour.journals.publicknowledgeproject.org/index.php/i-jim/article/view/9875
[51] R. S. Al-Maroof, S. A. Salloum, A. Q. AlHamadand, and K. Shaalan, "Understanding an Extension Technology Acceptance Model of Google Translation: A Multi-Cultural Study in United Arab Emirates," *Int. J. Interact. Mob. Technol.*, 14(3), 157–178, 2020. https://onlinejour.journals.publicknowledgeproject.org/index.php/i-jim/article/view/11110
[52] M. Habes, S. A. Salloum, M. Alghizzawi, and C. Mhamdi, "The Relation Between Social Media and Students' Academic Performance in Jordan: YouTube Perspective," in *International Conference on Advanced Intelligent Systems and Informatics*, 2019, 382–392.
[53] P. Galbacs, *The Friedman-Lucas Transition in Macroeconomics: A Structuralist Approach*. Academic Press, 2020.
[54] M. Al-Emran, V. Mezhuyev, and A. Kamaludin, "PLS-SEM in Information Systems Research: A Comprehensive Methodological Reference," in *4th International Conference on Advanced Intelligent Systems and Informatics (AISI 2018)*, 2018, 644–653. https://doi.org/10.1007/978-3-319-99010-1_59

ASTES

Advances in Science, Technology and Engineering Systems Journal Vol. 5, No. 4, 381-387 (2020)

www.astesj.com

Special Issue on Innovative Research in Applied Science, Engineering and Technology

ASTESJ

ISSN: 2415-6698

Development of Soil Moisture Monitoring by using IoT and UAV-SC for Smart Farming Application

Sarun Duangsuwan*,[1], Chakree Teekapakvisit[1], Myo Myint Maw[2]

[1]*Information Engineering, Prince of Chumphon Campus, King Mongkut's Institute of Technology Ladkrabang, Bangkok, 86160, Thailand*

[2]*Department of Computer Engineering and Information Technology (CEIT), Mandalay Technological University (MTU), Mandalay, 05011, Myanmar*

ARTICLE INFO

Article history:
Received: 19 June, 2020
Accepted: 17 July, 2020
Online: 28 July, 2020

Keywords:
UAV-SC
IoT
Soil moisture monitoring
Mobile application
Smart farming

ABSTRACT

Soil moisture is a fundamental factor for smart farming that is used to control the water management system. In this paper, the unmanned aerial vehicle (UAV) small cell (UAV-SC) can provide Internet of things (IoT) as the hotspot mobility network, due to the minimum limitation energy of connected IoT. The development of ground sensor (GS) communicates to the UAV-SC called GS-UAV-SC model for soil moisture monitoring is proposed to smart farming. UAV-SC aims to fulfill the data collection task with a limitation of GSs power. In the experiment, the two case scenarios: Napier grass farm and Ruzi grass farm are implemented. The result of soil moisture status is demonstrated as an example of data in real time on a mobile application monitoring system. The proposed system is useful for users/farmers to know the soil moisture data quickly for smart farming applications.

1. Introduction

Recently, agricultural UAV or drones become one of the most useful agricultural instruments utilized in smart farming, especially in the ground sensing applications. The UAV is employed as a mobility hotspot in the area lacking of the communication network to collect the data of soil and corps in order to monitor and control the water management system for precision agriculture. The agricultural UAV with a combination of IoT sensors are preferred. At present, the IoT sensors detect temperature and moisture of the soil and send them to farmers by using the UAV. Therefore, the identification of locations that suffer from droughts, water scarcity, and dryness of soil profile is easily observed. It helps the farmers to take precautionary methods such as contouring, damming, draining the surface water, and curtailing for further irrigation. Small UAV, either copters or flat-winged models with a combination of IoT sensors are essential.

In [1], the authors firstly introduced UAV which plays a great role in the aerial imagery of soils, particularly soil characteristics. Drones are attractive because they can fly at a low attitude over the fields, as many times as requires in the short intervals to study the same location. The result in [1] showed that the UAV or drones are one of the common methods for obtaining high-resolution maps showing spatial and temporal changes in soil moisture. However, the UAV imagery with low resolution is not used consistently to evaluate a field experiment. In [2], the authors have shown that the precision of soil moisture measurement with the frequency domain reflection (FDR) method was highly accurate. However, the soil moisture FDR sensor type is still expensive. Therefore, the low-cost capacitive sensor and very low-cost resistive sensors have been investigated in [3]. The authors have presented that low-cost capacitive sensors with soil-specific calibration matched the performance of the secondary standard and could possibly be used for water management with limited effects on irrigation efficiency. Nowadays, most of soil moisture application is based on IoT networking [4] or wireless sensor networking (WSN) [5]. The objective is to automatically obtain the agricultural parameters without requiring human-to-human or human-to-computer.

2. Related Work

2.1. UAV-SC

Most of the wireless IoT nodes utilized in the agricultural environment limit power energy which leads to the propagation problem in the surrounding area. Interestingly, B. Liu et al. [6] have proposed to solve the resource allocation problem in their UAV and IoT. The UAV works as power distribution by using a dynamic gamin-based model for wireless power transfer

*Corresponding Author: Sarun Duangsuwan, KMITL Prince of Chumphon Campus, Tel: +66-99186-4411; Email: sarun.du@kmitl.ac.th

applications. The authors in [6] have illustrated that the power energy transfer of UAV depends on the amount of the density of IoT wireless nodes and they can be controlled by the power by using the dynamic game method. On the other hand, the proposed measurement aided dynamic planning algorithm in [7] can solve the problem-based of multiple IoT connectivity network. This algorithm can help to control the drone small cell (DSC) base station as a self-configuration on the fly regarding the cell being located and channel being used, based on the real-time measurement of network throughput. In addition, more increasingly, an optional mobile backhaul link might use the drone or UAV aided emergency network [8]. However, the problem-based such as the inter-cell interference should be considered. In [9], the multiple DSCs used for the several based stations were optimized by using the equivalent uniform density plane entity (EUDPE) method. The results indicated that the increase of the transmission power of drone did not necessarily improve coverage performance for the IoT connectivity. Similar to the drone base stations (DBSs) in [10], the authors proposed a realistic mathematical model for the joint optimization problem of DBS placement and IoT users. Path loss measurement for an air-to-ground channel was investigated in [10]. For the data monitoring system based on WSN with the large-scale area such as a coast or river [11], the authors considered to maximize data collection with given energy budgets for the drone and sensors. DroneTank [11], the UAV can determine the flight path and speed to conduct data collection. As mentioned in the works of literature, the UAV-SC for ground sensing is very important in the smart farming applications.

2.2. Smart Farming

Recently, the proposed AgriLogger has been implemented in Italy [12]. The aim is to build precision agriculture in the areas lacking data communication networks that can collect data and store the long periods and transmitted agrometeorological data, such as temperature and relative humidity. The drone is equipped with a payload, such as a wireless transceiver, radio transmitter, and GNSS receiver. Additionally, a communication link provides the narrowband IoT (NB-IoT) network to collect the data via cloud management. AgriLogger was able to collect and store for long periods estimated for more than ten years, and consistently, agrometeorological parameters data in a successful way would be great profit for agriculture. As well-known that the WSN technology is useful for precision agriculture as well as the IoT solution. There are several works focused on using WSN [13,14]. In [15], the authors have presented the technique and practice of precision agriculture. They implied that precision agriculture is to provide decision support systems based on multiple parameters impacted to the crops plantation such as soil moisture, water management, wind speed, and so on, by using WSN-based or IoT-based cloud computing. In [16], a secure IoT-based WSN framework for smart agriculture was described. The simulation results show that the proposed was more efficient compared to the IoT communication reliabilities. The network throughput was increased to 13.5 % and 38.5 % for the packets drop ratio, 13.5 % for the network latency, 16 % for the energy consumption, and 26 % for the routing overheard of smart agriculture.

SmartFarmNet [17] platform is an example application for smart agriculture in Australia by using IoT platform. It provides a scalable sensor data acquisition, analysis, and visualization platform for smart farming applications, based on IoT. Interestingly, this platform measures soil moisture at particular multiple depths and steams data from the physical sensors to monitor a phenomenon. By using the SmartFarmNet gateway to process soil moisture data which is close to the source, the cloud computing performs real-time analysis on incoming sensor data streams. For a platform of precision agriculture, SmartFarmNet is an existing model of smart agriculture based on IoT-based platform. Considering the IoT for smart farming, the IoT platform can help the farmer to predict the disease of the strawberry farm in [18]. However, the problem is the false detection probability of IoT sensors to the gateway. Then, the authors in [19] have presented a solution called SensorTalk to automatically detect the potential sensor failures and semi-automatically calibrate the aging sensors. The solution showed that the false detection probability of IoT sensors to the gateway was reduced to less than 0.7 %.

In related work of smart irrigation, IoT framework for smart irrigation such as data monitoring, preprocessing, fusion, synchronization, storage, and irrigation management enriched by the prediction of soil moisture was presented in [20]. Smart&Green was used to preprocess soil moisture data with outlier removal criteria and techniques of Zscore, MZscore, GESD, and Chauvenet to provide a more precise irrigation water needed in irrigation management. While the propose of IoT for the water management interestingly was presented in [21], WSN, LoRa, and ESP32 modules were used. The system retrieved real-time data and used them to determine the correct amount of water to be used in a garden. With this solution [21], it was possible to save up to 34 % of water with sensor data from temperature, humidity, and soil moisture, or up to 26 % with only temperature inputs. At present, the application of IoT in smart farming is rapidly emerging. A Long-range wide area network (LoRaWAN) based on IoT platform has introduced and called LoRaFarM [22]. The LoRaFarM platform has evaluated on a real farm in Italy. This system can collect data such as air, soil, temperature, and humidity. The advantage of the LoRa network is the long-range communication network and life-long battery of sensors, but it is still needed more gateways in the field. In [22], the design for the soil moisture sensor kit was proposed. The LoRaFarM hardware was designed by using the 1W solar-cell, solar charger, soil sensor, LoRa module at 868 MHz, and LiPo battery.

3. Proposed Model and Implementation

The GS-UAV-SC model for smart farming applications is shown in Figure 1. It can be noted that the IoT soil moisture GS kits were installed in the field, then, were connected to the UAV-SC to transfer data streaming to the internet. After that, the data are stored and computed on the cloud platform. Additionally, the farmer/user can control the UAV around the field in order to collect all data from every sensor. User can monitor the data via the application program interface (API) on the mobile application. This proposed model aims to compensate for the low energy from the multiple GSs connectivity.

The structure model of the soil moisture GS prototype is shown in Figure 2. It can be noted that this platform would be used in case of sunlight. Herein, the capacitive soil moisture was used in this study. By using the capacitive soil moisture GS, the capacitance is varied based on the water content present in the soil. The capacitance converted into voltage level basic from 1.2 V to 3.0 V

maximum. The advantage of capacitive soil moisture GS which is made of corrosion-resistant material is that it gives long service life. The structure model of the soil moisture GS prototype consists of five parts:

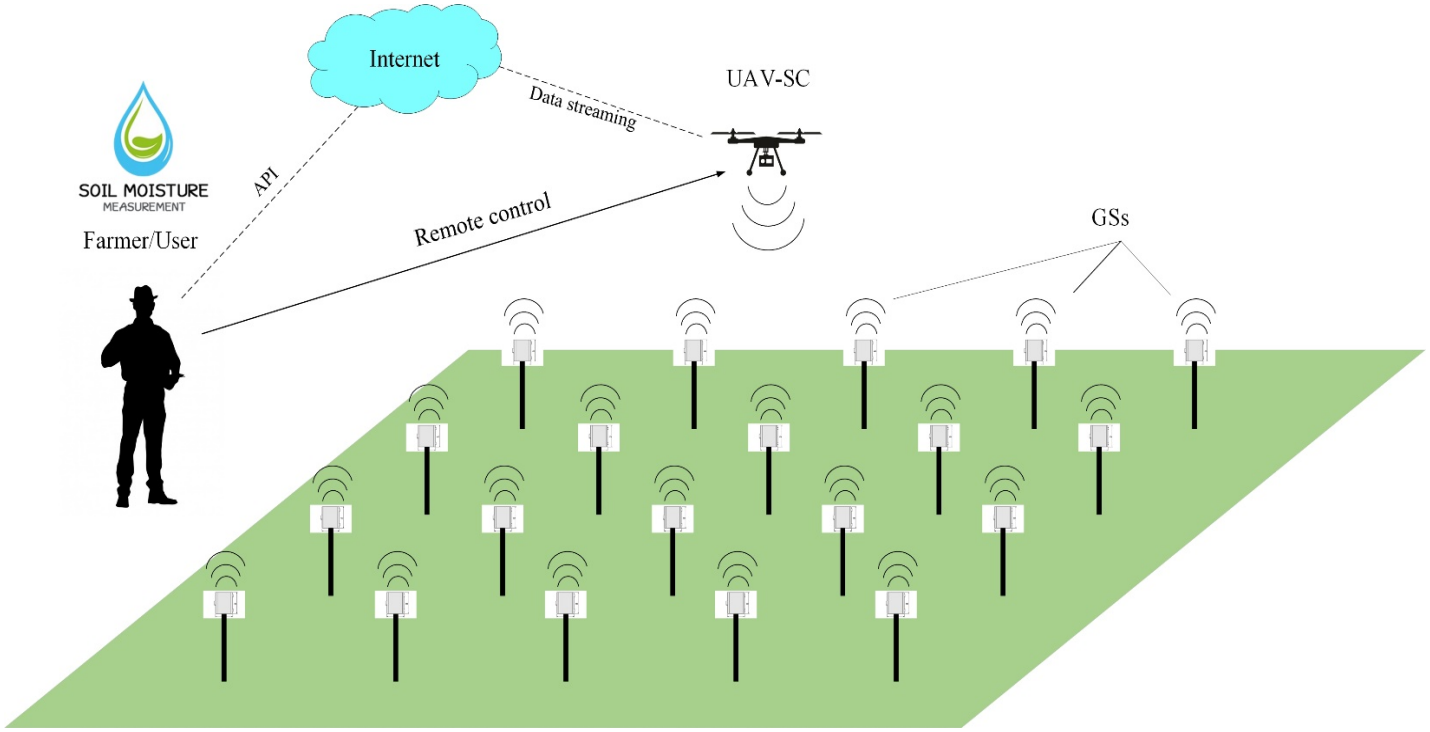

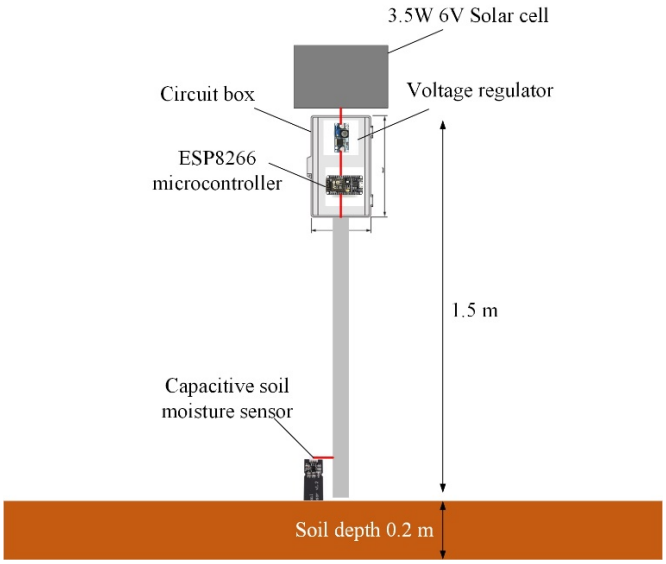

Figure 2: The structure model of soil moisture GS prototype.

2. Voltage regulator is DC to DC up/down LM2596 module, the maximum output current is 3 A, and the size is 50 mm wide and 37 mm length.
3. Microcontroller ESP8266 NodeMCU is used for controlling data from the soil moisture and transmitting to WiFi internet. The voltage is driven at 3.3 V and current consumption ranges from 70 mA to 240 mA. The transmitting power of microcontroller is 20 dBm, and it supports IEEE802.11 b/g/n.
4. Capacitive soil moisture sensor SKU: SEN0193, this module includes an on-board voltage regulator which gives an operating voltage range of 1.2 V to 3.0 V. The operating current is 5 mA. This module is an analog sensor which has 3-pins: A0 signal pin, positive pin +, and negative pin -. The depth of soil moisture sensor in the soil is 0.2 m according to the standard as shown Figure 2.
5. The material structure is made from aluminum pipe, and shield is inserted in the circuit box.

The implementation was conducted at the Tropical Animal Research Institute, Ramkhamhaeng University, Thailand. Figure 3(a) shows an example location of Napier grass farm and Ruzi grass farm in Figure 3(b) where the dimension of Napier grass farm is 25 m wide and 45 m length as shown in Figure 3(c) and Ruzi farm is 30 m wide and 50 m length in Figure 3(d). It is noted that these Napier and Ruzi grass are the main food of animals in the smart farm and 50 m of length in Figure 3(d). To note that, these Napier and Ruzi grass are mainly food of the animals within the smart farm.

3.1. Data Processing

The block diagram of data processing is shown in Figure 4. The quadcopter UAV is used for mobility and mounted with the WiFi transceiver. The WiFi transceiver radiates power to the GSs and is connected with the microcontroller ESP8266 NodeMCU module. After receiving the data from the capacitive soil moisture sensor, the ESP8266 NodeMCU transmits data to the internet, cloud computing, and cloud storage based on the Google firebase solution. Eventually, the soil moisture data is alerted to the mobile application.

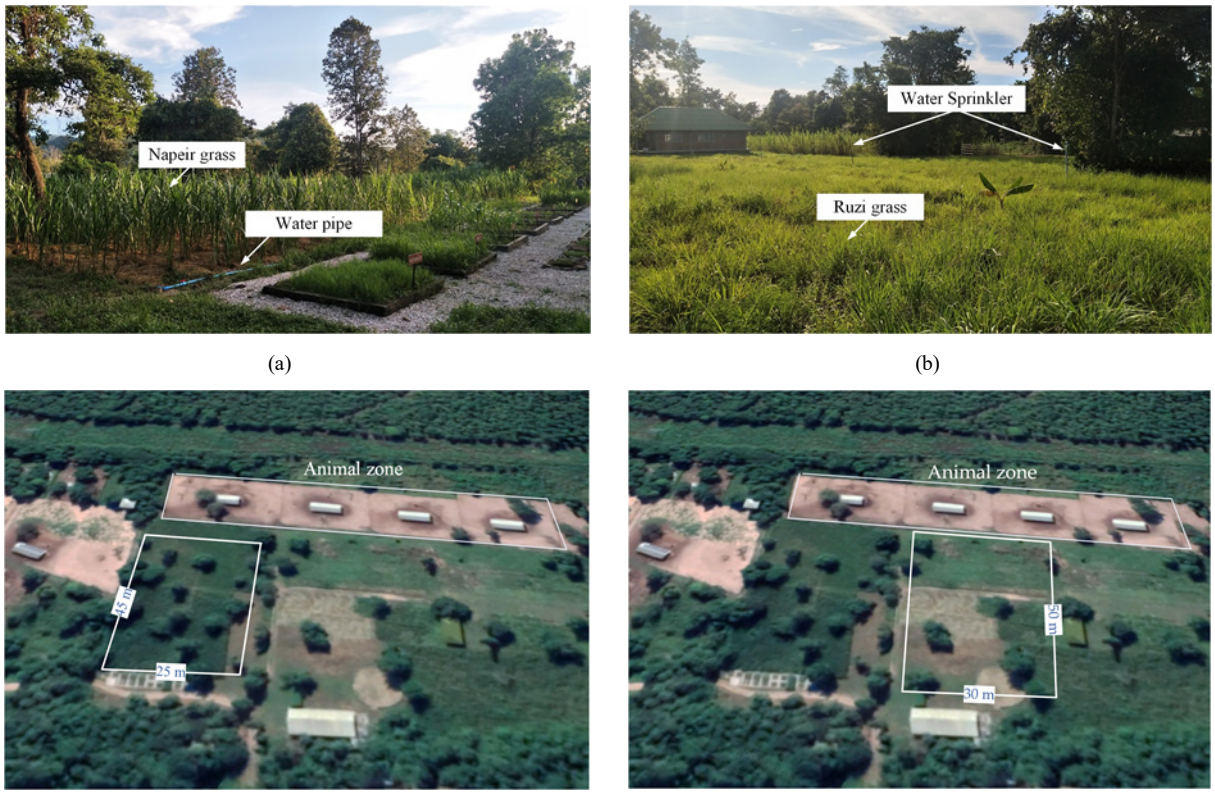

Figure 3: Smart farming of the Tropical Animal Research Institute, Ramkhamhaeng University: (a) Side view of Napier grass farm; (b) Side view of Ruzi grass farm; (c) Top view of Napier grass dimension; (d) Top view of Ruzi grass dimension.

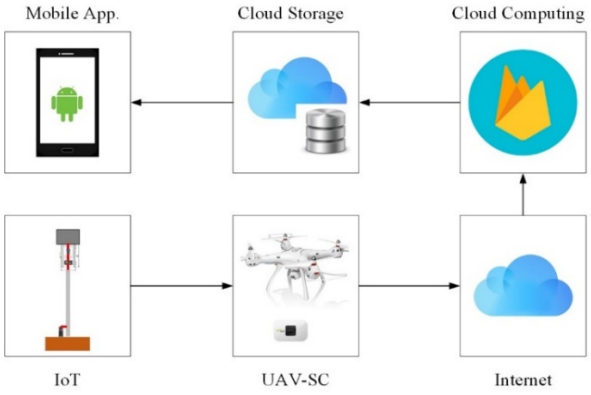

Figure 4: Block diagram of data processing.

The flowchart of the soil moisture monitoring process is shown in Figure 5. Under the condition of soil moisture, the level of the moisture is set to be alerted on the mobile application as follows:

- With the show “Dry” status, all sensors send the data as the range between 1 % to 45 %. It means that the soil is dry.
- With the show “Humid” status, all sensors send the data as the range from 46 % to 79 %. It means that the soil is humid.
- With the show “Wet” status, all sensors send the data as the range between 80 % and 100 % . It means that the soil is wet.

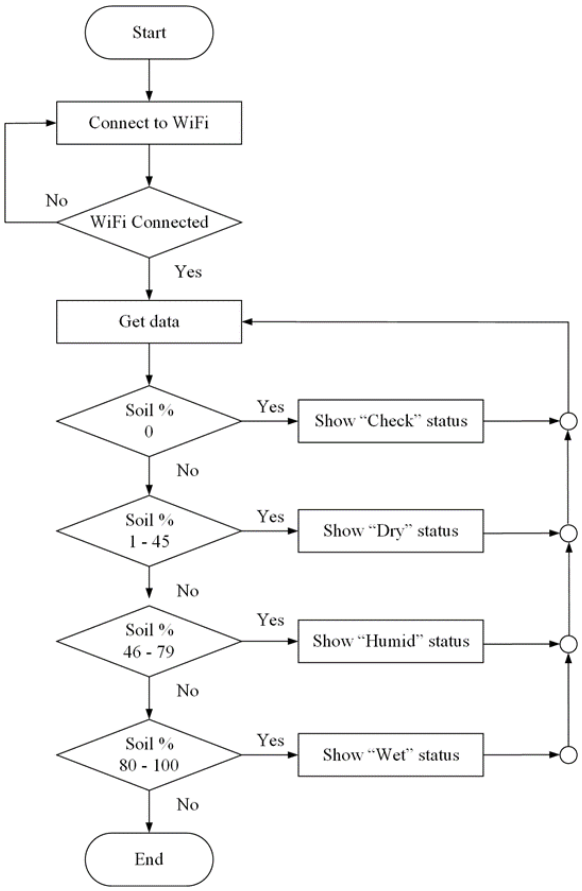

Figure 5: Flowchart of decision.

4. Experimental Setup

This section demonstrates the experimental setup in both Napier farm and Ruzi farm.

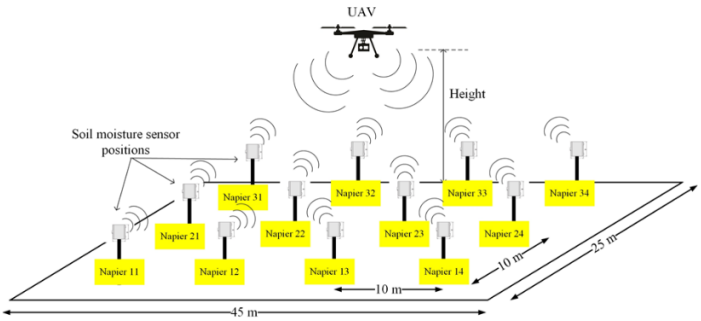

Figure 6: Experimental setup in Napier farm with 12 GSs.

: Real-time test in Napier farm.

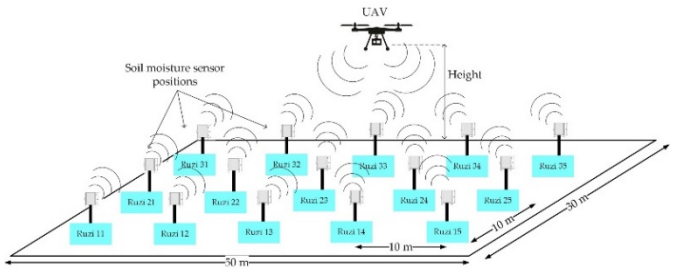

The experimental setup in Napier farm is demonstrated in Figure 6. The GSs are installed along the line of drip irrigation water systems in the field. The separation distance of each sensor is 10 m, and the position names are Napier11 to Napier34. Real-time test in Napier farm is shown in Figure 7. The flight time of the UAV is approximately 20 minutes, and the altitude is varied from 1 m to 10 m. For the sensor depth, it is a pin into the soil with about 0.2 m depth. The tested soil moisture GS kits are performed by the power supply from the solar cell panel in the day time. Therefore, the farmer/user can monitor the data in real time..

shown in Figure 8 and real-time test in Figure 9. It demonstrates the position of sensors in the field in which the number of GS is 15 positions. The GS sets as Ruzi11 to Ruzi35. The sensors installed along the line of the water sprinkler in the field. At the experiment, the UAV altitude was also varied from 1 m to 10 m. Note that the average temperature of all days of these locations was 40 degrees. As a result, both the Napier and Ruzi farms need more water spraying every day. Therefore, the GS-UAV-SC model is useful for the farmer/user to automatically control the on-off of the water management system in these agricultural farms.

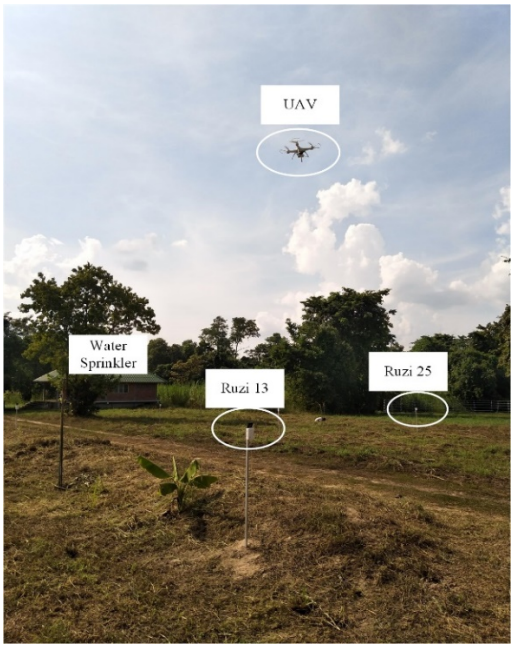

Figure 9: Real-time test in Ruzi farm.

5. Results and Discussion

Table 1: In case: Before opening the water system in Napier farm.

Positions	Soil moisture monitoring (%)					
Time	2.00PM	2.15PM	2.30PM	2.45PM	3.00PM	3.15PM
Napier 11	23	23	24	25	25	25
Napier 12	32	32	34	33	34	34
Napier 13	37	37	38	38	38	39
Napier 14	43	43	44	45	45	43
Napier 21	40	41	42	41	41	42
Napier 22	22	23	25	24	23	25
Napier 23	28	30	29	30	28	28
Napier 24	42	41	41	40	42	42
Napier 31	32	31	31	31	32	32
Napier 32	32	33	34	33	33	34
Napier 33	30	30	32	32	31	30
Napier 34	26	26	28	28	27	28

Table 2: In case: After opening the water system in Napier farm.

Positions	Soil moisture monitoring (%)					
Time	4.00PM	4.15PM	4.30PM	4.45PM	5.00PM	5.15PM
Napier 11	45	47	52	56	61	59
Napier 12	48	49	55	60	62	61
Napier 13	50	53	57	61	64	63
Napier 14	51	55	61	64	66	65
Napier 21	45	47	54	55	64	64
Napier 22	52	53	56	60	63	63
Napier 23	50	52	55	61	62	61
Napier 24	51	53	58	64	65	62
Napier 31	64	66	67	67	68	65
Napier 32	44	45	55	58	59	56
Napier 33	64	65	67	69	69	67
Napier 34	47	47	48	50	51	49

Table 3: In case: Before opening the water system in Ruzi farm.

Positions	Soil moisture monitoring (%)					
Time	2.00PM	2.15PM	2.30PM	2.45PM	3.00PM	3.15PM
Ruzi 11	21	20	20	18	19	20
Ruzi 12	21	20	19	20	19	21
Ruzi 13	25	25	26	27	26	25
Ruzi 14	31	30	30	31	30	31
Ruzi 15	32	32	33	34	33	34
Ruzi 21	16	16	15	16	16	18
Ruzi 22	13	14	15	16	17	17
Ruzi 23	25	26	26	27	28	28
Ruzi 24	31	30	31	30	30	31
Ruzi 25	33	34	33	34	34	33
Ruzi 31	12	13	14	14	15	16
Ruzi 32	15	14	15	18	17	18
Ruzi 33	22	23	22	23	23	25
Ruzi 34	0	0	0	0	0	0
Ruzi 35	0	0	0	0	0	0

Table 4: In case: After opening the water system in Ruzi farm.

Positions	Soil moisture monitoring (%)					
Time	4.00PM	4.15PM	4.30PM	4.45PM	5.00PM	5.15PM
Ruzi 11	38	46	47	48	48	47
Ruzi 12	46	48	51	53	52	51
Ruzi 13	46	48	53	56	54	54
Ruzi 14	52	53	55	57	56	55
Ruzi 15	48	49	54	57	58	56
Ruzi 21	46	48	51	52	53	54
Ruzi 22	79	80	81	79	74	71
Ruzi 23	53	54	59	60	62	59
Ruzi 24	45	46	52	54	55	53
Ruzi 25	47	49	54	54	54	53
Ruzi 31	52	54	60	61	59	57
Ruzi 32	49	51	55	55	56	54
Ruzi 33	46	48	51	52	53	51
Ruzi 34	0	0	0	0	0	0
Ruzi 35	0	0	0	0	0	0

Before the opening of the drip irrigation water system in Napier grass farm, soil moisture sensors were tested from 2 PM to 3:15 PM. The results of soil moisture sensors show that the data is in the range from 22 % to 42 % of the real-time monitoring. Therefore, the status was Dry status. After the opening of the drip irrigation water system for about forty-five minutes, it is observed that the soil moisture values were rapidly increased in the range of 45 % to 69 % as shown in Table 2. Thus, the "Humid" status was shown on the mobile application.

In Ruzi farm, the soil moisture values in Ruzi farm were in the range from 12 % to 34 % in Table 3 before opening the water sprinkler system, Therefore, the status showed as Dry. After the opening water sprinkler system about forty-five minutes in Ruzi farm, the results of soil moisture values were in the range from 38 % to 81 %. As a result, the status shown on mobile application was Dry, Humid, Wet, and Check status. And then, the capacitive soil moisture sensors were removed from the soil. Both Ruzi 34 and Ruzi 35 were 0 % with the "Check" status. The experiment data in Ruzi farm were collected on April 3, 2020.

The examples of mobile application on screen as real-time monitoring were shown in Figure 10 (a)-(b). The data collected at 4 PM is shown in Table 2 and Table 4. Figure 10 (a) and 10 (b) show the status of soil moisture values in Napier farm and Ruzi farm. The application is easily used and can be applied to control the water management (on-off) system both in Napier and Ruzi farms. It took just to 15 minutes to collect the data for the proposed model.

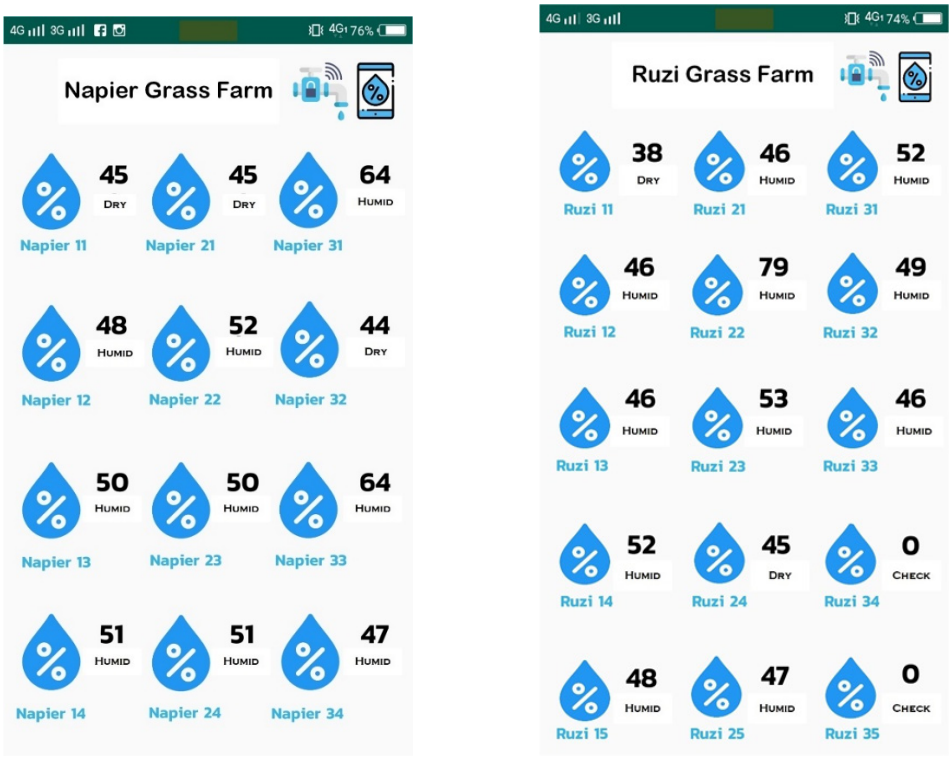

(a) (b)

Figure 10: Example of real-time monitoring on mobile application at 4 PM:

(a) On the screen in Napier farm. (b) On the screen in Ruzi farm.

6. Conclusion

In this paper, the proposed GS-UAV-SC model based on IoT and wireless communication connected network in smart farming has been implemented for soil moisture monitoring. The low-cost multiple GSs were designed as the ground sensing to monitor the soil moisture in the daylight both for Napier grass farm and Ruzi grass farm. The UAV-SC is equipped with the WiFi transceiver similar to the hotspot mobility and connected with the multiple GSs. This proposed smart farming system is called the GS-to-UAV-SC communication system. The implementation and results confirm that the UAV-SC can be applied as mobility transceiver to compensate for the low energy of GSs, including the real-time data that are designed to monitor soil moisture values on the mobile application. In future work, the optimization of path loss model for smart farming (SF) system will be implemented by the machine learning algorithms. .

Conflict of Interest

The authors declare that there is no conflict of interest regarding the publication of this paper.

Acknowledgment

This research was financially supported by the Academic Melting Pot, KMITL research fund. The authors would like to thank the Tropical Animal Research Institute, Ramkhamhaeng University, in Thailand, which was cooperative research in this work.

References

[1] C. M. Gevaert, J. Suomalainen, J. Tang, L. Kooistra, "Generation of Spectral-Temporal Response Surfaces by Combining Multispectral Satellite and Hyperspectral UAV Imaginary for Precision Agricultural Applications" IEEE J. of Selected Topics in Applied Earth Observations and Remote Sensing, **8**(6), 3140–3146, 2015. https://doi.org/10.1109/JSTARS.2015.2406339

[2] L. Chen, L. Zhangzhong, W. Zheng, J. Yu, Z. Wang, L. Wang, C. Huang "Data-Driven Calibration of Soil Moisture Sensor Considering Impacts of Temperature: A Case Study on FDR Sensors" Sensors, **19**(20), 1–11, 2019. https://doi.org/10.3390/s19204381

[3] S. Adla, N. K. Rai, S. H. Karumanchi, S. Tripathi, M. Disse, S. Pande "Laboratory calibration and performance evaluation of low-cost capacitive and very low-cost resistive soil moisture sensors" Sensors, **20**(2), 1–27, 2020. https://doi.org/10.3390/s20020363

[4] W. L. Chen, Y. B. Lin, Y. W. Lin, R. Chen, J. K. Liao, F. L. Ng, Y. Y. C. Liu, C. C. Wang, C. H. Chiu, T. H. Yen, "AgriTalk: IoT for Precision Soil Farming of Turmeric Cultivation" IEEE Internet of Things J., **6**(3), 5209–5223, 2019. https://doi.org/10.1109/JIOT.2019.2899128

[5] F. Viani, M. Bertolli, A. Polo, "Low-Cost Wireless System for Agrochemical Dosage Reduction in Precision Farming" IEEE Sensors J., **17**(1), 5–6, 2017. https://doi.org/10.1109/JSEN.2016.2622244

[6] B. Liu, H. Xu, X. Zhou, "Resource Allocation in Unmanned Aerial Vehicles (UAV)-Assisted Wireless-Powered Internet of Things" Sensors, **19**(8), 1–13, 2019. https://doi.org/10.3390/s19081908

[7] N. Lu, Y. Zhon, C. Shi, N. Cheng, B. Li, "Planning While Flying: A Measurement-Aided Dynamic Planning of Drone Small Cells" IEEE Internet of Things J., **6**(2), 2693–2705, 2019. https://doi.org/10.1109/JIOT.2018.2873772

[8] G. Castellanos, M. Deruyck, L. Martens, W. Joseph, "Performance Evaluation of Direct-Link Backhaul for UAV-Aided Emergency Networks" Sensors, **19**(15), 1–16, 2019. https://doi.org/10.3390/s19153342

[9] C. Dong, J. Xie, H. Dai, Q. Wu, Z. Qin, Z. Feng "Optimal Deployment Density for Maximum Coverage of Drone Small Cells" China Communications, **15**(5), 25–40, 2018. https://doi.org/10.1109/CC.2018.8387984

[10] A. Ahmed, M. Awais, T. Akram, S. Kulac, M. Alhussein, K. Aurangzeb, "Joint Placement and Device Association of UAV Base Stations in IoT Networks" Sensors, **8**(6), 1–16, 2019. https://doi.org/10.3390/s19092157

[11] R. Xoing, F. Shan, "DroneTank: Planning UAVs Flight and Sensors Data Transmission under Energy Constraints" Sensors, **18**(9), 1–19, 2018. https://doi.org/10.3390/s18092913

[12] M. Idbella, M. Iadaresta, G. Gagliarde, A. Mennella, S. Mazzoleni, G. Bonanomi, "AgriLogger: A New Wireless Sensor for Monitoring Agrometeorological Data in Areas Lacking Communication Networks" Sensors, **20**(6), 1–13, 2020. https://doi.org/10.3390/s20061589

[13] M. Bacco, A. Berton, A. Gotta, L. Caviglione, "IEEE 802.15.4 Air-Ground UAV Communications in Smart Farming Scenarios" IEEE Communication L. **22**(9), 1910–1913, 2018. https://doi.org/10.1109/LCOMM.2018.2855211

[14] F. Viani, M. Bertolli, A. Polo, "Low-Cost Wireless System for Agrochemical Dosage Reduction in Precision Farming" IEEE Sensors J., **17**(1), 5–6, 2017. https://doi.org/10.1109/JSEN.2016.2622244

[15] U. Shafi, R. Mumtaz, J. Garcia-Nieto, S. A. Hassan, S. A. Raza Zaidi, N. Iqbal, "Precision Agriculture Techniques and Practices: From Consideration to Applications" Sensors, **19**(17), 1–25, 2019. https://doi.org/10.3390/s19173796

[16] K. Haseeb, I. U. Din, A. Almogren, N. Islam, "An Energy Efficient and Secure IoT-based WSN Framework: An Application to Smart Agriculture" Sensors, **20**(7), 1–14, 2020. https://doi.org/10.3390/s20072081

[17] P. P. Jayaraman, A. Yavari, D. Geogakopoulos, A. Morshed, A. Zaslavsky, "Internet of Things Platform for Smart Farming: Experiences and Lessons Learnt" Sensors, **16**(11), 1–17, 2016. https://doi.org/10.3390/s16111884

[18] S. Kim, M. Lee, C. Shin, "IoT-based Strawberry Disease Prediction System for Smart Farming" Sensors, **18**(11), 1–17, 2018. https://doi.org/10.3390/s18114051

[19] Y. B. Lin, Y. W. Lin, J. Y. Lin, H. N. Hung, "SensorTalk: An IoT Device Failure Detection and Calibration Mechanism for Smart Farming" Sensors, **19**(21), 1–19, 2019. https://doi.org/10.3390/s19214788

[20] N. G. S. Campos, A. R. Rocha, R. Gondim, T. L. Coelho da Sliva, D. G. Gomes, "Smart & Green: An Internet-of-Things Framework for Smart Irrigation" Sensors, **20**(1), 1–25, 2020. https://doi.org/10.3390/s20010190

[21] A. Gloria, C. Dionisio, G. Simoes, J. Cardoso, P. Sebastiao, "Water Management for Sustainable Irrigation Systems using Internet-of-Things" Sensors, **20**(5), 1–14, 2020. https://doi.org/10.3390/s20051402

[22] G. Codelippi, A. Cilfone, L. Davoli, G. Ferrari, "LoRaFarM: a LoRaWAN-based Smart Farming Modular IoT Agriculture" Sensors, **20**(7), 1–24, 2020. https://doi.org/10.3390/s20072028

ASTES

Advances in Science, Technology and Engineering Systems Journal Vol. 5, No. 4, 388-396 (2020)

www.astesj.com

Special Issue on Innovative Research in Applied Science, Engineering and Technology

ASTESJ

ISSN: 2415-6698

The Role of KM in Enhancing AI Algorithms and Systems

Hani AlGhanem[1], Mohammad Shanaa[1], Said Salloum[1,2,*], Khaled Shaalan[1]

[1]*Faculty of Engineering &IT, The British University in Dubai, 345015, United Arab Emirates*

[2]*Research Institute of Sciences & Engineering, University of Sharjah, 27272, United Arab Emirates*

ARTICLE INFO

Article history:
Received: 24 June, 2020
Accepted: 14 July, 2020
Online: 28 July, 2020

Keywords:
Knowledge management
Artificial intelligence
AI algorithms

ABSTRACT

Knowledge Management processes present a vital role in improving AI systems and algorithms. Many studies and reviews were carried out to examine the relationship between KM processes and AI systems. However, studies were focusing on specific methods and the impact on some AI algorithms, neglecting the role of other KM processes and how it may affect the AI system to achieve the objective, which reduces the adoption in some organizations. The current study shows the relation between KM processes and AI systems from a higher perspective, giving different options to apply other KM processes for the same AI algorithm to reduce any implementation challenges and enhance the adoption level. The review looks into 16 studies collected from a different database from 2014 to 2019. The main finding of the research was the massive impact of some KM processes like knowledge acquisition and knowledge creation on the different types of AI systems and algorithms to give an additional option for organizations during the implementation. Additionally, the research finds that most of the studies agree on the positive relationship between knowledge management processes and the role-plays to enhance AI systems and algorithms. Finally, the study shows a decrease in the number of researches done for this topic in the selected databases, which can be enhanced by other researchers by examining other databases to increase results accuracy.

1. Introduction

Knowledge plays an essential role in the maintenance of organization business [1], as it can be explained as one of the most critical factors that companies need to maintain their business in the market [2]–[4], also knowledge considered as a valuable intangible resource. It includes all the ideas, concepts, data, technologies stored in the human brain [5]. Knowledge has many properties and can be summarized as 1) can be created by personnel, 2) dilatable, 3) can be saved in individuals brain or any other document storage or computerized storage, 4) can be stored in specific orders for easy of retrieving it when needed, 5) can be shared with others, 6) forgettable and can be lost [6]. Recently, the attention of KM has been evolved dramatically as many pieces of research, consultants, and specialists focus on organizational knowledge management in order to overcome the challenges that faced organizations [7], [8].

Knowledge management is considered a new domain for government institutes, which used to coordinate between all of the human resources, technological resources, organization structure, and environment to improve organization strategies [5]. Besides, KM exerted an effective role in educational practices [9]–[12]. While [13] collect the agreed definition of knowledge management as "creation, communication, and application of knowledge." Moreover, consider a vital tool to improve organizational processes. The primary purpose of KM is described by [14] "to improve the systematic handling of knowledge and potential knowledge within the organization". AI is the way to build a software program that can imitate the human brain in many mental procedures and processes, including learning, thinking, building perception, natural language processing, innovation, and complex issues resolution [15]. AI can be employed in many applications that required thinking and analysis, using AI tools such as statistical and mathematical methodologies to build computer understanding and machine learning in the same way as human thinking and acquiring knowledge. In their study of intelligent vehicles, they assert that the usefulness of feeding back the generated knowledge form the test result of smart vehicles to AI systems in order to improve it, so the AI system can learn more

*Corresponding Author: Said Salloum, University of Sharjah, UAE.
Tel: +971507679647 Email: ssalloum@sharjah.ac.ae

and provide better results[10]. In [16] they assert on the importance of the data warehouse to store organizational knowledge, and these data warehouses play an essential role in the application of artificial intelligent in general and decision support systems in specific, furthermore, Data/open data is considered a booster for the Information technology industry [17].

This review study raises the following four research questions:

1. What are the primary knowledge management processes studied, and how it is impacting AI systems?
2. What are the leading AI algorithms and systems reviewed in the studies collected?
3. What research methods have been used in finding the relation between knowledge management processes and AI systems?
4. How active is the topic of knowledge management impact on AI during the last five years, across the research databases?

The remainder of the review is split as follows: Section 2 containing a literature review, research methodology discussed in section 3. Section 4 demonstrates the findings and results achieved from the in-depth analysis of the articles reviewed. Finally, the review is concluded in section 5.

2. Literature review

Nobody could deny the role of information systems in our daily lives [18], [19]. Knowledge management plays a vital role in accelerating the wheels of information systems [20]–[22]. The initial show of knowledge management return to the 80s as came along with AI and expert systems, then it spread out between businessmen, academics, and consultants, in the last ten year big companies like telecommunication has many success factors, and one of the critical factors is the knowledge that gained from employees experience, stakeholders, customers, and competitors. This knowledge provides the companies with a strategic and sustainable competitive advantage by building an organizational culture having active knowledge management in general and knowledge sharing in specific [23].

A study by [24] explains that knowledge management tools are used to help in knowledge generation, documentation, and sharing. KM tools are used to make managing the knowledge is easier by implementing IT technologies to create, organize, and share knowledge, which helps to improve organization operation. KM tools can be classified into four groups; the first one is tools to discover knowledge and to build the knowledge structure, which concentrates on the current knowledge and the existing one, and to make available in a well-structured format and easy to access by linking the information, ideas, and experiences. The second one is tools for knowledge processing, which can be defined as the workflow of how to deal with information and knowledge by filter, store, and analyze it. The third one is tools used for share and transfers the knowledge between individuals, which included organization local intranet or internet; furthermore, it can be extended to public online forums, wiki which make the organization issues resolving the environment having. The fourth and final one is tools used to analyzing and applying the knowledge, which includes a wide range of applications, including intelligent agents, expert systems, and many others that help in decision making.

After reviewing 20 styles of KM frameworks in the period 1991 to 2015, In [25] conclude a unified KM framework which includes the five primary processes, the first one is knowledge transfer that focuses how the knowledge and information are being moved from one individual/organization to another using interaction between people or organizations in a written or verbal way through traditional ways of using technological way. The second one is storing the knowledge in a suitable storage device, and nowadays it is stored electronically as documents or into databases; storing the knowledge is essential; because knowledge can be lost, especially the tacit knowledge. The third one is knowledge application, is the way how to get benefit from the stored knowledge and employ it to improve organization innovation, processes, performance to build a continuous competitive advantage, and this can be done using knowledge application software like expert system, intelligent agents, decision-making systems. The fourth one is knowledge creation, which is come by converting explicit and tacit using different ways like internalization, combination, externalization, socialization. Also, knowledge can be created by interviewing the experts and knowledge exchange between individuals or by documenting the organizational work procedure. The fifth and last one is knowledge acquisition; this is the process of getting knowledge from outside of the organization and uses it within the organization's knowledge base, like knowledge gained from customers, competitors, or suppliers.

Many tools can be used and present AI, such as Intelligent Agents, Business intelligence, gadgets dashboard, and expert systems [15]. While [26] define the intelligent agents as "an autonomous system that can obtain synergy effects by combining a practical user interface, on the one hand, and an intelligent system based on Artificial Intelligence, Neural Networks, and fuzzy theory, on the other hand.".

An intelligent agent is defined as a computer system that can understand the environment that its existence in and interact based on the received data and predefined rules [27]. Intelligent agents can be categorized into different groups; the first one is the collaborative or non-collaborative, the collaborative mean that intelligent agents do a sequence of operation that one agent starts after the previous one finish his task. The second one is the profitable economy agents, which focus on the stock market and online trading by doing automatic deals and decisions. The third one is online assistant agents that can learn from the user experience. While the fourth one is called mobile agents as it can be used over the internet, for example, it can play a role in load balancing on specific servers [26].

The concept of Business intelligence (BI) was first introduced in the 90s and nowadays become widely used mainly in business to support decision making (Watson, H.J. and Wixom, B.H., 2007). BI provides a user interface that enables users to analyze and drill down the data into the information to extract and useful knowledge and data that needed to help in tacking a decision using a friendly geographical interface including charts, aggregates, and statistics [28].

The expert system is known as the first kinds of AI Implementation and can be used on an organizational level or personality level. Usually, an expert system consists of a

knowledge base module which used to keep all information and data related to issues solving. While fact base module contains some categorized information about specific cases, usually it used to build the final result, explanation module, which provides the steps that used in order to reach a specific solution depending on facts/ knowledge base. Finally, a presentation module responsible for providing all data to end-users in a human-readable and structured format [15]. There are two significant modules of expert systems, which are 1) knowledge-base which can build using fuzzy or first-order logic. So expert systems can fit the electronic governments due to the nature of e-government problems [29]. So expert systems consider and an application of knowledge management as it helps in decision making and problem-solving [30].

Neural Networks, including ANN, RNN, and CNN, simulates the human neural nerves, and it uses learning from provided data and experiments to build the network model and to find the unseen patterns within these data. Neural Networks, including ANN, RNN, and CNN, considered a robust algorithm to predict and forecast cretin scenario cases [31]. Artificial neural networks and data mining work in parallel for the CRM system in order to generate knowledge about customers' behaviors and to predict their willingness to purchase specific items [32]. Additionally, in [33] study, they express the importance of using knowledge management in order to feed the AI system as it is essential for personal characterization, which used to improve public safety using the decision tree algorithm.

It is essential to having a KM feeding to AI systems, which can help to improve AI in call center domains by helping call center agents to find the best resolution for the caller and customer, but KM should have reliable data and source of information. Machine learning (ML) can be employed by reading the history of customer chat conversation and previously solved issues with customers to prepare suggested answers to be used by customer services representative with the ability to customize the prepared answers by ML[24].

According to a study by [34] use many AI algorithms and implement it in a knowledge management system specifically in knowledge extraction to predict Heart failure for patients, among nine classifiers, the results come by employing Random forests algorithm with a range between 10 to 100 trees. Also, in [35] within the same medical domain, they use various AI algorithms, and one of them is the random forests, which is defined as a group of random and parallel created decision trees. The output of this algorithm is considered the average of the output of all decision trees within the forest.

Based on the studies that exist in the literature, most of the reviews are focusing on the direct impact on the knowledge management process to AI systems and algorithms, despite the cost or the possibility of implementing the idea within the organizations. Ignoring other criteria like cost has a negative impact, as seen in one of the studies that, despite the positive effect of system output to enhance performance and data accuracy, the cost of implementing these systems was a significant obstacle to adopt it. These facts encourage us to study the researches available to highlight this missing point and to assist researchers in focusing more on the implementation and adoption of the relation. Additionally, our study gives other available options for Knowledge Management processes, which can help in enhancing AI systems and algorithms.

3. Methodology

The systematic review provides a way to explorer all published papers, chapters, and articles to remove any biased conclusions [36]–[44]. While researches that do not consider a systematic way might lead to higher risk by selecting certain studies that support the author's point of view only and eliminate other points of view [45]. Also, Systematic review gives the reader the latest explored knowledge available in the entire literature for a specific research area or question [46]–[48].

A study by [49] summarize the process of systematic review in six steps. 1) Starting by specifying the research questions or the hypothesis that needs to be tested. 2) Then an inclusion/ exclusion criteria to be determined in order to filter the collected papers based on that criteria. 3) After that, a thorough search for all papers related to the research question to be collected from all available databases by defining the strategy and keywords for the search. 4) review all the retrieved papers from the previous step and evaluate the quality of the papers based on the title, abstract, or the conclusion; this step will eliminate all the un-related papers. 5) Data mining and extraction from the non-eliminated papers from the previous step using thorough reading and analysis of the paper according to research questions. 6) Finally, doing data analysis and answer the research questions providing shreds of evidence from the selected papers, and supported by literature review.

The systematic review is used to understand the impact of applying knowledge management processes in improving the decision making systems for health care [39]. The study utilizes a four steps approach to finalize the selected papers for the review. The steps used in the study succeeded in eliminating papers that were not related to the research questions. Additionally, the study explains in a table, the research methodology and findings from each of the selected papers. However, the table did not show the direction (positive/negative) for each paper and country of implementation as these details may impact the implementation of knowledge management in healthcare decision making systems if applied to countries with different rules and regulations.

Finally, the authors find that following the steps from [40], will help in achieving the paper goals.

Table 1: Inclusion and exclusion criteria.

Inclusion	Exclusion
Should be related to knowledge management Methodologies, processes, or lifecycle.	Articles published before 2014.
Should be related to artificial Intelligent Algorithms, or Techniques.	Related to Knowledge management, but not linked to Artificial Intelligent.
Should be related to the government domain or related to the general domain (without specific domain mentioned).	Related to Artificial intelligence but not linked to Knowledge management.

3.1. Inclusion/exclusion criteria

For the collected paper, it filtered in or out based on certain criteria, which are summarized in Table 1.

So, the above Table 1 shows the criteria that need to be considered when preparing the papers for the systematic review, so the result after applying the inclusion and exclusion criteria will be a list of papers that will be used in this study.

3.2. Data sources and search criteria

In order to collect the papers that are considered in these systematic reviews, a list of keywords was used or a combination of it using "And" operations. These keywords are "Knowledge management", "Artificial intelligent", government, "Artificial Intelligence", "e-Government". These keywords were used in different publication databases, including "ArticleFirst", "Electronic Collections Online", "Emerald Group Publishing Limited", "Google Scholar", and "Worldcat". The total numbers of retrieved papers were 239 .the first exclusion based on the year of publication and all papers before 2014, so 109 papers were eliminated. Two papers were found as duplicated. The remaining papers were 130. After applying all criteria from the inclusion and exclusion table, the remaining number of papers is 16. and listed in Table 2, which contain the source of the paper, details about knowledge management process, artificially intelligent algorithms or system, the research method that used in the paper, the country that targeted by the study, the target domain, the database that collected from and brief and summary about the paper and the main idea behind it.

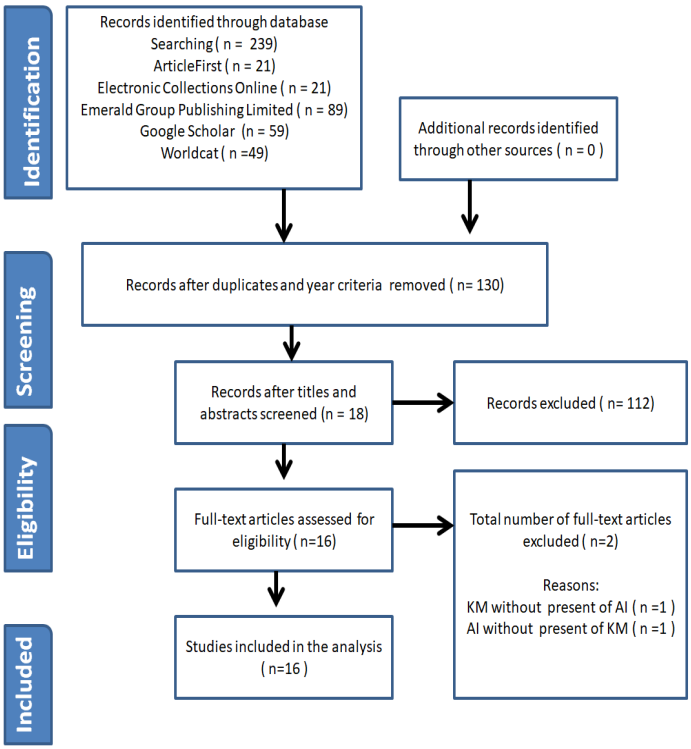

Figure 1: Process of selection papers.

Figure 1 shows the main phases of paper selection in systematic review starting by identifying the databases and collected numbers of each database; also, it explains that there are no additional sources of papers, from screening phase all duplicated papers and year criteria applied to filter out un-needed papers. The eligibility phase came to check the content of the papers if it fit and contain the research required info or not. Moreover, the final phase came to include the remaining papers in the study and analyze it

3.3. Quality assessment

In the systematic review, there is a concern about the quality of the collected papers, even inclusion and exclusion criteria applied, but it is not enough to check the quality of paper contents. A quality test should be conducted as strong evidence of good papers quality can tell how strong is the conclusion can be made [50]. So to check the quality of the papers, a quality assessment checklist was defined as shown in Table 2. For scoring purposes, there will be three values; if the answer to the question is yes, then the score will be 1; if the answer is no, then the score will be 0; if the answer is partially presented, then the score will be 0.5.

Table 2: A quality assessment checklist.

#	Question
1	Are the research aims clearly specified?
2	Are the Knowledge/KM considered by the study clearly specified?
3	Is the AI considered by the study clearly specified?
4	Do the results add to the literature?
5	Does the study add to your knowledge or understanding?

Based on the scoring criteria and Table 2, for each paper, a score between 0 to 5. By applying the quality assessment for all the 16 papers, a result shows in Table 3, P1 to P16 is a list of papers in the same order of papers list in table 4 main table. The results show that all papers are in excellent quality, so all of the 16 papers will be included in the analysis.

Table 3: Quality assessment result.

Source	Q1	Q2	Q3	Q4	Q5	Total	%
P1	1	0.5	1	0.5	1	4	80%
P2	1	1	1	1	1	5	100%
P3	1	1	0.5	1	1	4.5	90%
P4	1	0.5	1	1	1	4.5	90%
P5	1	1	1	1	1	5	100%
P6	1	1	0.5	1	1	4.5	90%
P7	1	1	1	1	1	5	100%
P8	0.5	1	1	1	1	4.5	90%
P9	1	1	0.5	1	0.5	4	80%
P10	0.5	0.5	1	1	1	4	80%
P11	1	1	1	1	1	5	100%
P12	1	1	0.5	1	1	4.5	90%
P13	1	1	1	1	1	5	100%
P14	1	1	1	1	1	5	100%
P15	1	1	1	1	1	5	100%
P16	1	1	1	1	1	5	100%

3.4. Data coding and analysis

The analysis section depends on the six steps suggested by [51] for a systematic review. In the initial phase, this paper analyzed the relationship and the quality of coded characteristics. Initially, the authors list the main Knowledge management processes for the papers reviewed. In addition to AI Algorithms and Systems, Research database (e.g., WorldCat, Emerald, and others), study direction (Positive, Negative, Neutral), Target Organization (public, private), and country. During the first analysis phase, authors excluded all papers which do not directly describe the impact of knowledge management on AI algorithms and systems. The authors analyzed all documents by dividing all studies between the authors and manually examine the articles. Secondly, the authors reviewed the papers on a high level and start excluding duplicate papers, and papers not on direct relation to this paper topic based on title and abstract screening. After that, the authors deep analyze the remaining researches and start to exclude papers that are not eligible based on a full review and quality assessment questions defined. Finally, 16 papers were selected as they match the quality criteria. Table 4 present the selected papers with the coding characteristics for each paper. The table reflects the analysis done for each paper in rows, by specifying the KM process discussed in the paper, the AI algorithm or system used, and the source research database. Additionally, the table stating the type of research methodology used in each study, the country research used within, and target type audience. Finally, the table illustrated the direction for the paper (Negative/Positive) and added the findings from each study.

Table 4: Analysis of knowledge management research articles with regard to AI algorithms and systems

#	Ref.	KM Process	AI Algorithm / AI Systems	Method	Country
P1	[52]	Knowledge Application /Decision making	Neural Networks including ANN, RNN, and CNN	Survey	USA
P2	[15]	Knowledge Discovery	1) Expert Systems 2) Multi-agent systems 3) Business Intelligence 4) Performance Dashboards	Case Study	Poland
P3	[53]	Knowledge Creation	1) Natural Language Processing 2) Machine-learning techniques 3) Human intelligence	Experimental	General
P4	[31]	Knowledge Application /Decision making	Neural Networks including ANN, RNN, and CNN	Interviews and Experimental	Iran
P5	[54]	Knowledge Creation	AI in General	Experimental	China
P6	[55]	Knowledge Acquisition	Ontology and XML	Experimental	Italy
P7	[29]	Knowledge Creation	AI in General	Case Study	Bangladesh
P8	[33]	Knowledge Application /Decision making	Decision Trees C4.5	Experimental	Colombia
P9	[56]	Knowledge Application /Decision making	Chatbot	Case Study	General
P10	[57]	1) Knowledge-Creating, 2) Knowledge Acquisition 3) Knowledge Sharing	Expert Systems	Literature Review	KSA
P11	[58]	1) Knowledge Acquisition 2) Knowledge Sharing	1) Fuzzy Logic 2) Case-based reasoning	Case study	Taiwan
P12	[59]	Knowledge Acquisition	Fuzzy Logic	Literature Review	Brazil
P13	[60]	Knowledge Acquisition	1) Neural Networks including ANN, RNN, and CNN 2) Support Vector Machines 3) Genetic Algorithms 4) Rough sets 5) Fuzzy Systems	Literature Review	General
P14	[61]	Knowledge Acquisition	1) Expert System 2) Deep Learning	Case study	Australia
P15	[34]	Knowledge-Creating,	Prediction model	Experimental and comparison study	Greece
P16	[35]	Knowledge-Creating,	Prediction model	Experimental	Bangladesh

4. Results and discussion

This systematic review is summarizing 16 articles published between 2014 and 2019 in Google scholar, Emerald, and WorldCat databases on regards to the impact of knowledge management processes in improving AI systems. The findings of this review discussed the following five questions:

4.1. RQ1: What are the primary knowledge management processes studied, and how it is impacting AI systems?

Different studies were done to investigate the impact of knowledge management processes in enhancing the AI systems and algorithms. Table 5 describes the knowledge management processes involved in the study captured, and the frequency of using the method in each study. It is noticeable that knowledge acquisition is the most common processes used to enhance AI systems (N = 6), followed by both knowledge creation and knowledge application/decision-making process (N = 6), knowledge sharing (N = 2), and Knowledge discovery with the least number of studies (N = 1). Referring to Table 4, it seems that knowledge application and decision-making processes have a positive impact on Neural Networks, including ANN, RNN, and CNN [31], Decision Trees [33], and Chatbots [56]. On the other hand, [52] argued that knowledge management application and decision making could have some negative impact on Neural Networks, including ANN, RNN, and CNN, in some applications.

Table 5: Knowledge management processes in the studies reviewed.

Source	Knowledge Application /Decision making	Knowledge Discovery	Knowledge Creation	Knowledge Acquisition	Knowledge Sharing
[52]	X				
[15]		X			
[53]			X		
[31]	X				
[54]			X		
[55]				X	
[29]			X		
[33]	X				
[56]	X				
[57]			X	X	X
[58]				X	X
[59]				X	
[60]				X	
[61]				X	
[53]			X		
[31]			X		

Additionally, it has been noticed that the Knowledge creation process has a positive impact on Natural Language Processing, Machine Learning, Human Intelligence [54], on Expert Systems [57], and on AI algorithms in general [29], [62].

Furthermore, the most knowledge management process impacting the AI systems as per the collected studies are knowledge acquisition and knowledge creation, as it is affecting Fuzzy Logic systems [58]–[60], Expert systems [57], [61], Neural Networks including ANN, RNN, and CNN Support Vector Machines, Genetic Algorithms, Rough sets [60], Deep Learning [61], Ontology and XML [55], and case-based reasoning [58]. Also, Knowledge Discovery seems to have a positive impact on Expert Systems, Multi-agent systems, Business Intelligence, Performance Dashboards [15]. Finally, the Knowledge Sharing process has a positive impact on Expert systems [57], Fuzzy Logic, and Case-based reasoning [58].

4.2. RQ2: What are the leading AI algorithms and systems reviewed in the studies collected?

Referring to Figure 2, it is noticeable that Expert systems, Neural Networks including ANN, RNN and CNN, and Fuzzy logic algorithms are taking the lead in the number of studies collected (N = 3), followed by general AI study (N = 2), and finally, other AI algorithms and Systems, Genetic Algorithms, Rough sets, Case-based reasoning, Human Intelligence, Machine Learning techniques, Chatbot, Decision Tree, Ontology and XML, Natural Language Processing, Performance Dashboards, Business Intelligence and Multi-language system (N = 1).

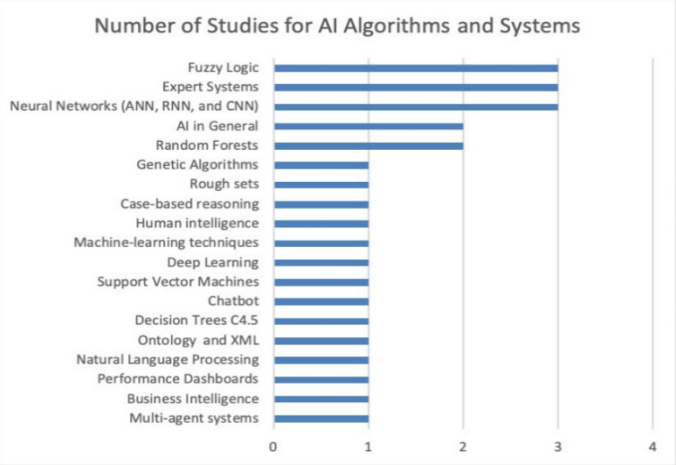

Figure 2: Number of Studies for AI Algorithms and systems.

4.3. RQ3: What research methods have been used in finding the relation between knowledge management processes and AI systems?

Analyzing Table 4 shows multiple research methods been used to find the relation between knowledge management processes, and AI algorithms and systems. Studies use Survey, Case Study, Experimental, Interviews, and Literature Review to perform the required analysis. Figure 3 presents the percentage and number of studies for each methodology. The experimental method takes the lead with seven studies with 44%. Followed by Case Study with five studies and 33%, followed by Literature Review with three studies and **18**%, and finally, the lowest two methods used are surveys and interviews with one research each and 6%.

4.4. RQ4: How active is the topic of knowledge management impact on AI during the last five years, across the research databases?

Looking to the year of publication, and by analyzing Figure 4, we notice a drop in the number of researches studied the relationship between knowledge management and AI algorithms and systems since 2014. The highest number of papers was in 2014 (N = 5), then from 2015 to 2017 there with the same number of researches (N = 2), followed by 2018 (N = 2), and finally in 2019 increased to two pieces of research (N = 3).

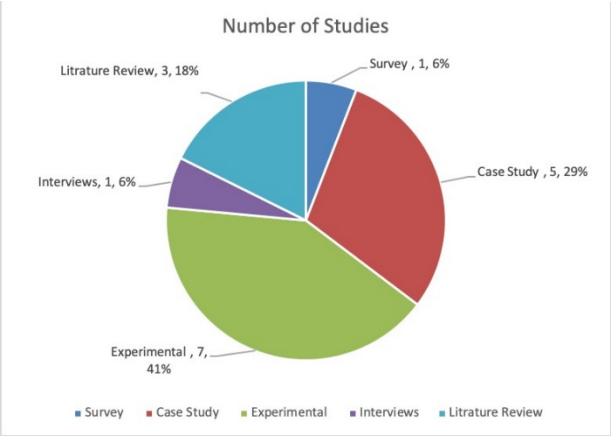

Figure 3: Research Methodology

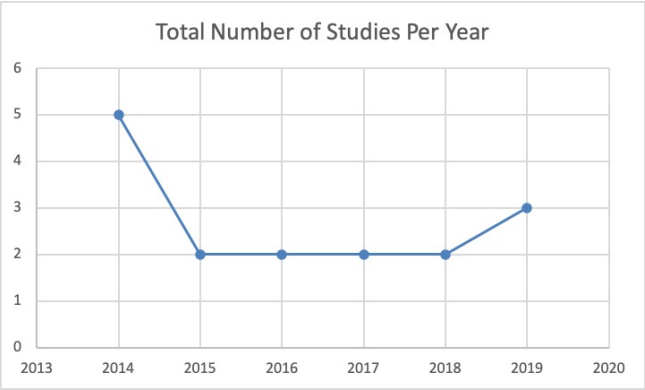

Figure 4: Total number of studies per year

Figure 5 shows how the Worldcat database is popular in having this topic as it has at least one paper every year from 2014 to 2019. The analysis indicates that Worldcat and Emerald have the top number of studies in 2014 (N = 2), followed by Google scholar (N = 1). In 2015, and 2016, Worldcat was the only database with studies related to the topic. In 2017, both Worldcat and Emerald had one research and appeared on both years.while in 2018, both Worldcat and google scholar database with one study for each related to the topic. Finally, in 2019, Worldcat, Emerald, and google Scholar had one research and appeared in each.

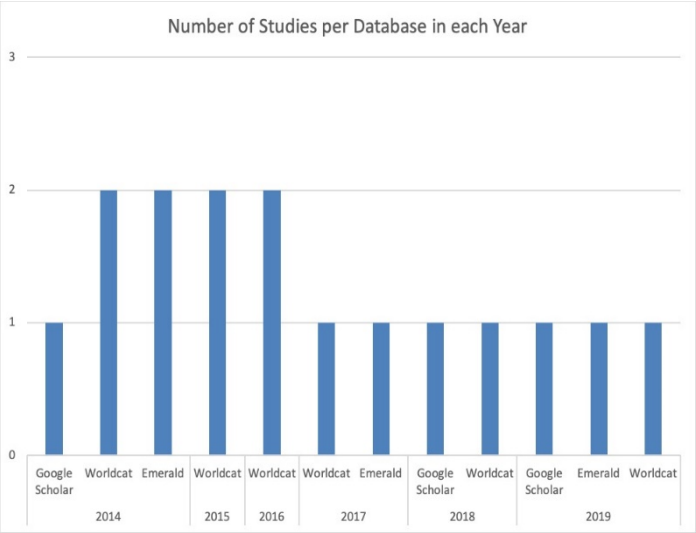

Figure 5: Number of studies per database in each year

Figure 6 describes the relationship between Knowledge management processes and the AI systems and algorithms that can be enhanced or impacted. This is also aligned with the previous discussion of the impact of knowledge acquisition on more number of AI systems and algorithms. Knowledge acquisition can passivity enhance Neural Networks, including ANN, RNN and CNN, Support Vector Machines, Genetic Algorithms, and rough sets, as also described in the study done by [60]. Both [58], [60] also agree that Knowledge acquisition can enhance Fuzzy Systems. Additionally, [61] added that knowledge acquisition could improve Expert systems and Deep learning by having a training way for the algorithms to enhance the outputs. Finally, based on Figure 4, we notice that the number of researches done for the relation between KM and AI systems is decreasing each year, comparing to the studies done in 2014.

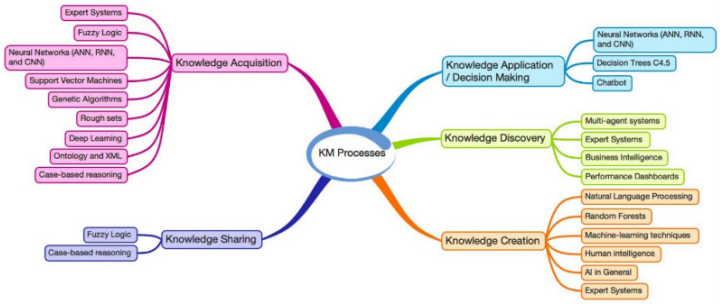

Regarding managerial insight, this paper provides a clear understanding of how each stage of knowledge management plays a role in enhancing AI Algorithms. Furthermore, this paper provides Practitioners, including software solutions architectures, digital transformation framework designers, and knowledge management, a solid base to get benefits from their knowledge management and employee the right AI algorithms to increase the benefits by using the right algorithms at the right KM stage.

5. Conclusion

The role of Knowledge Management processes in improving AI algorithms and systems was discussed in multiple studies. The paper used systematic review as an approach to determine the relationship between KM and how it affects AI systems and algorithms. This paper followed the six steps summarized by [51], to apply for a systematic review of selected papers. As a result, 16 papers were selected as they fit the requirements and selection criteria defined by the authors. Applying the quality assessment questions on all reviewed papers helped in filtering only high-quality researches, which discussed the selected topic. However, and in some scenarios, authors need to be careful while putting the filtering questions as it could lead to bias in selecting papers based on the expected outcome, not the real results. On the other hand, this paper agreed that knowledge acquisition has a positive impact on enhancing Deep learning and Expert systems related to record-keeper knowledge management in Australia, which increases the job inside offices [61].

In reference to Table 5, an analysis was done to classify the studies referring to Knowledge Management processes in enhancing AI algorithms and systems. It is noticeable that knowledge acquisition is the most common process to improve AI systems. This is in alignment with the studies done by [60], [61], which agree on the positive impact of knowledge acquisition on different AI systems and algorithms. Previous Knowledge management process papers studied the relation with AI systems

and algorithms and focusing on specific AI system or algorithm. In this study, we tried to show the link between KM and AI systems looking from the higher picture, and showing that some KM processes can work not only for specific AI algorithms or methods, but it can also help in improving other AI algorithms. This can help researchers to identify other options to enhance an AI system by checking multiple options for a more cost-effective way if the current process used is having high implementation costs. Analysis finding illustrates the impact of knowledge management acquisition as the most used process to enhance the different type of AI systems and Algorithms. It also highlights that knowledge creation is the second option for improving AI systems. The analysis also shows that although some KM processes like knowledge application may have a positive impact on performance and data accuracy, it can have a negative impact on implementation due to high-cost requirements [52]. This research can suggest other KM processes as an option to achieve the required objectives, which may have less cost for implementations.

The limit of this study was on the implementation cost related to KM processes within AI systems as it will defer from an organization to another, based on the requirements and objectives required to achieve. Another limitation was due to the small number of studies done to find the relation between KM and AI systems, which limited the study outputs and may affect results accuracy. Future research may extend and improve the result of this research by increasing the number of databases that may have more studies related to the topic. Additionally, future researches can add a quality assessment question during the filtering steps to identify the degree or weight for the improvement in percentage; each KM process can give to AI algorithms and systems. For example, researches can highlight the results of how much improvement can KM process like knowledge acquisition give for AI Algorithm like Support Vector Machines. Furthermore, a detailed recommendation table can be created to highlight the best KM processes that can be used for each AI algorithm or system with expected improvement percentage and cost. Finally, this paper can be used as a foundation to prepare a comprehensive mapping table for the KM processes used to improve AI algorithms and systems.

It is beyond the scope of this paper to examine the actual implementation of the KM roles on AI algorithms, but it is recommended to make a real case study for an organization that has an existing knowledge management system or need to build a new knowledge management system. Moreover, to check how the theoretical results are supported in a practical case study.

Acknowledgment

This work is a part of a project undertaken at the British University in Dubai.

References

[1] S. A. Salloum, M. Al-Emran, and K. Shaalan, "The Impact of Knowledge Sharing on Information Systems: A Review," in *13th International Conference, KMO 2018*, 2018. https://doi.org/10.1007/978-3-319-95204-8_9

[2] F. O. Omotayo and M. O. Salami, "Use of Social Media for Knowledge Sharing Among Students," *Asian J. Inf. Sci. Technol.*, 8(2), 65–75, 2018.

[3] K. S. Ahlam Wahdan, Sendeyah Hantoobi, Said A. Salloum, "A systematic review of text classification research based ondeep learning models in Arabic language," *Int. J. Electr. Comput. Eng.*, 10(6), 6629–6643, 2020. http://doi.org/10.11591/ijece.v10i6.pp%25p

[4] S. S. B Al Kurdi, M Alshurideh, "Investigating a theoretical frameworkfore-learning technology acceptance," *Int. J. Electr. Comput. Eng.*, 10(6), 6484~6496, 2020. http://doi.org/10.11591/ijece.v10i6.pp%25p

[5] P. López-Portillo, V. González, E. René, R. Hidalgo, and J. Alberto, "Knowledge management metrics for Public Organizations: A literature review-based proposal," *arXiv Prepr. arXiv1609.09541*, 2016. https://arxiv.org/abs/1609.09541

[6] S. Satyanarayan and G. Azumah, "Operationalisation of knowledge management practices in r&d activity in multinational organisations," in *Proceedings of the 12th Management International Conference: Managing Sustainability, Portorož, Slovania*), 23–26, 2011.

[7] H. A. Nasiruzzaman, R. Qudaih, and D. Ahmad, "Project success and knowledge management (km) practices in Malaysian institution of higher learning (IHL)," *J. Educ. Vocat. Res.*, 4(5), 159–164, 2013. https://doi.org/10.22610/jevr.v4i5.114

[8] C. Rusuli, R. Tasmin, J. Takala, and H. Norazlin, "Knowledge Management Process At Malaysian University Libraries: A Review," *Int. J. Soc. Sci.*), 1–16., 2012

[9] M. A. Arpaci, I., Al-Emran, M., Al-Sharafi, "The impact of knowledge management practices on the acceptance of Massive Open Online Courses (MOOCs) by engineering students: A cross-cultural comparison, Telematics and Informatics.," 2020. https://doi.org/10.1016/j.tele.2020.101468

[10] M. Al-Emran and V. Mezhuyev, "Examining the Effect of Knowledge Management Factors on Mobile Learning Adoption Through the Use of Importance-Performance Map Analysis (IPMA)," in *International Conference on Advanced Intelligent Systems and Informatics*), 449–458, 2019. https://doi.org/10.1007/978-3-030-31129-2_41

[11] M. Al-Emran, V. Mezhuyev, and A. Kamaludin, "An Innovative Approach of Applying Knowledge Management in M-Learning Application Development: A Pilot Study," *Int. J. Inf. Commun. Technol. Educ.*, 15(4), 94–112, 2019. DOI: 10.4018/IJICTE.2019100107

[12] M. Al-Emran, V. Mezhuyev, and A. Kamaludin, "Towards a conceptual model for examining the impact of knowledge management factors on mobile learning acceptance," *Technol. Soc.*, 2020. https://doi.org/10.1016/j.techsoc.2020.101247

[13] W. Bodrow and V. Magalashvili, "It-Based Purpose-Driven Knowledge Visualization.," in *ICSOFT (PL/DPS/KE/MUSE)*), 194–197, 2007.

[14] P. Heisig, "Harmonisation of knowledge management–comparing 160 KM frameworks around the globe," *J. Knowl. Manag.*, 13(4), 4–31, 2009. DOI: https://doi.org/10.1108/13673270910971798

[15] P. Ziuziański, M. Furmankiewicz, and A. Sołtysik-Piorunkiewicz, "E-health artificial intelligence system implementation: case study of knowledge management dashboard of epidemiological data in Poland," *Int. J. Biol. Biomed. Eng.*, 8), 164–171, 2014.

[16] H. R. Nemati, D. M. Steiger, L. S. Iyer, and R. T. Herschel, "Knowledge warehouse: an architectural integration of knowledge management, decision support, artificial intelligence and data warehousing," *Decis. Support Syst.*, 33(2), 143–161, 2002. https://doi.org/10.1016/S0167-9236(01)00141-5

[17] H. AlGhanem, A. Mustafa, and S. Abdallah, "Knowledge and Human Development Authority in Dubai (KHDA) Open Data: What Do Researchers Want?," in *European, Mediterranean, and Middle Eastern Conference on Information Systems*), 58–70, 2019,. https://doi.org/10.1007/978-3-030-44322-1_5

[18] C. Mhamdi, M. Al-Emran, and S. A. Salloum, *Text mining and analytics: A case study from news channels posts on Facebook*, 740. 2018. https://doi.org/10.1007/978-3-319-67056-0_19

[19] M. Al-Emran, S. Zaza, and K. Shaalan, "Parsing modern standard Arabic using Treebank resources," in *2015 International Conference on Information and Communication Technology Research, ICTRC 2015*, 2015. DOI**:** 10.1109/ICTRC.2015.7156426

[20] M. Al-Emran and T. Teo, "Do knowledge acquisition and knowledge sharing really affect e-learning adoption? An empirical study," *Educ. Inf. Technol.*, 2019. https://doi.org/10.1007/s10639-019-10062-w

[21] M. Al-Emran, V. Mezhuyev, A. Kamaludin, and M. AlSinani, "Development of M-learning Application based on Knowledge Management Processes," in *2018 7th International conference on Software and Computer Applications (ICSCA 2018)*, 2018. https://doi.org/10.1145/3185089.3185120

[22] M. Al-Emran, V. Mezhuyev, and A. Kamaludin, "Students' Perceptions towards the Integration of Knowledge Management Processes in M-learning Systems: A Preliminary Study," *Int. J. Eng. Educ.*, 34(2), 371–380, 2018. https://dialnet.unirioja.es/servlet/articulo?codigo=6872062

[23] S. Banerjee, "Knowledge Management and Organizational Performance: The Case of a Telecommunication Organization in India.", 2018.

[24] S. Al-Hawamdeh, "Knowledge management: re-thinking information management and facing the challenge of managing tacit knowledge," *Inf. Res.*, 8(1), 1–8, 2002.

[25] M. M. Shongwe, "An analysis of knowledge management lifecycle

frameworks: Towards a unified framework," *Electron. J. Knowl. Manag.*, 14(3, p. 140, 2016.
[26] D. S. Kim, C. S. Kim, and K. W. Rim, "Modeling and design of intelligent agent system," *Int. J. Control. Autom. Syst.*, 1(2), 257–261, 2003.
[27] D. Foster, C. McGregor, and S. El-Masri, "A survey of agent-based intelligent decision support systems to support clinical management and research," in *proceedings of the 2nd international workshop on multi-agent systems for medicine, computational biology, and bioinformatics*), 16–34, 2005.
[28] C. M. Olszak and E. Ziemba, "Approach to building and implementing business intelligence systems," *Interdiscip. J. Information, Knowledge, Manag.*, 2(1), 135–148, 2007.
[29] M. S. Hossain, P. Zander, M. S. Kamal, and L. Chowdhury, "Belief-rule-based expert systems for evaluation of e-government: a case study," *Expert Syst.*, 32(5), 563–577, 2015. https://doi.org/10.1111/exsy.12110
[30] H. Vacik, C. Torresan, T. Hujala, C. Khadka, and K. Reynolds, "The role of knowledge management tools in supporting sustainable forest management," *For. Syst.*, 22(3), 442–455, 2013.
[31] A. Azadeh, K. Darivandi Shoushtari, M. Saberi, and E. Teimoury, "An Integrated artificial neural network and system dynamics approach in support of the viable system model to enhance industrial intelligence: The case of a large broiler industry," *Syst. Res. Behav. Sci.*, 31(2), 236–257, 2014. https://doi.org/10.1002/sres.2199
[32] H. Y. Lam, G. T. S. Ho, C.-H. Wu, and K. L. Choy, "Customer relationship mining system for effective strategies formulation," *Ind. Manag. Data Syst.*, 114(5), 711–733, 2014. https://doi.org/10.1108/IMDS-08-2013-0329 Download as .RIS
[33] V. H. Masías, M. A. Valle, J. J. Amar, M. Cervantes, G. Brunal, and F. A. Crespo, "Characterising the Personality of the Public Safety Offender and Non-offender using Decision Trees: The Case of Colombia," *J. Investig. Psychol. Offender Profiling*, 13(3), 198–219, 2016. https://doi.org/10.1002/jip.1451
[34] E. E. Tripoliti *et al.*, "HEARTEN KMS–A knowledge management system targeting the management of patients with heart failure," *J. Biomed. Inform.*, 94, p. 103203, 2019. https://doi.org/10.1016/j.jbi.2019.103203
[35] N. Nahar and F. Ara, "Liver disease prediction by using different decision tree techniques," *Int. J. Data Min. Knowl. Manag. Process*, 8(2), 1–9, 2018.
[36] S. A. S. Salloum and K. Shaalan, "Investigating students' acceptance of E-learning system in Higher Educational Environments in the UAE: Applying the Extended Technology Acceptance Model (TAM)." The British University in Dubai, 2018.
[37] S. A. Salloum, A. Qasim Mohammad Alhamad, M. Al-Emran, A. Abdel Monem, and K. Shaalan, "Exploring students' acceptance of e-learning through the development of a comprehensive technology acceptance model," *IEEE Access*, 7, 2019. DOI**:** 10.1109/ACCESS.2019.2939467
[38] S. F. S. Alhashmi, M. Alshurideh, B. Al Kurdi, and S. A. Salloum, "A Systematic Review of the Factors Affecting the Artificial Intelligence Implementation in the Health Care Sector," in *Joint European-US Workshop on Applications of Invariance in Computer Vision*), 37–49, 2020. https://doi.org/10.1007/978-3-030-44289-7_4
[39] S. K. Al Mansoori S., Salloum S.A., "The Impact of Artificial Intelligence and Information Technologies on the Efficiency of Knowledge Management at Modern Organizations: A Systematic Review.," *Al-Emran M., Shaalan K., Hassanien A. Recent Adv. Intell. Syst. Smart Appl. Stud. Syst. Decis. Control. vol 295. Springer, Cham*, 2021. https://doi.org/10.1007/978-3-030-47411-9_9
[40] S. K. Areed S., Salloum S.A., "The Role of Knowledge Management Processes for Enhancing and Supporting Innovative Organizations: A Systematic Review.," *Al-Emran M., Shaalan K., Hassanien A. Recent Adv. Intell. Syst. Smart Appl. Stud. Syst. Decis. Control. vol 295. Springer, Cham*, 2021. https://doi.org/10.1007/978-3-030-47411-9_8
[41] S. K. AlShuweihi M., Salloum S.A., "Biomedical Corpora and Natural Language Processing on Clinical Text in Languages Other Than English: A Systematic Review.," *Al-Emran M., Shaalan K., Hassanien A. Recent Adv. Intell. Syst. Smart Appl. Stud. Syst. Decis. Control. vol 295. Springer, Cham*, 2021. https://doi.org/10.1007/978-3-030-47411-9_27
[42] S. K. Almansoori A., AlShamsi M., Salloum S.A., "Critical Review of Knowledge Management in Healthcare.," *Al-Emran M., Shaalan K., Hassanien A. Recent Adv. Intell. Syst. Smart Appl. Stud. Syst. Decis. Control. vol 295. Springer, Cham*, 2021. https://doi.org/10.1007/978-3-030-47411-9_6
[43] S. K. Habeh O., Thekrallah F., Salloum S.A., "Knowledge Sharing Challenges and Solutions Within Software Development Team: A Systematic Review.," *Al-Emran M., Shaalan K., Hassanien A. Recent Adv. Intell. Syst. Smart Appl. Stud. Syst. Decis. Control. vol 295. Springer, Cham*, 2021. https://doi.org/10.1007/978-3-030-47411-9_7
[44] S. K. Yousuf H., Lahzi M., Salloum S.A., "Systematic Review on Fully Homomorphic Encryption Scheme and Its Application.," *Al-Emran M., Shaalan K., Hassanien A. Recent Adv. Intell. Syst. Smart Appl. Stud. Syst. Decis. Control. vol 295. Springer, Cham*, 2021. https://doi.org/10.1007/978-3-030-47411-9_29
[45] R. French and P. Brocklehurst, "The effect of pregnancy on survival in women infected with HIV a systematic review of the literature and meta-analysis," *BJOG An Int. J. Obstet. Gynaecol.*, 105(8), 827–835, 1998. https://doi.org/10.1111/j.1471-0528.1998.tb10226.x
[46] D. M. Rousseau, J. Manning, and D. Denyer, "11 Evidence in management and organizational science: assembling the field's full weight of scientific knowledge through syntheses," *Acad. Manag. Ann.*, 2(1), 475–515, 2008. https://doi.org/10.5465/19416520802211651
[47] N. Al-Qaysi, N. Mohamad-Nordin, and M. Al-Emran, "Employing the technology acceptance model in social media: A systematic review," *Educ. Inf. Technol.*), 1–42, 2020. https://doi.org/10.1007/s10639-020-10197-1
[48] M. Fatehah, V. Mezhuyev, and M. Al-Emran, "A Systematic Review of Metamodelling in Software Engineering," in *Recent Advances in Intelligent Systems and Smart Applications*), 3–27, Springer, 2021. https://doi.org/10.1007/978-3-030-47411-9_1
[49] F. F. Tránsito, M. R. Helena, J. G. P. Francisco, and A. M. V. José, "The systematic review of literature in LIS: An approach," in *ACM International Conference Proceeding Series*, 02-04-Nove), 291–298, 2016. https://doi.org/10.1145/3012430.3012531
[50] L. Victor, "Systematic reviewing," *Soc. Res. Updat.*, 54(1), 1–4, 2008.
[51] T. Ferreras Fernández, H. Martín-Rodero, F. J. García-Peñalvo, and J. A. Merlo Vega, "The systematic review of literature in LIS: an approach," 2016. https://doi.org/10.1145/3012430.3012531
[52] O. Alsetoohy, B. Ayoun, S. Arous, F. Megahed, and G. Nabil, "Intelligent agent technology: what affects its adoption in hotel food supply chain management?," *J. Hosp. Tour. Technol.*, 2019. https://doi.org/10.1108/JHTT-01-2018-0005
[53] X. Liu, C. Guo, and L. Zhang, "Scholar metadata and knowledge generation with human and artificial intelligence," *J. Assoc. Inf. Sci. Technol.*, 65(6), 1187–1201, 2014. https://doi.org/10.1002/asi.23013
[54] L. Li *et al.*, "Artificial intelligence test: a case study of intelligent vehicles," *Artif. Intell. Rev.*, 50(3), 441–465, 2018. https://doi.org/10.1007/s10462-018-9631-5
[55] G. Boella, L. Di Caro, L. Humphreys, L. Robaldo, P. Rossi, and L. van der Torre, "Eunomos, a legal document and knowledge management system for the web to provide relevant, reliable and up-to-date information on the law," *Artif. Intell. Law*, 24(3), 245–283, 2016. https://doi.org/10.1007/s10506-016-9184-3
[56] O. Smilansky, "The Real Benefits of Artificial Intelligence:Adding AI to the contact center enables rapid information retrieval, leading to a better experience for both agents and customers," *Cust. Relatsh. Manag.*, 21 (11)), 28–31, 2017.
[57] A. Y. Al-Aama, "Technology knowledge management (TKM) taxonomy: using technology to manage knowledge in a Saudi municipality," *Vine*, 44(1), 2–21, 2014. https://doi.org/10.1108/VINE-12-2012-0052
[58] K. L. T. Choy *et al.*, "An intelligent case-based knowledge management system for quality improvement in nursing homes," *VINE J. Inf. Knowl. Manag. Syst.*, 48(1), 103–121, 2018. https://doi.org/10.1108/VJIKMS-01-2017-0001
[59] A. Sheffer Corrêa, A. de Assis Mota, L. Toledo Moreira Mota, and P. Luiz Pizzigatti Corrêa, "A fuzzy rule-based system to assess e-government technical interoperability maturity level," *Transform. Gov. People, Process Policy*, 8(3), 335–356, 2014. https://doi.org/10.1108/TG-08-2013-0028
[60] H. M. Said and A.-B. M. Salem, "Exploiting Computational intelligence Paradigms in e-Technologies and Activities," *Procedia Comput. Sci.*, 65), 396–405, 2015.
[61] G. Rolan, G. Humphries, L. Jeffrey, E. Samaras, T. Antsoupova, and K. Stuart, "More human than human? Artificial intelligence in the archive," *Arch. Manuscripts*, 47(2), 179–203, 2019. https://doi.org/10.1080/01576895.2018.1502088
[62] Z. Li, W. M. Wang, G. Liu, L. Liu, J. He, and G. Q. Huang, "Toward open manufacturing: A cross-enterprises knowledge and services exchange framework based on blockchain and edge computing," *Ind. Manag. Data Syst.*, 118(1), 303–320, 2018.

ASTES

Advances in Science, Technology and Engineering Systems Journal Vol. 5, No. 6, 416-422 (2020)

www.astesj.com

Special Issue on Innovative Research in Applied Science, Engineering and Technology

ASTESJ

ISSN: 2415-6698

The Probe Mark Discoloration on Bond Pad and Wafer Storage

Wen-Fei Hsieh*, Henry Lin, Vincent Chen, Irene Ou, Yung-Song Lou

Ardentec Cooperation Quality Assurance, No. 3, Gongye 3 rd Rd., Hsin-Chu Industrial Park, Hukou Township, Hsinchu County 30351, Taiwan, R.O.C.

ARTICLE INFO

Article history:
Received: 31 August, 2020
Accepted: 15 October, 2020
Online: 20 November, 2020

Keywords:
Probe Mark Discoloration
Fluorine Contamination
Wafer Storage

ABSTRACT

In this report, a probe mark discoloration with donut/circle shape was found. The corrosion formed on Aluminum bond pads. The SEM/EDS, TEM/EELS & AES surface techniques were used to identify this corrosion product. All these material analysis results pointed out the role of fluorine to this discoloration. The HAST testing, all the chip samples obtained from wafer center/middle area, were simulated to have been exposed in air for 1 year. HAST test result showed no fluorine source came from the center/middle zones of impact wafers. Another full wafer-level FOSB storage test showed the source of corrosive fluorine came from wafer itself. EDS mapping results, from extreme wafer edge zone, indicated the fluorine element distribution. The mechanism of this novel discoloration was proposed. However, more evidences were necessary for understanding the formation of donut discoloration corrosion.

1. Introduction

In order to obtain semiconductor device electrical performance, the circuit probing (CP) tests were performed by pin probing on bond pad before device package process. The typical bond pad materials are Aluminum (Al) with low content of silicon and copper to improve the resistance of electron migration. The interconnection from aluminum pad surface to external interface frame play a critical role in semiconductor package process. It is well known the Aluminum would form corrosion protective oxide film in oxygen condition. However, in the past three decades, the formation of fluorine (F) corrosive film on aluminum bond pad surface [1,2] and non-stick on pad (NSOP) failure issue that induced broad quality issues concern were reported by some researchers before. [3-7] These corrosive film was found to suffer semiconductor reliability. The early researches indicated two main root causes for these fluorine contained contamination. One is the fluorinated silicone glass (FSG) film could release fluorine into closed spacing, and then contaminate the bond pad surface. [1] The FSG layer is still an important low K dielectric layer used in device process, so the F leakage from FSG layer is still a unavoidable issue in semiconductor dielectric layer process. The second fluorine source is the fluorine embedded on Al pad surface, and the fluorine residue from previous pad etching and cleaning gas. [9] So the fluorine source for contamination divided into two groups, direct F embedded on Al top surface, and the indirect F from FSG layer. Therefore, the wafer storage become an important factor for fluorine contamination. The early F-induced contamination studies focused on the morphology and mechanism to induce corrosion product. No probe mark and electric testing effects were reported before. P. Chang [8] had stated the early probe mark discoloration study of yellow discoloration Al bond pad corrosion. However, the probe mark discoloration had not been fully report yet. [10, 11] In this paper, the donut/circle discoloration corrosion and a compressive study would be present.

In the beginning of this case, the probe mark discoloration was found at the stage of blue tape. All the impacted wafers finished all the CP tests, and stored in the Front Opening Shipping Box (FOSB) for more than two months. There are two types of probe mark discoloration forming on the bonding pad surface. Figure 1 (a) and (c) show these typical circle/donut discoloration optical microscope (OM) photos. The special feature of discoloration morphology is that probe mark is the center of cyclic/donut center. The OM inspection for discoloration corrosion indicated most of the corrosion was cyclic, and only few was donut shaped. Figure 1 (b) show that two touchdown would not induce two discoloration. The size of cyclic discoloration is not constant, however, the largest diameter of a suffered wafer, up to 35 um, is nearly the same. With the help of full wafer dice Auto Vision Inspection (AVI), most of the corrosive dice locate near the wafer edge zone. The worst fail rate would reach up to 15-18% of all the available dice.

*Corresponding Author: Wen-Fei Hsieh, Email: michael.hsieh@ardentec.com

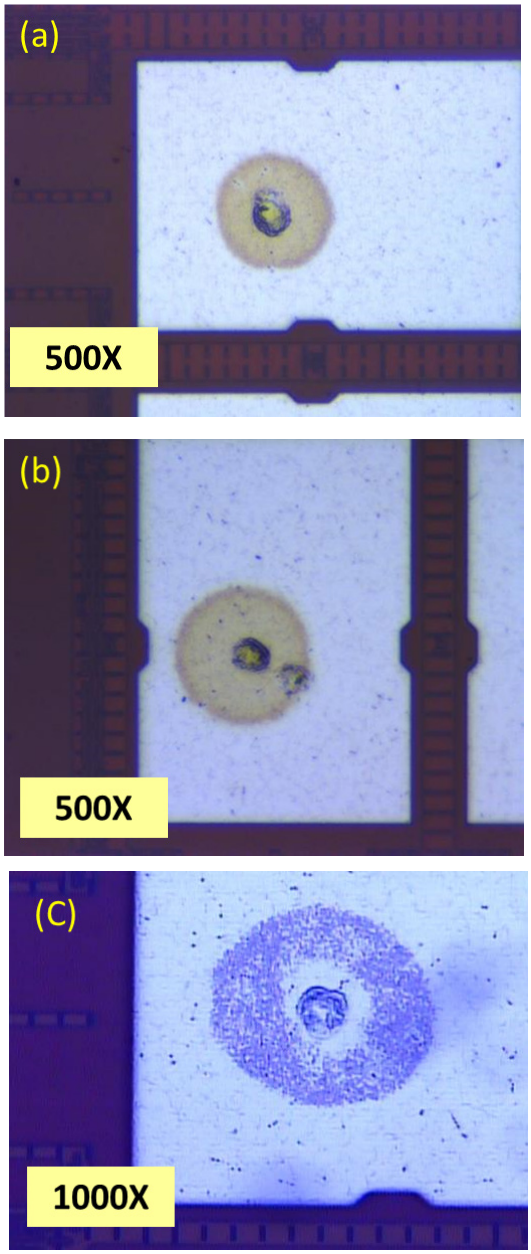

Figure 1: (a) show the typical probe mark discoloration OM image. (b) show the formation of discoloration on Al pad under dual pin touch down. No second discoloration is found. (c) show donut-shaped probe mark discoloration. To clearly show donut shape discoloration, (c) was magnified to 1000X, that is larger than Figure 1 (a) & (b).

2. Experiments and Results

In this study, the samples were checked in plane-view & cross-sectional approaches. The Scanning Electron Microscopy (SEM) images was obtained by 5 KeV electron energy. And the Energy Dispersive Spectrum (EDS) result was obtained by 10 KeV electron energy. Transmission Electron Microscopy (TEM) operated at 200 KeV with Electron Energy Loss Spectrum (EELS). SEM and TEM could get the information of morphology and corresponding EELS analysis for the normal and abnormal locations. Auger Electron Spectroscopy (AES) is a traditional surface analysis technology for bond pad corrosion case. So AES depth profile results would be included.

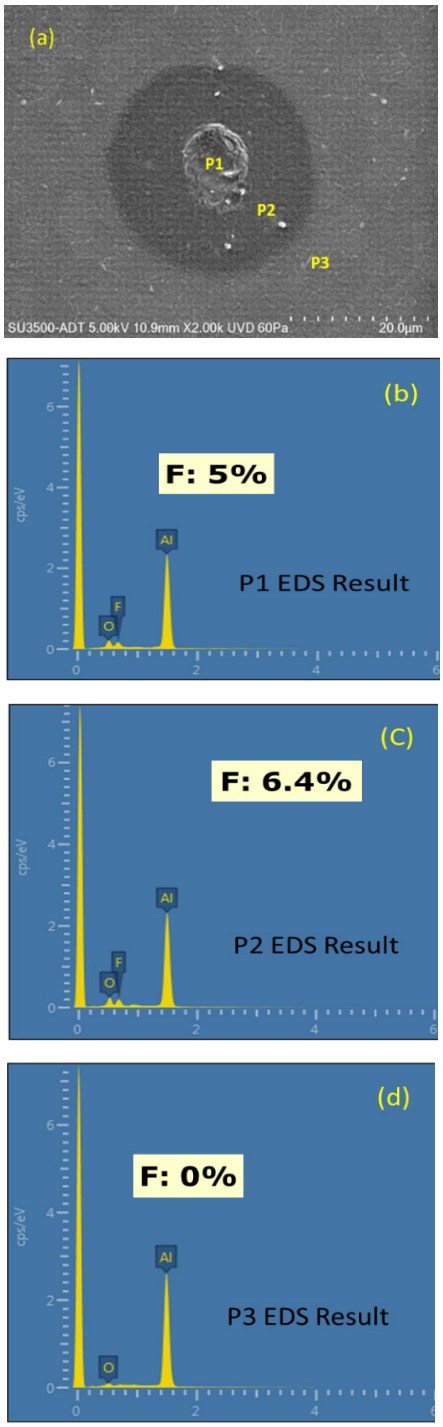

Figure 2: (a) is the SEM micrograph of probe mark discoloration corrosion. P1 is the zone of probe mark. P2 is the discoloration zone. P3 is the normal Al pad surface. (b),(c) & (d) the corresponding EDS analysis result of P1 to P3 various zones on Al pad surface. The oxygen element was found for each locations. The Fluorine was only found at the discoloration zones.

Based on the literature review, the various storage conditions would impact corrosion behavior. Highly Accelerated Stress Test (HAST) was applied with test conditions of temperature at 130ºC and RH 85% for 21 hours. This test is to simulate all the bond pad exposed in air without Nitrogen Cabinet storage or Moisture Barrier Bag (MBB) storage for 1 year. This test would be helpful to evaluate the impacted dies corrosion behavior. The secondary storage test, full wafer deposited in the regular FOSB, is to identify

the standard FOSB storage effect, and find out the source of F element.

2.1. SEM/EDS Analysis Results

Figure 2 show the top-view SEM photo and corresponding EDS analysis results of various feature locations on Al pad surface. The SEM photo clearly show the boundary of discoloration boundary on Al pad surface. Based on the SEM inspection, the rough size of this discoloration was more than 25 micro meter. The probe mark and corresponding discoloration zone were easily identified. The SEM photo also show various morphology of probe mark surface deformation. According to the EDS results of discoloration zone, the P1 & P2 of Fig. 2(a), where fluorine and oxygen contents are found on the center and middle of circle region. No Fluorine element was detected for normal P3 Al pad surface. The content of fluorine element, 5-6 %, is noted. That is, the probe mark discoloration is a kind of aluminum-fluorine-oxygen corrosion. As for the normal zone, aluminum oxide form on Al pad surface. Since this novel corrosion product has not been fully reported before, the EDS analysis is helpful to improve the key role of fluorine element.

Figure 3 show the OM photo and its corresponding EDS result. P1 to P4 of Figure 3(a) are the various locations of donut-shaped discoloration on Al pad surface. P1 is the probe mark zone. P2 is the cyclic annular zone without discoloration. P3 is the cyclic annular zone with discoloration corrosion. And P4 is the normal Al pad surface. The EDS result clearly indicate fluorine element is only found at the discoloration corrosive zone. No fluorine is found at P1- probe mark, P2- cyclic annular without discoloration, and P4 - normal Al pad surface zones. Based on these donut-shaped discoloration EDS results, the root cause of the discoloration event is due to fluorine contamination. However, due to the basic characteristic of high energy electron stopping power, the X-ray signal of EDS analysis is collected not only from Al pad top surface, but also the larger undersurface bulk volume. The distribution of fluorine element could not be identified by this EDS analysis. TEM and AES are necessary for further identification.

2.2. TEM/EELS Analysis Results

The cross-sectional TEM inspection is helpful to identify the thickness variation of corrosion film. Figure 4 show the full cross sectional TEM inspection photo of discoloration area. The thickness of discoloration corrosion film is just a few nm. Therefore, it could not be clearly identified by Figure 4. The magnified TEM photo indicate the thickness of discoloration film is uniform except for probing mark zone. Figure 5 show the High Angle Annular Dark Field (HAADF) TEM image of discoloration film structure. The HAADF image indicate the thickness of circle shape discoloration is within 5 nm. The corresponding Electron Energy Loss Spectrum (EELS) line scan results show the F & O distribution of this Al-O-F film. The fluorine is found on the top surface of corrosion film. No F & O could deeply penetrate into the Al. Figure 4 show the corrosion film of probe mark is complex. Figure 6 show the high magnification cross-sectional TEM image and its corresponding EELS data of probe mark oxidation. The variation of corrosion film thickness might be up to over 10X. The thicker film formed on probe mark zone is also the AL-O-F compound as other discoloration zone. The EELS fine structure analysis indicate discolored Al_2O_3 spectrum is a combination of

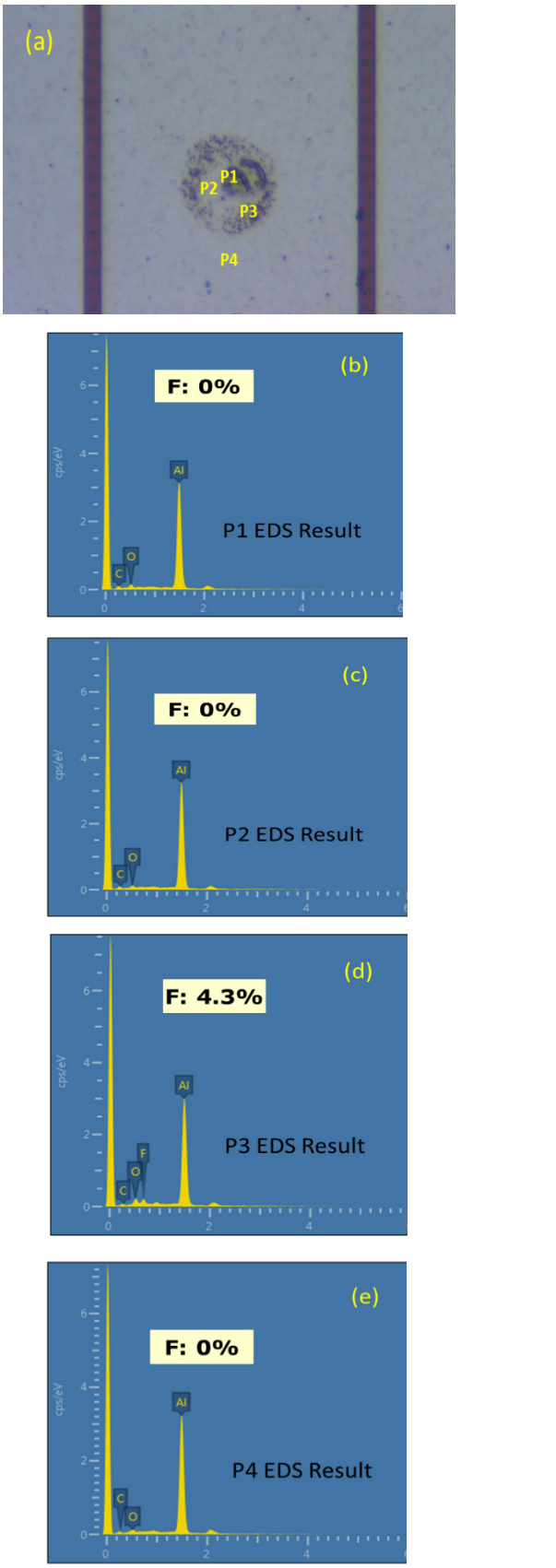

Figure 3: (a) is the OM image of donut-shaped probe mark discoloration. P1 is the zone of probe mark. P2 is the annular zone without discoloration. P3 is the annular zone with discoloration. P4 is the normal Al pad surface. (b), (c), (d) & (e) the corresponding EDS analysis results of various zones on bond pad surface. Fluorine is only found at the cyclic annular discoloration zone.

pure Al_2O_3 with OF_3. That is, the fluorine diffuse into the Aluminum oxide film. F atom form a new bonding to replace O bonding. These new formed Al-O-F must be less protective than original Al_2O_3 film.

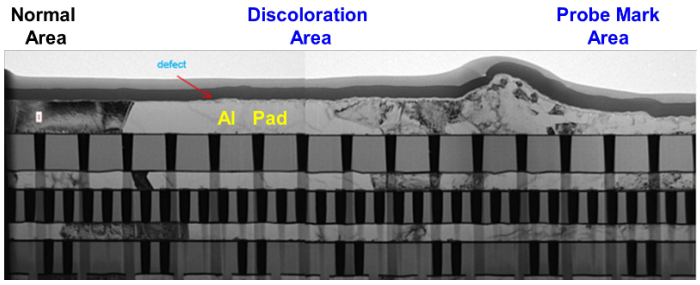

Figure 4: The low magnification full cross-sectional TEM image of discoloration defect corrosion.

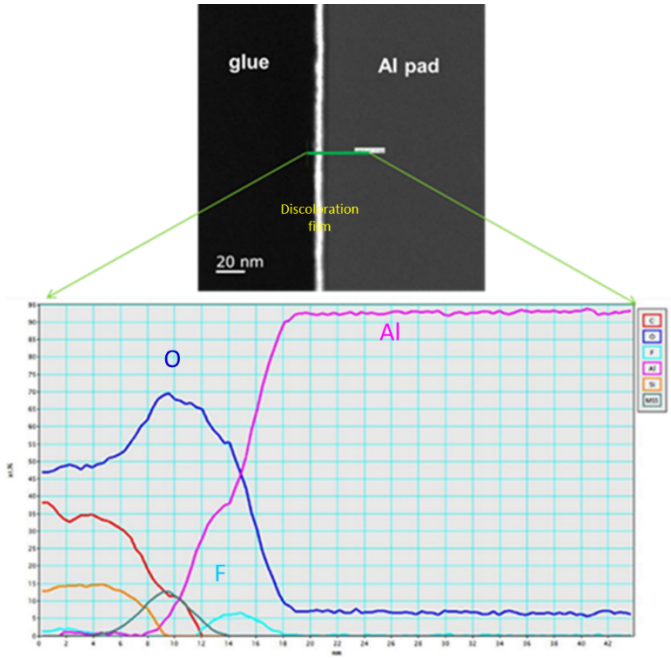

Figure 5: The cross sectional HAADF TEM image of discoloration zone and its corresponding EELS line scan result. The line scan result clearly show the distribution of fluorine and Oxygen just on the Al pad top surface.

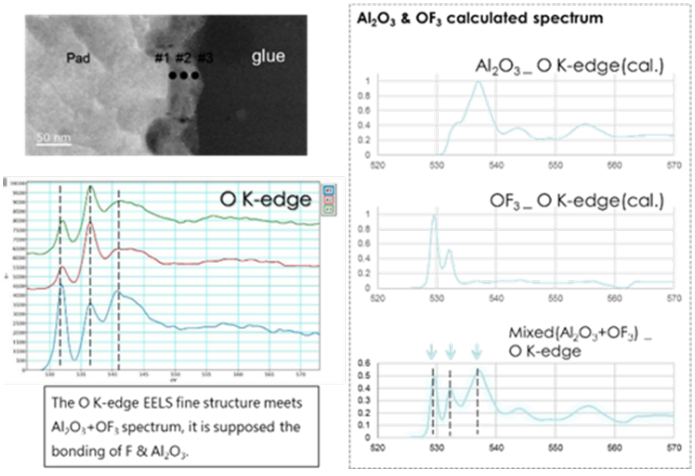

Figure 6: The TEM image and EELS data of probe mark discoloration defect film & its corresponding simulation EELS spectrum.

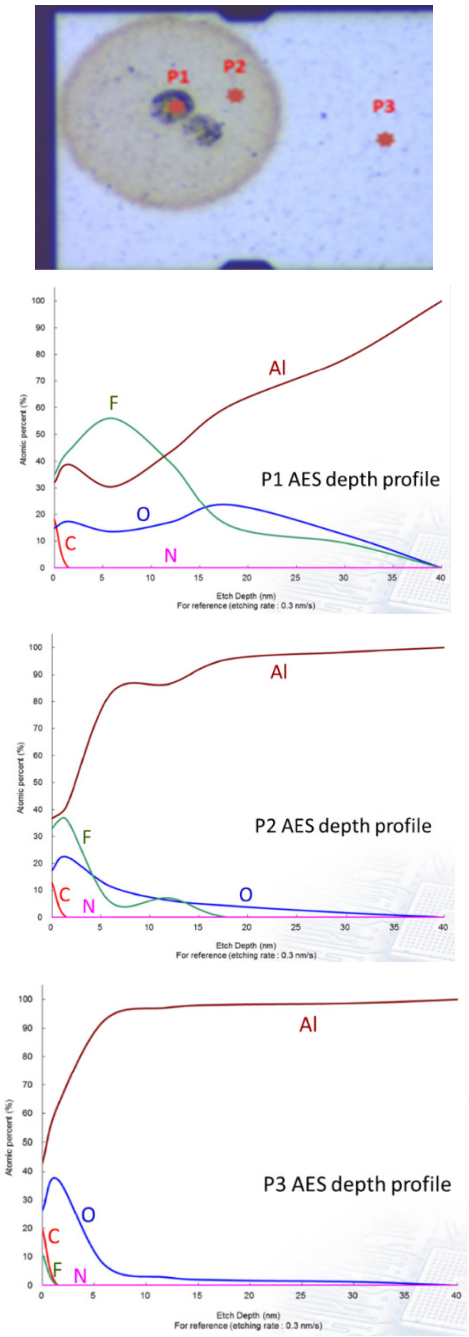

Figure 7: The OM photo and the corresponding AES depth profile of P1, P2 & P3, the P1, P2, & P3 are marked on discolored Al pad surface. P1 is the probe mark zone. P2 is the discoloration zone. P3 is the normal Al pad surface. The F element is found to co-exist with Al_2O_3 at discoloration zones.

2.3. AES Analysis Results

For a long time, the AES analysis is treated as the standard technology for Al pad surface contamination. Figure 7 (b) to (d) show the specific Auger Electron Spectrum (AES) depth profile result of normal/discoloration area of bond pad surface. The AES result indicate the main elements of probe mark and cyclic discoloration area are Al, F, and O. That is the same as previous EDS & EELS results. The AES depth profile results, P1, P2 & P3 of Figure 7, show the discoloration corrosion film is the F element co-existed with AlxOy. BTW, X-ray Photon Spectrum (XPS) is also an available surface analysis technology for oxidation state of

Al compound. However, due to the X-ray focusing capability limitation, XPS is not used in this bond pad case. The Secondary Ion Mass Spectrum (SIMS) analysis meet the similar limitation.

Two key factors decide the success of this contamination Failure Analysis. The first one is to identify the component of the corrosion product. The second one, sometimes it is more critical in probe testing FAB daily operation, is to find out the corrosion/contamination source, and then to stop this event.

Based on previous material analysis finding, the probe mark discoloration contamination is a special type of Al-F-O corrosion. Since the nature protective Al-O film would automatically form on bond pad top, therefore, the fluorine element play an important role in this corrosion event. Where do the fluorine come from? How do this discoloration develop?

The fluorine induced corrosion on Al bond pad is not an new issue[1,2]. The source of fluorine might come from wafer itself or external environment. The fluorine come from wafer itself is supposed to be the etching residue on Al pad surface.[9] The F-contained etching gas, like CF4, is broadly used in Al pad process loop. The fluorine element is supposed to easily residue on Al pad top surface after etching. Generally speaking, the 5 % fluorine residue on Al pad surface is regarded as a safe margin. However, the previous AES depth profile data indicate no fluorine element is found below 1.5nm of top surface on no discoloration area of Al pad. The source of fluorine need to clarify. Therefore, two various storage tests are necessary to find out the fluorine source. The first storage tests, HAST, the dice-level test is a high temperature corrosion accelerated test. The second test, FOSB storage test, is a full wafer-level test under daily standard storage operation. The experiment results show as below:

2.4. HAST Storage Test Result

In order to clarify the effects of long time storage and probing touchdown number on this corrosion. Four groups of various die samples were applied for the HAST. The nine discolored and nine normal dice were the first and secondary groups for HAST. The nine dice, with five and twenty probing touchdowns, set as the third and the forth groups. Therefore, in this HAST, total four groups dice obtained from impacted wafers were tested. The HAST testing preformed at the condition of temperature 130ºC and RH 85% for 21 hours. All the dice samples simulated to have exposed in air without N2 cabinet storage or MBB bag storage for 1 year. Table 1 consolidate the result of HAST storage test. The result of group one and two indicate that there is no visual change, by 100% OM inspection, after HAST storage simulation testing. No probe mark discoloration corrosion size increase after HAST. The secondary group data indicate no probe mark discoloration would form. The result of third and four group imply that the heavy deformation on Al pad surface would not automatic induce discoloration corrosion. According to the previous analysis, the fluorine is necessary for the formation of discoloration. The HAST result show no extra fluorine source exist in HAST tested dice.

Table 1: The HAST testing Result. Four various samples were tested. The size of all samples are die level. The discoloration dice show no deterioration after the test. No other tested dice show clear change. In this table, Y means discoloration; and N means no discoloration.

Group	1	2	3	4
Samples	Discolored 2 touchdown	Normal 2 touchdown	Normal 5 touch down	Normal 20 touch down
Dice Quantity	9	9	9	9
Discolored Before	Y	N	N	N
Discolor After	Y	N	N	N
Result	Discolor no deterioation	No Discolor	No Discolor	No Discolor

2.5. FOSB Storage Test Result

Based on the previous HAST result, all these dice were obtained from wafer center or middle area, and no extra fluorine was found. The FOSB storage test preformed for the full wafers deposited in normal FOSB at room temperature. The Ardentec AVI inspection was applied for the tested wafer before FOSB storage testing. Then these wafers, after some storage time, would be viewed by Ardentec standard AVI checking to identify the discoloration behavior on the same Al pad. After 4 weeks' storage time, obvious variation was found. Figure 8 clearly indicate the variation of two OM photos. The probe mark discoloration would deteriorate in FOSB storage test. That is to say, the fluorine-induced corrosion in the FOSB volume would be continuous. It is a manifest evidence the source of F element enhancing discoloration corrosion is due to the full wafers FOSB storage. The HAST result indicated no extra F was found from wafer center and middle area. Therefore, the source of F element of FOSB test is highly suspected to be the wafer edge or wafer extreme edge area. The EDS mapping was an excellent technology to show the various element distribution of semiconductor top surface. It would be helpful to identify the distribution of fluorine element of abnormal wafer extreme edge area.

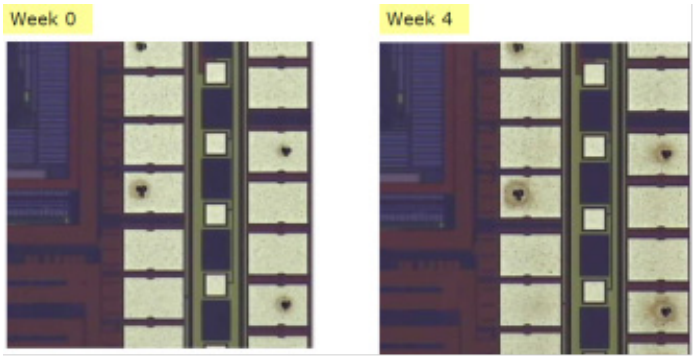

Figure 8: show the OM inspection result after FOSB storage test. The original probe mark discoloration is the OM micrograph on the left. After 4 week's FOSB storage, the size of probe mark discoloration became larger. The right hand side OM photo clearly show this deterioration.

Figure 9 show the EDS mapping result of extreme edge area of discoloration wafer. The EDS data clearly show the distribution of F, Al and other main elements on semiconductor wafer top surface. And the original location of this EDS mapping, the right hand side OM photo of Figure 9, was obtained at the extreme edge of full

wafers. There is a clear boundary between extreme edge, the upper part of OM image, and the internal die area. The fluorine-induced corrosion source is clearly identified from extreme edge of full wafers. It is supposed that the FSG layers exposed to FOSB space would be the F source of this corrosion.

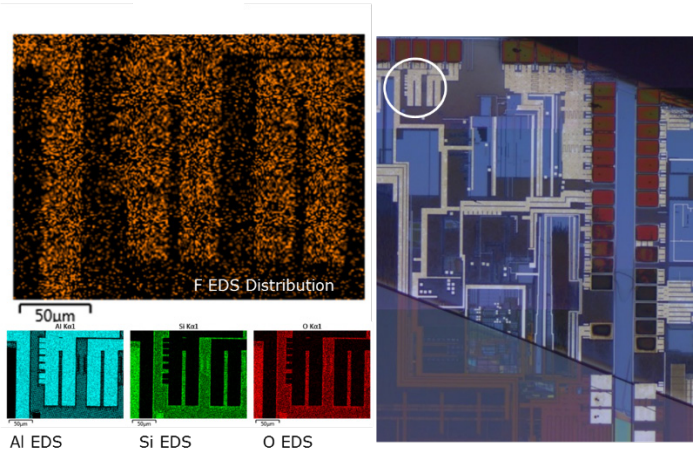

Figure 9: The EDS mapping result of Al pad on the discoloration wafer extreme edge area. The left hand side EDS mapping result show the distribution of F, Al, Si and O. The white circle area of right-hand side OM image shows the location of this EDS area of the wafer.

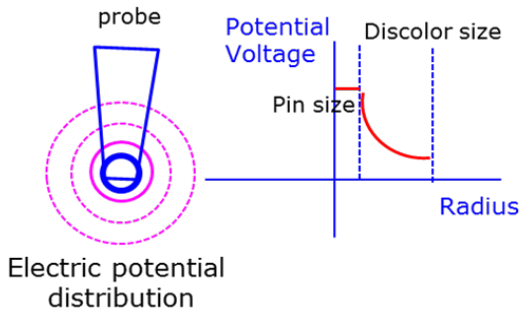

Figure 10: The critical CP testing and electrical testing potential field effect on Al bond pad surface.

The mechanism of this probe mark discoloration was proposed as follow: The CP testing would activate the embed fluorine. The formation of fluorine-contained oxide film induce this special discoloration.

The special point of this novel discoloration is the corrosion morphology with probe mark as its center. Some factors inducing the fluorine activation would spontaneously lead the probe mark as the discoloration cyclic center. In the beginning, the CP probing action would induce a permanent mechanical damage on the Al bond pad surface. This damage produce great deformation and heavy strain on the Al pad top surface, and this deformation and strain region, chemical activated, would be full of dislocation-like defects. The second mechanical effect was that probing test itself would break down the original protective Al-O film, and then create large amount of fresh aluminum surface. Both the mechanical effects would induce extremely active sites on Al pad surface. These would be easily for fluorine to react with Aluminum. The other impact of the probing action is the corresponding electric field potential, built by Circuit Probing test, would have an effect on the surrounding area of probe mark under the voltage/current variations. Under certain temperature, like the temperature of 125ºC setting at CP testing, and humidity, the fluorine contamination would be excited. Here the water is supposed to play an important role, leading to forming of hydrogen and oxygen, and after serial chemical reaction with fluorine, the AlxOyFz compound form. This kind of AlxOyFz compound is the discoloration by OM inspection. The threshold activation energy for all the chemical reactions was limited by electric potential field built by testing program, therefore, electric potential field introduced the circle shape discoloration region centered by probe mark. Figure 10 show the electric potential field distribution build by probing test.

The formation of probe mark discoloration on Al pad surface was not just due to single factor. There are three complex factors to induce this corrosion. The first factor is the sufficient fluorine supply in wafer storage environment. The fluorine might come from bond pad top surface or wafer inter metal dielectric layer. The second one is the environmental condition. The suitable temperature and enough humidity are critical to accelerate the fluorine corrosion reaction. The third factor induce probe mark discoloration formation was the probing touchdown and its sequential current and electric field. According the early study [3], the Al-O-F compound on Al pad surface show different morphology as this corrosion event. No previous report had pointed this Al-O-F compound discoloration morphology with probe mark as its circle center. Therefore, the characteristic of this contamination closely related to electric probing test condition. Then this novel probe marked discoloration need to combine all the above corresponding factors. These factors are materials property, wafer testing/storage environments and probing testing. Figure 11 show this idea.

According to the above mechanism, the formation of probe mark discoloration could stop in some ways. The material itself decide the source of fluorine. Therefore, the content of fluorine embedded on bond pad top surface or the distribution of fluorine on wafer edge is an important index to find the fluorine source. Since in CP and FT daily operation, no fluorine contained chemical materials are used. The CP & FT Fab is better to take them into regular monitor index for future discoloration event.

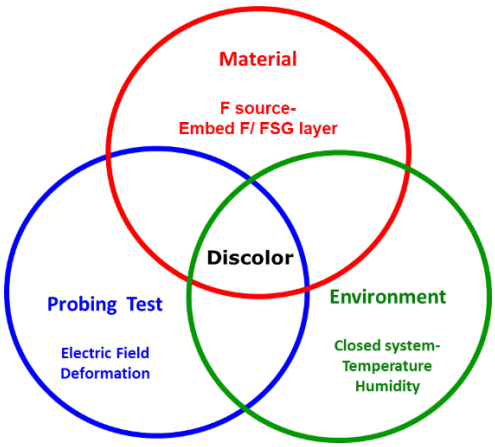

Figure 11: The factors to induce bond pad probe mark discoloration. These critical factors are material property, probing test and environment.

In the previous discoloration mechanism, the formation of donut shaped discoloration corrosion would be a weak point. Since the material analysis of donut discoloration indicate the fluorine

contained discoloration would only form on the ring zone, and no other discoloration would form on the other Aluminum pad surface. Therefore, the idea, discoloration originally form at probe mark area, and then fluorine diffusion to deteriorate discoloration, would not fully explain the formation of donut-shaped discoloration corrosion film. The EDS analysis result of donut-shaped discoloration imply that no fluorine exist at probe mark area. This impressive result also indicate the probe mark area with heavily deformation and high dislocation density would not spontaneously form corrosive fluorine contained Al-O-F film. The limitation of fluorine supply might be the key factor for this donut-shaped discoloration. There is no enough fluorine to form Al-O-F film on probe mark area, but enough fluorine to form Al-O-F film on annular area of Al top surface. In this system, there are two fluorine source, the embed fluorine and leakage form FSG. It is supposed that the embed fluorine would spontaneously form Al-O-F during CP testing under suitable electric potential activation. The fluorine supply from FSG leakage would be slowly deteriorate the corrosion due to diffusion into spacing is a time consuming process. That is to say, discoloration might be separate into two stages. In the first stage, embed fluorine play the key role in Al-O-F corrosion film formation. As for the secondary stage, the fluorine accumulation, leakage from FSG, and diffusion to Al-O-F interface play the key role. The secondary stage is a time consuming stage, therefore, storage environment is the controlled factor at this stage. The formation of cyclic discoloration corrosion would be that there is enough embed fluorine on the Al bond pad surface, and following with enough fluorine from FSG layer. As for the donut shaped discoloration, it would be that no enough embed fluorine on bond pad surface, so there is no complete cyclic discoloration formation. The key factor for donut-shaped discoloration formation is the supply of fluorine. No fluorine to react with Al metal. This explain that no Al-O-F film form at probe mark area and the formation of annular corrosion film. The possible root cause for donut discoloration might due to fluorine source complete consumption. However, no experiment would prove this proposal now.

3. Conclusions

- A new donut/circle shaped discoloration on Al bond pad is reported.
- Based on SEM/EDS, TEM/EELS and AES analysis results, the novel discoloration is due to form an Aluminum fluorine-oxide compound. The fluorine plays a key role in the formation of probe mark discoloration.
- With the help of HAST, FOSB storage test, and EDS mapping, the source of fluorine of this case is found.
- Since probe mark is the center of circle for discoloration, the formation of this corrosion is closely relative with the CP electric field.

Conflict of Interest

The authors declare no conflict of interest for this work. Formal "Conflict of Interest" document file is attached.

Acknowledgment

The authors would like to thank Polly Liu and Alex Si for their long time effort on discoloration impacted wafer management, and Berton Hsieh and Wei-Cheng Chen for their long time supporting on FA analysis.

References

[1] K. Ernst, D. Grman, R. Hauert, E. Holländer "Fluorine-induced corrosion of Aluminum microchip bond pads", Surface and Interface Analysis, **21**(10), 691 – 696, 2004, doi: 10.1002/sia.740211003

[2] W. A. P. Claassen and P. Krarner, "Aluminum Corrosion in the IC-MOS Production Line", Internal Report. Philips, Nijmegen, 1988.

[3] H. Younan, Shailesh Redkar, Lau Chi-Kwan and Mo Zhiqiang, " A Study on Non-Stick Aluminum Bond Pads due to Fluorine Contamination using SEM, EDS, TEM, IC, Auger, XPS & TOP-SIMS Techniques". in The Proceeding from the 28th International Symposium for Testing & Failure Analysis (ISTFA 2002), Phoenix, USA, 495-504, 2002.

[4] H. Younan, Shailesh Redkar, Ron Dickinson, and Peh Shirley, "A study on Fluorine-Induced Corrosion on Microchip Aluminum Bond Pads". in The Proceeding from the 29th International Symposium for Testing & Failure Analysis (ISTFA 2003), Phoenix USA, 249-255, 2003, doi: 10.1002/ sia.740211003

[5] K. Ernst, R. Hauert, E. Holländer, "The Fluorine-induced corrosion of Aluminum microchip bond pads", Surface and Interface analysis, vol.21, 691-696, 1994, doi: 10.1002/sia.740211003

[6] R.S. Sethu, "Reducing non-stick on pad for wire bond: A review" Australian Journal of Mechanical Engineering, **9**(2), 147-160, 2012, doi: 10.7158/M11-771.2012.9.2

[7] H. Younan, Nistala Ramesh Rao and Teong Jennifer, "Studies of Fluorine-induced Corrosion and Defects on Microchip Al Bond pads and Elimination Solutions" in The Proceedings from the 34th International Symposium for Testing and Failure Analysis, Portland USA, 285-290, 2008, doi: 10.1361/cp2008istfa285

[8] P.Chang, H.L Hsiao, C.H Cheng, S.I.Chu, H.W.Tai, Y.Y Shieh, C.Y Sun, "Investigation of Fluorine Induced Probe Marker Discoloration," in *2013* IEEE 15th Electronics Packaging Technology Conference (EPTC 2013), Singapore, 139-142, 2013, doi: 10.1109/EPTC.2013.6745700

[9] J.H. Linn, W. E. Swartz Jr., "An XPS study of the plasma etching of aluminum with CCl4", Spectroscopy Letters, **18**(5), 335-352, 1985, dio: 10.1080/00387018508062236

[10] W.F. Hsieh, Henry Lin, Vincent Chen, Irene Ou and Y.S. Lou, "The Investigation of Fluorine Induced Novel Probe Marker Discoloration", in The Proceeding from the 44th International Symposium for Testing & Failure Analysis (ISTFA 2018), Phoenix USA, 413-417, 2018.

[11] W. F. Hsieh, H. Lin, V. Chen, I. Ou and Y. S. Lou, "The probe marker discoloration on Al pad and wafer storage," 2019 IEEE 26th International Symposium on Physical and Failure Analysis of Integrated Circuits (IPFA), Hangzhou, China, 1-4, 2019, doi: 10.1109/IPFA47161.2019.8984909.

ASTES

Advances in Science, Technology and Engineering Systems Journal Vol. 5, No. 5, 426-433 (2020)

www.astesj.com

Special Issue on Innovative Research in Applied Science, Engineering and Technology

ASTESJ

ISSN: 2415-6698

Shape Optimization of Planar Inductors for RF Circuits using a Metaheuristic Technique based on Evolutionary Approach

Imad El Hajjami[*,1], Bachir Benhala[1], Hamid Bouyghf[2]

[1]*Faculty of Sciences, Moulay Ismail University, Meknes, 50050, Morocco*

[2]*FSTM Mohammedia, Hassan II University, Casablanca, 20000, Morocco*

ARTICLE INFO

Article history:
Received: 14 July, 2020
Accepted: 08 September, 2020
Online: 21 September, 2020

Keywords:
Optimization
Integrated Inductors
Evolutionary Algorithms
Quality Factor
RF Circuits

ABSTRACT

In this article, we concentrate on the use of a metaheuristic technique based on an Evolutionary Algorithm (EA) for determining the optimal geometrical parameters of spiral inductors for RF circuits. For this purpose, we have opted for an optimization procedure through an enhanced Differential Evolution (DE) algorithm. The proposed tool allows the design of optimized integrated inductors not only with a maximum quality factor(Q), but also with a maximum self-resonant frequency (SRF), and a minimum surface area, in addition to being adapted to any model of any technology. This paper presents also a comparison between performances of the optimized inductors (inductor square shape and inductor circular shape), in terms of the quality factor, SRF, and circuit size. For the purpose of mitigating the impact of parasitic effects, design basics have been taken into consideration. Then, in order to investigate the efficacy of evaluated results, an (EM) simulator has been employed.

1. Introduction

Integrated Inductors are of paramount importance elements, layout-optimization for spiral inductors has been the focus issue of several studies for the last few years, as for application, the four main characteristics that are required for the design of spiral inductors are: high inductance, high current capability, energy density, and low losses, with the inductors properties being identified by its geometrical and technological parameters [1].

For the sizing of spiral inductors, the designer should consider three main parameters [2], [3], the inductance value which is one of the most sensitive parameters, then, the quality factor (Q), and finally the self-resonant frequency (SRF).

Many works have been conducted for the sake of modeling and optimizing of spiral inductors. Formulation, modeling, and implementation remain the main steps for designing an integrated inductor [4], [5]. However, to ameliorate the optimization, the operation could be repeated many times till an acceptable solution is found.

Metaheuristic's techniques are especially applied to the optimal sizing of analog circuits [6], such techniques have proven to be efficient in solving difficult problems because they necessitate less time to converge and yield better solutions.

In this field, the methods mostly used are EA: 'Evolutionary Algorithms ' [7], such as the Differential Evolution (DE) Algorithm [8], and the Genetic Algorithm (GE) [9], [10], but in the last two decades, a new group of nature-inspired heuristic optimization algorithms have been introduced as SI: 'Swarm Intelligence Techniques', such as Ant Colony Optimization (ACO) [11], [12], Gravitational Search Algorithm (GSA) [13], Artificial Bee Colony (ABC) [14], Dragonfly Algorithm (DA) [15], Particle Swarm Optimization (PSO) [16], Grey Wolf Optimizer (GWO) [17], and Bacterial Foraging Optimization (BFO) [18].

Nevertheless, for the sake of achieving the optimal sizing of the (RF) spiral inductors, the Differential Evolution (DE) is to be the focus technique in this paper since it has been widely used in circuit design in the last decade.

In order to design circular and square spiral inductors for operating frequencies around 2.5 GHz, the inductor π-model has been embedded in the improvement device.

The next sections of the paper layout introduce as follows: Section 2 is devoted to the descriptions of the inductor π-model used, afterward, section 3 provides the synopsis of the DE

[*]Corresponding Author: Imad El hajjami, i.elhajjami@edu.umi.ac.ma

algorithm, while the optimal values of DE parameters have been determined by a proposed technique. Then, section 4 highlights the inductor sizing-optimization method, the technological parameters, and the design constraints as well, besides, the optimization results are presented, where analytical results obtained with DE are investigated by ADS momentum simulation software. Last and not least, the conclusion is offered in section 5.

2. Planar Spiral Inductors

All the shapes of spiral inductor known by four main geometrical parameters, the spacing between lines (s), the number of turns (n), the line width (w), and the outer length of a side (d_{out}), while the inner length of a side (d_{in}) defined by: $d_{in} = (d_{out} - 2.(n .(s + w) - s))$.

There are other important geometry parameters such the inductor length, while: $L = 4.n.d_{avg}$ for the square shape, and $L = 4.n.d_{avg}$ for the circular shape, then, the inductor area: $A=d_{out}^2$, and finally, the average diameter: $d_{avg} = 0.5.(d_{out} + d_{in})$.

Layouts of the circular and the square inductor have been showing respectively in Figure 1 and Figure 2 [19].

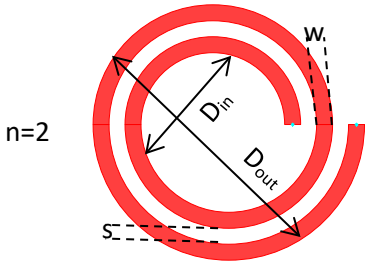

Figure 1: Layout of the Circular Integrated Inductor

2.1. The electrical Model of Integrated Inductors

It is important, thus, to present the expressions of the electrical model components for the inductor π-model, Figure 3 presented the electrical circuit for this type, while, C_s, C_{si}, C_{ox}, R_s, and R_{si} are respectively the substrate capacitance, the series capacitance between the spiral and the metal underpass, the substrate-oxide capacitance, the series resistance, and the substrate resistance, these parameters are determined by equations (1 2,3,4,5,6,7,8, 9):

$$C_{ox} = \frac{l.\omega.\varepsilon_{ox}}{2.t_{ox}} \quad (1)$$

$$C_s = \frac{(n.\varepsilon_{ox}).w^2}{t_{ox,m1-m2}} \quad (2)$$

$$C_{si} = \frac{C_{sub}.l.w}{2} \quad (3)$$

$$C_{sub} = \frac{\varepsilon_{sub}}{h_{sub}} \quad (4)$$

$$R_{si} = \frac{2}{(G_{sub}.l.w)} \quad (5)$$

$$G_{sub} = \frac{\sigma_{sub}}{h_{sub}} \quad (6)$$

$$R_s = \frac{l}{\sigma_m.\delta.\omega\left(1 - \exp\left(-\frac{t}{\delta}\right)\right)} \quad (7)$$

$$\delta = V\frac{2}{\omega.\mu.\sigma} \quad (8)$$

$$\sigma_m = \frac{1}{t.R_{sh}} \quad (9)$$

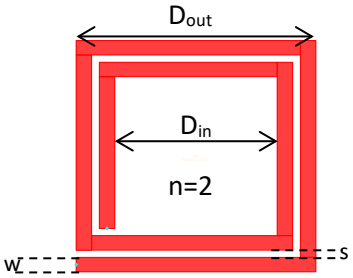

Figure 2: Layout of the Square Integrated Inductor

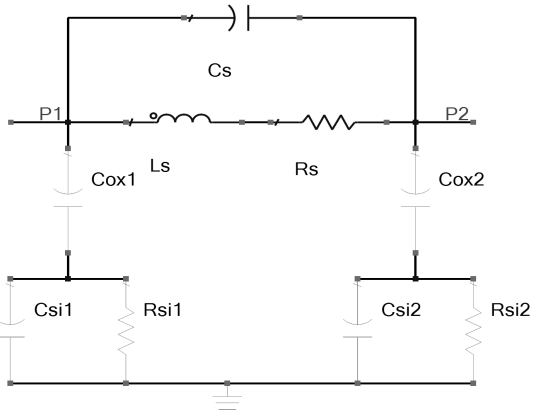

Figure 3: Integrated Inductor Electrical π -Model

where (t) is the turn thickness, (t_{ox}) is the oxide thickness between the spiral and the substrate, (σ_m) is the conductivity of the metal, (ω) is the frequency, ($t_{ox, M1-M2}$) is the oxide thickness between the spiral and the under-pass, (ε_{ox}) is the oxide permittivity, (G_{sub}) is the substrate conductance per unit area, (C_{sub}) is the substrate capacitance per unit area, (h_{sub}) is the substrate height, (σ_{sub}) is the substrate conductivity, (δ) is the skin depth, (μ) is the magnetic permeability of free space, and finally, (R_{sh}) is the sheet resistance.

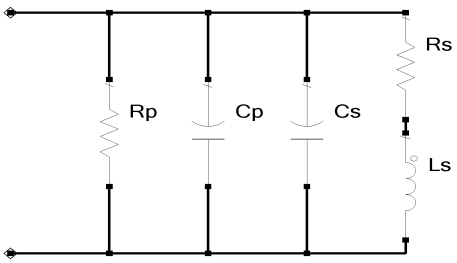

Figure 4: The Parallel π-Equivalent Circuit of Integrated Inductors

A similar inductor model has been shown in Figure 4, the quality factor (Q) was calculated by equations (10) and (11), where (C_p) is the shunt capacitance, and (R_p) is the shunt resistance.

$$Rp = \frac{1 + (\omega . Rsi(Csi + Cox))^2}{Rsi . \omega^2 . Cox^2} \quad (10)$$

$$Cp = \frac{(\mathrm{Cox} + Rsi^2 . \omega^2 (\mathrm{Csi} + \mathrm{Cox}) \mathrm{Csi} . \mathrm{Cox})}{1 + (Rsi . \omega (Csi + Cox))^2} \quad (11)$$

2.2. Inductance Ls

The model of the inductance L_s for the square inductor is expressed [19], [20] in equation (12):

$$Ls = \beta . dout^{\alpha 1} . w^{\alpha 2} . davg^{\alpha 3} . n^{\alpha 4} . s^{\alpha 5} \quad (12)$$

$\beta = 0.00166, \quad \alpha 2 = -0.125 \quad \alpha 4 = 1.83$
$\alpha 1 = -1.33, \quad \alpha 3 = 2.50, \quad \alpha 5 = -0.022$

The expression of the inductance L_s for the circular inductor is given in equation (13) [21]:

$$Ls = \frac{\mu_0 . n^2 . d_{avg} . c_1}{2} \left(\ln \left(\frac{c_2}{\rho} \right) + c_3 . \rho + c_4 . \rho^2 \right) \quad (13)$$

$c_1 = 1.00 \quad c_3 = 0.00$
$c_2 = 2.46 \quad c_4 = 0.20$

The coefficients c_i, β, and α_i are not depending on the technology but on the structure of the inductor. With ρ is the fill ratio, inductances in nH, and dimensions in µm.

The expression of the inductance for a given frequency (f) for two ports [20] defined as follow:

$$L = \left(\frac{1}{2\pi f} \right) . imag \left(\frac{1}{-Y(2,1)} \right) \quad (14)$$

2.3. The Quality factor (Q)

The quality factor is presented as follows:

$$Q = 2\pi * Energy\ stored / energy\ dissipated \quad (15)$$

The Q-Factor can be formed as:

$$Q = \left(\omega . \frac{Ls}{Rs} . \frac{2 . Rp}{2 . Rp + Rs . \left(\left(\omega . \frac{Ls}{Rs} \right)^2 + 1 \right)} \right) \times \left(1 - (Cs + 0{,}5 . Cp) . \left(\frac{Rs^2}{Ls} + \omega^2 . Ls \right) \right) \quad (16)$$

An ideal inductor has an infinite Quality factor [19].

When the peak magnetic energy is the same as the electric energy, the Q-Factor is equal to zero, this phenomenon is defined as the self-resonant frequency phenomena.

The energy stockpiled in the inductor is attached to the imaginary part of the input admittance (Y_{in}), whereas the real part of (Y_{in}) is proportional to the energy dissipated in resistances, with this approach is abridged to [20]:

$$Q = \frac{imag(-Y(1,1))}{Real(Y(1,1))} \quad (17)$$

3. The Differential Evolution Algorithm

It is possible to say that the DE algorithm, as is the genetic algorithm, is a population-based using identical operators' mutation, crossover, and selection. However; what makes the genetic algorithms yield a better solution is the fact that it builds on the crossover operation while the DE builds on the mutation one [8].

At the beginning of the DE process, the population of the n-pop solution vectors is randomly selected. This population is then ameliorated by stratifying mutation, crossover, and selection operators. First, the algorithm uses the mutation process as its search mechanism. Then, the DE uses crossover (recombination) operators, and the child vector that takes parameters from one parent more than the other. Afterward, a selection process is carried out in order to change the parent vectors if their fitness is less than of the newly generated child vectors. This three-stage process is repeated until a better solution is found [22].

The principal steps of the DE algorithm are defined mathematically as follows:

3.1. Mutation

For each objective vector $x_{j,k}$,a mutant vector is generated by (18):

$$v_{j,k+1} = x_{r1,k} - \beta \times (x_{r2,k} - x_{r3,k}) \quad (18)$$

where $j, r_1, r_2, r_3 \in \{1, 2, \ldots, NP\}$ are arbitrary chosen and must be different from each other. In equation (18), *(β)* is the scaling factor which affects the difference vector $(x_{r2,k} - x_{r3,k})$.

3.2. Crossover

The trial vector is produced by the mixture of the parent vector with the mutated vector:

$$u^i_{j,k+1} = v^i_{j,k+1} \quad if \quad (rand \leq Pc) \quad (19)$$
$$u^i_{j,k+1} = x^i_{j,k} \quad if \quad (rand > Pc)$$

where (P_c) is the crossover probability parameter.

3.3. Selection

The comparison between a parent and its identical offspring called the selection and can be expressed as:

$$x_{j,k+1} = u_{j,k+1} \quad if\ g(u_{j,k+1}) \leq g(x_{j,k}) \quad (20)$$
$$x_{j,k+1} = x_{j,k} \quad for\ Otherwise$$

where $g_{(x)}$ is the objective function value of the trial vector. The DE algorithm can be declared in 1:

3.4. The DE Algorithm Parametrization

To determine the optimal values of DE parameters, the Ackley function presented in equation (21) was investigated for 100 population and 1000 number of iterations.

Algorithm 1: Differential Evolution Algorithm

Begin
T=0;
Generate the initial population of individuals N;
Evaluate $g\ (x_{j,\ k})$
For *each individual i in the population* **do**
Choose r_1, r_2, r_3 within the range [1, N] randomly;
For *each parameter j* **do**
Generate the mutant vector with equation (18) ;
Generate a new vector with equation (19);
end for
if $g\ (u_{j,\ k+1}) \leqslant g\ (x_{j,\ k})$ **then**
$x_{j,k+1} = u_{j,k+1}$
else
$x_{j,k+1} = x_{j,k}$
end if
end for
T=T+1;
end

$$f(x) = -20.e^{-0.2\sqrt{\frac{\sum_{i=1}^{n} x_i^2}{n}}} + e^{\frac{\sum_{i=1}^{n}(\cos(2\pi x_i))}{n}} + 20 + e^1 \tag{21}$$

The Ackley function has one global minimum at: f (x_j) = 0; for x_j = (0 , … , 0).

The function evaluated on $x_j \in [-32, 32]$ for all (j = 1 , … , 32) .

Figure 5 displays the variation of fitness convergence according to the crossover probability P_c and the upper bound of the scaling factor $beta_{max}$ (with the lower bound of the scaling factor-beta $_{min}$ equal to 0,1). The cost function versus the number of iterations presented in Figure 6.

From Figure 5, the values of DE parameters that gave the best convergence are presented in Table 1.

4. Inductors Sizing

In the following section, we aim to maximize the Q-Factor for a specific value of the inductance for two structures, square and circular, by combining the inductor π-model and the DE optimization procedure. Afterward, simulations with ADSEM are adopted.

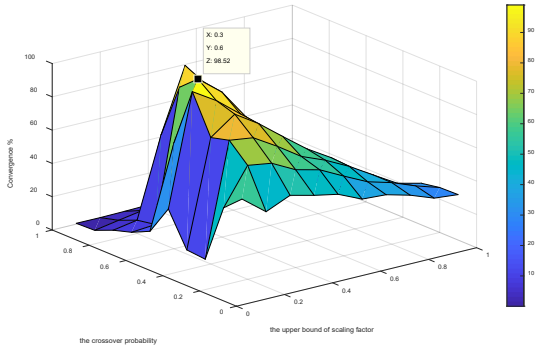

Figure 5: Convergence Rate versus the Crossover Probability and the Upper Bound of the Scaling Factor, with $beta_{min}$=0.1.

4.1. Constraints of the study

To minify the parasitic phenomena [20], [23], the liaison between geometry parameters in (22) is well respected as a sort of included design-rules [20], [23].

$$0.2 \leq \frac{din}{dout} \leq 0.8, \qquad 5w \leq din \tag{22}$$

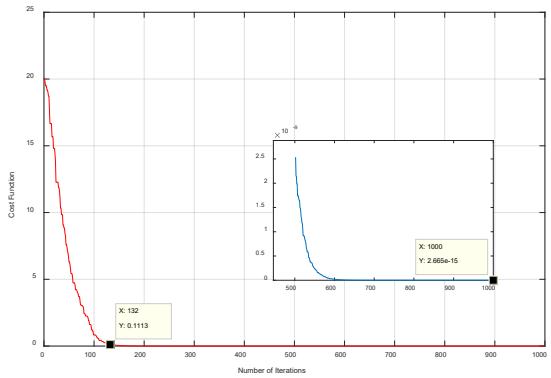

Figure 6: The Cost Function versus the Number of Iterations for the Ackley Function.

Table 1: Parameters Values of the Differential Evolution Algorithm.

Parameter	Value
The crossover probability	0.6
The lower bound of the scaling factor	0.1
The upper bound of the scaling factor	0.3
Population size	100
The number of iterations	500

• *The SRF Constraint*

The condition for a minimum self-resonant frequency which SRF ≥ SRF_{min} can be formed as [20]:

$$\left((2\pi SRF_{Min})^2.Ls.(Cp+Cs) + \frac{(Rs^2.(Cs+Cp))}{Ls}\right) \leq 1 \tag{23}$$

4.2. Optimization Procedure

The goal of this optimization is to find the optimum geometrical parameters of the spiral inductor to get a higher value of Q-Factor, the problem can be formulated as follows:

Find: $D = (Dout, w, s, n)$ (24)
To maximize: Q
Subject to:

$$g_1(x) = Ls = Ls_{req}$$
$$g_2(x) = Q \geq Q_{Min}$$
$$g_3(x) = SRF_{Min} \leq SRF$$
$$g_4(x) \leq 0, g_5(x) \leq 0, g_6(x) \leq 0, g_7(x) \leq 0$$
$$g_8(x) = n_{Min} \leq n \leq n_{Max}$$
$$g_9(x) = s_{Min} \leq s \leq s_{Max}$$
$$g_{10}(x) = w_{Min} \leq w \leq w_{Max}$$
$$g_{11}(x) = Dout_{Min} \leq Dout \leq Dout_{Max}$$

The objective function for the DE was defined as the following:

$$Fcost(x) = \left(\frac{1}{Q} + 10^9(L - Lsreq)\right).P(x) \quad (25)$$

Where :

$$P(x) = \prod_{i=3}^{i=7} Pi(x) \quad (26)$$

Or

$$Pi(x) = 1 + s_i \quad if\ g_i(x) > 0 \quad (27)$$
$$Pi(x) = 1 \quad for\ otherwise$$
$$s_3 = s_4 = s_5 = s_6 = s_7$$

where (s_i) is the penalty coefficient, and P(x) is the sum of constraints.

Constraints $g_8(x)$, $g_9(x)$, $g_{10}(x)$, and $g_{11}(x)$ are boundary constraints, as result, they can be examined, while the DE was not allowed to generate a candidate vector farther these limitations.

Equations of constraints $g_4(x)$, $g_5(x)$, $g_6(x)$, and $g_7(x)$ have been shown in Table 2.

4.3. Results and Discussions

In the following, we will be adopting a sizing of square and circular inductors, with distinct values of the inductance Ls_{req} in the field beyond 2.5 GHz, as shown in Table 3 the technological and physical parameters have been well presented, while Table 4 represents the geometry parameter boundaries.

The details of the optimization have been presented in Table 5 and Table 6. On aim to verify our procedure, Figure 7 gives the cost function versus the number of iterations for square inductors, in this case, the constraint for minimum self– resonant frequency is added as SRF_{min}=22 GHz. The optimization results of the maximum Q-Factor and area (A) for both circular and square inductors versus the inductance obtained using the DE algorithm are presented in Figure 8.

The Q-Factor versus frequency for each value of the inductance has been shown in Figure 9 and Figure 10. The simulation using momentum software has also been shown in Figure 11, Figure 12, Figure 13, and Figure 14.

The comparison between optimization results and simulations is presented in Table 7 and Table 8.

Table 2: Equations of Constraints.

Constraint	Equation
$g_4(x)$	(D_{in}/D_{out})-0.8
$g_5(x)$	0.2-(D_{in}/D_{out})
$g_6(x)$	(2.n+1).(s+w)-D_{out}
$g_7(x)$	(5.w-D_{in})

Table 3: The values of technological parameters.

Symbol	Parameter	Value
t	Metal thickness	2.8 µm
σ	Metal conductivity	4×10^7 Ω/m
ρ	Substrate resistivity	0.2 Ω.m
t_{sub}	Substrate thickness	600 µm
t_{ox}	The thickness of the oxide	6.42 µm
ε_r	The relative permittivity of the silicon	11,9
µ	The magnetic permeability of free space	$4\pi \times 10^{-7}$ H/m
$t_{ox_m1\text{-}m2}$	Oxide thickness between spiral and underpass	0.66 µm
ε_r	The relative permittivity of the Oxide	4
ε_0	Permittivity of vacuum	8.85×10^{-12} F/m

Table 4: Sizing Variables and their Allowable Ranges.

Sizing variable	Lower bound	Upper bound
w	1 µm	12 µm
d_{out}	140 µm	280 µm
s	2 µm	2.5 µm
n	1.50	12.00

Table 5: Optimization Results of Circular Inductors using the DE Algorithm.

Ls_{req}	Ls_{An}	D_{out}	w	s	n	Q
1.00	1.00	166.12	12.00	2.38	3.50	8.26
3.00	3.00	220.00	12.00	2.32	5.50	11.44
5.00	5.00	238.85	11.30	2.03	7.00	12.91
7.00	7.00	261.11	11.10	2.00	8.00	13.34
9.00	9.00	268.03	10.13	2.00	9.00	12.90
11.00	11.00	265.34	8.81	2.00	10.00	12.16
13.00	13.00	280.00	8.60	2.00	10.50	11.57
15.00	15.00	273.35	7.66	2.00	11.50	11.13

Table 6: Optimization Results of Square Inductors using the DE Algorithm.

Ls_{req}	Ls_{An}	D_{out}	w	s	n	Q
1.00	1.05	140.00	12.00	2.00	2.50	9.74
3.00	2.97	201.00	11.99	2.00	3.50	13.13
5.00	4.99	230.00	10.14	2.00	4.00	13.22
7.00	7.00	240.00	8.37	2.00	4.50	12.48
9.00	9.00	250.20	7.69	2.00	5.00	12.28
11.00	11.00	260.00	7.45	2.00	5.50	12.21
13.00	13.00	267.00	7.24	2.00	6.00	12.01
15.00	15.00	272.00	7.01	2.00	6.50	11.69

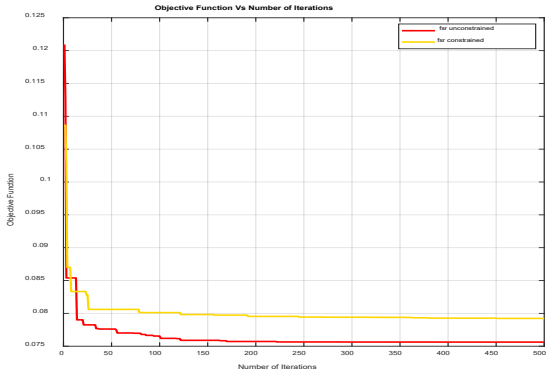

Figure 7: The Objective Function versus Iterations Number for a Square Inductor.

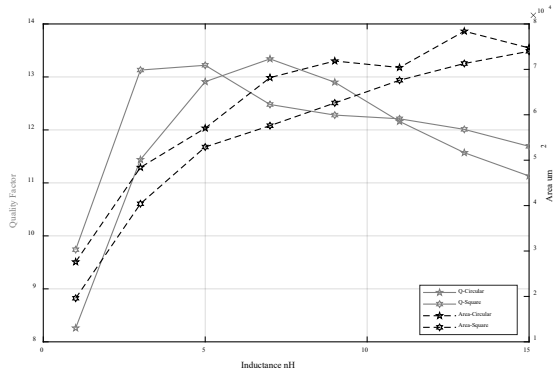

Figure 8: The Quality Factor and Inductors Area versus Inductance.

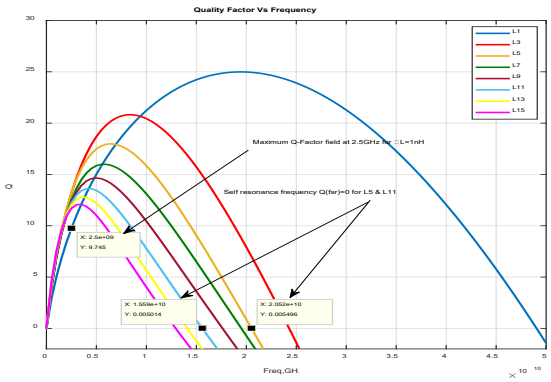

Figure 9: The Quality Factor of Square Inductors versus Frequency.

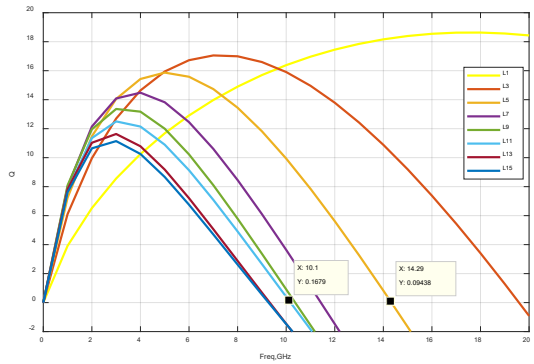

Figure 10: The Quality Factor of Circular Inductors versus Frequency.

What the results show is that when the inductance value increases, the quality factor decreases, and the self-resonant frequency decreases as well.

However, the results are very good in terms of the circuit's size, and the constraints are very robust.

The DE algorithm provides better results concerning the circuit's size and has a faster convergence as shown in the results.

We can notice that the simulation of square inductors is very accurate, with an error below 8.50% for the inductance value, and 5.21% for the quality factor for L_s less than 11 nH. It is possible to explain the increase of the error when the value of inductance is greater than 11 nH, in that we have taken similar limits of geometrical parameters for all values of the inductance, when the value of L_s has augmented, the number of turns became higher and D_{out} increased with a small percentage, in such circumstances, the quality factor decreases owing to the parasitic phenomena effects, this problem can be solved by increasing the parameters of the allowable range in the proportion of the outer diameter.

As for the circular inductor, generally, the error is below than 5.66% for inductance value, and 21.56% for the quality factor, Although, this type has the shortest perimeter, and with a circular configuration, a higher quality factor (Q) is obtained. Yet, this type shows a response to the parasitic phenomena effects.

We notice through the simulation that the circular inductor is not significantly affected by parasitic phenomena in terms of the self-resonant frequency. From Figures 10 and 13, we observe that the inductor of L_s equal to 11 nH reaches its maximum of Q-Factor when $f_{max} \sim 2$ GHz, the area on the left of f_{max}, is an area where the Q-Factor is fundamentally affected by the magnetic induced losses, skin and proximity effects, and the DC resistance [24],[25]. On the opposite side of f_{max}, in addition to the preceding effects, the Q-Factor is also affected by the substrate noise coupling [23]. The evaluated SRF equal to 10.1 GHz, and the SRF obtained via simulation equal to 8.5 GHz, at this time, the Q-Factor is equal to 0, starting from this point, the peak magnetic energy is less than the electric energy, due to the perturbation of this last because of the parasitic phenomena.

The layout constraints for circular inductors required extensive research, in order to mitigate the parasitic phenomena effects.

Moreover, the degradation of the Q-Factor can be seen more clearly for square inductors, from Figures 9 and 11, for L_s equal to 11 nH, the Q-Factor equal to 0 when the evaluated SRF equal to 15.59 GHz and the SRF obtained via simulation equal to 7 GHz, we conclude that this type is extremely influenced by the parasitic phenomena.

Table 7: Comparison between Optimization Results and Momentum Simulations for Circular Inductors.

Ls_{An}	Ls_{EM}	ϵ%	Q_{AN}	Q_{EM}	ϵ%
1.00	1.25	25.00	8.26	9.20	11.80
3.00	2.96	1.33	11.44	10.82	5.41
5.00	4.81	3.80	12.91	11.34	12.16
7.00	6.72	4.00	13.34	10.94	16.50
9.00	8.49	5.66	12.90	11.29	12.48
11.00	11.32	2.90	12.16	9.86	18.91
13.00	13.28	2.15	11.57	9.40	18.75
15.00	15.35	2.33	11.13	8.73	21.56

Table 8: Comparison between Optimization Results and Momentum Simulations for Square Inductors.

Ls_{An}	Ls_{EM}	ϵ%	Q_{AN}	Q_{EM}	ϵ%
1.05	0.96	8.50	9.74	10.09	3.59
2.97	2.78	6.39	13.13	13.65	3.96
4.99	4.74	5.01	13.22	13.66	3.32
7.00	6.78	0.80	12.48	13.97	4.25
9.00	8.72	3.14	12.28	13.12	5.21
11.00	10.79	1.90	12.21	12.15	0.49
13.00	12.74	2.00	12.01	10.81	10.00
15.00	14.85	1.00	11.69	9.67	17.27

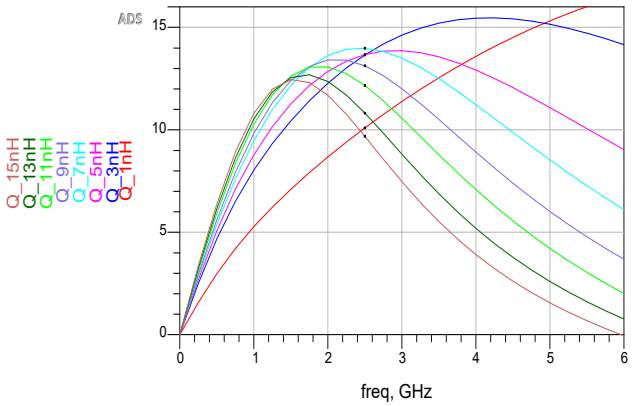

Figure 11: Simulation of the Quality Factor versus Frequency in Momentum for Square Inductors.

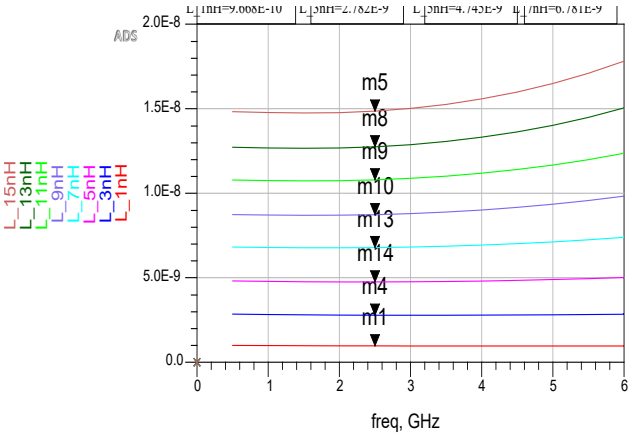

Figure 12: Simulation of the Inductance versus Frequency in Momentum for Square Inductors.

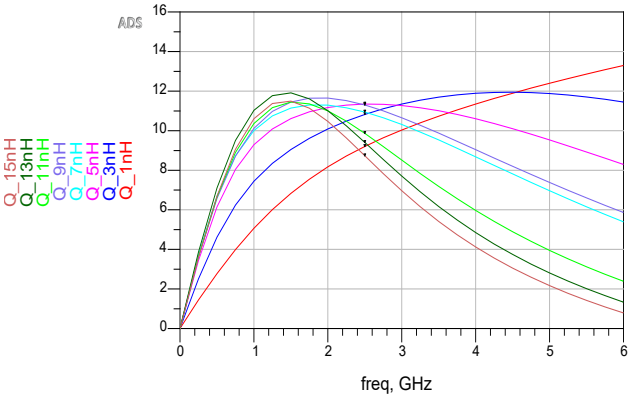

Figure 13: Simulation of the Quality Factor versus Frequency in Momentum for Circular Inductors.

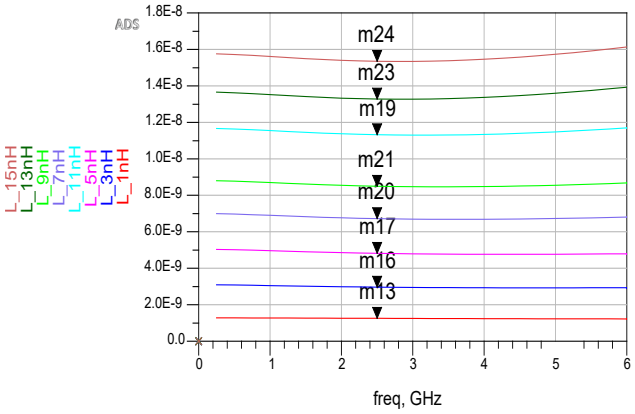

Figure 14: Simulation of the Inductance versus Frequency in Momentum for Circular Inductors.

5. Conclusion

For dealing with the optimal sizing of spiral inductors for (RF) circuits, we proposed on this paper an application of the Differential Evolution (DE) algorithm. Two inductor structures have been optimized i.e. shape square and shape circular, with a maximum Q-Factor, a maximum self-resonant frequency (SRF), and a minimum surface area. The performances of optimized inductors showed good results in terms of the Q-Factor, with the square inductor presenting a higher SRF and a smaller area (A) than the circular one.

The π-model does not allow for the assimilation of noises parasitic effects in a good way, leading to a lower SRF value, that is why we are focusing on using the double π-model, instead, for the integrated inductors optimal sizing.

References

[1] J. M. Lopez-Villegas, J. Samitier, C. Cane, P. Losantos, J. Bausells, "Improvement of the quality factor of RF integrated inductors by layout optimization," IEEE Transactions on Microwave Theory and Techniques, **48**(1), 76–83, 2000, https://doi.org/10.1109/22.817474

[2] H. M. Hsu, K. Y. Chan, H. C. Chien, H. C. Kuan, "Analytical design algorithm of planar inductor layout in CMOS technology," IEEE Transactions on Electron Devices, **55**(11), 3208–3213, 2008, https://doi.org/10.1109/TED.2008.2004248

[3] J. N. Burghartz, B. Rejaei, "On the design of RF spiral inductors on silicon," IEEE Transactions on Electron Devices, **50**(3), 718–729, 2003, https://doi.org/10.1109/TED.2003.810474

[4] Y. Yorozu, M. Hirano, K. Oka, Y. Tagawa, "Improvement of the quality factor of RF integrated inductors by layout optimization," IEEE Transactions on Microwave Theory and Techniques, **48**(1), 76–83, 2000, https://doi.org/10.1109/22.817474

[5] S. Abi, H. Bouyghf, A. Raihani, B. Benhala, "Swarm intelligence optimization techniques for an optimal RF integrated spiral inductor design," in 2018 International Conference on Electronics, Control, Optimization and Computer Science (ICECOCS), Kenitra, Morocco, 1–7, 2018, https://doi.org/10.1109/ICECOCS.2018.8610524

[6] P. Siarry, Z. Michalewicz, Advances in metaheuristics for hard optimization, Natural Computing Series, Springer, 2008.

[7] M. Crepinsek, S. H. Liu, M. Mernik, "Exploration and exploitation in evolutionary algorithms: A survey," ACM Computing Surveys, **45**(3), Article 35, 2013, https://doi.org/10.1145/2480741.2480752

[8] R. Storn, K. Price, "Differential evolution: A simple and efficient heuristic for global optimization over continuous spaces," J. Global Optimization, **11**(4), 341–359, 1997, https://doi.org/10.1023/A:1008202821328

[9] A. El Beqal, B. Benhala, I. Zorkani, "A Genetic algorithm for the optimal design of a multistage amplifier," International Journal of Electrical and Computer Engineering, **10**(1), 129–138, 2020, http://doi.org/10.11591/ijece.v10i1.pp129-138

[10] M. Mitchell, An introduction to genetic algorithms, The MIT Press, 1998.

[11] B. Benhala, "Sizing of an inverted current conveyors by an enhanced ant colony optimization technique," in 2016 Conference on Design of Circuits and Integrated Systems (DCIS), Granada, Spain, 1–5, 2016, https://doi.org/10.1109/DCIS.2016.7845271

[12] L. Kritele, B. Benhala, I. Zorkani, "Ant Colony Optimization for Optimal Low-Pass Filter Sizing," in: E. G. Talbi, A. Nakib. (Eds.), Bioinspired Heuristics for Optimization, Studies in Computational Intelligence, Springer, Cham, 283–299, 2019, https://doi.org/10.1007/978-3-319-95104-1_18

[13] E. Rashedi, H. Nezamabadi, S. Saryazdi, "GSA: A gravitational search algorithm," Information Sciences, **179**(13), 2232–2248, 2009, https://doi.org/10.1016/j.ins.2009.03.004

[14] C. J. Lin, M. L. Huang, "Modified artificial bee colony algorithm for scheduling optimization for printed circuit board production," Journal of Manufacturing Systems, **44**(1), 1–11, 2017, https://doi.org/10.1016/j.jmsy.2017.04.006

[15] S. Mirjalili, "Dragonfly algorithm: A new meta-heuristic optimization technique for solving single-objective, discrete, and multi-objective problems," Neural Computing and Applications, **27**(4), 1053–1073, 2016, https://doi.org/10.1007/s00521-015-1920-1

[16] B. Benhala, P. Pereira, A. Sallem, Focus on swarm intelligence research and applications, Nova Science Publishers, 2017.

[17] S. Mirjalili, S. M. Mirjalili, A. Lewis, "Grey wolf optimizer," Advances in Engineering Software, **69**, 46–61, 2014, https://doi.org/10.1016/j.advengsoft.2013.12.007

[18] K. M. Passino, "Biomimicry of bacterial foraging for distributed optimization and control," IEEE control systems Magazine, **22**(3), 52–67, 2002, https://doi.org/10.1109/MCS.2002.1004010

[19] C. P. Yue, C. Ryu, J. Lau, T. H. Lee, S. S. Wong, "A physical model for planar spiral inductors on silicon," in International Electron Devices Meeting, Technical Digest, San Francisco, USA, 155–158, 1996, https://doi.org/10.1109/IEDM.1996.553144

[20] S. S. Mohan, M. del Mar Hershenson, S. P. Boyd, T. H. Lee, "Simple accurate expressions for planar spiral inductances," IEEE Journal of Solid-State Circuits, **34**(10), 1419–1424, 1999, https://doi.org/10.1109/4.792620

[21] B. Rejaei, J. L. Tauritz, P. Snoeij, "A predictive model for si-based circular spiral inductors," in Topical Meeting on Silicon monolithic integrated circuits in RF systems, Ann Arbor, 148–154, 1998, https://doi.org/10.1109/SMIC.1998.750210

[22] D. Karaboga, B. Akay, "A comparative study of Artificial Bee Colony algorithm," Applied Mathematics and Computation, **214**(1), 108–132, 2009, https://doi.org/10.1016/j.amc.2009.03.090

[23] P. Pereira, M. H. S. Fino, F. V. Coito, M. V. Neves, "RF integrated inductor modeling and its application to optimization-based design," Analog Integrated Circuits and Signal Processing, **73**, 47–55, 2011, https://doi.org/10.1007/s10470-011-9682-x

[24] J. Aguilera, R.Berengue, Design and test of integrated inductors for RF applications, Dordrecht: Kluwer Academic Publishers, 2004.

[25] Y. Cao , R. A. Groves, X. Huang, N. D. Zamdmer, and al, "Frequency-independent equivalent-circuit model for on-chip spiral inductors," IEEE Journal of Solid-State Circuits, **38**(3), 419–426. 2003, https://doi.org/10.1109/JSSC.2002.808285

ASTES

Advances in Science, Technology and Engineering Systems Journal Vol. 5, No. 5, 434-443 (2020)

www.astesj.com

Special Issue on Innovative Research in Applied Science, Engineering and Technology

ASTESJ

ISSN: 2415-6698

New Algorithm for the Development of a Musical Words Descriptor for the Artificial Composition of Oriental Music

Mehdi Zhar*, Omar Bouattane, Lhoussain Bahatti

SSDIA Laboratory, Ecole Normale Supérieur de l'Enseignement Technique (ENSET), Mohammedia, 28810, Morocco

ARTICLE INFO

Article history:
Received: 14 July, 2020
Accepted: 08 September, 2020
Online: 21 September, 2020

Keywords:
Artificial Intelligence
Music
Musical Grammar
Alphabets
¼ de ton
Filtering

ABSTRACT

The Music Composition Library of the great composers constitutes an intellectual heritage. This article introduces an algorithm of artificial Oriental composing music based on the descriptors determined on a large learning base to automatically write Oriental music as the logic identical to any composer. Musical words are called a grammatical alphabet. Each word derived is created with the descriptors through its very own alphabet by crossing a number of filters removing all improper combinations and maintaining the features correctly responding with each filtering process while honoring the grammar of oriental music. A musical word is a combination of a rhythmic word and a symbolic word.

1. Introduction

Over the last years, Methods of experimental studies applied to the musical field have improved considerably. Only think of an ever-increasing amount of music sites that stream. There are nearly as many options to catalog and label music recordings as there are websites today. What features may be used to execute these processes though? What elements of the song will be taken into consideration when deciding descriptors used and What is the essence of music composing?

There is currently no method or rationale for an artificial arrangement for oriental music in a composer's style and manner. In comparison, numerous analyses have been established in the sense of occidental music.

Musical composition is an art based on the learning baggage that the composer learns implicitly by listening to a varied set of musical styles, we suppose that in the human being there are natural algorithms that allow in a very intelligent way to analyze, calculate and measure the stored data on a natural learning basis in effort to allow new creations and innovations, and we suppose that is the case of composer who produces new musical phrases.

Based on this idea that our work will reposition itself. The oriental music artificial by appealing to the ideas and thoughts of the great composers of history such as Mohammed ABDELWAHAB, Farid el ATTRACHE and others.

We present here a profound model of the algorithmic composition of the monophonic oriental melodies centered on a description from musical scores in alphabet form controlled by a number of compositional rules allowing for the production of words to constitute musical pieces. We extend the previous model to two distinct tasks: quantifying attributes and writing derivative words, which constitutes a song. The remainder of the paper is structured as follows: In section 2, we discuss the prior works as state-of-the-art on the collection of artificial music composition. Section 3 is devoted to our method modeling. The algorithm in question is developed in section 4. Section 5 is dedicated to Test and validate results. Finally, in section 6, we conclude this article and propose future work related to it.

2. State of the Art

The first studies of mathematical description for compositional music are related according to the literature to (Pierre Barbaud) [1]. From 1957 on, this style of music often referred to like electronic music or automated composition, brought the technical fascination that the Illiac String Quartet Suite created by both the author Lejaren Hiller and also the theorist Leonard M Isaacson, a work produced at the University of Illinois using the Illiac IV (Illinois Accumulator) computer [2]. Many plays consequently in display throughout the day. Use of Markov chains and stochastic processes by combining different theoretical properties that lead to composition [3]-[5]. According to [6], Single process systems will not appear to be successful, a network which is writing songs with harmonic attachment and other models of music composition has

*Corresponding Author Mehdi ZHAR, Email: mehdi.zhar@gmail.com

been presented in [7]-[11]. In the Blues style [12] we find an approach that helps producing monophonic songs of chord progression. Another idea is outlined in a device that produces F0 contour dynamically whenever a partition is provided out of an automated learning frame. This is expressed as a mathematical black box forming a contour of F0 with required characteristics like naturalness & expressiveness [13]. Using the well-established uniform distance from compression as a reference feature, which genetic algorithms can use to produce music automatically in a known style [14]. Neural networks in the thinking process might be helpful [15]-[20]. Neural networks in the thought process could help with more specifics [21]-[25]. A model considers melody and rhythm in tandem when modeling the relation among these two features, this method allows for the creation of fascinating full melodies or suggests alternative a series have broken harmony in accordance with the features of the splitting itself [26]. The classification of the oriental notes was suggested in [27] for identification by a system for modeling a musical sound by collecting a set of harmonic features representing the greatest knowledge found in this sound. Another method of audio classification was described in [28] enhancing the extraction of features using of constant transformation model, including initial musical context-related to audio features where notes occur. The simulation of a lute's sounds is discussed in [29]. Another model that considers notes as abstract functions, we find in [30], an eastern note and a quarter-tone scale pattern. In [31], an automated composition process of eastern music, which allows the generation of derived terms, based on the original features of a selected composer. In [32], the studies highlighted functionalities of SVM on a common songs database of 409 sounds of 16 groups, a comparison of SVM-based distinction Guo was established with other traditional methods, while proposing a new audio recovery criterion, called Boundary Deviation (DFB). [33] work on automated singer identification by distinguishing instrumental and singing sounds using audio information such as timbre parameters, pitch level, mel frequency cepstral coefficients (MFCC), linear predictive coefficients (LPC) and Indian video songs (IVS) audio signal loudness. In [34], an examination of the influence of texture choice on the identification of automated music genres and a novel K-Means-based texture filter aimed at distinguishing different sound textures in each album. The results indicate that the capture of texture heterogeneity within songs is necessary in order to improve the classifier accuracy and also reveal that the K-Means texture selection is capable of achieving substantial improvements over all the baseline using fewer textures per track than that of the other texture selectors examined and that the use of multiple texture representation makes for more possibilities. In [35] authors suggest a new paradigm for the classification of songs, integrating a Bidirectional Recurrent Neural Network dependent attention system. It also incorporates two focus-based models (serial focus and parallel attention). Compared to sequential attention, the parallel focus becomes more robust and the studies yield better results. In [36] an algorithm that illustrates a hierarchical structure from a series of discrete signs by replacing the repeated sentences with a grammatical method generating the sentence. In [37] a study of language identification in the field of artificial intelligence. In [38] a vertical partitioning model based on the Decision Tree mechanism for rhythmic music.

3. Modeling

To grasp the composer's logic composition of opera, symphony or something similar of Arabic musical art, it seems impossible to research a musical score as a whole, although our concept is to research the form and logic of which each word of the partition was composed, recognizing that there are N bars in the piece (play). measures are taken as words and word series forms a musical phrase. Original terms contain some amount of specific information that could be used in artificial compositions as input features. with more precision, our concept is based on the study of the word belonging to a musical piece, the word can contain relevant information forming a thought of the composer that we can decipher using the descriptors, this will allow us to reuse these parameters in order to artificially compose music while respecting the laws applied to the original word

3.1. Originality of Arabic Music

Students learn repertoire and technical methods through oral practice conveyed by a teacher. He evolves after some mastery of those components and places himself in the improvisation game and in the art of making music. He builds on the background of the components conveyed to him as well combine them so according to his desires, or even from that he creates variations that enrich a common repertoire. That oral tradition stays one of the most important elements of the understanding and pedagogy of Eastern music. Hence it is essential to have clear control of rhythmic and melodic structures to compose and analyze Eastern music. Students study melodic parts and never present them precisely as originally recorded. Professional Arabic musicians, like Indian professional musicians and American Jazz musicians, add musical innovations or improvisations to established pieces. Improvisations may be pretty long, converting 10-minute song into one-hour presentations, and often have nothing in common with the initial model. Carries different understanding of what constitutes a specific artist (in the last century, the older aesthetic frame lived side by side with a new aesthetic of modernization and creativity, leading to new combinations and fusions). One could sum up the traditional aesthetics as follows: A professional musician is required to memorize a vast repertoire of tunes, musical words, ornamental techniques, etc., while rarely playing the same song the same manner. Individuality and originality are important-but it can only be appreciated to the degree that it generates and expands hereditary awareness.

3.2. The Alphabet

We consider in our method two alphabets, one rhythmic alphabet, and one symbolic alphabet.

3.2.1 The Symbolic Alphabets

There are seven basic notes (C, D, E, F, G, A, B, S) in both Western and Arabic music plus (S) silence, which is known as a tone. But the peculiarity of the Oriental world comes from the fact that a quarter-tone is present, a note can be assigned to one of five states instead of one of three as in occidental music.

Figure 1: Notes states

Name of notes in traditional Arab vocabulary:

Table 1: Arabic Note Name

Name of Common Arabic Notes	Name of Occidental Notes
ELYAKAH	G (low)
ELTIK YAKAH	G+
ELQARAR ELHISAR	G#/ Ab
ELQARAR ELTIK HISAR	G#+/ Ab-
ELOUCHAÏRAN	A
ELQARAR ELNIM ADJAM	A+
ELQARAR ELADJAM	Bb
ELIRAQ	Bb+
ELQAOUACHT	B
ELTIK ELQAOUACHT	B+
ELRAST	C
ELNIM ELZIRKOULAH	C+
ELZIRKOULAH	C#/Db
ELTIK ELZIRKOULAH	C#+/Db-
ELDOUKAH	D
ELNIM ELKOURDI	Eb-/D+
ELKOURDI	Eb
ELSIKAH	Eb+
ELBOUZALIK	E
ELTIK ELBOUZALIK	E+/F-
ELDJAHARKAH	F
ELNIM ELHEDJAZ	F+/Gb-
ELHEDJAZ	F#/Gb
ELTIK ELHEDJAZ	G-/F#+
ELNAOUA	G (medium)

Bearing in mind the infinity of tones, we inferred infinity of musical notes. Human ear hears frequencies varying between 20 Hz (weakest frequency) to 20,000 Hz (maximum frequency), music culture artists defined this principle in a representation of musical keys.

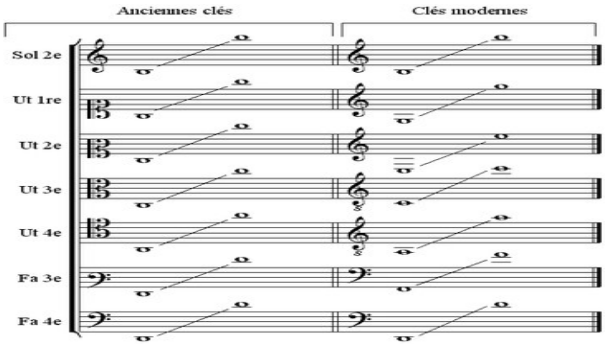

Figure 2: Note range

For this post, for each note, we'll find five states and seven different pitches.

Symbolic Alphabet Matrix:

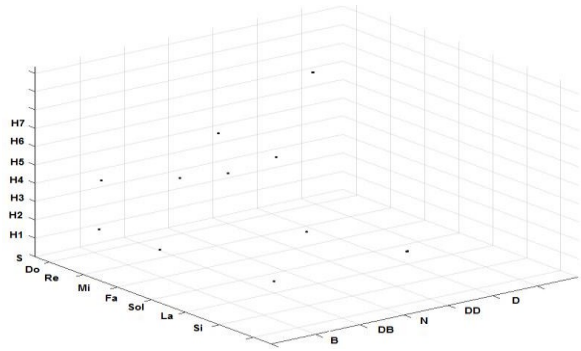

Figure 3: Matrix of the symbolic alphabet

3.2.2 *Ranges Representation*

A scale represents a subset of the alphabet consisting of seven notes of its derivatives plus the (S) silence. We may identify each spectrum at a 49-symbol height representing the terms and their heights. Finally, we have a number of symbols equal to 50.

Maqam:

Improvisation is not a free-for-all of Arabic literature. It must express a specific musical mode (known as maqam), that further means even more than playing on a given scale; so every maqam has a large vocabulary of idiomatic harmonic phrases as well as ornaments which the performer must perfect. Therefore, modulations are required (mood and scale changes), and melodies are required to be opened and closed, for some improvisation in a specific maqam.

Maqam is the term applied to the Eastern music scales, that title means the set of tonal intervals of the seven fundamental notes (as well as five notes in the sense of Eastern pentatonic scales). Scales are named by a note which even the sound was interrupted. oriental Maqam is different from the occidental ones as they are composed of a quarter of a tone while they are still smooth and sharp.

Example of Maqam RAST:

Figure 4: RAST Maqam

In Arabic, Maqam Rast is the title of a maqam (musical mode) and associated music systems. Rast is a Persian term that signifies "true" or "correct." Rast is known as the fundamental maqam in both Iranian and Eastern music, in the very same manner as major scale in occidental music, but in detail, it is unique from the major scale (the big scale is actually kind of like Ajam Maqam). Rast includes a third half flat with a seventh-scale half flat degree.

Tone Interval of Main Maqam:

This table contains our own work to define the interval of oriental maqam.

Table 2: The Interval of Maqam

Rast Genre	Tone Interval of Maqam
Rast	1 - 3/4 - 3/4 - 1 - 1 - 3/4 - 3/4
Kirdane	3/2 - 1/4 - 3/4 - 1 - 1 - 3/4 - 3/4
Sazkar	3/2 - 1/4 - 3/4 - 1 - 1 - 3/4 - 3/4

Suznak	1 - 3/4 - 3/4 - 1 - 1/2 - 3/2 - 1/2
Nairuz	1 - 3/4 - 3/4 - 1 - 3/4 - 3/4 - 1
Yakah	1 - 3/4 - 3/4 - 1 - 3/4 - 3/4 - 1
Dalanshine	1 - 3/4 - 3/4 - 1 - 1 - 3/4 - 3/4
Suzdalara	1 - 3/4 - 3/4 - 1 - 1 - 1/2 - 1
Mahur	1 - 3/4 - 3/4 - 1 - 1 - 1 - 1/2
Bayati Genre	
Bayati	3/4 – 3/4 - 1 - 1 - 2/1 - 1 - 1
Bayati Shuri	3/4 - 3/4 - 1 - 1/2 - 3/2 - 1/2 - 1
Husayni	3/4 - 3/4 - 1 -1 - 3/4 - 3/4 - 1
Muhayyar	3/4 - 3/4 - 1 - 1 - 1/2 - 1 - 1
Nikriz Genre	
Nikriz	1 - 2/1 - 1,5 - 2/1 - 1 - 2/1 - 1
Nawa Athar	1 - 2/1 - 1,5 - 2/1 - 2/1 - 1,5 - 1/2
Athar Kurd	1/2 - 1 - 3/2 - 1/2 - 1/2 - 3/2 - 1/2
Nahawand Genre	
Nahawand	1 - (1/2) / 1 - 1-1 - (1/2) / 1 - 1,5 - 2/1
Farahfaza	1 - 1/2 - 1 - 1 - 1/2 - 3/2 - 1/2
Nahawand Murassa	1 - 1/2 - 1 - 1/2 - 3/2 - 1/2 - 1
Ushaq Masri	1 - 1/2 - 1 - 1 - 3/4 - 3/4 - 1
Hijaz Genre	
Hijaz	1/2 - 1,5 - 1/2 - 1-2 - 1/2 - 1 - 1
Hijazkar	1/2 – 3/2 - 1/2 - 1 - 1/2 - 3/2 - 1/2
Shadd Araban	1/2 – 3/2 - 1/2 - 1 - 1/2 - 3/2 - 1/2
Shahnaz	1/2 – 3/2 - 1/2 - 1 - 1/2 - 3/2 - 1/2
Suzidil	1/2 – 3/2 - 1/2 - 1 - 1/2 - 3/2 - 1/2
Zanjaran	1/2 - 1 - 1/2 - 1 - 3/2 - 1/2 - 1
Kurd Genre	
Kurd	2/1 - 1 - 1 - 1 - 2/1 - 1 - 1
Hijazkar Kurd	1/2 - 1 - 1 - 1 - 1/2 - 1 - 1
Sikah Genre	
Sikah	3/4 - 1 - 1 - 4/3 - 4/3 - 1 – 3/4
Houzam	3/4 - 1 - 2/1 - 1,5 - 1/2 - 1 – 3/4
Rahat al-Arwah	3/4 - 1 - 2/1 - 1,5 - 1/2 - 1 – 3/4
Iraq	3/4 - 1 - 3/4 - 3/4 - 1 - 1 - 3/4
Awj Iraq	3/4 - 1 - 1/2 - 3/2 - 1/2 - 3/2 - 1/4
Bastanikar	3/4 - 1 - 3/4 - 3/4 - 1/2 - 3/2 - 1/2
Mustaar	5/4 - 1/2 - 1 - 1/2 - 1 - 1 - 3/4
Ajam Genre	
Ajam	1 - 1 - 2 - 1 - 1 - 1 - 1/2
Ajam Ouchayrane	1 – 1 - 1/2 - 1 - 1 - 1 - 1/2
Shaouq Afza	1 - 1 - 1/2 - 1 - 1/2 - 3/2 - 1/2
Independents Maqam	
Maqam Jiharkah	1 - 1 - 1/2 - 1 - 1 - 3/4 - 3/4
Maqam Lami	1/2 - 1 - 1 - 1/2 - 1 - 1 - 1
Maqam Saba	3/4 – 3/4 - 2/1 - 1,5 - 2/1 - 1 - 1
Maqam Saba Zamzam	1/2 - 1 - 1/2 - 3/2 - 1/2 - 1 - 1/2
Maqam Sikah Baladi	3/4 - 1 - 3/4 - 1/2 - 1/2 - 3/4 - 1

The scale reduces the number of available alphabets; also, every scale does have its own alphabet specified by the tonal intervals by considering the silence S also as a note into account.

Standard range: A{s, q1; q2; q3; ...; q49} pentatonic range: A{s, q1; q2; q3; ...; q35}.

3.2.3 The Rhythmic Alphabet

A musical note's shape-or number-defines its duration, and it shapes the musical rhythm by integrating the various durations. There are many types of note and specific silences or figures: Round, White, Black, Eighth, Sixteenth, Sixteenth, Triple Eighth, Quadruple Eighth, dotted notes, etc.

Example:

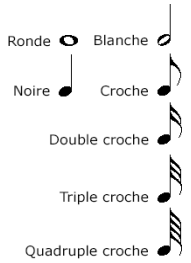

Figure 5: Rhythmic alphabet

Every note pattern's rhythm has always been worth twice as much as that which follows. We should find, in our analysis, the following set of durations (1/16, 3/32, 7/64, 1/48.1/48.1/48, 1/8, 3/16, 7/32, 1/24.1/24.1/24, 1/4, 3/8, 7/16, 1/12.1/12.1/12, 1/2, 3/4, 7/8, 1/6.1/6.1/6, 1, 3/2, 7/4, 1/3.1/3.1/3, 2, 3, 7/2, 2/3.2/3.2/3, 4, 6, 7, 4/3.4/3.4/3)

Every musical word is a mixture of symbols belongs to a symbolic alphabet and also has a length belongs to a rhythmic alphabet; the construction of musical words refers to the concatenation of a number of symbolic alphabets aligned to their rhythmic alphabet.

4. Proposed Algorithms

We suggest two algorithms: the first feeds a research base with calculated descriptors and second produces measurements involving derived terms that, while taking into account the grammar of western music, follow the same constraints as the original words in the study base.

4.1. Learning Steps

We will present a learning algorithm in this section, based on descriptors we described before. Those descriptors constitute the necessary details about a score's musical metric. 11 information's piece of fundamental for extracting from the initial term while respecting laws of Eastern musical grammar, condition of distance among the notes shall be regulated by scale, note and, note figures.

The measure in the first sense is a segmentation of the interval between musical discourse. In other words, measure is the separation of a musical piece into equal parts of the same duration.

Vertical bars on the staff show this section named measuring bars. This is determined by a certain number of periods-times being units for period calculation. Furthermore, the metric should be used as a broader unit of measurement that requires multiple periods in this respect.

Figure 6: The Measure

A bar includes two kinds of information, essential information describing the form of the music (rhythm, harmony, polyphony), and details of expression called nuances. In Western music, nuance is a symbol indicating the relative strength of note, a phrase, or a whole passage of a musical composition. During their performance, the nuances permit the musician to reproduce the dynamics of the work.

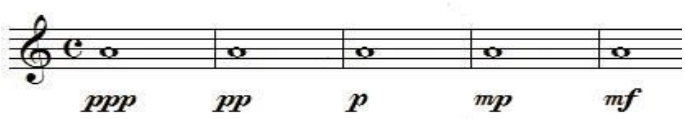

Figure 7: The Nuances

In comparison, the use of variations is almost absent in Arabic music. The peculiarity of oriental music lies with the fact that, in an ensemble, each musician will perform the same song but with different nuances. For this reason, nuances are excluded from this work.

Figure 8: The Absence of Nuances

4.1.1 *Proposed Learning Algorithm*

The proposed algorithm consisting of browsing a piece of music from an entered score, determining the descriptors, and then feeding a chronologically ordered learning base. This will allow us to have a database containing calculated features preventing initial words, the parameters stored in different tables constitute the thoughts of the composers but it is presented in a mathematical way including for each musical piece: the composer, the chosen scale, the chosen rhythm, the number of notes in a word, the sum of the intervals detected, the largest interval between two consecutive notes, and the smallest interval between two consecutive notes, the greatest duration of a note referring to the word concerned, the smallest duration of a note belonging to the word in question, the greatest pitch of note pertaining to the word and the smallest pitch of a note which belongs to that word and the pitch of the first note referring to the word concerned.

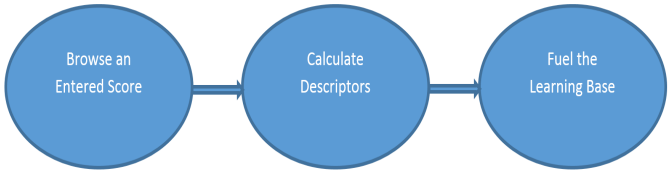

Figure 9: The Learning Algorithm

4.1.1.1 *Representation of Descriptors*

We identified eleven descriptors:

- **Nnote:** Notes numbers.
- **Gnote:** Maqam (indicated on armor, taken on consideration alterations the first and the last note of partition).
- **Snote:** Sum of tonal intervals among notes (depending on Maqam).
- **Gd:** Largest tonal interval among two notes (in terms of the Maqam).
- **Pd:** Smallest tonal interval among two notes (in terms of the Maqam).
- **R:** Rhythm
- **Dnote:** Longest note duration (in terms of the Maqam).
- **Pnote:** Shortest note duration (in terms of Rhythm)
- **Hnote:** First note pitch of the term.
- **Gh:** Highest height of the word.
- **Ph:** Lowest height of the word.

4.1.1.2 *Browse an Entered Score*

The algorithm beginning checks the score's first/last notes to determine the scale's main note then checks the rhythm (R) and starts measuring each note's length consecutively and as per the specified time unit. When sum of durations of note achieves the rhythm, the system Sees the previous sequence as a term, and then goes on to next one.

R = Rhythm

I = duration note for I = 0 to I = R → I=in + in+1

When terminal segmentation is complete, the system moves to descriptor estimating.

4.1.1.3 *Calculation of the descriptors of each word:*

The Algorithm for each segmented term:

1. Calculate the Nnote number.
2. checks the presence on the basis of the main note previously mentioned of the seven deferential notes constituting the Maqam, and measures distances (tonal interval) among them to conclude the Maqam
3. Calculates for each term, sum of the intervals tones among notes.
4. For each sentence, the system calculates the larger Gd, and between two sentences, the smallest tonal interval Pd.
5. For each term the system determines, largest duration Dnote and smallest one Pnote.

4.1.1.4 *Power supply for the learning base*

The algorithm takes each word to be a sequence (Gh, Ph, Note, Pnote, Hnote, Gnote, R, Dnote Snote, Pd, Gd). Feeding takes place on a learning base, which comprises the structure as follow:

1. Symbolic terms matrix table of heights.

2. Rhythmic alphabet table.
3. Ranges table.
4. Table of composers.
5. Pieces table
6. Descriptors and words table
7. Worktables.

4.2. Composition

The proposed model aims to create derivative words automatically in terms of the music descriptors contained in the database. First, the method starts by splitting the rhythmic word from symbolic word and by milking each one in a particular way. A collection of rules for calculating distance and filtering is implemented to create derived terms, then the system proceeds to a concatenation operation at the end, the entire process is rebooted N times to produce a similar musical song in the chosen composer's style of composition. It is sort of a continuation of the composer's thinking.

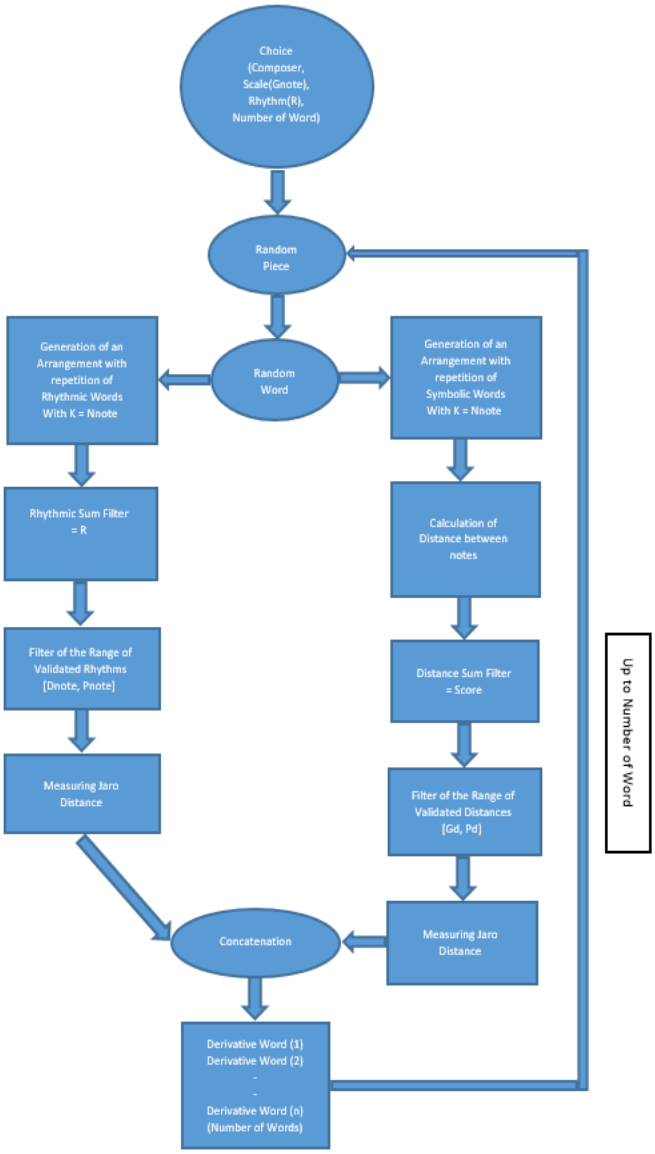

Figure 10: The Composition Algorithm

Option of (composer, scale, rhythm): In effort to create derived words, three essential elements (composer, scale, rhythm) should be filling at the beginning. the selection of Maqam will decide the rules applied to both the measure and the rhythm and will determine the size of measures.

RANDOM Piece: Randomly the algorithm selects a piece from among many pieces selected by a filter (composer, scale, rhythm).

RANDOM Measurement: Randomly the algorithm selects a measurement then retrieves its descriptors from multiple measurements of same piece.

4.2.1 The Symbolic Word

Generation repetition arrangement: All combinations are generated by the algorithm: n^k with k = Gnote scale note and specified by [Gh and Ph].

Calculation of distances between notes: Each of the 2 successive notes represents a distance, and the algorithm measures each distance by the scale concerned.

Filter on sum of distances = Score: If the distances between notes have been determined, the algorithm calculates the sum of all distances that constitute the term. All terms including Snote (word-derived) ! = Snote (original word) are excluded.

Filter of the range of validated distances [Gd, Pd]: The algorithm holds the terms [Gd, Pd] valued by distances.

Filtering by Measuring the Jaro Distance: In effort to choose words which is much less similar than the initial symbolic word, all words produced honoring all conditions and rules must be placed in competition.

The Jaro Similarity simj of two given strings

$$sim_j = \begin{cases} 0 & \text{if } m = 0 \\ \frac{1}{3}\left(\frac{m}{|s_1|} + \frac{m}{|s_2|} + \frac{m-t}{m}\right) & \text{otherwise} \end{cases} \quad (1)$$

where:

- |Si| is the length of sting Si;
- m is the number of matching characters
- t is half the number of transpositions

Two characters from S1 and S2 become considered matching even if they are similar and not further than the:

$$\left\lfloor \frac{\max(|s_1|, |s_2|)}{2} \right\rfloor - 1. \quad (2)$$

4.2.2 Rhythmic word

Generation of an arrangement with repetition: The method generates all different variations in rhythm as the same method as symbolic terms: n^k with k = Nnote.

Rhythm sum filter = R: The algorithm calculates sum of all distances which make up the term. All terms including R (word derivative)! = R (original word) are excluded.

Filter of the range of validated rhythms [Dnote, Pnote]: The system preserves terms whose letters respect [Dnote, Pnote].

Filtering by Measuring the Jaro Distance: All the words produced that comply with all laws and conditions should be placed in competition to prioritize terms that are less similar to the initial rhythmic word

Concatenation of *Symbolic word* and *Rhythmic word:*

Concatenation: The system randomly selects a derived word from the list of preserved terms and derived rhythmic term from the list of preserved rhythmic terms and combines the two.

The system reboots many times up to the **No** words.

5. Process Implementation

In this section, we are interested in generating a musical score by respecting laws and rules defined before. We have chosen to compose music by appealing to the thoughts of Mohammed ABDELWAHAB and this through his musical words that he composed before. all the musical libraries of different composing artists are considered intellectual heritage. in our algorithm, we try to create derived words from initial words.

Generation of pieces:

1. four words: Composer = Mohammed ABDELWAHAB; Maqam = Nahawand ; R = 4/4.
2. six words: Composer = Mohammed ABDELWAHAB; Maqam = Bayati ; R = 4/4.
3. Two words: Composer = Mohammed ABDELWAHAB; Maqam = Nahawand; R = 4/4.

5.1. Table of original words randomly selected from the learning base

Table 3: Original Words Randomly Selected from the Learning Bases

Composers	R	Maqam	Songs	Initial words
Mohammed abdelwahab	C	ELNAHAWAND	Al Fan	2do(2)1sib(2)1sol(2)
			Elfantazy	3/2mib(2)1/2re(2)3/4mib(2)1/4 re(2)3/4mib(2)1/4re(2)
			Elfan	1/2sib(2)1/2do(2)1/2re(2)1/2mi b(2)2fa(2)
			Elfan	3/2mib(3)1/2re(3)1st(3)1/4re(3)1/4re(3)1/4mib(3)1/4fa(3)1/4s ol(2)
			Limta Zaman	1sol(2)2sol(2)2sol(2)1fa(3)
		ELBAYATI	Elfantazy	1/2re(2)1/2mib(2)1/2fa(2)1/2fa (2)1/2sol(1)3/4mib(2)1/4re(2)1/ 2do(2)1/2re(2)
			Limta Zaman	1sol(2)1/2lab(2)1/2sib(2)1lab(2)1sol(2)
			Elfantazy	3/2sol(1)1/2fa(2)3/2lab(1)1/2so l(1)
			Ya mousafir Wahdak	1/2sol(2)1/2do(2)1/2sib(2)1/2la db(2)1sol(2)1st(2)
			Manaa Sali	1sib(2)1ladb(2)1/2sib(2)1/2sib(2)1/2do(2)1/2sib(2)1/2ladb(2)
			Ya mousafir Wahdak	1/2re(2)1/2mib(2)1/2re(2)1/2re (2)1/2do(2)1/2sib(2)1/2do(2)1/ 2do(2)1/2sib(2)1/2ladb(2)
			Manaa Salie	1s(0)1do(2)1sib(2)1do(2)
			Manaa Salie	3/2re(2)1/2do(2)1sib(2)1ladb(2)
			Ya mousafir wahdak	1sol(2)1ladb(2)1sib(2)1do(2)
		ELNAHAWAND	Elfantazy	1/4lab(1)1/4sol(1)1/2fa(2)1/4fa (2)1/4fa(2)1/2mib(2)1/4fa(2)1/ 4fa(2)1/4mib(2)1/2re(2)1/4mib (2)1/2do(2)
			Alfan	2sib(2)1lab(2)3/4sol(2)1/4lab(2)

5.2. Table of Calculated Descriptors

Table 4: Calculated Descriptors

	Calculated Descriptors								
Initial Words	Nnote	Snote	Gd	Pd	Dnote	Pnote	Hnote	Gh	Ph
2do(2)1sib(2)1sol(2)	3	2,5	1,5	1	2	1	2	2	2
3/2mib(2)1/2re(2)3/4mib(2)1/4re(2)3/4mib(2)1/4re(2)	6	2,5	0,5	0,5	1,5	0,25	2	2	2
1/2sib(2)1/2do(2)1/2re(2)1/2mib(2)2fa(2)	5	3,5	1	0,5	2	0,5	2	2	2
3/2mib(3)1/2re(3)1re(3)1/4re(3)1/4mib(3)1/4fa(3)1/4sol(2)	7	3	1	0	1,5	0,25	3	3	2
1sol(2)2sol(2)1fa(3)	3	1	1	0	2	1	2	3	2
1/2re(2)1/2mib(2)1/2fa(2)1/2sol(1)3/4mib(2)1/4re(2)1/2do(2)1/2re(2)	8	7	2	0,5	1,5	0,25	2	2	1
1sol(2)1/2lab(2)1/2sib(2)1lab(2)1sol(2)	5	3	1	0,5	1	0,5	2	2	2
3/2sol(1)1/2fa(2)3/2lab(1)1/2sol(1)	4	3	1,5	0,5	1,5	0,5	1	2	1
1/2sol(2)1/2do(2)1/2sib(2)1/2ladb(2)1sol(2)1re(2)	6	8,5	3,5	0,75	1	0,5	2	2	2
2sib(2)1lab(2)3/4sol(2)1/4lab(2)	4	2	1	0,5	2	0,25	2	2	2
3/2mib(2)1/2re(2)3/4mib(2)1/4re(2)3/4mib(2)1/4re(2)	6	2,5	0,5	0,5	1,5	0,25	2	2	2
1sib(2)1ladb(2)1/2sib(2)1/2do(2)1/2sib(2)1/2ladb(2)	6	4,25	1	0,75	1	0,5	2	2	2
1/2re(2)1/2mib(2)1/2re(2)1/2do(2)1/2sib(2)1/2do(2)1/2sib(2)1/2ladb(2)	8	5,75	1	0,5	0,5	0,5	2	2	2
1s(0)1do(2)1sib(2)1do(2)	4	2	1	1	1	1	2	2	2
3/2re(2)1/2do(2)1sib(2)1ladb(2)	4	2,75	1	0,75	1,5	0,5	2	2	2
1/4lab(1)1/4sol(1)1/2fa(2)1/4sol(1)1/4fa(2)1/2mib(2)1/4fa(2)1/4mib(2)1/2re(2)1/4mib(2)1/4re(2)1/2do(2)	12	9	1	0,5	0,5	0,25	1	2	1
1sol(2)1ladb(2)1sib(2)1do(2)	4	2,5	1	0,75	1	1	2	2	2

5.3. Generation of an Arrangement with Repetition of Symbolic Words with k=Nnote

Table 5: Generation of arrangement with repetition of symbolic words with k=Note

Generation of 3375 symbolic term with n = 15, k=3, Gh=3 and Ph=2			
DO2,DO2,	DO2,RE	DO2,FA	DO2,LAB2,L
DO2,DO2	2,SOL3	2,RE3	AB2,LAB2
DO2,DO2,	DO2,RE	DO2,FA	DO2,LAB2,S
DO2,RE2	2,LAB3	2,MIB3	IB2
DO2,DO2,	DO2,RE	DO2,FA	DO2,LAB2,D
DO2,MIB2	2,SIB3	2,FA3	O3
DO2,DO2,	DO2,MI	DO2,FA	DO2,LAB2,R
DO2,FA2	B2,DO2	2,SOL3	E3
DO2,DO2,	DO2,MI	DO2,FA	DO2,LAB2,MI
DO2,SOL2	B2,RE2	2,LAB3	……

5.4. Example of Symbolic Derived Words Meeting the Conditions for the Original Word 1sol(2)2sol(2)1fa(3)

Table 6: Example of Symbolic Derived word

	W1	W2	W3
Word1	RE2	DO2	S
Word2	RE2	DO2	DO2
Word3	RE2	RE2	DO2
Word4	RE2	MIB2	RE2

All features generated respect the rule: Distance Sum Filter = Score; Filter of the Range of Validated Distances [Gd, Pd], and the Measuring of Jaro Distance to choose the derived word with the least similarity to the original word.

In the end, operation of RANDAM is executed to choose a single word among the words respecting all the conditions and this to reduce the probability of falling on the same word the next iteration.

5.5. Generation of an arrangement of rhythmic words with k=Nnote

Table 7: Generation of Arrangement of Rhythmic Words with K=Nnote

Generation of 125 rhythmic term with n = 5, k =3, Dnote=2 and Pnote=1			
1;1;1,5	1;2;1,5	1,5;1;1,5	1,75;1,75;1,5
1;1;1,75	1;2;1,75	1,5;1;1,75	1,75;1,75;1,75
1;1;1	1;2;1	1,5;1;1	1,75;1,75;1
1;1;2	1;2;2	1,5;1;2	1,75;1,75;2
1;1,5;1	1,5;1;1	1,5;2;1	1,75;1;1
1;1,5;1,5	1,5;1;1,5	1,5;2;1,5	1,75;1;1,5
1;1,5;1,75	1,5;1;1,75	1,5;2;1,75	1,75;1;1,75
1;1,5;1	1,5;1;1	1,5;2;1	1,75;1;1
1;1,5;2	1,5;1;2	1,5;2;2	1,75;1;2
1;1,75;1	1,5;1,5;1	1,75;1;1	1,75;2;1
1;1,75;1,5	1,5;1,5;1,5	1,75;1;1,5	1,75;2;1,5
1;1,75;1,75	1,5;1,5;1,75	1,75;1;1,75	1,75;2;1,75
1;1,75;1	1,5;1,5;1	1,75;1;1	1,75;2;1
1;1,75;2	1,5;1,5;2	1,75;1;2	1,75;2;2
1;1;1	1,5;1,75;1	1,75;1,5;1	1;1;1
1;1;1,5	1,5;1,75;1,5	1,75;1,5;1,5	1;1;1,5
1;1;1,75	1,5;1,75;1,75	1,75;1,5;1,75	1;1;1,75
1;1;1	1,5;1,75;1	1,75;1,5;1	1;1;1
1;1;2	1,5;1,75;2	1,75;1,5;2	1;1;2
1;2;1	1,5;1;1	1,75;1,75;1	……

5.6. Example of rhythmic derived words meeting the conditions for the original word 1sol(2)2sol(2)1fa(3)

Table 8: Example of Symbolic Derived Words

Filtering with R = 4		
W1	W2	W3
1	1	2
1	3/2	3/2
1	2	1
3/2	1	3/2
3/2	3/2	1
2	1	1

5.7. Filtering with Jaro Distance

Table 9: Filtering Based on Jaro Distance

Filtering With Jaro Distance		
W1	W2	W3
1	1	2
1	3/2	3/2
1	2	1
3/2	1	3/2
3/2	3/2	1
2	1	1

5.8. Concatenation of Symbolic Word and Derived Word

The last operation consists of concatenating respectively the derived symbolic words with the derived rhythmic words.

Table 10: Example of Concatenated Word

Concatenated Word		
3/2	1	3/2
RE2	MIB2	RE2
3/2RE(2)	1MIB(2)	3/2RE(2)

5.9. Partition generated

Figure 11: Automatic Generated Music

6. Conclusion and Future Works

The proposed algorithm permitted us to produce musical words that constitute parts from the descriptors we described, each word generated through its own alphabet according to the laws relating to this term by crossing a collection of filters that held only the correct words. We have been attempting to address the theory of the composition of known Arabic music composers. The result obtained and demonstrated in an artificially and automatically generated and written piece of music, shows that the machine can be an artist and we can guarantee the continuity of the composer's thoughts, On the other hand, this area of artificial composition of oriental music still needs to be developed, we suggest the incorporation of the principle of alterations identified by the existence in a word of a foreign text, The meaning of an immediate change of scale, taking into account the relations between the terms and the introduction of the patterns of the ranges according to their definition, taking into account the unique changes in each range.

Conflict of Interest

The authors declare no conflict of interest.

Acknowledgment

The H2020 Project SybSPEED, N 777720, supports this work.

References

[1] P. Barbaud, R. Philippe, "L'ordinateur et la musique," Communication & Langages, **3**(1), 17–25, 1969, doi:10.3406/colan.1969.3744.

[2] C.A. Wamser, C.C. Wamser, "Lejaren A. Hiller, Jr.: A Memorial Tribute to a Chemist-Composer," Journal of Chemical Education, **73**(7), 601, 1996, doi:10.1021/ed073p601.

[3] C. Ames, "The Markov Process as a Compositional Model: A Survey and Tutorial," Leonardo, 22(2), 175–187, 1989, doi:10.2307/1575226.

[4] K. Jones, "Compositional Applications of Stochastic Processes," 1981, doi:10.2307/3679879.

[5] D.P. Kingma, J. Ba, "Adam: A Method for Stochastic Optimization," ArXiv:1412.6980 [Cs], 2017.

[6] G. Papadopoulos, G. Wiggins. "Ai methods for algorithmic composition: A survey, a critical view and future prospects," In AISB Symposium on Musical Creativity, pages 110-117, Edinburgh, UK, 1999, doi.org/10.1080/17513472.2012.738554.

[7] J.D. Fernandez, F. Vico, "AI Methods in Algorithmic Composition: A Comprehensive Survey," Journal of Artificial Intelligence Research, **48**, 513–582, 2013, doi:10.1613/jair.3908.

[8] P.M. Todd, "A Connectionist Approach to Algorithmic Composition," Computer Music Journal, **13**(4), 27–43, 1989, doi:10.2307/3679551.

[9] K.M. Kitani, H. Koike, ImprovGenerator : Online Grammatical Induction for On-the-Fly Improvisation Accompaniment, Proceedings of the International Conference on New Interfaces for Musical Expression, 469–472, 2010, doi:10.5281/zenodo.1177827.

[10] P. Worth, S. Stepney, "Growing Music: Musical Interpretations of L-Systems," in: Rothlauf, F., Branke, J., Cagnoni, S., Corne, D. W., Drechsler, R., Jin, Y., Machado, P., Marchiori, E., Romero, J., Smith, G. D., and Squillero, G., eds., in Applications of Evolutionary Computing, Springer, Berlin, Heidelberg: 545–550, 2005, doi:10.1007/978-3-540-32003-6_56.

[11] M.C. Mozer, "Neural Network Music Composition by Prediction: Exploring the Benefits of Psychoacoustic Constraints and Multi-scale Processing," Connection Science, **6**(2–3), 247–280, 1994, doi:10.1080/09540099408915726.

[12] D. Eck, J. Schmidhuber, "Finding temporal structure in music: blues improvisation with LSTM recurrent networks," in Proceedings of the 12th IEEE Workshop on Neural Networks for Signal Processing, 747–756, 2002, doi:10.1109/NNSP.2002.1030094.

[13] J. Franklin, "Computational models for learning pitch and duration using lstm recurrent neural networks". In Proceedings of the Eighth International Conference on Music Perception and Cognition (ICMPC8), Adelaide, Australia. Causal Productions, 2004. doi: 10.1007/978-3-319-55750-2.

[14] M. Alfonseca, M. Cebrián, A. Ortega, "Evolving computer-generated music by means of the normalized compression distance," in Proceedings of the 5th WSEAS international conference on Simulation, modelling and optimization, World Scientific and Engineering Academy and Society (WSEAS), Stevens Point, Wisconsin, USA: 343–348, 2005.

[15] S. Hochreiter, "The Vanishing Gradient Problem During Learning Recurrent Neural Nets and Problem Solutions," International Journal of Uncertainty, Fuzziness and Knowledge-Based Systems, **06**(02), 107–116, 1998, doi:10.1142/S0218488598000094.

[16] F.A. Gers, J. Schmidhuber, F. Cummins, "Learning to Forget: Continual Prediction with LSTM," Neural Computation, **12**(10), 2451–2471, 2000, doi:10.1162/089976600300015015.

[17] A. Graves, A. Mohamed, G. Hinton, "Speech recognition with deep recurrent neural networks," in 2013 IEEE International Conference on Acoustics, Speech and Signal Processing, 6645–6649, 2013, doi:10.1109/ICASSP.2013.6638947.

[18] J. Chung, C. Gulcehre, K. Cho, Y. Bengio, "Empirical evaluation of gated recurrent neural networks on sequence modeling," NIPS 2014 Workshop on Deep Learning, December, 2014.

[19] K. Cho, B. van Merriënboer, C. Gulcehre, D. Bahdanau, F. Bougares, H. Schwenk, Y. Bengio, "Learning Phrase Representations using RNN Encoder–Decoder for Statistical Machine Translation," in Proceedings of the 2014 Conference on Empirical Methods in Natural Language Processing (EMNLP), Association for Computational Linguistics, Doha, Qatar: 1724–1734, 2014, doi:10.3115/v1/D14-1179.

[20] R. Jozefowicz, W. Zaremba, I. Sutskever, "An empirical exploration of recurrent network architectures," in Proceedings of the 32nd International Conference on International Conference on Machine Learning - **37**, JMLR.org, Lille, France: 2342–2350, 2015.

[21] Y. LeCun, Y. Bengio, G. Hinton, "Deep learning," Nature, **521**(7553), 436–444, 2015, doi:10.1038/nature14539.

[22] J. Schmidhuber, "Deep Learning in Neural Networks: An Overview," Neural Networks, **61**, 85–117, 2015, doi:10.1016/j.neunet.2014.09.003.

[23] I. Sutskever, O. Vinyals, Q.V. Le, "Sequence to sequence learning with neural networks," in Proceedings of the 27th International Conference on Neural Information Processing Systems - **2**, MIT Press, Cambridge, MA, USA: 3104–3112, 2014.

[24] A. Graves, "Generating Sequences With Recurrent Neural Networks," ArXiv:1308.0850 [Cs], 2014.

[25] T.J. Sejnowski, "The unreasonable effectiveness of deep learning in artificial intelligence," Proceedings of the National Academy of Sciences, 2020, doi:10.1073/pnas.1907373117.

[26] F. Colombo, S.P. Muscinelli, A. Seeholzer, J. Brea, W. Gerstner, "Algorithmic Composition of Melodies with Deep Recurrent Neural Networks," ArXiv:1606.07251 [Cs, Stat], 2016, doi:10.13140/RG.2.1.2436.5683.

[27] L. Bahatti, M. Zazoui, O. Bouattane, A. Rebbani, "Short-Term Sinusoidal Modeling of an Oriental Music Signal by Using CQT Transform," Journal of Signal and Information Processing, **04**(01), 51, 2013, doi:10.4236/jsip.2013.41006.

[28] L. Bahatti, O. Bouattane, M. Zazoui1, A. Rebbani, Fast Algorithm for In situ transcription of musical signals : Case of lute music, ResearchGate, 2020.

[29] L. Bahatti, A. Rebbani, O. Bouattane, M. Zazoui, "Sinusoidal features extraction: Application to the analysis and synthesis of a musical signal," in 2013 8th International Conference on Intelligent Systems: Theories and Applications (SITA), 1–6, 2013, doi:10.1109/SITA.2013.6560805.

[30] B. Marzouki, Application of Arithmetic and Cyclic Groups to Music, First International conference on mathematics and applications. Department of Mathematics and Informatics Faculty of Sciences Oujda, 2013.

[31] M. Zhar, O. Bouattane, L. Bahatti, "New Algorithm For The Development Of A Musical Words Descriptor For The Artificial Synthesis Of Oriental Music," in 2020 1st International Conference on Innovative Research in Applied Science, Engineering and Technology (IRASET), 1–8, 2020, doi:10.1109/IRASET48871.2020.9092157.

[32] Y. Zhu, Z. Ming, Q. Huang, "SVM-Based Audio Classification for Content-Based Multimedia Retrieval," in: Sebe, N., Liu, Y., Zhuang, Y., and Huang, T. S., eds., in Multimedia Content Analysis and Mining, Springer, Berlin, Heidelberg: 474–482, 2007, doi:10.1007/978-3-540-73417-8_56.

[33] T. Ratanpara, N. Patel, "Singer identification using perceptual features and cepstral coefficients of an audio signal from Indian video songs," EURASIP Journal on Audio, Speech, and Music Processing, **2015**(1), 16, 2015, doi:10.1186/s13636-015-0062-9.

[34] J.H. Foleis, T.F. Tavares, "Texture selection for automatic music genre classification," Applied Soft Computing, **89**, 106127, 2020, doi:10.1016/j.asoc.2020.106127.

[35] Y. Yu, S. Luo, S. Liu, H. Qiao, Y. Liu, L. Feng, "Deep attention based music genre classification," Neurocomputing, **372**, 84–91, 2020, doi:10.1016/j.neucom.2019.09.054.

[36] C.G. Nevill-Manning, I.H. Witten, "Identifying Hierarchical Structure in Sequences: A linear-time algorithm," Journal of Artificial Intelligence Research, **7**, 67–82, 1997, doi:10.1613/jair.374.

[37] E.M. Gold, "Language identification in the limit," Information and Control, **10**(5), 447–474, 1967, doi:10.1016/S0019-9958(67)91165-5.

[38] S. Guggari, V. Kadappa, V. Umadevi, A. Abraham, "Music rhythm tree based partitioning approach to decision tree classifier," Journal of King Saud University - Computer and Information Sciences, 2020, doi:10.1016/j.jksuci.2020.03.015.

ASTES

Advances in Science, Technology and Engineering Systems Journal Vol. 5, No. 4, 477-487 (2020)

www.astesj.com

Special Issue on Innovative Research in Applied Science, Engineering and Technology

ASTESJ

ISSN: 2415-6698

Study of the Effect of Abnormalities in the External Ear Inducing Hearing Problems

Jihane Melloui*, Jamila Bakkoury, Omar Bouattane

SSDIA Laboratory, ENSET of Mohammedia, Hassan II University of Casablanca, Mohammedia, 28830, Morocco

ARTICLE INFO

Article history:
Received: 30 June, 2020
Accepted: 17 July, 2020
Online: 09 August, 2020

Keywords:
Tinnitus
Ear canal
Acoustic model
Anomaly
Resonant frequency

ABSTRACT

Tinnitus is a phenomenon for which the patient hears sound in the absence of any external sound source. To this day, there is no cure for this phantom sound perception. But it can be masked temporarily to help relief the patient's pain. In order to allow this, a better understanding of the phenomenon is needed. A validated acoustic model of the outer ear developed by the authors is used in this study. This model allows to study the effect of the presence of an anomaly (a cavity, a swelling or a foreign fluid) in the human auditory canal. These anomalies are modeled as a modification of the section of the ear canal or as an alternation of the medium of sound propagation in the ear canal. A parametric study involving the position, width and height of the anomaly as well as the sound velocity in the ear canal is conducted. The results obtained make it possible to conclude on the effect of each parameter on the frequency response of an auditory canal with anomaly.

1. Introduction

Tinnitus is the perception of a sound for which there is no external stimulus; patients suffering from it perceive a sound which may take the form of ringing, buzzing, beeping, hissing or whooshing [1]. This condition can impair one or both ears. According to national health surveys, almost 10 per cent of adults endure a form of tinnitus [2]. The prevalence of tinnitus among employees subject to workplace noise is 15 per cent [3].

This condition has consequences that can be continuous or intermittent, long-term or short-term, with a sudden or incremental occurrence. This can also be associated with the cardiac or respiratory rhythm. Its magnitude also changes during the day, with a period of morning calm and an evening or nightly rise (nocturnal rhythm) [4].

In addition, tinnitus is related not only to alternation in the auditory system such as speech perception, localization of sound and auditory attention [5-8], but also to affective disorders such as depression or anxiety, insomnia, confusion and lower quality of life [9-11].

There is no official classification of tinnitus recognized by all scientists and doctors. The most common types are two: One dividing tinnitus by manifestation (objective or subjective tinnitus) and the other defining it by the potential cause of tinnitus [12].

Objective tinnitus is the rarest but also the easiest to identify. It is a perceived pulsatile sound produced by the body (vascular or muscular cause) which the examiner may also hear. This type of tinnitus represents about 10 per cent of cases of tinnitus. The 90 per cent remaining are subjective [13].

Subjective tinnitus is only heard by the patient. The frequency perceived does not come from the body, but from one or more body system failures that may be from the cortex to the external auditory canal [14]. It can be caused by ear problems (tinnitus aurium) or cerebral problems (tinnitus cerebri) [1]. This tinnitus is a perceived sensation in the absence of any outer physical source (phantom sound) and its source is hard to determine [14]. It is characterized as persistent after continuous occurrence for 6 months [15].

The symptom of tinnitus can be induced by multiple causes and is often accompanied by loss of hearing at high frequencies linked to ageing. Different parts of the hearing system can cause tinnitus, such as the outer ear [16]. For example, an excessive ear wax can cause pressure in the ear canal and causes a change in the resonance frequency at the eardrum.

According to the second type of classification (potential cause of tinnitus) and, as in [17], the origin of tinnitus may be categorized as:

- Otological origin: The auditory system (external, middle or inner ear) or the auditory nerve. In this case, tinnitus is usually accompanied by hearing loss and sometimes dizziness.
- Central origin: The relay level of central auditory canal;

*Corresponding Author: Jihane Melloui, jihane.melloui@gmail.com

- Non otological origin: vascular, muscular, cerebral or cervical;
- Unknown origin: if no lesion and no other symptom are detected.

Several efforts have been made in the past to suppress or treat tinnitus. Some of these interventions included the use of drugs for the treatment of tinnitus [18-19]. In some serious cases, the sensation was eliminated by taking drastic actions, like cutting a specific nerve into the ear [20]. This completely removes the ability to hear using that ear.

The improved understanding of tinnitus physiopathological processes during the last decade has opened the way for many medical therapeutic researches [21-25]. The most common treatments used for tinnitus managing are cognitive and behavioral therapy (CBT), tinnitus retraining therapy (TRT) and sound therapy (SD)[26-31].

Cognitive and behavioral therapy is based on the premise that "what matters is not what happens to us, but how we do it." [25]. In fact, this treatment does not enhance tinnitus appreciation, but allows the individual to ignore it by emotional adjustments and behavioral changes [26].

Tinnitus retraining therapy is one of the most common techniques for managing tinnitus. Its neurophysiological model indicates that the limbic mechanism plays an important role in the perception of tinnitus [27]. The TRT principle is based on the patient's ability to become accustomed to the tinnitus signal.

Sound therapy is a program that uses external sound to manage tinnitus either via acoustic or electric stimulation [24]. It offers relief from tinnitus for both the short and long term. This treatment aims to minimize patient perception, effectively reducing the signal-to-noise ratio of tinnitus to ambient or surrounding noise [29-31].

Previous tinnitus suppression attempts involved the use of electrical stimulation [32]. In practice, it does not suppress tinnitus, but rather tries to mask the current tinnitus sound with another sound produced by the electrical stimuli. The key purpose of electrical stimulation is to eliminate tinnitus without any additional sound being applied. The direct electrical currents used cause severe damage to the biological tissue and can therefore not be used in the long term [32].

This problem can be fixed by means of an approach in which the tinnitus patient is subjected to a hearing test of varying pitches to determine the frequency of the perceived tinnitus sound. A noise generator (white noise, filtered noise, pink noise, ambient sounds ...) is used to mask tinnitus [24, 33]. This generator provides signals both above and below the specified tinnitus frequency.

The corresponding frequency of tinnitus was between 9000 and 11000 Hz for 86 per cent of the 771 patients in an experiment led by Johnson in [34]. The median tinnitus frequency of the 29 patients taking part in Neff's experiment [33] was 4046 Hz with a standard deviation of 2212,25 Hz. In Reavis experiment [29] on 20 participants, the mean frequency of tinnitus was 6929 Hz with a standard deviation of 2090 Hz.

It should be mentioned that such treatments do not heal tinnitus, but rather superimpose stimulus on the original tinnitus symptom in an attempt to mask the perceived sound. Given the multidisciplinary aspect of the condition, it is better to merge approaches for better results [35-37]. A deeper understanding of the tinnitus syndrome is required to make these masking methods more effective. To this end, further investigations must be carried out into causes that stimulate the phantom frequencies and the loss of hearing at high frequencies.

In this study, an analysis is carried out with the intention of further understanding the effect of certain anomalies that induce tinnitus on the resonance frequency of the human outer ear. An acoustic model previously developed by authors is used in the current research by inserting various diseases or anomalies into it, either through introducing acoustic resonators or by acting on some of its parameters.

The anomalies investigated are those that can lead to:

- A change of section at any position along the ear canal;
- A change in the propagating medium of the sound wave in the outer ear [38].

The introduction of a resonator simulating a swelling makes it possible to model, for example, an excessive presence of earwax, a pimple, an infection or a foreign body in the ear canal (Figure 1). The addition of an acoustic resonator simulating a cavity can make it possible to model anomalies such as lesions of the ear canal. The presence of a foreign fluid in the ear canal can be modeled by acting on the wave propagation velocity parameter in the outer ear. If this fluid is water, the swimmer's ear disease can be mentioned.

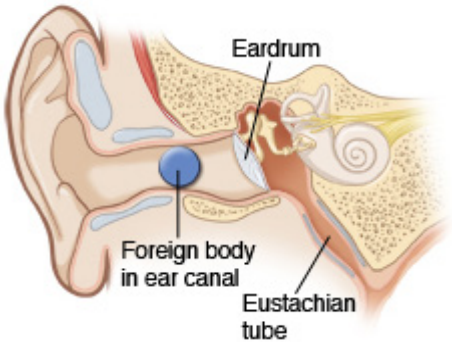

Figure 1: External auditory canal with a foreign body

2. Acoustic model of the outer ear

2.1. Outer ear

The outer ear plays a very significant function in the transmission of human sensory information from the environment to the tympanic membrane. It functions as a low frequency filter, a resonator for the middle range and direction dependent filter on high frequencies to enhance spatial awareness [39].

By providing a narrow entrance to the auditory system, the external ear protects the eardrum from mechanical damage. It provides directional amplification of the incident sound pressure level. It also transforms the incoming sound spectrum which was subjected to diffraction and amplifies acoustic waves at higher

frequencies [40]. These properties makes that the ear plays a significant role in spatial hearing.

In an attempt to comprehend these characteristics, it is better to divide the external ear system into its functional elements: the head, torso and pinna acting as diffraction bodies, the concha and the ear canal acting as acoustic resonators, and the eardrum providing an acoustic termination.

Such components must be seen as part of an integrated network, since they work together to transfer sound pressure from the free field to the middle ear entrance, depending on the frequency, direction and anatomy of the hearing system. Human ear models can provide a better understanding of how the human ear responds when it is artificially stimulated.

An acoustic model taking account of this integration is previously developed by authors [41] and is used in this paper to model anomalies present in the outer ear. This model is presented briefly in Figure 2. The purpose of this study is to examine the impact of anomalies on the external ear function. This is done by comparing the frequency response of a healthy external ear to an external ear with an anomaly.

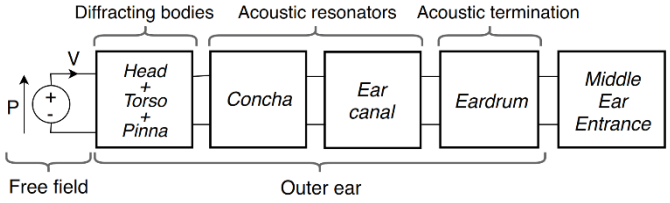

Figure 2: Acoustic Model of the External Ear

2.2. Outer ear acoustic model

The acoustic model presented associates with each part of the outer ear an acoustic resonator modeled by a transfer matrix. These transfer matrices can model a segment of the concha, auditory canal or even the eardrum. These resonators can have several forms (Figure 3) and are used, in this study, to model segments of the ear canal as well as abnormalities present in the outer ear. The corresponding transfer matrix of the outer ear (with or without anomaly) is obtained by multiplying the transfer matrixes of each segment.

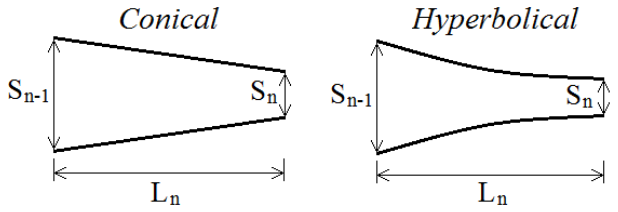

Figure 3: Acoustic resonator segment of different forms with parameters

The ear canal is divided into several segments (Figure 4), the number of segments depends on the precision sought in the calculation. A detailed study of the form as well as the optimal number of segments to approach with good precision the actual shape of the auditory canal is carried out previously by the authors in [41]. This model adopts the sound pressure p_i and the mass velocity v_i as the two state variables for linking the two ports of the i-th acoustic resonator.

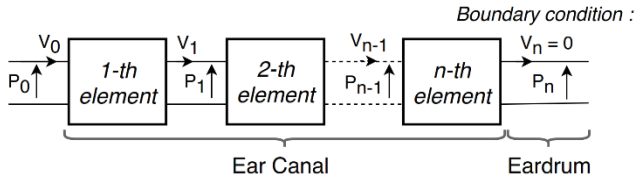

Figure 4: Segments of the ear canal acoustic model and boundary conditions

As illustrated in Figure 4, p_0 and v_0 represent the acoustic pressure and the mass velocity at the input of first resonator coming from the free field. The acoustic pressure and the mass velocity p_n and v_n are the outputs of the acoustic model of the outer ear which is also the entrance of middle ear. At the output of the n-th resonator, v_n=0 simulates the infinite impedance of the tympanic membrane since it behaves as an obstacle. This is used as a boundary condition for calculating the frequency response of the model.

The transfer matrix of the conical acoustic resonator T_C is described in (1). The section parameters are shown in Figure 3.

$$T_C = \frac{1}{1+\gamma L_n}\begin{bmatrix} T_{1C} & T_{2C} \\ T_{3C} & T_{4C} \end{bmatrix} \tag{1}$$

where:

$$T_{1C} = \cos(K L_n) + \frac{\gamma}{K}\sin(K L_n)\ ;\ T_{2C} = -j\frac{c}{S_{n-1}}\sin(K L_n)\ ;$$

$$T_{3C} = \frac{-j S_n}{cK}\left[\frac{-\gamma^2 L_n}{1+\gamma L_n}\cos(K L_n) + \left(K + \frac{\gamma^2}{(1+\gamma L_n)K}\right)\sin(K L_n)\right]\ ;$$

$$T_{4C} = \frac{S_n}{S_{n-1}}\left(\cos(K L_n) - \frac{\gamma}{(1+\gamma L_n)K}\sin(K L_n)\right) \tag{2}$$

$$\gamma = \frac{1}{L_n}\left(\sqrt{S_n/S_{n-1}} - 1\right) \tag{3}$$

The wave number K (in radius/m) takes into account the attenuation of the sound in the human ear as advised in [42]. It should be mentioned that this segment can be used to model uniform acoustic resonator simply by taking S_n equal to S_{n-1}. The transfer matrix of the hyperbolical acoustic resonator T_H is described in (4).

$$T_H = e^{\delta L_n}\begin{bmatrix} T_{1H} & T_{2H} \\ T_{3H} & T_{4H} \end{bmatrix} \tag{4}$$

where:

$$T_{1H} = \cos(K_h L_n) - \frac{\delta}{K_h}\sin(K_h L_n)\ ;\ T_{2H} = -j\frac{c}{S_{n-1}}\frac{K}{K_h}\sin(K_h L_n)$$

$$T_{3H} = \frac{-j K S_n}{K_h c}\sin(K_h L_n)\ ;\ T_{4H} = \cos(K_h L_n) + \frac{\delta}{K_h}\sin(K_h L_n) \tag{5}$$

$$K_h = \sqrt{K^2 - \left(\frac{\ln(S_n/S_{n-1})}{2L_n}\right)^2} \tag{6}$$

$$\delta = \frac{\ln(S_n/S_{n-1})}{2L_n} \tag{7}$$

The acoustic model is applied to two of the 15 auditory canals published by Stinson et al. [43], referred to in "Canal 4" and "Canal 6." Canal 4 and Canal 6 are measured from the right ear of a man and the left ear of a woman, respectively. Therefore, this study takes into account both ears and the sex of the individual.

Complete anatomy of the canals studied is available in [43]. The dimensions of the acoustic resonator segments and the variation in diameter over the length of both canals are shown in Figures 5 and 6.

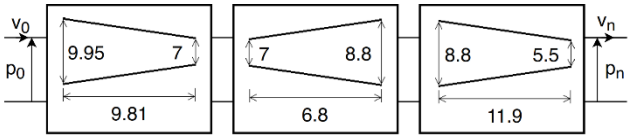

Figure 5: Parameters of the acoustic model of "Canal 4"

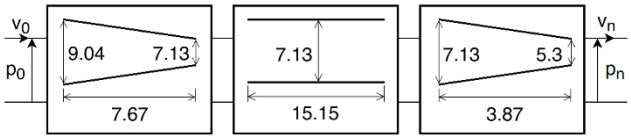

Figure 6: Parameters of the acoustic model of "Canal 6"

Canal 4 has a length of 28.51 mm and canal 6 has a length of 26.69 mm. Despite the fact that these lengths are of the same order of magnitude, there is a very different variation in the section along the ear canal. Both canals are modeled using three acoustic resonators in series. This allows to approach with good precision the true forms of these ear canals. Other segments of acoustic resonators are injected thereafter in order to model anomalies present in these healthy auditory canals.

3. Anomaly modeling

The normal function of transmission of the ear is compromised by alterations in its anatomy. It can be due to individual differences or technical blockages, such as foreign body parts, hearing aid implants, infections or tympanic membrane perforation.

The anomalies studied are those that can cause a difference in the section at any location along the external auditory canal or an alternation in the sound propagation medium in the outer ear. The first type of anomalies, consisting of an obstacle present in the ear canal, may be modeled by swelling or cavities. The parameters concerning this type of anomaly are presented in Figure 7. The second type can be modeled by the presence of a fluid in the auditory canal, which would cause the sound transmission medium to change from the air to the fluid contained in the auditory canal. These abnormalities can cause the resonance frequency of the ear to alter.

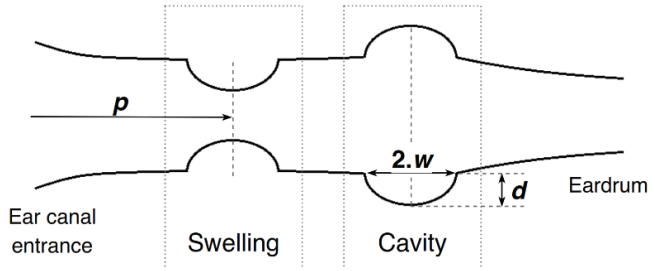

Figure 7 : Parameter definition of anomalies that change the section of the ear canal

Acoustic models of canals 4 and 6 are those of healthy outer ears into which these anomalies will be introduced (Figure 8). Each anomaly is modeled considering its shape. It is modeled by two acoustic resonators in series which can have a conical, hyperbolic or even a uniform section. Given the nature of the obstacle type anomaly studied in this paper, it is modeled using two segments of hyperbolic acoustic resonators as shown in Figure 7.

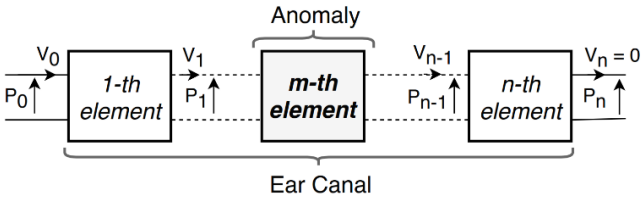

Figure 8 : Insertion of an acoustic resonator modeling anomaly in a healthy auditory canal model

A parametric analysis will be carried out using the acoustic model acquired (auditory canal with anomaly). In this analysis, the effect of position "p", width "w" and depth "d" of the obstacle type anomaly on the frequency response of the outer ear is investigated. The second type of anomaly concerns the study of the effect of the propagation speed of sound "c" in the ear canal.

Parameters "p" and "w" are expressed as a function of the total length "L" of the ear canal. The position values of the anomaly investigated in this work are 0.2L, 0.35L, 0.5L, 0.65L and 0.8L. The values considered for the anomaly width are 0.05L, 0.1L, 0.15L, 0.2L and 0.25L. The depth parameter "d" is expressed as a function of the width of the anomaly to hold the anomaly in proportion. This parameter can be set to 0.5w, 0.75w, 1w, 1.25w and 1.5w. In order to simulate the different levels of severity of the diseases that cause the presence of fluid in the ear canal, the speed of sound "c" parameter can be set to 350, 500, 650, 800 and 950m/s. This results in a test matrix of 65 cases.

Only one case is presented in Figure 9 given the large number of cases studied. This acoustic model of the "Canal 4" ear canal has a swelling of a width of w = 0.15L and a height of d = 1w at a distance of p = 0.65L from the entrance of the auditory canal. The same procedure applies in the other cases. In cases of abnormalities involving the presence of foreign fluids in the ear canal, the dimensions of the model are similar to those of the healthy model shown in Figures 5 and 6 (only the speed of sound parameter is modified).

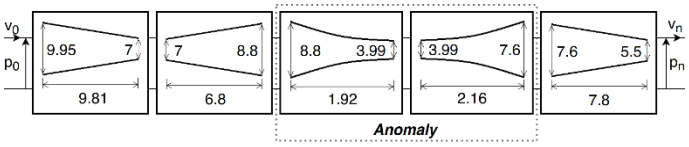

Figure 9 : Acoustic resonator modeling a swelling anomaly (p=0.65L, w=0.15L and d=1w) present in auditory canal « Canal 4 »

4. Results and discussion

The sound pressure level (SPL) presented in (8) is computed using Matlab. The results are reported in two formats: figures and tables. The figures show the variation in sound pressure level with frequency. The numerical values of the resonance frequencies as well as the gains at these frequencies are presented in the tables to improve the readability of the results.

$$SPL = 20 \log \left| \frac{p_n}{p_0} \right| \quad (8)$$

4.1. Effect of the propagation medium

Figure 10 shows the effect of the medium of sound propagation, which is characterized by the speed of sound "C", on the frequency response of the auditory canal. In this simulation, the greater the value of "C", the greater the volume of fluid contained in the ear.

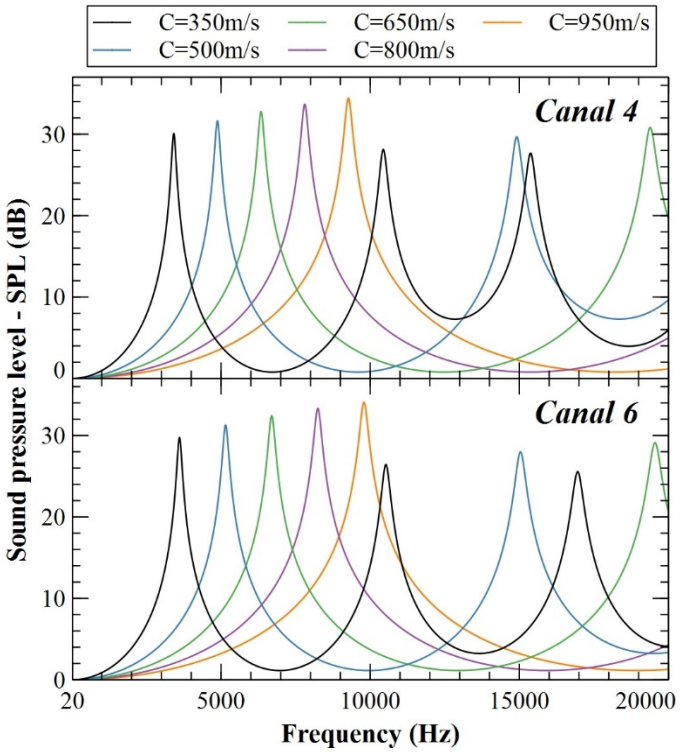

Figure 10 : Frequency response of Canal 4 and Canal 6 to different sound speed values

In the case of "Canal 4", it can be shown from Figure 10 that the first resonant frequency occurred at 3416, 4898, 6341, 7811 and 9272 Hz at sound velocity of 350, 500, 650, 800 and 950 m/s, respectively. The first resonant frequency for "Canal 6" is 3626, 5154, 6688, 8246 and 9793 Hz, respectively, at 350, 500, 650, 800 and 950 m/s.

It can be observed that only the ear canals with a propagation medium inducing a sound speed of 350, 500 and 650 m/s have a second resonant frequency. This resonant frequency for "Canal 4" is 9413, 14935 and 19388 Hz, respectively, at 350, 500 and 650 m/s. For "Canal 6", these values are 10529, 15037 and 19556 Hz at sound velocity of 350, 500 and 650 m/s, respectively.

For the third resonant frequency, only the canal providing a propagating medium with a sound velocity of 350 m/s is concerned. "Canal 4" resonates at 15383 Hz and "Canal 6" resonates at 16960 Hz. These ear canals are healthy canals.

These results show that the presence of fluid in the ear canal tends to reduce the number of resonant frequencies of the ear canal in the audible band. The resonance frequency values obtained for "Canal 6" are higher than those found for "Canal 4". That is due to the disparity in the physiology of these two auditory canals. The presence of a foreign fluid in the ear canal leads to an increase in the speed of sound propagation in this canal, which has a significant effect on the frequency of the resonance. Indeed, the frequency of resonance rises with the speed of sound propagation.

Considering the first resonance frequency, it can be reported that the gains at these frequencies for canals 4 and 6 are almost identical. This gain ranges by an order of magnitude from 30 dB at a sound transmission speed of 350 m/s to 34 dB at a speed of 950 m/s. From these findings, it can be assumed that an increase in the amount of fluid in the ear canal leads to an increase in the sound pressure level.

4.2. Effect of anomaly position

In order to study the effect of the position of a cavity or swelling on the frequency response of the human auditory canal, the parameters of the anomaly width "w" shall be set to 0.15L and the depth or height "d" of the anomaly shall be set at 1w.

Figure 11 indicates the evolution of the SPL as a result of the frequency in the audible band. This concerns the case of swollen auditory canals with various anomaly positions. Figure 12 shows that of auditory canals with a cavity. Table 1 indicates the relative deviation between the resonance frequency findings for a healthy canal and canals with anomaly. The table further shows the variations in SPL observed at these frequencies. It should be noted that for the calculation of these deviations, a healthy auditory canal is used as a reference for all the canals with anomaly.

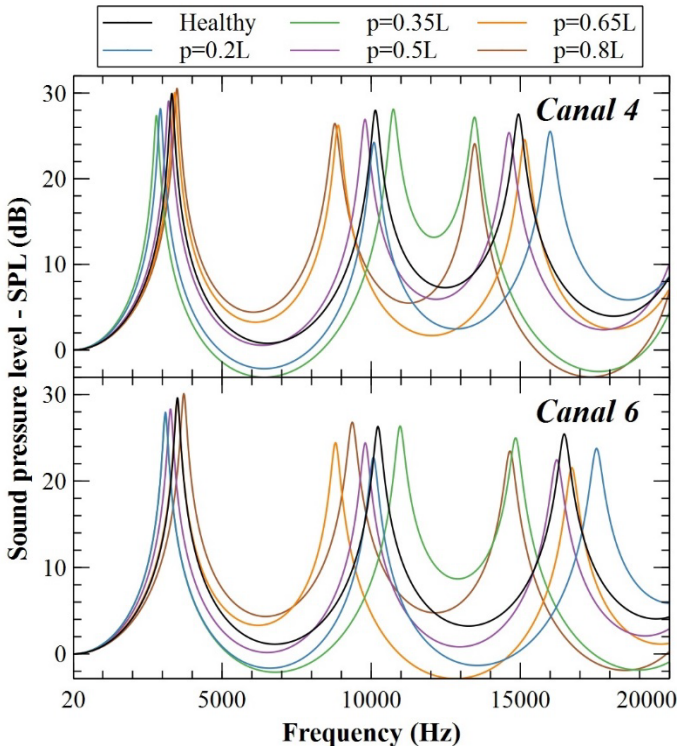

Figure 11 : Frequency response of the auditory canals with a swelling anomaly of different positions p (w= 0.15L and d=1w)

A negative SPL for the swelling located at 0.2L and 0.35L in "Canal 4", for the frequency bands [4918-7890] Hz and [4592-8344] Hz can be seen from the reading of Figure 11. In these same bands, gains for anomalies of positions 0.65L and 0.8L are significantly higher than those of the healthy canal. Between

15500Hz and 19100Hz, the frequency response of the canals with anomalies at 0.35L and 0.8L is almost identical and presents negative gains.

The frequency response of "Canal 6", consisting of a 0.2L and 0.35L swelling, shows negative gains in the [5200-8400] Hz band. Same observation for 0.35L and 0.8L in the frequency band [17000-20000] Hz. There are also negative gains for swelling cases in the 0.2L and 0.65L positions in the [12365-14774] Hz and [10951-14664] Hz bands, respectively. The healthy ear canal amplifies the sound of these frequencies. When such abnormalities have occurred, we find that this ear canal starts to decrease the sounds heard at these frequencies.

According to Figure 11 and taking into account the results obtained for "Canal 4", there are maximum differences of -18.77, -22.82, -10.74, -21.6 and -24.77 dB between the SPL curve of the healthy canal and those of the auditory canals with anomalies at positions 0.2L, 0.35L, 0.5L, 0.65L and 0.8L, respectively. These differences are observed at 14924, 14947, 10175, 10156 and 14955 Hz frequencies at 0.2L, 0.35L, 0.5L, 0.65L and 0.8L respectively. Negative deviations mean that the sound perceived at these frequencies is reduced. This can lead to a slight loss of hearing.

Absolute variations of 15.39, 18.12, 9.26, 19.04 and 20.01 dB between the healthy canal SPL and the canals with anomaly positions of 0.2L, 0.35L, 0.5L, 0.65L and 0.8L, respectively. Such variations are found at 16021, 13464, 9754, 8886 and 8768 Hz frequencies for 0.2L, 0.35L, 0.5L, 0.65L and 0.8L, respectively. Similar observations may be made from "Canal 6". Indeed, results show very similar variations but with slightly higher frequencies (of the order of 1500 Hz). These positive variations (amplification) may lead to an over-sensitivity to sounds having these frequencies in some cases and for some patients.

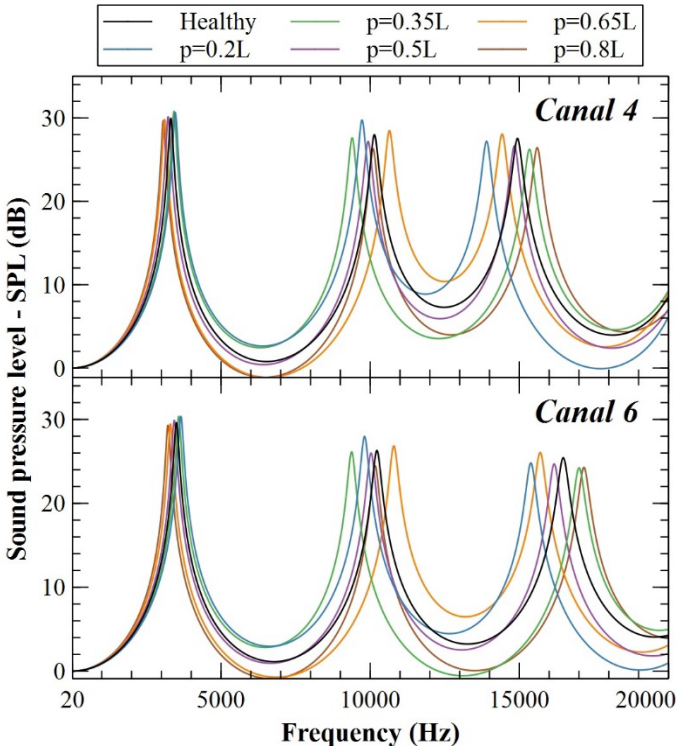

Figure 12 : Frequency response of the auditory canals with a cavity anomaly of different positions p (w= 0.15L and d=1w)

Figure 12 shows that the auditory canals 4 and 6 with a cavity type anomaly do not generally have negative SPL values. From this figure and taking into consideration the obtained results for "Canal 4", the maximum differences are -18.88, -16.68, -7.54, -12.92 and -14.65 dB between the healthy canal SPL and the auditory canals with 0.2L, 0.35L, 0.5L, 0.65L and 0.8L location anomalies, respectively. Those very variations are found at 14962, 10162, 10197, 10113 and 14911 Hz frequencies at 0.2L, 0.35L, 0.5L, 0.65L and 0.8L respectively.

Absolute differences of 15.91, 16.02, 6.15, 12.74 and 12.53 dB between the healthy canal SPL and the canal with anomalies of 0.2L, 0.35L, 0.5L, 0.65L and 0.8L respectively. These differences are observed at frequencies 13886, 9374, 9875, 10673 and 15630 Hz for positions 0.2L, 0.35L, 0.5L, 0.65L and 0.8L respectively.

For "Canal 6", these SPL differences are of the same order of magnitude for all the studied cases. However, these differences are observed at higher frequencies of approximately 1500 Hz at 0.2L and 0.8L positions, 6000 Hz at 0.5L and 0.65L positions and almost similar at 0.35L position.

This confirms the observation obtained from the swollen ear canals. However, the variations found for the anomaly of the cavity are smaller than those reported for the anomaly of the swelling.

Table 1: Effect of the position of swelling and cavity anomalies on frequency response for canal 4 and 6

		Resonant frequencies			SPL at resonant frequencies		
		RF-1	RF-2	RF-3	SPL (RF-1)	SPL (RF-2)	SPL (RF-3)
Canal 4							
	Healthy	3317 Hz	10140 Hz	14940 Hz	29,96 dB	28,00 dB	27,54 dB
Swelling	**p=0.2L**	-11,6%	-0,49%	7,10%	-5,94%	-13,4%	-7,33%
	p=0.35L	-15,6%	5,92%	-9,84%	-8,68%	0,39%	-1,27%
	p=0.5L	-3,26%	-3,41%	-2,14%	-3,00%	-3,86%	-7,88%
	p=0.65L	2,89%	-12,3%	1,34%	0,30%	-6,29%	-10,8%
	p=0.8L	5,19%	-13,4%	-9,84%	1,97%	-5,57%	-12,5%
Cavity	**p=0.2L**	4,49%	-4,08%	-6,96%	2,37%	6,25%	-1,23%
	p=0.35L	3,11%	-7,34%	2,68%	2,77%	-1,39%	-4,68%
	p=0.5L	-2,68%	-2,05%	-0,67%	0,60%	-2,89%	-3,20%
	p=0.65L	-6,33%	5,03%	-3,41%	-0,53%	1,75%	1,92%
	p=0.8L	-7,54%	-0,39%	4,42%	-0,90%	-6,04%	-4,03%
Canal 6							
	Healthy	3504 Hz	10230 Hz	16470 Hz	29,61 dB	26,30 dB	25,43 dB
Swelling	**p=0.2L**	-14,0%	-1,56%	6,62%	-5,64%	-13,6%	-6,53%
	p=0.35L	-11,5%	7,23%	-9,90%	-6,62%	0,19%	-1,77%
	p=0.5L	-6,65%	-4,18%	-1,52%	-4,36%	-7,19%	-11,7%
	p=0.65L	-0,20%	-13,9%	1,58%	-0,91%	-7,11%	-15,3%
	p=0.8L	6,14%	-8,45%	-10,9%	1,69%	1,86%	-7,75%
Cavity	**p=0.2L**	4,22%	-4,09%	-6,56%	2,60%	6,35%	-2,44%
	p=0.35L	2,11%	-8,33%	3,28%	2,57%	-0,61%	-4,76%
	p=0.5L	-2,11%	-1,96%	-1,82%	0,91%	-1,18%	-2,87%
	p=0.65L	-5,74%	5,47%	-4,68%	-0,51%	2,05%	2,48%
	p=0.8L	-8,11%	-0,59%	4,25%	-1,05%	-6,92%	-4,52%

The calculation of the relative deviations found in Table 1 uses the results reported for healthy auditory canal cases as a reference. Results presented in this table show that for the first resonance frequency (RF-1) and for the swelling case, there is a maximum deviation of -15.6% for "Canal 4" with an anomaly at position 0.35L and a maximum deviation of -14% for "Canal 6" with an anomaly at position 0.2L. In the case of a cavity, there is a maximum deviation of -7.54% for "Canal 4" with an anomaly located at 0.8L and a maximum deviation of -8.11% for "Canal 6" with an anomaly located at 0.8L.

In the case of the second resonance frequency (RF-2) and in the case of swelling, there is a maximum deviation of -13.4% for "Canal 4" with an anomaly at 0.8L and a maximum deviation of -13.9% for "Canal 6" with an anomaly at 0.65L. In the case of a cavity, there is a maximum deviation of -7.34% for "Canal 4" with an anomaly at position 0.35L and a maximum deviation of -8.33% for "Canal 6" with an anomaly at position 0.35L.

There is a maximum deviation of -9.84% in the third resonance frequency (RF-3) and for the swelling anomaly in "Canal 4" with an anomaly at 0.35L and 0.8L. For "Canal 6", one can observe a deviation of -9.9% for an anomaly located at 0.35L and a maximum deviation of -10.9% for an anomaly at 0.8L. In the case of cavity, there is a maximum deviation of -6.96% for "Canal 4" with an anomaly located at 0.2L and a maximum deviation of -6.56% for "Canal 6" with an anomaly at 0.2L.

It can be deduced that a decrease of the first resonance frequency may be caused by a swelling located at the entry of the auditory canal or a cavity situated towards the tympanic membrane. The result is completely reversed at the second resonance frequency. A swelling effect causes a drop of this frequency at the input and output of the auditory canal for the third resonance frequency. A cavity acts in the same way at the end of the auditory canal.

The effect of anomalies on the SPL at resonance frequencies can also be observed from Table 1. For auditory canals with swelling, there is a maximum deviation of -13.4% corresponding to the SPL at RF-2 for "Canal 4" with an anomaly at 0.2L and a maximum deviation of -15.3% corresponding to the SPL at RF-3 for "Canal 6" with an anomaly at 0.65L. For the auditory canals with a cavity, a maximum deviation of 6.25% corresponding to the SPL at RF-2 for "Canal 4" with an anomaly at position 0.2L and a maximum deviation of -6.92% corresponding to the SPL at RF-2 for "Canal 6" with an anomaly at position 0.8L are observed.

These deviation values remain low, which means that, unlike the swelling anomaly, this anomaly has little effect on the amplitude of the resonance peaks of the ear canal.

4.3. Effect of anomaly width

The parameter of the anomaly location "p" is set to 0.5L and the depth or height "d" is set to 1w to evaluate the influence of the width "w" of a swelling or cavity on the frequency response of the human auditory canal. Figure 13 shows the results obtained for canals 4 and 6 consisting of a swelling with values of different widths. Figure 14 displays the findings for the case of a cavity. Table 2 describes the relative deviations of the resonant frequency and the SPLs at these frequencies, taking as a reference the healthy auditory canal.

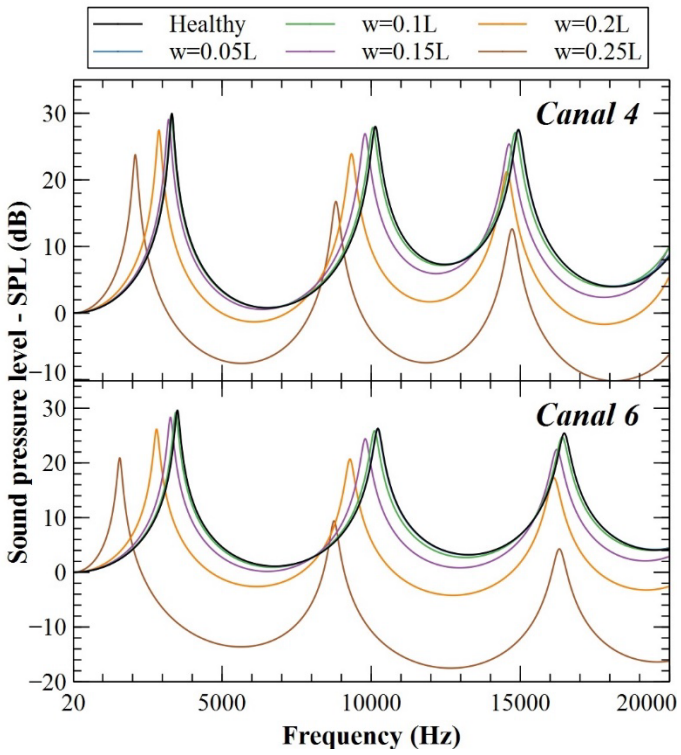

Figure 13 : Frequency response of the auditory canals with a swelling anomaly of different widths w (p= 0.5L and d=1w)

Figure 13 indicates negative magnitudes relating to the reduction of SPL through the ear canal with swelling. These values are -7.55, -7.46 and -10.15 dB, observed in the case of an anomaly of width of 0.25L in "Canal 4" in the frequency bands [3197-7972] Hz, [9666-13960] Hz and [15438-20000] Hz respectively. The anomaly of 0.2L width is also affected by this effect, but at a smaller scale. Therefore, one can assume that the greater the width of the swelling, the greater the risk of hearing loss.

In the case of "Canal 6", negative gains are noted for anomalies of width 0.2L and width 0.25L for frequency bands [4589-7607] Hz, [10776-14626] Hz and [17637-20000] Hz, and [2288-8398] Hz, [9102-16050] Hz and [16564-20000] Hz respectively. The maximum values observed for the 0.25L width anomaly in the bands mentioned above are -13.62, -17.51 and -16.38 dB. By comparing, on the one hand, the width of these frequency bands and, on the other hand, the minimum SPL values for canals 4 and 6, it can be concluded that "Canal 6" is more affected by a swelling anomaly than "Canal 4". This is because of their different anatomies.

Maximum absolute deviations between the healthy "Canal 6" SPL curve and those of the swollen canals with anomaly widths 0.05L, 0.1L, 0.15L, 0.2L and 0.25L are -0.52 dB at 10347 Hz, -4.31 dB at 10309 Hz, -12.7 dB at 10262 Hz, -22.76 dB at 10246 Hz and -38.37 dB at 10238 Hz, respectively. Positive deviation values are also observed and are 0.42 dB at 10070 Hz, 3.35 dB at 10025 Hz, 9.21 dB at 9764 Hz, 15.88 dB at 2797 Hz and 18.52 dB at 1548 Hz for swollen "Canal 6" with anomaly widths of 0.05L, 0.1L, 0.15L, 0.2L and 0.25L, respectively.

It can be deduced from these values that the SPL reduces exponentially with an increase in the width of the swelling.

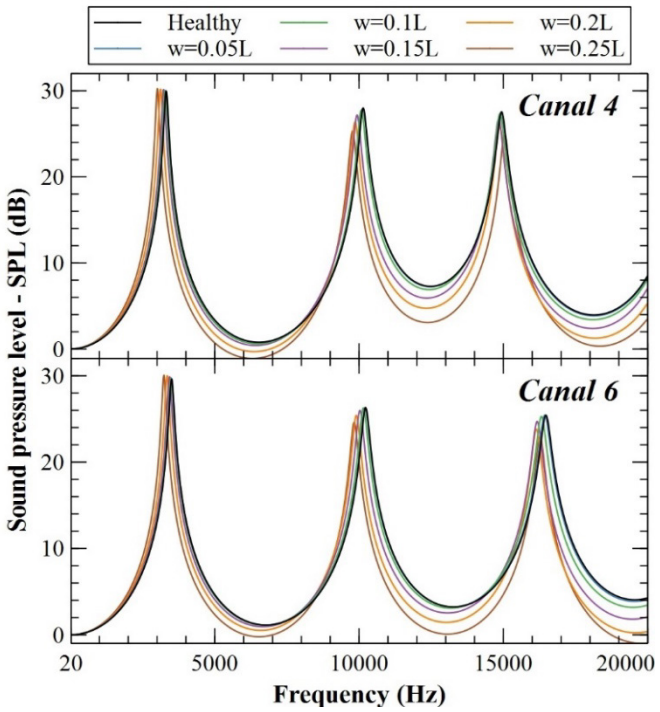

Figure 14 : Frequency response of the auditory canals with a cavity anomaly of different widths w (p= 0.5L and d=1w)

Figure 14 shows that auditory canals 4 and 6 with an anomaly of the cavity type have no negative SPL values. This is in agreement with the observation made in the study of the effect of the anomaly position.

From this figure and taking into consideration the obtained results for “Canal 6”, the maximum absolute deviations are -0.98, -4.34, -8.42, -10.06 and -12.61 dB measured between the healthy canal SPL and the auditory canals with 0.05L, 0.1L, 0.15L, 0.2L and 0.25L width anomalies, respectively. Those variations occurs at 16629, 16580, 16545, 16544 and 10265 Hz frequencies for 0.05L, 0.1L, 0.15L, 0.2L and 0.25L widths respectively. As in the majority of the cases studied, it can be noted that the maximum absolute deviations occur at high frequencies.

For similar anomaly widths, the cavity effect is much less pronounced than swelling effect. This is because the swelling presents an obstacle in the ear canal, while the cavity presents a wider opening of the latter. This observation can easily be made by comparing the shape of the curves in Figures 13 and 14.

Figure 14 also shows that the difference between the SPL curves on the healthy canal and the anomaly canals increases exponentially with the "w" width. It can be deduced that this effect is much more present in the case of swelling anomalies by comparing the differences obtained.

Results presented in Table 2 show that the maximum relative deviations for resonance frequencies RF-1 and RF-2 are observed for an anomaly of a width of 0.25L. That applies to the two types of abnormalities investigated (swelling and cavity). The first resonance frequency (RF-1) for the swelling case presents a maximum deviation of -36.9% and -55.2% for “Canal 4” and “Canal 6”, respectively. In the case of a cavity, there is a maximum deviation of -9.29%, -7.56% for “Canal 4” and “Canal 6”, respectively.

Table 2: Effect of the width of swelling and cavity anomalies on frequency response for canal 4 and 6

		Resonant frequencies			SPL at resonant frequencies		
		RF-1	RF-2	RF-3	SPL (RF-1)	SPL (RF-2)	SPL (RF-3)
Canal 4							
	Healthy	3317 Hz	10140 Hz	14940 Hz	29,96 dB	28,00 dB	27,54 dB
Swelling	**w=0.05L**	0,03%	0,00%	-0,07%	-0,20%	0,04%	-0,15%
	w=0.1L	-0,63%	-0,79%	-0,74%	-0,93%	-0,61%	-1,67%
	w=0.15L	-3,26%	-3,41%	-2,14%	-3,00%	-3,86%	-7,88%
	w=0.2L	-13,0%	-7,88%	-2,61%	-8,38%	-14,6%	-22,91%
	w=0.25L	-36,9%	-13,0%	-1,41%	-20,63%	-40,2%	-54,18%
Cavity	**w=0.05L**	-0,18%	-0,10%	-0,07%	0,07%	-0,14%	-0,07%
	w=0.1L	-1,15%	-0,59%	-0,40%	0,30%	-0,89%	-0,76%
	w=0.15L	-2,68%	-2,05%	-0,67%	0,60%	-2,89%	-3,20%
	w=0.2L	-5,85%	-2,74%	-0,40%	0,73%	-5,79%	-6,25%
	w=0.25L	-9,26%	-3,59%	0,66%	0,97%	-9,57%	-9,77%
Canal 6							
	Healthy	3504 Hz	10230 Hz	16470 Hz	29,61 dB	26,30 dB	25,43 dB
Swelling	**w=0.05L**	-0,29%	-0,20%	0,00%	-0,24%	-0,23%	-0,31%
	w=0.1L	-1,66%	-1,17%	-0,36%	-1,32%	-1,71%	-2,79%
	w=0.15L	-6,65%	-4,18%	-1,52%	-4,36%	-7,19%	-11,72%
	w=0.2L	-19,9%	-9,19%	-2,06%	-11,65%	-21,4%	-32,05%
	w=0.25L	-55,2%	-14,4%	-0,97%	-29,35%	-64,3%	-83,20%
Cavity	**w=0.05L**	-0,11%	-0,20%	-0,18%	0,17%	0,08%	0,04%
	w=0.1L	-0,66%	-0,78%	-0,91%	0,54%	-0,11%	-0,63%
	w=0.15L	-2,11%	-1,96%	-1,82%	0,91%	-1,18%	-2,87%
	w=0.2L	-4,42%	-3,18%	-2,00%	1,28%	-3,38%	-6,41%
	w=0.25L	-7,56%	-3,89%	-1,21%	1,52%	-6,46%	-9,99%

In the case of the second resonance frequency (RF-2) and for swelling anomaly, there is a maximum deviation of -13% and -14.4% for “Canal 4” and “Canal 6”, respectively. In the case of a cavity, there is a maximum deviation of -3.59% and -3.89% for “Canal 4” and “Canal 6”, respectively.

There is a maximum deviation of -2.61% in the third resonance frequency (RF-3) for the swelling anomaly of width 0.2L in “Canal 4”. For “Canal 6”, one can observe a deviation of -2.06% for an anomaly of the same width. In the case of cavity, there is a maximum deviation of -6.67% for “Canal 4” with an anomaly of width 0.15L and a maximum deviation of -2% for “Canal 6” with an anomaly of width 0.2L.

From these deviations, it can be deduced that the effect of the increase in the anomaly width is the maximum for RF-1. This effect is less pronounced for RF-2 and less so for RF-3. It should be noted that the effect on RF-3 is insignificant, regardless of the type of anomaly and its width. However, the influence of this anomaly has a major effect on the SPL at this frequency (RF-3).

The maximum relative deviations of the SPL at resonance frequencies is observed at the third resonance frequency (RF-3). Its value is -9.77% and -9.99% for “Canal 4” and “Canal 6”, respectively in the case of a cavity. In the case of swelling

anomaly, there is a maximum deviation of -54.8% and -83.20% for "Canal 4" and "Canal 6", respectively. From these values, it can be noted that the drop in SPL caused by an increase in anomaly width is very significant, especially at the third resonance frequency.

4.4. Effect of anomaly height/depth

The anomaly position parameter "p" is set to 0.5L and the width "w" is set to 0.15L in order to evaluate the influence of the height/depth "d" of the swelling or cavity on the frequency response of the human auditory canal. In the case of a swelling anomaly, the parameter "d" being studied is called height, and in the case of a cavity anomaly, one can talk about the depth.

Figure 15 shows the results obtained for canals 4 and 6 consisting of a swelling with values of varying heights. Figure 16 shows the data for the cavity case. Table 3 illustrates the relative deviations of the resonant frequency and the SPLs at these frequencies, taking as a reference the healthy auditory canal.

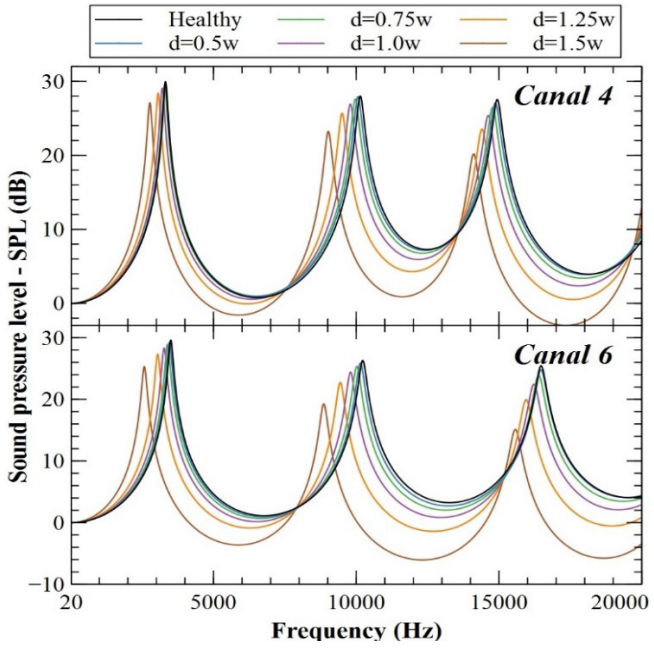

Figure 15 : Frequency response of the auditory canals with a swelling anomaly of different heights d (p= 0.5L and w=0.15L)

Figure 15 indicates negative magnitudes relating to the reduction of SPL through the ear canal with swelling. The maximum of these values, in "Canal 4", are -1.58 and -2.96 dB, observed in the case of an anomaly of 1.50w height in the frequency bands [4737-7026] Hz and [15776-18849] Hz respectively. Thus, the greater the swelling height, the more risk of hearing loss can be expected.

In the case of "Canal 6", at frequency bands [5381-7195] Hz, [11601-13834] Hz and [18210-20000] Hz, negative SPL values are noted for anomalies of height 1.25w. Same finding for the anomaly of the 1.50w height in the [4127-7510] Hz, [10037-14501] Hz and [16630-20000] Hz frequency bands. The maximum values observed for the 1.25w height anomaly in the above mentioned bands are -0.865, -1.4 and -0.53 dB, respectively. The maximum values measured for the anomaly of 1.50w height are -3.62, -6.05 and -5.77 dB, respectively.

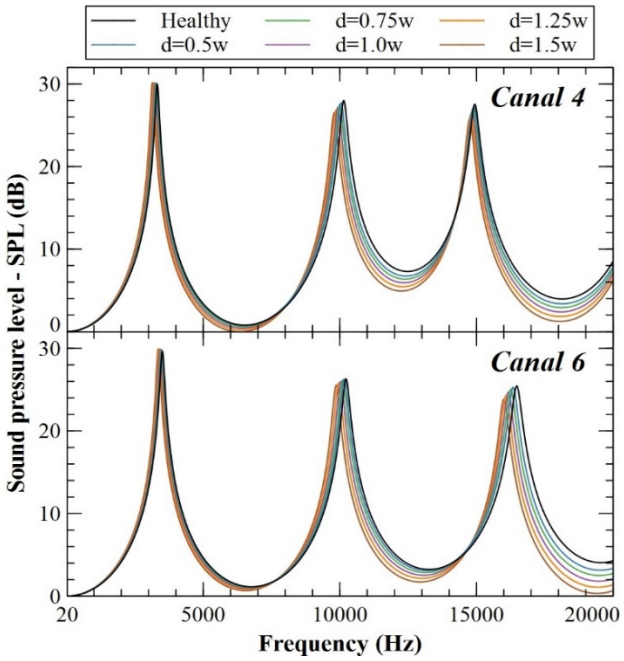

Figure 16 : Frequency response of the auditory canals with a cavity anomaly of different depths d (p= 0.5L and w=0.15L)

Table 3: Effect of the height/depth of swelling and cavity anomalies on frequency response for canal 4 and 6

		Resonant frequencies			SPL at resonant frequencies		
		RF-1	RF-2	RF-3	SPL (RF-1)	SPL (RF-2)	SPL (RF-3)
Canal 4							
	Healthy	3317 Hz	10140 Hz	14940 Hz	29,96 dB	28,00 dB	27,54 dB
Swelling	**d=0.5w**	0,24%	-0,79%	-0,47%	-0,87%	-0,36%	-1,71%
	d=0.75w	-0,9%	-1,71%	-1,07%	-1,67%	-1,46%	-3,92%
	d=1.00w	-3,26%	-3,41%	-2,14%	-3,0%	-3,86%	-7,88%
	d=1.25w	-7,60%	-6,26%	-3,55%	-5,24%	-8,25%	-14,49%
	d=1.5w	-16,5%	-11,0%	-5,49%	-9,55%	-17,0%	-26,7%
Cavity	**d=0.5w**	-0,63%	-0,89%	-0,20%	0,43%	-1,04%	-0,98%
	d=0.75w	-1,60%	-1,46%	-0,47%	0,53%	-1,89%	-1,96%
	d=1.00w	-2,68%	-2,05%	-0,67%	0,60%	-2,89%	-3,20%
	d=1.25w	-3,92%	-2,71%	-0,94%	0,63%	-4,04%	-4,65%
	d=1.5w	-5,28%	-3,40%	-1,20%	0,63%	-5,25%	-6,28%
Canal 6							
	Healthy	3504 Hz	10230 Hz	16470 Hz	29,61 dB	26,30 dB	25,43 dB
Swelling	**d=0.5w**	-1,37%	-0,78%	0,06%	-1,28%	-1,63%	-2,63%
	d=0.75w	-3,22%	-2,05%	-0,49%	-2,47%	-3,69%	-5,98%
	d=1.00w	-6,65%	-4,18%	-1,52%	-4,36%	-7,19%	-11,72%
	d=1.25w	-13,0%	-7,7%	-3,16%	-7,7%	-13,54%	-21,55%
	d=1.5w	-26,4%	-13,3%	-5,40%	-14,52%	-26,77%	-40,54%
Cavity	**d=0.5w**	-0,57%	-0,68%	-0,79%	0,61%	-0,11%	-0,55%
	d=0.75w	-1,26%	-1,27%	-1,28%	0,81%	-0,53%	-1,53%
	d=1.00w	-2,11%	-1,96%	-1,82%	0,91%	-1,18%	-2,87%
	d=1.25w	-3,11%	-2,74%	-2,31%	1,01%	-2,02%	-4,44%
	d=1.5w	-4,25%	-3,57%	-2,85%	1,05%	-2,97%	-6,21%

It should be mentioned that the frequency bands mentioned above in the case of anomaly of 1.25w height are far more restricted than that of anomaly of 1.50w height. It can be seen from these values that the influence of the height of the anomaly is less significant than the other effects studied, but remains quite important especially for the swelling case.

As in the study of the effect of the position and the width of the anomaly, the SPL curve presents no negative values in the case of the auditory canals in the presence of a cavity (Figure 16). Curves obtained for auditory canals with anomalies show greater deviations for "Canal 6" than for "Canal 4". This can be easily confirmed by reading Figure 16 and Table 3.

Considering the results shown in Figure 16 for "Canal 6", the maximum absolute deviations are -3.82, -6.15, -8.42, -10.51 and -12.38 dB measured between the healthy canal SPL and the auditory canals with 0.5w, 0.75w, 1w, 1.25w and 1.50w depth anomalies, respectively. Those variations occurs at 16589, 16567, 16545, 16535 and 16530 Hz frequencies for 0.5w, 0.75w, 1w, 1.25w and 1.50w depths respectively. It can be noted that the maximum absolute deviations occur at high frequencies for all considered cases. These deviations are observed at an almost identical frequency (around 16550 Hz) for all studied cases. This can also be shown that these differences correlate linearly with increasing depth d parameter.

By taking into account, for example, the results of the swelling case in "Canal4" available in Table 3, it can be observed that the deviations in resonance frequency varies from -0.24% for the height of 0.1w to -16.5% for the height of 1.5w. This shows that the resonance frequency varies linearly with the height / depth of the anomaly. It can also be found that the SPL deviation at the resonance frequency varies from -0.87% at a height of 0.1w to -9.55% at a height of 1.5w. This shows that the SPL at resonance frequency varies in an exponential manner with the height/depth of the anomaly.

Reading from Table 3, maximum relative deviations in terms of frequency resonance and SPL at those frequencies are all observed for 1.5w, which is the highest depth/height value considered in the analysis. In the case of "Canal4" with a 1.5w depth swelling, the deviation is -16.5%, -11%, -5.49% at the first, the second and the third resonant frequencies respectively. The deviation in SPL is -9.55%, -17%, -26.7% at the first, the second and the third resonant frequencies respectively.

The effect of increasing the anomaly depth is most pronounced for RF-1. This effect is less significant for RF-2 and even less for RF-3. The opposite effect is observed with respect to the SPL at these frequencies. The same observation can be made from both canals (4 and 6) as well as the two anomalies (cavity and swelling).

5. Conclusion

An investigation is conducted in this paper with the purpose of better understanding the influence of some abnormalities which may cause tinnitus. A previously developed and validated acoustic model associates an acoustic resonator with each part of the outer ear. Such resonators can have several forms which may be used to model a human auditory canal. The model is used for adding various anomalies into it, either by incorporating acoustic resonators or by operating on the parameters of it. The abnormalities examined are those that may induce a change in the external auditory canal section, or an alternation in the external ear 's sound transmission medium.

The acoustic model is applied to two auditory canals that are found in the literature where anomalies are inserted. A parametric study is conducted taking into account the influence of an anomaly's location, width and depth simulating an obstacle on the outer ear's frequency response. This research also discusses the influence of the propagation speed of sound in the ear canal to model a form of ear condition like swimmer's ear. This is done by contrasting the frequency response of a healthy external ear to an external ear with an anomaly.

It can be concluded in the light of the results that the presence of fluid in the ear canal tends to decrease its number of resonant frequencies in the audible band. The more fluid the ear canal has, the higher the resonant frequency and the higher the sound pressure level at it.

A swelling at the entrance of the auditory canal or a cavity at the end of it may result in a significant drop in the first resonance frequency value. The finding at the second frequency of resonance is entirely inverted. A swelling effect causes this frequency to drop for the third resonance frequency at the input and output of the auditory canal. A cavity at the end of the auditory canal functions in the same way. The auditory canal SPL's response decreases exponentially with an increase in the anomaly's width. The effect of the anomaly width increase is the maximum for first resonant frequency. The drop in SPL at third resonance frequency is the most significant.

The effect of the anomaly's height is less significant than the other parameters studied, but remains very important especially for the case of swelling. For this case, the more the height of the anomaly, the more probability of hearing loss can be expected. The deviation between the resonant frequency for the healthy canal and the one with anomaly correlate linearly with increasing height/depth parameter. However, the deviation of the SPL at resonance frequency varies exponentially with the height/depth.

Across all the cases analyzed, it is observed that, when contrasting it with the swelling anomaly, the cavity has less effect on the frequency response of the auditory canal. This is due to the fact that the swelling in the ear canal presents an obstacle while the cavity presents a wider opening. The frequency response of auditory canals with the same anomaly is not identical. This amounts to the disparity of their anatomies.

All anomalies cause changes in SPL, resulting in increases in some frequency ranges and, at the same time, attenuation in other ranges. This can lead to hearing loss or over-sensitivity to sound having these frequencies. This could lead to tinnitus with severities that rely on the physiology and psychology of the individual.

References

[1] C. Coelho, R. Santos, Roberto, K. Campara, R. Tyler, "Classification of Tinnitus" Otolaryngologic Clinics of North America, **S0030-6665**(20), 30052–9, 2020. https://doi.org/10.1016/j.otc.2020.03.015

[2] J. M. Bhatt, H. W. Lin, N. Bhattacharyya, "Prevalence, severity, exposures, and treatment patterns of tinnitus in the United States" JAMA Otolaryngol Head Neck Surg., **142**(10), 959–965, 2016. https://doi.org/10.1001/jamaoto.2016.1700

[3] E. A. Masterson, C. L. Themann, S. E Luckhaupt, J. Li, G. M. Calvert, "Hearing difficulty and tinnitus among US workers and non-workers in 2007" American Journal of Industrial Medicine, **59**(4), 290–300, 2016. https://doi.org/10.1002/ajim.22565
[4] E. Josse, Les acouphènes. Traitement par l'hypnose, Resilience-pys, 2006.
[5] K. J. Trevis, N. M. McLachlan, S. J. Wilson, "Cognitive Mechanisms in Chronic Tinnitus: Psychological Markers of a Failure to Switch Attention" Frontiers in psychology, **7**, 2016. https://doi.org/10.3389/fpsyg.2016.01262
[6] D. Ivansic, O. Guntinas-Lichius, B. Müller, G. F. Volk, G. Schneider, C. Dobel, "Impairments of Speech Comprehension in Patients with Tinnitus-A Review" Frontiers in aging neuroscience, **9**, 2017. https://doi.org/10.3389/fnagi.2017.00224
[7] P. Hyvärinen, "Neurophysiologically-based approaches to tinnitus diagnostics and treatment," Ph.D Thesis, Aalto University, 2016.
[8] L. Jagoda, N. Giroud, P. Neff, A. Kegel, T. Kleinjung, M. Meyer, "Speech perception in tinnitus is related to individual distress level - A neurophysiological study" Hearing Research, **367**, 48–58, 2018. https://doi.org/10.1016/j.heares.2018.07.001
[9] B. Langguth, A. B. Elgoyhen, "Current pharmacological treatments for tinnitus" Expert Opinion on Pharmacotherapy, **13**(17), 2495–2509, 2012. https://doi.org/10.1517/14656566.2012.739608
[10] D. A. Colucci, "Insomnia and Tinnitus: A Worrisome Cycle" The Hearing Journal, **70**(6), 43–45, 2017. https://doi.org/10.1097/01.HJ.0000520670.39014.4c
[11] S. Weidt, A. Delsignore, M. Meyer, M. Rufer, N. Peter, N. Drabe, T. Kleinjung, "Which tinnitus-related characteristics affect current health-related quality of life and depression? A cross-sectional cohort study" Psychiatry Research, **237**, 114–121, 2016. https://doi.org/10.1016/j.psychres.2016.01.065
[12] T. Rodebaugh, E. Lenze, "Tinnitus" JAMA, **323**, 2020. https://doi.org/10.1001/jama.2020.0697
[13] E. Coulon, "Les acouphènes ou l'impossible silence: étiologie, physiopathologie et tentatives de traitement, " Ph.D Thesis, Mixed Faculty Of Medicine And Pharmacy Of Rouen, 2002.
[14] I. Adamchic, T. Toth, C. Hauptmann, M. Walger, B. Langguth, I. Klingmann, P. A. Tass, "Acute effects and after-effects of acoustic coordinated reset neuromodulation in patients with chronic subjective tinnitus" NeuroImage: Clinical, **15**, 541–558, 2017. https://doi.org/10.1016/j.nicl.2017.05.017
[15] B. Mazurek, H. Olze, H. Haupt, A. J. Szczepek, "The more the worse: the grade of noise-induced hearing loss associates with the severity of tinnitus" International Journal of Environmental Research and Public Health, **7**(8), 3071–3079, 2010. https://doi.org/10.3390/ijerph7083071
[16] O. Zagólski, "Management of Tinnitus in Patients with Presbycusis" International Tinnitus Journal, **12**(2), 175–178, 2006.
[17] N. Julien, O. Sterkers, "Les acouphènes" La vie médicale, **16**, 661–667, 1990.
[18] P. S. Guth, J. Risey, W. Briner, P. Blair, H. T. Reed, G. Bryant, C. Norris, G. Housley, R. Miller, "Evaluation of amino-oxyacetic acid as a palliative in tinnitus" Annals of Otology, Rhinology, and Laryngology, **99**(1), 74–79, 1990. https://doi.org/10.1177/000348949009900113
[19] R. Salvi, E. Lobarinas, W. Sun, "Pharmacological Treatments For Tinnitus: New And Old" Drugs of the future, **34**(5), 381–400, 2009. https://doi.org/10.1358/dof.2009.034.05.1362442
[20] E. C. Nam, R. Lewis, H. H. Nakajima, S. N. Merchant, R. A. Levine, "Head rotation evoked tinnitus due to superior semicircular canal dehiscence" The Journal of Laryngology & Otology, **124**(3), 333–335, 2010. https://doi.org/10.1017/S0022215109991241
[21] D. M. Baguley, D. McFerran, D. Hall "Tinnitus" The Lancet, **382**(9904), 1600–1607, 2013. http://doi.org/10.1016/S0140-6736(13)60142-7
[22] R. F. Cima, D. Kikidis, B. Mazurek, H. Haider, C Cederroth, A. Noreña, A. Lapira, A. Bibas, D. Hoare, "Tinnitus healthcare: a survey revealing extensive variation in opinion and practices across Europe" BMJ Open, **10**, 2020. http://doi.org/10.1136/bmjopen-2019-029346
[23] F. Zamiri, M. Moosapour, R. Hoseinabadi, "Tinnitus Treatments and Managements" Global Journal of Otolaryngology, **13**(5), 01–04, 2018. https://doi.org/10.19080/GJO.2018.13.555874
[24] R.S Hallam, S.C Jakes, C. Chambers, R. Hinchcliffe, "A comparison of different methods for assessing the intensity of tinnitus" Acta Otolaryngol, **99**, 501–508, 1985. https://doi.org/10.3109/00016488509182253
[25] H. Selye, Du rêve à la découverte, Éditions de La Presse, 66–68, 1973.
[26] T. Fuller, R. F. Cima, B. Langguth, B. Mazurek, J. Vlaeyen, D. Hoare, Cognitive behavioural therapy for tinnitus, Cochrane Database of Systematic Reviews, 2020. http://doi.org/10.1002/14651858.cd012614.pub2
[27] P. J. Jastreboff, "25 Years of tinnitus retraining therapy" HNO, **63**, 307–311, 2015. https://doi.org/10.1007/s00106-014-2979-1
[28] C. Formby, R. Scherer, "Rationale for the Tinnitus Retraining Therapy Trial" Noise & health, **15**, 134–142, 2013. https://doi.org/10.4103/1463-1741.110299
[29] K. M. Reavis, V. S. Rothholtz, Q. Tang, J. A. Carroll, H. Djalilian, F. G. Zeng, "Temporary suppression of tinnitus by modulated sounds" Journal of the Association for Research in Otolaryngology : JARO, **13**(4), 561–571, 2012. https://doi.org/10.1007/s10162-012-0331-6
[30] R. Soleimani, M. M. Jalali, T. Hasandokht, "Therapeutic impact of repetitive transcranial magnetic stimulation (rTMS) on tinnitus: a systematic review and meta-analysis" European archives of oto-rhino-laryngology, **273**(7), 1663–1675, 2016. https://doi.org/10.1007/s00405-015-3642-5
[31] M. Pedemonte, Chapter 7 – Tinnitus treatment during sleep, The auditory system in sleep 2nd edition, 2018. https://doi.org/10.1016/B978-0-12-810476-7.00007-5
[32] ATA Newsletter, American Tinnitus Association, **10**(1), 1–4, 1985.
[33] P. Neff, L. Zielonka, M. Meyer, B. Langguth, M. Schecklmann, W. Schlee, "Comparison of Amplitude Modulated Sounds and Pure Tones at the Tinnitus Frequency: Residual Tinnitus Suppression and Stimulus Evaluation" Trends in hearing, 23, 1–16, 2019. https://doi.org/10.1177/2331216519833841
[34] R. M. Johnson, J. Fenwick, "Masking Levels (Minimum Masking Levels) and Tinnitus Frequency" The Journal of Laryngology & Otology, **98**(S9), 63–66, 1984. https://doi.org/10.1017/S1755146300090132
[35] M. Ralli, A. Greco, R. Turchetta, G. Altissimi, M. de Vincentiis, G. Cianfrone, "Somatosensory tinnitus: Current evidence and future perspectives" Journal of International Medical Research, **45**(3), 933–947, 2017. https://doi.org/10.1177/0300060517707673
[36] G. Shekhawat, K. Kobayashi, G. Searchfield, "Methodology for studying the transient effects of Transcranial Direct Current Stimulation combined with Auditory Residual Inhibition on Tinnitus" Journal of Neuroscience Methods, **239**, 28–33, 2014. https://doi.org/10.1016/j.jneumeth.2014.09.025
[37] H. Teismann, A. Wollbrink, H. Okamoto, G. Schlaug, C. Rudack, C. Pantev, "Combining transcranial direct current stimulation and tailor-made notched music training to decrease tinnitus-related distress--a pilot study" PloS one, **9**(2), 1–11, 2014. https://doi.org/10.1371/journal.pone.0089904
[38] J. Melloui, O. Bouattane, J. Bakkoury, "Study of the effect of a cause of tinnitus on the resonant frequency of the outer ear" in 1st International Conference on Innovative Research in Applied Science, Engineering and Technology (IRASET), Meknes, Morocco, 2020. https://doi.org/10.1109/IRASET48871.2020.9092217
[39] B. B. Ballachanda, "Theoretical and applied external ear acoustic" Journal of the American Academy of Audiology, **8**(6), 411–420, 1998.
[40] E. A. G. Shaw, Acoustical Characteristics of the Outer Ear, Encyclopedia of Acoustics, M.J. Crocker (Ed.), 1325–1335, 2007. https://doi.org/10.1002/9780470172537.ch105
[41] J. Melloui, O. Bouattane, J. Bakkoury, "Acoustic model of the human outer ear" International Journal of Engineering & Technology, **7**(4), 3286–3293, 2018. https://doi.org/10.14419/ijet.v7i4.15842
[42] H. Hudde , A. Engel, "Measuring and modeling basic properties of the human middle ear and ear canal. Part II: Ear canal, middle ear cavities, eardrum, and ossicles" Acta Acustica united with Acustica, **84**(5), 894–913, 1998.
[43] M.R. Stinson, B.W. Lawton, "Specification of the geometry of the human ear canal for the prediction of sound-pressure level distribution" The Journal of the Acoustical Society of America, **85**(6), 2492-2503, 1989. https://doi.org/10.1121/1.397744

ASTES

Advances in Science, Technology and Engineering Systems Journal
Vol. 5, No. 5, 478-484 (2020)
www.astesj.com
Special Issue on Innovative Research in Applied Science, Engineering and Technology

ASTES Journal
ISSN: 2415-6698

Contextual Word Representation and Deep Neural Networks-based Method for Arabic Question Classification

Alami Hamza[*,1], Noureddine En-Nahnahi[1], Said El Alaoui Ouatik[1,2]

[1]*LISAC Laboratory, Faculty of Sciences Dhar El Mahraz, Sidi Mohamed Ben Abdellah University, PO Box 1796, Fez 30003, Morocco*

[2]*Laboratory of Engeneering Sciences, National School of Applied Sciences, Ibn Tofail University, Kenitra, Morocco*

ARTICLE INFO

Article history:
Received: 01 July, 2020
Accepted: 05 September, 2020
Online: 24 September, 2020

Keywords:
Arabic Question Classification
Contextual Word Representation
ELMo
RNN
CNN

ABSTRACT

Contextual continuous word representation showed promising performances in different natural language processing tasks. It stems from the fact that these word representations consider the context in which a word appears. But until recently, very little attention was paid to the contextual representations in Arabic question classification task. In the present study, we employed a contextual representation called Embeddings from Language Models (ELMo) to extract semantic and syntactic relations between words. Then, we build different deep neural models according to three types: Simple models, CNN and RNN mergers models, and Ensemble models. These models are trained on Arabic questions corpus to optimize the cross entropy loss given questions representations and their expected labels. The dataset consists of 3173 questions labeled according the Arabic taxonomy and an updated version of the Li & Roth taxonomy. We performed various comparisons with models based on the widely known context-free word2vec word representation. These evaluations confirm that ELMo representation achieves top performances. The best model scores up to 94.17%, 94.07%, 94.17% in accuracy, macro $F1$ score, and weighted $F1$ score, respectively.

1 Introduction

Question Answering Systems (QAS) have become one of the most popular information retrieval applications. These systems enable automatic answering to natural questions. This involves several parts functioning jointly to extract exact response, considering a user's question. A typical QAS is composed of three main components: 1) Question processing performs Question Classification (QC) and keywords extraction; 2) Passage retrieval apply information retrieval techniques to extract the passages that most probably contains the answer; 3) Answer processing processes the extracted passages and formulate the answer in natural language. A proper QC method enhances the performance of QAS by omitting insignificant answer candidates. In [1], the authors showed that 36.4% of errors made by QAS are associated to the QC. Despite the progress in different English natural language processing domains due to machine learning models, Arabic questions classification must address countless challenges owing to the lack of labeled corpora and difficulties associated to the complex morphology of this language, such us the absence of capital letters, the presence of diacritical marks, and its inflectional and derivational nature.

A typical QC method based on machine learning is composed of three main steps: 1) question preprocessing; 2) question representation; and 3) question classification. Previous works [2] represented words with term frequency-inverse document frequency (TF-IDF) method. This latter neglects relationships between words inside a question resulting in poor question representation. This restrictions led the authors [3] to use a continuous distributed word embeddings model [4]. This word representation ignores the context word yet it has the up side of considering both semantic and syntactic relations between words.

In this paper, we build question embedding by using a contextual representations namely Embeddings from Language Models (ELMo) [5]. Unlike the well known word2vec [4] representation that not consider the context, ELMo representation is able to compute word representation considering the word's context. In addition, we build various models according to three types: Simple models, CNN and RNN mergers models, and Ensemble models. The simple models are based on global max pooling, CNN, and RNN without any CNN/RNN combination. The CNN and RNN mergers models combine CNN and RNN layers to extract automatically more features from word representations. The Ensemble models predict

[*]Corresponding Author: Alami Hamza, Sidi Mohammed Ben Abdellah University, Morocco hamza.alami1@usmba.ac.ma

the probability of class labels by mixing the probability scores from different models. Our evaluations confirm that contextual representations show a good effects on Arabic question classification, and ensemble models based on word2vec and ELMo representations achieves top performances since they scored up to 94.17%, 94.07%, 94.17% in regards to accuracy, macro $F1$ score, and weighted $F1$ score.

The rest of the paper is structured as follows: Section 2 provides a brief overview of the previous works on Arabic question classification; Section 3 reveals our method for Arabic question classification which is based on contextual word representation; Section 4 presents the performance evaluations and the comparison results of various models; Finally, Section 5 concludes and gives future works and perspectives.

2 Related works

Numerous researches proposed methods for Arabic question classification. We introduce some of these methods in the following paragraphs.

In [6], the authors created a question answering system particularly for the holy Quran. Questions are represented by a set of terms, every term comprises both a part of speech tag and a stem of a word. They introduced a new taxonomy especially for classifying the question associated to the holy Quran. A support vector machine (SVM) classifier was trained on 180 training questions and tested with 3-folds cross validation on 50 questions. The obtained accuracy was about 77.2%.

In [7], the authors pursued a rule based approach to build their Arabic question classifier. The authors employed the NOOJ [1] tool to develop the Arabic linguistic rules that characterize question. They prepared a set of 200 questions for training questions and a set of 200 questions for test. They observed recall and precision are 93% and 100%, respectively.

In [2], the authors performed a comparison between two well known algorithms, SVM and Multinomial Naive Bayes, for Arabic question classification. In order to represent questions into vector space model, the TF-IDF method was applied. They trained the models with 300 training questions and tested on 200 questions. The best results were achieved by the SVM model which scored 100%, 94%, and 97% on precision, recall, and F1-measure.

In [3], the authors suggested a new Arabic taxonomy motivated from Arabic linguistic rules. They applied the continuous distributed word representation proposed in [4, 8, 9] to represent words. This representation captures semantic and syntactic relations between words. Various models including SVM, XGBoost, logistic regression were trained to classify questions given their words vectors. They built a dataset that contains 1041 questions for training and 261 questions for testing. The best performances were scored with the SVM model. It achieved 90%, 91%, 90%, and 90% on accuracy, precision, recall, and F1 score.

These works added on the progress of Arabic question classification methods. Nevertheless, the sizes of the datasets used in these studies were relatively small. Also, the TF-IDF representation has several drawbacks such us the word representation is sparse and huge, the semantic and syntactic relations between words can not be captured. What's more, the enriched word2vec representation calculates static word vectors neglecting the context were a word appears. Thus, a word with multiple meaning (polysemy phenomena) is misrepresented. Finally, the method based on linguistic rules proposed by [7] is highly impacted by the dataset used to extract rules and demands greater time and rules to consider additional Arabic question types.

[1] http://www.nooj-association.org/

3 Method

Our method is composed of three main steps including preprocessing, question representation, and questions classification.

3.1 Preprocessing

Our preprocessing pipeline is composed of two main steps: 1) punctuation and non Arabic words removal; 2) questions tokenization. Unlike standard pipelines of text preprocessing which perform stop words removal, we keep these words since they contain valuable information and are involved during the question classification. For instance, the words *Why* and *Who* are essential to identify the question type.

3.2 Question representation

To represent questions into a vector space format, we use the ELMo representation introduced in [5, 10]. All the words included into a question are passed to a neural network that is composed of two main layers: 1) one dimensional convolutional neural network with different filter sizes that computes word embeddings based on its character level embeddings; 2) a stack of two Bidirectional LSTM (BiLSTM) layers. The network is trained with large textual corpora to optimize language model objective. Thus, the ELMo representation of a word k, given by $\mathbf{ELMo}_k$, is calculated by the next equation:

$$\mathbf{ELMo}_k = \frac{1}{3}\sum_{j=0}^{2} \mathbf{h}_{k,j}^{(LM)} \quad (1)$$

where $\mathbf{h}_{k,j}$ is the output of the hidden layers j of the neural network. Figure 1 depicts the overall design of the ELMo technique. In order to calculate contextual word representation, we used the pre-trained word representation presented by [10, 11]. The model is trained with a set of 20-million-words data randomly picked from the Arabic Wikipedia corpus. Every word in represented by an 1024 dimension vector.

A question Q, that is a succession of l words, is modeled by the later matrix:

$$\mathbf{Q} = [\mathbf{ELMo}_{word_1}, ..., \mathbf{ELMo}_{word_l}] \quad (2)$$

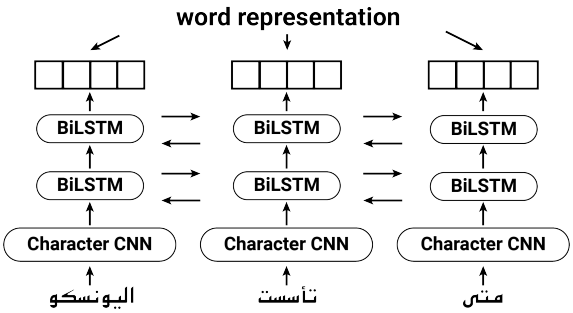

Figure 1: The overall architecture of Embeddings from Language Models

3.3 Questions classification

We constructed several neural network models on top of ELMo embeddings for Arabic questions classification. The goal is to investigate the behavior of contextual representation with diverse neural network architectures. In the course of training, the parameters of the ELMo model are fixed and the remainder of the parameters are optimized according the categorical cross entropy loss denoted by the equation:

$$J(\theta) = -\frac{1}{T}\sum_{t=1}^{T}\left[y_t \log \hat{y}_t + (1 - y_t)\log\left(1 - \hat{y}_t\right)\right] \tag{3}$$

where y_t is the true class label, $\hat{y}_t$ is the predicted class label, and T is the count of a taxonomy's classes.

3.3.1 ELMo with global max pooling

Our primary model consists of a pile of layers including input layer, global max pooling layer and a softmax layer. The input layer represents the input features which are questions embeddings calculated with the ELMo model. The global max pooling catches the more important characteristics. The softmax layer maps these features to a vector of probabilities. Figure 2 depicts the explained architecture.

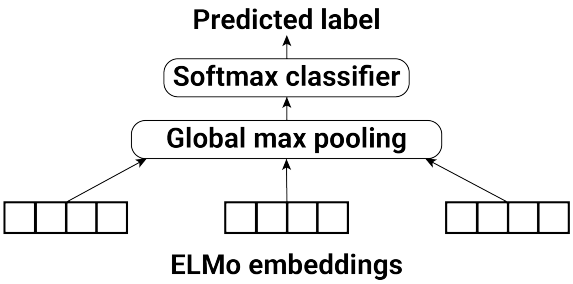

Figure 2: ELMo with global max pooling model

3.3.2 ELMo with global max pooling and dense layer

Based on the model described in the previous subsection 3.3.1 and with the purpose of extracting more features, we included a dense layer among the softmax layer and the global max pooling layer. Figure 3 illustrates the described architecture.

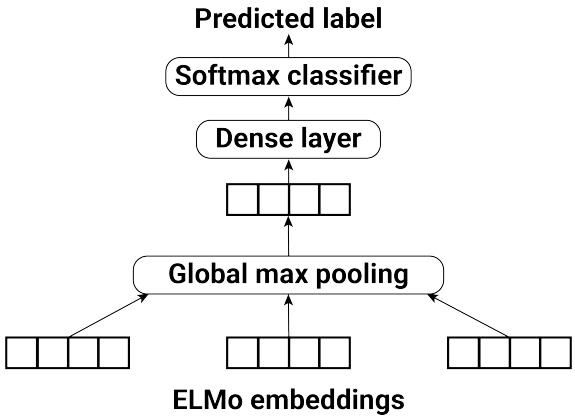

Figure 3: ELMo with global max pooling and dense layer model

3.3.3 ELMo with last hidden state of a GRU layer

To extract additional features, we included a Gated Recurrent Unit (GRU) layer that can handle sequential data and extract helpful information. Let denote Q a question represented by $Q = [w_1, w_2, ...w_k]$ where k the number of word vectors within Q and w_i is the i-th word vector of the question. GRU processes the data word-by-word according to the time-step from the past to the future. At each time step the current hidden state is computed as follows:

$$r_t = \text{sigmoid}\left(W_r \cdot [h_{t-1}, w_t]\right) \tag{4}$$

$$z_t = \text{sigmoid}\left(W_z \cdot [h_{t-1}, w_t]\right) \tag{5}$$

$$\tilde{h}_t = \tanh\left(W_{\tilde{h}} \cdot [r_t \odot h_{t-1}, w_t]\right) \tag{6}$$

$$h_t = (1 - z_t) \odot h_{t-1} + z_t \odot \widetilde{h}_t \tag{7}$$

The output of the final hidden state is passed to the softmax layer to compute the probabilities of belonging to each class label. Figure 4 presents the described architecture.

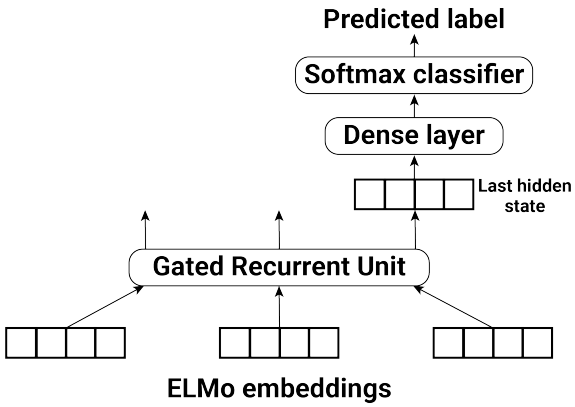

Figure 4: ELMo with last hidden state of a GRU layer model

3.3.4 ELMo with GRU and global max pooling

This model considers all the time steps from the GRU layer. It applies a global max pooling to extract the most important features

from every words within a question. The architecture of the model is illustrated in Figure 5.

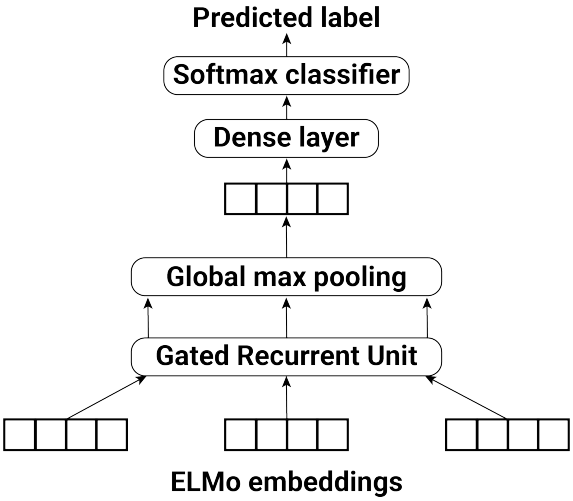

Figure 5: ELMo with GRU and global max pooling model

3.3.5 ELMo with CNN and global max pooling

Convolutional Neural Networks (CNN) proved good performances in both computer vision and NLP fields. These models extract new features applying 1 dimensional convolution on word neighbours. Figure 6 illustrates the model architecture. Let $w_i \in \mathbb{R}^p$ the p dimensional word representation corresponding to the i-th word in the question. A question of length k, which is padded when necessary, is represented by the following equation:

$$Q = [w_1, w_2, ...w_k] \tag{8}$$

where Q the question matrix. New features $m \in \mathbb{R}^{k-n+1}$ are produced by applying a convolution to each window of n words. The window size n vary between 2 to 5 thus we compute for each widow size a feature map. We then apply global max pooling [12] to capture the most important features. We concatenate these features and apply a softmax layer to classify the question.

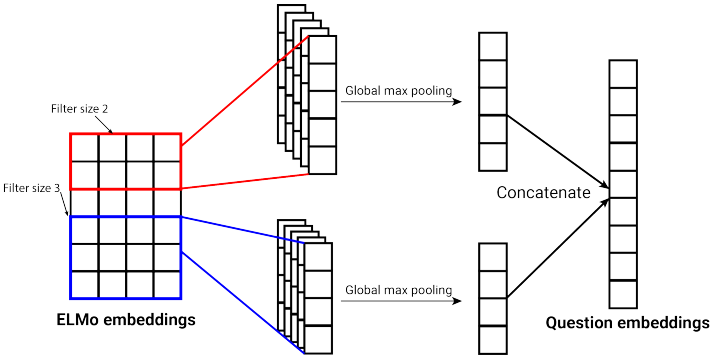

Figure 6: Multiple filters CNN with global max pooling

3.3.6 ELMo with CNN, GRU, and global max pooling

This model apply a convolution filters on top of ELMo embeddings. This operation results in a number of features maps equals to the number of filters used. Next, each features map is passed to GRU layers. The question embeddings is then the concatenation of the outputs of a set global max pooling functions applied on top of each hidden states of GRU layers. Finally, a softmax function is applied to classify the question. Figure 7 illustrates the architecture of this model.

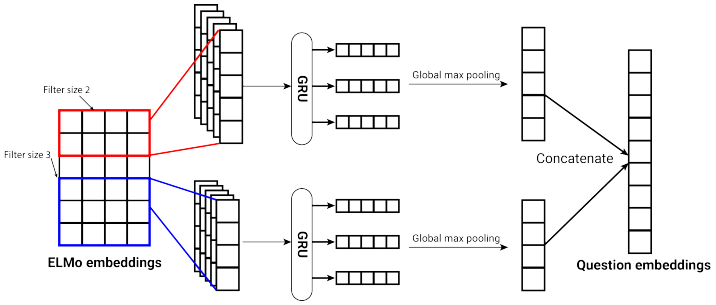

Figure 7: Multi filters CNN and GRU layers

3.3.7 ELMo with GRU, CNN, and global max pooling

The architecture of this model is similar to the architecture described in section 3.3.6. The only change is we apply first a GRU layer then convolution operations with different filter. Figure 8 presents the general architecture of this model. Various convultions with filter size between 2 to 5 are applied to the hidden states of the GRU layer. Next, a global max pooling is applied to extract the most important features for each filter features. Finally, the outputs of the global max pooling functions are concatenated to build the question embeddings.

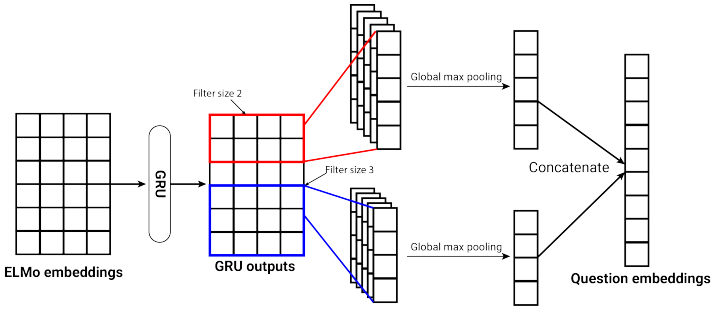

Figure 8: GRU and multi filters CNN model

3.3.8 Ensemble Models

An ensemble model aggregates the prediction of diverse models results in once final prediction for unseen data. We applied two ensemble models including mean scores-based ensemble and max scores-based ensemble. The mean scores-based model computes the average of the probability scores predicted by each model the class label with the highest probability score is assigned to the question. The max scores-based model pick the class label with the highest probability across all the predicted scores from different model.

4 Experimental results

4.1 Questions Classification Dataset

The dataset consists of 3173 Arabic questions. These questions are manually labeled with an application created by our team. We picked randomly 80% (2538) of questions as training set and 20% (635) of questions as testing set. Table 1 and Table 2 show the distribution of the class labels.

Table 1: Distribution of classes in the Arabic questions dataset

Classes	#	Classes	#
(Human...) العاقل	602	(Entity...) غير العاقل	1084
(Status...) حال الشيء و هيئته	121	(Location) المكان	450
(Time) الزمان	318	(Numbers) العدد	304
(Yes/No) التصديق	294		

Table 2: Distribution of classes in the Arabic questions dataset

Classes	#	Classes	#
Abbreviation	22	Description	709
Entity	468	Human	627
Location	453	Numeric	600
Yes/No	294		

4.2 Experimental settings

Considering that we deal with a multi-class classification problem, we use three measures to evaluate every model. The measures contain accuracy, macro F1 score and weighted F1 score. We employed widely known libraries including Scikit-learn, Tensorflow 2.0 and Keras libraries to construct and evaluate every single model [13, 14]. In the interest of reducing the internal covariate shift and the training time, we utilize layer normalization [15]. We fixed the batch size at 32 questions and the epochs at 1000 iterations for each model. We retained the model that achieves the optimal loss on training set. Our experiments are completely carried out in Google Colaboratory[2].

4.3 Simple models evaluation

We segment the proposed models into three sets including simple models, CNN and RNN mergers, ensemble models. The first set contains simple models that are composed with global max pooling, convolutions, and recurrent neurones layers. These model do not contain any type of combination between convolutions and recurrent neurones layers. The second set is named CNN and RNN mergers where convolutions and recurrent features are merged. The last models apply ensemble methods to build the question classification performance.

We evaluate our simple models with two different word representation: 1) The context-free word representation, designated by enriched word2vec with subword information [16], which embeds a word into a 300 dimensional vector. This technique possesses the capability to catch semantic and syntactic relationships among words. At the same time, it do not take into account the word in context; and 2) The contextual word representation ELMo [5] which calculates a 1024 dimensional vector for each word. This representation regards the context of word resulting in an enhanced question embeddings. Table 3 and Table 4 shorten the achieved performances with both the Arabic taxonomy and the updated Li & Roth taxonomy. In the event of the Arabic taxonomy, the ELMo representation surpasses the enriched word2vec representation in regards to accuracy, macro F1 score, and weighted F1 score. Nonetheless, this come at the expense of the lower size of the words' vectors. Lastly, the model which consists of ELMo embeddings, GRU layer, and global max pooling layer achieves the best performances outlined by 93.86%, 93.37%, and 93.84% on accuracy, macro F1 score, and weighted F1 score. In the event of the updated Li & Roth taxonomy, word2vec based models handle better the imbalanced dataset problem. The model that have word2vec embeddings as inputs and composed of GRU and global max pooling achieves 87.24% in terms of macro F1 score. The model composed of ELMo embeddings, CNN, and global max pooling scored top results in terms of accuracy and weighted F1 score.

Table 3: Performance measures (accuracy, macro F1 score, and weighted F1 score) of simple models with Arabic taxonomy

	Accuracy	*macro F1 score*	*weighted F1 score*
W2V + Global max pooling	78.74%	78.38%	78.64%
W2V + Global max pooling + dense	82.99%	82.86%	82.92%
W2V + Last hidden state of GRU	92.44%	92.74%	92.45%
W2V + GRU + Global max pooling	92.76%	92.96%	92.75%
W2V + CNN + Global max pooling	90.55%	91.00%	90.56%
ELMo + Global max pooling	86.77%	88.25%	86.83%
ELMo + Global max pooling + dense	88.03%	89.03%	88.11%
ELMo + Last hidden state of GRU	91.97%	92.12%	91.96%
ELMo + GRU + Global max pooling	**93.86%**	**93.37%**	**93.84%**
ELMo + CNN + Global max pooling	90.70%	91.12%	90.65%

Table 4: Performance measures (accuracy, macro F1 score, and weighted F1 score) of simple models with the updated Li & Roth taxonomy

	Accuracy	*Macro F1 score*	*Weighted F1 score*
W2V + Global max pooling	76.54%	65.61%	76.32%
W2V + Global max pooling + dense	81.73%	70.51%	81.68%
W2V + Last hidden state of GRU	91.65%	85.50%	91.56%
W2V + GRU + Global max pooling	92.13%	**87.24%**	92.05%
W2V + CNN + Global max pooling	89.13%	85.87%	88.97%
ELMo + Global max pooling	80.94%	71.87%	80.52%
ELMo + Global max pooling + dense	84.72%	76.51%	84.86%
ELMo + Last hidden state of GRU	91.50%	82.31%	91.69%
ELMo + GRU + Global max pooling	91.97%	82.67%	92.03%
ELMo + CNN + Global max pooling	**92.28%**	82.78%	**92.33%**

4.4 CNN and RNN mergers evaluation

We test out CNN and RNN mergers with the word2vec and ELMo word representations. These models have the ability to extract more valuable features from raw data. Table 5 presents the results of the CNN and RNN mergers with the Arabic taxonomy. The model that takes ELMo embeddings as inputs and apply GRU then CNN achieves the best scores 94.01%, 93.60%, and 93.98% in terms of accuracy, macro F1 score, and weighted F1 score. Besides, Table 6 shows that the word2vec word representation with Li & Roth taxonomy scored the best results 91.81% accuracy, 88.32% macro F1 score, and 91.84% weighted F1 score. However, the model

[2]https://colab.research.google.com/

architecture remains the same. Thus, the evaluation confirms that applying GRU layer followed by CNN layer is better than applying CNN layer then GRU layer for Arabic question classification.

Table 5: Performance measures (accuracy, macro F1 score, and weighted F1 score) of the CNN and RNN mergers with the Arabic taxonomy

	Accuracy	*Macro F1 score*	*Weighted F1 score*
W2V+CNN+GRU+Global Max Pooling	90.71%	90.91%	90.68%
W2V+GRU+CNN+Global Max Pooling	92.44%	92.47%	92.43%
ELMo+CNN+GRU+Global Max Pooling	91.02%	90.96%	91.03%
ELMo+GRU+CNN+Global Max Pooling	**94.01%**	**93.60%**	**93.98%**

Table 6: Performance measures (accuracy, macro F1 score, and weighted F1 score) of the CNN and RNN mergers with the updated Li & Roth taxonomy

	Accuracy	*Macro F1 score*	*Weighted F1 score*
W2V+CNN+GRU+Global Max Pooling	91.02%	86.16%	90.92%
W2V+GRU+CNN+Global Max Pooling	**91.81%**	**88.32%**	**91.84%**
ELMo+CNN+GRU+Global Max Pooling	90.87%	81.24%	90.86%
ELMo+GRU+CNN+Global Max Pooling	91.65%	84.87%	91.75%

4.5 Ensemble models evaluation

Finally, we evaluate the ensemble models based on the mean scores and the max scores obtained by classifier models with the best performances. Table 7 and Table 8 present the result of the ensemble model based on the GRU + CNN + Global Max Pooling model with Arabic and Li & Roth taxonomies, respectively. We notice that the ensemble method surpasses simple models and CNN and RNN mergers in the case of Arabic taxonomy. However, for Li & Roth taxonomy the mean scores-based ensemble model achieved the best results in terms of accuracy and weighted F1 score. The GRU + Global Max Pooling achieves the best performance according to the macro F1 score.

Table 7: GRU + CNN + Global Max Pooling ensemble model with Arabic taxonomy

	Accuracy	**Macro F1 score**	**Weighted F1 score**
Mean scores-based Ensemble	94.17%	94.07%	94.17%
Max scores-based Ensemble	94.17%	94.07%	94.17%

Table 8: GRU + CNN + Global Max Pooling ensemble model with Li & Roth taxonomy

	Accuracy	**Macro F1 score**	**Weighted F1 score**
Mean scores-based Ensemble	**92.60%**	**86.52%**	**92.69%**
Max scores-based Ensemble	92.44%	86.39%	92.54%

4.6 Discussion

From the one hand we discuss the obtained results for the Arabic taxonomy. The ELMo contextual word representation performs better than the word2vec context free word representation. The simple models evaluation shows that the GRU a recurrent neural network architecture is more appropriate than CNN for Arabic question classification. The CNN and RNN mergers evaluation confirms that the stack GRU/CNN achieves better results than the stack CNN/RNN. Besides, the ensemble models build with the word2vec and ELMo embeddings impact positively the performance of the Arabic question classification task. On the other hand, the classifiers trained with Li & Roth taxonomy shows different behaviors. The simple models evaluation reveals that the ELMo representation with CNN + Global Max Pooling model has top performances in terms of accuracy and weighted F1 score while the word2vec representation with GRU + Global Max Pooling model has the top performance in terms of macro F1 score. Thus, the latter model is able to handle imbalanced data problem more appropriately. The CNN and RNN mergers evaluation supports that word2vec with the stack GRU/RNN model is better than ELMo embeddings with RNN/GRU model. Finally, ensemble models improve the accuracy and the weighted F1 score but not the macro F1 score.

To conclude, the Arabic taxonomy works well with contextual representation ELMo and ensemble models while the model choice with Li & Roth taxonomy is related to the performance, e.g., if the objective is to optimize the accuracy of the question classification task then the ensemble model is more appropriate.

5 Conclusion

In this work, we built various Arabic question classifier based on simple models, CNN and RNN mergers and Ensemble methods. We trained these models with both context free word representation word2vec [4, 16] and contextual word representation ELMo [5, 10]. The latter has the upside to compute, for a word, a vector that catch semantic and syntactic meaning by considering its context. Ability that the enriched wor2vec model can not perform. We compared the performances of the proposed models with two different question taxonomies including Arabic taxonomy and Li & Roth taxonomy. From the one side, the experiments on questions labeled with Arabic taxonomy showed that contextual representation achieved promising results 94.01% accuracy, 93.60% macro F1 score and 93.98% weighted F1 score. Along with, ensemble methods improve the results slightly since it scored the top performances 94.17% accuracy, 94.07% macro F1 score and 94.17% weighted F1 score. On the other side, for questions labeled with Li & Roth taxonomy the top classifier in terms of macro F1 score (87.24%) was built based on word2vec and GRU + Global Max Pooling model. The mean score-based ensemble model scored 92.60% accuracy and 92.69% weighted F1 score which are the best obtained results in terms of accuracy and weighted F1 score. Thus, the the model choice with Li & Roth taxonomy is related to the performance the classifier needs to optimize more

As perspectives, we arrange to expand this work by building other Arabic question answering system components including the passage retriever and the answer processing modules. First, we plan to construct a module that aims to retrieve the most similar passages to a question based on contextual representation. Next, We intend to integrate these context aware representations in the answer processing module. Finally, we project to build an Arabic question answering system based on components that integrate contextual word embeddings, which have the capabilities of extracting syntactic and semantic relation of a word considering its context, to enhance further their performances.

Conflict of Interest The authors declare no conflict of interest.

References

[1] D. Moldovan, M. Paşca, S. Harabagiu, M. Surdeanu, "Performance issues and error analysis in an open-domain question answering system," ACM Transactions on Information Systems, **21**(2), 133–154, 2003, doi:10.1145/763693.763694.

[2] W. Ahmed, B. A. P, "CLASSIFICATION OF ARABIC QUESTIONS USING MULTINOMIAL NAIVE BAYES." International Journal of Latest Trends in Engineering and Technology Special Issue SACAIM, 82–86, 2016.

[3] A. Hamza, N. En-Nahnahi, K. A. Zidani, S. E. A. Ouatik, "An arabic question classification method based on new taxonomy and continuous distributed representation of words," Journal of King Saud University - Computer and Information Sciences, 2019, doi:https://doi.org/10.1016/j.jksuci.2019.01.001.

[4] P. Bojanowski, E. Grave, A. Joulin, T. Mikolov, "Enriching Word Vectors with Subword Information," Trans. Assoc. Comput. Linguistics, **5**, 135–146, 2017.

[5] M. E. Peters, M. Neumann, M. Iyyer, M. Gardner, C. Clark, K. Lee, L. Zettlemoyer, "Deep Contextualized Word Representations," in M. A. Walker, H. Ji, A. Stent, editors, Proceedings of the 2018 Conference of the North American Chapter of the Association for Computational Linguistics: Human Language Technologies, NAACL-HLT 2018, New Orleans, Louisiana, USA, June 1-6, 2018, Volume 1 (Long Papers), 2227–2237, Association for Computational Linguistics, 2018, doi:10.18653/v1/n18-1202.

[6] H. Abdelnasser, M. Ragab, R. Mohamed, A. Mohamed, B. Farouk, N. El-Makky, M. Torki, "Al-Bayan: an arabic question answering system for the holy quran," in Proceedings of the EMNLP 2014 Workshop on Arabic Natural Language Processing (ANLP), 57–64, 2014.

[7] H. M. Al Chalabi, S. K. Ray, K. Shaalan, "Question classification for Arabic question answering systems," in Information and Communication Technology Research (ICTRC), 2015 International Conference on, 310–313, IEEE, 2015.

[8] T. Mikolov, I. Sutskever, K. Chen, G. S. Corrado, J. Dean, "Distributed Representations of Words and Phrases and their Compositionality," in C. J. C. Burges, L. Bottou, Z. Ghahramani, K. Q. Weinberger, editors, Advances in Neural Information Processing Systems 26: 27th Annual Conference on Neural Information Processing Systems 2013. Proceedings of a meeting held December 5-8, 2013, Lake Tahoe, Nevada, United States, 3111–3119, 2013.

[9] T. Mikolov, K. Chen, G. Corrado, J. Dean, "Efficient Estimation of Word Representations in Vector Space," in Y. Bengio, Y. LeCun, editors, 1st International Conference on Learning Representations, ICLR 2013, Scottsdale, Arizona, USA, May 2-4, 2013, Workshop Track Proceedings, 2013.

[10] W. Che, Y. Liu, Y. Wang, B. Zheng, T. Liu, "Towards Better UD Parsing: Deep Contextualized Word Embeddings, Ensemble, and Treebank Concatenation," in D. Zeman, J. Hajic, editors, Proceedings of the CoNLL 2018 Shared Task: Multilingual Parsing from Raw Text to Universal Dependencies, Brussels, Belgium, October 31 - November 1, 2018, 55–64, Association for Computational Linguistics, 2018, doi:10.18653/v1/k18-2005.

[11] A. Kutuzov, M. Fares, S. Oepen, E. Velldal, "Word vectors, reuse, and replicability: Towards a community repository of large-text resources," in Proceedings of the 58th Conference on Simulation and Modelling, 271–276, Linköping University Electronic Press, 2017.

[12] R. Collobert, J. Weston, L. Bottou, M. Karlen, K. Kavukcuoglu, P. P. Kuksa, "Natural Language Processing (Almost) from Scratch," J. Mach. Learn. Res., **12**, 2493–2537, 2011.

[13] M. Abadi, A. Agarwal, P. Barham, E. Brevdo, Z. Chen, C. Citro, G. S. Corrado, A. Davis, J. Dean, M. Devin, S. Ghemawat, I. Goodfellow, A. Harp, G. Irving, M. Isard, Y. Jia, R. Jozefowicz, L. Kaiser, M. Kudlur, J. Levenberg, D. Mané, R. Monga, S. Moore, D. Murray, C. Olah, M. Schuster, J. Shlens, B. Steiner, I. Sutskever, K. Talwar, P. Tucker, V. Vanhoucke, V. Vasudevan, F. Viégas, O. Vinyals, P. Warden, M. Wattenberg, M. Wicke, Y. Yu, X. Zheng, "TensorFlow: Large-Scale Machine Learning on Heterogeneous Systems," 2015, software available from tensorflow.org.

[14] M. Abadi, P. Barham, J. Chen, Z. Chen, A. Davis, J. Dean, M. Devin, S. Ghemawat, G. Irving, M. Isard, M. Kudlur, J. Levenberg, R. Monga, S. Moore, D. G. Murray, B. Steiner, P. Tucker, V. Vasudevan, P. Warden, M. Wicke, Y. Yu, X. Zheng, "TensorFlow: A system for large-scale machine learning," in Proceedings of the 12th USENIX Symposium on Operating Systems Design and Implementation (OSDI '16), 265–283, 2016.

[15] L. J. Ba, J. R. Kiros, G. E. Hinton, "Layer Normalization," CoRR, **abs/1607.06450**, 2016.

[16] E. Grave, P. Bojanowski, P. Gupta, A. Joulin, T. Mikolov, "Learning Word Vectors for 157 Languages," in N. Calzolari, K. Choukri, C. Cieri, T. Declerck, S. Goggi, K. Hasida, H. Isahara, B. Maegaard, J. Mariani, H. Mazo, A. Moreno, J. Odijk, S. Piperidis, T. Tokunaga, editors, Proceedings of the Eleventh International Conference on Language Resources and Evaluation, LREC 2018, Miyazaki, Japan, May 7-12, 2018, European Language Resources Association (ELRA), 2018.

ASTES

Advances in Science, Technology and Engineering Systems Journal Vol. 5, No. 3, 478-486 (2020)

www.astesj.com

Special Issue on Innovative Research in Applied Science, Engineering and Technology

ASTESJ

ISSN: 2415-6698

Monte Carlo Estimation of Dose in Heterogeneous Phantom Around 6MV Medical Linear Accelerator

Zakaria Aitelcadi[1,*], Mohamed Reda Mesradi[1], Redouane El Baydaoui[1], Ahmed Bannan[1], Abdennacer Ait Ayoub[2], Kamal Saidi[1], Saad Elmadani[1]

[1]*Hassan First University of Settat, High Institute of Health Sciences, Laboratory of Sciences and Health Technologies, 26000, Settat, Morocco*

[2]*Clinique spécialisée Menara, 40000, Marrakech, Morocco*

ARTICLE INFO

Article history:
Received: 12 May, 2020
Accepted: 18 June, 2020
Online: 20 June, 2020

Keywords:
Monte Carlo
MLC
GATE
Artefacts
PTO
Heterogeneous
ECLIPSE
AAA

ABSTRACT

In this work, we completed a validation of the Varian Clinac IX equipped with the High Definition Multi-Leaf Collimator (HD 120 MLC) instead of the removable jaws, using GATE Monte Carlo Platform version 8.2. We validated the multileaf collimator (MLC) geometry by simulating two dosimetric functions (Percentage Depth Dose (PDD) and Dose Profile (DP)), for 6MV photon beam energy and different field sizes (3x3, 4x4, 6x6, 8x8, 10x10, 12x12, 15x15, and 20x20 cm²). We then compared the results with measurements realized with two detectors, namely the cylindrical ionization chamber and the micro-diode PTW silicon. By applying the Relative Dose Difference method (RDD), we noted a less than 2% and 1% agreement for the field sizes (10x10, 12x12, 15x15, 20x20 cm²) and (3x3, 4x4, 6x6, 8x8 cm²) respectively. Moreover, to evaluate the relevance of Monte Carlo method in a heterogeneous media, particularly in small field sizes (1x1, 2x2, 3x3 cm²), we have simulated three clinical studies based on the Physical Test Objects (PTOs) that are the equivalent slabs of lung and bone included in a water phantom. We noticed that the simulated PDDs exhibit two significant irregularities in the interface between water and lung. To eliminate these phenomena, we have used the "setMaxStepSizeInRegion" parameter implemented in GATE. We also noticed an important difference of 5% corresponding to the small field sizes, between homogeneous and heterogeneous simulated PDDs. We used the RDD method in this case as well. Moreover, we observed a difference between 1-4% between the simulated PDDs and the calculated ones by ECLIPSE Treatment Planning System (TPS). These results indicate that GATE (8.2) is useful in dosimetry with heterogeneous situations as well such as bone and lung.

1. Introduction

In clinical radiotherapy, most TPS are calibrated in a homogeneous media with densities equal to 1. However, some organs have strong heterogeneities such as bone and lung. Hence a better precision requires a corrective dose in conventional TPS. In this context, Monte Carlo simulations present a real alternative allowing enhanced precision related to the transport of high energy photons, particularly in heterogeneous media. However, complex MC simulations require a great amount of computing resources and are time-consuming. Consequently, the optimization of the computation time is necessary. In our study, we used lung and bone equivalent slabs included in a water phantom as Physical Test Objects (PTOs).

Moreover, modern radiotherapy also uses complex beam shapes. For this purpose, we modeled a Varian Clinac IX 6MV photon beam energy with the High Definition Multi-Leaf Collimator (HD 120 MLC). This instrument can hold up to 120 pairs of leaves that move independently to allow the output of a complex beam shape. In practice, there are three types of MLCs, namely type A (e.g. Scanditronix and Siemens) [1], type B (e.g. Elekta) [2] and type C (e.g. Varian) [3]. The three are distinguished by their leaf's size, speed of movement, and the

*Corresponding Author: Zakaria Aitelcadi, z.aitelcadi@gmail.com

transmission factor related to their arrangement and their geometry.

In this study, we have used the PTOs to evaluate the relevance of the MC method in the case of small radiation fields used in the context of small tumors. We realized this objective in two parts. In the first part, we have modeled a Varian Clinac IX 6MV photon beam energy to take into account the MLC based on our previous work [4] and using the geometric data provided by the manufacturer [3]. Thus, we compared the simulated dosimetric functions (PDD and DP) for different field sizes (3x3, 4x4, 6x6, 8x8, 10x10, 12x12, 15x15 and 20x20 cm²) to the measured ones using the RDD method [5]. In the second part, we have simulated three PTOs geometries (water+bone, water+lung, and water+bone+lung). Then we compared the PDDs of the heterogeneous media with the homogeneous ones. We also compared the simulated PDDs with the ones calculated by ECLIPSE TPS, based on the Anisotropic Analytic Algorithm (AAA). Finally, we've been interested in the optimization of the artefact phenomenon at the interfaces.

2. Material and Methods

2.1. Measurements including the HD 120 MLC

In this study, the Varian Clinac IX 6MV photon beam we used is equipped with the High-Definition Multi-Leaf Collimator (HD 120 MLC). PDD measurements were made at 100 cm of the Source Surface Distance (SSD), with a pitch of 0.1 mm in a depth between 0 and 5 cm in water and 1 mm for depths greater than 5 cm. In the case of DP, we chose 0.1 mm as a pitch in the penumbra region. In measurements with fields greater than or equal to 4x4cm² a cylindrical ionization chamber (Exradin type A28), with a volume of 0.125 cm^3 was used, while for fields less than 4x4cm^2, measurements were carried out using a micro-diode silicon detector PTW with a volume of 0.03 cm^3 placed in a Doseview standard 3D solid water phantom of Standard Imaging.

2.2. HD 120 MLC modelling

The geometry and components materials of the HD 120 MLC have been implemented in GATE (V8.2) code using the manufacturer's data [3]. It is formed by two blocks (A and B) that can hold 60 independent leaves oriented according to the Y-axis. Each block holds 28 external leaves «half leaves» (0.5 cm width) and 32 internal «quarter leaves» (0.25 cm width). They both are placed at 100 cm from the source [6,7]. Furthermore, the ends of the leaves are rounded with a 16 cm radius, their thickness is 6.9 cm and they are spaced from each other with a distance of 0.0047 cm.

The 32 internal leaves are positioned according to an alternative pattern (Figure 2): a drop with its fine end oriented towards the source (or "Target leaf") then its neighbor whose fine end is oriented this time towards the isocenter of the accelerator (or «Isocenter leaf»), these two types of leaves differ by the distance tongue and groove which is worth 0.1 and 0.01 cm respectively to create a vertical play between the tongue of a leaf and the groove of the adjacent leaf [8].

Besides, in GATE (V8.2), we introduced four types of leaves (quarter isocenter, quarter target, half isocenter, and half target) (Figure 2). Which we located them at the origin of the marker placed in the entrance of the photon target. Then the leaves were repeated with the possibility of rotation and translation around their center and Y axis, and X, Y, and Z respectively. Figure 3 shows the GATE model of the Varian Clinac IX, including the HD 120 MLC [8].

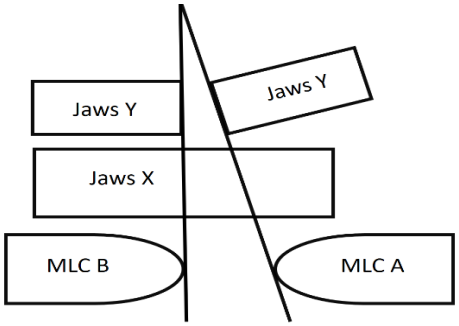

Figure 1: Varian Clinac MLC illustration

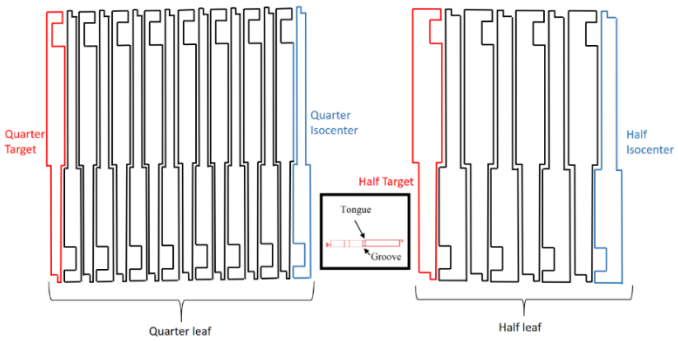

Figure 2: Schematic presentation of the HD 120 MLC, with Target and Isocenter leaf for each type

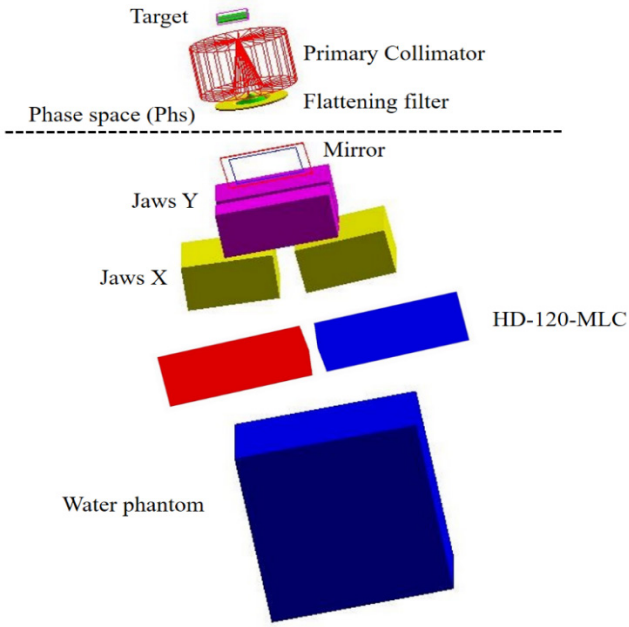

Figure 3: Varian Clinac IX accelerator head GATE modeled including the HD 120 MLC

On the other hand, in GATE (V8.2), the dosimetric functions (PDD and DP) corresponding to the different field sizes (3x3, 4x4, 6x6, 8x8, 10x10, 12x12, 15x15 and 20x20 cm²) were realized using the "DOSE ACTOR". PDD was normalized at depth (D_{max}) where the deposited dose is maximal. We compared the simulation results with those measured using the RDD method [6]. The latter consists of evaluating the relative dose difference between an experimental value and a theoretical reference value using equation 1. The dose difference should be less than 3% in the build-up region and less than 1% for most depths ranging from maximum dose depth (D_{max}) to 30 cm. In equation 1, Dc is the calculated absorbed dose, and D_m is the measured dose (reference). Indeed, to obtained good statistic 9.10^9 particles were generated from a phase space (Phs) previously used as a source [4] and directed into a water phantom of the same size used in measurements.

$$RDD\ (\%) = 100 * \frac{D_c - D_m}{D_m} \quad (1)$$

Table 1: Material characteristics for lung and bone equivalent slabs

Materials	Density (g/cm^3)	Width (cm)	Composition (%)
Lung slab	0.31	10	H (8.31), C (60.08), N (2.71), O (23.04), Mg(4.8), Cl(1.02)
Bone slab	1.91	5	H (3.30), C (25.37), N (0.91), O (35.28), Mg(3.36), P (8.82), Cl(0.03), Ca(22.91)

2.3. Heterogeneity Study

In this work, we conducted a study of heterogeneity using the two PTOs (lung and bone equivalent slabs). The three heterogeneous geometries studied are illustrated in Figure 4. The Phantom 1 includes a lung equivalent slab with a size of (30 x 30 x 10 cm^3) placed at 5 cm from the entrance. The Phantom 2 contains a slab bone with a size of (30 x 30 x 5 cm^3) placed at 5 cm. The Phantom 3 includes two slabs: bone and lung located at 5 cm and 10 cm respectively.

To evaluate the ability of GATE to predict the dose distribution in a heterogeneous media, we compared the simulated PDDs with the three phantoms with a homogenous one. This concern six different fields sizes (1x1, 2x2, 3x3, 10x10, 15x15 and 20x20 cm²). In GATE, the composition and the density of lung and bone equivalent slabs were given by the manufacturer (Table 1). We compared GATE results with the ones obtained with the ECLIPSE TPS by applying the RDD method. We note that we used the same GATE geometry in ECLIPSE and that calculations were performed using the AAA algorithm [9,10].

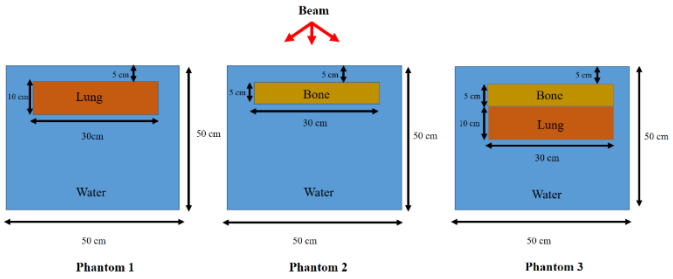

Figure 4: Two PTOs geometries using for three different studies

3. Results and Discussion

3.1. Static validation of the HD 120 MLC

Figures 5 and 6 show the simulated PDDs and DPs compared to those measured for the field sizes (3x3, 4x4, 6x6, 8x8, 10x10, 12x12, 15x15, and 20x20 cm²). Table 2 illustrates the results of this comparison. We note that the PDD results exhibit an agreement of less than 2% for the most points, while with the DP results the differences are around 1% in the build-up region and 2% outside. These simulations indicate that the accuracy with MLC is better than with the removable jaws used in our previous work [4].

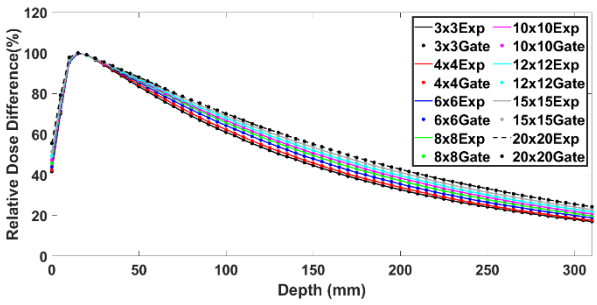

Figure 5: PDDs defined by the 120 HD MLC for different field sizes

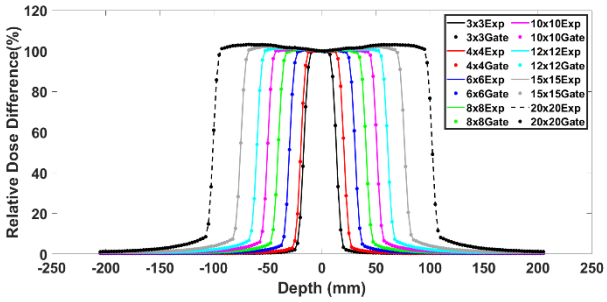

Figure 6: DPs defined by the 120 HD MLC for different field sizes

3.2. Heterogeneity study

3.2.1. Artefact phenomenon

In the literature, few studies were interested in the artefact phenomenon observed in MC simulations at the boundary between two biological matters [11], for example between water and lung. For this purpose, we simulated the PDD using phantom 1. The results indicated two significant irregularities in the

interface between water and lung (Figure 7). The "setMaxStepSizeInRegion" is the key factor for this phenomenon provided in GATE. It is defined as the maximal step size of charged particles. Thus, we performed simulations by varying this parameter within the range of 10-50 µm. Table 3 shows the calculation time for each value corresponding to a step of 10 µm. Adjusting the "setMaxStepSizeInRegion" with the recommended cutoff value [4], the two artefacts are gone.

Table 2: Average RDD between (PDD & DP) calculated and measured ones for different field sizes

Field sizes (cm^2)	RDD (%)	
	PDD	DP
3x3	0.1666	0.1952
4x4	0.1836	0.1936
6x6	0.258	0.4256
8x8	0.3839	0.8934
10x10	0.5289	0.9612
12x12	0.7145	1.0142
15x15	0.9236	1.0958
20x20	1.0147	1.3541

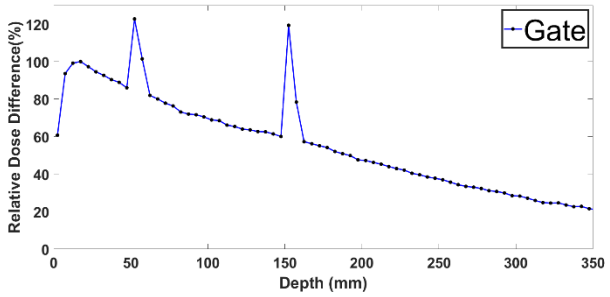

Figure 7: Artefact phenomenon in the boundaries between Water and Lung equivalent slab for 10x10 cm² field size

Table 3: CPU timing for “"setMaxStepSizeInRegion" values

“setMaxStepSizeInRegion” value (µm)	CPU timing (h)
10	30
20	**20**
30	48
40	53
50	59

3.2.2. *Heterogeneity study compared to homogenous one*

In Figure 8, the fact that the lung has a weaker density, this doesn't lead to any change in the PDD in region 1 therefore, the two PDD curves (water and water-lung) are almost identical for all field sizes studied in this region. In region 2, the photon’s attenuation is weaker, and the fact that in small fields (1x1, 2x2, and 3x3 cm²) there is almost no lateral electron equilibrium, lung PDDs are lower than the one in water. This electronic disequilibrium is due to the Compton effect [12]. Indeed, when the electron range produced by the Compton Effect is half of the field size, the electrons produced will transfer their energies outside the radiation field from where the electronic balance is lost. However, for a large field sizes (10x10, 15x15 and 20x20 cm²) the photons’ attenuation and the lateral electron equilibrium becomes significant. This is due to the field sizes increase, consequently, lung PDDs become relatively higher than the ones in the water. Indeed, in region 3, the fact that for all field sizes, the PDDs in the lung are relatively higher than ones in the water, is mainly due to the lower density of lung in region 2.

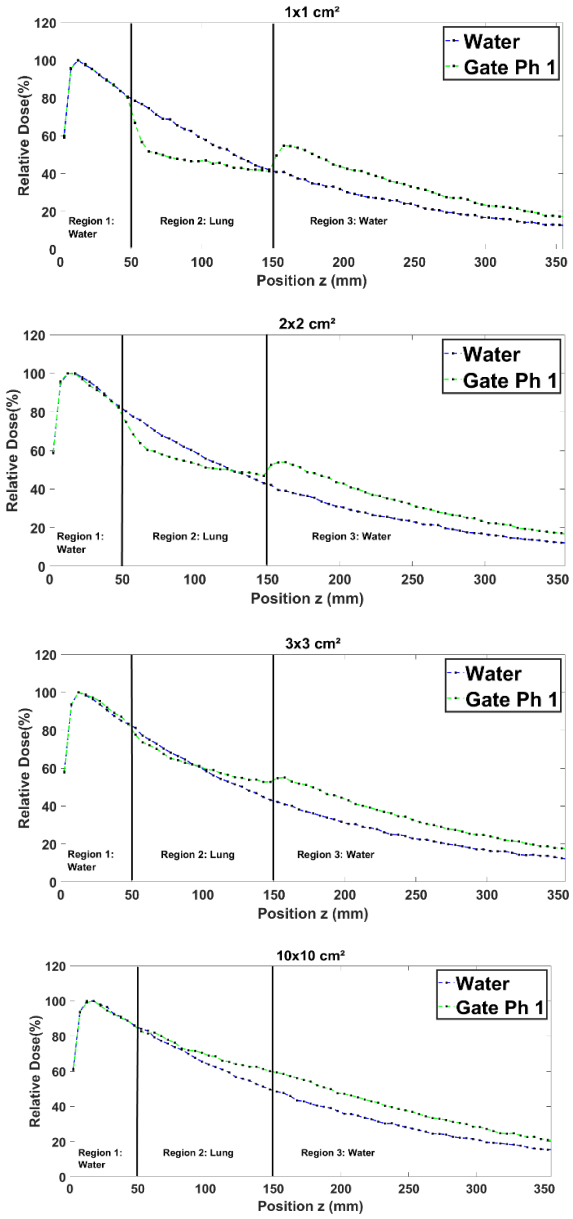

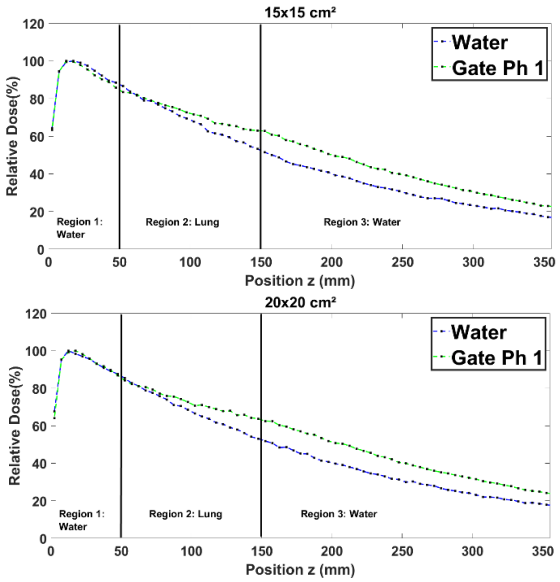

Figure 8: Comparison between the PDD in a homogenous phantom with phantom 1 for 1x1, 2x2, 3x3, 10x10, 15x15 and 20x20 cm² field sizes.

Figure 9 shows that in region 1, for all field sizes the presence of bone seems to not affect the PDDs curves. In region 2, although bone has a higher attenuation coefficient, the related PDDs seem to be relatively weaker than the ones in the water. This is observed for all field sizes, owing to the Compton scattering effect [12]. Indeed, in region 3, the higher attenuation coefficient of bone in region 2, makes that PDDs in bone are still relatively weaker than the ones in water for all field sizes.

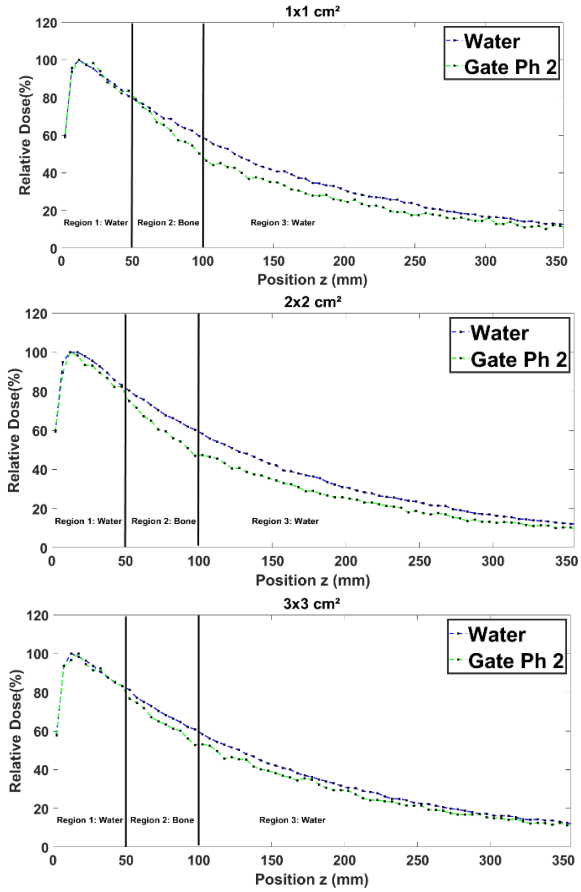

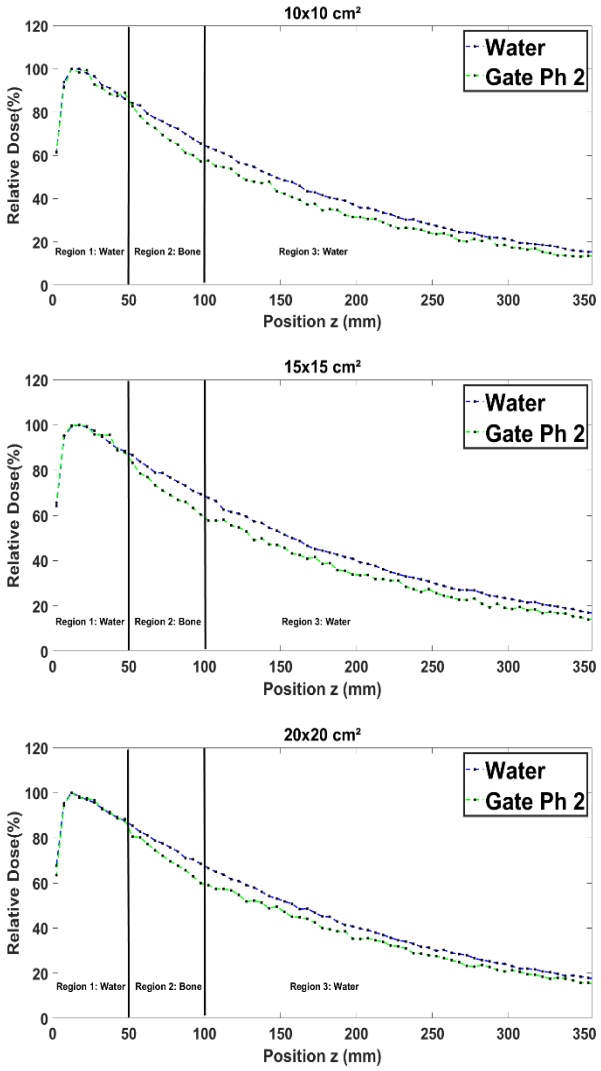

Figure 9: Comparison between the PDD in a homogenous phantom with phantom 2 for 1x1, 2x2, 3x3, 10x10, 15x15 and 20x20 cm² field sizes.

Figure 10 shows that in region 1 the two PDDs curves are almost identical, despite the presence of the two bone and lung slabs. In regions 2 and 3, the related PDDs seem to be relatively weaker than the ones in the water, owing to the Compton scattering effect and the low density of lung. This is observed for all field sizes. In region (4) the fact that for all field sizes, the PDDs in the presence of lung and bone are relatively higher than the ones in water alone, results primarily to the low density of lung in region 3.

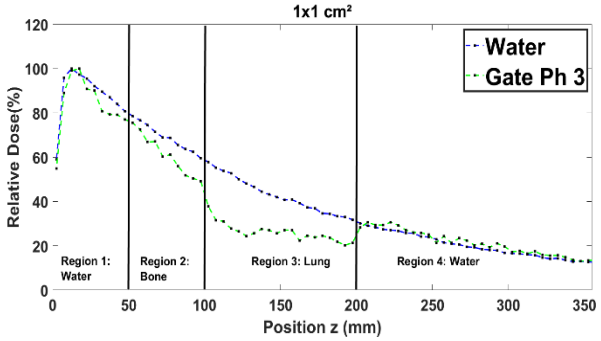

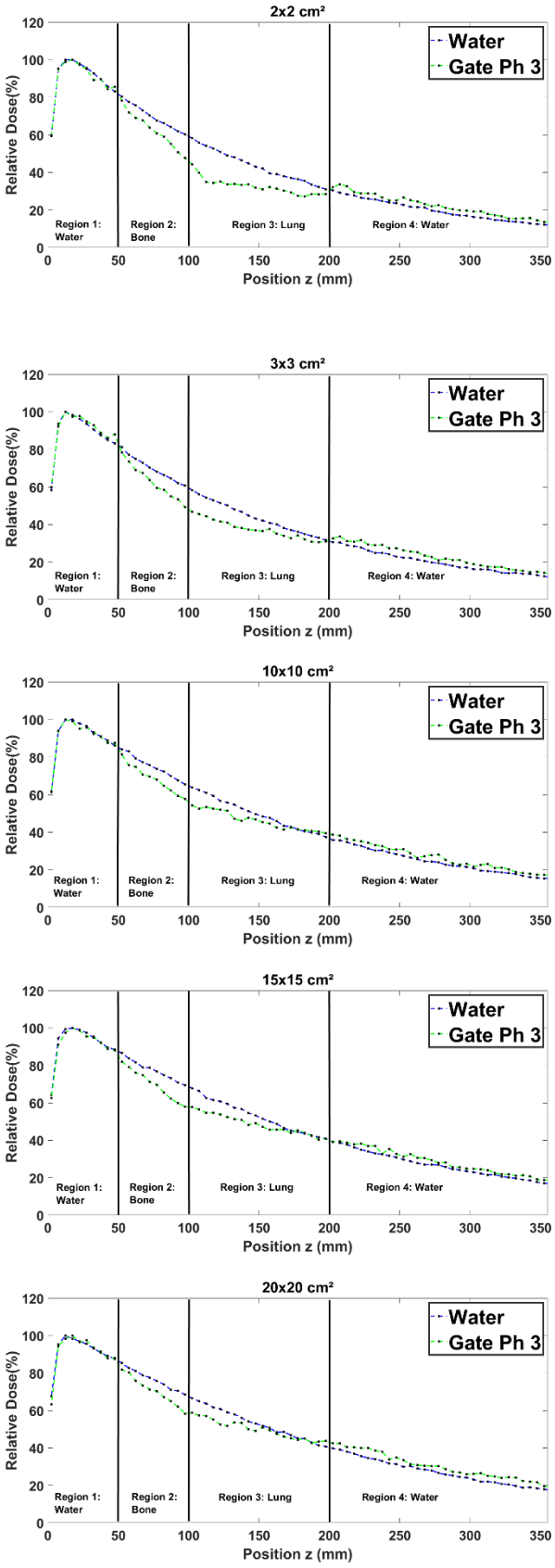

Figure 10: Comparison between the PDD in a homogenous phantom with phantom 3 for 1x1, 2x2, 3x3, 10x10, 15x15 and 20x20 cm² field sizes.

3.2.3. *Heterogeneity comparison study between GATE and ECLIPSE (AAA)*

Figure 11 shows that the PDDs obtained by ECLIPSE and GATE from Phantom 1 are in general closely similar with a difference less than 1%, except for the 1x1 cm² field where ECLIPSE PDD exceeds GATE by 4.02%. This can be explained by the fact that ECLIPSE does not take into account the lateral electronic equilibrium in lung slab for very small fields. Table 4 presents the average RDD of the PDDs calculated by ECLIPSE and simulated by GATE for Phantom 1.

Table 4: Average RDD between GATE and ECLIPSE (AAA) PDDs for different field sizes in phantom 1

Field sizes (cm²)	RDD (%)
1x1	4.02
2x2	0.83
3x3	1.27
10x10	1.68
15x15	0.53
20x20	0.63

Figure 12 shows that in region 1, the PDDs obtained from Phantom 2, are in general closely similar for all field sizes. In region 2, we note a difference of 1 to 5% explained by the fact that ECLIPSE overestimates the energy deposited by secondary electrons in bone slab [13]. Table 5 presents the average RDD of the PDDs for Phantom 2.

Table 5: Average RDD between GATE and ECLIPSE (AAA) PDDs for different field sizes in phantom 2

Field sizes (cm²)	RDD (%)
1x1	0.26
2x2	1.31
3x3	2.31
10x10	4.08
15x15	4.03
20x20	3.75

Figure 13 shows that in region 1, the PDDs obtained from Phantom 2, are in general closely similar for all field sizes. In region 2, for small field sizes, ECLIPSE PDDs exceed the GATE ones by more than 4%. This is because ECLIPSE overestimates the energy deposited by secondary electrons in bone slab [13]. On the other hand, for field sizes greater than or equal to (10x10 cm²) the deference is 2%, owing to the presence also of lung in region 3. Table 6 presents the average difference for PDDs calculated and measured by applying the RDD method.

Table 6: Average RDD between GATE and ECLIPSE (AAA) PDDs for different field sizes in phantom 3

Field sizes (cm²)	RDD (%)
1x1	4.23
2x2	4.59
3x3	3.61
10x10	2.00
15x15	1.91
20x20	1.74

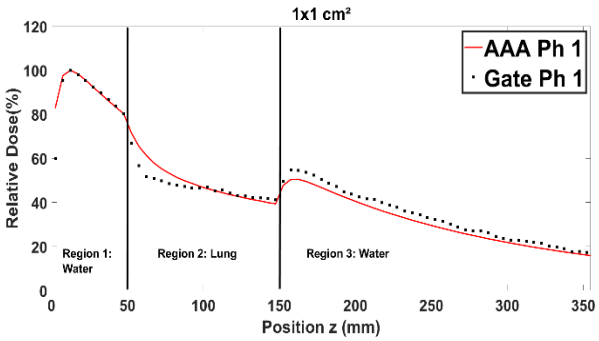

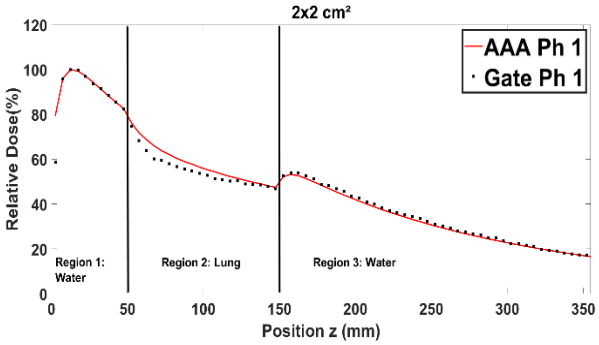

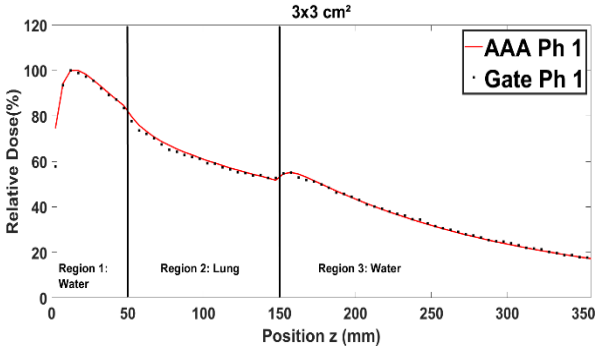

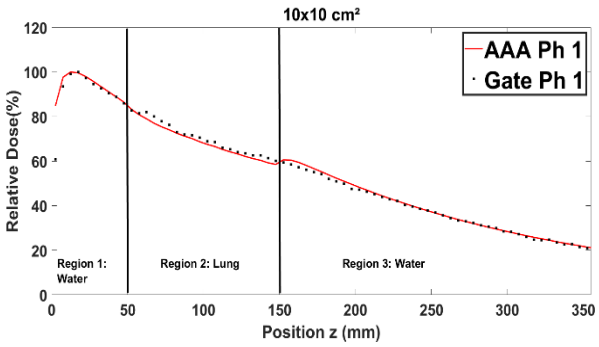

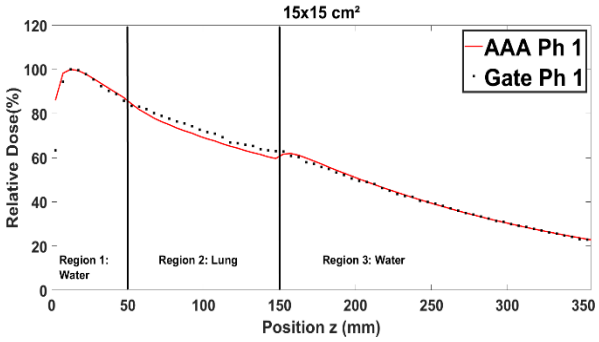

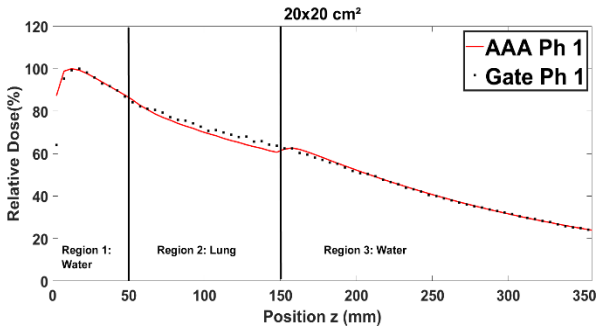

Figure 11: Comparison between GATE and ECLIPSE (AAA) PDDs in phantom 1 for 1x1, 2x2, 3x3, 12x12, 15x15 and 20x20 cm² field sizes.

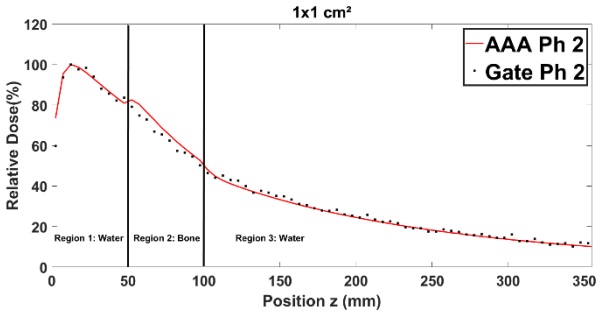

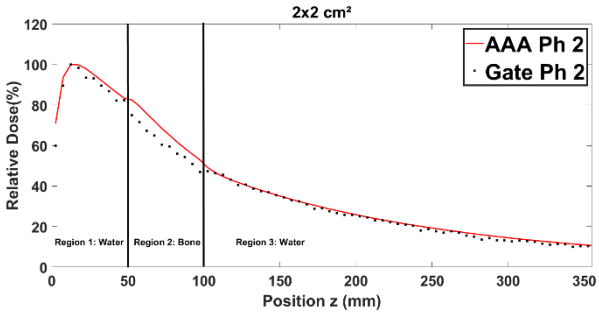

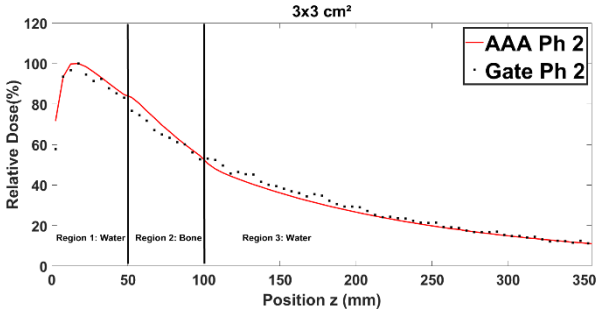

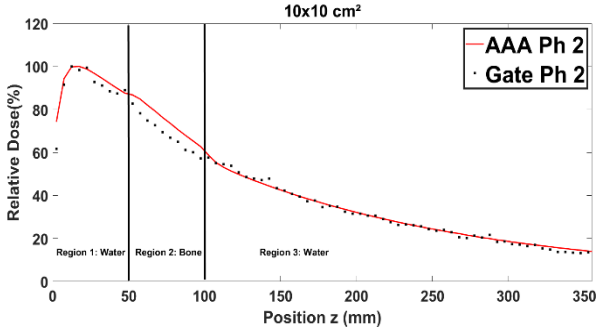

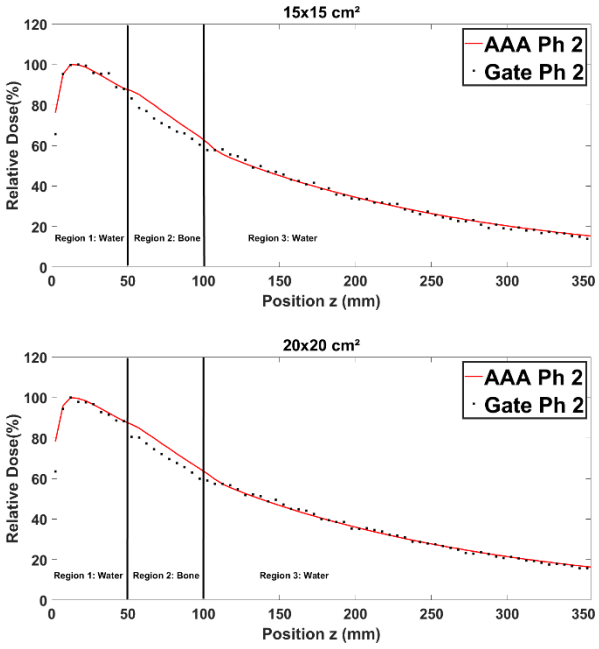

Figure 12: Comparison between GATE and ECLIPSE (AAA) PDDs in phantom 2 for 1x1, 2x2, 3x3, 12x12, 15x15 and 20x20 cm² field sizes.

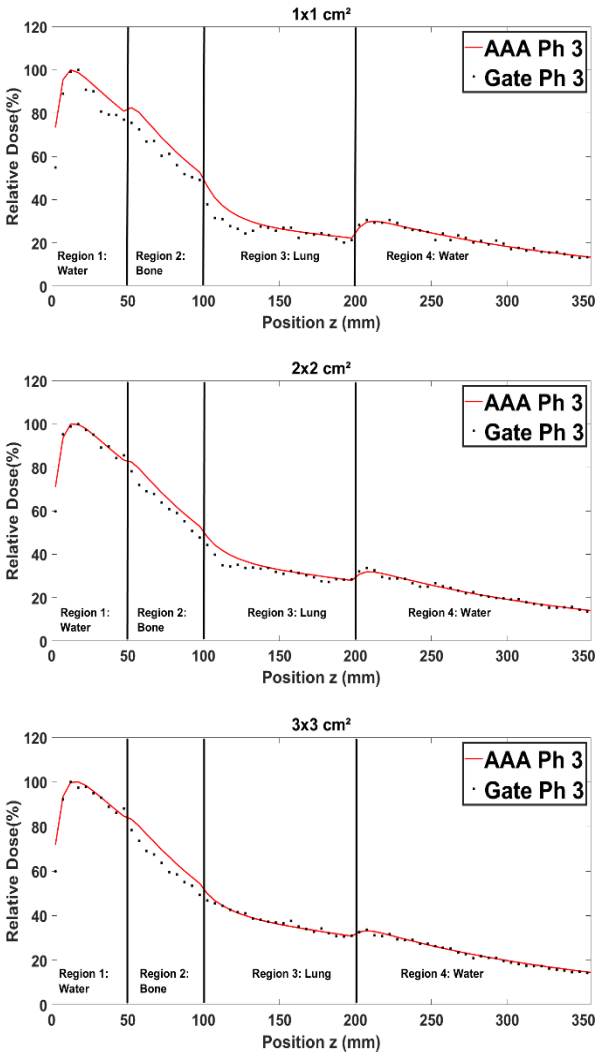

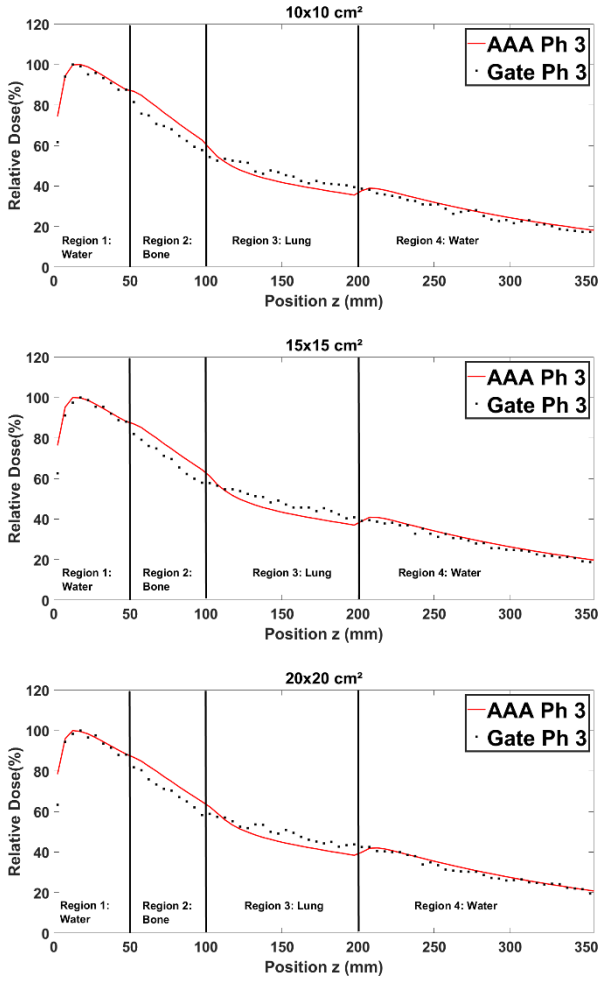

Figure 13: Comparison between GATE and ECLIPSE (AAA) PDDs in phantom 3 for 1x1, 2x2, 3x3, 12x12, 15x15 and 20x20 cm² field sizes.

4. Conclusion

In addition to our previous work, in this study, we successfully used the up-to-date version of GATE 8.2 to simulate the High Definition Multi-Leaf Collimator (HD 120 MLC) using the manufacturers'. We performed the MLC validation by comparing the dosimetric functions (PDD and DP) measured in a water phantom with those simulated for different field sizes using, the relative dose difference method (RDD). Results show an agreement of less than 2% between simulated and measured functions. On the other hand, we demonstrated by using three studies based on the Physical Test Object (PTOs), the capacity of GATE 8.2 code to reproduce the dosimetric function in heterogeneous media such as lung and bone. Moreover, we showed that GATE exceeds ECLIPSE in the assessment of dose in heterogeneous media, since the latter does not take into account the lateral electronic disequilibrium. Indeed, the optimization of the "setMaxStepSizeInRegion" parameter in GATE led to eliminate the phenomenon of artefact in the interface between lung and bone. In conclusion, the static validation of our MLC 120 HD model, as well as the results of the dose distribution in heterogeneous media will lead us in future research for a dynamic

validation to test the feasibility of the clinical application of the Monte Carlo simulations.

Conflict of Interest

We declare that we have no conflict of interest.

References

[1] AAPM. Basic applications of multileaf collimators. report of the AAPM radiation therapy committee Task Group No 50 AAPM Report No 72 (Madison, WI: American Institute of Physics by Medical Physics Publishing). 2001.

[2] Heath, E, Seuntjens, J. Development and validation of a BEAMnrc component module for accurate Monte Carlo modelling of the Varian dynamic Millennium multileaf collimator. Phys Med Biol 2003;48(24):4045-4063. https://doi.org/10.1088/0031-9155/48/24/004

[3] Michael K. Fix, Werner Volken, Daniel Frei, Daniel Frauchiger, Ernst J. Born and Peter Manser, Monte Carlo implementation, validation, and characterization of a 120 leaf MLC. Med. Phys., 38(10) : 5311-5320, 2011. https://doi.org/10.1118/1.3626485

[4] Z. Aitelcadi, A. Bannan, R. El baydaoui, MR. Mesradi, A. Halimi, S. Elmadani, Feasibility of external radiotherapy dose estimation in homogenous phantom using monte carlo modeling. JATIT, 98(8) :1151-1162, 2020.

[5] Cho S.H., Vassiliev O.N., Lee S., Liu H.H., Ibbott G.S., and Mohan R. Reference photon dosimetry data and reference phase space data for the 6 mv photon beam from varian clinac 2100 serie linear accelerators. Med. Phys., 32(1) :137–148, 2005. https://doi.org/10.1118/1.1829172

[6] Huq, MS, Das, IJ, Steinberg, T, Galvin, JM. A dosimetric comparison of various multileaf collimators. Phys Med Biol 2002;47(12):N159-170. https://doi.org/10.1088/0031-9155/47/12/401

[7] J. V. Siebers, P. J. Keall, J. O. Kim, and R. Mohan, "A method for photon beam Monte Carlo multileaf collimator particle transport," Phys. Med. Biol. 47(17), 3225 (2002). https://doi.org/10.1088/0031-9155/47/17/312

[8] C. Borges, M. Zarza-Moreno, E. Heath, N. Teixeira and P. Vaz, Monte Carlo modeling and simulations of the High Definition (HD120) micro MLC and validation against measurements for a 6MV beam. Med.Phys., 39(1), 2012. https://doi.org/10.1118/1.3671935

[9] Fogliata, A, Vanetti, E, Albers, D, et al. On the dosimetric behaviour of photon dose calculation algorithms in the presence of simple geometric heterogeneities: comparison with Monte Carlo calculations. Phys Med Biol 2007;52(5):1363-1385. https://doi.org/10.1088/0031-9155/52/5/011

[10] Panettieri, V, Barsoum, P, Westermark, M, Brualla, L, Lax, I. AAA and PBC calculation accuracy in the surface build-up region in tangential beam treatments. Phantom and breast case study with the Monte Carlo code PENELOPE. Radiother Oncol 2009;93(1):94-101. https://doi.org/10.1016/j.radonc.2009.05.010

[11] Poon, E., Verhaegen, F., 2005. Accuracy of the photon and electron physics in GEANT4 for radiotherapy applications. J. Med. Phys., 2005, 32(6), 1696–1711. https://doi.org/10.1118/1.1895796

[12] L.A.R. da Rosa, S.C. Cardoso, L.T. Campos, V.G.L. Alves, D.V.S. Batista, A.Facure, Percentage depth dose evaluation in heterogeneous media using thermolumiescent dosimetry. JOURNAL OF APPLIED CLINICAL MEDICAL PHYSICS, 11(1), 2010, 117-127. https://doi.org/10.1120/jacmp.v11i1.2947

[13] Cardoso SC, Alves VGL, da Rosa LAR, Campos LT, Batista DVS, Facure A, Monte Carlo Simulation of Bony Heterogeneity Effects on Dose Profile for Small Irradiation Field in Radiotherapy. PLoS ONE. 2010; 5(5): e10466. https://doi.org/10.1371/journal.pone.0010466

ASTES

Advances in Science, Technology and Engineering Systems Journal Vol. 5, No. 3, 487-492 (2020)

www.astesj.com

Special Issue on Innovative Research in Applied Science, Engineering and Technology

ASTESJ

ISSN: 2415-6698

5G mm-wave Band pHEMT VCO with Ultralow PN

Abdelhafid Es-Saqy[*,1], Maryam Abata[1], Mohammed Fattah[2], Said Mazer[1], Mahmoud Mehdi[3], Moulhime El Bekkali[1], Catherine Algani[4]

[1]*AIDSESL, Sidi Mohamed Ben Abdellah University, 30050, Morocco*

[2]*EST, My Ismail University, 50050, Morocco*

[3]*ML, Lebanese University, 6573/14, Lebanon*

[4]*ESYCOM, Gustave Eiffel University, CNAM, 75003, France*

ARTICLE INFO

Article history:
Received: 21 May, 2020
Accepted: 07 June, 2020
Online: 20 June, 2020

Keywords:
pHEMT VCO
Local Oscillator
Low Phase Noise
MMIC VCO
5G VCO

ABSTRACT

Oscillator phase noise (PN) has a strong impact on the spectral purity of the RF signal in wireless systems and is, therefore, a main challenge when designing a local oscillator. In this paper, we propose a new approach for designing a low PN oscillator based on the Time-Invariant Linear Model of phase noise. It leads on voltage-controlled oscillator (VCO) simulated good performances: a low phase noise (PN) near -123.2 dBc/Hz@1MHz offset from the carrier, an output power of 3.26 dBm, and an output signal frequency ranging from 27.98 GHz to 29.67 GHz. Low power-consumption (51mW) and small size (0.237 mm^2) benefit from MMIC UMS foundry (United Monolithic Semiconductors) and 0.15 µm-pHEMT GaAs technology.

1. Introduction

The development of fifth-generation mobile networks (5G) is currently of great interest for telecommunication firms. This new generation will be the gateway to self-driving cars, virtual and augmented reality, Internet of Things, and other future technologies [1], therefore, it requires large contiguous blocks of spectrum.

The microwave frequency spectrum has become fully occupied with time. Therefore, in order to fulfill the explosive increase in broadband transmission requirements, new frequency allocation is needed for 5G applications. This new generation of mobile communications should allow download speeds up to 10Gbit/s, with a latency less than 1ms [2]. Fortunately, there are large frequency bands in the mmWave range that are not devoted to any other application [3]. Delegates at the World Radiocommunication Conference 2019 (WRC-19) identified five additional mm-Wave frequency bands for the deployment of 5G networks: [24.25-27.5 GHz], [37-43.5 GHz], [45.5-47 GHz], [47.2-48.2] and [66-71 GHz] [4].

In order to transpose the IF (Intermediate Frequency) signal to RF (Radio Frequency), or vice versa, wireless communication systems (Figure 1) require one or more local oscillators (LO). Thus, the local oscillator has strong impact on the spectral purity of the transmitted or received signal. Therefore, the design of LO with high purity is a major challenge. Many researchers have addressed the issue of phase noise in oscillators and have suggested several solutions to overcome this limitation [5-7], however, the impact of the proposed methods remains very limited, in term of phase noise performance, and does not meet the requirements of the new generation 5G.

In reference [5], the authors proposed an innovating architecture using two coupled VCOs and exhibiting -121.4 dBc/Hz @1MHz frequency offset Phase Noise for a chip area of 1.55 mm^2. In reference [6] a phase noise varying from -100 to -96 dBc/Hz@100kHz has been achieved, while the VCO core equals to 1 mm^2. And finally, the authors of reference [7] presented an architecture composed of four Colpitts VCOs and three millimeter-wave selectors, the phase noise varies from -100.7 dBc/Hz to -95.3 @ 1 MHz offset, while the chip size exceeds 3.7 mm^2.

*Corresponding Author: Abdelhafid Es-Saqy, abdelhafid.essaqy@usmba.ac.ma

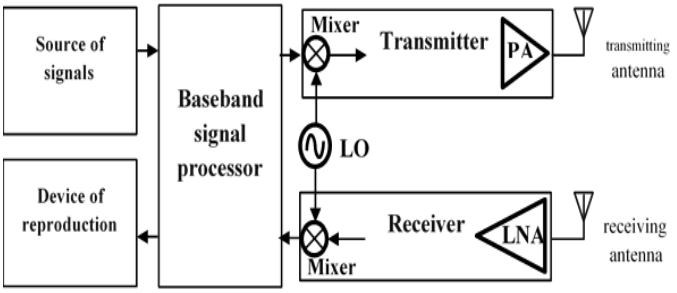

In this paper, we propose a new approach for designing a low PN oscillator presented previously in reference [8]. It is based on the Time-Invariant Linear Model (TILM) of PN [6, 8], and applied to design a MM-wave band VCO. Simulations show that the proposed architecture exhibits an extremely low phase noise level associated to a small size, compared to the ones published recently in the literature.

This paper is organized as follows. In section 2, we introduce the device technology. In section 3, a phase noise analysis is presented in order to extract an electrical model. The fourth section is dedicated to the proposed VCO architecture, while the fifth section presents the simulation results. Then we conclude.

2. GaAs pHEMT technology: PH15 UMS process

In last years, the development of III-V semiconductor materials for microwave devices has been sustained. Among these III-V semiconductors, gallium arsenide (GaAs) is the precursor, with better electronic and physical properties than silicon such as a higher electron mobility. GaAs Pseudomorphic High Electron Mobility Transistors (pHEMT) (Figure 2) are currently base of MMIC (Monolithic microwave integrated circuit) circuits thanks to mature technologies.

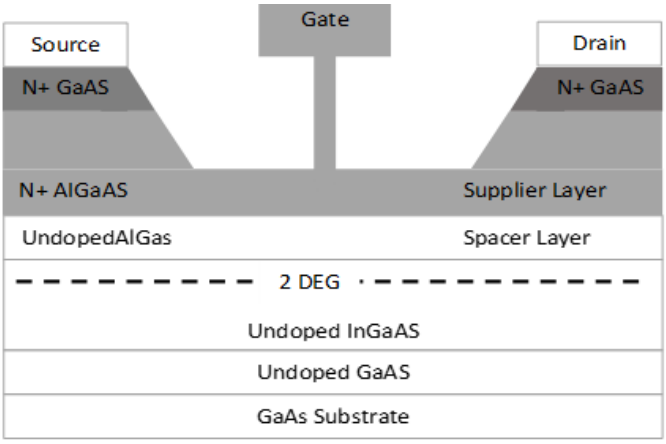

Due to the development of these transistors, local oscillators [9], power amplifiers [10, 11], mixers [12], and frequency multipliers [13] have shown improved performances. The 5G mm-wave VCO circuit, presented in this paper, is designed using the commercial UMS foundry (PH15 process). PH15 technology is based on a classical pseudomorphic AlGaAs/InGaAs/GaAs HEMT structure shown in Figure 2. This 5G mm-wave process features typically 110 GHz-f_T cut-off frequency, 640mS/mm peak transconductance, 220 mA/mm maximum drain current, -0.7 V pinch-off voltage and beyond 4.5 V gate-drain breakdown voltage. As the gate length is 0.15 µm, we take 30 µm-gate width. The PH15 process includes two metal interconnect layers, TaN resistors of 30 Ω/square, SiN MIM capacitors of 330 pF/mm^2, airbridge and via holes. Table 1 shows typical datas of the pHEMT transistor [14].

Table 1: Typical data of the pHEMT Transistor

Parameter	Value
Power Density	300 mW/mm
Gate Length	0.15 µm
Ids (gm max)	220 mA/mm
Ids sat	550 mA/mm
V_{BDS}	> 4.5 V
Cut off frequency	110 GHz
Vpinch	-0.7 V
Gm max	640 mS/mm
Noise	0.5 dB @ 10 GHz 1.9 dB @ 60 GHz
Gain	14 dB @ 10 GHz 6 dB @ 60 GHz

3. Voltage Controlled Oscillator Phase Noise

In wireless communication systems, a pure sine wave at a single frequency is an ideal case, i.e., a Dirac delta function at a single frequency. However, additive noise from propagation environment and circuits modulates the oscillator, introducing frequency fluctuations. These fluctuations spread the signal power at adjacent frequencies of the carrier frequency resulting in noise sidebands (Figure 3), generally named phase noise since it can be, in the time domain, represented as a random variation of the phase.

Recent wireless communication systems require radio frequency carriers of very high spectral purity. The quality of the VCO becomes a determining factor in the quality of the entire system. It would be very difficult to transmit a signal at very high frequencies and with complex modulations without a very low PN VCO.

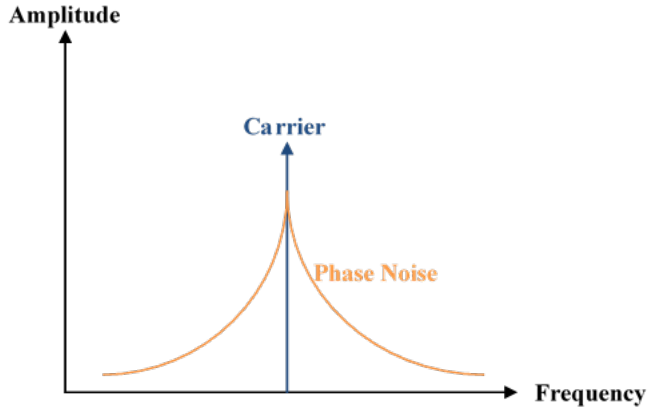

The up-converted amplitude noise is a critical source to phase noise, but there are other contributors of phase noise in a LO [15], we cite for example: flicker noise, 1/*f* noise, thermal noise and shot noise. In order to design a LO that combines both low PN

and small size, it is mandatory to find the relationship between PN and the circuit parameters. This relationship is given by the equation (1) [6]:

$$L(f_0, \Delta f) = \frac{2kT}{C} \cdot \frac{f_0}{Q} \cdot \frac{1+F}{A_0^2} \cdot \frac{1}{\Delta f^2} \qquad (1)$$

where $L(f_0, \Delta f)$ is the single sideband phase noise (SSPN) at Δf offset frequency from the carrier f_0, k is Boltzmann constant, T is the absolute temperature, C is the resonator capacitance value, Q is the resonator quality factor, F is noise factor and A_0 is the output signal amplitude.

From equation 1, PN of the LO is reduced when increasing the quality factor of the resonator circuit, in order to improve the amplitude of the output signal [6] or increasing the value of the capacitance of the circuit. In this work, we focused on a capacitance increase. Therefore, a capacity C1 has been added, in order to enhance the capacitance value of the resonator circuit and thus improve the PN. However, as the oscillation frequency depends on the circuit capacitance, the inductance value L1 must be reduced to keep the oscillation frequency value (figure 5).

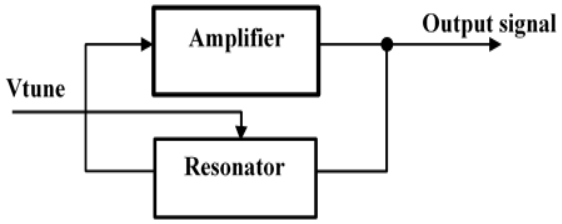

Figure 4: Synoptic diagram of a VCO

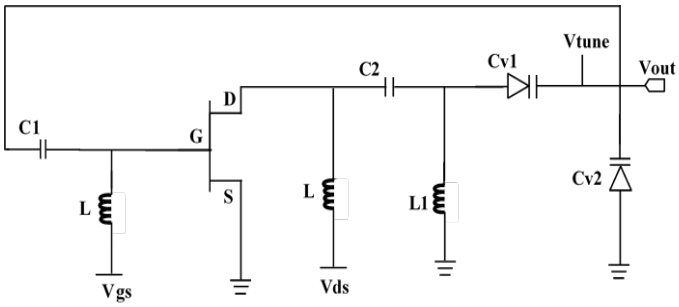

4. Voltage Controlled Oscillator Design

4.1. Colpitts Architecture

An oscillator (Figure 4) can be modeled by an amplifier to compensate for the energy losses, and a resonator to select the oscillation frequency [13]. The tank circuit of the Colpitts Oscillator contains a capacitive divider (two capacitors in series) and an inductance L1, while the amplifier circuit is composed of transistors with their bias elements. In [16], two varactors Cv1 and Cv2 replace fixed capacitors for purpose of tune the oscillation frequency with Vtune (figure 5). The simulation results of this VCO Colpitts show a varying oscillation frequency between 26.6 and 28.85 GHz, a PN near -96.07 and -113.07dBc/Hz@100kHz and @1MHz offset frequency respectively, and a fundamental output power of 9 dBm @ Vtune= 6 V. Although the VCO has an acceptable FoM of -172.82dBc/Hz, the PN must be improved to fulfill the 5G requirements.

4.2. Low PN VCO Architecture

In order to design a best performing VCO, an innovative architecture is proposed, studied and designed in this work. This circuit is based on the back-to-back structure of the varactors presented in [5] and on the Colpitts structure studied in [13] and [16]. Therefore, we maintained the same active part used in [13] and [16] and a capacity C1 has been added to the resonator circuit in order to enhance the capacitance value of the resonator circuit (Figure 6).

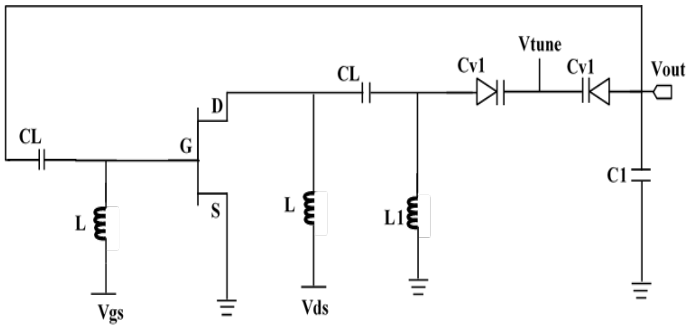

Graphs in Figure 7 show the variation of the capacitance of the resonator versus the control voltage Vtune with and without C1. From the two graphs, we can observe that the capacitance value of the circuit is clearly increased.

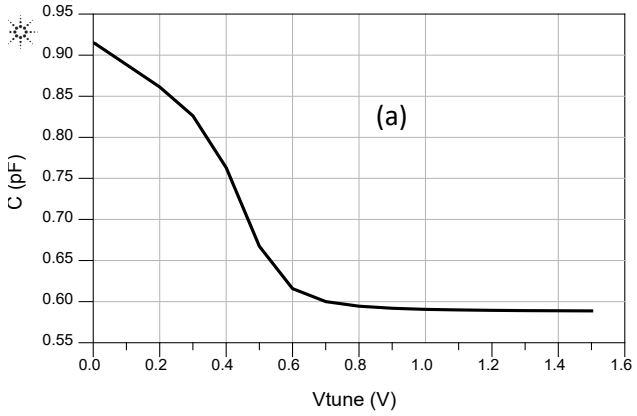

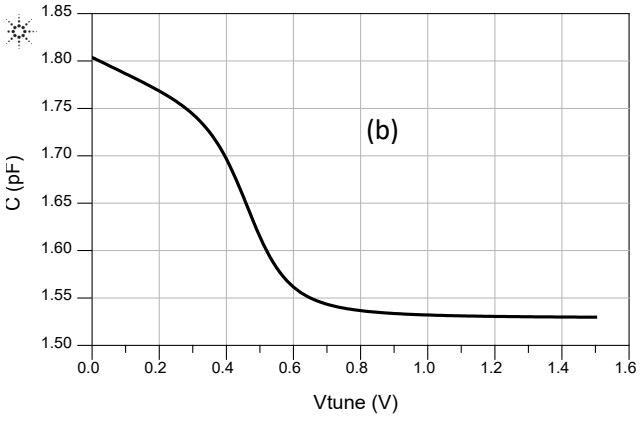

4.3. pHEMT VCO Layout

At mm-wave frequencies, parasitic capacitances and inductances can have a strong impact on the final Voltage Controlled Oscillator circuit performance. For this reason, a number of optimization steps were carried out before the final VCO layout presented in Figure 8.

The GaAs technology is multilayered. The chip dimensions are 0.56 x 0.423 mm^2, for a surface area of 0.237 mm^2. We can note that it is an extremely compact circuit compared to the architectures recently published in the literature [7, 13, 17-19].

5. Voltage Controlled Oscillator Simulation

The first step when designing an oscillator is to check the convergence of the circuit. Figure 9 shows that at 28 GHz the loop gain is 1.122 and the phase is 0.048 so both oscillation conditions in amplitude and phase are satisfied.

Simulation results on an electrical simulator software, show that the delivered signal is a sine wave (Figure 10) varying between 27.98 GHz and 29.67 GHz (Figure 11). Therefore, the tuning range (TR) is 1.69 GHz (about 6% of central frequency).

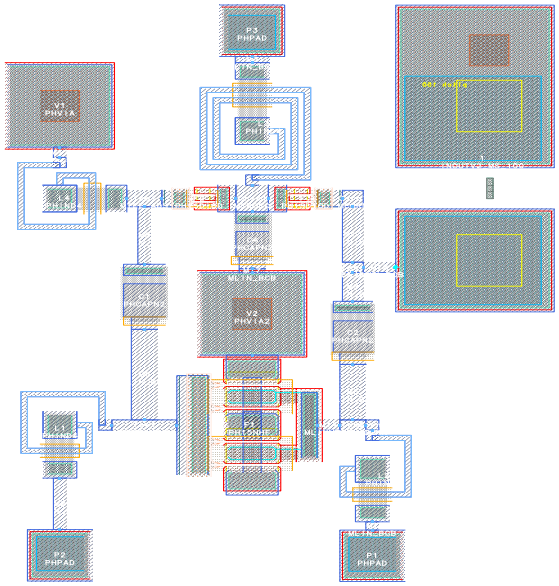

At the frequency 28.97 GHz (Vtune = 2.00 V), phase noise equals to -113.073, -133.078 and -153.07 dBc/Hz @ 100kHz, 1MHz and 10MHz offset frequency respectively (Figure 12). We can deduce that is an ultra-low PN level. Nevertheless, this architecture has an ultra-low PN only in a small tuning range part (around 28.95 GHz) (Figure 13), outside, the PN level is increased by 15 dB, i.e. the PN increases until it reaches the value -133.3 dBc/Hz @10MHz offset. Anyway, the PN of this architecture remains low compared to the other architectures recently published.

The fundamental output power is 3.26 dBm, on the other hand, at the first and second harmonics, it is equals to -18.8 dBm -14.2 dBm, respectively. Thus, the first and second harmonic rejections are 22.05 dB and 17.45 dB respectively (Figure 14). The DC power consumption is about 51 mW.

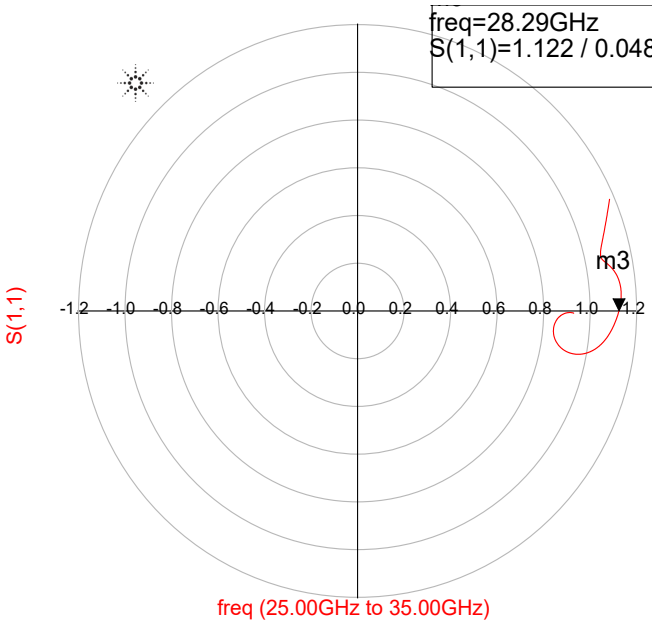

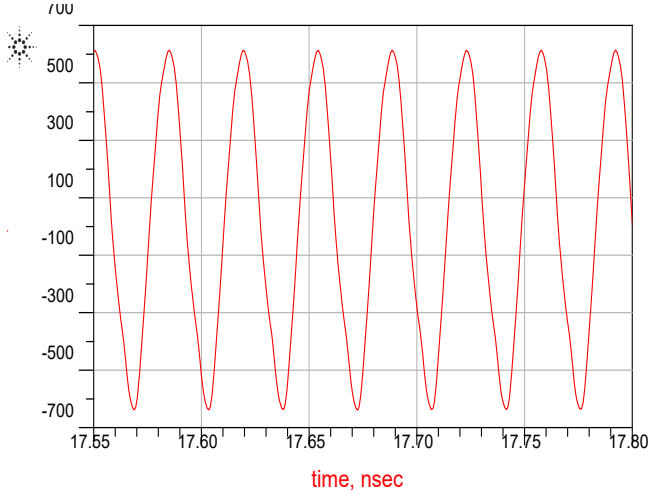

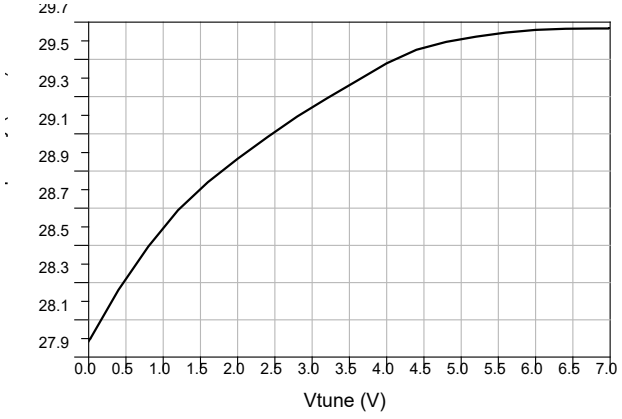

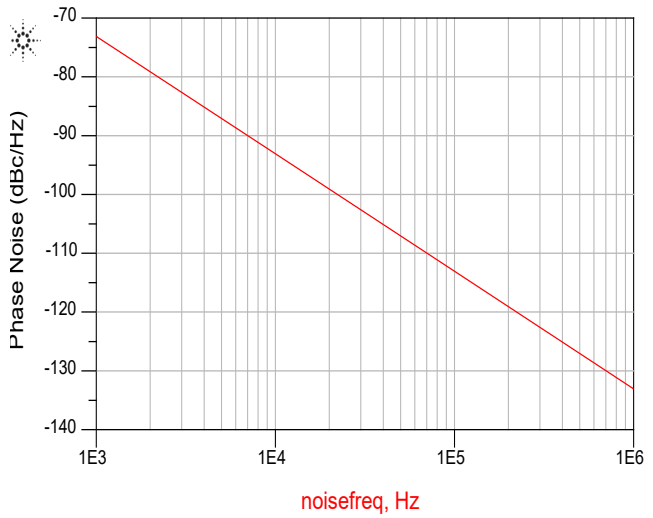

Figure 12: Single Sideband Phase Noise for Vtune=2 V

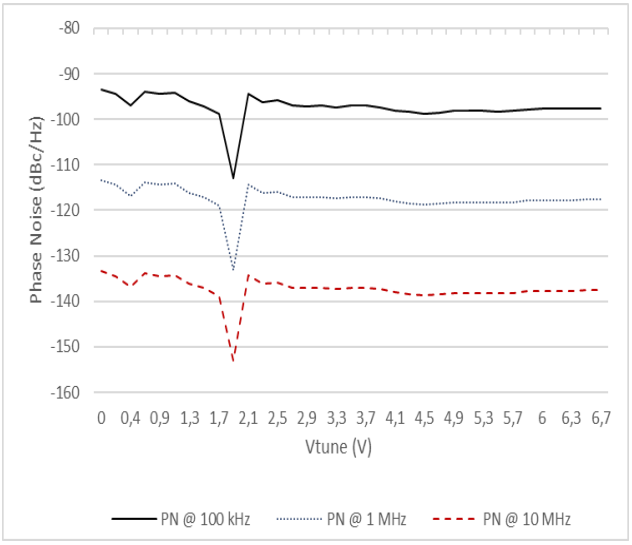

Figure 13: Single Sideband Phase Noise versus Vtune

6. Analysis of the simulation results

Table 2 presents the performance of the designed LO architecture compared to other architectures recently published in the literature. The PN of our architecture is 21.2 dB lower than the architecture proposed in [17] and beyond 22.5 dB, 22.1 dB and 14 dB lower than the architecture designed in [7], [13] and [18] respectively. Our VCO also has a relatively a wide tuning frequency range of about 1.67 GHz and a high fundamental output power of 3.26 dBm. The circuit consumption is quite low, less than half the DC power consumed by the VCO circuits studied in [7] and [19]. Finally, our LO has a good FoM of -195.3 dBc/Hz and is very small chip size compared to other architectures [7, 17-19].

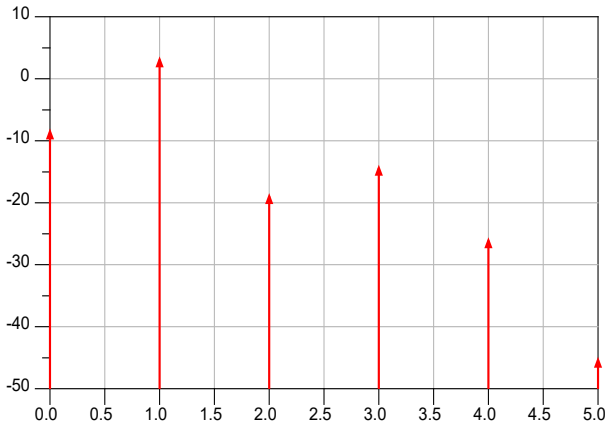

Table 2: Performance of different VCOs recently published in the literature

Ref.	Oscillation frequency (GHz)	DC power consumption (mW)	Fundamental output power (dBm)	PN (dBc/Hz) @1MHz	FoM** (dBc/Hz)	Chip area (mm^2)	Technologie
[17]	28.3	-	11.8	-102	-	0.5	0.15 µm pHEMT
[7]	29.4	124.6	4.5	-100.7	-169.11	3.75	0.13 µm SiGeBiCMOS
[13]	28.02	96	5	-100.9	-180.37	0.25	0.15 µm GaAs pHEMT
[19]	27.7	122	9.75	-113.16	-181.06	0.515	0.15 µm GaAs pHEMT
[18]	28.1	20	-	-109.2	-184.2	0.24	22 nm CMOS
This work	28.8	51	3.26	-123.2*	-195.3	0.237	0.15 µm GaAs pHEMT

(*) The average value of PN

$$(**) \quad \text{FoM} = L(f_0, \Delta f) + 10\log(P_{disp}) - 20\log\left(\frac{f_0}{\Delta f}\right)$$

Where $L(f_0, \Delta f)$ is the PN $@\Delta f$ offset from the f_0 and P_{disp} is the DC power consumption of the circuit in mW.

7. Conclusion

A new design approach for a low PN VCO is proposed, studied, and validated in this paper. This approach has enabled the design of a LO for the 5G mm-Wave band of low PN of -123.2 dBc/Hz @1MHz offset frequency from carrier, with a TR of 1.69 GHz, a fundamental output power of about 3.26 dBm associated to low DC power consumption.

References

[1] B. Dzogovic, B. Santos, T. Van Do, B. Feng, T. Van Do, and N. Jacot, "Bringing 5G Into User's Smart Home" in 2019 IEEE Intl Conf on Dependable, Autonomic and Secure Computing, Intl Conf on Pervasive Intelligence and Computing, Intl Conf on Cloud and Big Data Computing, Intl Conf on Cyber Science and Technology Congress, Fukuoka, Japan, 2019.https://doi.org/10.1109/DASC/PiCom/CBDCom/CyberSciTech.2019.00145.

[2] D. Milovanovic and Z. Bojkovic, "5G Mobile Networks: What is Next?" International Journal of Communications, 4, 1-5, 2019.

[3] G. Kang, S. Jiang, and Z. Zhao, "Research on millimeter wave spectrum planning for 5G" J. Phys. Conf. Ser., 1345, 1-5, 2019. https://doi.org/10.1088/1742-6596/1345/3/032040.

[4] International Telecommunication Union, "Key outcomes of the World Radiocommunication Conference 2019" ITU News Magazine, 6, 1-56, 2019.

[5] J. Hyvert, D. Cordeau, and J.-M. Paillot, "Analysis and design of a very low phase-noise Ku-band coupled VCO using a modified cascode architecture in 0.25 µm SiGe:C BiCMOS technology" Microelectron. J., 75, 137–146, 2018. https://doi.org/10.1016/j.mejo.2018.04.002.

[6] L. Romanò, V. Minerva, C. Samori, and M. Pagani, "Low Phase Noise, Very Wide Band SiGe Fully Integrated VCO" in 12th Gallium Arsenide applications symposium, Amsterdam, 2004.

[7] G. Cheng, Z. Li, Z. Li, T. Han, and M. Tian, "A 22-to-36.8 GHz low phase noise Colpitts VCO array in 0.13-µm SiGe BiCMOS technology" Microelectron. J., 88, 79–87, 2019. https://doi.org/10.1016/j.mejo.2019.04.004.

[8] A. Es-Saqy, M. Abata, S. Mazer, M. Fattah, M. Mehdi, M. El Bekkali, C. Algani, "Very Low Phase Noise Voltage Controlled Oscillator for 5G mm-wave Communication Systems" in 2020 1st International Conference on Innovative Research in Applied Science, Engineering and Technology (IRASET), Meknes, Morocco, 2020. https://doi.org/10.1109/IRASET48871.2020.9092005

[9] A. Es-saqy, M. Abata, M. Fattah, S. Mazer, M. Mehdi, M. El bekkali, "Study and Design of a MMIC Voltage Controlled Oscillator for 5G mm-wave band Applications" Int. J. Adv. Trends Comput. Sci. Eng., 9(2), 2124–2129, 2020. https://doi.org/10.30534/ijatcse/2020/186922020.

[10] H. Lee, W. Lee, T. Kim, M. Helaoui, F. M. Ghannouchi, and Y. Yang, "6–18 GHz GaAs pHEMT Broadband Power Amplifier Based on Dual-Frequency Selective Impedance Matching Technique" IEEE Access, 7, 66275–66280, 2019. https://doi.org/10.1109/ACCESS.2019.2917699.

[11] Y. Chen, C.-N. Chen, C.-C. Chiong, and H. Wang, "A Compact 40-GHz Doherty Power Amplifier With 21% PAE at 6-dB Power Back Off in 0.1um GaAs pHEMT Process" IEEE Microw. Wirel. Compon. Lett., 29(8), 545–547, 2019. https://doi.org/10.1109/LMWC.2019.2925716.

[12] C. Wang, D. Hou, J. Chen, and W. Hong, "A Dual-Band Switchable MMIC Star Mixer" IEEE Microw. Wirel. Compon. Lett., 29(11), 737–740, 2019. https://doi.org/10.1109/LMWC.2019.2940637.

[13] M. Kim, K. Choi, and J. Kim, "W-Band Backward Distributed Frequency Doubler Using GaAs 0.15 um pHEMT Process," IEEE Microw. Wirel. Compon. Lett., 29(6), 400–402, 2019. https://doi.org/10.1109/LMWC.2019.2913307.

[14] PH15-UMS MMIC Foundry, 2015-2016 Foundry Brochures.

[15] A. Hajimiri, "A General Theory of Phase Noise in Electrical Oscillators" IEEE JOURNAL OF SOLID-STATE CIRCUITS, 33(2), 179-194, 1998.

[16] A. Es-Saqy, M. Abata, S. Mazer, I. Halkhams, M. Mehdi, and C. Algani, "Comparative Study Between Hartley and Colpitts VCO for 5G MM-Wave Band Applications" in 2019 7th Mediterranean Congress of Telecommunications (CMT), Fès, Morocco, 2019. https://doi.org/10.1109/CMT.2019.8931343.

[17] B. Piernas, K. Nishikawa, T. Nakagawa, and K. Araki, "A compact and low-phase-noise Ka-band pHEMT-based VCO" IEEE Trans. Microw. Theory Tech., 51(3), 778–783, 2003. https://doi.org/10.1109/TMTT.2003.808584.

[18] M. A. Shehata, M. Keaveney, and R. B. Staszewski, "A 184.6-dBc/Hz FoM 100-kHz Flicker Phase Noise Corner 30-GHz Rotary Traveling-Wave Oscillator Using Distributed Stubs in 22-nm FD-SOI" IEEE Solid-State Circuits Lett., 2(9), 103–106, 2019. https://doi.org/10.1109/LSSC.2019.2929326.

[19] A. Es-Saqy, M. Abata, M. Mehdi, S. Mazer, M. Fattah, M. El bekkali, C. Algani, "28 GHz Balanced pHEMT VCO with Low Phase Noise and High Output Power Performance for 5G mm-Wave Systems" Int. J. Electr. Comput. Eng., 10(5), 2020. http://doi.org/10.11591/ijece.v10i5.pp%25p.

Advances in Science, Technology and Engineering Systems Journal Vol. 5, No. 6, 489-496 (2020)

www.astesj.com

Special Issue on Innovative Research in Applied Science, Engineering and Technology

ASTESJ

ISSN: 2415-6698

An Adaptive Nonlinear Sensorless Controller of Doubly Fed Induction Generator Driven By Wind Turbine

Radouane Ourhdir*, Mohammed Rachidi

Department of Electromechanical Engineering, Ecole Nationale Supérieure des Arts et Métiers, Moulay Ismail university, Meknès, BP 4024, Morocco

ARTICLE INFO

Article history:
Received: 01 July, 2020
Accepted: 07 September, 2020
Online: 20 November, 2020

Keywords:
Doubly fed induction generator (DFIG)
Control Wind Power Generation
Rotor speed observer
Unknown Aerodynamic Torque
Unknown Rotor Winding Resistance
Adaptive control projection operator
Lyapunov Theory

ABSTRACT

In this study, an adaptive nonlinear sensorless controller for doubly fed induction generator (DFIG) driven by a wind turbine is proposed. The aim is to maximize the extracted power by tracking the wind turbine optimal torque-speed characteristic without the need for rotor speed measurement. This controller ensures a satisfactory tracking of both stator flux and rotor speed. It considers the detailed model of DFIG in an arbitrary (d–q) rotating frame without any simplifying assumption. An observer provides the rotor speed estimation incorporated in the control loop. To guarantee the system stability under parametric uncertainties like the aerodynamic torque and the rotor winding resistance, which harms the efficiency and the robustness of the controller, update laws are established to estimate the uncertain parameters. Lyapunov's theory is used to prove the system stability. The proposed adaptive sensorless controller validity is demonstrated by simulation in Matlab/Simulink environment. The robustness of the controller is confirmed by the comparison between the same controller with and without adaptation.

1. Introduction

Recently, using wind energy to produce electricity has been gradually grabbing the attention of many researchers, thanks to its cleanliness and dependability. Because of its smaller power electronic components rating and its wide speed operation range, the DFIG is seen as the most used wind turbine generator [1–3]. The DFIG rotor windings are connected to the electrical grid via rotor and grid side converters (RSC and GSC) and RL filter, whereas the stator windings are immediately related to the electrical grid as illustrated by Figure 1. In the last decade, many researchers giving much focus and interest to the field of sensorless control of DFIG-based wind turbine (DFIG-WT)[4–7]. In this control strategy, the DFIG-WT systems operate without the need to use the speed sensor, which lowers the whole system cost and enhance its overall reliability by minimizing the number of components that are susceptible to failure.

There has been some research about sensorless control using proportional-integral (PI) loops such as [8,9]. The latter mainly relied on assumptions that the flux or stator voltages are constant, and the stator resistance is negligible. However, these assumptions are useless under grid faults or load variations. Furthermore, the small resistance of the stator may cause an incorrect damped dynamics of the stator flux [10].

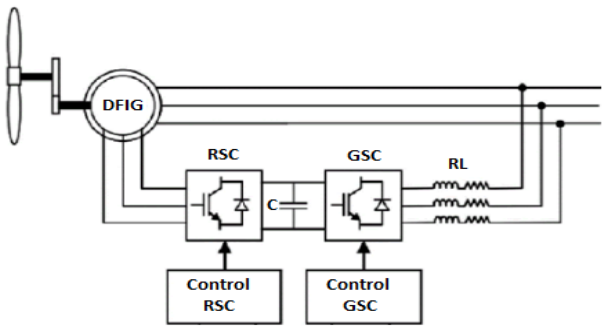

Figure 1: Schematic representation of grid connected DFIG-WT system

For the most control strategies, if the actual values do not correspond to the parameters and variables of DFIG-WT used in the control law, it could result in a failure of the closed-loop control. So, when some parameters and variables are difficult to be measured, some strategies based on estimation theory are important to generate a pertinent control. The frequency, the

*Corresponding Author: Radouane Ourhdir, radouane.ourhdir@edu.umi.ac.ma

temperature and the magnetic saturation may cause the change of DFIG parameters [11]. Therefore, the online parameter estimation or disturbance observer is compulsory to have high precision control.

Much research has addressed the control of DFIGs during parameter variation [12–14]. On the other hand, the modeling and the control of WT is not an easy task, particularly when large scale WTs, in megawatts, are considered [15,16]. Hopefully, to minimize the drive train vibration and to develop the quality of the extracted power, some works use the estimation theory in order to take into consideration the uncertainties arose from the aerodynamic torque, particularly in the stage of the maximum power point tracking (MPPT) [17].

The main focus of this work is to elaborate an adaptive sensorless control for the rotor side converter (RSC), this controller takes into consideration the detailed model of DFIG. Update laws in real-time are established to deal with the parameter uncertainties. To preserve the objectives of the MPPT without the need to use rotor speed sensor , a speed observer is incorporated in this controller. The remaining of this research paper displays as follows: The second section revolves around the model of the DFIG-WT system. The third section puts forward the suggested nonlinear controller: For the start, we present the proposed rotor speed observer. Afterward, we introduce our sensorless controller design, and we point out to the control laws of DFIG, and update laws for the speed observer, as well as the estimated rotor resistance and aerodynamic torque, which are competed using the Lyapunov theory. The last section considers simulation results and discussion. At last, we wrap up by drawing some concluding remarks.

2. DFIG-WT model

2.1. Wind turbine model

Based on wind turbine aerodynamic[18], The power captured from the wind can be expressed as :

$$P_t = \frac{1}{2}\rho\pi R^2 C_p(\lambda,\beta)\, v^3 \tag{1}$$

where ρ is the air density, R is the blade radius and v is the wind speed. The wind power coefficient $C_p(\lambda,\beta)$ depens on the design the blades; is a function of pitch angle β and tip speed ratio λ (TSR).
where:

$$\lambda = \frac{R\,\omega}{G\,v} \tag{2}$$

In which ω is the mechanical generator speed and G is the gearbox ratio. In the basis of the wind turbine design [18], the expression of power coefficient is:

$$C_p(\lambda,\beta) = c_1\left(\frac{c_2}{\lambda_i} - c_3\beta - c_4\right)\exp\left(-\frac{c_5}{\lambda_i}\right) + c_6\lambda \tag{3}$$

where:

$$\frac{1}{\lambda_i} = \frac{1}{\lambda + 0.08\beta} - \frac{0.035}{\beta^3 + 1}$$

The coefficients c_1-c_6 are listed in Table 1.

Table 1: Values of coefficients c1-c6

c_1	c_2	c_3	c_4	c_5	c_6
0.5176	116	0.4	5	21	0.0068

When the pitch angle β remains unchanged, there is an optimum tip ratio $\lambda = \lambda_{opt}$ that maximizes the power coefficient C_p, In this study, we assume that $\beta = 0$ .So the MPPT is achieved by the control of the generator speed. Conforming to (2) the mechanical speed that optimize the extracted power is:

$$\omega^* = \frac{G\lambda_{opt}}{R_t}\, v \tag{4}$$

2.2. Induction generator model

Employing the flux-linkage and voltage equations of the induction generator [19], the state variables of DFIG in an arbitrary reference frame rotating at speed ω_0 include d-q rotor currents and stator fluxes i_{dr}, i_{qr}, $\varphi_{ds}, \varphi_{qs}$, and generator speed ω .The considered 5th-order state-space representation of DFIG can be expressed as:

$$\begin{cases} \dfrac{d\varphi_{ds}}{dt} = u_{ds} - \alpha\varphi_{ds} + \omega_0\varphi_{qs} + \alpha M i_{dr} \\ \dfrac{d\varphi_{qs}}{dt} = u_{qs} - \alpha\varphi_{qs} - \omega_0\varphi_{ds} + \alpha M i_{qr} \\ \dfrac{di_{dr}}{dt} = \dfrac{1}{\sigma}u_{dr} - \dfrac{R_r}{\sigma}i_{dr} - \alpha\beta M i_{dr} + (\omega_0 - \omega)i_{qr} \\ \qquad - \beta u_{ds} + \alpha\beta\varphi_{ds} - \beta\omega\varphi_{qs} \\ \dfrac{di_{qr}}{dt} = \dfrac{1}{\sigma}u_{qr} - \dfrac{R_r}{\sigma}i_{qr} - \alpha\beta M i_{qr} - (\omega_0 - \omega)i_{dr} \\ \qquad - \beta u_{qs} + \alpha\beta\varphi_{qs} + \beta\omega\varphi_{ds} \\ \dfrac{d\omega}{dt} = -\dfrac{f}{J}\omega + \dfrac{T_t}{J} - \mu\left(\varphi_{qs}i_{dr} - \varphi_{ds}i_{qr}\right) \end{cases} \tag{5}$$

with:

$$\sigma = L_r\left(1 - \frac{M^2}{L_r L_s}\right), \quad \beta = L_r\frac{M}{\sigma L_s}, \quad \mu = \frac{M}{JL_s}, \quad \alpha = \frac{R_s}{L_s}$$

T_t is the mechanical torque. The rest of the parameters of DFIG-WT system are given in Table 2, Appendix B.

3. Control design

3.1. Speed observer

Achievement of MPPT strategy requires a quick convergence of the mechanical rotor speed to its optimal value. An observer is proposed to estimate the actual rotor speed of DFIG.

$$\dot{\hat{\omega}} = -\frac{f}{J}\hat{\omega} + \frac{\hat{T}_t}{J} - \mu\left(\varphi_{qs}i_{dr} - \varphi_{ds}i_{qr}\right) + \eta \tag{6}$$

Measurement of the rotor currents and the stator fluxes are compulsory for the latter observer; it relies also on the estimated aerodynamic torque $\hat{T}_t$ and the term η which will be elaborated by the means of the Lyapunov approach.

3.2. Reference Signals

Supposing that; the d-q rotating frame is aligned with the stator flux vector as in [20]. In our case, we consider that the stator flux vector is associated with the d-axis of the d-q reference frame giving:

$$\varphi_{qs} = 0;\ \varphi_{ds} = \Psi^* \tag{7}$$

Based on the assumption (7) illustrated by Figure 2, the expressions of the reference signals in the steady-state condition of DFIG can be established:

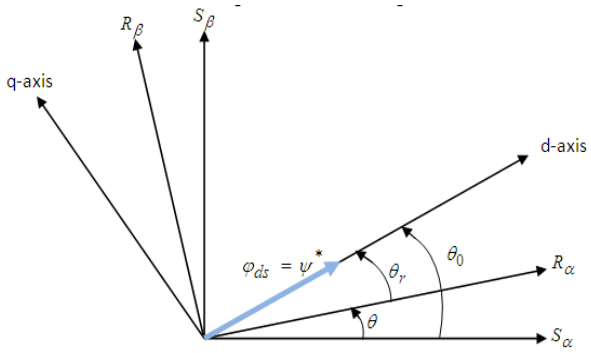

Figure 2: Determination of angles for the DFIG in d-q reference frame

Taking into consideration the latter assumption (7), and according to the first equation of (5), the reference of the direct rotor current can be expressed as follows:

$$i_{dr}^* = \frac{\Psi^*}{M} - \frac{u_{ds}}{\alpha M} + \frac{1}{\alpha M}\frac{d\Psi^*}{dt} \tag{8}$$

From the 5th equation of the system (5), the reference of the quadratic rotor current is established by replacing the aerodynamic torque by its estimate and incorporating a feedback saturation function [21], which relies on the estimated and reference rotor speed:

$$i_{qr}^* = \frac{1}{\mu\Psi^*}\left(-k_\omega sat\left(\hat{\omega} - \omega^*\right) + \frac{f}{J}\omega^* - \frac{\hat{T}_t}{J} + \frac{d\omega^*}{dt}\right) \tag{9}$$

where:

$$sat(y) = \begin{cases} 0.1 & if \quad y \geq 0.1 \\ y & if \quad -0.1 \prec y \prec 0.1 \\ -0.1 & if \quad y \leq -0.1 \end{cases}$$

The saturation function sat(y) has a finite limit at infinity; it is a linear, odd, and differentiable function in a neighborhood of the origin. To satisfy the assumption (7), the d-q reference frame must rotate at a specific speed ω_0 which is expressed using the second equation of (5):

$$\omega_0 = \dot{\theta}_0 = \frac{u_{qs} + \alpha M i_{qr}^*}{\Psi^*} \tag{10}$$

3.3. Control and update laws

The rotor speed sensor has some weak points concerning robustness, maintenance, cost, and cables linking the speed sensor and the control block. Any incorrect value provided by the rotor speed sensor may significantly harm the defined control targets and it can also destroy the system stability. Besides, accurate modeling of the aerodynamic torque is not an easy task, and the rotor winding resistance may vary up during operation due to the heating of the generator. That is to say that it constitutes uncertain parameters for the model which can affect the system stability. Yet, to ensure the system stability and maintain the control objectives in the presence of uncertainties and without needing to measure the rotor speed, the system closed-loop stability is examined to extract the expressions of the additional term η used in the speed observer, and the update laws of the estimated rotor resistance and aerodynamic torque. In this study, we assume that the aerodynamic torque and rotor resistance are unknown and vary slowly with time and should be estimated. To this purpose, the error variables can be introduced as follows:

$$\begin{cases} \tilde{\omega} = \omega - \omega^* \\ \tilde{\varphi}_{ds} = \varphi_{ds} - \Psi^* \\ \tilde{\varphi}_{qs} = \varphi_{qs} \\ \tilde{i}_{dr} = i_{dr} - i_{dr}^* \\ \tilde{i}_{qr} = i_{qr} - i_{qr}^* \\ e_\omega = \hat{\omega} - \omega \\ \tilde{R}_r = R_r - \hat{R}_r \\ \tilde{T}_t = T_t - \hat{T} \end{cases} \tag{11}$$

Using equations (5), (6), (7), (8), (9), (10) and (11) the system of the error dynamics can be expressed as follows:

$$\begin{cases} \dot{\tilde{\varphi}}_{ds} = -\alpha\tilde{\varphi}_{ds} + \omega_0\tilde{\varphi}_{qs} + \alpha M\tilde{i}_{dr} \\ \dot{\tilde{\varphi}}_{qs} = -\alpha\tilde{\varphi}_{qs} - \omega_0\tilde{\varphi}_{ds} + \alpha M\tilde{i}_{qr} \\ \dot{\tilde{i}}_{dr} = \frac{u_{dr}}{\sigma} - \frac{R_r}{\sigma}i_{dr} - \alpha\beta M i_{dr} + (\omega_0 - \omega)i_{qr} \\ \qquad - \beta u_{ds} + \alpha\beta\varphi_{ds} - \beta\omega\varphi_{qs} - \frac{di_{ds}^*}{dt} \\ \dot{\tilde{i}}_{qr} = \frac{u_{qr}}{\sigma} - \frac{R_r}{\sigma}i_{qr} - \alpha\beta M i_{qr} - (\omega_0 - \omega)i_{dr} \\ \qquad - \beta u_{qs} + \alpha\beta\varphi_{qs} + \beta\omega\varphi_{ds} - \frac{di_{qs}^*}{dt} \\ \dot{\tilde{\omega}} = -\frac{f}{J}\tilde{\omega} + \frac{\tilde{T}_t}{J} - \mu\tilde{\varphi}_{qs}i_{dr} + \mu\tilde{\varphi}_{ds}i_{qr} + \mu\Psi^*\tilde{i}_{qr} \\ \dot{e}_\omega = -\frac{f}{J}e_\omega - \frac{\tilde{T}_t}{J} + \eta \end{cases} \tag{12}$$

In order to have a compact error dynamic system, the error variables e_d and e_q are considered instead of $\tilde{i}_{dr}$ and $\tilde{i}_{qr}$:

$$\begin{cases} e_d = \tilde{\varphi}_{ds} + \frac{\tilde{i}_{dr}}{\beta} \\ e_q = \tilde{\varphi}_{qs} + \frac{\tilde{i}_{qr}}{\beta} \end{cases} \tag{13}$$

The error dynamics in (12) becomes:

$$\begin{cases} \dot{\tilde{\varphi}}_{ds} = -(\alpha + \alpha\beta M)\tilde{\varphi}_{ds} + \omega_0\tilde{\varphi}_{qs} + \alpha\beta M e_d \\ \dot{\tilde{\varphi}}_{ds} = -(\alpha + \alpha\beta M)\tilde{\varphi}_{qs} - \omega_0\tilde{\varphi}_{ds} + \alpha\beta M e_q \\ \dot{e}_d = \dfrac{u_{rd}}{\beta\sigma} - \dfrac{\tilde{R}_r}{\beta\sigma} i_{dr} + \left(\varphi_{qs} + \dfrac{i_{qr}}{\beta}\right)e_\omega + \eta_{0d} \\ \dot{e}_q = \dfrac{u_{rq}}{\beta\sigma} - \dfrac{\tilde{R}_r}{\beta\sigma} i_{qr} - \left(\varphi_{ds} + \dfrac{i_{dr}}{\beta}\right)e_\omega + \eta_{0q} \\ \dot{e}_\omega = \dfrac{f}{J} e_\omega - \dfrac{\tilde{T}_t}{J} + v \end{cases} \quad (14)$$

where:

$$\eta_{0d} = -\frac{\hat{R}_r}{\beta\sigma} i_{dr} - \alpha M i_{dr}^* + (\omega_0 - \hat{\omega})\frac{i_{qr}}{\beta} - (\hat{\omega} - \omega_0)\varphi_{qs} + \alpha\Psi^* - u_{ds} - \frac{1}{\beta}\left(\frac{\dot{\Psi}^*}{M} - \frac{1}{\alpha M}\frac{du_{sd}}{dt} + \frac{1}{\alpha M}\frac{d^2\Psi^*}{dt^2}\right)$$

$$\eta_{0q} = -\frac{\hat{R}_r}{\beta\sigma} i_{qr} - \alpha M i_{qr}^* - (\omega_0 - \hat{\omega})\frac{i_{dr}}{\beta} + (\hat{\omega} - \omega_0)\varphi_{ds} + \omega_0\Psi^* - u_{qs} - \frac{1}{\beta}\left[-\frac{\dot{\Psi}^*}{\mu\Psi^{*2}}\left(-k_\omega sat(\hat{\omega} - \omega^*) + \frac{f}{J}^* - \frac{\hat{T}_t}{J} + \dot{\omega}^*\right) + \frac{1}{\mu\Psi^*}\left(-k_\omega \frac{d}{dt} sat(\hat{\omega} - \omega^*)(\dot{\hat{\omega}} - \dot{\omega}^*) + \frac{f}{J}\dot{\omega}^* - \frac{\dot{\hat{T}}_t}{J} + \ddot{\omega}^*\right)\right]$$

The expression of the stator direct voltage derivative $\frac{du_{sd}}{dt}$ is detailed in Appendix A. we construct a Lyapunov function for the system (14) as:

$$V = \frac{1}{2}\left(\tilde{\varphi}_{ds}^2 + \tilde{\varphi}_{qs}^2 + z_d^2 + z_q^2\right) + \frac{1}{2}\lambda e_\omega^2 + \frac{\gamma}{J} e_\omega \tilde{T}_t + \frac{\gamma^2}{\lambda J^2}\tilde{T}_t^2 + \frac{1}{2}\delta\tilde{R}_r^2 \quad (15)$$

where λ, γ and δ are positive design parameters given in Appendix B. The derivative of V along with the time gives

$$\dot{V} = -\alpha\left[\tilde{\varphi}_{ds}^2 + \tilde{\varphi}_{qs}^2\right] - \alpha M\beta\left[\tilde{\varphi}_{ds}^2 + \tilde{\varphi}_{qs}^2\right] + \alpha M\beta\left[e_d\tilde{\varphi}_{ds} + z_q\tilde{\varphi}_{qs}\right] + \tilde{T}_t\left[v\frac{\gamma}{J} - \frac{2\gamma^2}{\lambda J^2}\dot{\hat{T}}_t\right] + \tilde{R}_r\left[-\frac{e_d i_{dr}}{\sigma\beta} - \frac{z_q i_{qr}}{\sigma\beta} - \delta\dot{\hat{R}}_r\right] + e_\omega\left[e_d\left(\varphi_{qs} + \frac{i_{qr}}{\beta}\right) - e_q\left(\varphi_{ds} + \frac{i_{dr}}{\beta}\right) + \lambda v - \frac{\gamma}{J}\dot{\hat{T}}_t\right] + z_q\left[\eta_{0q} + \frac{u_{qr}}{\sigma\beta}\right] + z_d\left[\eta_{0d} + \frac{u_{dr}}{\sigma\beta}\right] - \frac{\lambda f}{J}e_\omega^2 - \frac{\gamma}{J^2}\tilde{T}_t^2 - \left[\frac{\lambda}{J} + \frac{\gamma f}{J^2}\right]\tilde{T}_t e_\omega \quad (16)$$

It's obvious that:

$$\left(\frac{e_d}{2} - \varphi_{ds}\right)^2 + \left(\frac{e_q}{2} - \varphi_{qs}\right)^2 \geq 0 \quad (17)$$

From (17), we can get the following inequality:

$$\left[-\tilde{\varphi}_{ds}^2 - \tilde{\varphi}_{qs}^2 + e_d\tilde{\varphi}_{ds} + e_q\tilde{\varphi}_{qs}\right] \leq \frac{e_d^2 + e_q^2}{4} \quad (18)$$

The control laws are derived as:

$$\begin{cases} u_{dr} = -\sigma\beta\left[\dfrac{\alpha M\beta}{4} e_d + \eta_{0d} + k e_d\right] \\ u_{qr} = -\sigma\beta\left[\dfrac{\alpha M\beta}{4} e_q + \eta_{0q} + k e_q\right] \end{cases} \quad (19)$$

We define the dynamics of the rotor resistance as

$$\dot{\hat{R}}_r = \Pr oj\left[-\frac{1}{\delta}\left[\frac{e_d i_{dr} + e_q i_{qr}}{\sigma\beta}\right], \hat{R}_r\right] \quad (20)$$

where $\Pr oj[g, \hat{R}_r]$ is the projection algorithm[22], which is specified in our case by

$$\dot{\hat{R}}_r = \begin{cases} g & if\ \ R_{rm} \leq \hat{R}_r \leq R_{rM} \\ g & if\ \hat{R}_r < R_{rm}\ \ and\ g \geq 0 \\ g & if\ \hat{R}_r > R_{rM}\ \ and\ g \leq 0 \\ g\left[1 - \dfrac{R_{rm}^2 - \hat{R}_r^2}{R_{rm}^2 - (R_{rm} - \varepsilon_1)^2}\right] & if\ \ \hat{R}_r < R_{rm}\ and\ \ g < 0 \\ g\left[1 - \dfrac{\hat{R}_r^2 - R_{rM}^2}{(R_{rM} + \varepsilon_1)^2 - R_{rM}^2}\right] & if\ \ \hat{R}_r > R_{rM}\ and\ \ g > 0 \end{cases} \quad (21)$$

with R_{rM} and R_{rm} are the upper and the lower bound values of R_r, respectively, and ε_1 is an arbitrary positive constant such that $R_{rm} - \varepsilon_1 \geq 0$.

We define the update laws of the additional term and the aerodynamic torque as

$$\eta = \begin{cases} \varsigma = \dfrac{2}{\lambda}\left[e_q\left(\varphi_{ds} + \dfrac{i_{dr}}{\beta}\right) - e_d\left(\varphi_{qs} + \dfrac{i_{qr}}{\beta}\right)\right] & if\ \hat{T}_t \leq T_{tM} \\ \varsigma = \dfrac{2}{\lambda}\left[e_q\left(\varphi_{ds} + \dfrac{i_{dr}}{\beta}\right) - e_d\left(\varphi_{qs} + \dfrac{i_{qr}}{\beta}\right)\right] & if\ \hat{T}_t > T_{tM} \\ & and\ \dfrac{dP(\hat{T}_t)}{dt}\varsigma \leq 0 \\ \dfrac{\varsigma}{1 + P(\hat{T}_t)} & Otherwise \end{cases} \quad (22)$$

$$\dot{\hat{T}}_t = \begin{cases} \chi = \dfrac{J}{\gamma}\left[e_q\left(\varphi_{ds} + \dfrac{i_{dr}}{\beta}\right) - e_d\left(\varphi_{qs} + \dfrac{i_{qr}}{\beta}\right)\right] & if\ \hat{T}_t \leq T_{tM} \\ \chi = \dfrac{J}{\gamma}\left[e_q\left(\varphi_{ds} + \dfrac{i_{dr}}{\beta}\right) - e_d\left(\varphi_{qs} + \dfrac{i_{qr}}{\beta}\right)\right] & if\ \hat{T}_t > T_{tM} \\ & and\ \dfrac{dP(\hat{T}_t)}{dt}\chi \leq 0 \\ \dfrac{1 + P(\hat{T}_t)}{1 + P(\hat{T}_t)}\chi & Otherwise \end{cases} \quad (23)$$

where:

$$P(\hat{T}_t) = \frac{\hat{T}_t^2 - T_{tM}^2}{2\varepsilon_2\hat{T}_{tM} + \varepsilon_2^2} \quad (24)$$

with T_{tM} is the upper bound value of T_t and ε_2 is an arbitrary positive constant. Substituting (18), (19), (21), (22) and (23) in (16), the time derivative of (15) becomes:

$$\dot{V} \le -\alpha\left(\tilde{\varphi}_{ds}^2 + \tilde{\varphi}_{qs}^2\right) - \underbrace{\left[k - \frac{\alpha\beta M}{4}\right]}_{C}\left(e_d^2 + e_q^2\right) - \lambda\frac{f}{J}e_\omega^2 - \left(\frac{\lambda}{J} + \gamma\frac{f}{J^2}\right)\tilde{T}_t e_\omega - \frac{\gamma}{J^2}\tilde{T}_t^2 \quad (25)$$

The time derivative of (15) can be written in the following way:

$$\dot{V} \le -\min\{\alpha, C\}\left(\tilde{\varphi}_{ds}^2 + \tilde{\varphi}_{qs}^2 + e_d^2 + e_q^2\right) - \lambda\frac{f}{J}e_\omega^2 - \left(\frac{\lambda}{J} + \gamma\frac{f}{J^2}\right)\tilde{T}_t e_\omega - \frac{\gamma}{J^2}\tilde{T}_t^2 \quad (26)$$

Since $\tilde{T}$ and $\tilde{R}_r$ has been designed using a projection algorithm (bounded), from (15) and (26) we can establish that the functions $\tilde{\varphi}_{ds}$, $\tilde{\varphi}_{qs}$, e_d, e_q and e_ω are bounded on $[0, \infty)$. Consequently, from (14) it's clear that $\dot{\tilde{\varphi}}_{ds}$, $\dot{\tilde{\varphi}}_{qs}$, $\dot{e}_d$, $\dot{e}_q$ and $\dot{e}_\omega$ are bounded on $[0, \infty)$. So the functions $\tilde{\varphi}_{ds}$, $\tilde{\varphi}_{qs}$, e_d, e_q and e_ω are uniformly continuous on $[0, \infty)$, as a result, from(13) it can be seen that $\dot{\tilde{i}}_{dr}$, $\dot{\tilde{i}}_{qr}$, $\ddot{\tilde{i}}_{dr}$ and $\ddot{\tilde{i}}_{qr}$ are bounded, and the functions $\dot{\tilde{i}}_{dr}$, $\dot{\tilde{i}}_{qr}$ are also uniformly continuous on $[0, \infty)$.

The closed loop of the system (14) is determined based on (19), (21), (22) and (23) as:

$$\begin{cases} \dot{\tilde{\varphi}}_{ds} = -(\alpha + \alpha\beta M)\tilde{\varphi}_{ds} + \omega_0\tilde{\varphi}_{qs} + \alpha\beta M e_d \\ \dot{\tilde{\varphi}}_{qs} = -(\alpha + \alpha\beta M)\tilde{\varphi}_{qs} - \omega_0\tilde{\varphi}_{ds} + \alpha\beta M e_q \\ \dot{e}_d = -\left(k + \frac{\alpha\beta M}{4}\right)e_d - \frac{\tilde{R}_r}{\sigma}e_d + \frac{\tilde{R}_r}{\sigma}\tilde{\varphi}_{ds} \\ \qquad + e_q e_\omega + \frac{i_{qr}^*}{\beta}e_\omega - \frac{i_{dr}^*}{\sigma\beta}\tilde{R}_r \\ \dot{e}_q = -\left(k + \frac{\alpha\beta M}{4}\right)e_q - \frac{\tilde{R}_r}{\sigma}e_q + \frac{\tilde{R}_r}{\sigma}\tilde{\varphi}_{qs} - e_d e_\omega \\ \qquad -\left(\Psi^* + \frac{i_{dr}^*}{\beta}\right)e_\omega - \frac{i_{qr}^*}{\sigma\beta}\tilde{R}_r \end{cases} \quad (27)$$

We can put the last five equations of (27) in the following form:

$$\begin{aligned} \dot{x}(t) &= [A(t) + B(t)]x(t) + C(t)z(t) \\ \dot{z}(t) &= Dz(t) + Ex(t) + Fw(t) \\ \dot{w}(t) &= Gx(t) \end{aligned} \quad (28)$$

where:

$$x(t) = \left[\tilde{\varphi}_{ds}, \tilde{\varphi}_{qs}, e_d, e_q\right]^T \; ; \; z(t) = \left[e_\omega, \tilde{R}_r\right]^T \; ; \; w(t) = \tilde{T}_t$$

and

$$A(t) = \begin{pmatrix} -(\alpha + \alpha\beta M) & \omega_0 & \alpha\beta M & 0 \\ -\omega_0 & -(\alpha + \alpha\beta M) & 0 & \alpha\beta M \\ 0 & 0 & -\left(k + \frac{\alpha\beta M}{4}\right) & 0 \\ 0 & 0 & 0 & -\left(k + \frac{\alpha\beta M}{4}\right) \end{pmatrix}$$

$$B = \begin{pmatrix} 0 & 0 & 0 & 0 \\ 0 & 0 & 0 & 0 \\ \frac{\tilde{R}_r}{\sigma} & 0 & -\frac{\tilde{R}_r}{\sigma} & e_\omega \\ 0 & \frac{\tilde{R}_r}{\sigma} & -e_\omega & -\frac{\tilde{R}_r}{\sigma} \end{pmatrix} \quad C = \begin{pmatrix} 0 & 0 \\ 0 & 0 \\ \frac{i_{qr}^*}{\beta} & -\frac{i_{dr}^*}{\sigma\beta} \\ -\left(\Psi^* + \frac{i_{dr}^*}{\beta}\right) & -\frac{i_{qr}^*}{\sigma\beta} \end{pmatrix}$$

$$E = \begin{pmatrix} 0 & 0 & \frac{2}{\lambda}f_1\left(\varphi_{ds} + \frac{i_{dr}}{\beta}\right) & -\frac{2}{\lambda}f_1\left(\varphi_{ds} + \frac{i_{dr}}{\beta}\right) \\ 0 & 0 & -f_2\frac{i_{dr}}{\delta\sigma\beta} & -f_2\frac{i_{qr}}{\delta\sigma\beta} \end{pmatrix}$$

$$F = \begin{pmatrix} -\frac{1}{J} \\ 0 \end{pmatrix} \; ; \; D = \begin{pmatrix} -\frac{f}{J} & 0 \end{pmatrix}$$

$$G = \begin{pmatrix} 0 & 0 & f_3\frac{J}{\gamma}\left(\varphi_{qs} + \frac{i_{qr}}{\beta}\right) & -f_3\frac{J}{\gamma}\left(\varphi_{ds} + \frac{i_{dr}}{\beta}\right) \end{pmatrix}$$

with $f_i, i = 1,2,3,$ are bounded functions such that $0 \le f_i \le 1$

Since the functions $\tilde{\varphi}_{ds}, \tilde{\varphi}_{qs}, e_d, e_q, e_\omega$ are bounded, so for all $t \ge t_0$ $A(t), B(t), C(t), D(t), E(t), F(t)$ and $G(t)$ are bounded, with $\|A(t)\| \le A_M$, $\|B(t)\| \le B_M$, $\|C(t)\| \le C_M$, $\|D(t)\| \le D_M$, $\|E(t)\| \le E_M$, $\|F(t)\| \le F_M$, $\|G(t)\| \le G_M$

From (15), the function $V(t)$ can be put into the following inequation:

$$\alpha_1\left(\|x\|^2 + \|z\|^2 + \|w\|^2\right) \le V \le \alpha_2\left(\|x\|^2 + \|z\|^2 + \|w\|^2\right) \quad (29)$$

The time derivative of $V(t)$ (26) can be written in the following way:

$$\dot{V} \le -a_3\|x\|^2 - a_4\|w\|^2 + a_5\|w\|\|z\| \quad (30)$$

with:

$$a_3 = \min\{\alpha, k\}, \; a_4 = \frac{\gamma}{J^2}, \; a_5 = -\left(\frac{\lambda}{J} + \frac{\gamma f}{J^2}\right)$$

According to the proof of lermma 2.1 in [23], the origin $x = 0, z = 0; w = 0$ of (28) is locally exponentially stable.

4. Simulation Results

Simulation of the detailed model of 3MW DFIG-WT using the proposed adaptive nonlinear sensorless controller is performed in MATLAB/Simulink environment, the parameters and characteristics of the latter DFIG-WT along with the design parameters are given in Table 2, and Table 3, Appendix B.

The estimation and tracking performance of the adaptive sensorless controller is shown using a variable wind speed of $(8.5\ m/s)$ mean value as depicted in Figure 3. To show the robustness of the proposed adaptive sensorless controller against the aerodynamic torque and the rotor winding resistance variation the tracking performance for both the sensorless controller with [24] and without adaptation at constant wind speed $(9\ m/s)$ has been compared in Figure 4. The simulation is performed with the variation of the mechanical torque and the rotor winding resistance described by:

$$T_t = \begin{cases} T_t & for\ t \le 20s \\ 0.5T_t & for\ t > 20s \end{cases} \quad (31)$$

$$R_r = \begin{cases} R_r & for\ t \le 10s \\ 1.5R_r & for\ t > 10s \end{cases} \quad (32)$$

From Figure 3 (a) and 3 (b) the actual rotor speed varies in accordance with the wind speed, which confirms the effectiveness of the MPPT. Figure 3 (c) shows a good tracking performance of the stator quadratic current. According to Figure 3(d) it can be noticed that the estimated torque recovers the applied unknown torque. Similarly, from Figure 3(e) it can be observed that the estimated rotor resistance quickly converges to its true profiles. In Figure 4 the adaptive nonlinear sensorless controller performance is shown by the comparison of the proposed adaptive sensorless and the sensorless controller proposed in [24]. From Figures 4 (a) and 4 (b) it is noted that the stator flux and the rotor speed tracking errors sustain small perturbations caused by the unknown rotor resistance and the unknown aerodynamic torque, but they converge to zero quickly as soon as the estimates of R_r , and T_t converges to their actual values. Whereas in the case of control without adaptation Figures 4 (c) and 4 (d) the rotor speed and the stator flux don't track anymore their references after variation of the rotor resistance and the aerodynamic torque.

When the actual values do not correspond to their references, the closed loop system is exposed to failure, which destroys the control objectives. These results confirm the robustness of our controller regarding to the rotor resistance variation along with the aerodynamic torque.

5. Conclusion

This paper presents an adaptive nonlinear sensorless controller for DFIG-WT to maximize the wind energy extracted under parametric uncertainties and unknown rotor speed. The simulation performed in Matlab/Simulink environment illustrates the good results provided by the controller regarding the good tracking capability of the rotor speed and stator flux, in addition to correct estimation of the unknown rotor speed, aerodynamic torque, and the rotor resistance. Also, the comparison result between the same controller with and without adaptation shows the effectiveness of this work.

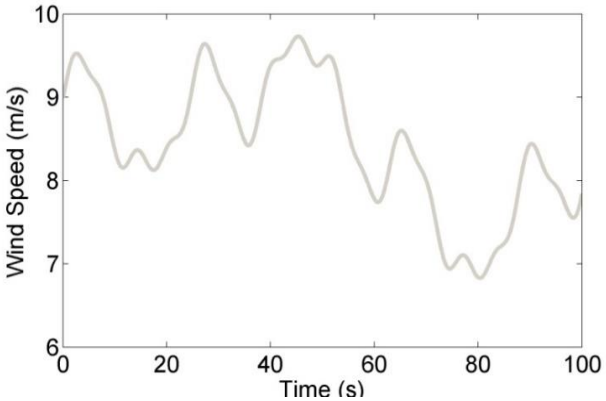

(a) Time varying wind speed

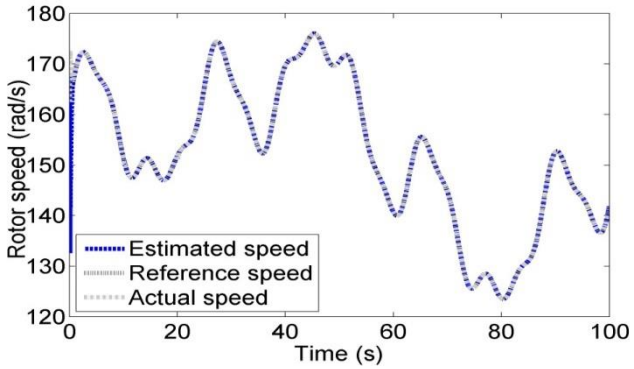

(b) Actual, Reference and estimated rotor

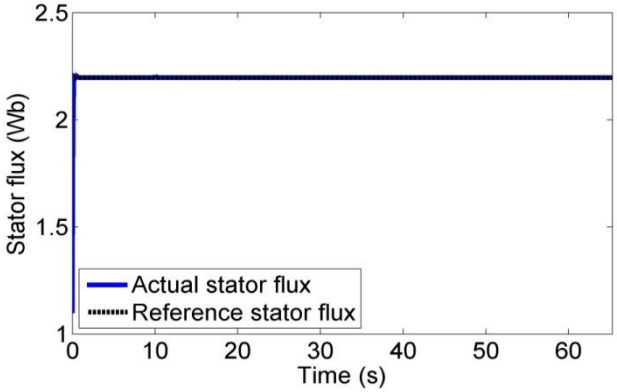

(c) The Actual and reference stator flux

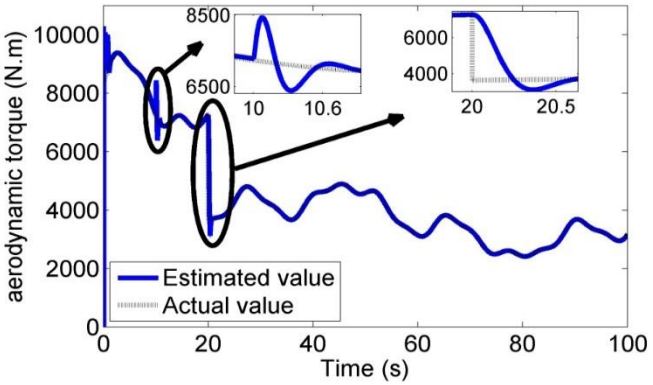

(d) The aerodynamic torque and its estimate

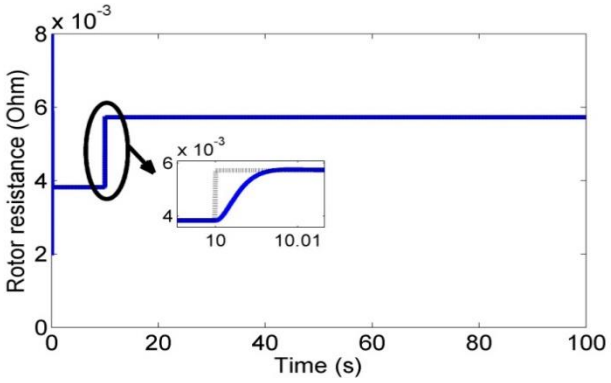

(e) The rotor resistance and its estimate

Figure 3: Comparison of tracking performance s under unknown parameters Changes occur at t=10s $\Delta R_r = 50\%$, t=10s $\Delta T_t = -50\%$ and at t=20s

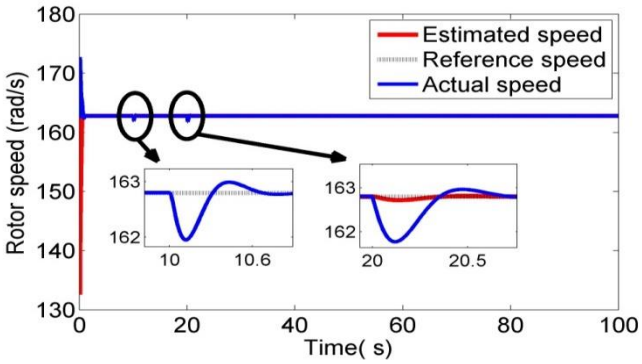

(a) Actual, Reference and estimated rotor speed with adaptation

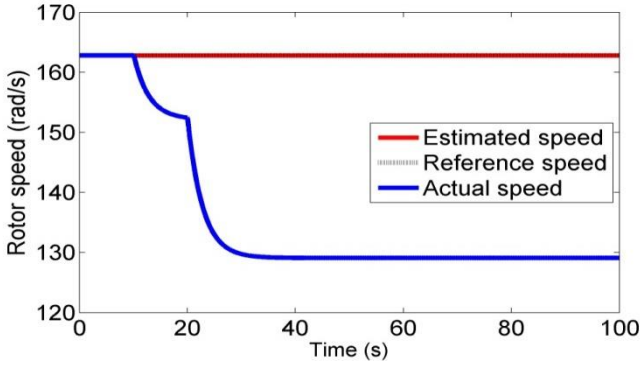

(b) Actual, Reference and estimated rotor speed without adaptation

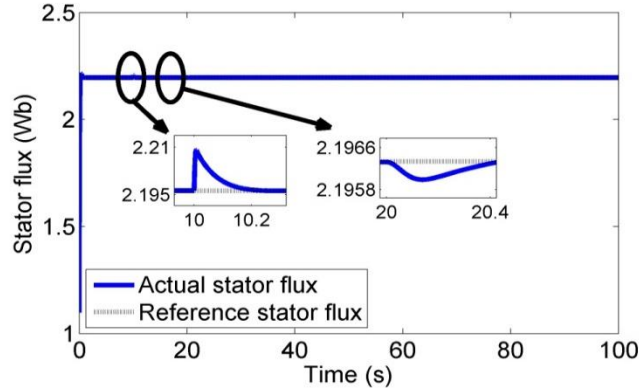

(c) The Actual and reference stator flux with adaptation

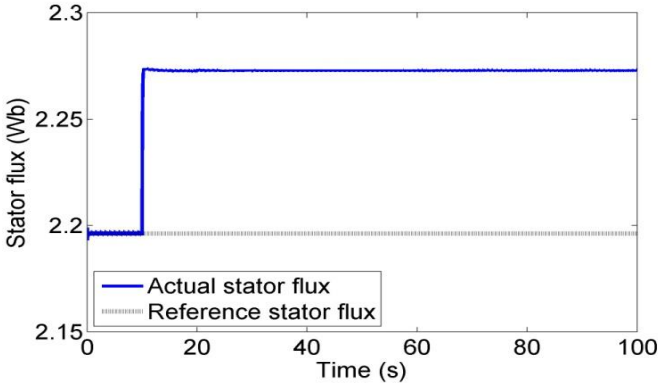

(d) The Actual and reference stator flux without adaptation

Figure 4: Comparison of tracking performances under unknown parameters
Changes occur at t=10s $\Delta R_r = 50\%$, t=20s $\Delta T_l = -50\%$

References

[1] G.M. As, "Doubly fed induction generator uising back-to-back PWM converters and its application to variable- speed wind-energy generation," 1996.

[2] S. Müller, M. Deicke, R.W. De Doncker, "Doubly fed induction generator systems for wind turbines," IEEE Industry Applications Magazine, **8**(3), 26–33, 2002, doi:10.1109/2943.999610.

[3] G. Boroumandjazi, B. Rismanchi, R. Saidur, "Technical characteristic analysis of wind energy conversion systems for sustainable development," ENERGY CONVERSION AND MANAGEMENT, **69**, 87–94, 2013, doi:10.1016/j.enconman.2013.01.030.

[4] A.B. Ataji, Y. Miura, T. Ise, H. Tanaka, "A Rotor-Current-Based Slip Angle Estimator for Grid-Connected Doubly Fed Induction Generator Requiring the Stator Inductance only," IEEE Transactions on Power Electronics, **32**(6), 4827–4838, 2017, doi:10.1109/TPEL.2016.2598441.

[5] L.Y. Lu, N.F. Avila, C.C. Chu, T.W. Yeh, "Model Reference Adaptive Back-Electromotive-Force Estimators for Sensorless Control of Grid-Connected DFIGs," IEEE Transactions on Industry Applications, **54**(2), 1701–1711, 2018, doi:10.1109/TIA.2017.2765300.

[6] M.W. Kalaga Mbukani, N. Gule, "Comparison of high-order and second-order sliding mode observer based estimators for speed sensorless control of rotor-tied DFIG systems," IET Power Electronics, **12**(12), 1–11, 2019, doi:10.1049/iet-pel.2018.6225.

[7] R.M. Prasad, M.A. Mulla, "Position-sensorless direct torque control of grid-connected DFIG with reduced current sensors," Sadhana - Academy Proceedings in Engineering Sciences, **45**(1), 2020, doi:10.1007/s12046-020-1275-x.

[8] H. Becheri, I.K. Bousserhane, A. Harrouz, I. Colak, K. Kayisli, "Sensorless Control of Wind Turbine Conversion Equipped with a DFIG Using MPPT Strategy," Proceedings - 2018 IEEE 18th International Conference on Power Electronics and Motion Control, PEMC 2018, (3), 605–610, 2018, doi:10.1109/EPEPEMC.2018.8522002.

[9] E.H. Abdou, A.R. Youssef, S. Kamel, M.M. Aly, "Sensorless Wind Speed Control of 1.5 MW DFIG Wind Turbines for MPPT," 2018 20th International Middle East Power Systems Conference, MEPCON 2018 - Proceedings, 700–704, 2019, doi:10.1109/MEPCON.2018.8635209.

[10] B. Yang, L. Jiang, L. Wang, W. Yao, Q.H. Wu, "Nonlinear maximum power point tracking control and modal analysis of DFIG based wind turbine," International Journal of Electrical Power & Energy Systems, **74**, 429–436, 2016, doi:10.1016/j.ijepes.2015.07.036.

[11] G.E.-P. and R.E.-P. López-García , F. Beltran-Carbajal, "A Review of RFO Induction Motor Parameter Estimation Techniques," **18**(2), 271–283, 2003.

[12] J.M. Mauricio, A.E. Leon, A. Gomez-Exposito, J.A. Solsona, "An Adaptive Nonlinear Controller for DFIM-Based Wind Energy Conversion Systems," IEEE Transactions on Energy Conversion, **23**(4), 1025–1035, 2008.

[13] A. Susperregui, I. Lizarraga, J. Jugo, G. Tapia, "Automated control of doubly fed induction generator integrating sensorless parameter estimation and grid synchronisation," IET Renewable Power Generation, **8**(1), 76–89, 2014, doi:10.1049/iet-rpg.2013.0045.

[14] R. Ourhdir, M. Rachidi, "Adaptive input-output feedback linearization control of doubly-fed induction machine in wind power generation," International Review of Automatic Control, **12**(1), 11–20, 2019, doi:10.15866/ireaco.v12i1.15619.

[15] J.M. Pinar Pérez, F.P. García Márquez, A. Tobias, M. Papaelias, "Wind turbine reliability analysis," Renewable and Sustainable Energy Reviews, **23**(March), 463–472, 2013, doi:10.1016/j.rser.2013.03.018.

[16] X. Jin, W. Ju, Z. Zhang, L. Guo, X. Yang, "System safety analysis of large wind turbines," Renewable and Sustainable Energy Reviews, **56**, 1293–1307, 2016, doi:10.1016/j.rser.2015.12.016.

[17] F. Liu, D. Li, P. Li, Y. Song, "Quadratic Optimal Tracking Control of Wind Turbine Systems," IFAC-PapersOnLine, **48**(28), 502–507, 2015, doi:10.1016/j.ifacol.2015.12.178.

[18] S. Heier, GRID INTEGRATION OF WIND ENERGY GRID INTEGRATION OF WIND ENERGY ONSHORE AND OFFSHORE.

[19] I. Press, L. Shafer, G.W. Arnold, D. Jacobson, ANALYSIS OF ELECTRIC MACHINERY AND DRIVE SYSTEMS.

[20] G. Abad, J. López, M.A. Rodríguez, L. Marroyo, G. Iwanski, Doubly Fed Induction Machine: Modeling and Control for Wind Energy Generation, 2011, doi:10.1002/9781118104965.

[21] R. Marino, P. Tomei, C.M. Verrelli, Induction Motor Control Design, 2010, doi:10.1007/978-1-84996-284-1.

[22] L. Praly, "Adaptive Nonlinear Regulation: Estimation from the Lyapunov Equation," IEEE Transactions on Automatic Control, **37**(6), 729–740, 1992,

doi:10.1109/9.256328.
[23] R. Marino, G.L. Santosuosso, P. Tomei, "Robust adaptive observers for nonlinear systems with bounded disturbances," IEEE Transactions on Automatic Control, **46**(6), 967–972, 2001, doi:10.1109/9.928609.
[24] R. Ourhdir, M. Rachidi, "Nonlinear sensorless control of doubly fed induction generator in wind power generation," 2020 1st International Conference on Innovative Research in Applied Science, Engineering and Technology, IRASET 2020, **2**(1), 2020, doi:10.1109/IRASET48871.2020.9091997.

Appendix A. Frame transformation and u_{ds} derivative

The direct and quadratic components of the stator voltage in the (d,q) reference frame can be expressed as follows:

$$\begin{pmatrix} u_{ds} \\ u_{qs} \end{pmatrix} = \begin{pmatrix} \cos\theta_0(t) & \sin\theta_0(t) \\ -\sin\theta_0(t) & \cos\theta_0(t) \end{pmatrix} \begin{pmatrix} u_{\alpha s} \\ u_{\beta s} \end{pmatrix} \quad (A.1)$$

where (α, β) stand for the fixed reference frame and θ_0 the electrical angle of the (d, q) rotating reference frame to the (α, β) one, see Figure 2. The components of the stator voltage in (α, β) are:

$$\begin{pmatrix} u_{\alpha s} \\ u_{\beta s} \end{pmatrix} = \underbrace{\sqrt{\frac{2}{3}} \begin{pmatrix} 1 & -\frac{1}{2} & -\frac{1}{2} \\ 0 & \sqrt{\frac{3}{2}} & -\sqrt{\frac{3}{2}} \end{pmatrix}}_{T} \begin{pmatrix} u_{as} \\ u_{bs} \\ u_{cs} \end{pmatrix} \quad (A.2)$$

In which T is the Concordia matrix transformation, and u_{as}, u_{bs} and u_{cs} are the 3-phases stator voltage giving by :

$$\begin{pmatrix} u_{as} \\ u_{bs} \\ u_{cs} \end{pmatrix} = V_m \begin{bmatrix} \sin(\omega_s t) \\ \sin\left(\omega_s t - \frac{2\pi}{3}\right) \\ \sin\left(\omega_s t + \frac{2\pi}{3}\right) \end{bmatrix} \quad (A.3)$$

Using the conventional derivative proprieties for scalar, vector and matrix, we can obtain the direct stator voltage component derivative $\frac{du_{ds}}{dt}$ used in (14). From (A.1) the expression of the direct stator voltage is:

$$u_{ds} = \begin{pmatrix} \cos\theta_0(t) & \sin\theta_0(t) \end{pmatrix} \begin{pmatrix} u_{\alpha s} \\ u_{\beta s} \end{pmatrix}$$

From (A.2), (A.3) and (10), the derivative of u_{ds} is given by:

$$\begin{aligned} \frac{du_{sd}}{dt} &= \begin{bmatrix} u_{as} & u_{bs} & u_{cs} \end{bmatrix} T^T \frac{u_{qs} + \alpha M i_{qr}^*}{\Psi^*} \begin{bmatrix} -\sin\theta_0(t) \\ \cos\theta_0(t) \end{bmatrix} \\ &+ \begin{bmatrix} \cos\theta_0(t) & \sin\theta_0(t) \end{bmatrix} T \omega_s V_m \begin{bmatrix} \sin\left(\omega_s t + \frac{\pi}{2}\right) \\ \sin\left(\omega_s t - \frac{\pi}{6}\right) \\ \sin\left(\omega_s t - \frac{5\pi}{6}\right) \end{bmatrix} \end{aligned} \quad (A.4)$$

$$\cos\theta_0(t) = \frac{\varphi_{\alpha s}}{\sqrt{\varphi_{\alpha s}^2 + \varphi_{\beta s}^2}} \text{ and } \sin\theta_0(t) = \frac{\varphi_{\beta s}}{\sqrt{\varphi_{\alpha s}^2 + \varphi_{\beta s}^2}}$$

Appendix B. characteristics/parameters of 3 MW DFIG-WT and the adaptive sensorless controller

Table 2: Characteristics and parameters of DFIG-WT

Parameter	Definition	Value
	Induction generator	
P_{rat}	Rated power	$3\,MW$
U	Rated stator voltage	$690\ V$
ω_s	Stator angular frequency	314 rad/s
p	Number of pole pairs	2
R_r	Rotor winding resistance	0.00382 Ω
R_s	Stator winding resistance	0.00297 Ω
L_r	Rotor inductance	0.0122 H
L_s	Stator inductance	0.0122 H
M	Mutual inductance	0.01212 H
	Wind Turbine	
R	Blade Radius	$45\ m$
G	Gearbox ratio	100
$C_{p\max}$	Maximal Power coefficient	0.48
λ_{opt}	Optimal Tip Speed Ratio(TSR)	8.14
	Generator and Turbine	
J	Moment of inertia	$254\ kg.m^2$
f	Dumping coefficient	0.24
f_r	grid frequency	50 Hz
U	grid voltage	$690\ V$

Table 3: parameters of the adaptive sensorless controller

Parameter	Value
k	6000
k_ω	100
δ	70000
γ	0.0098
T_{tM}	10000
R_{rm}	$0.5R_r$
R_{rM}	$2R_r$
ε_1	$0.001R_r$
ε_2	5

ASTES

Advances in Science, Technology and Engineering Systems Journal Vol. 5, No. 4, 523-530 (2020)

www.astesj.com

Special Issue on Innovative Research in Applied Science, Engineering and Technology

ASTESJ

ISSN: 2415-6698

Damage Accumulation Model for Cracked Pipes Subjected to Water Hammer

Zakaria Mighouar*, Laidi Zahiri, Hamza Khatib, Khalifa Mansouri

SSDIA Laboratory, Hassan II University of Casablanca, ENSET of Mohammedia, Mohammedia, 28830, Morocco

ARTICLE INFO

Article history:
Received: 30 June, 2020
Accepted: 22 July, 2020
Online: 09 August, 2020

Keywords:
Damage accumulation
Fatigue life
Loading sequence
Pipe
Semi-elliptical crack
Variable amplitude loading
Water hammer

ABSTRACT

During service, oil and gas pipelines may be exposed to cyclical loads during service, which may lead to a structural failure. Failure is due in most cases to cracks in the structure. Mechanics of the propagation of surface cracks pose a serious challenge and, therefore, models are required to help analyze it. In this study, a nonlinear model is proposed to estimate the accumulation of fatigue damage in the case of defected pipes subjected to a water hammer. The studied pipes are in the presence of a semi-elliptical longitudinal surface crack. This numerical model allows the load sequence to be considered when the structure is under variable amplitude loading. The validated model is used in a parametric analysis, the purpose of which is to determine the influence of the fluid transported and the defect parameters on the evolution of the accumulated damage. The results allow the conclusion of the parameters that have the most impact on the harmfulness of the crack defect as well as the most dangerous cracks in the case of a pipe subjected to water hammer.

1. Introduction

Oil and gas pipelines may be exposed to cyclic loads during service which could provoke failure. Failure of pipes could endanger human life, which is why manufacturers comply with very strict safety requirements. Nonetheless, the exploitation of welded structures still presents the risk of catastrophic failures. Failure is in most cases due to the existence of cracks at stress concentration zones such as inclusions, dents and weld defects [1].

Surface cracks, as well as inclusions, dents, corrosion damage, and cracks of the welding bead region, result in the most frequent defects in the welded structures. The propagation of surface cracks presents a substantial problem. Its mechanics need therefore to be studied after its initiation [2]-[4]. Possible crack propagation mechanisms of the welded structures, through the weld metal (WM), the base metal (BM) and the heat-affected-zone (HAZ), should be analyzed for safe operations [4]-[5].

Mechanical elements subjected to variable amplitude loading are susceptible to failure during operation because of fatigue. Load interaction takes place in this case [6]-[7]. When contrasted with the constant amplitude case, the applied sequence load could be responsible for accelerated or delayed crack growth [8]-[11]. Therefore it is necessary, in these conditions, to use an accurate and fast prediction method of fatigue life [12]-[13].

*Corresponding Author: Zakaria Mighouar, zakaria.mighouar@gmail.com

If sudden changes in pressure of the fluid occur in a pressurized system, then the defect of the pipe becomes even more dangerous [14]. When the flow velocity is changed sharply, the kinetic energy is forcibly converted into pressure energy that causes large and rapid changes in pressure inside the pipe. In the pipeline network, this pressure disturbance is propagated at high speed in a form of pressure wave [14]-[16].

The change in pressure caused by this effect, known as the water hammer, may lead to serious failures or leaks, particularly dangerous in the case of large transport systems [16]-[18]. The pipeline operators must characterize the level of risk associated with the threat once the defect has been identified, with the objective of making the right decision quickly [19]. This paper aims to propose a simple but effective nonlinear model to estimate the fatigue damage accumulation in longitudinal welded pipe structures subjected to water hammer wave pressures. This numeric model considers the effect of the loading sequence when the structure is under variable amplitude loading.

After validation of the model against results in the literature, an analysis is carried out to assess the effect of several parameters on the evolution of the fatigue damage accumulation. This study takes into account the location of a semi-elliptical longitudinal surface crack (base metal, weld metal and heat affected zone), its dimensions, its position (internal and external) and the transported fluid (water, light oil and heavy oil). This study will also shed light on the most harmful crack defects.

2. Fatigue failure

Fatigue is a process that, in the event of stresses or deformations varying over time, alters the local properties of a material. This may be magnified by surface irregularities, defects or structural discontinuities [20]. The major phases of structural fatigue failure are the formation of a crack called initiation, the steady propagation of crack followed by a rapid and unstable fracture of the structure [1], [3], [7].

In order to develop predictive capabilities, various theories have been advanced to characterize the fracture process, such as Linear Elastic Fracture Mechanics (LEFM) and Elastic-Plastic Fracture Mechanics (EPFM) [21]. LEFM is more appropriate for predicting material failure when the load response is elastic and the fracture response is brittle [22].

Fracture mechanics can be useful in predicting the life of components that are subject to time-dependent crack growth mechanisms. The cracking rate can be correlated with fracture mechanics parameters, such as the stress-intensity factor (SIF) and the critical crack size (a_C). Failure can be estimated if the fracture toughness of the material (K_{IC}) is known.

Paris et al. [23] initially suggested that the crack growth rate (da/dN) could be associated with the stress intensity factor range (ΔK) if the material is subjected to variable loading of constant amplitude (1). The material coefficients (C) and (m) are obtained experimentally.

$$\frac{da}{dN} = C\,\Delta K^m = C\left(K_{MAX} - K_{MIN}\right)^m \quad (1)$$

C, m: Paris law constants which depends on the material
K_{MIN}: Minimum stress intensity factor (MPa.m$^{0.5}$)
K_{MAX}: Maximum stress intensity factor (MPa.m$^{0.5}$)

Several experiments have shown that the length of the crack varies exponentially as a function of the number of cycles [1], [4], [9]. From this, it can be concluded that crack growth is rather slow until the final phase of fatigue life, where a relatively short number of cycles could lead to rapid crack growth resulting in failure. The initial crack length appears to be a very significant parameter for fatigue life assessment.

Numerous crack growth models have been suggested to predict the fatigue life of the structures. These models relate (da/dN) to the amplitude of stress or the maximum stress that can be expressed by the stress intensity factor.

Paris' Law is the simplest fatigue crack growth equation that gives the rate of fatigue crack growth [23]. A modified form which uses the effective stress to account for the crack closure [24-25] can be written as in (2).

$$\frac{da}{dN} = C\left(0.25\,K_{MAX} + 0.5\,K_{MIN} + 0.25\frac{{K_{MIN}}^2}{K_{MAX}}\right)^m \quad (2)$$

Crack closure is a fatigue loading phenomenon where, even if an external load is acting on the material, the contact is maintained between the opposite faces of the crack [7]. With an increase in load, a critical value of stress intensity factor (K_{OP}) is achieved when the crack is "open" (Figure 1).

Previous work by the authors [25] outlines the process of calculating the SIF where the correction factors for the analytical model have been introduced (2). These factors are used to enhance the results obtained in the case of high internal pressure and help to take into account the position of the crack (internal or external).

This process will be used in this paper to propose a method for assessing damage caused by a longitudinal semi-elliptical crack present in a metallic pipe. This pipe is considered to be subject to variable amplitude loading (internal pressure) caused by the water hammer phenomenon.

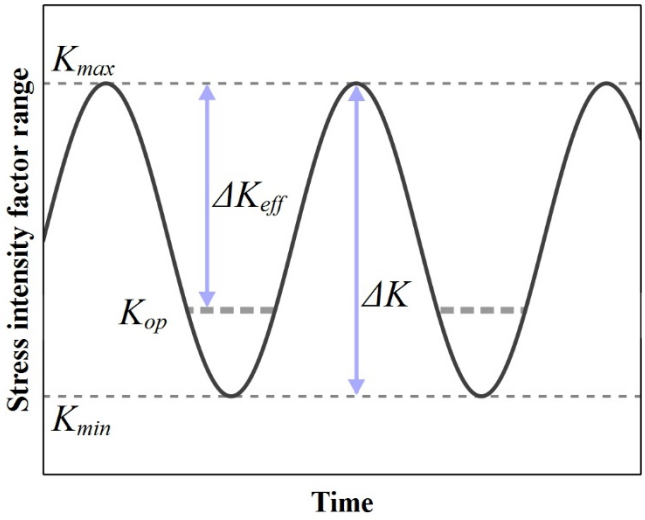

Figure 1: Crack closure effect

3. Damage accumulation model

Fatigue loading of pipeline structures varies by nature. Figure 2 shows a typical operating pressure spectrum for a pipeline. During fatigue loading, the pipeline material undergoes alterations resulting in damage [26]-[28]. It is therefore essential that models explicitly take into account the variability of fatigue loading.

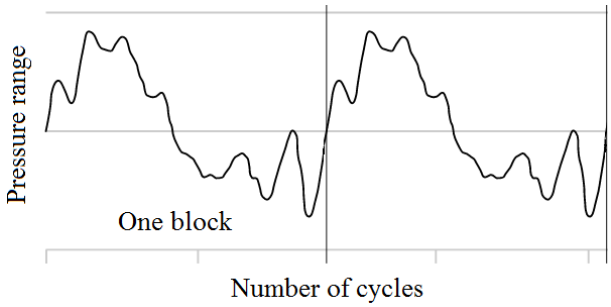

Figure 2: Typical operation pressure spectrum

The models used to describe fatigue-related damage accumulation can currently be classified into two categories: linear and non-linear approaches. Palmgren-Miner rule (3) is a linear damage accumulation approach that is widely used in engineering equipment because of its simplicity [29]. Damage (D) per stress level is estimated to be the ratio of the number of cycles (n) to the estimated lifetime of fatigue (N). Total damage is given by summing all estimated damage values. The summation should be equal to 1 or a given critical value as a failure criterion.

$$D = \frac{n}{N} \tag{3}$$

It is well known that the Palmgren-Miner Rule does not take into account the load sequences, load conditions and load interaction effects [30]. Many methods of fatigue damage accumulation have been suggested to fix the downside of this rule, and a large number of these models are based on nonlinear accumulation laws [31]-[33]. Load sequences and interaction effects are, in general, very important issues in the fatigue damage accumulation.

The main purpose of this paper is to propose a nonlinear model for fatigue damage accumulation based on fracture mechanics parameters. In this numerical model, the effect of the load interaction is considered. This damage model is described in equation (4). The stress intensity factor (K_I) and the crack depth (a) for a given stress level are estimated using a model developed by authors in [25]. This model allows the calculation of damage induced by a single pressure cycle and is defined as the maximum value between the ratio (a/t) and (K_I/K_{IC}), where (t) is the thickness of the pipe wall.

The damage accumulation values vary between a minimum value and 1 (or a specified critical value). The minimum value corresponds to the damage value calculated with the initial crack size. The value 1 signifies the rupture of the pipe.

$$D = \max\left(\frac{a}{t}; \frac{K_I}{K_{IC}}\right) \tag{4}$$

In the case where the value of 1 is caused by the ratio (a/t), it can be concluded that the propagation of the crack induces a leak in the structure. Otherwise, we will conclude that there has been a break (K/K_{IC} ratio equal to 1).

The model (4) alone does not allow to estimate the damage induced by an entire pressure spectrum. This model is intended to be used in an algorithm described in Figure 3. This allows the load interaction effect to be taken into account when the pipe is subjected to static or variable loading.

The algorithm for calculating accumulated damage developed hereby is based on the work of Thun et al. [34]. They estimate the damage accumulation using an analytical model. In this paper, the approach is based on numerical calculation of the damage accumulation and is illustrated in Figure 3. In this Figure, the pressure peak (p_i) is applied for (n_i) cycles. This algorithm is developed using C language and permits to estimate the damage accumulation after the application of (Nb_Blocks) cycles. Each cycle comprises (k) pressure peaks. The pressure peaks correspond to the sudden variation of the internal pressure in the pipe due to the phenomenon of water hammer.

The first step of the algorithm consist on calculating the damage (D_1) due to the first pressure peak (p_1) and the corresponding number of cycles (n_1) is estimated using the proposed damage model (4). This damage (D_1) is used to compute ($N_{2,equ}$) that induce the same damage but this time using the second pressure peak ((p_2) in this case). This step converts the previous damage into equivalent cycles.

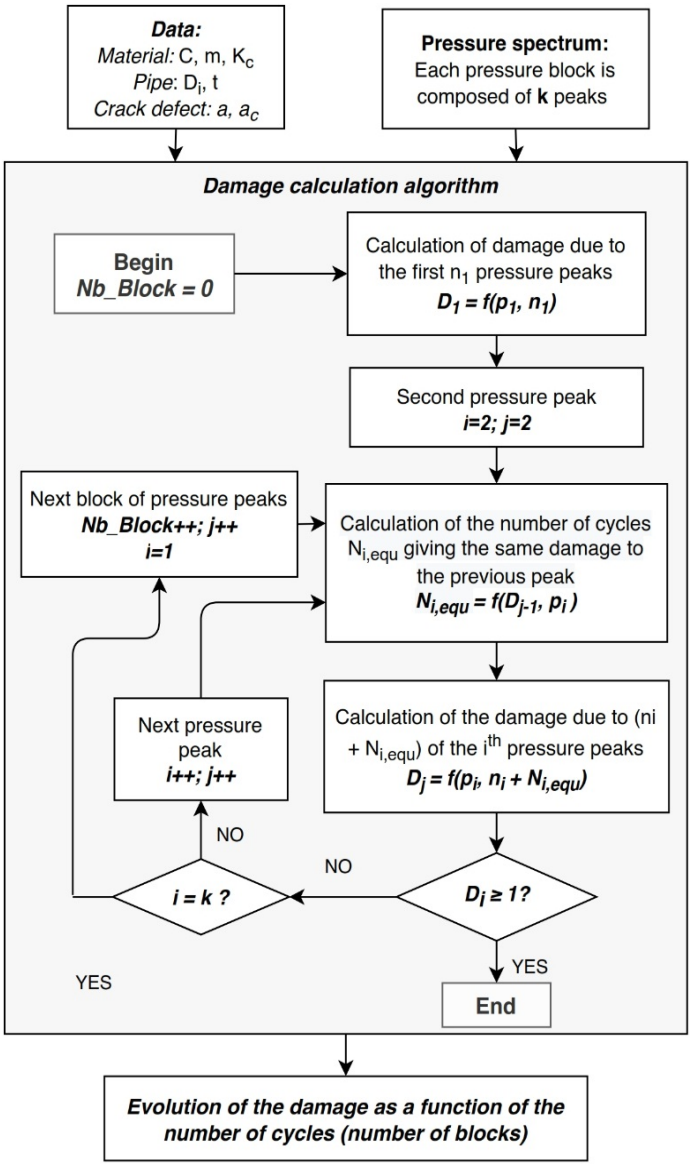

Figure 3: Damage accumulation algorithm

To calculate the damage (D_2) after the second pressure peaks (p_2) (and the previous ones), the number of cycles (N_2) for the second stress level is added to ($N_{2,equ}$). The damage model (4), taking the dimensions of the crack and the constant amplitude pressure p_2 for ($n_{2+N2,equ}$) cycles as parameters, is used to estimate D_2.

The same steps apply for the following pressure peaks until reaching the last peak of the block. As long as the value of the calculated damage does not exceed the critical value (here 1), the algorithm continue by resuming to the first pressure peaks and incrementing the number of cycles by 1 (one block equal to one cycle). The value of the estimated damage takes the previous damages into consideration on the basis of this concept.

It should be noted that, this model takes as input the pressure spectrum due to water hammer. This can be achieved by solving a system of equations that describes the transient flow of fluid in the pipe using the Method of Characteristics (MOC) [14, 17, 18, 25]. A more detailed study is led by authors in [25]. Only the results needed to build the study will be presented in this paper.

4. Water hammer

The water hammer is one of the most significant examples of a transient flow in pressurized pipelines. The history of the study of this phenomenon dates back to the 19th century [35]. The first approaches to mathematical formulation resulted in the most common formula that relates the variation in maximum pressure (Δp) to the change in fluid velocity before and after a sudden valve shift (Δv) [35] as mentioned in (5). Where (ρ) is fluid density, and (c) is wave propagation celerity.

$$\Delta p = \rho \cdot c \cdot \Delta v \tag{5}$$

The above method is a useful description of the phenomenon from a practical point of view. In view of its simplicity, equation (5) has made it possible for transient flow cases in elastic pipes, to estimate the maximal pressure range due to the water hammer. This has been seen to be satisfactory for many years. While this formulation is still common, more complex and accurate descriptions of the phenomenon have been developed.

The mathematical description of transient flow in pipelines is expressed by a set of two partial differential equations [14, 25, 35], i.e. the continuity equation (6), the momentum equation (7). It is applicable in the case of elastic pipe and describes the analytical pattern of the water hammer model for compressible fluid flow.

$$\frac{\partial p}{\partial t} + \rho c^2 \frac{\partial V}{\partial x} = 0 \tag{6}$$

$$\frac{\partial V}{\partial t} + \frac{1}{\rho}\frac{\partial p}{\partial x} + \frac{\lambda V|V|}{2D_i} = 0 \tag{7}$$

Where:
p: fluid pressure (MPa)
V: Instantaneous fluid velocity (m/s)
t: Time (s)
x: One-dimensional axis (m)
λ: Darcy-Weisbach friction coefficient
D_i: Internal pipe diameter (m)

The method of characteristics (MOC), characterized by rapid convergence and high accuracy of estimation outcomes, can be used to easily resolve this partial differential equation system [36-37]. In the computation, the initial conditions used are p_0=56.05MPa and V_0=1.2m/s. The value of p_0 corresponds to the nominal pressure and V_0 corresponds to the fluid velocity at the inlet of the pipe.

The obtained curves, using the MOC, describe the pressure variation of the fluid within the pipe as time-based. Fatigue life can only be predicted through the proposed numerical approach using pressure variation against the number of cycles. In an earlier study [37], it is detailed about how to convert time-based pressure spectrum to pressure spectrum according to the number of cycles by applying filters.

In this way, the pressure spectrum caused by the water hammer phenomenon can be estimated when a valve is suddenly closed/opened. Thus, the effect of this dynamic load on crack defects in the metallic pipe is simulated and the time for calculation is greatly optimized.

Three separate fluids are included in this study, their characteristics are shown in Table 1. Figure 4 shows the pipe dimensions. The pipe is made from the material API X52 with a Young modulus of 200GPa and a Poisson ratio of 0.3. As the pressure considered in this study does not exceed the specified minimum yield strength (SMYS), a linear elastic behavior of the material is considered. The friction factor λ is 0.019.

Table 1: Characteristics of the studied fluids [25]

Fluid	ρ (kg/m³)	C (m/s)
Water	998,2	1366,03
Light Oil	813	1463,21
Heavy Oil	962	1105,13

Figure 4: Pipe dimensions

Figure 5 indicates the outcome of that process for the three separate fluids when the valve opens and closes. The pressure drops to 26.85, 26.36 and 25.98 MPa during the sudden closing of the valves for water, light oil and heavy oil respectively.

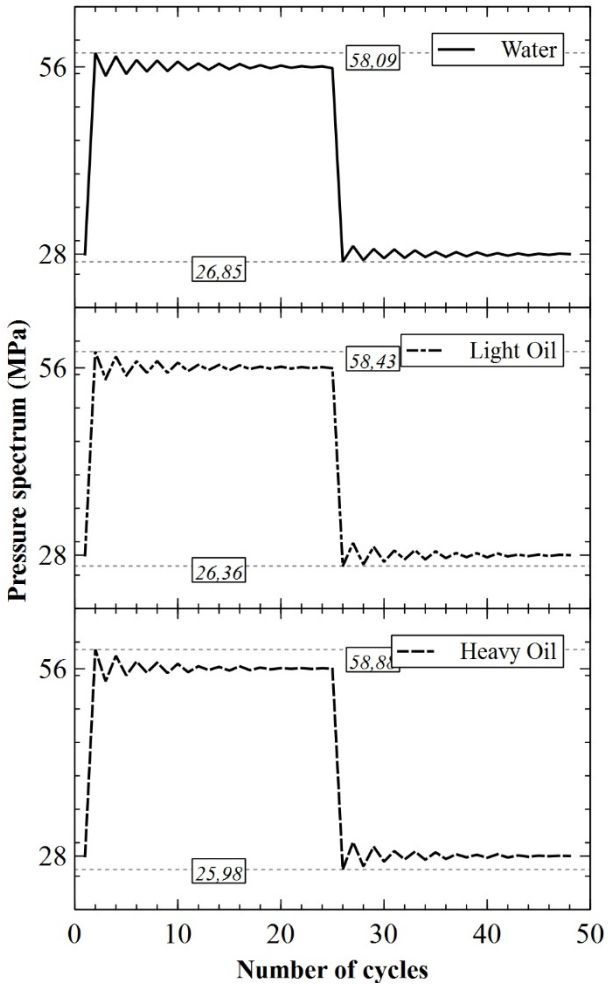

Figure 5: Filtered water hammer pressure waves for three different fluids (One block of pressure spectrum)

The maximum pressures reached are 3.73, 4.34 and 5.14% higher than the nominal pressure (56.05 MPa) of the fluid for water, light oil and heavy oil respectively. The simple equation (5) predicts increases in pressure due to the effect of water hammer of 2.43, 2.12 and 1.89% for water, light oil and heavy oil respectively.

This shows that taking more proper method to estimate pressure variation in case of water hammer when estimating the life of pipes will allow more reliable results. These pressures spectrums represent one block of variable amplitude pressure range. This can be used to assess the effect of water hammer in the case of different fluids on the integrity of the pipe structure.

The method used to calculate the pressure difference induced by water hammer provides results superior to those predicted by (5). Note that (5) does not provide any information on the cycles count until water hammer waves are attenuated. It is therefore important for industrialists to use a more accurate method, taking into account the effect of the water hammer. This is particularly important for the analysis of defects in highly pressurized pipeline structures.

5. Validation study

In order to validate the damage estimation approach proposed in this paper, we will compare the results obtained from our model with those published by Zoran [38, 39]. Pipe and fluids properties will be adapted for this purpose.

The proposed approach will be compared in the case of the two types of loading: constant (Figure 6) and variable (Figure 7) amplitude loading. In both cases, the pipe contains an internal semi-elliptical crack in longitudinal orientation. Initial crack size is 0.4 mm for all cases with a ratio (crack depth / crack width) equal to 0.4. In the case of constant amplitude loading, the evolution of the propagation of the crack is calculated for four internal pressures: 40, 50, 65 and 75MPa. The results are shown in Figure 6. One can see from the Figure 6 that the evolution of the number of cycles as a function of the crack depth obtained from the proposed model follows that of the literature.

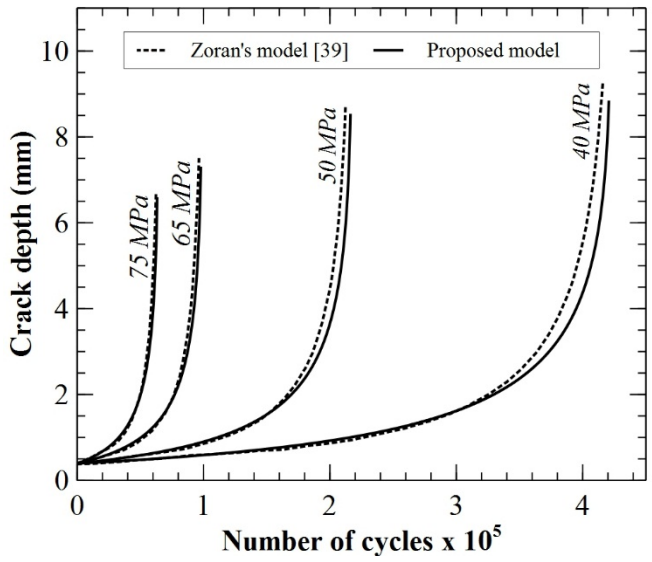

Figure 6: Crack propagation vs. number of cycle in the case of constant amplitude pressure spectrum

In the case of variable amplitude loading, Zoran [39] defined two types of loadings, one heavy and one medium. Five standardized pressure values (20, 35, 45, 60 and 70 MPa) are considered for each type of loading.

In Figure 7, the references EP70, EP60, EP45, EP35, and EP20 are kept the same from that of the literature. For example, in the codification EP70, 70 represents the equivalent pressure range of the pipe [39].

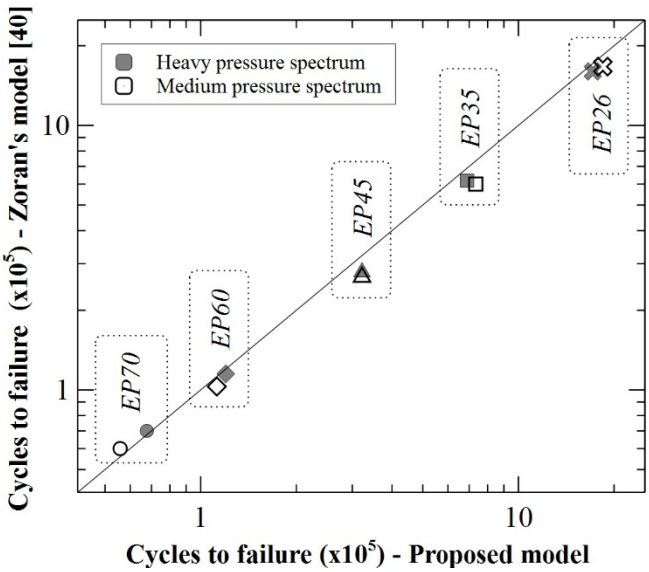

Figure 7: Crack propagation vs. number of cycle in the case of variable amplitude pressure spectrum

As shown in Figures 6 and 7, the deviance between the results obtained from the model developed and those of the literature remain acceptable. Which validated the proposed model.

6. Parametric study

In order to study the effect of the water hammer on the severity of the crack defect in the pipe, 54 cases will be investigated. In all cases, the initial crack depth is the same and equal to 3.25 mm. A semi-elliptical surface crack is the defect being studied.

The proposed algorithm (Figure 3) takes as input the pressure spectrum presented in Figure 5 to simulate a pipe transporting water, light oil and heavy oil. The crack dimensions (a/c) are 0.4, 0.6 and 0.8. The ratio (a/c) corresponds to the ratio crack depth to crack width.

The crack is considered to be located in the base metal, the welding metal and the heat-affected-zone. The parameters of the Paris Law (C and m) along with the critical stress intensity factor used for each zone are shown in Table 2. The process for obtaining the Paris Law and K_{IC} parameters can be found in [40] and [41] respectively. The position of the crack (internal or external) is also being studied.

Table 2: Material properties

Material	C[40]	m[40]	K_{IC} [41] (MPa.m$^{0.5}$)
Base metal	3.3 e-09	2.74	53.36
HAZ	1.13 e-09	3.25	53.36
Weld metal	1.04 e-09	3.28	61.02

7. Results and discussion

Figures 8, 9 and 10, along with Table 3, present the results of the numerical damage estimation model developed and validated hereby. The curves show an exponential evolution of the damage until the rupture or leakage of the structure (when the damage accumulation is equal to unity). This is typical for the propagation of longitudinal cracks in the metal pipe under cyclic pressure.

In order to obtain readable curves, Figure 8 groups together the evolutions of the damage accumulated only for the internal surface cracks present in pipes transporting water. This curve will allow us to evaluate the effect of the crack dimension on the evolution of the damage accumulation. Figure 9 contains the results of the accumulated damage for cracks of dimension (a/c) of 0.4 present in pipes transporting water. This will allow us to evaluate the effect of the crack position (internal or external) on the evolution of the damage. Figure 10 regroups the evolutions of the accumulated damage for the internal surface cracks of dimensions a/c of 0.4. This will allow us to evaluate the effect of the fluid transported by the pipeline on the evolution of the damage of the crack defect. Table 3 presents the number of cycles to fatigue for all of the studied cases.

All the curves start with a damage value of 0.237, which corresponds to the initial crack depth (3.25mm) divided by the thickness of the pipe (13.7mm). This shows that for all the cases studied in this paper and for the first peak of the pressure spectrum, we obtain a value of (a/t) greater than (K/K_{IC}).

In the following, the lower value of the crack dimension is used as a reference for the calculation of the deviations (the results for a/c equal to 0.8 to calculate the deviation for the cracks a/c equal to 0.6 and likewise for a/c equal to 0.6 and 0.4).

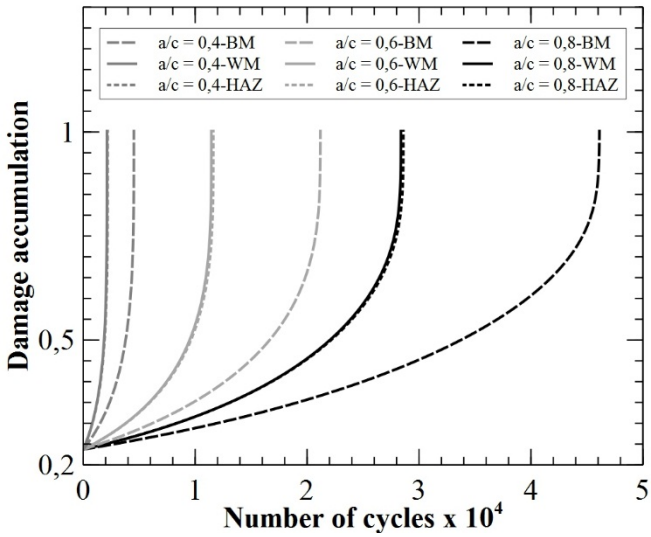

Figure 8: Effect of crack dimensions on the damage accumulation for water and internal cracks

It can be noted from reading the Figure 8 that, for the cracks located in the base material, a drop of -54% in term of fatigue life if crack dimension a / c evolves from 0.8 value to 0.6. From a/c = 0.6 to 0.4, a drop of -78.6% is observed. For the cracks located in the weld material, one notices a drop in fatigue life of -59.7% and -81.5% for respectively the crack with a/c dimension of 0.6 and 0.4. In the case of crack located in the heat affected zone, one notices a fall of -59.4% and -81.3% for respectively the crack with a/c dimension of 0.6 and 0.4. These values of deviations are very close to those observed in the case of a crack located in the welding material.

From these values of deviations, one can clearly see the important effect of the dimension of the crack and more precisely the ratio (a/c) on the fatigue lifetime. In fact, the lower the (a/c) ratio, the more harmful the crack.

From Figure 9, and if we take this time as reference of deviations the values obtained for the internal surface cracks, we observe a difference of + 26.8%, + 31.5% and + 39.4% compared to external surface cracks for defects located in the base material, in the weld material and in the heat-affected area, respectively. This confirms the fact that internal surface cracks are more harmful than external cracks (with same dimensions), regardless of the type of load or the material in which it is located.

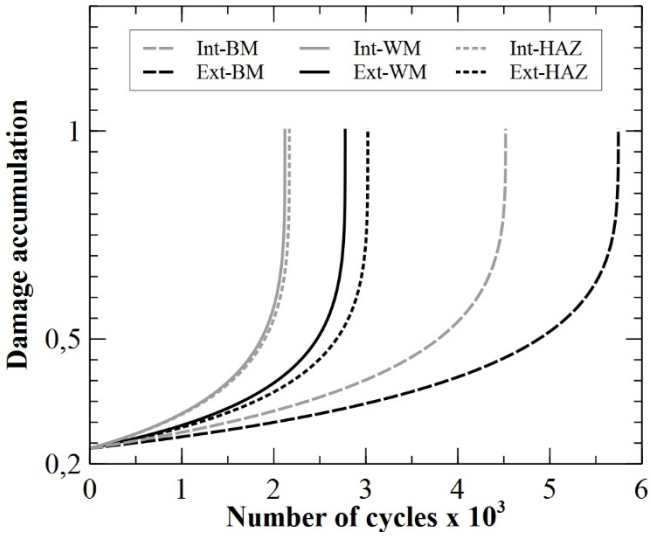

Figure 9: Effect of the position of the crack on the damage accumulation for crack with a/c of 0.4 and water

From a simple reading of Figure 10, we can notice that the evolution of the accumulated damage in the case of a cracked pipe transporting light oil is very close to that obtained for the pipe transporting heavy oil.

Let us take as reference of calculation of the deviations the results obtained in the case of crack present in a pipe transporting water. There is a difference of almost -6.9%, -8.15% and -8.1% in terms of fatigue life between the values obtained for the pipe transporting water and the pipes transporting oil (light or heavy) for cracks located in the base material, the weld material and in the heat-affected area, respectively.

This shows that the transported fluid has an effect on the evolution of the damage and therefore on the propagation of the crack. Admittedly, the effect of the fluid is not as pronounced as the other parameters studied. But if one seeks to obtain a precise evaluation of the damage induced by a defect on the structure, this parameter should not be neglected.

Let us consider the case of an internal crack of dimension (a/c) of 0.4 present in a pipe transporting heavy oil. From Figures 8, 9

and 10 as well as Table 3, the crack defect in the weld material has a deviation of -54.5% in terms of fatigue life compared to a crack in the base material. By taking the same reference, the crack located in the heat affected zone presents a deviation of -53.39%.

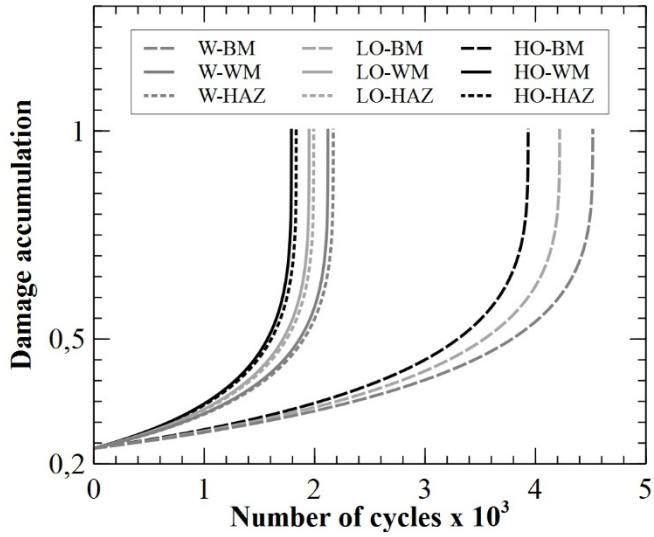

Figure 10: Effect of transported fluid on the damage accumulation for internal crack with dimension of 0.4

It is concluded that the crack is much more harmful when it is located in the weld material or the HAZ than when it is located in the base material. The most harmful crack remains that located in the welding material.

Table 3: Number of cycles to fatigue for all the studied cases

		Number of cycles to fatigue (cycles)					
		Base Metal		Weld Metal		HAZ	
	a/c	Int.	Ext.	Int.	Ext.	Int.	Ext.
Water	0,4	4531	5744	2118	2785	2168	3023
	0,6	21194	28211	11447	15846	11618	17009
	0,8	46117	64454	28382	41250	28600	43965
Light Oil	0,4	4218	5453	1944	2607	1991	2831
	0,6	18790	25506	10006	14127	10161	15170
	0,8	38939	55498	23628	35024	23822	37344
Heavy Oil	0,4	3931	5093	1787	2409	1832	2618
	0,6	16677	22688	8760	12432	8904	13360
	0,8	32914	47016	19701	29354	19881	31322

Int.: Internal cracks. Ext.: External cracks

8. Conclusion

A nonlinear model was proposed to estimate the accumulation of fatigue damage in cracked pipes subjected to water hammer. This model allows for the load sequence to be taken into consideration when the structure is subjected to variable amplitude loading, but can also be used in the case of constant amplitude loading.

The model uses the pressure spectrum calculated using the method of characteristics as input. It is based on an algorithm that allows the load sequence to be taken into account. This algorithm uses a mathematical model of the stress intensity factor that incorporates correction factors. One factor is used to improve the accuracy of the results in the case of high stress, and the other allows the crack location (internal or external) to be taken into account.

After validation of the model against results from the literature, it is used in a parametric study. The objective of this study is to evaluate the effect of certain parameters on the evolution of accumulated damage with the number of fatigue cycles. These parameters are the fluid transported by the pipe (water, light oil and heavy oil), the position (external and internal), the dimension (expressed by the ratio depth of the crack to the width of the defect) and the location of a semi-elliptical crack (base metal, weld metal and heat affected zone). These are the parameters that have the greatest impact on the harmfulness of the crack defect.

On the basis of the results achieved, the significant effect of the crack dimension and, more precisely, the ratio (a/c) on accumulation damage can be clearly seen. In fact, the lower the ratio (a/c), the more harmful the crack is. Internal surface cracks are found to be more harmful than external cracks, regardless of the type of load or material in which they are located. When located in the welding material or in the heat-affected zone, the surface crack is far more harmful than when located in the base material. The most harmful crack is the one in the welding metal.

The effect of the transported fluid is not as pronounced as the other parameters studied, but this parameter should not be neglected if the objective is to obtain a precise assessment of the damage caused by a structural defect.

This model will be used in further studies to analyze the effect of other types of crack defects on the integrity of a pipe structure subjected to a water hammer or even a high internal pressure.

References

[1] L. Zahiri, Z. Mighouar, H. Khatib, K. Mansouri, B. Salhi, “Fatigue life analysis of dented pipes subjected to internal pressure” International Review of Mechanical Engineering, **11**(8), 587–596, 2017. https://doi.org/10.15866/ireme.v11i8.12089

[2] M. A. N. Beltrão, E. M. Castrodeza, F. L Bastian, “Fatigue crack propagation in API 5L X-70 pipeline steel longitudinal welded joints under constant and variable amplitudes” Fatigue & Fracture of Engineering Materials & Structures, **34**(5), 321–328, 2011. https://doi.org/10.1111/j.1460-2695.2010.01521.x

[3] K. Pawan, M. Mamookho, S. Srijan, D. Aniket, “Prediction of the Propagation of Fatigue Cracks in Part-Through Cracked Pipes with CASCA and FRANC2D” Transactions of the Indian Institute of Metals, 2020. https://doi.org/10.1007/s12666-020-01886-z

[4] S. A. Barter, L. Molent, P. White, B. Dixon, “ Recent Australian full-scale F/A-18 fatigue tests” Structural Integrity and Life, **9**(2), 89–112, 2009.

[5] M. Manjgo, A. Sedmak, B. Grujić, “Fracture and fatigue behaviour of NIOMOL 490K welded joint” Structural Integrity and Life, **8**(3), 149–158, 2008.

[6] B. K. C. Yuen, F. Taheri, “Proposed modifications to the Wheeler retardation model for multiple overloading fatigue life prediction” International Journal of Fatigue, **28**(12), 1803–1819, 2006. https://doi.org/10.1016/j.ijfatigue.2005.12.007

[7] K. D. Singh, K. H. Khor, I. Sinclair, “Finite element and analytical modeling of crack closure due to repeated overloads” Acta Materialia, **56**(4), 835–851, 2008. https://doi.org/10.1016/j.actamat.2007.10.046

[8] M. A. Meggiolaro, J. T. P. de Castro, “On the dominant role of crack closure on fatigue crack growth modeling” International Journal of Fatigue, **25**(9-11), 843–854, 2003. https://doi.org/10.1016/S0142-1123(03)00132-4

[9] H. Dirik, T. Yalçinkaya, “Fatigue Crack Growth under Variable Amplitude Loading through XFEM” Procedia Structural Integrity, **2**, 3073–3080, 2016. https://doi.org/10.1016/j.prostr.2016.06.384

[10] K. Kurmoiartseva, P. Trusov, “Multilevel description of damage accumulation in titanium and titanium alloys” in AIP Conference Proceedings, **2053**, 030032, 2018. https://doi.org/10.1063/1.5084393

[11] L. Muys, J. Zhang, N. Micone, W. De Waele, S. Hertelé, "Cycle-by-cycle simulation of variable amplitude fatigue crack propagation" International Journal Sustainable Construction & Design, **8**(1), 2017. https://doi.org/10.21825/scad.v8i1.6808
[12] A. Vojdani, G. Farrahi, "Reliability assessment of cracked pipes subjected to creep-fatigue loading" Theoretical and Applied Fracture Mechanics, **104**, 1–12, 2019. https://doi.org/10.1016/j.tafmec.2019.102333
[13] J. R. Mohanty, B. B. Verma, P. K. Ray, "Prediction of fatigue crack growth and residual life using an exponential model. Part II: mode-I overload induced retardation" International Journal of Fatigue, **31**(3), 425–432, 2009. https://doi.org/10.1016/j.ijfatigue.2008.07.018
[14] A. Kodura, P. Stefanek, K. Weinerowska-Bords, "An Experimental and Numerical Analysis of Water Hammer Phenomenon in Slurries" Journal of Fluids Engineering, **139**(12), 1–9, 2017. https://doi.org/10.1115/1.4037678
[15] C. Cristoffanini, M. Karkare, M. Aceituno, "Transient Simulation of Long Distance Tailings and Concentrate Pipelines for Operation Training" in SME Annual Meeting/Exhibit, Salt Lake City, UT, 210–214, 2014.
[16] M. Kandil, A. M. Kamal, T. El-Sayed, "Effect pipes material on water hammer" International Journal of Pressure Vessels and Piping, **179**, 2019. https://doi.org/10.1016/j.ijpvp.2019.103996
[17] T. Wang, J. Jiang, G. Lan, "Research on Accumulator for Water Hammer Protection of Long-Distance Slurry Transportation Pipelines" in Sixth International Symposium on Fluid Machinery and Fluid Engineering (ISFMFE), Wuhan, China,1–6, 2014.
[18] W. Wan, W. Huang, "Water hammer simulation of a series pipe system using the MacCormack time marching scheme" Acta Mechanica, **229**, 3143–3160, 2018. https://doi.org/10.1007/s00707-018-2179-2
[19] T. Vilkys, V. Rudzinskas, O. Prentkovskis, J. Tretjakovas, N. Visniakov, P. Maruschak, "Evaluation of Failure Pressure for Gas Pipelines with Combined Defects" Metals, **8**(5), 346, 2018. https://doi.org/10.3390/met8050346
[20] A. Okab, K. Alkhazraji, A. Gatta, "Influence of Pressure and Thermal Parameters on Stresses Analysis of Pressurized and Cracked Pipes" Oriental Journal of Chemistry, **35**(6), 1640–1646, 2019. https://doi.org/10.13005/ojc/350604
[21] H. F. B. de Oliveira Dias, Failure Assessment on Effects of Pressure Cycle Induced Fatigue on Natural Gas Pipelines, Instituto Superior Técnico, 2014.
[22] A. A. Griffith, "The Phenomena of Rupture and Flow in Solids" Philosophical Transactions of the Royal Society of London, **221**(582–593), 163–198, 1921. https://doi.org/10.1098/rsta.1921.0006
[23] P. C. Paris, F. A. Erdogan, "Critical Analysis of Crack Propagation Laws" Journal of Basic Engineering, **85**(4), 528–533, 1963. https://doi.org/10.1115/1.3656901
[24] W. Elber, "Fatigue crack closure under cyclic tension" Engineering Fracture Mechanics, **2**, 37–45, 1970. https://doi.org/10.1016/0013-7944(70)90028-7
[25] Z. Mighouar, L. Zahiri, H. Khatib, K. Mansouri, Z. El Majid, "Effect of Water Hammer on Pipes Containing a Crack Defect" International Journal of Mechanical & Mechatronics Engineering, **18**(3), 25–31, 2018.
[26] A. Benin, S. Nazarova, A. Uzdin, "Designing Scenarios of Damage Accumulation" in International Scientific Conference Energy Management of Municipal Facilities and Sustainable Energy Technologies, 600–610, 2019. https://doi.org/10.1007/978-3-030-19868-8_57
[27] J. M. Torrenti, G. Pijaudier-Cabot, J. M. Reynouard, Mechanical Behaviour of Concrete, John Wiley and Sons, Inc., 185–223, 2013. https://doi.org/10.1002/9781118557587
[28] A. Belegundu, S. Nayak, J. Loverich, M. Grissom, "Vibration-Based Damage Accumulation Modeling" in 28th Conference on Mechanical Vibration and Noise, Charlotte, North Carolina, USA, 2016. https://doi.org/10.1115/DETC2016-59106
[29] M. A. Miner, "Cumulative damage in fatigue" Journal of Applied Mechanics, **12**(3), 159–164, 1945.
[30] S. P. Zhu, H. Z. Huang, Z. L. Wang, "Fatigue life estimation considering damaging and strengthening of low amplitude loads under different load sequences using fuzzy sets approach" International Journal of Damage Mechanics, **20**(6), 876–899, 2011. https://doi.org/10.1177/1056789510397077
[31] B. Isojeh, M. El-Zeghayar, F. Vecchio, "Concrete Damage under Fatigue Loading in Uniaxial Compression" ACI Materials Journal, **114**, 225–235, 2017. https://doi.org/10.14359/51689477
[32] H. Gao, H. Huang, S. Zhu, Y. Li, R. Yuan, "A Modified Nonlinear Damage Accumulation Model for Fatigue Life Prediction Considering Load Interaction Effects" The Scientific World Journal, 2014. https://doi.org/10.1155/2014/164378
[33] S. R. Maitra, K. S. Reddy, L. S. Ramachandra, "Stress Intensity Factor Based Damage Prediction Model for Plain Concrete under Cyclic Loading" Journal of Materials in Civil Engineering, **30**(7), 2018. https://doi.org/10.1061/(ASCE)MT.1943-5533.0002289
[34] H. Thun, U. Ohlsson, L. Elfgren, "A deformation Criterion for Fatigue of Concrete in Tension" Structural Concrete, **12**(3), 187–197, 2011. https://doi.org/10.1002/suco.201100013
[35] B. E. Wylie, V. L. Streeter, L. Suo, Fluid Transients in Systems, Englewood Hills, Prentice Hall, NJ, 1993.
[36] M. Dallali, M.A. Guidara, M.A. Bouaziz, C. Schmitt, E. Haj-Taieb, Z. Azari, "Accuracy and security analysis of transient flows in relatively long pipelines" Engineering Failure Analysis, **51**, 69–82, 2015. https://doi.org/10.1016/j.engfailanal.2015.03.001
[37] Z. Mighouar, L. Zahiri, H. Khatib, K. Mansouri, "Numerical Modeling Of Water Hammer Pressure Waves In Steel Pipes" in 1st International Conference on Innovative Research in Applied Science, Engineering and Technology (IRASET), Meknes, Morocco, 2020. https://doi.org/10.1109/IRASET48871.2020.9092171
[38] D. P. Zoran, "Fatigue Crack Growth Prediction For Pipes With Known Initial Crack" Trends in the Development of Machinery and Associated Technology, 461–464, 2013.
[39] D. P. Zoran, "Assessment Of Fatigue Crack Growth In Pipes Subjected To Variable Loading" Trends in the Development of Machinery and Associated Technology, 109–112, 2014.
[40] L. Zahiri, Z. Mighouar, H. Khatib, K. Mansouri, B. Salhi, "Fatigue Behavior Of Longitudinal Welded Pipes Subjected To Cyclic Internal Pressure, Containing Welding Defects" International Journal of Mechanical Engineering & Technology, **9**(3), 560–569, 2018.
[41] A. Belalia, A Rahmani, G. B. Lenkey, G. Pluvinage, Z. Azari, "Dynamic characterization of API 5L X52 pipeline steel" Key Engineering Materials, **498**, 15–30, 2012. https://doi.org/10.4028/www.scientific.net/KEM.498.15

ASTES

Advances in Science, Technology and Engineering Systems Journal Vol. 5, No. 5, 526-535 (2020)

www.astesj.com

Special Issue on Innovative Research in Applied Science, Engineering and Technology

ASTESJ

ISSN: 2415-6698

Multi Closed-loop Adaptive Neuro-Fuzzy Inference System for Quadrotor Position Control

Halima Housny[1], El Ayachi Chater[*,2], Hassan El Fadil[1]

[1]*Electrical Engineering, National School of Applied Sciences, Ibn Tofail University, Kénitra 14000, Morocco*

[2]*Electrical Engineering, Higher School of Technology, Mohammed V University, Salé 11060, Morocco*

ARTICLE INFO

Article history:
Received: 01 August, 2020
Accepted: 15 September, 2020
Online: 26 September, 2020

Keywords:
Adaptive neuro-fuzzy inference system
Quadrotor system UAVs
Intelligent control
Integral control

ABSTRACT

This paper deals with a multi closed-loop adaptive neuro-fuzzy inference system (ANFIS) design for the under-actuated quadrotor systems. First, the training data set for the fuzzy inference system is obtained using a proportional integral derivative controller. Then, an initial ANFIS controller is designed, where the integral control action is preserved in the multi-closed-cloop ANFIS for each quadrotor system state. Thereafter, scaling gains are added to the controller inputs/outputs, and a multidimensional PSO algorithm is used to tune all the control parameters. Besides, using a simulation example, the aerial vehicle performances are investigated in the presence of an unknown payload mass parameter. Specifically, the position tracking performances of the proposed multi closed-loop PSO-based ANFIS plus integral control strategy is compared with the classical PID, conventional ANFIS, and non-optimized ANFIS plus integral controllers. Thus, using the conducted simulation results, it results that the multi closed-loop PSO-based ANFIS plus integral can achieve perfect translational trajectory-tracking and ensure better attitude stabilization despite unknown quadrotor payload mass parameter. Therefore, the proposed new multi closed-loop PSO-based control strategy may be considered as an efficient controller when considering an arbitrary trajectory-tracking problem for the quadrotor system.

1. Introduction

In recent years, a growing number of researchers have been interested in quadrotor aerial vehicles as a result of their vertical take-off and landing (VTOL) ability, accurate hovering, good behavior even in case of severe maneuverability, and low cost. Then, the growing utilization of these unmanned aerial vehicles (UAV) has begun for all types of tasks. For instance, these aerial vehicles are commonly utilized in smart farming [1], real-time mapping while exploring confined spaces such as tunnels and mines [2], and air travel [3]. However, although the quadrotor has become a successful UAV, this aerial robot is an underactuated and coupled system. Thus, to control this nonlinear system, several approaches have been presented. However, designing an efficient control strategy for this aerial vehicle is still a difficult task. In the literature, different methods have been used to ensure the quadrotor flight stabilization. First, prominent control approaches for quadrotor attitude stabilization and trajectory-tracking control include the proportional-integral-differential (PID) controller [4]. However, despite this control approach could ensure flight stabilization for hovering state, it cannot stabilize the quadrotor in presence of external disturbances. Also, using a simplified dynamic model, the position control could be achieved using a nested loop based backstepping control strategy [5]. Furthermore, the backstepping technique was combined with integral control, which allows bringing together the backstepping robustness against disturbances, with the integral control robustness against model uncertainties (see *e.g.* [6], [7], and [8]). The result was an integral backstepping control (IBC) scheme that could be used for attitude stabilization as well as for trajectory tracking control. However, although the altitude control objective was ensured, the vehicle hovering still shows attitude oscillations (see *e.g.* [9]).

Besides, as a powerful tool for controlling nonlinear systems, many (integral) sliding mode controllers were designed for stabilizing the quadrotor attitude (see *e.g.* [10]). However, a persistent shattering effect was observed on the vehicle attitude, although the stable hovering was achieved. Therefore, due to its switching control behavior, which is not acceptable by quadrotor

[*]Corresponding Author: El Ayachi Chater, EST-UM5 Avenue Prince Heritier BP 227, Tel: +212-663318151; Email: elayachi.chater@um5.ac.ma

dynamics, perfect autonomous quadrotor flight cannot be ensured using a sliding mode control strategy. Then, to compensate for parameter uncertainty, many adaptive control strategies are also proposed for controlling the quadrotor position (see *e.g.* [11]), with satisfactory results despite the yaw angle was poorly stabilized.

Interestingly, several fuzzy logic controllers (FLC) are also proposed for the autonomous quadrotor flight control (see *e.g.* [12], [13]). Indeed, to achieve the attitude stabilization as well as position tracking control, fuzzy logic control is usually utilized. To test the proposed fuzzy control performances, a few results have shown that efficient position control may are obtained for smooth trajectory tracking, despite poor vehicle attitude stabilization. Roughly, using only fuzzy logic controllers, the quadrotor attitude and its vertical position control problem could be solved using a reduced intelligent fuzzy-based controller (see *e.g.* [14]). Specifically, combining the two above controllers with a metaheuristic optimization tool permits obtaining better performances. For instance, a PID-like structure consists of using a fuzzy controller that utilizes the error, its derivative, and its integral as input signals. Interestingly, each input is applied through a block whose gain is adjustable. Moreover, the control action (*i.e.* the controller output) may also be applied through a block whose gain could be tuned. Thus, using an optimization algorithm, all the scaling-gains could be independently adjusted, which allows improving the controller performances. Namely, the provided simulation results show good attitude stabilization and stable reference trajectory tracking for the (*x,y,z*)-position and ψ-yaw rotation (see *e.g.* [15] [16]). However, the robustness of the proposed controllers was not sufficiently highlighted. Besides, artificial neural networks (ANN) have shown their effectiveness in controlling unmanned aerial vehicles [17]. Specifically, the fuzzy logic controller utilizes expert knowledge in establishing the rule-base [18], while artificial neural networks learn system operations utilizing neurons in almost a similar way the human beings do [19]. Interestingly, a new control strategy denoted adaptive neuro-fuzzy inference system (ANFIS) has appeared, which allows benefiting from FLC as well as ANN control approaches. For instance, using quadrotor tests, the ANFIS was shown to be as good as a type-2 fuzzy controller [20]. Then, compared to conventional proportional-integral-differential control, a multi-disturbance simulation scenario has shown that the ANFIS controller can enhance the quadrotor trajectory-tracking performances [21]. Indeed, to implement its inner fuzzy inference subsystem, the ANFIS approach can construct its knowledge utilizing training data from any classical controller. Interestingly, while designing the ANFIS controller, adding (input-output) scaling-gains can improve the control system robustness, which necessitates using an optimization or teaching-learning algorithm [22]. Especially, the particle swarm optimization still proves its high efficiency in ANFIS design, whether for tuning the membership functions [23] or for tuning the rule base of the inference mechanism [24].

Considering the above presentation, this work presents the ANFIS design steps for controlling a quadrotor UAV whose payload mass parameter is assumed to be unknown during the aerial vehicle flight. Thus, we first present the learning ANFIS controller design step, where the necessary training data set is collected from a classical proportional-integral-differential controller. Then, the other ANFIS design steps are described in detail. Specifically, this work presents an improved structure of the ANFIS control strategy, namely the multi closed-loop ANFIS plus integral control action, where an additional integral control action is shown to be improving the quadrotor control system performances. Roughly, as the steady-state operation of a quadrotor is hovering, it results that an integral control can compensate for unmodeled dynamics and parameter deviations. For this reason, the initial integral control action is maintained as an additional component in the proposed ANFIS, which makes the proposed control strategy a new multi closed-loop control structure [25]. Then, to improve the ANFIS performances, the state error signals are applied to the controller inputs through linear blocks whose scaling factors could be optimized. Besides, after the optimization process, the resulting control system performances are compared to those obtained using a classical PID and the conventional (non-optimized) ANFIS controllers. It turns out that the multi closed-loop PSO-based ANFIS plus integral controller can show better tracking control performances and better compensation for external disturbances.

It is worth noticing that the ingredients of the proposed idea have been presented in previous authors' work [26]. However, the main idea of the present paper is fully rewritten to make the proposed control strategy concisely designed with a complete quadrotor system model, without using the small-angle assumption. Besides, to show the robustness and the effectiveness of the proposed multi closed-loop ANFIS plus integral control strategy, both internal, as well as external disturbances, are here taken into account and shown to be compensated for.

This work comprises five sections. First, the quadrotor mathematical model is described in section 2. Then, in section 3, the PSO-based adaptive neuro-fuzzy inference system plus integral design steps are described. To show the effectiveness of the enhanced ANFIS control strategy, a simulation example is provided and commented in section 4. Finally, a concluding summary ends the paper.

2. Quadrotor Mathematical Model

The main actuation of a quadrotor is based on the rotors that are equidistant from the vehicle center of gravity (COG). Thus, this aerial vehicle motion is usually controlled utilizing the relative speed of its four actuators. However, the three rotations around the (φ, θ, ψ) Euler angles, and the linear motions along the (x, y, z) three axes, make the quadrotor a six-degree-of-freedom (6DOF) system. For this reason, the quadrotor is said under-actuated because it has only four control inputs.

2.1. Quadrotor kinematic model

The quadrotor is a symmetrical structure, which can rotate around its three axes. Then, studying its dynamics involves two frames. First, the body-fixed frame $\boldsymbol{\mathcal{F}}_B = \left(G, e_{bx}, e_{by}, e_{bz}\right)$, where G is the vehicle center of gravity. Then, the inertial frame $\boldsymbol{\mathcal{F}}_E = \left(O, e_{ix}, e_{iy}, e_{iz}\right)$, where O is an arbitrarily chosen origin in the space (see Figure 1).

Thus, w.r.t $\boldsymbol{\mathcal{F}}_E$ -frame, let $\boldsymbol{\xi} \coloneqq [x \quad y \quad z]^T$ denote the absolute vehicle CoG position, and $\boldsymbol{\eta} \coloneqq [\varphi \quad \theta \quad \psi]^T$ denote the vehicle attitude and orientation, where (φ , θ , ψ) denote respectively the roll, pitch, and yaw Euler angles. However, to

avoid the gimbal lock problem, let us consider the following usual assumption:

A1. $-\pi/2 < \varphi < \pi/2\,, -\pi/2 < \theta < \pi/2$

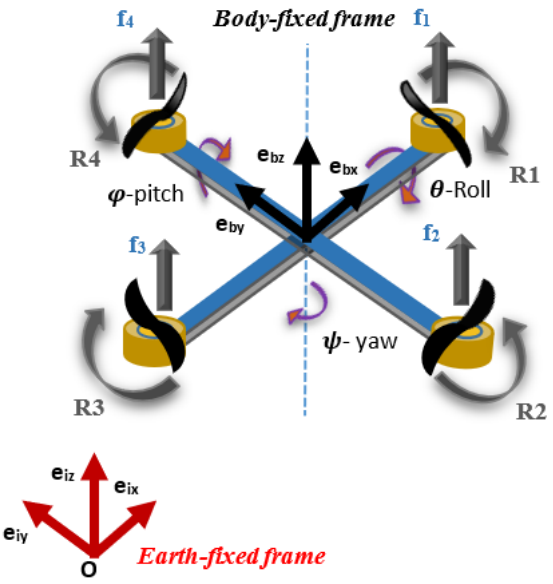

Figure 1: Quadrotor X-structure and frames

Now, let us notice that the well-known rotation matrix from $\mathcal{F}_B$-frame to $\mathcal{F}_E$-frame is given by [27]:

$$\boldsymbol{R}(\eta) = \begin{bmatrix} c_\theta c_\psi & s_\varphi s_\theta c_\psi - c_\varphi s_\psi & c_\varphi s_\theta c_\psi + s_\varphi s_\psi \\ c_\theta s_\psi & s_\varphi s_\theta s_\psi + c_\varphi c_\psi & c_\varphi s_\theta s_\psi - s_\varphi c_\psi \\ -s_\theta & s_\varphi c_\theta & c_\varphi c_\theta \end{bmatrix} \quad (1)$$

with $c_\alpha := cos(\alpha)\,, s_\alpha := sin(\alpha)$. This means that

$$\dot{\boldsymbol{\xi}} = \boldsymbol{R}(\eta)\boldsymbol{V_b} \quad (2)$$

where $\dot{\boldsymbol{\xi}} := [v_x \quad v_y \quad v_z]^T$ and $\boldsymbol{V}_b := [u \quad v \quad w]^T$ denote respectively the earth-fixed and body-fixed vehicle linear velocities.

Now, concerning angular velocities, the transformation matrix from the $\mathcal{F}_E$-frame to the $\mathcal{F}_B$-frame is denoted the transfer matrix and is given by [27]

$$\boldsymbol{T}(\eta) = \begin{bmatrix} 1 & 0 & -s_\theta \\ 0 & c_\varphi & s_\varphi c_\theta \\ 0 & -s_\varphi & c_\varphi c_\theta \end{bmatrix} \quad (3)$$

Then, it follows that

$$\boldsymbol{\Omega}_b = \boldsymbol{T}(\eta)\dot{\boldsymbol{\eta}} \quad (4)$$

where $\dot{\boldsymbol{\eta}} := [\dot{\varphi} \quad \dot{\theta} \quad \dot{\psi}]^T$ denotes the Euler angles rates, and $\boldsymbol{\Omega}_b := [p \quad q \quad r]^T$ denotes the body-fixed angular velocity.

2.2. Quadrotor dynamic model

Assuming that the quadrotor rotors do rotate at ω_i $(i = 1 \ldots 4)$, it results that each quadrotor actuator generates a thrust force that is given by $f_i := k{\omega_i}^2, (k > 0)$, w. r. t $\mathcal{F}_B$. Thus, the total upward thrust writes:

$$\boldsymbol{F}_b := [0 \quad 0 \quad T]^T \quad (5)$$

where $T := k\sum_{i=1}^{4} {\omega_i}^2$. Then, considering the $\mathcal{F}_E$-earth-fixed frame, and using solid mechanics, the total upward thrust writes:

$$\boldsymbol{F}_e := \boldsymbol{R}(\eta)\boldsymbol{F}_b \quad (6)$$

Thus, using Newton formalism for translational motions, the quadrotor translational dynamics are described by:

$$m\ddot{\boldsymbol{\xi}} = \boldsymbol{F}_e - \boldsymbol{W}_g \quad (7)$$

where m denotes the aerial vehicle total mass, and $\boldsymbol{W}_g$ denotes the quadrotor weight vector, which is given by:

$$\boldsymbol{W}_g := [0 \quad 0 \quad mg]^{\mathrm{T}} \quad (8)$$

where g stands for the gravity acceleration.

Now, to describe the aerial vehicle rotation motion, let us recall that the above thrust forces do also produce the following torques:

$$\boldsymbol{U}_\eta := [\tau_\varphi \quad \tau_\theta \quad \tau_\psi]^T, \quad (9)$$

with

$$\begin{bmatrix} \tau_\varphi \\ \tau_\theta \\ \tau_\psi \end{bmatrix} := \begin{bmatrix} kl(-{\omega_2}^2 + {\omega_4}^2) \\ kl(-{\omega_1}^2 + {\omega_3}^2) \\ d(-{\omega_1}^2 + {\omega_2}^2 - {\omega_3}^2 + {\omega_4}^2) \end{bmatrix} \quad (10)$$

where l denotes the distance between each rotor and the quadrotor center of mass. $(d > 0)$ denotes the drag constant.

Thus, using Newton formalism for rotational motions, the aerial vehicle rotation dynamics are described by:

$$\boldsymbol{J}\dot{\boldsymbol{\Omega}}_b = \boldsymbol{U}_\eta - \boldsymbol{\Omega}_b \times \boldsymbol{J}\boldsymbol{\Omega}_b \quad (11)$$

where $\boldsymbol{J} := diag(j_x, j_y, j_z)$ denotes the inertia matrix, and $\boldsymbol{\Omega}_b$ denotes the above body-fixed angular velocity defined in (4).

Then, let us notice that, using the following vectors:

$$\begin{cases} \boldsymbol{U} := [T \quad \tau_\varphi \quad \tau_\theta \quad \tau_\psi]^T \\ \boldsymbol{\Omega}_s := [{\omega_1}^2 \quad {\omega_2}^2 \quad {\omega_3}^2 \quad {\omega_4}^2]^T \end{cases} \quad (12)$$

and considering the following actuation matrix:

$$\mathbf{M}_a := \begin{bmatrix} k & k & k & k \\ 0 & -kl & 0 & kl \\ -kl & 0 & kl & 0 \\ -d & d & -d & d \end{bmatrix} \quad (13)$$

it results that the control distribution from the actuating motors may be described by:

$$U = \mathrm{M}_a \Omega_s \tag{14}$$

Ultimately, according to (4), (7), and (11), the quadrotor dynamics can be summarized as follows:

$$\begin{cases} \dot{x} = v_x \\ \dot{y} = v_y \\ \dot{z} = v_z \\ \dot{v}_x = (c_\varphi s_\theta c_\psi + s_\varphi s_\psi)\frac{T}{m} \\ \dot{v}_y = (c_\varphi s_\theta s_\psi - s_\varphi c_\psi)\frac{T}{m} \\ \dot{v}_z = (c_\varphi c_\theta)\frac{T}{m} - g \\ \dot{\varphi} = p + q\, s_\varphi\, t_\theta + r\, c_\varphi\, t_\theta \\ \dot{\theta} = q c_\varphi - r s_\varphi \\ \dot{\psi} = q\frac{s_\varphi}{c_\theta} + r\frac{c_\varphi}{c_\theta} \\ \dot{p} = \frac{\tau_\varphi}{j_x} + \frac{j_y - j_z}{j_x} qr \\ \dot{q} = \frac{\tau_\theta}{j_y} + \frac{j_z - j_x}{j_y} pr \\ \dot{r} = \frac{\tau_\psi}{j_z} + \frac{j_x - j_y}{j_z} pq \end{cases} \tag{15}$$

Now, considering the above quadrotor dynamics, and using enhanced fuzzy control strategies, our objective is guaranteeing the tracking-control of arbitrary ξ_{des} position for any ψ_{des} -yaw orientation, and ensuring the stabilization of (φ, θ) attitude angles, in presence of unknown aerial vehicle payload mass parameter.

3. Multi Closed-loop PSO-based ANFIS plus Integral Controller

3.1. Problem statement

From the above objective, let us design the system inputs, namely the vector $\boldsymbol{U} := [T \quad \tau_\varphi \quad \tau_\theta \quad \tau_\psi]^T$, which allows ensuring the tracking of $(x_{\mathrm{des}}, y_{\mathrm{des}}, z_{\mathrm{des}})$-reference trajectory for arbitrary ψ_{des} -yaw orientation, and the stabilization of (φ, θ) quadrotor attitude, despite random payload mass change during the vehicle flight, which also means a change of the matrix inertia. More concisely, we aim to stabilize the quadrotor system while tracking a position reference trajectory with the constraint to keep small overshoot and small rise and settling times, despite the presence of external disturbances. Then, it is worth noticing that because of quadrotor under-actuation, the control system structure may be designed using two control subsystems. Namely, an upstream control subsystem whose role is to ensure the reference trajectory tracking, and a downstream control subsystem whose role is stabilizing the vehicle attitude.

3.2. PSO-based ANFIS plus integral algorithm

Now, we briefly describe the proposed PSO-based adaptive neuro-fuzzy inference system plus integral (ANFIS+I) control strategy that is based on a Multi-Closed-loop ANFIS controller, where the additional control scaling gains are optimized using a multidimensional PSO algorithm. For clarity, algorithm 1 enumerates the main steps of the code to implement using a simulation tool (*e.g.* Matlab). For clarity, the methodology of the PSO-based ANFIS+I control design may be summarised using algorithm 1.

Algorithm 1: PSO-based ANFIS+I control algorithm

Collect training data
Generate ANFIS controller
ANFIS Enhancement with integral control
ANFIS+I scaling factors optimization using PSO

3.3. ANFIS architecture

The adaptive neuro-fuzzy inference system (ANFIS) algorithm was firstly introduced by Jang in 1993 [28], which was considered as an intelligent hybrid algorithm based on the benefits of both fuzzy logic control (FLC) and artificial neural network (ANN) approaches. The idea started from the fact that to design a suitable FLC for the considered plant, we need a minimum of knowledge upon the system functioning, which allows us to define the fuzzy rules of the controller. Then, we should define the membership function type and degree. For this reason, the design of this control is considered a complicated task despite the wide use of the FLC system in control engineering [29]. Thus, to compensate for the disadvantages of the FLC system, the artificial neural network (ANN) is also used. Roughly, the ANN algorithm may be utilized during the learning process, which can approximate an unknown function from the system inputs and outputs data set, using a multitude of neurons in a similar way of a human-being brain.

Indeed, through five layers of the ANN algorithm, the system output y is computed from $(x_1,\ x_2)$ inputs using several inference system parameters such as the fuzzy rules number and the membership function type and degree. For clarity, Figure 2 shows the ANFIS architecture model.

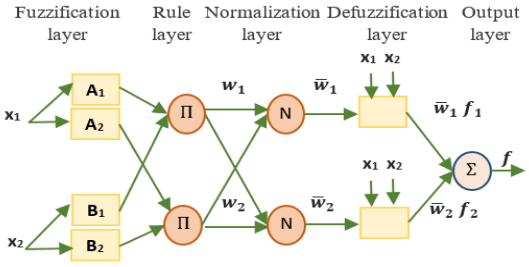

Figure 2: ANFIS architecture with two membership function

Now, the learning process of the ANFIS algorithm may be described as follows:

First, in the fuzzification layer, the output of each node is computed from the following equation:

$$\begin{cases} O_i^1 = \mu_{A_i}(x_1) \\ O_i^1 = \mu_{B_i}(x_2) \end{cases} \tag{16}$$

where (x_1, x_2) are the inputs, $(A_i\ ,\ B_i)$ are the node linguistic label, where i varies from 1 to the membership function number.

Then, to compute the output node of the second layer, we use the product of each input entering into the node as follows:

$$\begin{cases} O_j^2 = w_j \\ w_j = \mu_{A_i}(x_1) * \mu_{B_i}(x_2) \end{cases} \quad (17)$$

where j varies from 1 to the fuzzy rule number n and w_j is a rule-coefficient that stands for the firing strength.

Now, to compute the value of each node in the normalization layer, each firing strength is divided by the sum of all firing strength, which is denoted by the normalized firing strength according to the following equation:

$$\begin{cases} O_j^3 = \bar{w}_j \\ \bar{w}_j = \frac{w_j}{\sum_{j=1}^{9} w_j} \end{cases} \quad (18)$$

where j varies from 1 to n

Then, in the defuzzification layer, using the normalized firing strength $\bar{w}_j$ and the consequent parameters $\{p_j, q_j, r_j\}$, we compute a weighted value of each fuzzy rule using the following equation:

$$\begin{cases} O_j^4 = \bar{w}_j f_j \\ \bar{w}_j f_j = \bar{w}_j (p_j x_1 + q_j x_2 + r_j) \end{cases} \quad (19)$$

Thus, the final unique node value obtained in the output layer is computed by adding the incoming inputs according to the following equation:

$$O_1^5 = \sum_{j=1}^{n} \bar{w}_j f_j \quad (20)$$

3.4. ANFIS algorithm design

To design the ANFIS controller, the first step is the collection of learning data. Indeed, this learning process is very important while designing the ANFIS controller. In this work, we choose to select the training data set from a proportional-integral-differential controller. Then, benefiting from the symmetrical structure, to control the six-state quadrotor system, namely $(x, y, z, \varphi, \theta, \psi)$, only four P(I)D controllers are necessary. Roughly, similar PD controllers are used for the horizontal positions x and y, similar controllers are used for the attitude Euler angles φ and θ, a PID control structure is used for the quadrotor altitude z, and for controlling the ψ-yaw quadrotor orientation (see Figure 3). Then, to get the necessary training data for the ANFIS controller, the responses of the four P(I)D controllers are collected. Especially, in this work, the training data is a 3-dimensional vector, namely, the $(e, \dot{e})$ controller inputs and the y-controller output. Roughly, two steps are needed during the design of the ANFIS controller: the training and the testing process. Moreover, the initial training data is arbitrarily separated into a training data V_{train} (70% of initial data) and the testing data V_{test} (30% of initial data). Then, to transform the $(e, \dot{e})$-inputs into the y-output, we should select several parameters of the ANFIS algorithm.

Moreover, to approximate the fuzzy inference system (FIS) from the initial data set, the type and degree of the input-output membership functions (MFs) should be defined.

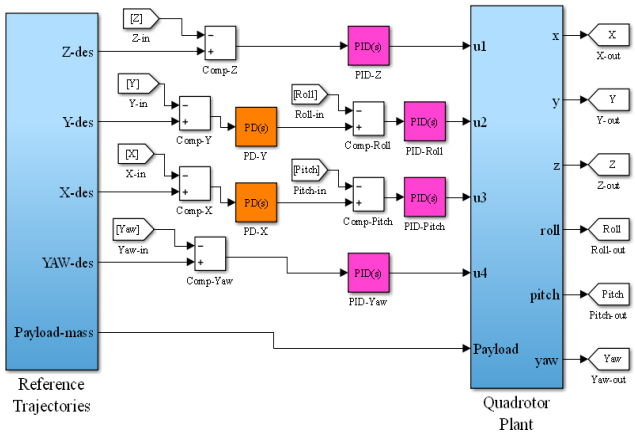

Figure 3: Quadrotor system controlled by the PD plus integral controllers

However, it is worth noticing that the choice of the membership functions degree significantly affects the necessary computational time for designing the controller. This means that choosing a small MFs degree is beneficial to the controller computing time. Then, in the proposed ANFIS controller, only three inputs MFs and three output MFs, are configured to implement each fuzzy inference system (FIS) of the controller. Furthermore, compared to other MFs types such as the trapezoidal, triangular, and bell, the Gaussian MFs type is characterized by the less complexity and high precision (see *e.g.* [30], and [31]). Thus, the (Gaussian) MFs that are chosen as inputs MFs type are defined by:

$$\mu_{A_i}(x) = e^{-\frac{(c_i - x)^2}{2\sigma_i^2}} \quad (21)$$

where $c_i(\sigma_i), (i = 1, 2, 3)$, are the center(width) of the fuzzy set for each MF. Finally, the other inference parameters are chosen as shown in Table 1:

Table 1: Inference system parameters

Fuzzy type	Defuzzification method	Inference engine
Takagi-Sugeno	*weighted average (wtaver)*	*prod-max*

Indeed, to design the ANFIS controller, we should select additional ANFIS parameters such as training epoch number n_{ep}, training error goal E_{train} and optimization method. Practically, we used the parameter values that are given in Table 2.

Then, in quadrotor system control, the trained ANFIS controller is used instead of the above controllers (see Figure 3).

3.5. Integral control action for ANFIS controller

Each of the four resulting ANFIS controllers has two inputs (the error, and its derivative $\dot{e}$) as shown in Figure 4. Then, the steady-state error cannot be removed because of the non-existence of internal integral control. For this reason, we associate each ANFIS controller with an integral control action to combine the benefits of the ANFIS controller and the integral control, which allows obtaining an enhanced and robust controller that is denoted ANFIS+I.

Table 2: ANFIS algorithm parameters

Training epoch number n_{ep}	Training error goal E_{train}	Optimization method
20	0	Last-squares and back-propagation gradient descent

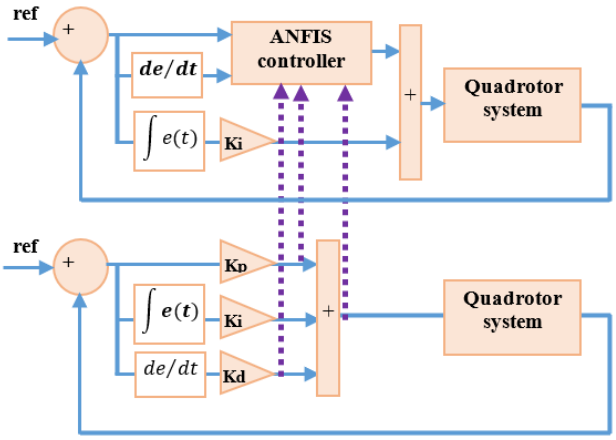

Figure 4: Selection of training data set for ANFIS controller

For this reason, two inputs of each initials controllers (error e , and its rate $\dot{e}$) are used to design the ANFIS controller while the integral action ($\int e(t)$) is maintained in the designed ANFIS controller with the same parameter K_i. Thus, due to the additional integral control, the controller results in a multi closed-loop control structure, which permits obtaining better performance for the quadrotor control system [25].

Furthermore, to enhance the performance of the ANFIS+I controller, three inputs and output scaling gains are added as shown in Figure 5. Then suitable values should be determined for each scaling gain. Specifically, as three scaling parameters should be simultaneously tuned for each ANFIS+I state-controller, in the next subsection, the multidimensional particle swarm optimization (PSO) algorithm is proposed.

3.6. Multidimensional PSO algorithm description

Based on the observation of birds flying, the particle swarm optimization (PSO) metaheuristic algorithm was initiated by J. Kennedy and R. C. Eberhart in 1997 [32]. Thus, the theory of this algorithm is based on the arbitrary choice of particles to design the initial population in a fixed search space [16]. Then, at each new iteration, a different population is selected according to the position and velocity of each particle.

Therefore, as stated by the next equations, the best values of the local and global fitness parameters are computed as follows:

$$\begin{cases} v_{ij}(\mathrm{t}+1) = w\, v_{ij}(\mathrm{t}) + \mathrm{c}_1 r_1 \left(\chi_{1,ij}(\mathrm{t}) - \chi_n(\mathrm{t})\right) \\ \qquad\qquad + \mathrm{c}_2 r_2 \left(\chi_{2,ij}(\mathrm{t}) - \chi_{ij}(\mathrm{t})\right) \\ \chi_{ij}(\mathrm{t}+1) = \chi_{ij}(\mathrm{t}) + v_{ij}(\mathrm{t}+1) \end{cases} \quad (22)$$

where $i = 1 \ldots n$ denotes the particle number of populations, $j = 1 \ldots m$ assigns the parameter to tune in dimension m. c_1 and c_2 denote the cognitive and social constants, respectively. r_1 and r_2 are arbitrary scalars in the interval [0,1]. w is the inertia weight that is used to balance the effect of the previous velocity to the actual value. Thus, at each specific time t, for each particle i in each dimension j, several parameters are to consider: the velocity v_{ij}^t, the position χ_{ij}^t, the local best fitness $\chi_{1,ij}^t$, and the global best fitness $\chi_{2,ij}^t$. Then, to design the four PSO-based ANFIS+I controller, a code was developed using Matlab Environment. The main steps of this code are presented in Algorithm 2.

Algorithm 2: Multidimensional PSO algorithm steps

Result: Optimum parameters

Set the search space, the particles number n, the number of iteration n_{iter};

Repeat:

Generate a random population

Evaluate the objective function

Evaluate the local and global best fitness

Compute the velocity and position of particles according to equation (22)

Until the maximum number of iterations (n_{iter}) is reached

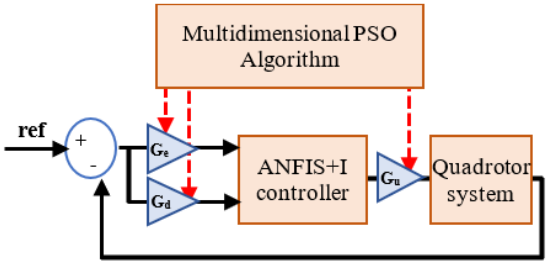

Figure 5: ANFIS+I controller scaling gains tuning using multidimensional PSO algorithm

The objective is to find the optimal values of the PSO-based ANFIS+I scaling gains for each controlled state (x, z, φ, and ψ) (see Figure 5). Then, the optimization algorithm starts by selecting the multidimensional PSO parameters such as the population number (n), the tune dimension (m), the maximum iterations number (n_{iter}), and the search space.

In this work, to reduce the tuning dimension using the multidimensional PSO algorithm, we utilize the same PSO-based ANFIS+I controller for the horizontal position x and y as well, and for the attitude angle φ and θ as well, which permits simplifying the optimization dimension to three scaling factors G_e, G_d and G_u for only four ANFIS+I controllers. Thus, dimension m could be reduced to twelve parameters. Besides, we choose 500 as the population number, 5 as the maximum number of iterations, and [0.1 , 5] as bounds of the search space.

Then, the optimization process starts by initializing a random population p_{ij} , where i ($1 \le i \le n$) represents a population particle, and j ($1 \le j \le m$) denotes the number of tuned parameters. Then, at each iteration k ($1 \le k \le n_{iter}$) , the algorithm generates a new population p_{ij} after evaluating the best local and global fitness, which is based on computing two parameters: position and velocity of each particle according to equation (22). Of course, these computations are repeated until the

maximum of iteration number ($i.e\ n_{iter}$) is reached and the smallest value of the objective function criterion is obtained. Thus, the algorithm ends and provides the suitable scaling gains that correspond to an optimal ANFIS+I controller.

3.7. Objective function criterion choice

As described in the above subsection, the multidimensional PSO algorithm role is to optimize the scaling gains of the (four) ANFIS+I controllers, which ends by obtaining a minimum value of an objective function criterion. For this reason, several criteria can be used such as the overshoot (Mp), the settling time (Ts), the rise time (Tr) [20], the integral of absolute error (IAE), the integral of squared error (ISE), the integral of time-weighted squared error ($ITSE$), and the integral of time-weighted absolute error ($ITAE$) [33]. However, IAE and ISE objective function criteria do ignore the time when computing the difference between the desired signal and the actual signal (*i.e,* error e), which could result in high settling time and unacceptable overshoot [34], while $ITAE$ and $ITSE$ objective function criteria do compute the error through the time and allow improving the system performances.

Therefore, in this work, we use the well-known $ITAE$ objective function criterion. Then, for each state, to evaluate the ANFIS+I scaling gains, we consider the $ITAE$ criterion that is defined by:

$$ITAE = \int_0^\infty t|e(t)|\,dt \qquad (23)$$

4. Simulation Results

In this section, the simulation tests are provided to show the efficiency of the proposed PSO-based ANFIS+I controller. For clarity, the quadrotor system parameters are given in Table 3 [4].

To check the robustness of the proposed control strategy, four different controllers are implemented for controlling the quadrotor system.

Table 3: Quadrotor system parameters

Symbol	Description	Value
g	Gravitational acceleration	9.81 m.s^{-2}
m	Quadrotor mass	0.65 Kg
l	Distance from center to motor	0.23 m
j_x	Moment of inertia about x-axis	7.5 10^{-3} Kg.m^2
j_y	Moment of inertia about y-axis	7.5 10^{-3} Kg.m^2
j_z	Moment of inertia about z-axis	1.3 10^{-2} Kg.m^2
k	Propeller force constant	3.13 10^{-5} N.s^2
d	Propeller torque constant	7.5 10^{-7} N.s^2

First, we collect the training data set that is used to design the fuzzy inference system. Thus, the first simulation scenario consists in controlling the quadrotor system by the classical PID control approach. For simplicity, for each quadrotor state ($\varphi, \theta, \psi, x, y, z$), the suitable control parameters are determined using the Matlab PID Tuner. These parameters are summarized in Table 4.

Thereafter, the ANFIS controller is implemented using the data collected from the quadrotor system dynamic response when it is controlled by the PID control approach. In this step, an initial ANFIS controller is designed using the generated fuzzy inference system. Roughly, two MATLAB functions are available: *genfis1*, which returns the initial membership functions set, and *anfis*, which gives the fuzzy inference system.

Table 4: Parameters of PID controller

	x	y	z	φ	θ	ψ
k_p	0.011	-0.011	3.09	0.4	0.4	3.7
k_i	0	0	1.5	0.15	0.15	7.5
k_d	0.12	-0.12	4.5	0.11	0.11	0.56

Then, to improve the ANFIS controller, we kept the initial integral control action in the designed controller, which allows guaranteeing more robustness to the closed-loop system.

In the next step, to improve the quadrotor control system performances, we use the multidimensional PSO algorithm to optimize the ANFIS+I scaling gains ($i.$e G_e, G_d , and G_u). Table 5 gives the value of the obtained scaling gains for each quadrotor state after the optimization process.

Table 5: ANFIS+I scaling gains tuned by multidimensional PSO algorithm

	x	y	z	φ	θ	ψ
G_e	4.82	-4.82	2.21	4.56	4.56	4.26
G_d	0.73	-0.73	1.26	0.36	0.36	2.66
G_u	4.4	-4.4	2.31	0.95	0.95	2.21

For comparison purposes, Table 6 shows the performance results of the four control strategies: classical PID, ANFIS (without the integral control, (non-optimized) ANFIS+I, and multidimensional PSO-based ANFIS+I controllers.

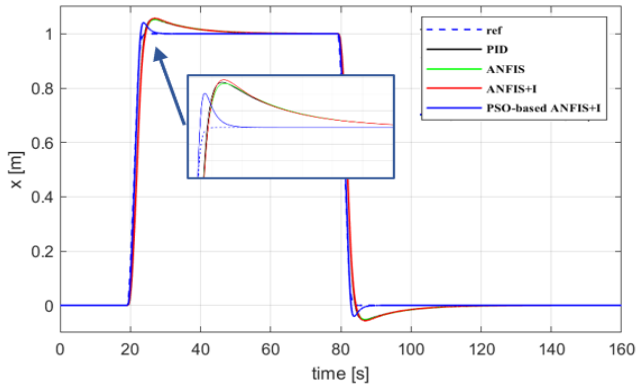

Figure 6: x-state tracking control response

Figures 6, 7, and 8 show the simulation results for x, y, and z quadrotor system states, respectively. The comparison of the four control strategies permits claiming that the PSO-based ANFIS+I controller can provide better control performances than the other control strategies. Except for the altitude (z) rise time, the proposed controller gives the smallest overshoot and the minimum rise and settling times.

For simplicity, the ψ-yaw reference trajectory was chosen to be null. Then, from Figures 9, 10, and 11, it is shown that quadrotor Euler angles, namely (φ, θ, ψ) are very small, which means that the three quadrotor rotational motions are well stabilized.

Table 6: Performances of the PID, ANFIS, ANFIS+I, and PSO-based ANFIS+1

		PID	ANFIS	ANFIS+I	PSO-based ANFIS+I
x	$M_p(\%)$	5.17	5.05	5.47	4.08
	$T_r(s)$	2.9	3.006	3.02	2.4
	$T_s(s)$	26.5	26.7	26.5	15.24
	$ITAE$	1.003	0.99	1.01	0.15
y	$M_p(\%)$	5.17	5.04	5.47	4.08
	$T_r(s)$	2.9	3.006	3.02	2.4
	$T_s(s)$	26.5	26.79	26.5	15.24
	$ITAE$	1.49	1.49	1.5	0.24
z	$M_p(\%)$	6.95	4.04	7.008	0.61
	$T_r(s)$	1.68	1.75	1.68	1.8
	$T_s(s)$	8.23	8.11	8.24	6.05
	$ITAE$	0.47	0.35	0.47	0.10

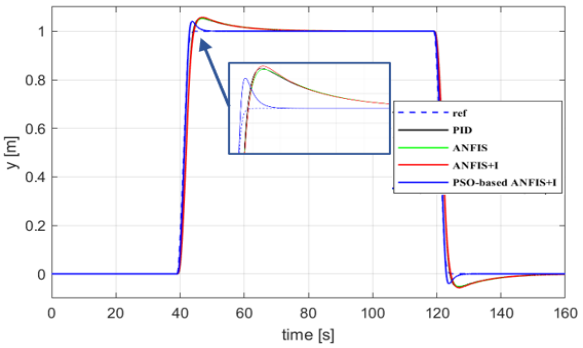

Figure 7: y-state tracking control response

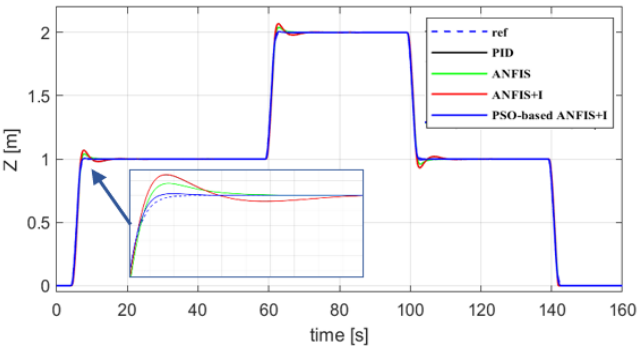

Figure 8: z-state tracking control response

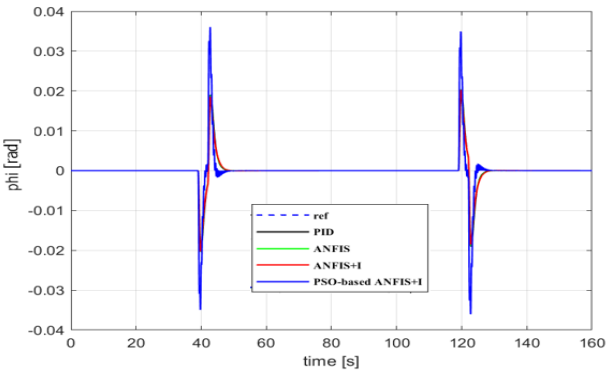

Figure 9: φ-state tracking control response

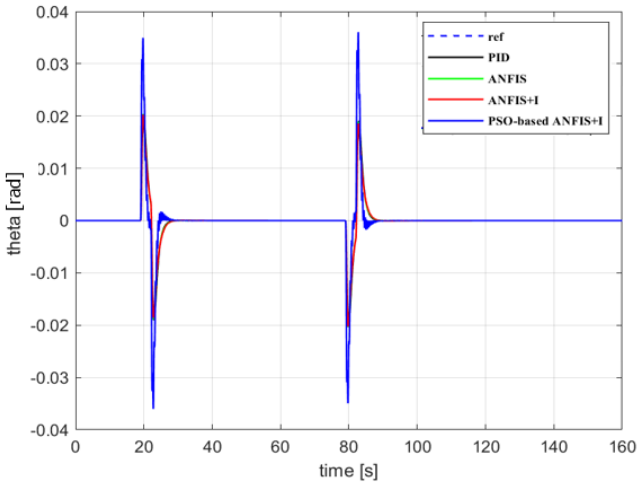

Figure 10: θ-state tracking control response

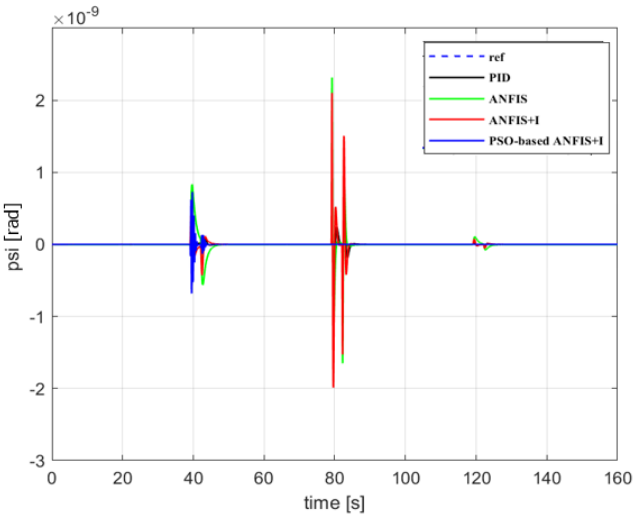

Figure 11: ψ-state tracking control response

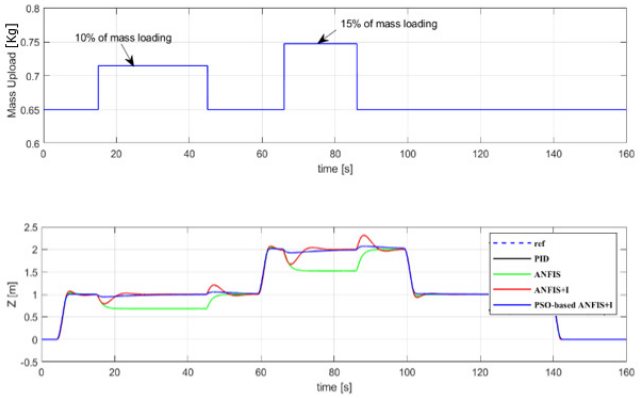

Figure 12: Mass payload disturbance rejection

Besides, additional simulation tests have been performed to evaluate the robustness of the proposed control strategy for the quadrotor system trajectory-tracking. Specifically, a payload mass has been added to the quadrotor system as an (unknown) external disturbance. Then, Figure 12 shows the effects on the quadrotor altitude z of 10% and 15% of total mass change, respectively. It is clearly shown that, in the case of the proposed controller, the fact

that the aerial vehicle's total mass could be modified during the air travel has almost no effect upon the tracking quality. This means that the proposed controller can efficiently compensate for external static-like disturbances.

Then, from the above simulation examples, it results that the multi closed-loop PSO-based ANFIS+I control strategy can ensure the best control performances in comparison with the other control strategies, namely it generates the smallest overshoot and the smallest rise and settling times as well.

5. Conclusion

In this paper, a PSO-based adaptive neuro-fuzzy inference system plus integral (ANFIS+I) control is proposed as a new intelligent controller for the quadrotor trajectory tracking control problem. First, to collect the necessary training data set, a classical PID (tuned) controller is implemented for the quadrotor system. Then, to achieve good robustness, the (initial) integral control action is preserved in the control structure in addition to the generated ANFIS controller. Moreover, scaling gains are added to the ANFIS inputs-output, and optimized using the minimization of the *ITAE* objective function criterion. Thus, the new control strategy denoted multidimensional PSO-based ANFIS plus integral is designed. To show the effectiveness of the proposed controller, several simulation tests are provided. Namely, in comparison with the traditional PID, the ANFIS controller, ANFIS plus integral control, it is shown that the proposed control strategy can ensure better time-domain performances in case of trajectory tracking problem for the quadrotor system. Particularly, the proposed controller can efficiently compensate for unknown mass modification with the smallest overshoot and good attitude stabilization. Therefore, the multi closed-loop ANFIS+I controller, where the scaling gains are optimized using the multidimensional PSO-algorithm, can be considered as an additional control strategy to solve the position tracking problem for the quadrotor system.

References

[1] U.R. Mogili, B. Deepak, "Review on application of drone systems in precision agriculture," Procedia Computer Science, 133, 502–509, 2018. doi:10.1016/j.procs.2018.07.063.

[2] E. Kaufman, K. Takami, Z. Ai, T. Lee, "Autonomous Quadrotor 3D Mapping and Exploration Using Exact Occupancy Probabilities," in 2018 Second IEEE International Conference on Robotic Computing (IRC), IEEE: 49–55, 2018. doi:10.1109/IRC.2018.00016.

[3] X. Liang, Y. Fang, N. Sun, H. Lin, "Dynamics analysis and time-optimal motion planning for unmanned quadrotor transportation systems," Mechatronics, 50, 16–29, 2018. doi: 10.1016/j.mechatronics.2018.01.009.

[4] S. Bouabdallah, Design and control of quadrotors with application to autonomous flying, Ph. D Thesis, Epfl, 2007.

[5] E. de Vries, K. Subbarao, "Backstepping based nested multi-loop control laws for a quadrotor," in 2010 11th International Conference on Control Automation Robotics & Vision, IEEE: 1911–1916, 2010. doi: 10.1109/ICARCV.2010.5707890.

[6] S. Bouabdallah, R. Siegwart, "Full control of a quadrotor," in 2007 IEEE/RSJ International Conference on Intelligent Robots and Systems, IEEE: 153–158, 2007. doi: 10.3929/ethz-a-010039365.

[7] A. Poultney, P. Gong, H. Ashrafiuon, "Integral backstepping control for trajectory and yaw motion tracking of quadrotors," Robotica, **37**(2), 300–320, 2019. doi: 10.1017/S0263574718001029.

[8] E. Chater, H. Housny, H. El Fadil, "Robust Control Design for Quadrotor Trajectory Path Tracking," in 2019 8th International Conference on Systems and Control (ICSC), IEEE: 21–26, 2019. doi: 10.1109/ICSC47195.2019.8950509.

[9] J.F. Guerrero-Castellanos, N. Marchand, A. Hably, S. Lesecq, J. Delamare, "Bounded attitude control of rigid bodies: Real-time experimentation to a quadrotor mini-helicopter," Control Engineering Practice, 19(8), 790–797, 2011. doi: 10.1016/j.conengprac.2011.04.004.

[10] M. Herrera, W. Chamorro, A.P. Gómez, O. Camacho, "Sliding mode control: An approach to control a quadrotor," in 2015 Asia-Pacific Conference on Computer Aided System Engineering, IEEE: 314–319, 2015. doi: 10.1109/APCASE.2015.62.

[11] M. Huang, B. Xian, C. Diao, K. Yang, Y. Feng, "Adaptive tracking control of underactuated quadrotor unmanned aerial vehicles via backstepping," in Proceedings of the 2010 American Control Conference, IEEE: 2076–2081, 2010. doi: 10.1109/ACC.2010.5531424.

[12] S.A. Raza, W. Gueaieb, "Fuzzy Logic based Quadrotor Flight Controller.," ICINCO-ICSO, 9, 105–112, 2009.

[13] E. Kayacan, R. Maslim, "Type-2 fuzzy logic trajectory tracking control of quadrotor VTOL aircraft with elliptic membership functions," IEEE/ASME Transactions on Mechatronics, **22**(1), 339–348, 2016. doi: 10.1109/TMECH.2016.2614672.

[14] M. Santos, V. Lopez, F. Morata, "Intelligent fuzzy controller of a quadrotor," in 2010 IEEE international conference on intelligent systems and knowledge engineering, IEEE: 141–146, 2010. doi: 10.1109/ISKE.2010.5680812.

[15] H. Housny, H. El Fadil, "New Deterministic Optimization Algorithm for Fuzzy Control Tuning Design of a Quadrotor," in 2019 5th International Conference on Optimization and Applications (ICOA), IEEE: 1–6, 2019. doi: 10.1109/ICOA.2019.8727622.

[16] H. Housny, H. El Fadil, "Fuzzy PID Control Tuning Design Using Particle Swarm Optimization Algorithm for a Quadrotor," in 2019 5th International Conference on Optimization and Applications (ICOA), IEEE: 1–6, 2019. doi: 10.1109/ICOA.2019.8727702.

[17] S. Bansal, A.K. Akametalu, F.J. Jiang, F. Laine, C.J. Tomlin, "Learning quadrotor dynamics using neural network for flight control," in 2016 IEEE 55th Conference on Decision and Control (CDC), IEEE, Las Vegas, NV, USA: 4653–4660, 2016, doi:10.1109/CDC.2016.7798978.

[18] F. Soares, J. Burken, T. Marwala, "Neural network applications in advanced aircraft flight control system, a hybrid system, a flight test demonstration," in International Conference on Neural Information Processing, Springer: 684–691, 2006. doi: 10.1007/11893295_75.

[19] A. Abraham, "Beyond integrated Neuro-fuzzy systems: reviews, prospects, perspectives and directions," School of Computing and Information Technology, Monash University, Victoria, Australia, 2002.

[20] P. Ponce, A. Molina, I. Cayetano, J. Gallardo, H. Salcedo, J. Rodriguez, "Experimental Fuzzy Logic Controller Type 2 for a Quadrotor Optimized by ANFIS," IFAC-PapersOnLine, **48**(3), 2435–2441, 2015, doi:10.1016/j.ifacol.2015.06.453.

[21] S. Rezazadeh, M.A. Ardestani, P.S. Sadeghi, "Optimal attitude control of a quadrotor UAV using Adaptive Neuro-Fuzzy Inference System (ANFIS)," in The 3rd International Conference on Control, Instrumentation, and Automation, IEEE, Tehran, Iran: 219–223, 2013, doi:10.1109/ICCIAutom.2013.6912838.

[22] O. Ghorbanzadeh, H. Rostamzadeh, T. Blaschke, K. Gholaminia, J. Aryal, "A new GIS-based data mining technique using an adaptive neuro-fuzzy inference system (ANFIS) and k-fold cross-validation approach for land subsidence susceptibility mapping," Natural Hazards, **94**(2), 497–517, 2018, doi:10.1007/s11069-018-3449-y.

[23] H.M.I. Pousinho, J.P.S. Catalao, V.M.F. Mendes, "Wind power short-term prediction by a hybrid PSO-ANFIS approach," in Melecon 2010-2010 15th IEEE Mediterranean Electrotechnical Conference, IEEE: 955–960, 2010. doi: 10.1109/MELCON.2010.5475923.

[24] J.P. da S. Catalão, H.M.I. Pousinho, V.M.F. Mendes, "Hybrid wavelet-PSO-ANFIS approach for short-term electricity prices forecasting," IEEE Transactions on Power Systems, **26**(1), 137–144, 2010. doi: 10.1109/TPWRS.2010.2049385.

[25] H. Housny, E. Chater, H. El Fadil, "Multi-Closed-Loop Design for Quadrotor path-Tracking Control," in 2019 8th International Conference on Systems and Control (ICSC), IEEE: 27–32, 2019. doi: 10.1109/ICSC47195.2019.8950659.

[26] H. Housny, H. El Fadil, "PSO-based ANFIS for quadrotor system trajectory-tracking control," in 2020 1st International Conference on Innovative Research in Applied Science, Engineering and Technology (IRASET), IEEE: 1–6, 2020. doi: 10.1109/ICSC47195.2019.8950659.

[27] R. Mahony, V. Kumar, P. Corke, "Multirotor Aerial Vehicles: Modeling, Estimation, and Control of Quadrotor," IEEE Robotics Automation Magazine, **19**(3), 20–32, 2012, doi:10.1109/MRA.2012.2206474.

[28] J.-S. Jang, "ANFIS: adaptive-network-based fuzzy inference system," IEEE Transactions on Systems, Man, and Cybernetics, **23**(3), 665–685, 1993. doi: 10.1109/21.256541.

[29] L.A. Zadeh, Fuzzy sets and applications, 1987.

[30] N. Talpur, M.N.M. Salleh, K. Hussain, "An investigation of membership functions on performance of ANFIS for solving classification problems," IOP Conference Series: Materials Science and Engineering, 226, 012103, 2017, doi:10.1088/1757-899X/226/1/012103.
[31] A. Sadollah, Introductory Chapter: Which Membership Function is Appropriate in Fuzzy System?, InTech, 2018, doi:10.5772/intechopen.79552.
[32] J. Kennedy, R.C. Eberhart, "A discrete binary version of the particle swarm algorithm," in 1997 IEEE International conference on systems, man, and cybernetics. Computational cybernetics and simulation, IEEE: 4104–4108, 1997. doi: 10.1109/ICSMC.1997.637339.
[33] T.K. Priyambodo, A. Dharmawan, O.A. Dhewa, N.A.S. Putro, "Optimizing control based on fine tune PID using ant colony logic for vertical moving control of UAV system," in AIP Conference Proceedings, AIP Publishing: 170011, 2016. doi: 10.1063/1.4958613.
[34] R.A. Krohling, J.P. Rey, "Design of optimal disturbance rejection PID controllers using genetic algorithms," IEEE Transactions on Evolutionary Computation, **5**(1), 78–82, 2001. doi: 10.1109/4235.910467.

ASTES

Advances in Science, Technology and Engineering Systems Journal Vol. 5, No. 4, 531-539 (2020)

www.astesj.com

Special Issue on Innovative Research in Applied Science, Engineering and Technology

ASTESJ

ISSN: 2415-6698

Development of an Adaptive HVAC Fuzzy Logic Controller for Commercial Facilities: A Case Study

Hamidi Meryem*, Bouattane Omar, Raihani Abdelhadi, Khalili Tajeddine

Signals, Distributed Systems and Artificial Intelligence Laboratory, ENSET, University Hassan II, Mohammedia, 28000, Morocco

ARTICLE INFO

Article history:
Received: 11 June, 2020
Accepted: 14 July, 2020
Online: 09 August, 2020

Keywords:
Fuzzy logic
Commercial building
Electrical consumption
EMS
HVAC

ABSTRACT

This paper is a case study of the integration of an energy management system (EMS) in a commercial building. A detailed analysis of this EMS's impact on energy consumption is presented. High energy demand is very common in commercial and industrial facilities. With this in mind, the present work aims to improve the energy consumption rate within a commercial facility by proposing an energy management system based on a central fuzzy logic controller. Thus, the central controller adapts the energy management to a pre-established schedule taking at consideration primarily the Heating, Ventilation and Air Conditioning (HVAC) of the targeted building.

1. Introduction

The energy consumption is growing considerably in recent years making global warming and climate change an everlasting threat. Commercial activities and individual lifestyles directly impact the energy demand [1], [2]. Therefore, it is very important to exploit energy in a more efficient way without altering the desired comfort [3]-[7]. Heating, Ventilation and Air-Conditioning systems (HVAC) maintain a good indoor air quality through adequate ventilation and provide thermal comfort. However, HVAC systems are among the most energy demanding components within buildings [1], [8]. These elements require about 40% of the overall energy demand causing an excessive and rapid increase in energy consumption leading to a harmful impact on the global environment [3], [9]. In addition, energy consumption is more substantial in residential and commercial facilities [10]. The energy consumption is around 18% in commercial buildings while it is 22% in residential ones for the same components architecture [2], [11]. This energy requirement is due to the poor design and thermic insolation of existing classic commercial buildings and population general behavior [2], [8], [12]. Consequently, new energy efficient technologies and applications are emerging as a key solution capable of facing the building performance challenge [7], [11]-[13]. Furthermore, researchers recently, focus on the management and control of energy in buildings using active control systems within the buildings [8]. Their primary interest is to realize sustainable energy savings, while improving the energy efficiency and maintaining a proper comfort conditions [14-19]. In this scope, the current work is a case study where we propose a new approach to optimally manage energy in a typical commercial facility. In this building, we establish a very specific controlling algorithm in order to reduce the energy consumption as much as possible. The integrated system targets basically the management of loads following various parameters. In addition to the electrical loads, the proposed controller takes account of other parameters such as the building architecture, customers flow, internal and external temperature, energy consumption behavior. The building architecture and load structure is first described. Then, the HVAC components and specification are briefly presented. Moreover, the energy saving methodology is described and the design and modeling of the Fuzzy logic controller is well depicted in addition to the simulation results and analysis.

2. Building description and component models

2.1. Outline description

In a commercial facility, the two main energy-consuming loads are light and the HVAC system. Figure 1 summarizes an analysis study conducted on commercial buildings of the same type with a surface between 1,000 m² and 3,000 m² and present the average loads consumption of these commercial buildings. As shown in Figure 1, the HVAC system consumes about 58% of the total energy; a huge amount compared with the other categories. The

*Corresponding Author: HAMIDI Meryem, meryem.ham@gmail.com +212 619 152 755

lighting system consumes about 17%, followed by office devices with 15% consumption and only 10 % for all the other instruments.

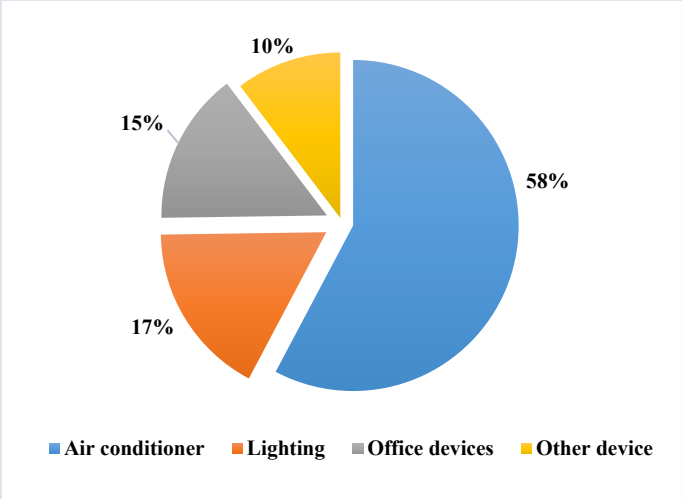

Figure 1: Electrical loads distribution in commercial buildings

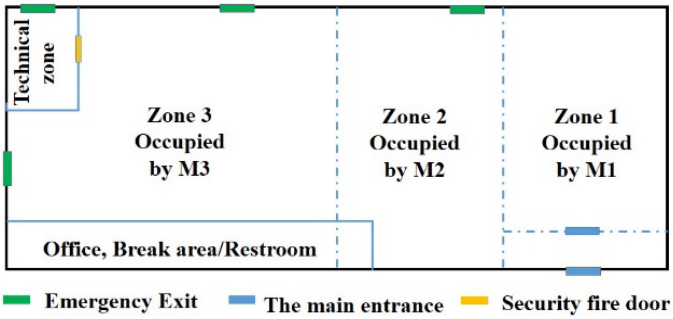

Figure 2: zoning of the HVAC system

The present case study studies a commercial building located at Oujda, Morocco (34° 40' 48" N, 1° 54' 36" W). Oujda city has a Mediterranean climate with a cold, rainy winter and a hot summer. The average annual temperatures are between 15°C and 20 °C. The average temperature in summer is 35 °C and can reach 40 °C. Unlike winter, the average temperature is 18 °C and minimal temperature can drop under 0°C. The building was opened in December 2016, extending over an area of 1600 m², the monthly average electrical consumption is 11879 kWh. The commercial building is equipped with LED lighting system. The HVAC system is divided to three Modules M1, M2 and M3 as presented in Figure 2. The first and second modules control 25 % of the buildings each, the third one is responsible for the rest. The electrical power of the HVAC system is 72KW in average, total power can be divided as follows:

$$M1 = M2 = 18\,KW$$

$$M3 = 2 * M2 = 2 * M1 = 36KW \quad (1)$$

In a typical commercial store environment, the parameters such as customer flow, collaborators number may be taken into consideration beside internal and external temperature. Indeed, these parameters can be used to assess more details related to the energy consumption. Different works have studied their effect on the overall user's comfort and building profitability [8, 15].

2.2. Modeling approach

So far, several reviews have been published on modeling methods [20-23], control approaches [24 - 26] and optimization techniques [26]. Besides HVAC systems simple modeling and practical energy savings, recent works target the evaluation of overall system performance [27]. The HVAC modeling techniques are widely discussed in the review study conducted in [28]. The presented models have been classified into three different categories physics-based model, data-driven model and gray-box model. Authors have concluded that each model category has both strengths and weaknesses and none of those models could be commonly used as HVAC system modeling. However, authors recommend to select the most suitable modeling technique based on the case study. In the present study, the modeling approach was carried out according to the commercial building specifications and the required energy (E_{req}) to meet the loads demand of the building. The global data taken at consideration consist of internal parameters (people, HVAC, lighting) and external ones (sun, air, moisture). Thus, the energy need can be written as:

$$E_{req} = E_{loss} - E_{gain} \quad (2)$$

Where E_{loss} represents the energy losses through envelope components of the building and E_{gain} depicts the ventilation/infiltration losses. The energy losses consist of energy transfer outwards from the building in terms of conduction (E_{cond}) through envelope components (roof, walls, glazing, ground), ventilation by the HVAC equipment (E_{equ}), and infiltration process (E_{inf}). This energy can be defined as:

$$E_{loss} = E_{cond} + E_{equ} + E_{inf} \quad (3)$$

While, energy gain is the useful energy to the building from occupants (E_{occ}), lighting equipment (E_{lig}) and sun (E_{sol}). This can be written as:

$$E_{gain} = E_{occ} + E_{lig} + E_{sol} \quad (4)$$

Based on the studied building specifications, some energy losses could be neglected for simplicity purposes. Therefore, the building conditioning system can be described by energy balance model [29] as follows:

$$T_{n+1}^{i} = \mu T_n^i + (1-\mu)(T_n^0 \pm \eta e_n / A) \quad (5)$$

Where T_n^i and T_n^0 are respectively the building inside and outside temperature at the time sequence n, T_{n+1}^i is the inside temperature at the time sequence $n+1$, e_n represents the electric power input at n. μ, η and A represent respectively the inertia factor, the overall thermal conductivity and the thermal conversion efficiency. The term "$\pm$" in "equation (5)" means that the operator "$-$" is used when the HVAC is on cooling mode and "$+$" when heating.

3. Energy saving Methodology

3.1. Energy repartition in typical buildings

Authors in [2] propose a review on large-scale energy saving studies. The work deals with the governments energy policies capable of generating noticeable energy savings. Authors also propose a scientific approach for quantifying the potential energy savings by improving the customer operations planning in

commercial buildings. The study associates between energy modeling techniques, studies on human behavior in buildings exploitation activities, surveying and sampling methods.

In commercial buildings, less than 50% of office equipment are switched off during off-work hours [1], [2]. In the present case, we also investigate the application of eco-energetic protocols in both operating and non-operating hours. The present study confirmed that the use of traditional eco-energy methods and protocols could save up to 60% of the monthly electric energy consumption. Moreover, authors in [3] confirmed that in HVAC systems, the average energy saving is generally 20–60%, lighting (20–50%), water heating (20–70%) and refrigeration (20–70%). Consequently, it is estimated that in new buildings, an energy economy of up to 50% can be achieved. In almost all cases, HVAC shows the highest share of energy savings, especially in small buildings where HVAC typically accounts for the major portion of the energy use [8], [2].

3.2. Operations time slots

The general electricity cost is not solely related to the total electricity consumption; the daily consumption periods noticeably affect the energy consumption budget [30]. The electricity consumption during a time slot is related to the number of costumers during that period and the classic exterior climate conditions.

In this work, the energy consumption fees are divided into three time slots, each one corresponds to a specific cost. According to [31], there are generally three classic time slots: Off-Peak hours, Peak hours, and Full hours. We have closely studied each period in order to understand the evolution of the energy consumption in each slot. This allows us to propose a schedule for the operation of the HVAC system. Table 1 illustrate the difference between the three time slots, and their consumption cost.

Table 1: General time slots in low voltage power subscription

Time slots	Period		Billing		Subscription cost (MAD/KVA)
	October - March	April-September	Cost (MAD/kWh)		
Peak-Off hours (T1)	22h-7h	23h-7h	C1	0,648	494
Peak hours (T2)	7h-17h	7h-18h	C2	0,886	
Full hours (T3)	17h-22h	18h-23h	C3	1,241	

Figure 3 presents records of the monthly consumption in the studied building. The available records in the study are dispatched on 6 months only: from December 2016 to May 2017.

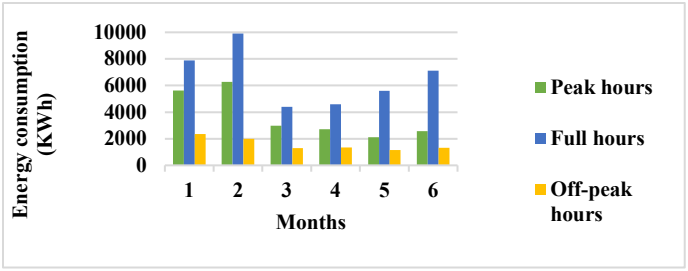

Figure 3: Energy consumption by slot in KWH

During winter season, we have an early sunset which causes a rapid drop in temperature in the evening. Figure 3 illustrates the impact of winter season on the consumption during the designed time slots. As the figure illustrates, the power consumption is at its peak during the Full hours between December and January. This change in consumption is due to the alteration in customers' flow which increases between 5 pm and 9 pm. On the other hand, during the Off-Peak hours, the energy consumption is very low because during closing time, the building consumes a minimum of the energy. The function cost in this system is essentially based on three variables and can be expressed as:

$$Cost = f(x_1, x_2, x_3) \tag{6}$$

Where x_1 is the actual operating time slot, x_2 is related to the number/costumer flow change and x_3 is related to the external temperature. The control system aims to reduce as much as possible the cost function (6). In order to grasp the whole concept, the cost function can be expressed in more details as follows:

$$Cost = T_1 * C_1 + T_2 * C_2 + T_3 * C_3 \tag{7}$$

Where T_i and C_i are variables related to the cost function factors. These variables are subject to seasonal changes and power generation cost in the region. "equation (6)" and "equation (7)" are related by the following equation:

$$x_i = T_i * C_i \quad i \in \{1, 2, 3\} \tag{8}$$

Figure 4 and 5 illustrate the variation of the costumer flow and external temperature from 8 am to 10 pm and during a whole 24h period respectively.

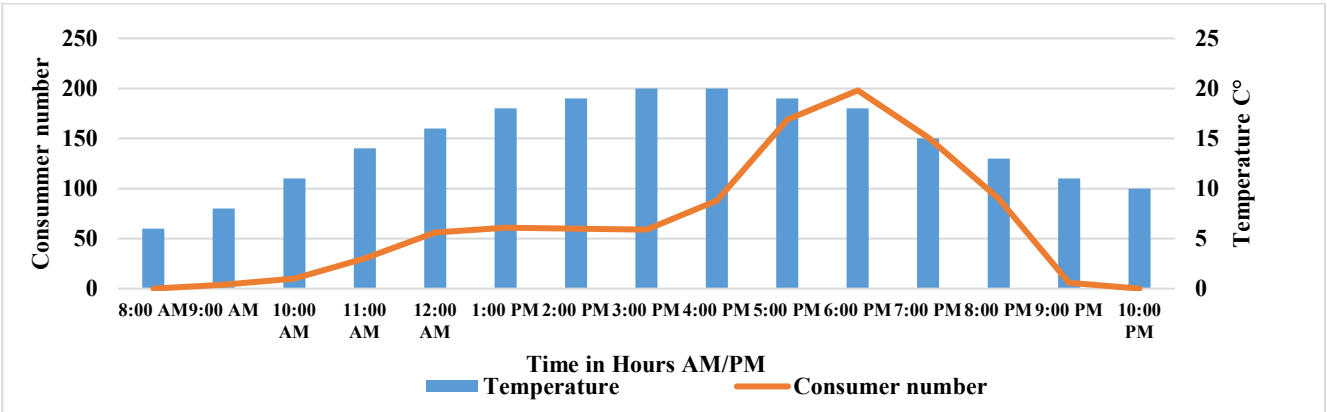

Figure 4: variation of costumer flow and external temperature from 8 am to 10 pm

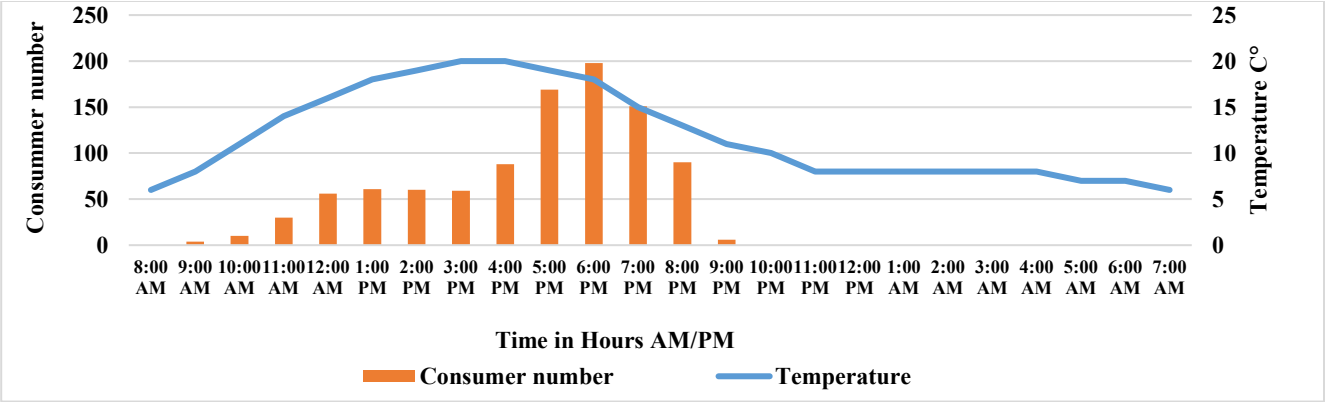

Figure 5 : variation of costumer flow and external temperature during a 24h period.

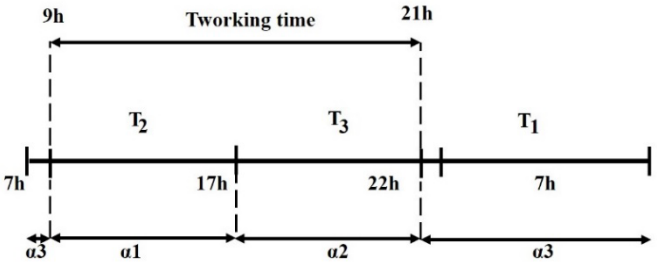

Figure 6: standard working day cost variables

The difference in costumers' flow in Figure 4 and 5 shows that controlling the HVAC system during off-work periods is not necessary and can guarantee a considerable energy savings. Furthermore, the work conditions, and costumers' availability are season dependent, thus, the total working time and periods of high activity change gradually along the year. Figure 6 shows the general segmentation of the working time and cost function factors for the studied case.

α_i are directly related to the cost function and represent the portion of time when energy can be represented as entirely consumed inside T_i slots.

$$Cost = g(\alpha_1, \alpha_2, \alpha_3) \quad (9)$$

On Figure 6 the total working time can be written as:

$$T_{workingtime} = \alpha_1(T_2) + \alpha_2(T_3) \quad (10)$$

Standard conditions in the present case study where $\alpha_1(T_2) = 8h$, $\alpha_2(T_3) = 4h$ and $\alpha_3(T_1) = 12h$, the total working time $T_{workingtime} = 12h$. At this point, it is clear that the working time, population condition and external conditions should be controlled depending on time segment. Authors in [32] the use of PID as control strategy for HVAC systems which resulted in in a high energy consumption. Whereas, in the same study, authors found that the use of HVAC control method presents the most promising results in terms of energy efficiency.

3.3. HVAC Controllers principle

The HVAC system being the key component to energy saving in commercial buildings, studies investigate multiple control strategies in order to encourage their implementation [8,28, 33]. Numerous recent studies have given an emphasis on improving the HVAC system through advanced control algorithms rather than classic control methods [28, 34]. Thus, some control strategies manage the HVAC system based on a day-ahead electricity price and outdoor temperature forecast [30]. Furthermore, existing controllers are generally classified into two major categories: predictive and adaptive controllers [16]. The study in [28] offers a critical overview of the modeling technics currently used in HVAC systems with regard to their applicability and acceptance in real practice, the study also summarizes the weaknesses, applications and services of the modeling technics. Authors in [27] present a study where they examine the performance of each HVAC unit, while evaluating the energy consumption and efficiency of each control technic (FLC, PID and simple ON/OFF time slots).

Control policies, also, can be categorized into two major types: model based and data driven [35]. Model-based control strategies require mathematical models as much as the building and the HVAC system specifications to generate minimal control rules. The data driven HVAC control strategies operate by adjusting the management parameters. In [28] authors offer a fairly global review on the different algorithms used to improve the HVAC energy management systems. Most used ones are the data mining algorithms, the Artificial Neutral Network (ANN) and the Support Vector Machine (SVM). The work in [27] compared between classic ON/OFF method, PID, Fuzzy logic, Agent based and neural network control. Related to the present case study, we have chosen to base the exploited control strategy on the fuzzy logic system given the promising results obtained [23-27]. Moreover, since the operation of HVAC systems is not linear, classic controllers not suitable for exploitation in such facilities. The common components of Fuzzy Logic Controller (FLC) attached to HVAC systems are well illustrated as block diagrams in various works [27, 36, 37].

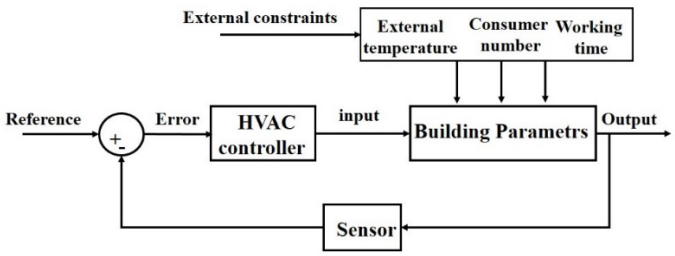

Figure 7: HVAC general control model

The implementation of fuzzy logic based methods requires a qualitative distribution of the inputs and outputs ranges by establishing a direct link to the different comfort zones sought for the clients visiting the facility. Several research works have analyzed this particular point, hence pushing us to adapting the same approach based on the facility's schedule in present case study [38, 39]. Figure 7 presents a control model of the studied building that depends on the external temperature, consumer number, working time. The three zones of the building are controlled via the Fuzzy logic program taking for each section the main three parameters described before.

4. The proposed design for the Fuzzy logic controller

4.1. Overall description of fuzzy logic controller

The temperature control is achieved by integrating several parameters such as temperature and humidity inputs[38, 39]. In this case study, we implemented two inputs in the designed model; temperature and number of clients. During the test period, we consider that time slots configuration remains unchanged [40- 42]. Figure 8 illustrates the design adopted in present case study. As it can be understood from the figure, temperature variations and clients' density inside the building are the inputs while the heating or cooling actions represent the outputs. This design is applied to each module zone M_i depending on costumers flow and the frequency of temperature variation.

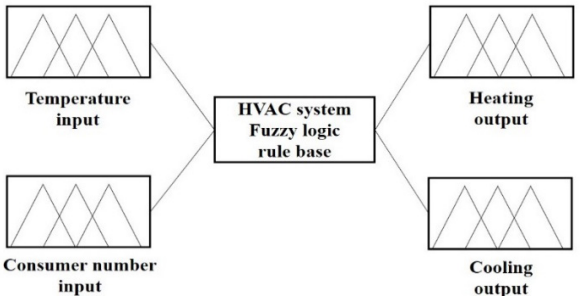

Figure 8: the proposed design of the fuzzy logic controller

In order to enhance the management strategy each of the customers' flow, opening hours and the temperature is regularly updated by keeping a close feed on present season and any other sudden variations such as vacation periods and time zone change.

4.2. Input variables' design

a) Membership function for the temperature management

In order to establish the membership of temperature variation inputs we used the local weather data registered over the previous year. The sections of temperature vary between very cold conditions when temperatures are less than 14°C and hot conditions when temperatures are above 38°C in Oujda city.

For the temperature membership function, it is divided into five ranges as described in Table 2. The "Too cold range" is reserved for any value below 14°C. For the "Cold" range between 7 and 23°C, "Warm" is the range of 15 and 30°C, the "Hot" range between 23 and 38 °C and the final range "Too Hot" above 38 °C. This segmentation was the key to designing the Ranges of temperature inputs in the fuzzy logic model as presented in Figure 9.

The definition or this partition of the membership function ranges, depends on the region and its climatic conditions. That means if we have another case of study in another region the value of the range may change in term of the variation of the local weather data.

Table 2 : Temperature membership functions

Membership functions	Range (C°)
Too cold	Below 14
Cold	7-23
Warm	15-30
Hot	23-38
Too Hot	Above 38

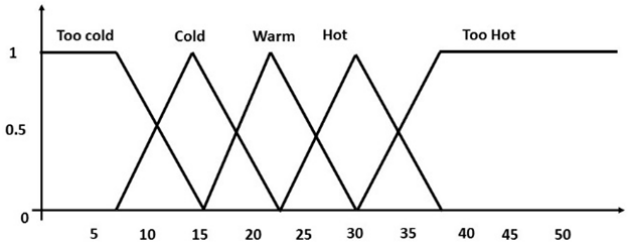

Figure 9 : Ranges of temperature inputs

b) Membership function for the costumers' flow

In this case of study costumers flow is a primary factor in the proposed commercial building EMS. In this perspective, Table 3 shows that the number of membership functions is organized into five categories of clients' density. The same process as the temperature input was applied for the consumer flow input.

Where the "Very low" range is reserved for 1 to 15 persons followed by the "Low" range between 10 and 30 persons, "Medium" range between 20 and 80 costumers, the "High" range between 60 and 150 peoples and the final range "Very high" is reserved for 120 to 250 costumers. The definition or this partition depends on the region, the building size and the most import the data of the costumers' flow of the previous years to define the average number of people in each single range. In Figure 10 presents the ranges of clients' density inputs implemented in fuzzy logic model.

Table 3 : Clients' density membership functions

Membership functions	Range (number)
Very low	1-15
Low	10-30
Medium	20-80
High	60-150
Very high	120- 250

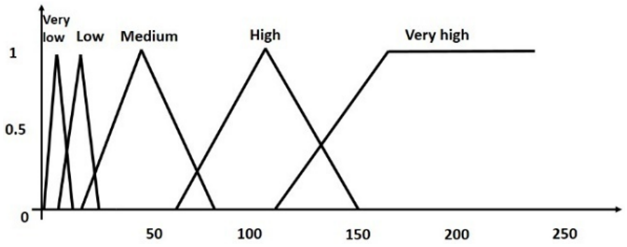

Figure 10: Ranges of clients' density inputs

4.3. Output variables' design

Membership functions and ranges are supposed to be similarly designed for each of the units M1, M2 and M3 constituting the HVAC system. Each unit is endowed with its own sensors and aeration control. The author in [17] describes the design of room temperature and humidity controller using Fuzzy Logic. He considered almost the same model of the distribution of the membership functions except that it was categorized in different ranges for cooling and heating functions.

Table 4 : Controller Output membership functions

Membership functions	Range
OFF	0-0.05
Slow	0-0.45
Medium	0.35-0.65
Fast	0.6-1

For this case of study, the Output membership function is organized in four ranges (OFF, Slow, Medium and Fast) into the interval of 0 and 1, either for the cooling or the heating controller output. The used control output in this case study is achieved by adopting two outputs with the same interval functions as illustrated on Table 4 and Figure 11.

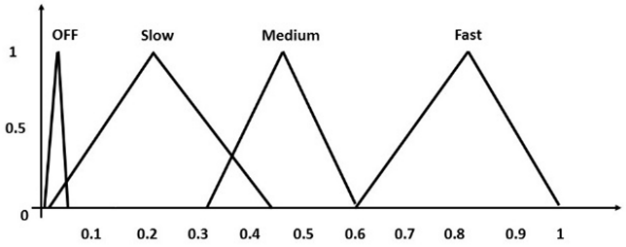

Figure 11: Fuzzy representation of the output membership

4.4. Rule base

The rule base describes the laws and conditions governing the activation of the heating/ventilation system in all the sections M_1, M_2 and M_3. Table 5 presents the fixed rules obtained after several operation tests in HVAC system. The control's rule base in Table 5, shows different possible decision making by the fuzzy logic system for different inputs range, and the considered decision that the fuzzy logic control will made based on the previous input and output membershi

For example, if the Number of consumers is high (between 120-250 consumer) and the temperature is Too Hot (above 39 °C), the decision of the fuzzy logic controller for the three units will be:

$$M1 = Cooling\ slow.$$

$$M2 = Cooling\ fast\ .$$

$$M3 = Cooling\ medium.$$

Figure 12 presents a planning example based on the fuzzy logic controller decision. Figure 12 presents a one planning example based on a recorded set of data during summer. During morning working hours M1, M2 and M3 are generally all occupied by workers and store staff, this is why they are all initially activated in order to guarantee minimum comfort conditions. Indeed, between 10h and 12h in the example above, M3 is activated using medium cooling mode because temperature is above 38°C and clients are between 30 and 50 individuals.

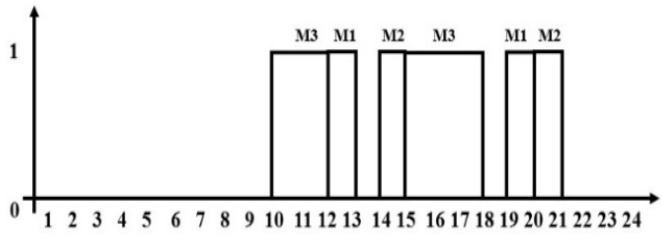

Figure 12 : Example of a HVAC control Schedule

From 12h to 13h, we notice that M3 is still activated but with a change in operating mode (cooling fast) and M1 is initiated in cooling medium. This decision is primarily related to the temperature and clients' number, however M1 will be rapidly switched off, because the controller anticipates the thermal exchange between the units of the building. The same procedure is followed throughout the day; the controller adapts the internal temperature to the external temperature and clients' number.

Table 5 : Control's rules base

Number of consumers	Temperature C°				
	Too cold	Cold	Warm	Hot	Too-Hot
Very low	M1=OFF M2= Heating slow M3= Heating Slow	M1=OFF M2=OFF M3=OFF	M1=OFF M2=OFF M3=OFF	M1=OFF M2=OFF M3=OFF	M1=OFF M2=OFF M3=OFF
Low	M1=OFF M2=OFF M3= Heating fast	M1=OFF M2=OFF M3= Heating fast	M1=OFF M2=OFF M3=OFF	M1=OFF M2= Cooling medium M3=OFF	M1=OFF M2=OFF M3= Cooling medium
Medium	M1=Heating slow M2=OFF M3= Heating medium	M1=OFF M2= Heating medium M3=OFF	M1=OFF M2=OFF M3=OFF	M1=OFF M2=OFF M3=OFF	M1=OFF M2=OFF M3=OFF
High	M1=OFF M2= Heating medium M3=OFF	M1=OFF M2= Heating slow M3=OFF	M1=OFF M2=OFF M3=OFF	M1=OFF M2=OFF M3= Cooling medium	M1= Cooling slow M2= Cooling medium M3= Cooling fast
Very high	M1=OFF M2=OFF M3=OFF	M1=OFF M2=OFF M3=OFF	M1=OFF M2= Cooling slow M3=OFF	M1=OFF M2= Cooling medium M3= Cooling fast	M1= Cooling slow M2= Cooling fast M3= Cooling medium

5. Study results and analysis

5.1. Impact of the proposed schedule on the fuzzy logic controller

Figure 13 illustrates the impact of adopting the fuzzy logic controller on electric consumption fees of the building, the first month corresponds to December 2016 and number 20 to July 2018.

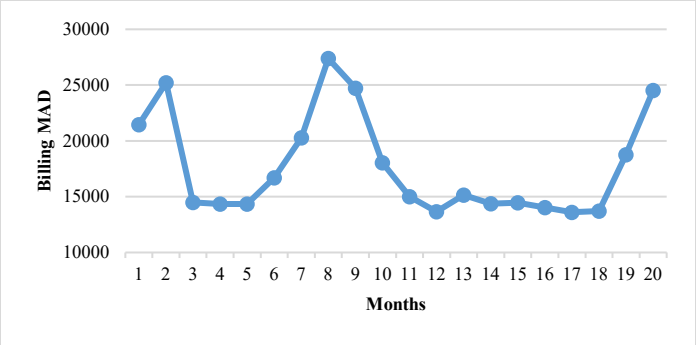

Figure 13: Monthly energy consumption fees in MAD

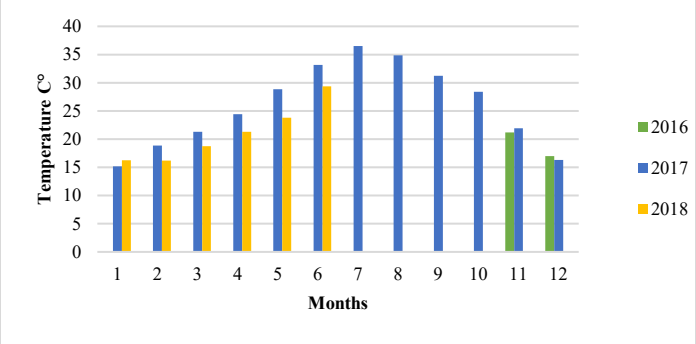

Figure 14: Collected temperature data of the city of Oujda [18].

The control model has been commissioned on June 2017, however it can be seen that there is an increase in power consumption in the month of July 2017 because of the high ambient temperature during the season period and laps of temporary suspension of the controller for technical adaptation. Moreover, the high energy consumption during summer season still poses a technical difficulty even after commissioning the proposed controller. Despite this stiffness we established that a steady decrease of 9.71% energy consumption has been achieved compared with the same period of the previous year. In Figure 14 month corresponds to January and number 12 to December of each corresponding year.

Related to the present case study, we can undoubtedly assume that promising and palpable results have been noticed after only two months from the first introduction of the fuzzy controller. After the first testing period it has been reported to us that the facility has achieved a 30% energy gain. Table 6 presents the recorded energy profit during the testing periods of 2017 and 2018. The recorded gains were calculated based on the following equations:

$$Profit\ E_b = \frac{\Delta E_b}{E_b} \tag{11}$$

$$Profit\ E_c = \frac{\Delta E_c}{E_c} \tag{12}$$

Where E_c is the energy consumption in KWh and E_b is the energy fees in MAD. As it can be seen on Table 6 substantial energy gains have been made which proves the efficiency of the developed controller.

5.2. System simulation and behavior

The ingenuity of the proposed controller is its ability to manage the three areas of the commercial building separately, while taking at consideration the thermal exchange between the three units.

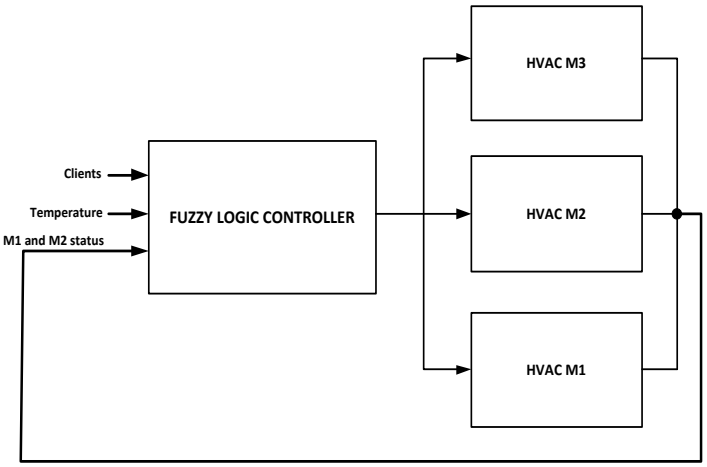

Figure 15: Simulation principle of the fuzzy logic controller

Table 6 : Recorded energy profit during testing periods of 2017 and 2018

Month	Energy consumption KWh		Profit	
	2017	2018	Profit (Ec)	Profit (Eb)
January	18178	8606	+ 52,66%	+43%
February	8673	8718	- 0,52%	+ 0,15%
March	8649	8338	+ 3,6%	+ 2,13%
April	8862	8128	+ 8,28%	+ 5,2%
May	11033	8387	+ 23,98%	+ 17,9%
June	14783	12651	+ 14,42 %	+ 7,42%
July	20494	17818	+ 13,06%	+ 10,41%

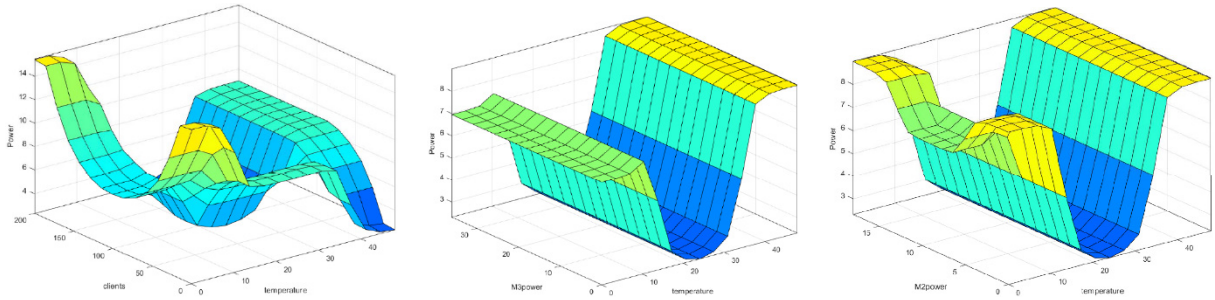

(a) (b) (c)

Figure 16: Variation of M1 HVAC power according to (a) ambient temperature and client's movement, (b) temperature and M3 HVAC power, (c) temperature and M2 HVAC power

Thus, the system, adapts the needed power for air conditioning purpose while exploiting at the same time the already deployed power in the other units. M3 requires the largest share of energy, this is why, during long periods of harsh temperature difference between the inside and the outside of the building, this unit is the main preserver of comfort inside the building. Figure 15 presents the simulation principle of the proposed controller. The controller doesn't simply adapt the inside ambient temperature based on defined set-points and external conditions, but it also exploits the possibility of under-powering M1 or M2 when the conditions are beneficial. Figure 16 presents all the possible cases for powering M1 based on the external temperature, clients' movement inside the store and power status of the HVAC system in M2 and M3.

As it can be seen on Figure 16 above, M1's HVAC system is only activated in extreme cases of temperature and clients' movement Figure 16 (a). Since the controller exploits the thermal exchange between the building units, power required in the middle of the day is greatly decreased. Furthermore, it can be noticed on Figure 16 (b) and (c) that during normal operating conditions, dissipated power of M1's HVAC system is greatly reduced, since M2 and M3 can help stabilize temperature inside the building.

6. Conclusion

In this paper, the design and implementation of a new Fuzzy logic controller was introduced into a commercial facility in Morocco. The case study presents how the building was functioning before and how the HVAC system was the primary drainer of energy during infrastructure analysis. The article describes how an appropriate modeling approach was designed in order to assess and quantify the energy loss during each month of the year. Furthermore, the article founded the energy saving methodology on existing research works. Thus, the working time was distributed into operating time slots, each with its own working characteristics defined by workers and visitor's dynamics. Particularly, in the present case study, special variables were introduced to cover the season time change and personnel interaction with the visitors and clients in the facility. This design allows the HVAC system to adapt automatically to the season without undergoing any change by the management team. During the design phase, input and output variable were carefully selected to minimize the number of uncontrolled events, especially during season shifts.

This case study showed very promising results in terms of energy saving and smoothness in HVAC control. For instance, the integration of this particular controller granted the facility a 20% steady energy savings during the first official test period. The presented controller can also help HVAC oversizing errors caused by classic design methodologies, thus limiting the maximum power subscription. Besides, by taking additional measures such as population flow control and energy efficiency ethics among working staff, a more substantial gain can be achieved. In the upcoming work, we intend to investigate how categorizing areas in the facility, each with its own control strategy, can affect the HVAC system in terms of energy economy.

References

[1] E. Delzendeh et al., "The impact of occupants' behaviours on building energy analysis: A research review" Renewable and Sustainable Energy Reviews, 80, 1061–1071. doi:10.1016/j.rser.2017.05.264.

[2] A. Elie, et al., "A Comprehensive Framework to Quantify Energy Savings Potential from Improved Operations of Commercial Building Stocks", Energy Policy, 67, avril 2014, 459-72. DOI.org, doi:10.1016/j.enpol.2013.12.031.

[3] V.S.K.V. Harish, A. Kumar, "A Review on Modeling and Simulation of Building Energy Systems" Renewable and Sustainable Energy Reviews, 56, avril 2016, 1272-92. DOI.org, doi:10.1016/j.rser.2015.12.040.

[4] P. Jianli, "A Survey of Energy Efficiency in Buildings and Microgrids using Networking Technologies", IEEE Communications Surveys & Tutorials, **16**(3), 2014, 1709-31. Doi:10.1109/SURV.2014.060914.00089.

[5] R. Rajeev et al., "Improving the Energy Efficiency of the Existing Building Stock: A Critical Review of Commercial and Institutional Buildings", Renewable and Sustainable Energy Reviews, 53, janvier2016, 1032-45. Doi:10.1016/j.rser.2015.09.084.

[6] C. Jinbao et al., "Improving Energy-Efficiency in Public Buildings in China: Challenges and Solutions", 2009 International Conference on Computational Intelligence and Software Engineering, IEEE, 2009, 1-5. Doi:10.1109/CISE.2009.5362887.

[7] E.G. Ochieng, "Integration of Energy Efficient Technologies in UK Supermarkets", Energy Policy, 67, avril 2014, 388-93. Doi:10.1016/j.enpol.2013.12.002

[8] L. Pérez-Lombard, "A review on buildings energy consumption information. Energy and Buildings", 40(3), 394–398. doi:10.1016/j.enbuild.2007.03.007

[9] A. Šimelytė, "Promotion of renewable energy in Morocco. Energy Transformation Towards Sustainability", 249–287, 2020. doi:10.1016/b978-0-12-817688-7.00013-6

[10] S. D'Oca, T. Hong, J. Langevin, "The human dimensions of energy use in buildings: A review", Renewable and Sustainable Energy Reviews, 81, 731–742, 2017. doi:10.1016/j.rser.2017.08.019

[11] L. Yanfei, Z. O'Neill, "A Critical Review of Fault Modeling of HVAC Systems in Buildings", Building Simulation, **11**(5), October 2018, 953-75, 2018. DOI.org, doi:10.1007/s12273-018-0458-4.

[12] A.M. Waseem, et al., "Computational Intelligence Techniques for HVAC Systems: A Review", Building Simulation, **9**(4), août 2016, 359-98. Doi:10.1007/s12273-016-0285-4.

[13] H.S. Mehdi, A Novel Intelligent Control of HVAC System in Smart Microgrid, Journal of Electrical Systems and Information Technology, **4**(2), septembre 2017, 299-309. Doi:10.1016/j.jesit.2017.01.005.

[14] N. Soares et al., "A Review on Current Advances in the Energy and Environmental Performance of Buildings towards a More Sustainable Built Environment", Renewable and Sustainable Energy Reviews, 77, September 845-60, 2017. DOI.org (Crossref), doi:10.1016/j.rser.2017.04.027.

[15] G.Y. Yasin et al., Design and Development of Advanced Fuzzy Logic Controllers in Smart Buildings for Institutional Buildings in Subtropical Queensland" Renewable and Sustainable Energy Reviews, 54, février 2016, 738-44, 2016. DOI.org, doi:10.1016/j.rser.2015.10.105.

[16] A.I. Dounis, Advanced control systems engineering for energy and comfort management in a building environment—A review. Renewable and Sustainable Energy Reviews, **13**(6-7), 1246–1261, 2009. doi:10.1016/j.rser.2008.09.015.

[17] Woods, Ruth, et al. «The Influence of Users Behaviour on Energy Use in European ShopingCentres: Influence Of User Behaviour on Energy Use » Sustainable Development, 25 (1), janvier 2017, 11-24. Doi:10.1002/sd.1638.

[18] O.A. Nisiforou, et al. Behaviour, Attitudes and Opinion of Large Entreprise Employees with Regard to their Energy Usage Hbaits and Adoption of Energy Saving Mesures, Energy and buildings, 55, decembre 2012, 299-311. Doi: 10.1016/j.enbuikd.2012.08.034.

[19] S. Janet, et al., The Energy Cultures Framework: Exploring the Role of Norms, Practices and Material Culture in Shaping Energy Behaviour in New Zealand ». Energy Research & Social Science, **7**, 117-23, 2015. Doi:10.1016/j.erss.2015.03.005.

[20] Invest in Morocco - Power Rates. http://www.invest.gov.ma/index.php?Id=34503&lang=en. Consulted the 17th of November, 2020.

[21] L.A. Zadeh, Fuzzy Sets, Information and Control, 338–353, (1965).

[22] S. Adnan, Electric vehicle power electronics cooling system pump control using fuzzy logic" nternational Journal of Advanced Computer Research, **7**(31), juin 2017, 111-20. Doi:10.19101/IJACR.2017.730019.

[23] A. Agarwal, A. Mishra, and M. Dixit, "Design of an Improved Fuzzy Logic based Control System for Washing Machines," **51**(8), 5–10, 2016

[24] M. Mongkolwongrojn, "Implementation of fuzzy logic control for air conditioning systems, In: Proceedings of 8th International Conference on Control, Automation and Systems, 313–321, 2005.

[25] G.Y. Yasin, et al., Recent Developments of Advanced Fuzzy Logic Controllers Used in Smart Buildings in Subtropical Climate, Energy Procedia, 61, 2014, 1021-24. Doi:10.1016/j.egypro.2014.11.1015.

[26] M.M. Gou, et al., Thermal Comfort Based Fuzzy Logic Controller, Building Services Engineering Research and Technology, **22**(4), 237-53, 2001. DOI.org (Crossref), doi:10.1177/014362440102200403.

[27] K. Mahmoud, Investigation of energy saving in HVAC systems : Modeling, simulation, and measurement using fuzzy logic controller ». 2018 IEEE International Conference on Industrial Technology (ICIT), IEEE, 445-50, 2018. DOI.org, doi:10.1109/ICIT.2018.8352218.

[28] A. Zakia, Modeling Techniques Used in Building HVAC Control Systems: A Review ». Renewable and Sustainable Energy Reviews, **83**, 64-84, 2018. DOI.org, doi:10.1016/j.rser.2017.10.044.

[29] C. Schweppe, Estia: A real-time consumer control scheme for space conditioning usage under spot electricity pricing. Computers & Operations Research, **18**(8), 751–765, 1991. doi:10.1016/0305-0548(91)90013-h

[30] Z. Yanyu et al., Multi-objective optimal control algorithm for HVAC based on particle swarm optimization ». Fifth International Conference on Intelligent Control and Information Processing, IEEE, 417-23, 2014. DOI.org, doi:10.1109/ICICI2014.7010290.

[31] A. Abdel-Hamid et al., Fuzzy Logic Control of Air-Conditioning System in Residential Buildings, Alexandria Engineering Journal, **54**(3), 395-403, 2015. Doi:10.1016/j.aej.2015.03.023.

[32] M. Abbas, M. Saleem Khan, Fareeha Zafar, « Autonomous Room Air Cooler Using Fuzzy Logic Control System, International Journal of Scientific & Engineering Research 2(5), 2011.

[33] M. Jamieson, "$3 Billion Opportunity: Energy Management in Retail Operations" , Schneider Electric executive summary, 1-6, 2014.

[34] R. Nikitha et al.,Token Based Scheduling for Energy Management in Building HVAC Systems ». Applied Energy, **173**, 67-79, 2016. DOI.org, doi:10.1016/j.apenergy.2016.04.023.

[35] G. Ali et al., HVAC System Energy Optimization Using an Adaptive Hybrid Metaheuristic,Energy and Buildings, **152**, 149-61, 2017. DOI.org, doi:10.1016/j.enbuild.2017.07.053.

[36] S. Jaw-Kuen et al., Fuzzy Controller for a Voltage-Regulated Solar-Powered MPPT System for Hybrid Power System Applications, Energies, **8**(5), 3292-312, 2015. DOI.org, doi:10.3390/en8053292.

[37] L. Bortoni-Anzures, et al., Fuzzy Controller for Automatic Steering in Heavy Vehicle Semi-Trailers, Ingeniería, Investigación y Tecnología, **14**(1), 1-9, 2013. DOI.org, doi:10.1016/S1405-7743(13)72220-0.

[38] B. Ben et al., Apportioning Energy Consumption in the Workplace: A Review of Issues in Using Metering Data to Motivate Staff to Save Energy, Technology Analysis & Strategic Management, **26**(10) 1196-211, 2014. Doi:10.1080/09537325.2014.978276.

[39] A. Christina, Co-Simulation of Fuzzy Control in Buildings and the HVAC System Using BCVTB, Advances in Building Energy Research, **12**(2), 195-216, 2018. Doi:10.1080/17512549.2017.1279077.

[40] Z. Ma, An Assessment for Energy Management in Retail Stores, Journal of Energy and Power Engineering, **12**(5), 2018. Doi:10.17265/1934-8975/2018.05.002.

[41] S. Steve, Reducing Energy Demand: A Review of Issues, Challenges and Approaches, Renewable and Sustainable Energy Reviews, 47, 74-82, 2015. Doi:10.1016/j.rser.2015.03.002.

[42] O. Dartevelle, " Énergie et commerces, conception et rénovation énergétiques des bâtiments", Les Cahiers de l'Urbanisme N° 70, Université catholique de Louvain Architecture et Climat Chargés de recherche p92-96, 2008.

ASTES

Advances in Science, Technology and Engineering Systems Journal Vol. 5, No. 4, 540-547 (2020)

www.astesj.com

Special Issue on Innovative Research in Applied Science, Engineering and Technology

ASTESJ

ISSN: 2415-6698

Human-Robot Multilingual Verbal Communication – The Ontological knowledge and Learning-based Models

Mohammed Qbadou[*,1], Intissar Salhi[1], Hanaâ El fazazi[1], Khalifa Mansouri[1], Michail Manios[2], Vassilis Kaburlasos[2]

[1]*Laboratory Signals, distributed systems and artificial intelligence, Mathematics & Computer Science, ENSET, Hassan II University of Casablanca, Casablanca, 28000, Morocco*

[2]*HUman-MAchines INteraction (HUMAIN) Lab, Department of Computer Science, International Hellenic University (IHU), Kavala Campus, GR-65404 Agios Loukas, Kavala, 65201, Greece*

ARTICLE INFO

Article history:
Received: 30 June, 2020
Accepted: 09 July, 2020
Online: 09 August, 2020

Keywords:
Natural language Processing
multilingual interaction
human-robot interaction
general ontology
LSTM Neural Networks

ABSTRACT

In their verbal interactions, humans are often afforded with language barriers and communication problems and disabilities. This problem is even more serious in the fields of education and health care for children with special needs. The use of robotic agents, notably humanoids integrated within human groups, is a very important option to face these limitations. Many scientific research projects attempt to provide solutions to these communication problems by integrating intelligent robotic agents with natural language communication abilities. These agents will thus be able to help children suffering from verbal communication disorders, more particularly in the fields of education and medicine. In addition, the introduction of robotic agents into the child's environment creates stimulating effects for more verbal interaction. Such stimulation may improve their ability to interact with pairs. In this paper, we propose a new approach for the human-robot multilingual verbal interaction based on hybridization of recent and performant approach on translation machine system consisting of neural network model reinforced by a large distributed domain-ontology knowledge database. We have constructed this ontology by crawling a large number of educational web sites providing multi-lingual parallel texts and speeches. Furthermore, we present the design of augmented LSTM neural Network models and their implementation to permit, in learning context, communication between robots and children using multiple natural languages. The model of a general ontology for multilingual verbal communication is produced to describe a set of linguistic and semantic entities, their properties and relationships. This model is used as an ontological knowledge base representing the verbal communication of robots with children.

1. Introduction

The great evolution of the theories and tools of artificial intelligence in addition to the technological achievements in the field of industrial robotics have contributed to the advent of intelligent robots endowed with physical as well as intellectual capacities. The efficient and rational integration of this kind of intelligent robots in real working environments in the presence of human beings is always a challenge and an important objective for the engineer as well as for the scientist. Several fields and sectors of application are directly concerned by this integration and consider it very promising for greater productivity and efficiency. Among these areas are mainly the industrial sectors and to a lesser but growing extent the education and health sectors. Especially for the education and health sectors, the most important aspect that determines the success or failure of this integration is the capacity for verbal interaction between humans and these intelligent robots. Indeed, verbal exchanges for these two sectors are essential for students' learning activities and for exchanges with patients during medical procedures. Verbal exchanges are even more important in the case of students or patients with special needs and especially in the case of autistic children.

[*] Corresponding Author: Mohammed QBADOU, 340 Cité Anfa, 28000, Mohammedia, Morocco, +212667514296 qbmedn7@gmail.com

This research work is part of this context and aims to produce generic models representing a solution to the problem of verbal interaction of intelligent robots with several groups of children who use different natural languages. We also provide an implementation and experimentation of these models by considering the case of three natural languages most formally used in the geographical area of North Africa in this case Arabic, French and English. Our models will allow a smart robot to be able, in real time, to detect and communicate in the natural language of the children in front. This will be of great use for teachers or tutors to carry out collaborative learning activities in which the robot will have the role of teacher, tutor or even of student.

The paper is outlined in a way that Section 2 gives a survey on human-robot interaction systems. The section 3 explains our architecture model that illustrate the main three transformation modules the robot must have to interact with humans in multiple natural languages. The three modules that compose the whole system have also been discussed. Section 4 give the details on the first module especially the description of the data structure used, a scraping approach we developed to extract the expected data of parallel text and audio corpus mainly as JSON file format. The end of this section provides the Extract-Transform-Load model describing the mapping operations of data and metadata from the corpus to the ontology database. In section 5, we show how we can improve the performance of the translation machine algorithm based on our ontological knowledge base. Section 6 provides a conclusion on the different aspects of our models and ends with a critical discussion in order to identify new avenues for future research.

2. Survey on Human-Robot interaction

2.1. Classes of Human-Robot interaction

In a common work environment, an intelligent robot can have two types of interaction with humans [1]: verbal or non-verbal. The first interaction form covers the production of emotions or meaning without use of words or speech but using only facial or body gestures. On the other hand, the second form necessarily involves the use of natural language expressions in the orally and/or written forms.

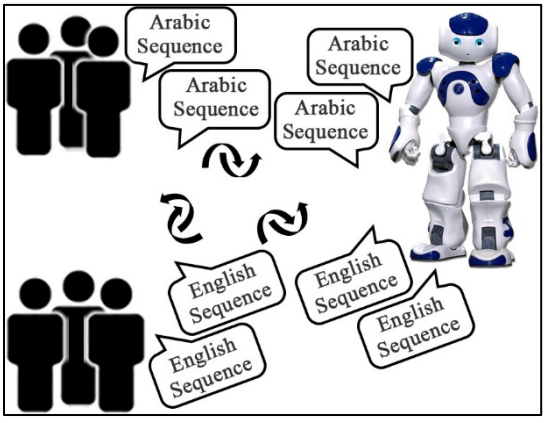

Figure 1: Human-Robot multilingual verbal communication

Figure 1 illustrates the key idea of our work where an intelligent robot is called to allow real-time verbal exchanges between two or more groups not speaking the same language and having to share a common experience of learning or therapy. The robot thus plays the role of mediator and communication interface between the different groups.

2.2. Overview of research findings on oral interactions between robotic agents and humans

In the last decade, several high-quality research studies have been conducted on problems related to the oral communication possibilities between robots and humans. This period was marked by a significant number of articles indexed in this area. The study of these references revealed the main guidelines relating to our work and the following three research areas namely: (1) smart robotics and cognitive [2]-[6], (2) knowledge systems and (3) ontological databases [7]-[10] and artificial intelligence and machine learning techniques [11]-[16].

These research works highlight the inability of conventional robotic systems to respond to rapid changes in technical and functional production requirements. They present as a solution to these problems, the introduction of cognitive robots in the production lines. These robots while being able to adapt quickly, they are also able to interact and collaborate with human operators.

3. General architecture for robot-human communication in multi-language context

3.1. Block diagram of our proposal system

Figure 2 describes our general-purpose showing that robot-human interactions pass essentially through four modular units: the control unit, the perception unit, the knowledge data management system and the multilingual communication interface including text and speech sequences. This last unit contains all the transformations applied to the input signals collected by the robot's exchange unit. The knowledge base unit gives the semantic support of the different transformations for the synthesis of the robot reactions. This last unit contains all the transformations applied to the input signals collected by the exchange units of the robot. The knowledge management unit provides the semantic support for these transformations for the synthesis of the robot's reactions.

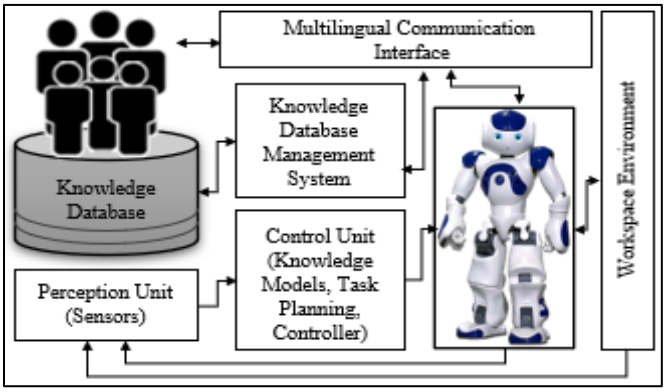

Figure 2: Block diagram of the proposed Human-Robot interaction system

3.2. Systemic model of verbal communication of robots based on an ontological knowledge database

The diagram in the figure 3 provides an integrated systemic representation of our approach which is built up into three large

independent parts, namely: (A) the devoted part for the construction and updating the text and audio parallel corpus links to the expandable list of languages, (B) the second part consisting in decisive phase which constitutes a driving force of construction and extension of our ontological knowledge database by the discovery of the entities and the relationships which connect them as well as their properties[10]. This engine also has the role of extracting all the occurrences associated with the entities found. (C) the third part constitutes the system of language identification, speech recognition and text translation.

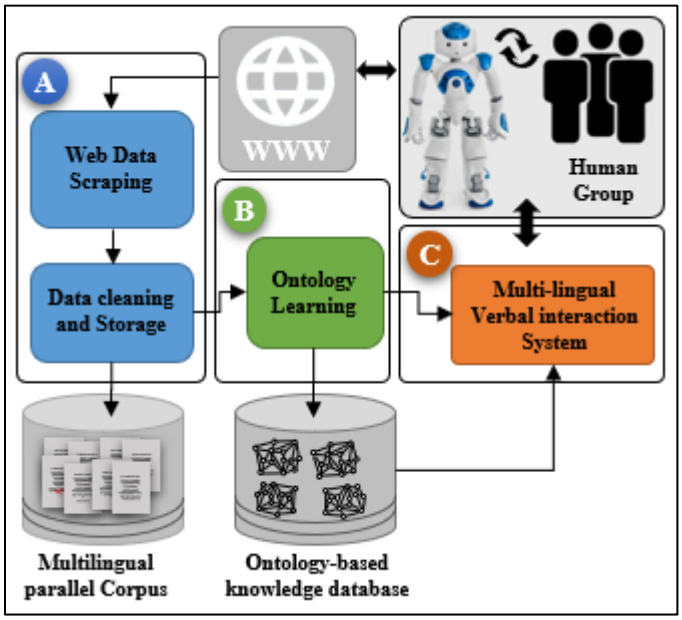

Figure 3: Architectural model of Human-Robot interaction system

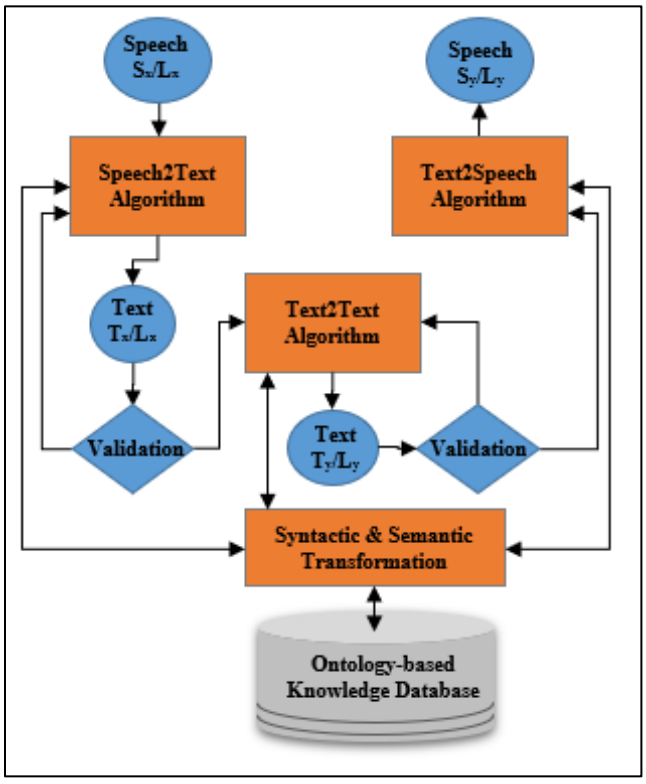

Figure 4: General model for Human-Robot multilingual verbal interactions

3.3. Specification diagram of Speech2speech algorithm using knowledge database

The objective of this module is the transformation of a given speech Sx, expressed in a language Lx, into an equivalent speech Sy expressed in another language Ly. This transformation is necessary to guarantee the exchange in a multi-language context. We have decomposed this transformation into three successive operations: (1) "Speech2Text": the transformation of the speech Sx into an equivalent text Tx and expressed in the same language Lx. (2) the transformation of the text Tx into an equivalent text Ty expressed in the language Ly and, (3) the transformation of the text Ty into an equivalent speech Sy expressed in Ly.

Figure 4 describes the sequence of the three operations and shows their relationship to the ontological knowledge management system. These operations are all based on the use of machine learning algorithms trained and validated by a high-quality dataset of parallel speeches and texts for the Arabic, French and English languages. The knowledge system also serves as a storage base [17] for all conversations collected or generated by the system.

3.4. Model of speech recognition and ontology-based tagging

Figure 5 describes the most complicated transformation in our system. It is carried out in five phases: firstly phase (1) dedicated to the pre-processing of the input speech in order to eliminate possible crudes by the application of filters and to segment it into pieces thanks to the application of techniques detection of breaks, framing and windowing. A second phase (2) consists of the application of an algorithm for identifying the language of speech. The results of these two phases are used by phase (3) which transforms each segment into a sequence of words thanks to the use of a neural network of the "multi-layer perceptron" type. semantic and contextual integration represents phase (4) and makes it possible by analysis and discovery of the semantic relationships provided by the ontological knowledge base. this completeness of the generated text also allows phase (5) to associate a set of tags with the speech that has just been processed.

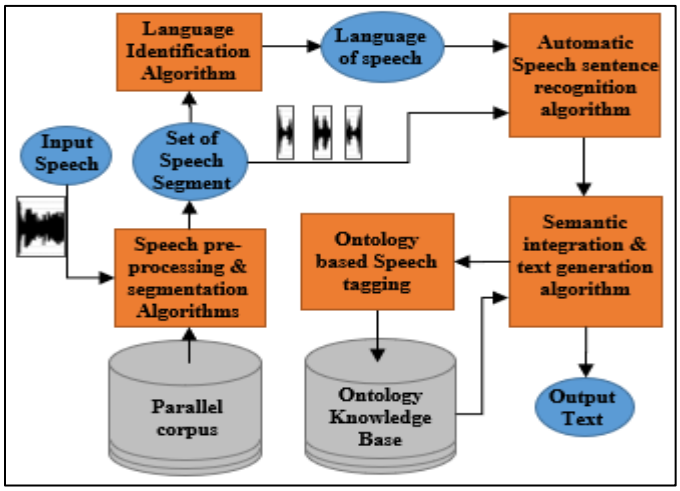

Figure 5: Speech recognition and text generation models

3.5. Language identification algorithm

The identification of the language of a speech is often done by selecting and analyzing a piece of this speech as reported in [8] and

[18]. As reported in [11]-[13] and [19], this identification may be done by a classification algorithm based on the automatic learning of a "deep neural network" trained using a multi-language speeches dataset recorded for several speakers. For its simplicity and the precision of its results, we chose the use of a classification algorithm based on the learning of a recurrent neural network (RNN) [20]. This learning is done on a large number of features generated by an extraction function based on the knowledge base.

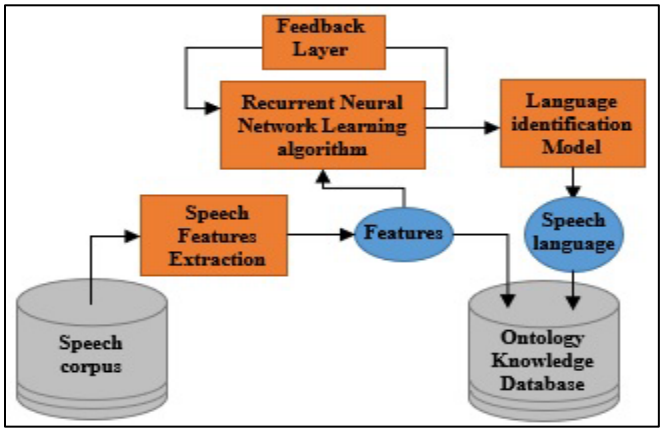

Figure 6: Ontology-based identification of the speech language

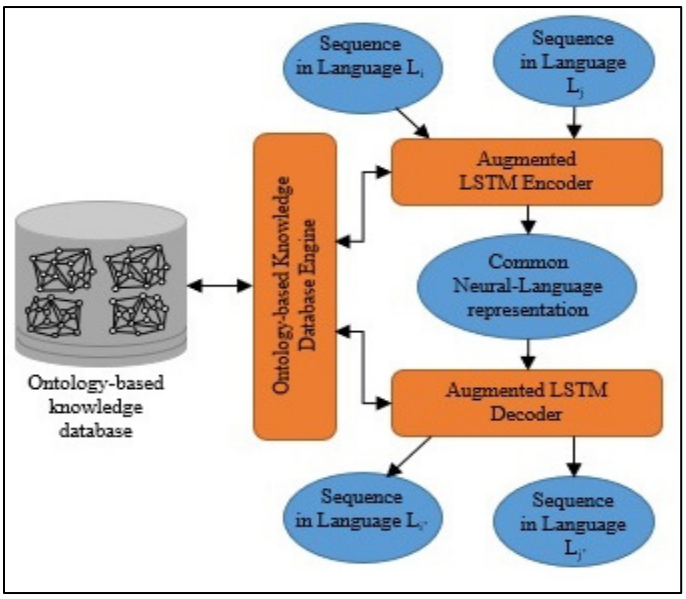

Figure 7: augmented LSTM Seq2Seq using ontology

To implement and test the models proposed in figures 5 and 6, we chose to create components programmed in Python and this for the range of these standard libraries in the fields of numerical calculation, machine learning and the field of processing of natural languages [21]. To define the corpus of speeches and parallel texts for the three languages considered, we identified a large list of websites offering free multilingual resources such as multilingual newspapers, online and multilingual tv channels, podcasts in lines in addition to forums and tweets of thematic conversations.

3.6. Text to Text Translation

Several works on the problem of automatic translation machine have been published. The most recent have adopted machine learning based on LSTM neural networks model with variants obtained by adding additional layers in order to improve the translation accuracy. Among recent approaches, we can notably cite "tree LSTM based methods with attention [14] and LSTM based methods with transformers [15]-[16]. As depicted in figure 8, our approach is based on the latest model whose learning is improved by the addition of a "labeling" module and reduction of the training dataset thanks to our ontological knowledge base.

The figure 7 describes the translation machine process in two steps and their interaction with the ontological knowledge database through the ontological engine. Thus, the input sequence message expressed in language Li is first encoded based on Long Short-Term Memory (LSTM) networks augmented algorithm [22] in a common representation that is independent to the source and the target languages. The second step performs the decoding in the target language according the second step of LSTM algorithm.

4. Ontology-based knowledge data representation

4.1. Ontology capabilities and usage

The formal modeling of knowledge on a field of activity and the representation of dependency relationships between its elements has always been a means expected by both engineers and scientists [23]. This modeling makes it possible to structure knowledge to serve as a knowledge base allowing to carry out new analytical studies and validate theories [10]. Among the models widely adopted by researchers stand out the ontological models. moreover, ontological models have a great capacity to represent semantic and contextual aspects relating to a domain [24]-[25]. Ontologies have an extensive use in Web applications where they are been considered as source of semantics with a rich and formal representations.

Thanks to these representations a large possibility in terms of reasoning mechanisms and, manipulation of data and metadata are possible [4]. For all these advantages, the ontological models are adopted in the fields of cognitive robotics and that of artificial intelligence. These possibilities also allow the management of knowledge relating to collaboration between robots and humans through verbal communication [7]. In this research work, we exploit all these possibilities through a domain ontology, as illustrated in figure 8, to serve as a model of a knowledge base for Human-Robot interaction system. This model should allow domain hierarchization into interest sub-domains (education, health, specific education, therapy, ...) [26]. Our model also provides the linguistic entities for natural language processing operations we have defined in section 3. We adopted OWL language to create and use our ontological knowledge database.

Figure 8 corresponds to the ontological model we designed. It represents a general ontology that represents several fields of knowledge, such as education, health and rehabilitation as examples. In connection with these domains, our ontological model also models the set of conversations that may occur between human and/or robotic agents. the detailed representation of the linguistic components of the conversations is also given by this model. the model represents a conversation as a set of textual or oral sequences. The ontology expresses the relationships between all the entities and their main properties.

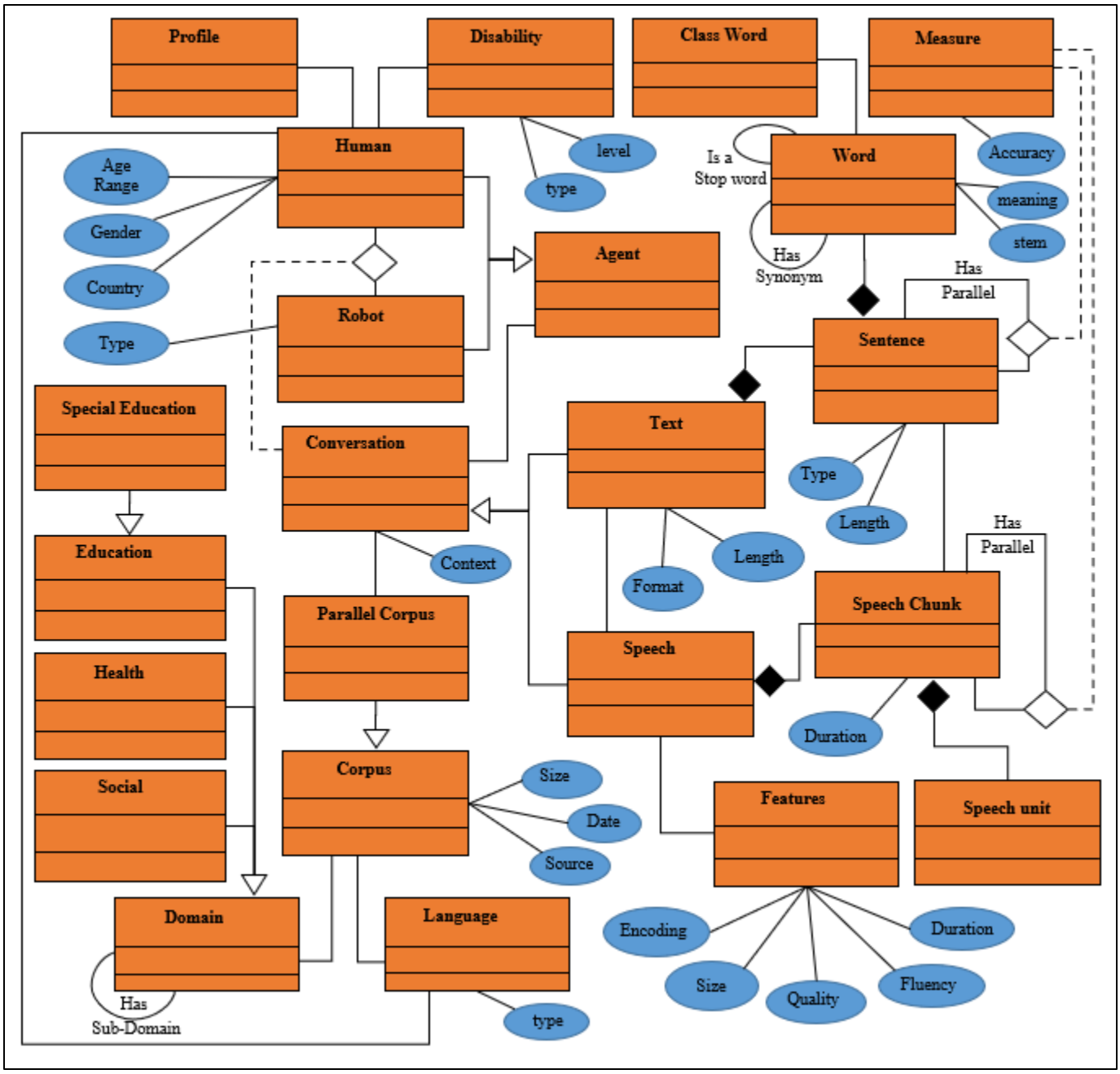

4.2. Ontology use for tagging sequences and reducing dataset

The ontology represented at figure 8 is used as a knowledge management system for managing information related to the human-robot verbal interactions and for help in capturing important multilingual interactions' features for a specific domain or sub-domain [9]. Indeed, building on a hierarchy of domains and sub domains of interactions and their links to a set of linguistic and semantic concepts, our ontology knowledge base allows extraction of relevant, reduced and contextual datasets that facilitate learning significantly. It also allows a relevant labeling of these datasets producing semantic learning attributes. The figure 9 shows the principle followed to favor the reduction of training datasets taking into account the hierarchy of domains.

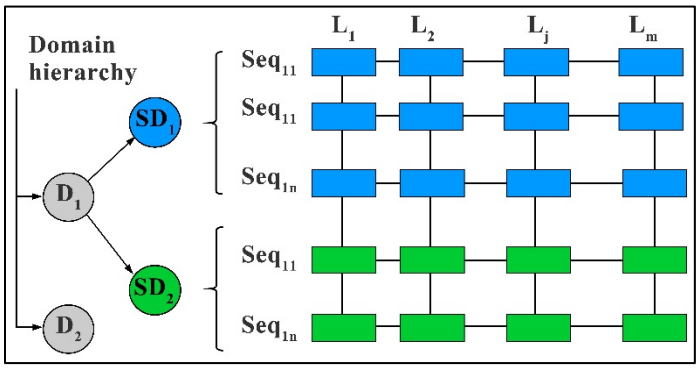

Figure 9: Dataset reduction and sequence tagging based on ontology

The exploitation of the domain hierarchy provided by our ontology allows to generate reduced and relevant dataset (table 1) according to the considered domain (education, therapy, ...)

Furthermore, an ontology-based feature optimization method is used to reduce significantly dimensionality of feature space [10]. Thus, we are able to extract dimension-reduced datasets of multilingual parallel texts for the training and validating the LSTM-based learning model. This method is conducted in two steps:

- As a first one, concepts of general ontology are generated by a transformation of the terms of vector space model, then the frequency weights of these concepts are calculated by the frequency weights of the terms.
- and according to the structure of the general ontology, similarity weights are associated then with the concept features.

5. Experiments and Results

5.1. The used dataset

The results published in this paper are obtained on a parallel dataset constructed for Arabic, French and English (Table 2). The choice of these languages reflects our objective of deploying the results in the Moroccan context where these three languages are dominant. The table groups together the main data characterizing the distribution of sentences in the dataset used.

Figure 10 provides a graphical representation of these results. This graph shows a very strong similarity of these results for the three languages considered.

5.2. Model training

The figure 11 shows the learning result of our LSTM neural network model. It shows in particular the list of layers created and the order in which they are connected with an LSTM layer and at the end the Dense layer which comes from the LSTM layer and which is responsible for producing the prediction of the outputs. The reshape functions have been used for successive dataset transformation from 2D to 3D format.

Table1: Parallel text dataset reduction based on domain hierarchies

Dom	SubD	N	En	Fr	Ar
D_1	$SubD_1$	1	Help	Aidez-moi	النجدة
		3	Jump	Saute	اقفز
		4	Run	Cours	اركض
		5	Stop	Arrête	قف
		..	…	…	…
	$SubD_2$	1	The verbal interaction	L'interaction verbale	التفاعل اللفظي
		2	Computer components	Composants de l'ordinateur	مكونات الكمبيوتر
			…	…	…

Table2: Multilingual Training dataset - Length sentences distribution

English		Arabic		French	
Count	120.0000	Count	120.0000	Count	120.0000
Mean	123.2437	Mean	123.2437	Mean	123.2437
Std	143.1298	Std	152.1779	Std	152.1779
Min	1.0000	Min	7.0000	Min	2.0000
25%	31.5000	25%	31.0000	25%	31.0000
50%	45.0000	50%	44.0000	50%	46.0000
75%	164.5000	75%	172.0000	75%	167.0000
Max	518.0000	Max	523.0000	Max	526.0000

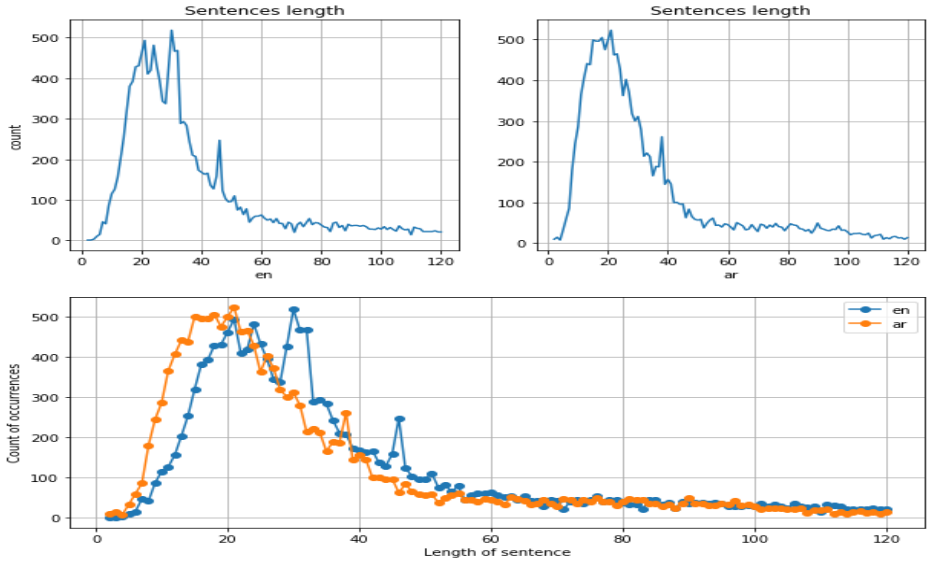

Figure 10: Distribution of the number sentence occurrences by length.

Layer (type)	Output Shape	Param #	Connected to
input_25 (InputLayer)	(None, None, 36)	0	
input_26 (InputLayer)	(None, None, 47)	0	
reshape_25 (Reshape)	(None, 120, 36)	0	input_25[0][0]
reshape_26 (Reshape)	(None, 120, 47)	0	input_26[0][0]
lstm_25 (LSTM)	[(None, 256), (None,	300032	reshape_25[0][0]
lstm_26 (LSTM)	[(None, 120, 256), (	311296	reshape_26[0][0] lstm_25[0][1] lstm_25[0][2]
dense_13 (Dense)	(None, 120, 47)	12079	lstm_26[0][0]
activation_13 (Activation)	(None, 120, 47)	0	dense_13[0][0]

Total params: 623,407
Trainable params: 623,407
Non-trainable params: 0

Figure 11: LSTM Model training life-cycle – model summary

6. Conclusion and future works

In this paper, we presented several models and algorithms for a new approach of the human robot multilingual verbal interaction. The strength of our method lies in the combination of the strength of ontological models in terms of semantic representation and their possibilities of reasoning and inference to the capacity of machine learning models based on the LSTM model. We perform the implementation of these models using the machine learning package named Keras and NLTK python framework. These implementations have been tested in a multi-agent environment made up of several robot and human agents which interact verbally according to a number of conversations in the three languages.

The development of new upgrades for our system will be the focus of our future research, we are also aiming to take action integrating human-robot interactions in the fields of therapy and special education with the purpose of accumulating data in these fields as well as emotional data, that would allow our robots to mimic human emotion expressed in facial expressions, choice of words and voice intonation as well as detect the emotional state of patients and act accordingly. In addition, we will consider implementing the proposed models in real situations of interaction between NAO robots and children, especially in the case of the two following areas: Therapeutic rehabilitation of children with specific needs and the educational system for this category of children.

Acknowledgment

This research has been partially supported by the project "CybSPEED: Cyber-Physical Systems for Pedagogical Rehabilitation in Special Education" H2020-MSCA-RISE-2017. This project has received funding from the European Union's Horizon 2020 research and innovation program under the Marie Skłodowska-Curie grant agreement No 777720.

References

[1] N. Mavridis, "A review of verbal and non-verbal human–robot interactive communication" Robotics and Autonomous Systems, Volume **63**(1), 22-35, 2015. https://doi.org/10.1016/j.robot.2014.09.031

[2] I. Kafiev, P. Romanov and I. Romanova, "Intelligent Mobile Robot Control in Linguistic Evaluation of Solution Options" in 2019 International Multi-Conference on Industrial Engineering and Modern Technologies (FarEastCon), Vladivostok, Russia, 2019. https://doi.org/10.1109/FarEastCon.2019.8934814

[3] R.R. Galin, R.V. Meshcheryakov, "Human-Robot Interaction Efficiency and Human-Robot Collaboration" Kravets A. (eds) Robotics: Industry 4.0 Issues & New Intelligent Control Paradigms. Studies in Systems, Decision and Control, **272**, Springer, Cham, 55-63, 2020. https://doi.org/10.1007/978-3-030-37841-7_5

[4] A. Angleraud et al., "Human-Robot Interactive Learning Architecture using Ontologies and Symbol Manipulation" In Proceedings of the 27th IEEE International Symposium on Robot and Human Interactive Communication, RO-MAN, Nanjing, 2018. https://doi.org/10.1109/ROMAN.2018.8525580

[5] K. Gaur, G.S.Virdi, "Smart Manufacturing with Robotic automation and Industry 4.0-A Review" in International Journal of Innovative Research in Science, Engineering and Technology, **7**(3), 2481-2486, March 2018. DOI:10.15680/IJIRSET.2018.0703082

[6] A. Perzylo et al., "SMErobotics: Smart Robots for Flexible Manufacturing" in IEEE Robotics & Automation Magazine, **26**(1), 78-90, March 2019. https://doi.org/10.1109/MRA.2018.2879747

[7] L. Howard, G. Paulo, F. Sandro, J. I. Olszewska, "Ontology for autonomous robotics" in 2017 26th IEEE International Symposium on Robot and Human Interactive Communication (RO-MAN), Lisbon, 189-194, 2017. https://doi.org/10.1109/ROMAN.2017.8172300

[8] S. Kobayashi, S. Tamagawa, T. Morita and T. Yamaguchi, "Intelligent Humanoid Robot with Japanese Wikipedia Ontology and Robot Action Ontology" in 2011 6th ACM/IEEE International Conference on Human-Robot Interaction (HRI), Lausanne, 417-424, 2011. https://doi.org/10.1145/1957656.1957811

[9] A. Zeyer, P. Bahar, K. Irie, R. Schlüter and H. Ney, "A Comparison of Transformer and LSTM Encoder Decoder Models for ASR" in 2019 IEEE Automatic Speech Recognition and Understanding Workshop (ASRU), SG, Singapore, 8-15, 2019. https://doi.org/10.1109/ASRU46091.2019.9004025

[10] M.M. Ali et al., "Ontology-based approach to extract product's design features from online customers' reviews" Computers in Industry, **116**, 103175,2020. https://doi.org/10.1016/j.compind.2019.103175

[11] D. Cruz-Sandoval et al., "Towards a Conversational Corpus for Human-Robot Conversations" in HRI '17 Companion March 06-09, Vienna, Austria, ACM, 99-100, 2017. http://dx.doi.org/10.1145/3029798.3038344

[12] K. Sugiura and K. Zettsu, "Rospeex: A cloud robotics platform for human-robot spoken dialogues" 2015 IEEE/RSJ International Conference on Intelligent Robots and Systems (IROS), Hamburg, 2015, 6155-6160, 2015. https://doi.org/10.1109/IROS.2015.7354254

[13] T. Kawahara "Spoken Dialogue System for a Human-like Conversational Robot ERICA" in D'Haro L., Banchs R., Li H. (eds) 9th International Workshop on Spoken Dialogue System Technology. Lecture Notes in Electrical Engineering, **579**. Springer, Singapore, 65-75, 2019. https://doi.org/10.1007/978-981-13-9443-0_6

[14] Z. Huang et al., "TRANS-BLSTM: Transformer with Bidirectional LSTM for Language Understanding" in arXiv:2003.07000 [cs.CL], 2019. https://arxiv.org/abs/2003.07000v1

[15] H. Li, A. Y. C. Wang, Y. Liu, D. Tang, Z. Lei and W. Li, "An Augmented Transformer Architecture for Natural Language Generation Tasks" in 2019 International Conference on Data Mining Workshops (ICDMW), Beijing, China, 1-7, 2019. https://doi.org/10.1109/ICDMW48858.2019.9024754

[16] W. Yu, M. Yi, X. Huang, X. Yi and Q. Yuan, "Make It Directly: Event Extraction Based on Tree-LSTM and Bi-GRU" in IEEE Access, **8**, 14344-14354, 2020. https://doi.org/10.1109/ACCESS.2020.2965964

[17] M.S.H. Ameur, Farid Meziane, Ahmed Guessoum, "ANETAC: Arabic Named Entity Transliteration and Classification Dataset" in arXiv:1907.03110v1 [cs.CL] 2019, https://arxiv.org/abs/1907.03110v1

[18] Y. Tanimoto et al., "Feature extraction and Classification of Learners using Multi-Context Recurrent Neural Networks" in 2019 IEEE 11th International Workshop on Computational Intelligence and Applications (IWCIA), Hiroshima, Japan, 77-82, 2019. https://doi.org/10.1109/IWCIA47330.2019.8955064

[19] M. Swain, A. Routray, P. Kabisatpathy, "Databases, features and classifiers for speech emotion recognition: a review," in. International Journal of Speech Technology, **21**, 93–120, 2018. https://doi.org/10.1007/s10772-018-9491-z

[20] M.A.A. Albadr, S. Tiun, F.T. "Spoken language identification based on the enhanced self-adjusting extreme learning machine approach" PLOS ONE, **13**(4), 2018. https://doi.org/10.1371/journal.pone.0194770

[21] M. H. Nehrir, C. Wang, Deep Learning with Python, Manning Publications Co, 2018.

[22] H.L. Yang HL et al., "A Personalization Recommendation Framework of IT Certification e-Learning System" in: Knowledge-Based Intelligent Information and Engineering Systems, **4693**, 50-57, 2007. https://doi.org/10.1007/978-3-540-74827-4_7

[23] J.J. Jung, H.G. Kim, GS. Jo, "Alignment-Based Preprocessing of Personal Ontologies on Semantic Social Network" in Knowledge-Based Intelligent Information and Engineering Systems, **4693**, 255-262, 2007. https://doi.org/10.1007/978-3-540-74827-4_33

[24] S.U. Ya-ru et al., "Agricultural Ontology Based Feature Optimization for Agricultural Text Clustering" Journal of Integrative Agriculture, **11**(5), 752-759, 2012. https://doi.org/10.1016/S2095-3119(12)60064-1

[25] K. Munir, M. Sheraz Anjum, "The use of ontologies for effective knowledge modelling and information retrieval" Applied Computing and Informatics, **14**(2), 116-126, 2018. https://doi.org/10.1016/j.aci.2017.07.003

[26] H. I. Krebs and N. Hogan, "Therapeutic Robotics: A Technology Push" in Proceedings of the IEEE, **94**(9), 1727-1738, 2006. https://doi.org/10.1109/JPROC.2006.880721

ASTES

Advances in Science, Technology and Engineering Systems Journal
Vol. 5, No. 5,578-591 (2020)
www.astesj.com
Special Issue on Innovative Research in Applied Science, Engineering and Technology

ASTES Journal
ISSN: 2415-6698

Numerical Study of Gas Microflow within a Triangular Lid-driven Cavity

Youssef Elguennouni[*,1], Mohamed Hssikou[2], Jamal Baliti[3], Mohammed Alaoui[1]

[1]*Moulay Ismail University of Meknes, Faculty of Sciences, Morocco*

[2]*University of Ibn Zohr, Faculty of Sciences, Agadir, Morocco*

[3]*University of Sultan Moulay Slimane, Polydisciplinary Faculty, Beni Mellal, Morocco*

ARTICLE INFO

Article history:
Received: 03 August, 2020
Accepted: 26 September, 2020
Online: 05 October, 2020

Keywords:
SRT-LBM
MRT-LBM
DSBC
BSBC
lid-driven
micro-cavity
Knudsen number
vortex

ABSTRACT

A rarefied gas flow is modeled inside two cases of triangular lid-driven microcavity using single (SRT) and multi-relaxation time (MRT) lattice Boltzmann approaches. In the first one, the right angle is in the top-left corner and the upper wall moves with positive horizontal velocity. However, in the second case, the right angle is in the bottom-left corner and the bottom wall moves with negative horizontal velocity. Unlike the classical form of square cavities, widely treated in the literature, the triangular form has a diagonal wall that affects the flow motion. At the moving wall, diffuse scattering boundary condition (DSBC) is employed while at the stationary sides, a combination of bounce-back and specular reflection boundary conditions (BSBC) is used. The computations are primarily performed in the slip and early transition regimes. The rarefaction effect, given by the Knudsen number (Kn) value, on the profiles of velocity components, is examined for both approaches. This study proves that for the higher values of Kn, the SRT-LBM approach cannot provide accurate results, particularly, near the inclined wall. However, the MRT-LBM approach confirms its validity even in the transition regime. A comparison with Direct Simulation Monte Carlo (DSMC) results for horizontal velocity contours shows the efficiency of the MRT-LBM approach than the SRT-LBM one which breaks down for rarefied flows.

1 Introduction

A complete description of gas microflows involved in the micro/nano-electro-mechanical systems (MEMS/NEMS) [1] remains a challenge for many researchers during the last decades. Lid-driven cavity flow is one of the classical benchmark problems of computational fluid dynamics (CFD) [2–5]. Such flow has been analyzed by various computational methods like the Navier-Stokes-Fourier equations (NSF) [6, 7], Direct Simulation Monte Carlo (DSMC) [7–10] and moment equations approach [6, 10, 11].

In micro-devices, gaseous flows undergoe non-equilibrium or rarefaction effects. The gas flow rarefaction degree is, usually, given by the Knudsen number (Kn) which is the ratio of gas-molecules mean free path (λ) and the characteristic length of the system (l) (see Fig. 1). The particle/wall collisions cease to be negligible against the particle/particle ones in the transition regime and the gas becomes rarefied. This situation takes place in many microfluidic and vacuum applications [12, 13].

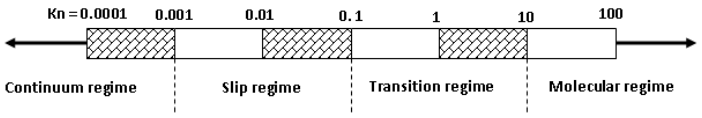

Figure 1: Flow regimes according to the Knudsen number.

To describe this kind of flows a kinetic based approach is needed. In order to save the computational time, the lattice boltzmann method (LBM) is used. This method was, first, inspired by the lattice gas automata (LGA) method for which the fluid is moving along the lattice. For both methods, the time, space, and velocities of the particles are discrete. The LGA model uses a six-speed hexagonal lattice, however, in LBM, the most used model for two-dimensional (D = 2) geometries is D2Q9 which is a square grid with nine discrete velocities (Q = 9). In recent years, LBM has become a promising alternative to simulate fluid flows and heat transfer problems. Unlike the classical CFD approaches, the LBM is a mesoscopic approach which combines the classical computational fluid

[*]Corresponding Author: Youssef Elguennouni, y.elguennouni@edu.umi.ac.ma

dynamics (CFD) and the kinetic description based on the Boltzmann equation. The method, therefore, ensures a relation between the macro and the microscopic descriptions of flow. Only a few studies that have investigated the effectiveness of this method and extend its ability to model hydrodynamic and rarefied flows [14–20]. However, the study of such flows requires a good choice and implementation of the boundary conditions (BC), which is a key step in the LBM simulation process. In the literature different BC are tested for various problems in order to capture non-equilibrium effects near the walls [21–25]. To solve the lattice Boltzmann equation (LBE), we used the well-known kinetic model of Bhatnagar–Gross–Krook (BGK) [26] which is the simplest and most widely used collision operator for the LBE. This operator is represented by a linear discretization of the relaxation of particle distribution function toward the Maxwell equilibrium state.

Application of LBM, under rarefaction conditions, to describe gas microflows is still a new field needing improvement to extend its applicability to this kind of flows. This study aims to simulate lid-driven gas flow in triangular micro-cavity. The results obtained by both approaches of LBM, SRT and MRT, are compared with those obtained by the DSMC method in the slip regime, usually encountered in MEMS devices [27]. The main simulation parameters are the Knudsen number (Kn) and the tangential momentum accommodation coefficient σ (TMAC). Unlike the DSMC method which needs a long computation time to give satisfactory results [28] and the extended macroscopic theory, like regularized 13 moment (R13), which the range of validity is limited [6, 29], the MRT-LBM proved its effectiveness for rarefied gas simulation.

2 Problem statement

In the current simulation, an isosceles right-angled triangular prism micro-cavity is considered with a large cross-sectional aspect ratio, the flow properties are independent of z-coordinate. In this study, the effect of any external body force is neglected. The gas flow can be considered within a two-dimensional enclosure of length scale $H = L$. According to the position of the moving wall, with a constant velocity U_0, two cases of the isosceles right triangle are considered in this study. In the first one, the right angle is in the top-left corner and the upper wall moves towards positive x-direction. However, in the second case, the right angle is in the bottom-left corner and the bottom wall moves in the negative x-direction (see Figs. 2).

3 Lattice Boltzmann models and boundary conditions

3.1 Boltzmann equation

In absence of external force, the behavior of gas flow is governed by the Boltzmann equation given by

$$(\partial_t + \mathbf{c}.\nabla_r) f = \Omega(f). \quad (1)$$

Where f is the distribution function and $\Omega(f)$ is the collision operator which represents the particles microscopic collision dynamics. In the BGK model, this operator is given by

$$\Omega(f) = -\frac{1}{\tau}(f - f^{eq}). \quad (2)$$

In which τ represents the relaxation time and f^{eq} is the Maxwell distribution function at the equilibrium state.

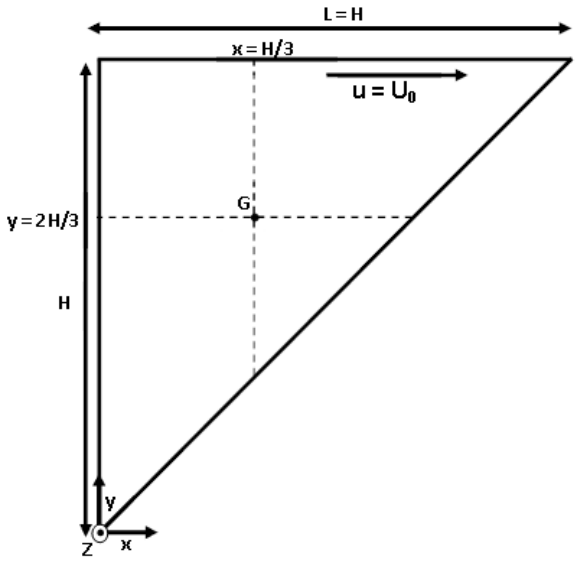

(a) Case (1)

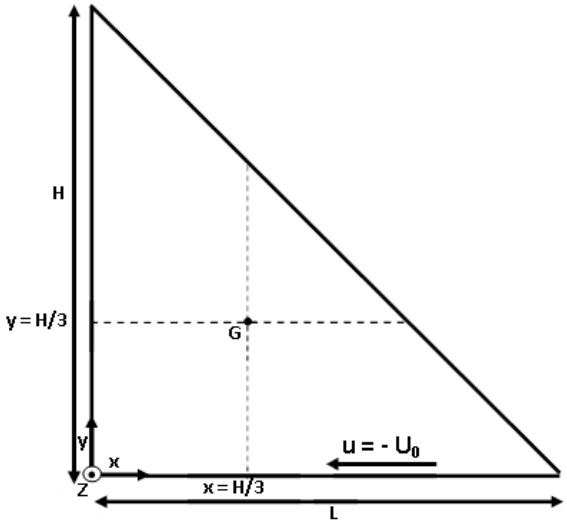

(b) Case (2)

Figure 2: Studied domain configuration.

3.2 Single relaxation time lattice Boltzmann method (SRT-LBM)

For distribution function density f a D2Q9 model with square grid is used in this study. According to the BGK model, the governing, lattice Boltzmann equation, for this distribution function, is written as

$$f_k(\mathbf{x} + \mathbf{c}_k\Delta t, t + \Delta t) = f_k(\mathbf{x}, t)(1 - \frac{\Delta t}{\tau}) + \frac{\Delta t}{\tau} f_k^{eq}(\mathbf{x}, t). \quad (3)$$

The Maxwell distribution function f_k^{eq} at the equilibrium state is written in the Taylor expansion as

$$f_k^{eq} = w_k \rho \left[1 + 3\frac{\mathbf{c}_k.\mathbf{u}}{c^2} + \frac{9}{2}\frac{(\mathbf{c}_k.\mathbf{u})^2}{c^4} - \frac{3}{2}\frac{\mathbf{u}^2}{c^2} \right]. \quad (4)$$

Where the weight factors w_k are $w_0 = 4/9$, $w_{1-4} = 1/9$, $w_{5-8} = 1/36$, and c is the lattice speed given by: $c = \frac{\Delta x}{\Delta t} = \frac{\Delta y}{\Delta t}$. The discrete scheme D2Q9 is characterized by

$$\begin{bmatrix} \mathbf{c}_{k,x} \\ \mathbf{c}_{k,y} \end{bmatrix} = c \begin{bmatrix} (0 & 1 & 0 & -1 & 0 & 1 & -1 & -1 & 1) \\ (0 & 0 & 1 & 0 & -1 & 1 & 1 & -1 & -1) \end{bmatrix}, \quad k = 0 - 8$$

The macroscopic values of density ρ and velocity $\mathbf{u} = (u, v)$, are computed by the following relations:

$$\rho = \sum_{k=0}^{8} f_k, \quad (5a)$$

$$\rho \mathbf{u} = \sum_{k=0}^{8} f_k \mathbf{c}_k. \quad (5b)$$

For rarefied flows, the ratio of the mean free path λ and the mean thermal velocity $\langle v \rangle = \sqrt{\frac{8RT}{\pi}}$ is equivalent to the relaxation time τ given by

$$\tau = \frac{\lambda}{\langle v \rangle} = \lambda \sqrt{\frac{\pi}{8RT}}. \quad (6)$$

In microfluidic devices, gas flows are characterized by their rarefaction degree given by the Knudsen number $Kn = \frac{\lambda}{H}$, where H is the total number of lattice nodes in the y-direction. Usually, we set $c = \sqrt{3RT} = 1$ for D2Q9 model, therefore [22]

$$\tau = \sqrt{\frac{3\pi}{8}} \lambda \cong KnH. \quad (7)$$

3.3 Multi-relaxation time lattice Boltzmann method (MRT-LBM)

The collision operator in the multi-relaxation time lattice Boltzmann method (MRT-LBM) is given by

$$M^{-1}\mathbf{S}\left[\mathbf{m}(\mathbf{x}, t) - \mathbf{m}^{eq}(\mathbf{x}, t)\right]. \quad (8)$$

Thus, the eq. (3) becomes,

$$f_k(\mathbf{x} + \mathbf{c}_k \Delta t, t + \Delta t) - f_k(\mathbf{x}, t) = -\mathbf{M^{-1}S}[\mathbf{m}(\mathbf{x}, t) - \mathbf{m}^{eq}(\mathbf{x}, t)]. \quad (9)$$

Where $\mathbf{m}(\mathbf{x}, t)$ is a vector of moments and $\mathbf{m}^{eq}(\mathbf{x}, t)$ is the corresponding one at the equilibrium state. The passage from the velocities space to the moments space and vice versa is obtained by the following linear transformations:
$\mathbf{m} = \mathbf{M}f$ and $f = \mathbf{M^{-1}m}$.
For D2Q9 scheme, the transformation matrix $\mathbf{M}$ is given by

$$M = \begin{bmatrix} 1 & 1 & 1 & 1 & 1 & 1 & 1 & 1 & 1 \\ -4 & -1 & -1 & -1 & -1 & 2 & 2 & 2 & 2 \\ 4 & -2 & -2 & -2 & -2 & 1 & 1 & 1 & 1 \\ 0 & 1 & 0 & -1 & 0 & 1 & -1 & -1 & 1 \\ 0 & -2 & 0 & 2 & 0 & 1 & -1 & -1 & 1 \\ 0 & 0 & 1 & 0 & -1 & 1 & 1 & -1 & -1 \\ 0 & 0 & -2 & 0 & 2 & 1 & 1 & -1 & -1 \\ 0 & 1 & -1 & 1 & -1 & 0 & 0 & 0 & 0 \\ 0 & 0 & 0 & 0 & 0 & 1 & -1 & 1 & -1 \end{bmatrix}$$

The moments vector $\mathbf{m}$ is:

$$|\mathbf{m}\rangle = \begin{pmatrix} \rho & e & \varepsilon & \rho u & q_x & \rho v & q_y & p_{xx} & p_{xy} \end{pmatrix}^T.$$

Where e is the energy, ε is the square of energy, $\mathbf{j} = (\rho u, \rho v)$ is the momentum of density, and $\mathbf{q} = (q_x, q_y)$ is the vector of heat flux. The stress tensor components are also p_{xx}, and p_{xy}.
The moments vector at the equilibrium state $\mathbf{m}^{eq}(\mathbf{x}, t)$ is given by

$$\mathbf{m^{eq}} = \begin{cases} m_0^{eq} = \rho \\ m_1^{eq} = -2\rho + 3(j_x^2 + j_y^2) \\ m_2^{eq} = \rho - 3(j_x^2 + j_y^2) \\ m_3^{eq} = j_x \\ m_4^{eq} = -j_x \\ m_5^{eq} = j_y \\ m_6^{eq} = -j_y \\ m_7^{eq} = j_x^2 - j_y^2 \\ m_8^{eq} = j_x j_y \end{cases} \quad (10)$$

In the moment space the collision matrix $\mathbf{S}$ is the diagonal matrix,

$$\mathbf{S} = \begin{pmatrix} 1 & 1.4 & 1.4 & 1.0 & 1.2 & 1.0 & 1.2 & s_7 & s_8 \end{pmatrix}.$$

Where $s_7 = s_8 = 1/\tau$. Note that by taking $s_k = 1/\tau, k = 0{-}8$, the MRT model is reduced to the SRT one.

3.4 Stationary and moving walls boundary conditions

Boundary conditions implementation plays a crucial role in gas flow simulation within micro-geometries. In the present study, a combination of bounce-back and specular boundary conditions (BSBC) is used at the stationary walls, however, diffuse scattering boundary conditions (DSBC) are imposed at the moving wall.

- *Combination of bounce-back and specular boundary conditions*

The BSBC is adopted by using the coefficient of the tangential momentum accommodation σ (TMAC) expressed by [30]

$$\sigma = \frac{M_i - M_r}{M_i - M_w}. \quad (11)$$

Where $M_{i,r,w}$ are the tangential momentum of molecules related, respectively, to the incident, reflected molecules, and wall. This coefficient ranges from 0 for pure specular reflection, to 1 which corresponds to the pure bounce-back one.

At the inclined wall, the boundary conditions using TMAC are as follows (see Fig. 3):

$$f_6 = f_8, \quad (12a)$$

$$f_2 = \sigma \times f_4 + (1 - \sigma) \times f_1, \quad (12b)$$

$$f_3 = \sigma \times f_1 + (1 - \sigma) \times f_4. \quad (12c)$$

- *Diffuse scattering boundary condition*

The DSBC is used to simulate fluid interactions at solid interfaces written as [31]

$$|(\mathbf{c}_k - \mathbf{u}_\mathbf{w}).\mathbf{n}|f_k = \sum_{(\mathbf{c}_{k'} - \mathbf{u}_\mathbf{w}).\mathbf{n}<0} |(\mathbf{c}_{k'} - \mathbf{u}_\mathbf{w}).\mathbf{n}|\Re_f(\mathbf{c}_{k'} \to \mathbf{c}_k) f_{k'}. \quad (13)$$

Where

$$\Re_f(\mathbf{c}_{k'} \to \mathbf{c}_k) = \frac{A_n}{\rho_\mathbf{w}} ((\mathbf{c}_k - \mathbf{u}_\mathbf{w}).\mathbf{n}) f_k^{eq}|_{\mathbf{u}=\mathbf{u}_\mathbf{w}}, \quad (14)$$

where k and k' refer to the reflected and incident directions of molecules, respectively, and $\mathbf{n}$ is the unit normal vector inward of the wall, and $\Re_f(\mathbf{c}_{k'} \to \mathbf{c}_k)$ is the scattering probability from the direction $\mathbf{c}_{k'}$ to $\mathbf{c}_k$. By satisfying zero normal flux condition across the wall, the coefficient of normalization A_n can be obtained by the following relation:

$$A_n = \rho_\mathbf{w} \frac{\sum_k |(\mathbf{c}_k - \mathbf{u}_\mathbf{w}).\mathbf{n}|f_k}{|(\mathbf{c}_k - \mathbf{u}_\mathbf{w}).\mathbf{n}|f_k^{eq} \sum_{k'} |(\mathbf{c}_{k'} - \mathbf{u}_\mathbf{w}).\mathbf{n}|f_{k'}}. \quad (15)$$

At the top wall, the unknown distribution functions are $f_{k=4/7/8}$ (see Fig. 3) can be determined from the known ones $f_{k=2/5/6}$ and $f_{k=4/7/8}^{eq}$ as shown in the DSBC (Eqs. (13)–(15)) by

$$f_{k=4/7/8} = \frac{A_n}{\rho_\mathbf{w}} f_{k=4/7/8}^{eq}(\rho_\mathbf{w}, \mathbf{u}_\mathbf{w})(f_2 + f_5 + f_6). \quad (16)$$

For the D2Q9 model, the coefficient A_n takes the value 6 [24].

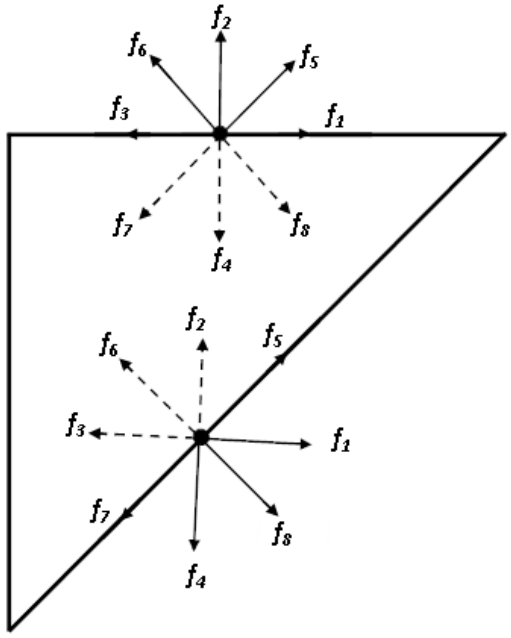

Figure 3: Gas-surface interaction at the top and inclined walls.

4 Results and discussion

All present simulations are carried out using a developed Fortran code. The SRT-LBM and MRT-LBM approaches are used to simulate lid-driven gas microflow in two configurations of triangular right micro-cavity isosceles (see Figs. 2). In the literature, the simulation of fluid microflows was made a lot for a square-section cavity [14–20]. However, a few studies were focused on the geometries with inclined sides [32–38]. Unlike most of these papers, based on the Reynolds number (Re), the rarefaction degree is expressed in this study according to the Knudsen number value (Kn).

4.1 Mesh independence study

For $Kn = 0.01$ and $\sigma = 0.5$, Table 1 shows mesh size effect on the x-velocity component at the center of the moving wall, while Figure 4 shows their effect on the profiles of u-velocity along the vertical line $x/H = 1/3$ and v-velocity along the horizontal line $y/H = 2/3$ for the case (1) using the SRT-LBM approach. Similarly, Figure 5 shows the profiles of u and v along the lines $x/H = 1/3$ and $y/H = 1/3$, respectively, for the case (2) by using the MRT-LBM approach. As shown, the grid size 300×300 is enough to offer good and reliable results.

Table 1: Effect of the mesh on the x-velocity component at the center of the moving wall for $Kn = 0.01$ and $\sigma = 0.5$.

Mesh	200×200	300×300	400×400
SRT-LBM for case (1)	0.9120	0.9116	0.9115
MRT-LBM for case (2)	-0.9057	-0.9061	-0.9062

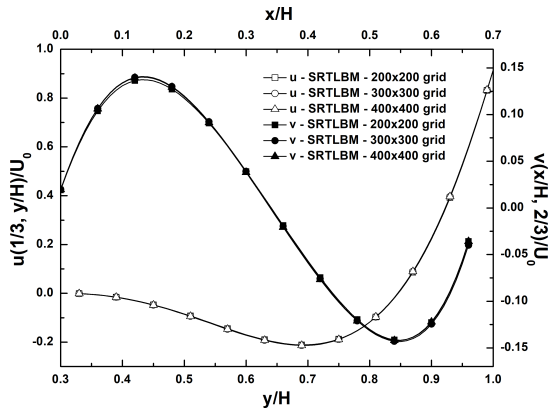

Figure 4: Profiles of u and v-velocity components along the lines $x/H = 1/3$ and $y/H = 2/3$, respectively, obtained by SRT-LBM for case (1).

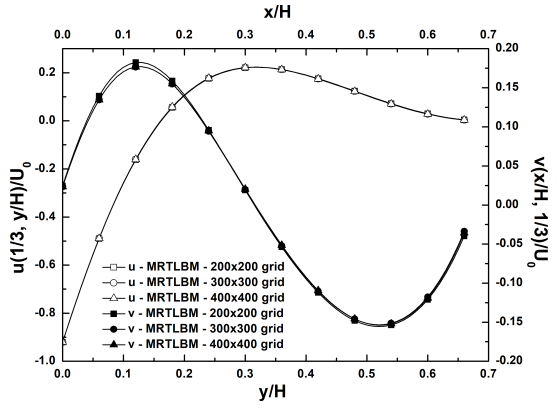

Figure 5: Profiles of u and v-velocity components along the lines $x/H = 1/3$ and $y/H = 1/3$, respectively, obtained by MRT-LBM for case (2).

4.2 Validation test

In order to ensure the validation of these models, a comparison is made with previous studies according to the widely used TMAC value ($\sigma = 0.7$) [14–16, 20] for both validation cases (square micro-cavity and a triangular micro-cavity (case(2)). At first, the profile of $u-$velocity for $Kn = 0.01$ and $Kn = 0.1$ along the vertical centerline are compared with the findings reported by Perumal et al. [14, 15] and Rahmati et al. [16] for a square micro-cavity (see Fig. 6a). Table 2 shows the location of the primary vortex center for $Kn = 0.01$ and $Kn = 0.1$. The results of the current study align well with those of Rahmati et al. [16, 17], and Tang et al. [18]. In the second validation case, u-velocity contours inside a triangular micro-cavity (case (2)) are confronted with those obtained by the DSMC method [38], the most confident and powerful method to study of such flows. Figures 6b and 7 show, respectively, the u-velocity component profiles for $x/H = 1/3$ and the u contours for $Kn = 0.01$ and $Kn = 0.1$. Table 3 shows the location of the primary vortex center according to the Knudsen number values $Kn = 0.01$ and $Kn = 0.1$. It is shown that MRT-LBM results are acceptable and approximate well, those of Roohi et al. [38], for which $U_0 = 100m/s$.

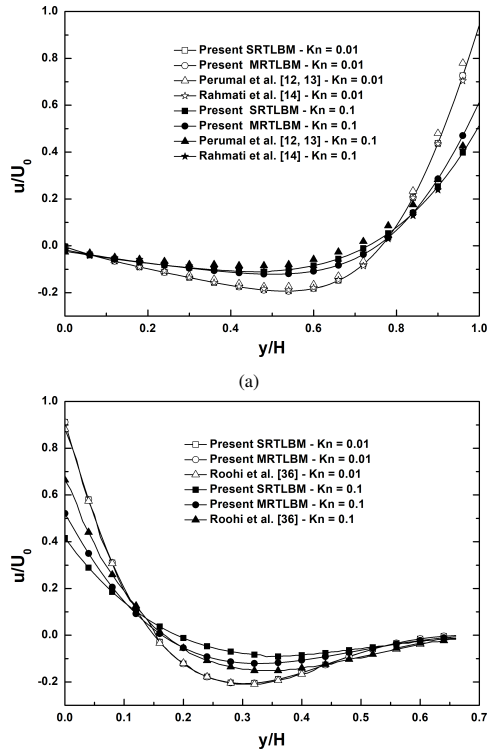

Figure 6: Profile of x-velocity for $Kn = 0.01$ and $Kn = 0.1$ (a) along the vertical centerline for square micro-cavity and (b) along the line $x/H = 1/3$ case (2) with a positive velocity $+U_0$.

4.3 Numerical results and analysis

In this work, the lid-wall moves with a fixed horizontal velocity $U_0 = 0.1$ for all simulations. To compare with and reproduce the results of Roohi et al. [38], the TMAC is taken $\sigma = 0.7$. Using the SRT-LBM and MRT-LBM methods, Figures 8 and 9 show the Knudsen number effect on the horizontal and vertical velocities profiles, respectively, for case (1) and case (2). The slip effect at the moving wall is more pronounced [14–17, 20, 38]. As predicted by the kinetic theory, the velocity slip vanishes at the continuum limit ($Kn = 0.007$), the gas-molecules velocity is almost equal the lid-velocity U_0. To evaluate both effects of rarefaction degree and TMAC value, Tables 4 and 5 show that as Kn and σ increase, the effects of non-equilibrium impact on the flow motion and the velocity slip evolve more importantly. For the first case, since the moving wall velocity is positive then the horizontal velocity component decreases to take negative values near the inclined wall, then increases to take positive values with y-coordinate beyond the primary vortex position. In that case, the lowest value of u/U_0 is located at $y/H = 0.7$ for $Kn = 0.007$ (see Figs. 8(a-b)). Similar and opposite behavior of u-component velocity is observed in the second case. The highest values of u/U_0 is located at $y/H = 0.32$ for $Kn = 0.007$ (see Figs. 9(a-b)). The vertical velocity-slip increases when Kn increases and it is more prominent by the SRT-LBM approach than by the MRT-LBM one [16, 20] (see Figs. 8(c-d) and 9(c-d)). The MRT-LBM method maintains its stability near the walls and the vertical slip-velocity can be captured even at the center of the inclined plane on the right (see Figs. 10b and 10d). However, for the SRT-LBM method, when the value of Kn increases fluctuations appear on and near the inclined wall. These fluctuations have a significant influence, especially for $Kn = 0.1$ (see Figs. 10a and 10c). For $Kn = 0.01$, 0.05, and 0.1, Table 6 shows the position of the primary and secondary vortices inside the micro-cavity for the first case. For both approaches, by increasing Kn, the primary vortex moves from right to left in the direction of x and from top to bottom in the direction of y. However, the secondary vortices at the bottom of the micro-cavity vanish and it cannot be captured using the SRT-LBM method while the MRT-LBM method retains their presence and these vortices undergo the same motion as the primary ones with Kn (see Figs. 12). For the value of TMAC $\sigma = 0.7$, these vortices are slightly shifted to the right with respect to the $\sigma = 0.5$ case. Table 7 presents the location of flow vortices in the second case. The primary vortex with Kn for both approaches moves from left to right in the direction of x and from bottom to top in the direction of y. But, SRT-LBM cannot retain its horizontal x-direction movement for $Kn = 0.1$. As in the case (1), unlike the SRT-LBM approach, the secondary vortices are well captured by MRT-LBM. These vortices move as the primary one along y-direction but in the opposite x-direction. Thus, unlike in the square-cavity, in the presence of an inclined wall, the flow stagnation points undergo two motion under rarefaction effects. For $\sigma = 0.7$, both types of vortices are moved in downward direction and shifted to the right with respect to the $\sigma = 0.5$ case. For different Knudsen numbers, the flow stagnation which corresponds to u/U_0 profiles intersection point remains the same (see Table 8, Figs. 8 (a-b) and Figs. 9(a-b)). The density ρ is also sensitive to the rarefaction degree and its value increases with Kn. An expected density has a great value near the upper-right and lower-left corners, for the cases (1) and (2), respectively (see Fig. 11a). To examine the required run time for both approaches, the profiles of velocity components at the gravity center of the micro-cavity (1) ($x = H/3, y = 2H/3$) are plotted as a function of the number of time steps for $Kn = 0.01$ and $\sigma = 0.7$. After approximately 10000-time steps number the velocity hits the steady-state (see Figs. 11b and 11c). Developed codes SRT-LBM and MRT-LBM are run on

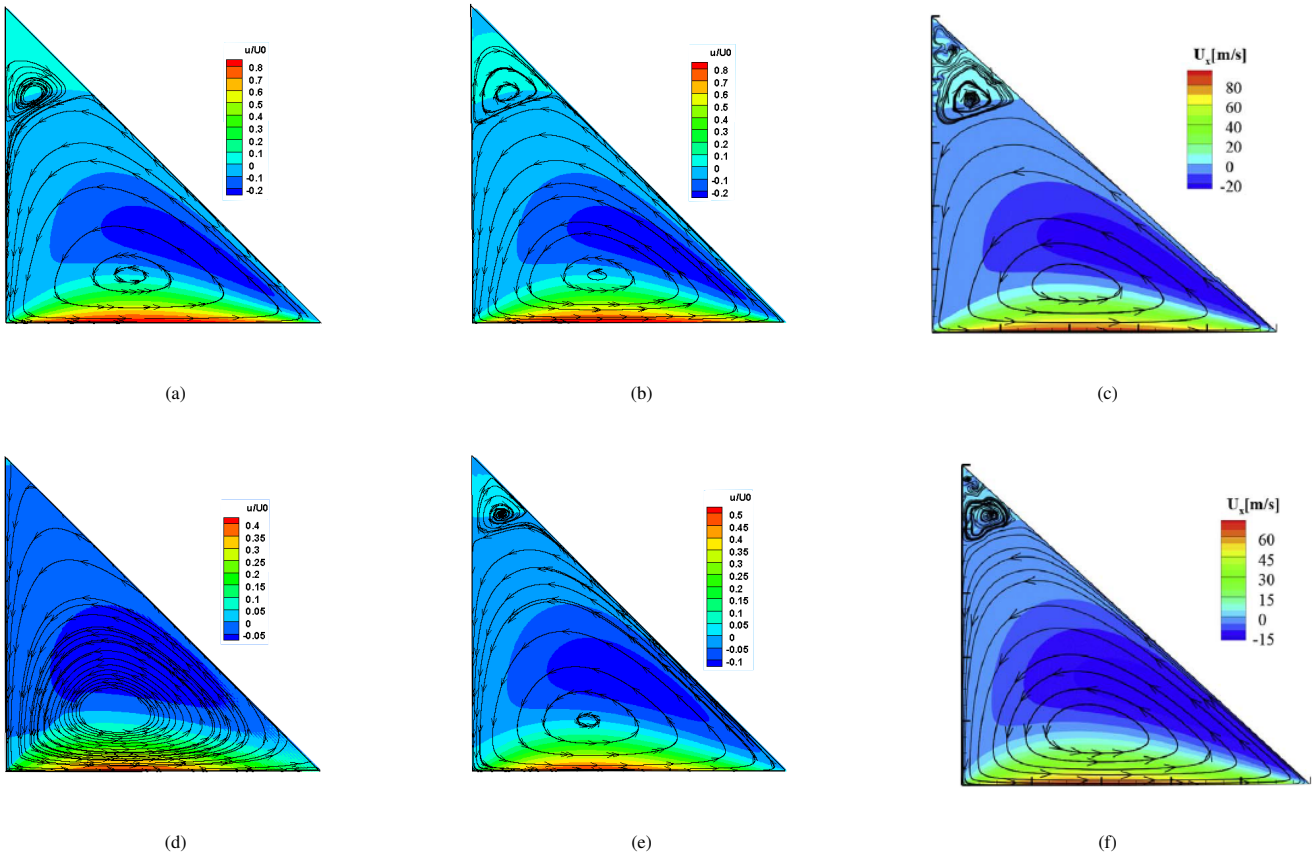

Figure 7: x-velocity streamlines and contours for $\sigma = 0.7$ - case (2) with a positive velocity $+U_0$. (a) SRT-LBM $-Kn = 0.01$ (b) MRT-LBM $-Kn = 0.01$ (c) Roohi et al. [38] $-Kn = 0.01$ (d) SRT-LBM $-Kn = 0.1$ (e) MRT-LBM $-Kn = 0.1$ (f) Roohi et al. [38] $-Kn = 0.1$.

Table 2: Primary vortex center locations for a square micro-cavity.

Kn	SRT-LBM	MRT-LBM	Rahmati et al. [16]	Rahmati et al. [17]	Tang et al. [18]
0.01	(0.5009, 0.7638)	(0.5030, 0.76378)	(0.5017, 0.7637)	(0.5022, 0.7663)	(0.5, 0.7633)
0.1	(0.5001, 0.7316)	(0.5041, 0.75336)	(0.5020, 0.7240)	(0.5023, 0.7570)	(0.5, 0.72)

Table 3: Primary vortex center locations for the triangular micro-cavity (case (2)).

Kn	SRT-LBM	MRT-LBM	Roohi et al. [38] - Monatomic	Roohi et al. [38] - Diatomic
0.01	(0.3979, 0.1525)	(0.3974, 0.1523)	(0.4209, 0.1520)	(0.4119, 0.1520)
0.1	(0.3529, 0.1888)	(0.3678, 0.1624)	(0.3799, 0.1659)	(0.3780, 0.1670)

the Intel (R) Core (TM) i5-3340 M CPU laptop @ 2.7 GHz and RAM 8.00 GB. To obtain accurate findings the MRT-LBM requires more processing time than the SRT-LBM [16, 20] due to the higher number of moments hired in the calculation to capture the effects of non-equilibrium (see Table 9). In Figures 12(a-i) the flow streamlines and u-velocity contours are plotted for $Kn = 0.007$, 0.05, 0.1, 1 and 3, respectively for $\sigma = 0.7$. As the increase in the Knudsen number, the streamlines take the wall shape and the secondary vortices observed for the lower Knudsen numbers vanish at the bottom of the micro-cavity (1) [14–16, 20]. In addition, the primary vortex undergoes a slight downward, and right-to-left movement with Kn growth. Also, u-velocity is sensitive to the degree of rarefaction and its value decreases as Kn increases. Figures 13 describe the flow streamlines, u and v-velocities contours for $Kn = 0.007$ and $Kn = 0.1$, respectively, by combining the cavity of case(1)/case(2) with their corresponding anti-symmetric cases. The segments connecting the primary and secondary vortices centers intersect at the center of the square micro-cavity, respectively (see Figs. 13(a-b)). The plots of the velocity components distributions, Figures 13(c-f), confirm the data anti-symmetric variation with respect to the square cavity center and their sensitivity to the rarefaction effect. So, by studying the two cases (1) and (2) we can deduce the characteristics of the gas flow in their corresponding anti-symmetrical forms.

Finally, it is shown that SRT-LBM loses its validity in the

transition regime while the results of the MRT-LBM method still remain convincing. To summarize the MRT-LBM method imposes itself as a good alternative for simulating the gas microflows usually encountered in the micro-devices.

Table 4: Slip effects on the x-velocity component $\frac{u(H/2,H)}{U_0}$ at the center of the moving wall - case (1).

Approaches	*Kn*	0.007	0.01	0.05	0.1
SRT-LBM	$\sigma = 0.5$	0.9372	0.91165	0.64171	0.41041
	$\sigma = 0.7$	0.93674	0.91076	0.63227	0.39725
MRT-LBM	$\sigma = 0.5$	0.93739	0.91214	0.67381	0.51394
	$\sigma = 0.7$	0.93692	0.91126	0.66554	0.50135

Table 5: Slip effects on the x-velocity component $\frac{u(H/2,0)}{U_0}$ at the center of the moving wall - case (2).

Approaches	*Kn*	0.007	0.01	0.05	0.1
SRT-LBM	$\sigma = 0.5$	-0.93045	-0.90587	-0.63838	-0.41238
	$\sigma = 0.7$	-0.92999	-0.90498	-0.62877	-0.39784
MRT-LBM	$\sigma = 0.5$	-0.93042	-0.90617	-0.67291	-0.51524
	$\sigma = 0.7$	-0.92998	-0.90531	-0.66484	-0.50287

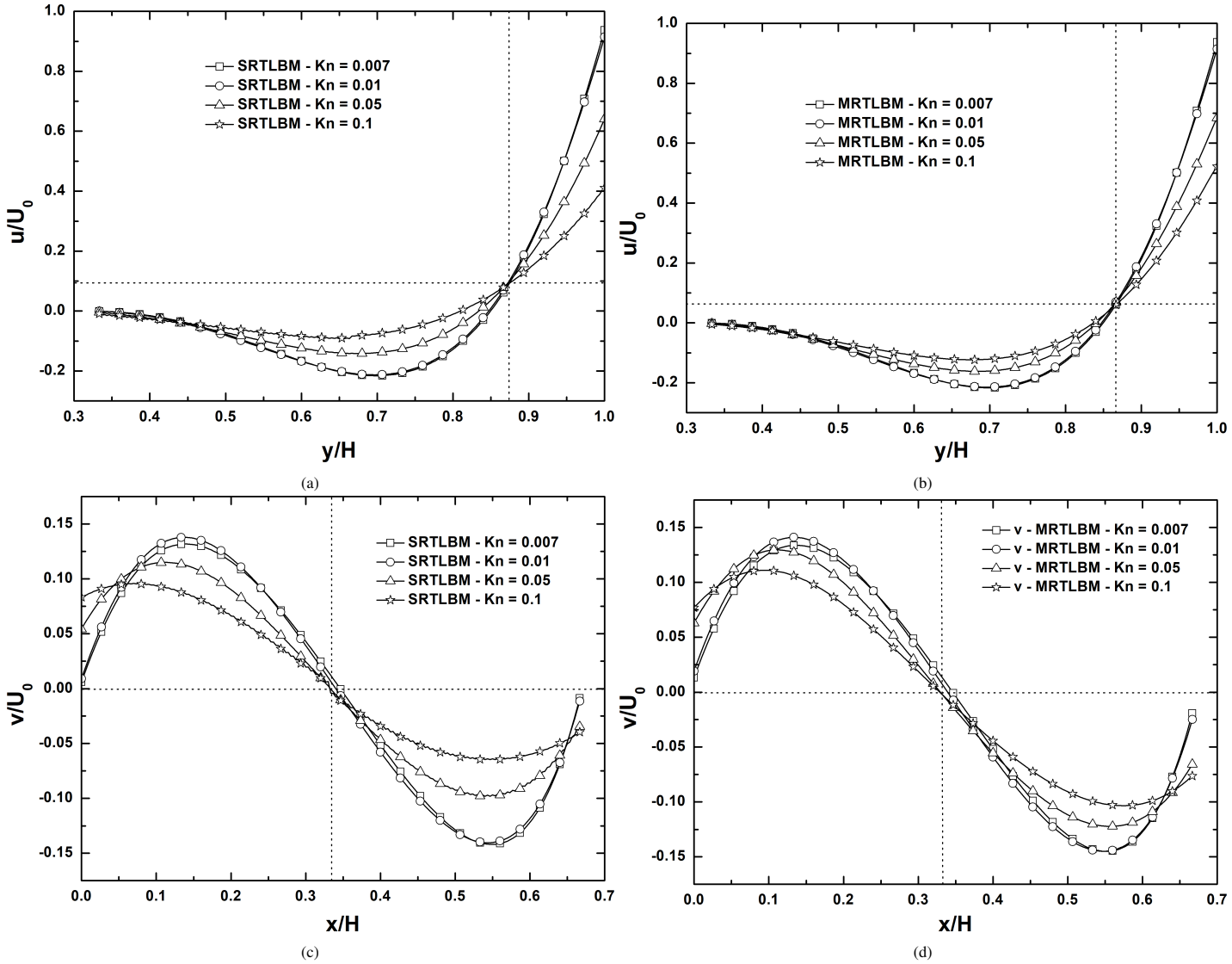

Figure 8: (a)-(b) x-velocity profile along the vertical line $x/H = 1/3$ and (c)-(d) profile of y-velocity along the horizontal line $y/H = 2/3$ at different Knudsen numbers for $\sigma = 0.7$ - case (1).

Table 6: Primary and secondary vortices locations for different values of Kn and σ - case (1).

Approaches \ Kn		0.01	0.05	0.1
SRT-LBM ($\sigma = 0.5$) **MRT-LBM**	Primary vortex	(0.3939, 0.8455)	(0.3697, 0.8298)	(0.3493, 0.8035)
	Secondary vortex	(0.0770, 0.2711)	– – – – –	– – – – –
	Primary vortex	(0.3933, 0.8458)	(0.3681, 0.8360)	(0.3660, 0.8298)
	Secondary vortex	(0.1101, 0.2572)	(0.0884, 0.1807)	– – – – –
SRT-LBM ($\sigma = 0.7$) **MRT-LBM**	Primary vortex	(0.3944, 0.8471)	(0.3713, 0.8351)	(0.3526, 0.8106)
	Secondary vortex	(0.0783, 0.2821)	– – – – –	– – – – –
	Primary vortex	(0.3938, 0.8473)	(0.3702, 0.8416)	(0.3681, 0.8377)
	Secondary vortex	(0.1124, 0.2669)	(0.1018, 0.2293)	(0.0910, 0.1878)

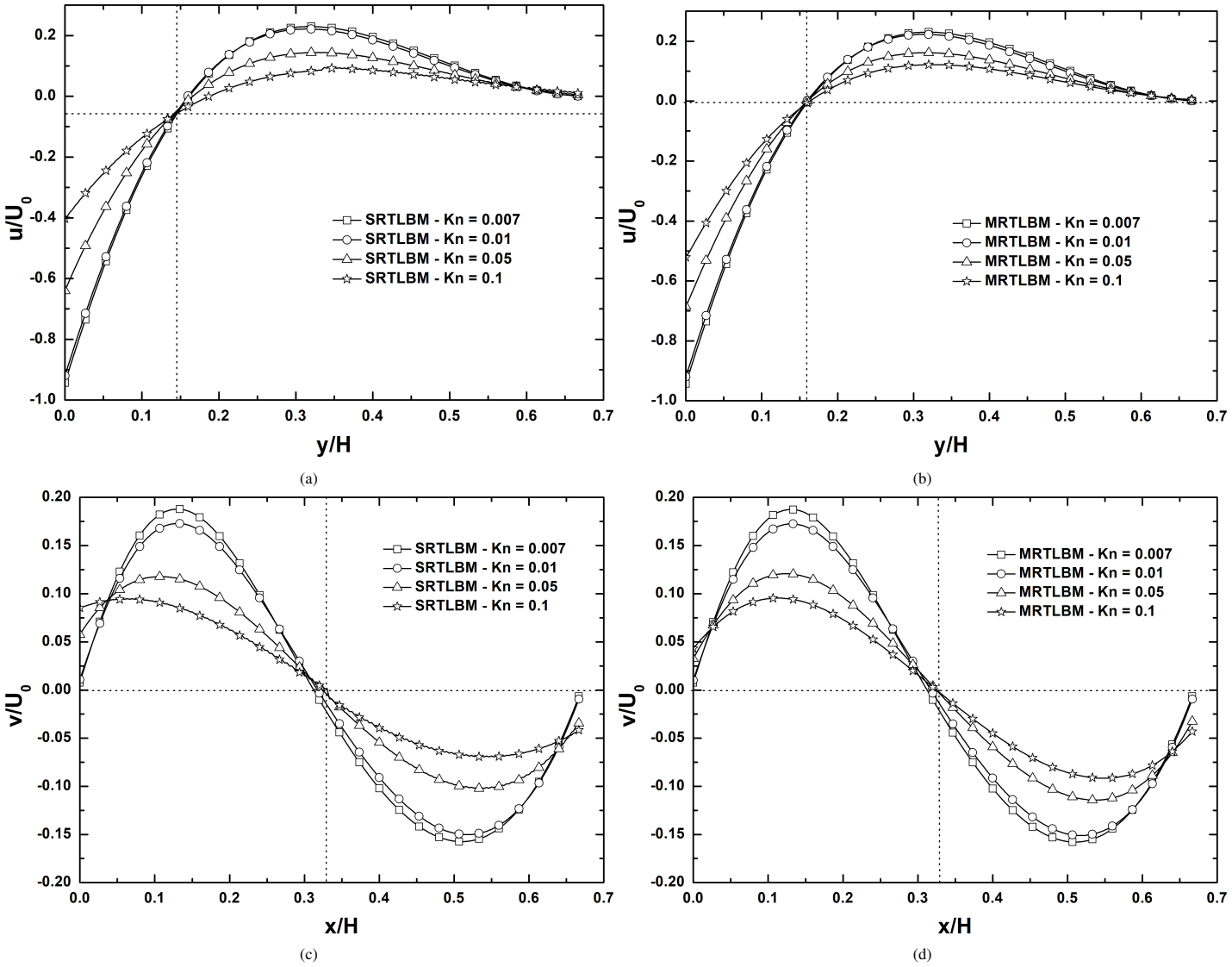

Figure 9: (a)-(b) x-velocity profile along the vertical line $x/H = 1/3$ and (c)-(d) profile of y-velocity along the horizontal line $y/H = 1/3$ at different Knudsen numbers for $\sigma = 0.7$ - case (2).

Table 7: Primary and secondary vortices locations for different values of Kn and σ - case (2).

Approaches \ Kn		0.01	0.05	0.1
SRT-LBM ($\sigma = 0.5$)	Primary vortex	(0.3275, 0.1616)	(0.3514, 0.1709)	(0.3379, 0.1944)
	Secondary vortex	(0.0871, 0.7438)	– – – – –	– – – – –
MRT-LBM	Primary vortex	(0.3272, 0.1612)	(0.3508, 0.1653)	(0.3537, 0.1709)
	Secondary vortex	(0.1069, 0.7517)	(0.0879, 0.8217)	– – – – –
SRT-LBM ($\sigma = 0.7$)	Primary vortex	(0.3296, 0.1597)	(0.3539, 0.1653)	(0.3404, 0.1870)
	Secondary vortex	(0.0896, 0.7329)	– – – – –	– – – – –
MRT-LBM	Primary vortex	(0.3293, 0.1594)	(0.3536, 0.1596)	(0.3555, 0.1630)
	Secondary vortex	(0.1098, 0.7417)	(0.1020, 0.7727)	(0.0912, 0.8133)

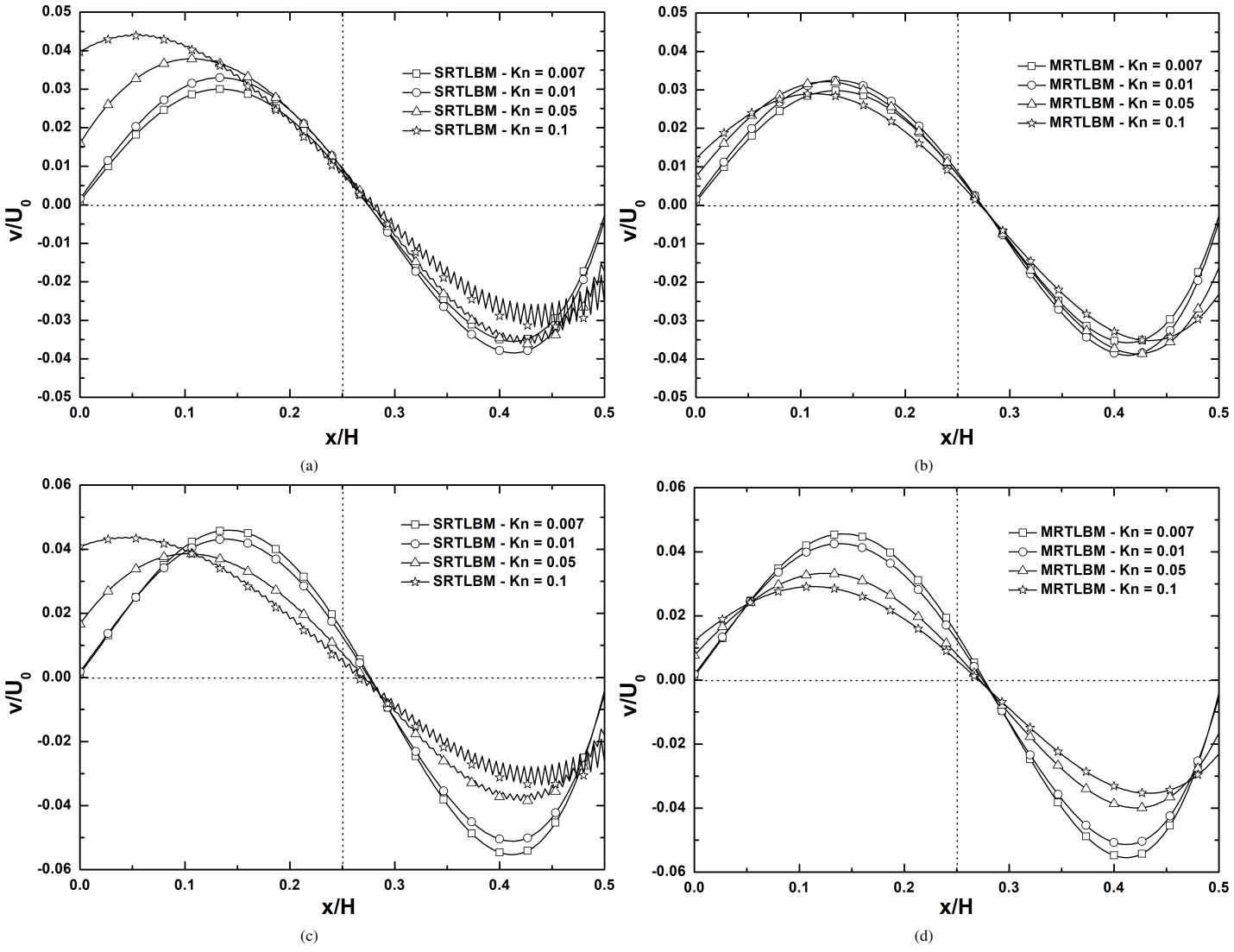

Figure 10: Profile of y-velocity along the horizontal line $y/H = 0.5$ at different Knudsen numbers for $\sigma = 0.7$ (a) SRT-LBM - case (1) (b) MRT-LBM - case (1) (c) SRT-LBM - case (2) and (d) MRT-LBM - case (2).

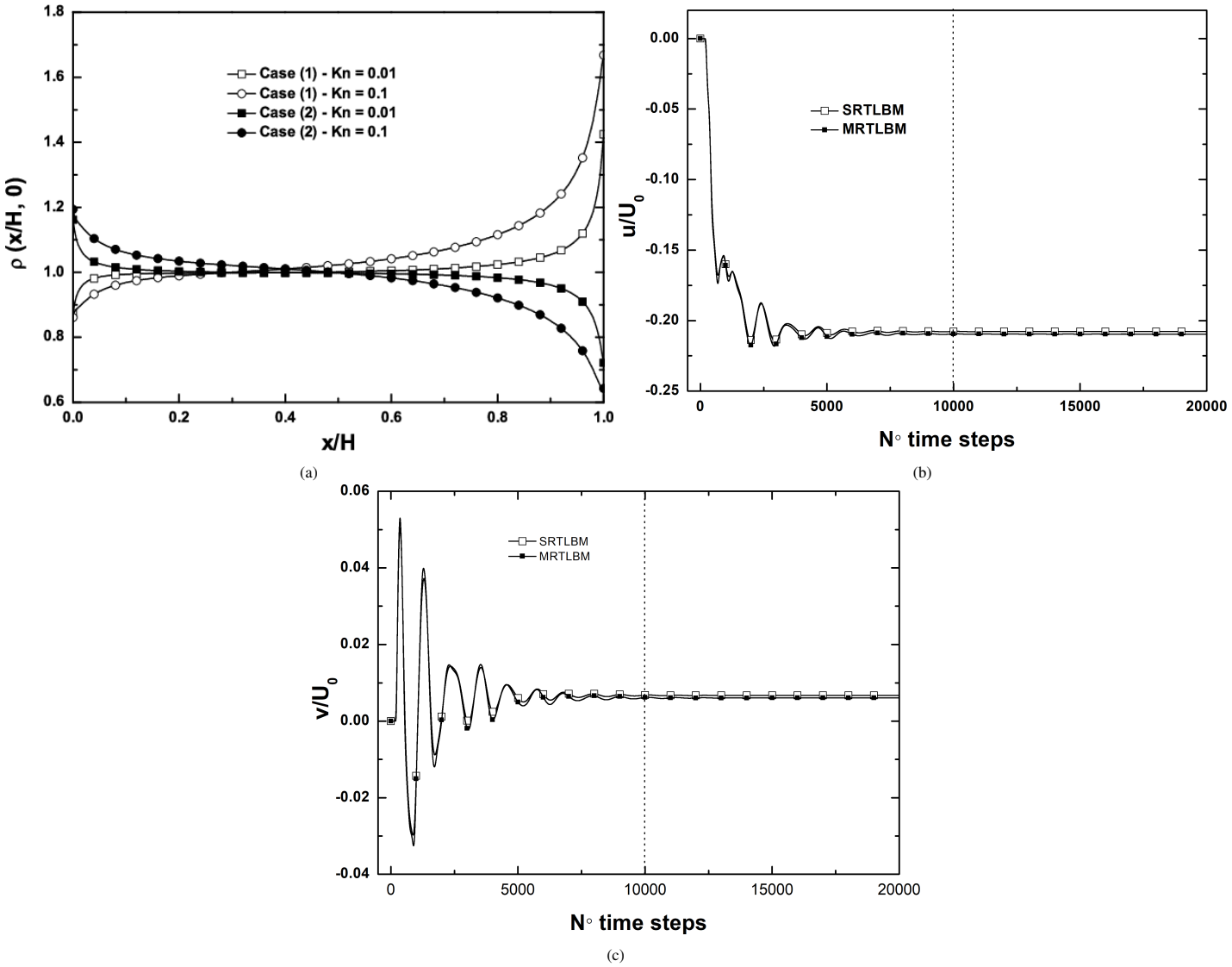

Figure 11: For $\sigma = 0.7$. (a) Density along the moving wall for $Kn = 0.01$ and $Kn = 0.1$ for both cases by using the MRT-LBM method and (b)-(c) Evolution of x and y-velocities at the center of gravity of the micro-cavity as a function of time for $Kn = 0.01$ by using both methods - case(1).

Table 8: Coordinates $(y/H, u/U_0)$ of the common intersection points at the line $x/H = 1/3$ for $\sigma = 0.7$.

Approaches \ Cases	Case (1)	Case (2)
SRT-LBM	(0.874, 0.094)	(0.145, −0.005)
MRT-LBM	(0.866, 0.064)	(0.159, −0.004)

Table 9: Execution time for 1000 iterations.

Approaches \ Mesh	**200 × 200**	**300 × 300**	**400 × 400**
SRT-LBM	10.4s	21.4s	37.3s
MRT-LBM	30.8s	65.4s	113.3s

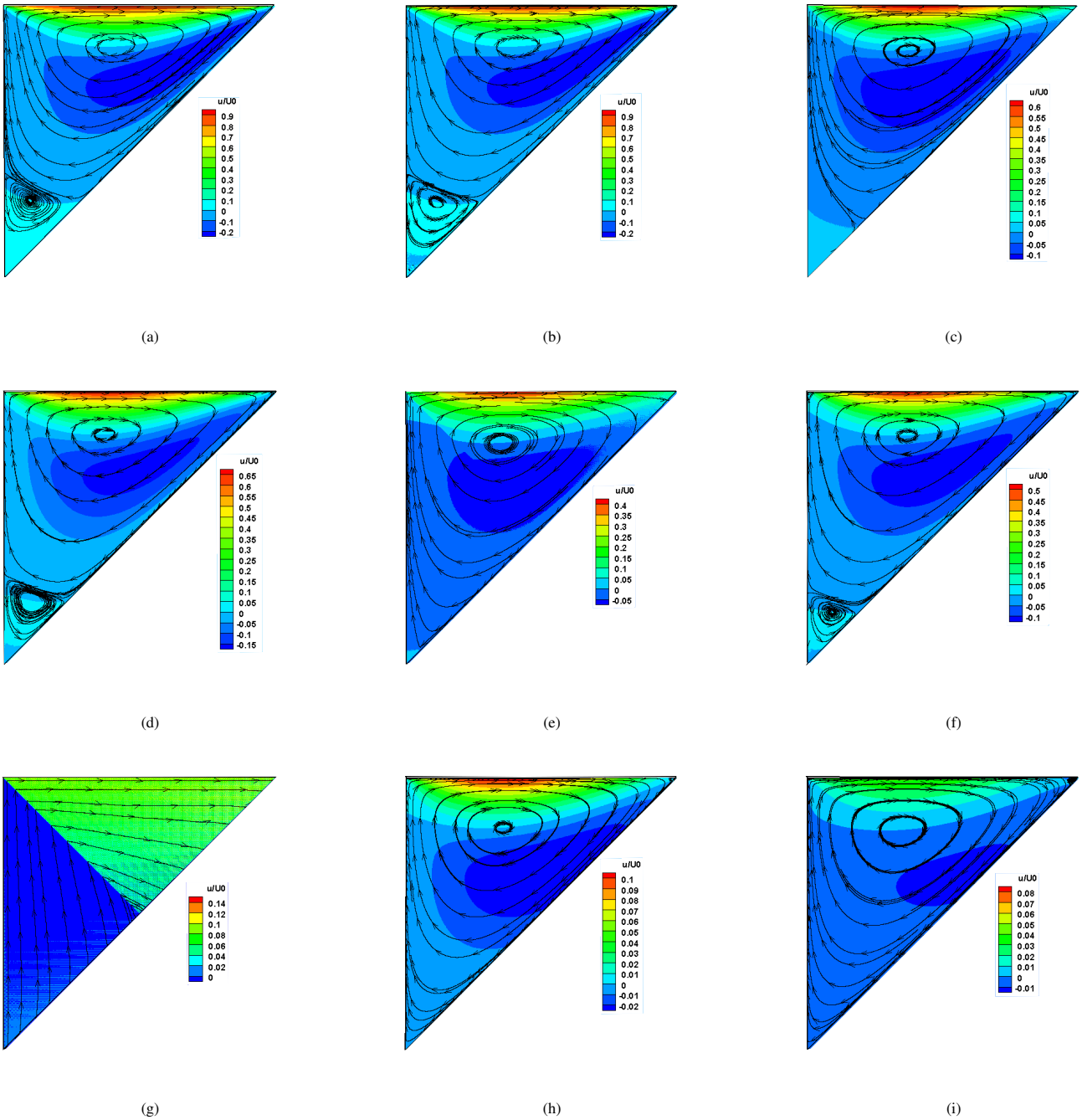

Figure 12: The flow streamlines and x-velocity contours for $\sigma = 0.7$ (case (1)) (a) SRT-LBM $-Kn = 0.007$ (b) MRT-LBM $-Kn = 0.007$ (c) SRT-LBM $-Kn = 0.05$ (d) MRT-LBM $-Kn = 0.05$ (e) SRT-LBM $-Kn = 0.1$ (f) MRT-LBM $-Kn = 0.1$ (g) SRT-LBM $-Kn = 1$ (h) MRT-LBM $-Kn = 1$ and (i) MRT-LBM $-Kn = 3$.

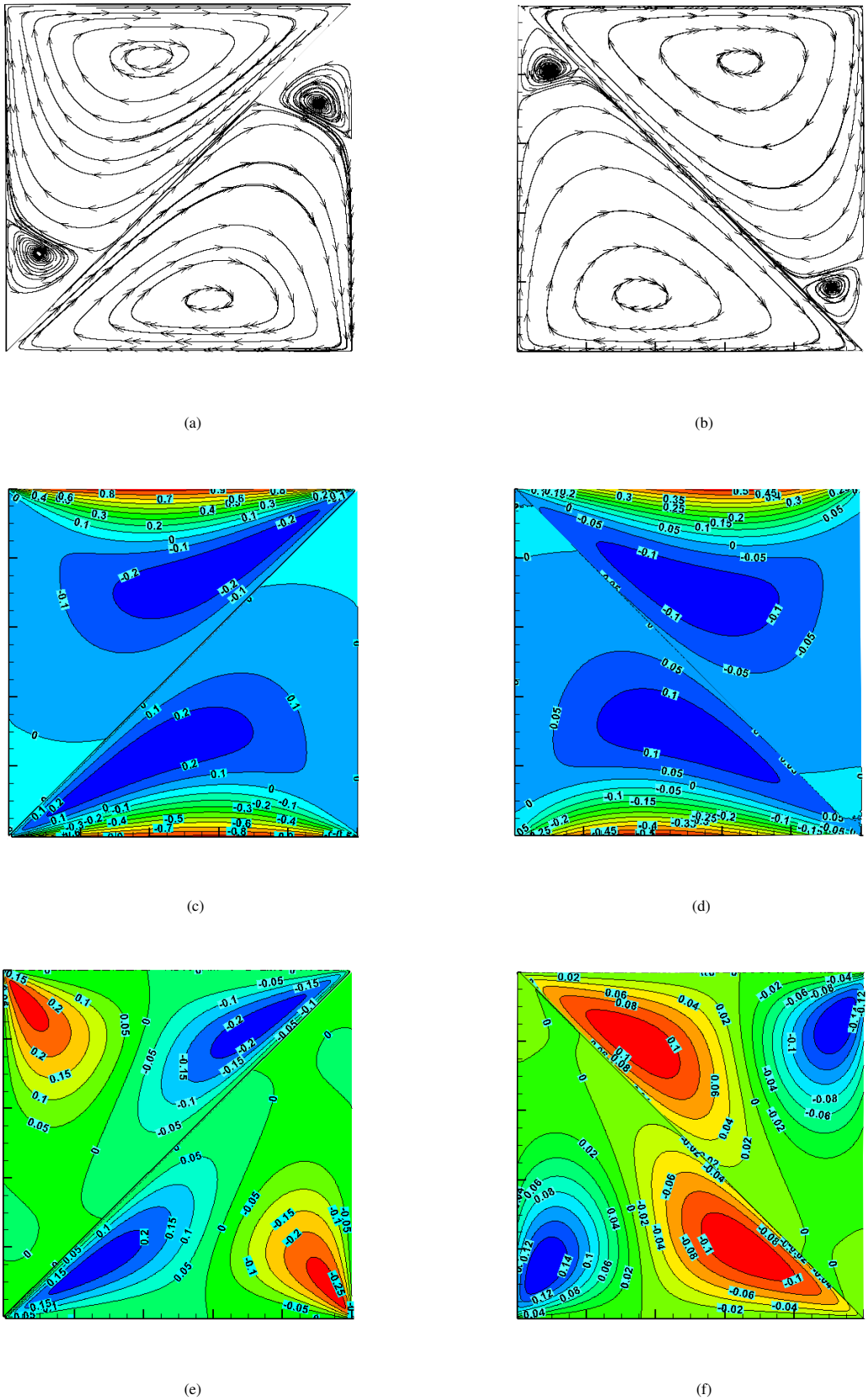

(a) (b)

(c) (d)

(e) (f)

Figure 13: The flow streamlines, x and y-velocities contours for $\sigma = 0.7$, respectively. (a, c and e) SRT-LBM $-Kn = 0.007$ (case (1) with its corresponding anti-symmetric shape) and (b, d and f) MRT-LBM $-Kn = 0.1$ (case (2) with its corresponding anti-symmetric shape).

5 Conclusion

In the current paper, a comparison between SRT-LBM and MRT-LBM confirms MRT-LBM method's ability to simulate rarefied gas flows. A lid-driven flow inside an isosceles triangular cavity is investigated numerically. The range of Knudsen numbers discussed is from the slip to the early transition regime. To capture non-equilibrium effects near the walls slip boundary conditions are used. It is clear that the SRT-LBM loses its validity with increasing the rarefaction degree while the MRT-LBM findings approximate well with those obtained by the DSMC method. To sum up, this research reveals many interesting characteristics of micro lid-driven microflows. In the slip regime, for small values of the Knudsen number, the results demonstrate that both methods are good alternatives, but in the transition regime, only MRT-LBM shows its capability to describe the gas microflows usually found in the MEMS/NEMS devices.

Nomenclature

H, L	Cavity height and length
t	Time
Kn	Knudsen number
Re	Reynolds number
R	Gas constant
c	Lattice speed
c_s	Speed of sound
$\mathbf{c}_k$	Lattice velocity vector
$\mathbf{u}$	Velocity vector
U_0	Velocity of the moving wall
f	Density distribution function
f_{eq}	Equilibrium density distribution function
w_k	Weight factors in the equilibrium distribution
M	Transformation matrix for D2Q9 scheme
$\mathbf{m}$	Moment vectors
$\mathbf{m}^{eq}$	Equilibrium moment vectors
S	Collision matrix
Greek Symbols	
λ	Mean free path
Δt	Time step
Δx, Δy	Lattice spacing in x and y directions
τ	Momentum relaxation time
σ	Tangential Momentum Accommodation Coefficient (TMAC)
ρ	Density

Conflict of Interest

The authors declared no potential conflicts of interest with respect to the research, authorship and publication of this article.

Acknowledgments

The authors wish to express their cordial thanks to the Editors and Reviewers for their valuable suggestions and constructive comments whish have served to improve the quality of this paper.

Funding

The authors received no financial support for the research, authorship and publication of this article.

References

[1] M. Gad-El-Hak, "The fluid mechanics of microdevices—the freeman scholar lecture," Journal of Fluids Engineering, Transactions of the ASME, **121**(1), 5–33, 1999, doi:10.1115/1.2822013.

[2] U. Ghia, K. N. Ghia, C. Shin, "High-Re solutions for incompressible flow using the Navier-Stokes equations and a multigrid method," Journal of computational physics, **48**(3), 387–411, 1982, doi:10.1016/0021-9991(82)90058-4.

[3] K. Ghasemi, M. Siavashi, "Three-dimensional analysis of magnetohydrodynamic transverse mixed convection of nanofluid inside a lid-driven enclosure using MRT-LBM," International Journal of Mechanical Sciences, **165**, 105199, 2020, doi:10.1016/j.ijmecsci.2019.105199.

[4] A. Bo, F. Mellibovsky, J. Bergadà, W. Sang, "Towards a better understanding of wall-driven square cavity flows using the lattice Boltzmann method," Applied Mathematical Modelling, **82**, 469–486, 2020, doi:10.1016/j.apm.2020.01.057.

[5] T. Huang, H.-C. Lim, "Simulation of Lid-Driven Cavity Flow with Internal Circular Obstacles," Applied Sciences, **10**(13), 4583, 2020, doi:10.3390/app10134583.

[6] J. Baliti, M. Hssikou, M. Alaoui, "Rarefaction and external force effects on gas microflow in a lid-driven cavity," Heat Transfer—Asian Research, **48**(1), 80–99, 2019, doi:10.1002/htj.21369.

[7] S. Mizzi, D. R. Emerson, S. K. Stefanov, R. W. Barber, J. M. Reese, "Effects of rarefaction on cavity flow in the slip regime," Journal of computational and theoretical nanoscience, **4**(4), 817–822, 2007, doi:10.1166/jctn.2007.2374.

[8] A. Mohammadzadeh, E. Roohi, H. Niazmand, "Simulation of Rarefied Gas Flow in Micro/Nano Cavity Using DSMC," in 10th Iranian Aerospace Society Conference, 2011.

[9] B. John, X.-J. Gu, D. R. Emerson, "Investigation of heat and mass transfer in a lid-driven cavity under nonequilibrium flow conditions," Numerical Heat Transfer, Part B: Fundamentals, **58**(5), 287–303, 2010, doi:10.1080/10407790.2010.528737.

[10] A. Mohammadzadeh, A. Rana, H. Struchtrup, "DSMC and R13 modeling of the adiabatic surface," International Journal of Thermal Sciences, **101**, 9–23, 2016, doi:10.1016/j.ijthermalsci.2015.10.007.

[11] A. Rana, M. Torrilhon, H. Struchtrup, "A robust numerical method for the R13 equations of rarefied gas dynamics: Application to lid driven cavity," Journal of Computational Physics, **236**, 169–186, 2013, doi:10.1016/j.jcp.2012.11.023.

[12] G. A. Bird, J. Brady, Molecular gas dynamics and the direct simulation of gas flows, volume 5, Clarendon press Oxford, 1994.

[13] F. Sharipov, Rarefied gas dynamics: fundamentals for research and practice, John Wiley & Sons, 2015.

[14] D. A. Perumal, G. V. Kumar, A. K. Dass, "Application of Lattice Boltzmann Method to Fluid Flows in Microgeometries." CFD letters, **2**(2), 2010.

[15] D. A. Perumal, V. Krishna, G. Sarvesh, A. K. Dass, "Numerical Simulation of Gaseous Microflows by Lattice Boltzmann Method," International Journal on Production and Industrial Engineering, **2**(1), 11, 2011.

[16] A. Rahmati, S. Niazi, "Application and comparison of different lattice Boltzmann methods on non-uniform meshes for simulation of micro cavity and micro channel flow," Computational Methods in Engineering, **34**(1), 97–118, 2015, doi:10.18869/ACADPUB.JCME.34.1.97.

[17] A. Rahmati, S. Niazi, "A multi relaxation time lattice Boltzmann method for simulation of flow in micro devices," in Proc. 19th Annual Int. Conf. on Mechanical Engineering, Birjand, Iran, 2011.

[18] G. Tang, W. Tao, Y. He, "Lattice Boltzmann method for gaseous microflows using kinetic theory boundary conditions," Physics of Fluids, **17**(5), 058101, 2005, doi:10.1063/1.1897010.

[19] G. Tang, W. Tao, Y. He, "Simulating two-and three-dimensional microflows by the lattice Boltzmann method with kinetic boundary conditions," International Journal of Modern Physics C, **18**(05), 805–817, 2007, doi:10.1142/S0129183107010577.

[20] Y. Elguennouni, M. Hssikou, J. Baliti, R. Ghafiri, M. Alaoui, "SRT-LBM and MRT-LBM comparison for a lid-driven gas microflow," in 2020 1st International Conference on Innovative Research in Applied Science, Engineering and Technology (IRASET), 1–6, IEEE, 2020, doi:10.1109/IRASET48871.2020.9092233.

[21] X. Nie, G. D. Doolen, S. Chen, "Lattice-Boltzmann simulations of fluid flows in MEMS," Journal of statistical physics, **107**(1-2), 279–289, 2002, doi:10.1023/A:1014523007427.

[22] C. Lim, C. Shu, X. Niu, Y. Chew, "Application of lattice Boltzmann method to simulate microchannel flows," Physics of fluids, **14**(7), 2299–2308, 2002, doi:10.1063/1.1483841.

[23] G. Tang, W. Tao, Y. He, "Thermal boundary condition for the thermal lattice Boltzmann equation," Physical Review E, **72**(1), 016703, 2005, doi:10.1103/PhysRevE.72.016703.

[24] X. Niu, C. Shu, Y. Chew, "Numerical Simulation of Isothermal Micro Flows by Lattice Boltzmann Method and theoretical analysis of the Diffuse scattering boundary condition," International Journal of Modern Physics C, **16**(12), 1927–1941, 2005, doi:10.1142/S0129183105008448.

[25] Q. Zou, X. He, "On pressure and velocity boundary conditions for the lattice Boltzmann BGK model," Physics of Fluids, **9**(6), 1591–1598, 1997, doi:10.1063/1.869307.

[26] P. L. Bhatnagar, E. P. Gross, M. Krook, "A model for collision processes in gases. I. Small amplitude processes in charged and neutral one-component systems," Physical review, **94**(3), 511, 1954, doi:10.1103/PhysRev.94.511.

[27] G. Karniadakis, A. Beskok, N. Aluru, Microflows and nanoflows: fundamentals and simulation, volume 29, Springer Science & Business Media, 2006.

[28] M. Hssikou, J. Baliti, Y. Bouzineb, M. Alaoui, "DSMC method for a two-dimensional flow with a gravity field in a square cavity," Monte Carlo Methods and Applications, **21**(1), 59–67, 2015, doi:10.1515/mcma-2014-0009.

[29] M. Hssikou, J. Baliti, M. Alaoui, "Extended macroscopic study of dilute gas flow within a microcavity," Modelling and Simulation in Engineering, **2016**, 2016, doi:10.1155/2016/7619746.

[30] Y. Zhang, R. Qin, Y. Sun, R. Barber, D. Emerson, "Gas flow in microchannels–a lattice Boltzmann method approach," Journal of Statistical Physics, **121**(1-2), 257–267, 2005, doi:10.1007/s10955-005-8416-9.

[31] S. Ansumali, I. V. Karlin, "Kinetic boundary conditions in the lattice Boltzmann method," Physical Review E, **66**(2), 026311, 2002, doi:10.1103/PhysRevE.66.026311.

[32] E. Erturk, O. Gokcol, "Fine grid numerical solutions of triangular cavity flow," The European Physical Journal Applied Physics, **38**(1), 97–105, 2007, doi:10.1051/epjap:2007057.

[33] F. Munir, N. A. Che Sidik, M. Rody, H. Zahir, M. Tahir, "Numerical simulations of shear driven square and triangular cavity by using Lattice Boltzmann scheme," World Academy of Science, Engineering and Technology, **70**, 190–194, 2010.

[34] F. A. Munir, M. I. M. Azmi, M. R. M. Zin, M. A. Salim, N. A. C. Sidik, "Application of lattice Boltzmann method for lid driven cavity flow," International Review of Mechanical Engineering, **5**(5), 856–861, 2011.

[35] M. Idris, C. Nor Azwadi, N. N. Izual, "Vortex structure in a two dimensional triangular lid-driven cavity," in AIP Conference Proceedings, volume 1440, 1078–1084, American Institute of Physics, 2012, doi:10.1063/1.4704323.

[36] M. Nazari, "LBM for modeling cavities with curved and moving boundaries," Modares Mechanical Engineering, **13**(5), 117–129, 2013.

[37] B. An, J. M. Bergadà Granyó, "Numerical study of the 2D lid-driven triangular cavities based on the Lattice Boltzmann method," in Proceedings of the 3rd Annual International Conference on Mechanics and Mechanical Engineering:(MME 2016), 945–953, Atlantis Press, 2016, doi:10.2991/mme-16.2017.133.

[38] E. Roohi, V. Shahabi, A. Bagherzadeh, "On the vortical characteristics and cold-to-hot transfer of rarefied gas flow in a lid driven isosceles orthogonal triangular cavity with isothermal walls," International Journal of Thermal Sciences, **125**, 381–394, 2018, doi:10.1016/j.ijthermalsci.2017.12.005.

ASTES

Advances in Science, Technology and Engineering Systems Journal Vol. 5, No. 6, 606-612 (2020)

www.astesj.com

Special Issue on Innovative Research in Applied Science, Engineering and Technology

ASTESJ

ISSN: 2415-6698

Fast and efficient Maximum Power Point Tracking controller for photovoltaic modules

Khalid Chennoufi*, Mohammed Ferfra

Department of Electrical Engineering, Mohammadia School of Engineers, Mohammed V University in Rabat, Rabat, PB765, Morocco

ARTICLE INFO

Article history:
Received: 31 July, 2020
Accepted: 06 November, 2020
Online: 24 November, 2020

Keywords:
Artificial Neural Network
Backstepping
MPPT
Double diode model
SEPIC

ABSTRACT

This paper presents an efficient Maximum Power Point Tracking (MPPT) controller for photovoltaic modules. The MPPT technique consists of a combination between backstepping controller and artificial neural network (ANN).The (ANN) has been employed to generate the optimum voltage, which corresponds to the maximum power voltage delivered by photovoltaic modules, while the backstepping controller is developed to track the generated voltage, by computing the duty cycle of the Single Ended Primary Inductor Converter (SEPIC). The control of the boost converter is based on Lyapunov stability analysis, and an integral action is added to increase system robustness. In order to prove the accuracy of the developed control a comparison between the proposed method and sliding mode was carried out. In addition the stability was evaluated under sudden variation of environmental conditions. The simulation was carried out in MATLAB software, the results shows that the proposed controller tracks the reference voltage within 25 ms, in addition the systems reacts to sudden environments change with no oscillations, which demonstrate the robustness of the proposed method.

1. Introduction

In recent years, the demand of electrical energy increases, which reduces the reserves of the conventional resources and increases the global warming, therefore the use of renewable energies is the only way to reduce the dependence on fossil fuels and ensure the energy security. In fact, photovoltaic energy is the most popular renewable energy source, however, the output power relies on weather conditions and the load. This led the researchers to present various algorithms that make photovoltaic modules operates in the maximum power point. Thus a various Maximum Power Point Tracking algorithms with different degrees of complexity and precision have been proposed in the literature [1-3]. The perturb and the observe, and incremental conductance [4], methods are often used due to their simplicity and ease of implementation, however their main drawback is the fluctuations around the point of maximum power.

Thus to overcome the oscillations issues and increase the performance of the tracking a combination between direct control methods and the nonlinear commands has been employed by the researchers.

In [5], Authors propose a maximum power point tracking controller for hybrid Photovoltaic - Wind energy system. The controller is developed by the combination of perturb & observe and Sliding Mode. P&O loop is used for the computation of the reference voltage, while Sliding Mode is designed to track this voltage by generating the control signal. The proposed method exhibits good convergence speed, but the main disadvantage is the oscillations around maximum power point.

In [6], Authors present a control of a single-phase Photovoltaic inverter using backstepping algorithm which track the desired voltage generated by Perturb and Observe method and adjust the duty cycle in order to operate in maximum power point. The error between the output and reference voltage was eliminated quickly, but some fluctuations have been observed in the desired operating point.

In [7], Authors propose a maximum power point tracking controller for Photovoltaic system. The controller is developed by the combination of Sliding Mode and Artificial Neural Network (ANN). The ANN is employed to generate the reference voltage, while Sliding Mode is designed to track this voltage by generating the control signal. The proposed method presents good

*Corresponding Author: Khalid Chennoufi, Tel: +212 668 01 15 90, khalidchennoufi@research.emi.ac.ma

performance; however, some oscillations is noticed around maximum power point.

In order to overcome fluctuation issues around maximum power point, this paper proposes a hybrid method, which consists of a backstepping controller combined to the Artificial Neural Network (ANN). The ANN is employed to generate the reference voltage, while backstepping controller is designed to adjust the duty cycle of the converter in order to track the desired voltage, which corresponds to the voltage of the Maximum Power Point, (Fig1).

In contrast of previous methods which adopt single diode model, the photovoltaic modelling was carried out using double diode model, as the modelling using single diode degrade at low irradiance. In addition the present work doesn't rely on any simplification which can compromise the accuracy of the controller modelling, furthermore the SEPIC converter was employed since it offer more advantages instead of the traditional converter.

The present paper is organized as follows. In Section 2, the modelling of the PV system is presented. The Section 3, presents the design of the proposed controller. The simulations and discussions are illustrated in Section 4.

2. Modelling of PV system

The Photovoltaic system proposed in this paper consists of a photovoltaic module connected to a resistive load through a Single ended primary converter as shown in Figure 1.

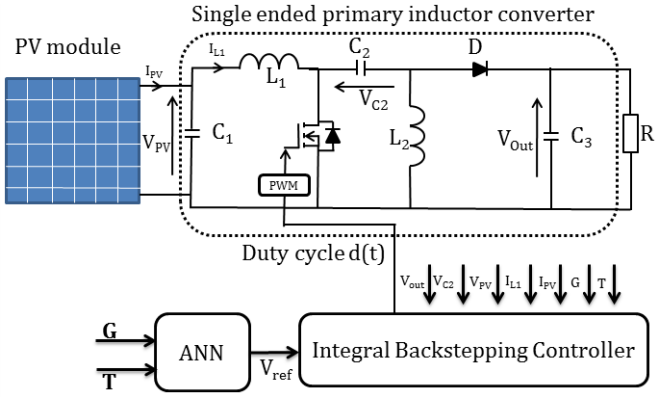

Figure 1: Illustration of the proposed Photovoltaic system.

Where V_{out}, V_{c2}, V_{PV} are the output voltage, the voltage across the capacitor C_2, and the photovoltaic voltage respectively, I_{pv} and I_{L1} are the photovoltaic and inductor 1 currents, While G and T are respectively the irradiation and the Temperature.

The datasheet parameters of the polycrystalline photovoltaic module KD 245 GH are presented in Table 1.

Table 1: PV module datasheet

Parameter	Value
Short-circuit current (I_{sc})	8.91(A)
Open circuit voltage (V_{oc})	36.9 (V)
Maximum current (I_m)	8.23 (A)
Maximum voltage (V_m)	29.8 (V)
Number of cells in series (N_s)	60
Temperature coefficient of current (k_i)	5.35×10^{-3} (A/K)
Temperature coefficient of voltage (K_V)	-0.133(V/K)

2.1. Modelling of the SEPIC converter

The SEPIC is an acronym of (single ended primary inductor converter), which is a DC-DC converter capable to operate as boost or buck mode [8], that offer the possibility to raise or decrease the voltage at the output [9]. In addition the SEPIC converter makes the PV system operate at its maximum power point with 'weak current ripples [10]. Furthermore it can work on any operating point by changing the duty cycle [11]. The converter is modelled mathematically based on these states [12] as shown in figure 2.

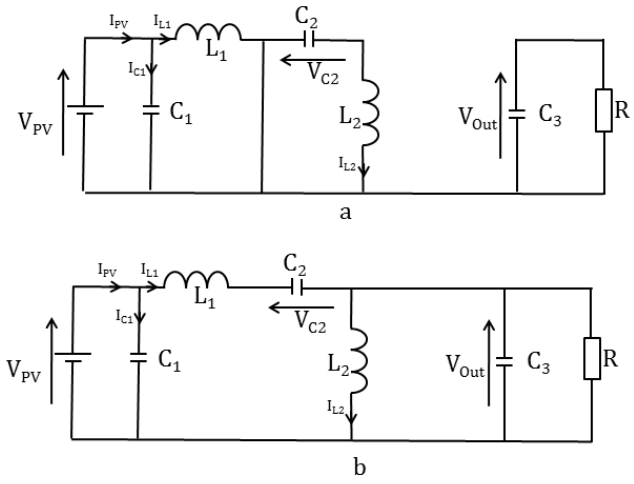

Figure 2: SEPIC converter circuit, (a) Equivalent circuit switch is ON (b) switch is OFF

When the commutator is on (u=1) as shown in figure 2-a. The capacitor C_3 supplies energy to the load and the energy stored in the inductances increases, the inductor L1 is alimented from the input while the inductor L_2 is feeded from the capacitor C_2. The representation of state space can be described as

$$\frac{dI_{L1}}{dt} = \frac{V_{PV}}{L_1} \quad (1)$$

$$\frac{dI_{L2}}{dt} = \frac{-V_{C2}}{L_2} \quad (2)$$

$$\frac{dV_{c2}}{dt} = \frac{I_{L2}}{C_2} \quad (3)$$

When the commutator is off (u=0) as shown in figure 2-b. The two inductors are discharged and the energy stored in the capacitors increases. The representation of state space can be written as:

$$\frac{dI_{L1}}{dt} = \frac{V_{PV} - V_{C2} - V_{out}}{L_1} \quad (4)$$

$$\frac{dI_{L2}}{dt} = \frac{V_{out}}{L_2} \quad (5)$$

$$\frac{dV_{C2}}{dt} = \frac{I_{L1}}{C_2} \quad (6)$$

The combination between the two state spaces can be expressed as:

$$\frac{dI_{L1}}{dt} = \frac{(u-1)V_{C2}}{L_1} + \frac{(u-1)V_{out}}{L_1} + \frac{V_{PV}}{L_1} \quad (7)$$

$$\frac{dV_{C2}}{dt} = \frac{(1-u)I_{L1}}{C_2} + \frac{uI_{L2}}{C_2} \quad (8)$$

$$\frac{dI_{L2}}{dt} = -\frac{dV_{C2}}{L_2} + \frac{(1-u)V_{out}}{L_2} \quad (9)$$

$$\frac{dV_0}{dt} = \frac{(1-u)I_{L1}}{C_3} + \frac{(u-1)I_{L2}}{C_3} - \frac{V_{out}}{RC_3} \quad (10)$$

where u=(0 or 1)

2.2. Modelling of the Photovoltaic module

In this work the modelling of a solar module is developed based on double diode model which is illustrated in figure 3, where the first diode describes the saturation currents due to diffusion mechanism, while the second diode describes the current due to recombination in the depletion zone.

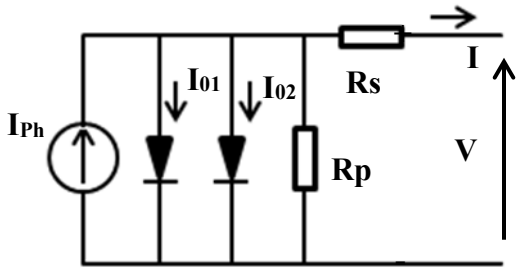

Figure 3: Illustration of the double diode model.

The output current of a solar cell is represented by:

$$I = I_{ph} - I_{01}\left(exp\left(\frac{V+R_sI}{a_1V_T}\right) - 1\right) - I_{02}\left(exp\left(\frac{V+R_sI}{a_2V_T}\right) - 1\right) - \frac{V+R_sI}{R_p} \quad (11)$$

The unknown parameters such as: a_1,a_2,I_{01},I_{02},I_{ph},R_s and R_p. are extracted using a combination between the equation of three main operating points which are, the open circuit voltage, the short circuit current and the maximum power point. The objective is to find the equations of I_{01}, I_{02}, R_p and I_{ph} which depend only of Rs, a1 and a2. The value of series resistance (Rs) and ideality factors (a_1,a_2) are obtained using a fast iteration by adjusting simulated and datasheet powers [13]. The extracted parameters are illustrated in Table 2.

The extracted parameters are integrated in a MATLAB algorithm to plot V-I and V-P curves as shown in Figs. 4, the simulation allow to predict the behaviour of the photovoltaic modules in different meteorological condition, thus when the temperature increases the open circuit voltage decrease while the short circuit current increase slightly which result a loss of generated power. On the other hand, when the solar irradiance increases both short circuit current and the open circuit voltage increase which raise the generated power.

Table 2: Extracted Parameters of KD 245GH module

Parameter	Value
a_1	1.005879
a_2	1.994120
I_{ph} (A)	8.931164
I_{01} (A)	3.906668×10^{-10}
I_{02} (A)	1.094485×10^{-06}
R_s (Ω)	0.286199
R_p (Ω)	120.495147

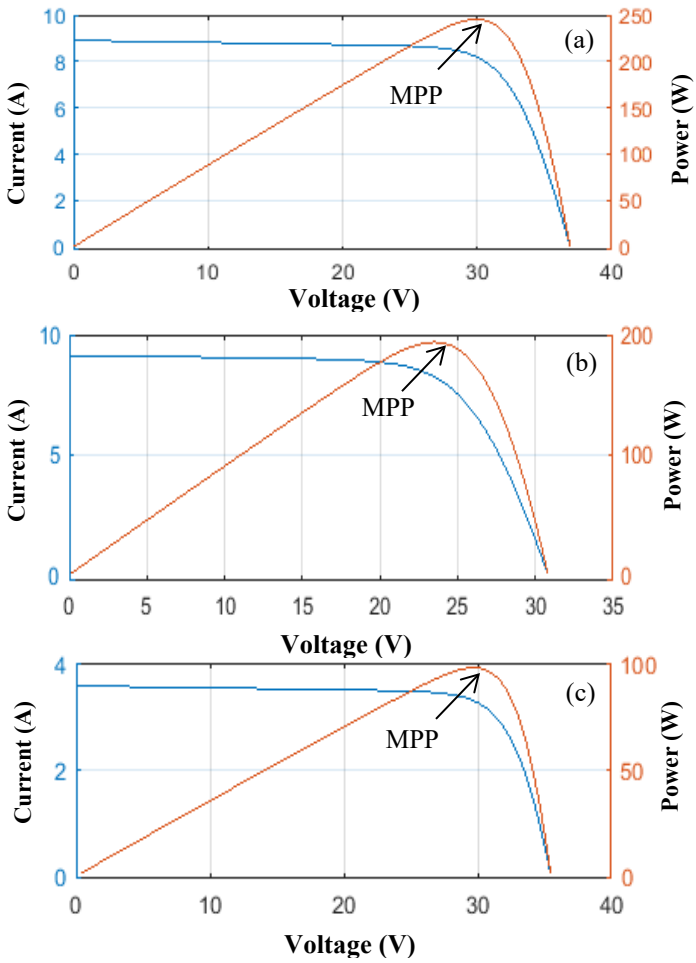

Figure 4: Generated current and power at 25°C - 1000 W/m² (a), 75°C - 1000 W/m² (b) and 25°C - 400 W/m² (c)

3. Proposed controller:

Figure 1 presents the schematic drawing of the proposed controller, it consists of a combination between Artificial Neural Network and backstepping controller. The ANN loop generates a voltage reference for every solar irradiation and temperature, which correspond to the maximum power point voltage, while the backstepping controller tracks the generated reference by adjusting the duty cycle.

3.1. Artificial Neural Network

Artificial neural network is a computational processing model based on artificial intelligence that is meant to simulate the functioning of a human brain , which consists of processing units interconnected by nodes [14]. The ANN architecture consists of three layers as shown in Figure 5, The input layer receives various forms and structures of information based on an internal weighting system, the hidden layer is where artificial neurons get an ensemble of weighted inputs and generates an output via an activation function, while and the output layer receives data from hidden layer and gives the results of the ANN [15, 16].

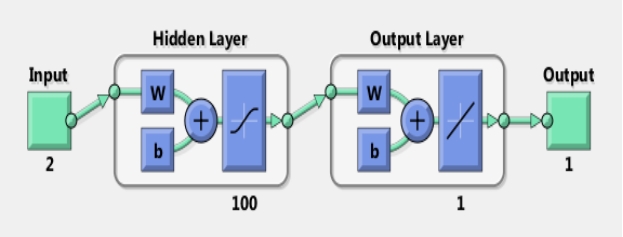

Figure 5: Proposed Neural network hierarchy

In this work the input layer was designed with two neurons, irradiation and the temperature, a database of 158 cases was created by increasing the irradiance by a step of 5 K from 278 K to 333 K and changing the irradiance for each temperature from 200 to 1050 W/m². The hidden layer was created with 100 neurons as shown in Figure 5. The output layer has only one neuron which corresponds to the voltage at maximum power of the 158 pair irradiance temperature.

3.2. Integral backstepping

The backstepping controller is designed to track the reference voltage generated by the artificial neural network by adjusting the duty cycle of the converter. The control law is generated based on Lyapunov stability analysis. The design of the controller is as follows:

The tracking error is defined as the difference between photovoltaic and reference voltages:

$$e_1 = Vpv - Vref \tag{12}$$

An integral action is added in order to improve the tracking precision as follow:

$$e = e_1 + \lambda e_{Int} \tag{13}$$

The tracking error becomes:

$$e = Vpv - Vref \quad + \lambda \int (Vpv - Vref)dt \tag{14}$$

Where λ is a positive constant

The modified Lyapunov function can be written as:

$$V_1 = \frac{1}{2} e_1^2 + \frac{\lambda}{2} e_{Int}^2 \tag{15}$$

The derivative of the (15) with respect to time is:

$$\dot{V}_1 = e_1 \left[(\dot{V}_{pv} - \dot{V}_{ref}) + \lambda \int (Vpv - Vref)dt \right] \tag{16}$$

To guarantee the asymptotic stability, the Lyapunov function has to be negative definite derivative:

$$\dot{V}_1 = -K_1 e_1^2 \tag{17}$$

where K_1 is a positive constant

The following equation is obtained:

$$\left[(\dot{V}_{pv} - \dot{V}_{ref}) + \lambda \int (Vpv - Vref)dt \right] = -K_1 e_1 \tag{18}$$

The photovoltaic current is given by:

$$I_{PV} = I_{C1} + I_{L1} \tag{19}$$

The derivative of photovoltaic tension can be written as:

$$\dot{V}_{pv} = \frac{I_{PV} - I_{L1}}{C_1} \tag{20}$$

The desired value of inductor current would be:

$$I_d = I_{PV} + C_1 \left[(K_1 e_1 - \dot{V}_{ref}) + \lambda \int (Vpv - Vref)dt \right] \tag{21}$$

where (I_d=I_{L1})

The second error represents the difference between the inductor and the desired current:

$$e_2 = I_{L1} - I_d \tag{22}$$

The derivative of Lyapunov function with respect to the time can be expressed as

$$\dot{V}_1 = e_1 \left[\left(\frac{I_{PV} - (e_2 + I_d)}{C_1} - \dot{V}_{ref} \right) + \lambda \int (Vpv - Vref)dt \right] \tag{23}$$

By using equation (18) and (20) the above equation can be written as

$$\dot{V}_1 = -k_1 e_1^2 - \frac{e_1 e_2}{C_1} \tag{24}$$

The time derivative of (22), using equation (9) can be written as:

$$\dot{e}_2 = \frac{1}{L_1} V_{pv} - \frac{1}{L_1} (1 - u)(V_{out} + V_{c2}) - \dot{I}_d \tag{25}$$

Where:

$$\dot{I}_d = \dot{I}_{PV} + C_1 \left[(K_1 e_1 - \ddot{V}_{ref}) + \lambda (Vpv - Vref) \right] \tag{26}$$

The derivative of photovoltaic current with respect to the time can be expressed as:

$$\dot{I}_{PV} = \frac{dI_{PV}}{dV_{PV}}\frac{dV_{PV}}{dt} \quad (27)$$

By differentiating the equation (11) with respect to the voltage the derivative of photovoltaic current is obtained:

$$\dot{I}_{PV} = \left[-\frac{I_{01}\exp\left(\frac{V + R_s I_{PV}}{a_1 V_T}\right)}{a_1 V_T} - \frac{I_{02}\exp\left(\frac{V + R_s I_{PV}}{a_2 V_T}\right)}{a_2 V_T} - \frac{1}{R_P}\right]\dot{V}_{PV} \quad (28)$$

In order to guarantee the asymptotic stability of the system and the convergence of the errors e_1 and e_2 to zero, a composite Lyapunov function V_2 is defined as:

$$V_2 = V_1 + \frac{1}{2}e_2^2 \quad (29)$$

The derivative of V_2 with respect to the time is:

$$\dot{V}_2 = \dot{V}_1 + e_2\dot{e}_2 \quad (30)$$

By using equation (24) the derivative of V_2 can be expressed as:

$$\dot{V}_2 = -K_1 e_1^2 + e_2\left[\frac{1}{L_1}V_{pv} - \frac{1}{L_1}(1-u)(V_{out} + V_{c2}) - \dot{I}_d - \frac{e_1}{C_1}\right] \quad (31)$$

The time derivative of Lyapunov function has to be negative definite:

$$\frac{1}{L_1}V_{pv} - \frac{1}{L_1}(1-u)(V_{out} + V_{c2}) - \dot{I}_d - \frac{e_1}{C_1} = -K_2 e_2 \quad (32)$$

where K_2 is a positive constant

The control law, which guarantees e_1, e_2 converges asymptotically to 0, is given by:

$$u = 1 - \left[V_{PV} + L_1\left(K_2 e_2 - \frac{e_1}{C_1} - \dot{I}_d\right)\right]\frac{1}{V_{C2} + V_0} \quad (33)$$

4. Simulation results

In order to study the performance of the proposed method, a simulation was carried out in Matlab software. The parameters of the simulation are illustrated in Table 3.

Table 3: Parameters of the SEPIC

Parameter	Value
Inductor 1 (L_1)	2.5 mH
Inductor 2 (L_2)	2.5 mH
Capacitor 1 (C_1)	4500 uF
Capacitor 2 (C_2)	79 µF
Capacitor 3 (C_3)	2400 µF
Constant (λ)	1
Constant (K_1)	10^4
Constant (K_2)	10^4
Load resistor (R)	50Ω
Switching frequency (f)	7 KHz

The system being simulated into different temperature and irradiation condition as shown in Figure 6, During the first case the [0s, 20s], the PV module is consider operating under the irradiation of the maximum power point while the temperature was raised to 318 K to simulate the temperature effect. In the second case [20s, 40s], the irradiation drop smoothly from 1000 W/m² to 600 W/m² while the temperature decrease between two consecutive levels from 318 k to 307 K. In the last case [40s, 60s], the temperature is considered constant in 298K while the irradiation increase among two successive stage to reach 1000 W/m² thus the PV module is considered operating in the maximum power point.

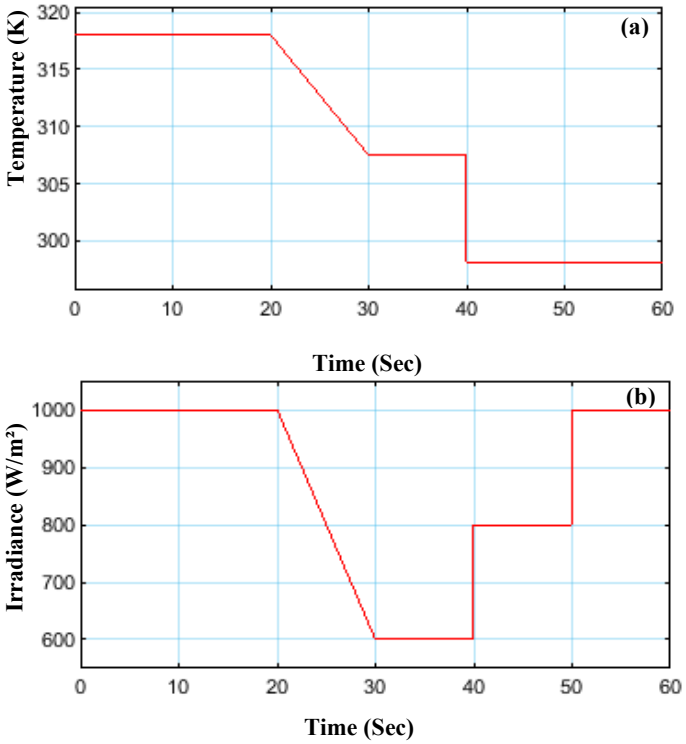

Figure 6: Temperature (a) and Irradiation (b)

Figure 7 shows that the variations in temperature and irradiation cause a slight variation in voltage and a large variation in current and power. By comparing the proposed method with the method proposed by [7] it can be seen that the proposed method bring reach the reference voltage in 25 ms, Figure (b), with high accuracy, in contrast the proposed method in [7] reaches the desired voltage with a delay of 60 ms with large oscillations. In addition the obtained curves exhibit fast and good reactions when sudden variation in temperature and irradiance occurs.

Figure 8 shows the output current, voltage and power of the PV module generated at the output of the SEPIC converter using the proposed method with the result proposed by [7]. As can be seen from the figures (a), (b) and (c), the obtained curves using sliding mode controller present large oscillations and the use of the proposed method allow reducing significantly the magnitude of the fluctuation, which guarantees good performance in the maximum point tracking.

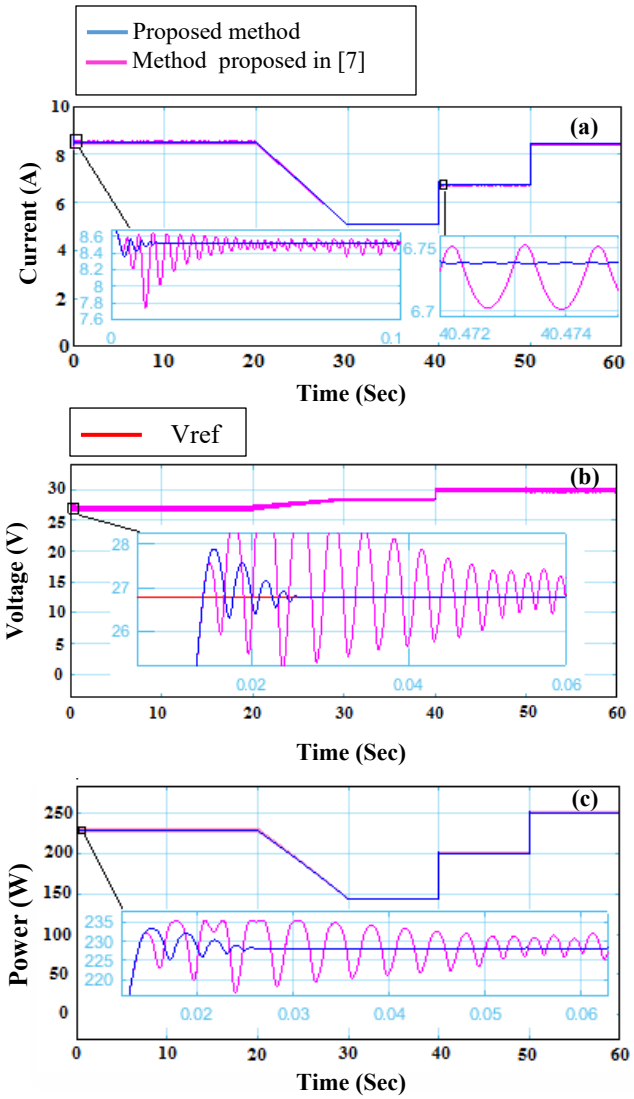

Figure 7: Photovoltaic Current (a), Voltage (b) and Power (c),

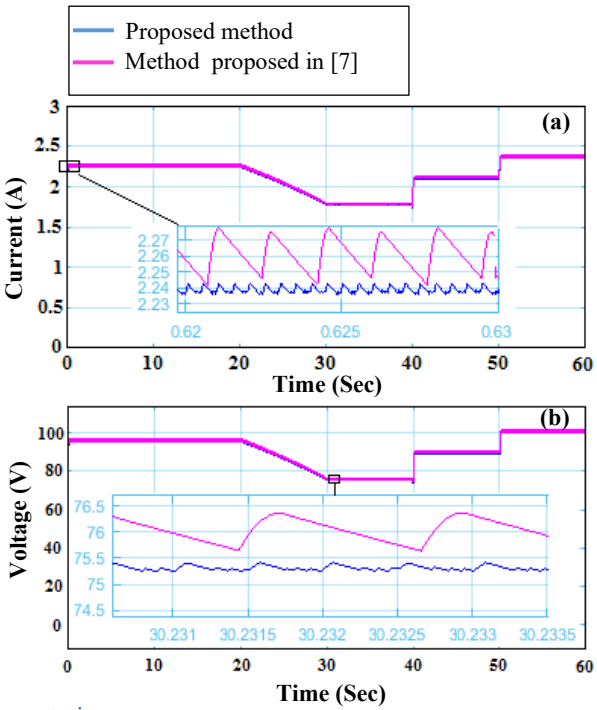

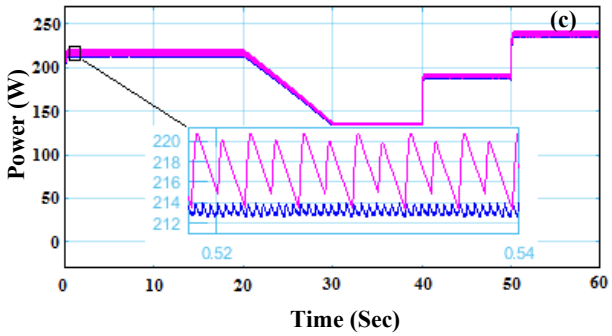

Figure 8: SEPIC output Current (a), Voltage (b) and Power (c).

5. Conclusion

In this paper an integral backstepping controller for maximum power point tracking is proposed. In order to increase the performance of tracking the controller was developed by combining backstepping controller and artificial neural network (ANN). The photovoltaic modelling was carried out using double diode model as the modelling using single diode degrade at low irradiance, and in order to reduce the current ripples the single ended primary inductor converter (SEPIC) has been employed. The simulation has been done in Matlab/Simulink software, the results show that the proposed method tracks the reference voltage with good accuracy and fast convergence speed, in addition the photovoltaic power reaches maximum power in less than 25 ms. Furthermore the obtained curves show that there are no oscillations in the output voltage, current and power. Thus the proposed method presents a fast and stable reaction when the environmental conditions changes, which confirms the effectiveness and the stability of the proposed method.

Conflict of Interest

The authors declare no conflict of interest.

References

[1] T. Esram, P.L. Chapman, "Comparison of photovoltaic array maximum power point tracking techniques," IEEE Transactions on Energy Conversion, **22**(2), 439–449, 2007, doi:10.1109/TEC.2006.874230.

[2] M.K. Dr S.R.Kapoor, "Comparison between IC and Fuzzy Logic MPPT Algorithm Based Solar PV System using Boost Converter," International Journal of Advanced Research in Electrical, Electronics and Instrumentation Engineering, **04**(06), 4927–4939, 2015, doi:10.15662/ijareeie.2015.0406007.

[3] J.P. Ram, T.S. Babu, N. Rajasekar, "A comprehensive review on solar PV maximum power point tracking techniques," Renewable and Sustainable Energy Reviews, 67, 826–847, 2017, doi:10.1016/j.rser.2016.09.076.

[4] M. Al-Dhaifallah, A.M. Nassef, H. Rezk, K.S. Nisar, "Optimal parameter design of fractional order control based INC-MPPT for PV system," Solar Energy, 159(June 2017), 650–664, 2018, doi:10.1016/j.solener.2017.11.040.

[5] O. Zebraoui, M. Bouzi, "Robust sliding mode control based MPPT for a PV/Wind hybrid energy system," International Journal of Intelligent Engineering and Systems, **11**(5), 290–300, 2018, doi:10.22266/IJIES2018.1031.27.

[6] O. Diouri, N. Es-Sbai, F. Errahimi, A. Gaga, C. Alaoui, "Modeling and Design of Single-Phase PV Inverter with MPPT Algorithm Applied to the Boost Converter Using Back-Stepping Control in Standalone Mode," International Journal of Photoenergy, **2019**, 2019, doi:10.1155/2019/7021578.

[7] S.A. Touil, N. Boudjerda, A. Boubakir, K. El Khamlichi Drissi, "A sliding mode control and artificial neural network based MPPT for a direct grid-connected photovoltaic source," Asian Journal of Control, **21**(4), 1892–1905, 2019, doi:10.1002/asjc.2007.

[8] W.M. Moussa, "Modeling and Performance Evaluation of a DC/DC SEPIC Converter," Proceedings of 1995 IEEE Applied Power Electronics Conference and Exposition, 1995, 1995, doi: 10.1109/APEC.1995.469096

[9] D. Adar, G. Rahav, S. Ben-Yaakov, "A unified behavioral average model of SEPIC converters with coupled inductors," Power Processing and Electronic Specialists Conference **1997**, 1997,doi: 10.1109/PESC.1997.616761

[10] E. Durán, M. Sidrach-De-Cardona, J. Galán, J.M. Andújar, "Comparative analysis of Buck-Boost converters used to obtain I-V characteristic curves of photovoltaic modules," PESC Record - IEEE Annual Power Electronics Specialists Conference, 2036–2042, 2008, doi:10.1109/PESC.2008.4592243.

[11] A.R. Kashyap, R. Ahmadi, J.W. Kimball, "Input voltage control of SEPIC for maximum power point tracking," 2013 IEEE Power and Energy Conference at Illinois, PECI 2013, 30–35, 2013, doi:10.1109/PECI.2013.6506030..

[12] R.W. Erickson, D. Maksimovic, Fundamentals of Power Electronics, 2nd Edition, 2001.

[13] K. Chennoufi, M. Ferfra, M. Mokhlis, "An accurate modelling of PV Modules based on two-diode model," Renewable Energy, 2020, https://doi.org/10.1016/j.renene.2020.11.085.

[14] N. Nambiar, R.S. Palackal, K. V. Greeshma, A. Chitra, "PV fed MLI with ANN based MPPT," 4th IEEE Sponsored International Conference on Computation of Power, Energy, Information and Communication, ICCPEIC 2015, 293–300, 2015, doi:10.1109/ICCPEIC.2015.7259478.

[15] S.Z. Hassan, H. Li, T. Kamal, J. Ahmad, M.H. Riaz, M. A. Khan, "Performance of Different MPPT Control Techniques for Photovoltaic Systems" in 5th International Conference on Electrical Engineering, UET Lahore, Pakistan from Feb. 15-16th, 2018, doi: 10.1109/ICEE.2018.8566713

[16] S.Z. Hassan, H. Li, T. Kamal, L. Khan, S. Mumtaz, "Neuro-Fuzzy Wavelet Based Adaptive MPPT Algorithm for Photovoltaic Systems" Energies, **10**(3), 2017, doi: 10.3390/en10030394

ASTES

Advances in Science, Technology and Engineering Systems Journal Vol. 5, No.5, 607-612 (2020)

www.astesj.com

Special Issue on Innovative Research in Applied Science, Engineering and Technology

ASTESJ

ISSN: 2415-6698

Experimental and Numerical Study of the Mechanical Behavior of Bio-Loaded PVC Subjected to Aging

Abdelghani Lakhdar*, Aziz Moumen, Laidi Zahiri, Mustapha Jammoukh, Khalifa Mansouri

SSDIA Laboratory, Hassan II University of Casablanca, ENSET of Mohammedia, 28830, Morocco

ARTICLE INFO

Article history:
Received: 10 July, 2020
Accepted: 19 September, 2020
Online: 05 October, 2020

Keywords:
PVC
Aging
Numerical modeling
Recycling
Coconut fibers
Cow horn fibers

ABSTRACT

Increased recycling of PVC has become a requirement in industrial and scientific research level. Several studies will be realized. To confirm and check the recycled materials performance, it will be important to go through numerical modeling, which consists not only in validating the results of the experiments, but also in predicting what happens when the material is loaded. PVC material is more used in different fields, that ultimately means, after service life, an increase in waste requiring a high recycling rate. This article presents an approach validating the aging model as well as a numerical analysis predicting the mechanical properties of PVC after aging. The analysis samples (rigid and flexible) PVC which are subject to two types of accelerated aging, allows to obtain an aging model. Numerical modeling of PVC after aging is carried out using the finite element method and has been able to confirm the results obtained experimentally. Predicting the mechanical properties of rigid PVC after aging loaded with coconut and cow horn fibers after a first recycling is made by the finite element method, Mori-Tanaka and Double inclusion models. The obtained results have showed an improvement in the mechanical characteristics of the PVC studied using this natural bio-loading with these two fibers which respect the environment and have a lower cost and more lightness.

1. Introduction

The waste of plastic products continues to increase due to increased use in recent years. Among these materials we find PVC which covers all sectors of economic activity [1–5]. It's the second position after polyethylene. The PVC tonnages recycled under Vinyl Plus between 1 January and 31 December 2016 by the initiatives of the EuPC Sector Groups, Sector Associations and Recovinyl [6] are growing, in particular for window profiles, flexible PVC and cables, which involve industrial and scientific research to study the actions of recycled PVC.

The recycling of PVC is becoming a current necessity in the industry in order to upgrade it. However, this process requires the addition of fillers on the aged PVC to improve the mechanical characteristics. Before attempting this process based in the difference method consisting in proposing and validating a model from tests by evaluating the difference between the performances measured experimentally and the performances simulated numerically as shown in the figure 1.

This method also makes it possible to check the expected performances by evaluating the difference between a specification and the tests, and to predict the performances from the models, by evaluating the difference between the simulated performances and the performances expressed in the experimental specifications. In this context, an artificial aging model was carried out experimentally and numerically validated by the finite element modeling.

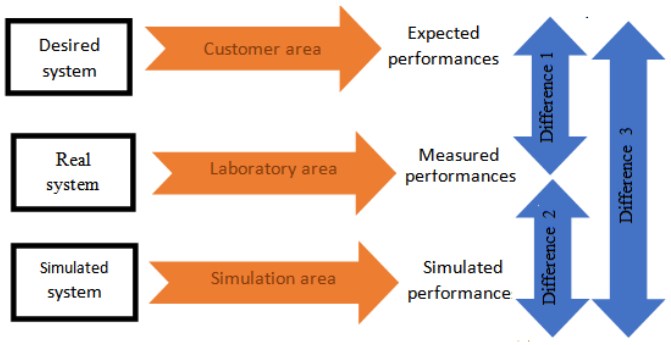

Currently, the recycling of PVC requires loading in order to ameliorate its mechanical characteristics. A variety of studies are focused on the bio loading of materials in view of the requirements in terms of sustainable development and the environment

*Corresponding Author: Abdelghani Lakhdar, lakhdarabdelghani11@gmail.com

In this study and using three numerical models, finite elements, Mori-Tanaka and Double inclusion [8, 9]. We will predict the behavior of bio-loaded PVC after aging. The fillers used are coconut and cow horn fibers.

The aim of the present study is to validate the aging model of PVC material experimentally and numerically, and to predict by a numerical modeling, the mechanical behavior of this material bio loaded.

2. Study of the PVC aging model

2.1. Description of the adopted aging model

2.1.1. Types of aging

Two types of aging are adopted. The Rigid and flexible PVC samples as illustrated in figure 2.

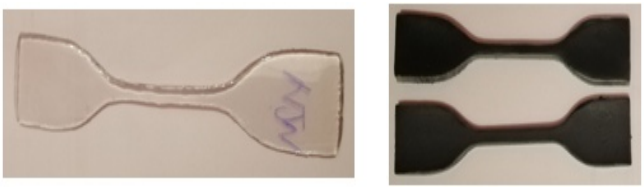

Figure 2: Flexible and rigid PVC specimen [3]

We took two configurations, accelerated artificial and under normal conditions aging at an average Moroccan temperature [3]. The figure 3 below shows the two types of aging

a) Aging by a constant temperature oven of 328.15 K
b) Aging by solar energy for 10h at average temperature T_{mean}= 300.15 K

Figure 3: aging configuration [3]

Table 1 illustrate that mean reference temperature is 300.15 K.

Table 1: Mean reference temperature in Morocco [3]

OUARZAZATE	Average temperature for 60 years	Maximum average temperature	Minimum average temperature	Record maximum temperature	Record minimum temperature	Average precipitation
unit	°K	°K	°K	°K	°K	°K
year	299.15	300.15	284.15	319.15	265.15	283.65
January	281.15	291.15	294.15	299.15	268.15	273.95
February	284.15	293.15	276.15	304.15	268.15	273.65
March	288.15	296.15	279.15	312.15	271.15	274.45
April	291.15	300.15	283.15	314.15	272.15	273.65
May	295.15	304.15	286.15	318.15	276.15	273.45
June	299.15	309.15	290.15	322.15	281.15	273.45
July	303.15	313.15	293.15	323.15	287.15	273.45
August	302.15	311.15	293.15	320.15	316.15	273.65
September	298.15	306.15	289.15	316.15	283.15	274.65
October	292.15	300.15	284.15	306.15	276.15	274.65
November	287.15	295.15	280.15	303.15	271.15	274.65
December	282.15	290.15	275.15	301.15	265.15	274.45

2.1.2. Results and discussion

After a tensile test carried out by the EZ-20 tensile machine (figure 4) and a numerical analysis using the finite element method, which is known for its strong ability to predict the behavior of more complex materials [10–19], on the flexible and rigid PVC samples after and before aging, the results obtained from the test are grouped together in the figures 5 and 6 and table 2.

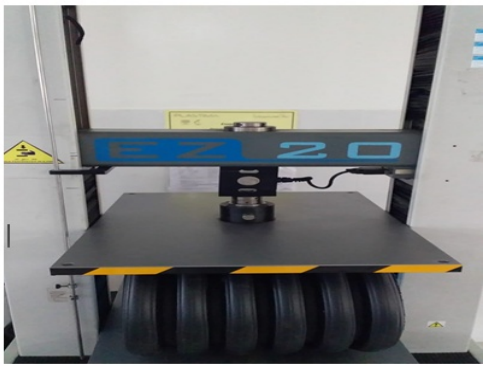

Figure 4: Tensile Testing machine EZ-20

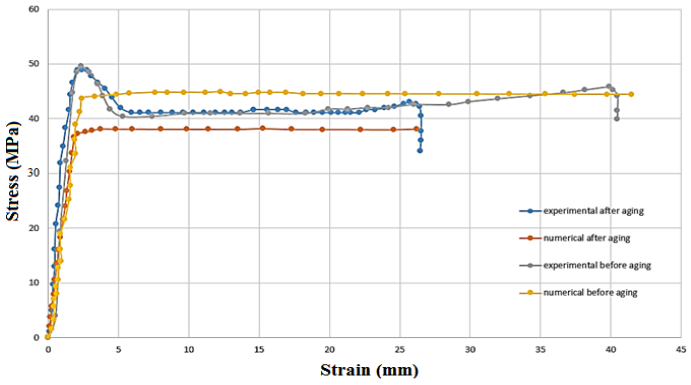

Figure 5: Tensile curves of rigid PVC before & after aging

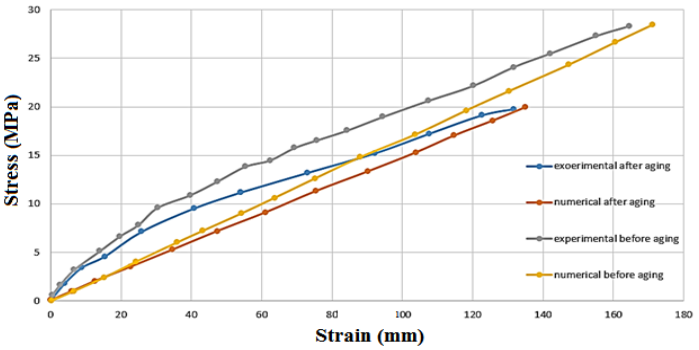

Figure 6: Tensile curves of flexible PVC before & after aging

Table 2: Experimental and numerical results

	Experimental Stress at break (MPa)	Numerical Stress at break (MPa)	Experimental Strain at break (mm)	Numerical Strain at break (mm)
Rigid PVC before aging	40	44	42	42
Rigid PVC after aging	34	37,5	26	26
Flexible PVC before aging	28	28	168	169
Flexible PVC after aging	20	20	135	135

We note that the stiffness of rigid PVC has changed slightly after aging and this is due to the inclination of the slope towards the elastic region. Its deformation potential before breaking has also been reduced. The flexibility of the flexible PVC is decreased at the elongation stage and become more rigid, its elastic limit is decreased.

Results of the analysis obtained numerically reveals that the numerical finite element modeling supports the findings already reported experimentally and that it is able to predict the mechanical behavior of more complex materials. The deformation ability of rigid PVC after aging has decreased, the stress at break for flexible PVC has decreased and the rigidity has increased because the deformation after aging is much less than before this process.

In order to return these products to their reference characteristics after many recycling, we have tried to establish a reference model for potential recycling studies.

Experimental research and numerical modeling were carried out using the finite elements approach on flexible and rigid PVC before and after aging.

Heat and ultraviolet rays are the key requirements for modifying the mechanical and thermal parameters of PVC, because the sensitivity of rigid PVC to these two conditions for 15 days, and 7 days for flexible PVC has been able to modify its mechanical characteristics.

3. Numerical Study of the Bio Loaded PVC

3.1. Numerical Models

3.1.1. Finite elements

This analysis is founded on the division of the bio composite by a good mesh and bringing together the sub-domains thereafter.

We will use the quadratic elements due to their efficiency of computation and the simplicity of convergence.

3.1.2. Mori-Tanaka

The mathematical model of this model is presented as follows:

$$\epsilon(x)= \xi(I,C_0) : \epsilon^*, \forall\ x \in (I) \qquad (16)$$

$\xi(I,C_0)$: Eshelby tensor

ϵ^* : The deformation acting the Eshelby volume.

The strain concentration tensor: $B^{\epsilon}= H^{\epsilon}(I,C_{fibers},C_{PVC})$ (17)

With:

$$H^{\epsilon}(\ I,\ C_{Fibers}\ ,\ C_{PVC}\ )= \{I +\ \xi(I,\ C_{Fibers}\ ):\ C^{-1}_{\circ Fibers}\ ):[\ C_{PVC} - C_{Fibers}]\}^{-1} \qquad (18)$$

H^{ϵ} : The fibers strain concentration tensor.

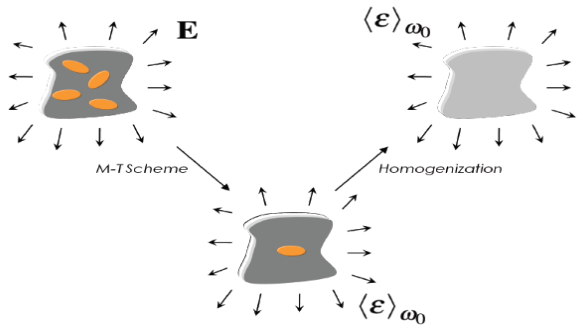

Figure 7: The Mori Tanaka model [8]

3.1.3. Double Inclusion

The strain concentration tensor in Coconut and cow horn fibers to its contour on the PVC matrix is presented by the following equation.

$$B^{\epsilon}= [(1-\xi(\upsilon_1))\ ((B_l^{\xi})^{-1} +\xi(\upsilon_1)(\ (B_v^{\xi})^{-1}]^{-1} \qquad (19)$$

With : $$\xi(\upsilon_1)=\frac{1}{2}\upsilon_1(1+\upsilon_1) \qquad (20)$$

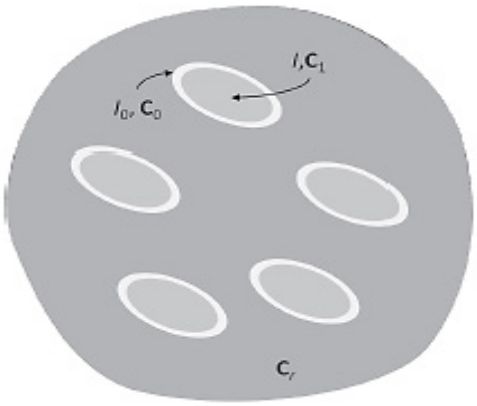

Figure 8: The Double inclusion model [9]

3.2. Bio loads

The loads used are from animal and natural origin, having a light density and a lower cost unlike classical loads affecting the environment. We will be interested in two types of loads in order to know their effect on the performance of PVC materials after aging

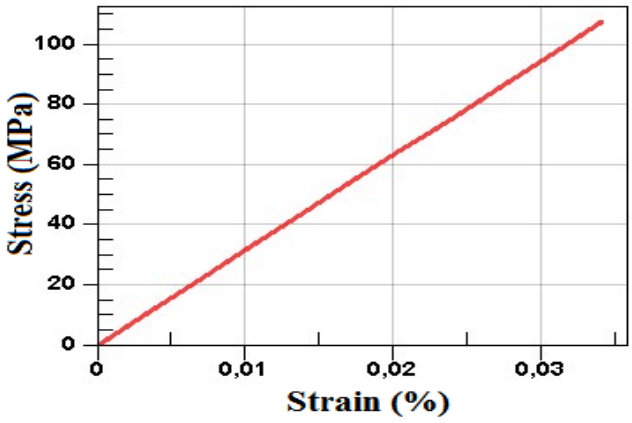

Figure 9: Tensile curve of the cow horns

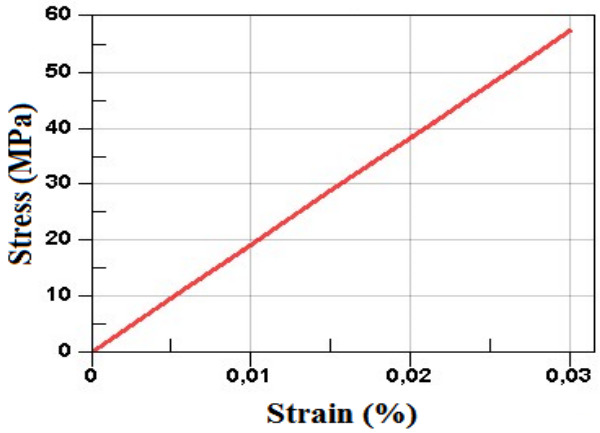

Figure 10: Tensile curve of the coconut

The two bio loads behave elastically with good values of the stresses at break and Young modulus as presented in the table 3.

Table 3: Numerical properties of cow Horns fibers in MPa

	Stress at break	Young modulus
Horn fibers	106.92	3148.4
Coconut fibers	57	1920

3.3. Results and Discussion

We studied in the previous chapter that the performances of PVC were modified after an accelerated aging which simulates reality. Before starting a first experimental recycling we will carry out a numerical modeling to predict what will happen.
The procedure consists in taking around10% of the two bio loads (cow horns and coconut), and adding it to PVC and comparing the results to see the improvements or degradations of the PVC material.

The idea is to find the material that will improve the performance of PVC and then use it as a bio load to improve recyclability. In what follows, we will simply choose rigid PVC as an object of this study

3.3.1. Internal Structure of the Bio loaded PVC

In this modeling, we choose a random distribution of coconuts and cow horns fibers in the PVC presented in figure 11 below

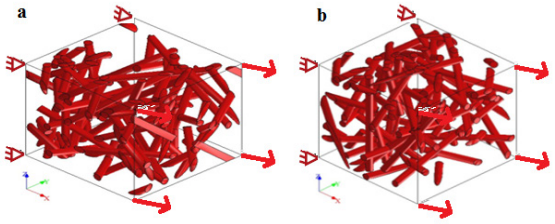

a) PVC bio laded by Coconuts b) PVC bio loaded by cow horns

Figure 11: internal structure of bio loaded PVC

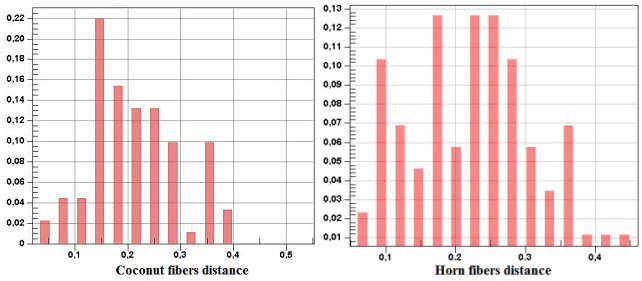

Figure 12: Ccoconut and horn fibers distance

The following table shows the statistical distance for the coconuts and cow horn fibers in PVC.

Table 4: coconuts and cow horn fibers distance

	Mean	Min	Max	Std dev
PVC bio loaded by Coconut	0.212	0.026	0.545	0.093
PVC bio loaded by Cow Horns	0.22	0.0538	0.455	0.0899

The meshes obtained by the numerical modeling of the coconut and cow horns are illustrated in Figure 13.

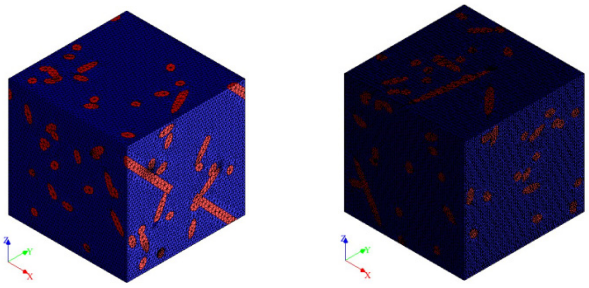

PVC bio laded by Coconuts PVC bio loaded by cow horns

Figure 13: PVC bio loaded mesh

The following table shows the parameters of mesh used in the present modeling.

Table 5: parameters of mesh

	Elements	Nodes	Size	Min size
PVC bio loaded by Coconut	330731	507283	0.029181	0.0058362
PVC bio loaded by Cow Horns	1449438	2182774	0.029181	0.0058362

We can deduce that the optimal percentage of the bio fillers in rigid PVC leading to better mechanical properties is 9.3Wt% for Coconut and 9.5 Wt% for Horn fibers.

Table 6: Number of fibers used and optimal content of bio loads

	Number of fibers	Content (Wt%)
PVC bio loaded by Coconut	31	9.3
PVC bio loaded by Cow Horns	32	9.5

We used two Rho and Gamma indicators for the two charging forms to check the consistency of the mesh, which are often used between 0 and 1 with better stability and convergence far from null.

We note that for Gamma it is between 0.6 and 1, whereas Rho is between 0.4 and 0.8, so they are far from 0 which verifies the mesh quality. Figures 14 and 15 demonstrate how those two indicators are distributed

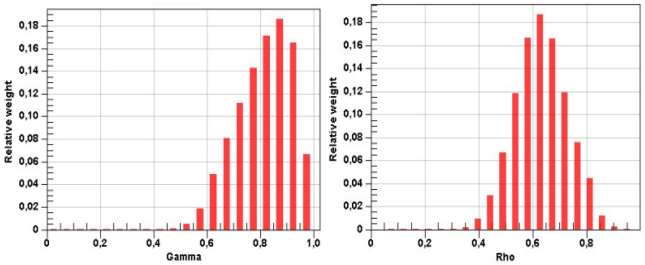

Figure 14: Gamma and Rho distribution of PVC bio loaded by Coconut

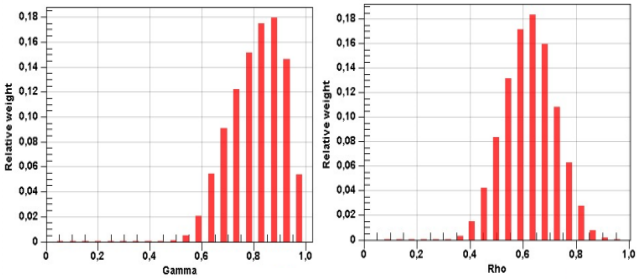

Figure 15: Gamma and Rho distribution of PVC bio loaded by Cow horns

Table 7 presents the average values obtained for Gamma and Rho criterion

Table 7: Average values of Gamma and Rho criterion

	Gamma criterion	Rho criterion
PVC bio loaded by Coconut	0.813	0.632
PVC bio loaded by Cow Horns	0.81	0.626

3.3.2. Effect of Bio loading on Rigid PVC

The three numerical models, finite elements, Mori-Tanaka and double inclusion illustrated in figures 16, 17 and 18 presents almost the same results as summarized in the table 8 and 9.

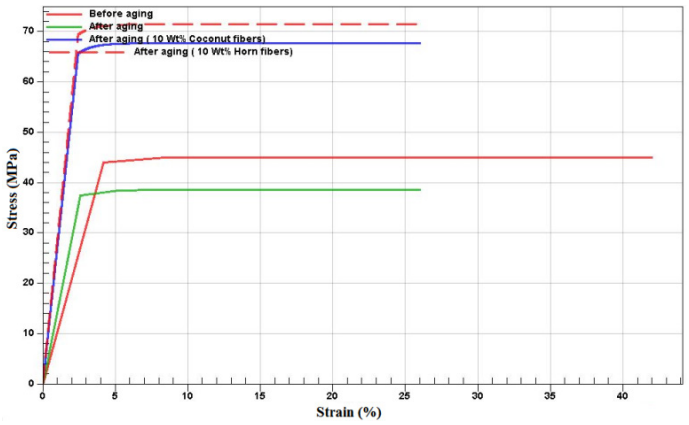

Figure 16: Tensile curve with the Finite element model

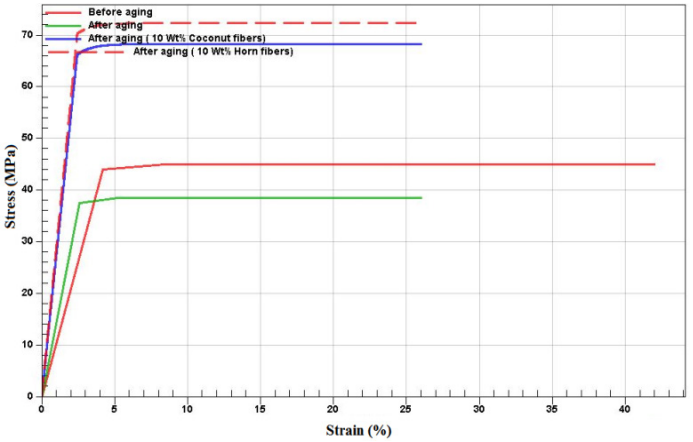

Figure 17: Tensile curves with the Mori-Tanaka model

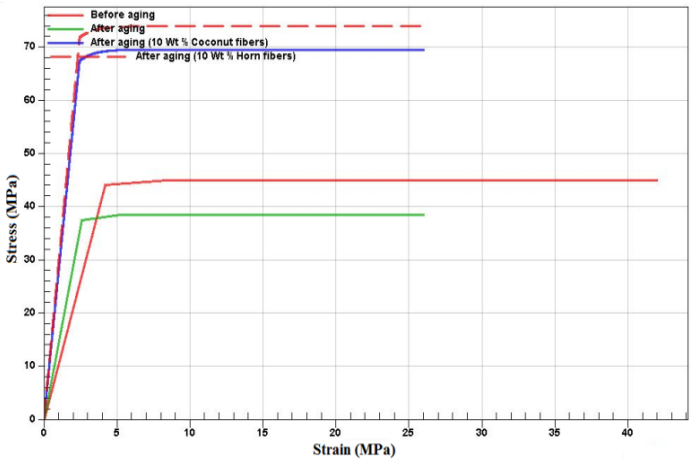

Figure 18: Tensile curves with the double inclusion model

Table 8: Numerical Stress at break in MPa obtained by different models for different content of Coconut fibers

Model	Content (Wt%)	Stress at break at
Mori-Tanaka	0	37.5
	10	68.521
Double inclusion	0	37.5
	10	69.799
Finite element	0	37.5
	9.3	68

Table 9: Numerical Stress at break in MPa obtained by different models for different content of Horn fibers

Model	Content (Wt%)	Stress at break at
Mori-Tanaka	0	37.5
	10	72.433
Double inclusion	0	37.5
	10	74.2
Finite element	0	37.5
	9.5	71.75

The analysis of the results obtained numerically for the different bio composites after a first aging show that the stresses at breakage improve by adding the two types of bio-loads compared to pre and post aging as shown in figures 16, 17, 18 and the tables 8 and 9.

Horn fibers have given better mechanical properties than coconut fibers. These results are validated by the different numerical models used. The numerical results show that the optimal percentages of Cow horns and Coconut fibers are 10 Wt% obtained by Mori-Tanaka and Double inclusion models and 9.3 Wt% obtained by the Finite element method for Coconut and 9.5 Wt% for cow horns fibers.

4. Conclusion

In this study, the mechanical behavior of flexible and rigid PVC pre and post aging was experimentally simulated and validated numerically. The submission of these PVCs to ultra violet rays and heat has caused the degradation of its performance. We then proceeded to bio loading rigid PVC after aging in order to compare its behavior with the pure state.

The modeling of these homogenizations are made by three numerical models, the finite element, Mori-Tanaka and Double inclusion models which have shown a power to predict the behavior of the bio loaded PVC after aging. The fillers used are Coconut and Cow horn fibers, resulting in an improvement in the performance characteristics of PVC after aging for an optimum percentage of around 10 percent Wt.

Cow horns fibers have given better mechanical properties than coconut fibers. These results are validated by the different numerical methods used.

Hence the improvement of the mechanical properties of rigid PVC after aging using this natural bio loading by these two fibers friendly to the environment and presenting a lower cost and more lightness.

In future works, we will opt for other numerical methods by simulating other natural bio loads and in different orientations of fibers in order to search for bio composites with better mechanical characteristics.

References

[1] E.T. Abdullah, S.M. Hasan, A.N. Naje, "Optical properties of PVC-MWCNT nano composites," 2013.

[2] A.M. El Sayed, W.M. Morsi, "Dielectric relaxation and optical properties of polyvinyl chloride/lead monoxide nanocomposites," Polymer Composites, **34**(12), 2031–2039, 2013.

[3] A. Lakhdar, M. Jammoukh, L. Zahiri, K. Mansouri, A. Moumen, B. Salhi, "Numerical and Experimental Study of the Behavior of PVC Material Subjected to Aging," in 2020 1st International Conference on Innovative Research in Applied Science, Engineering and Technology (IRASET), IEEE: 1–6, 2020.

[4] W. V Titow, Stabilisers: general aspects, Springer: 255–333, 1984.

[5] I. Janajreh, M. Alshrah, S. Zamzam, "Mechanical recycling of PVC plasticwaste streams from cable industry: A case study," Sustainable Cities and Society, **18**, 13–20, 2015.

[6] C.D.E.S. Activités, L. De Vinylplus, "RAPPORT D ' AVANCEMENT 2017," 2017.

[7] J.-L. Martinand, "La didactique des sciences," Revue Française de Pédagogie, **91**(1), 114–117, 1990.

[8] A. Moumen, M. Jammoukh, L. Zahiri, K. Mansouri, "Study Of The Optimal Micromechanical Behavior Of A Polymer Reinforced By Snail Shell Particles Using The Mori-Tanaka Numerical Model," in 2020 IEEE International conference of Moroccan Geomatics (Morgeo), 1–6, 2020, doi:10.1109/Morgeo49228.2020.9121908.

[9] S. Nemat, M. Hori, Micromechanics: overall properties of heterogeneous materials, 1993.

[10] A. Moumen, M. Jammoukh, L. Zahiri, K. Mansouri, "Numerical modeling of the thermo mechanical behavior of a polymer reinforced by horn fibers," International Journal of Advanced Trends in Computer Science and Engineering, **9**(4), 6541–6548, 2020, doi:10.30534/ijatcse/2020/342942020.

[11] P. Marimuthu, C. Kumar, "Finite element modelling to predict machining induced residual stresses in the end milling of hard to machine Ti6Al4V alloy," Periodicals of Engineering and Natural Sciences, **7**(1), 1–11, 2019.

[12] Ö.Y. Bozkurt, İ.C. Dai, Ö. Özbek, "The finite element analysis and geometry improvements of some structural parts of a diesel forklift truck," Periodicals of Engineering and Natural Sciences, **5**(2), 2017.

[13] S. Komurcu, A. Gedikli, "Numerical modelling of the in-plane loaded homogenized masonry walls," Periodicals of Engineering and Natural Sciences, **5**(3), 2017.

[14] J.J. Lee, E. Piersanti, K.-A. Mardal, M.E. Rognes, "A mixed finite element method for nearly incompressible multiple-network poroelasticity," SIAM Journal on Scientific Computing, **41**(2), A722–A747, 2019.

[15] M. Ghalandari, S. Bornassi, S. Shamshirband, A. Mosavi, K.W. Chau, "Investigation of submerged structures' flexibility on sloshing frequency using a boundary element method and finite element analysis," Engineering Applications of Computational Fluid Mechanics, **13**(1), 519–528, 2019.

[16] S.-F. Yin, S.-L. Xue, B. Li, X.-Q. Feng, "Bio–chemo–mechanical modeling of growing biological tissues: Finite element method," International Journal of Non-Linear Mechanics, **108**, 46–54, 2019.

[17] Y. Hong, Y. Yan, Z. Tian, F. Guo, J. Ye, "Mechanical behavior analysis of 3D braided composite joint via experiment and multiscale finite element method," Composite Structures, **208**, 200–212, 2019.

[18] J. Naveen, M. Jawaid, A. Vasanthanathan, M. Chandrasekar, Finite element analysis of natural fiber-reinforced polymer composites, Elsevier: 153–170, 2019.

[19] P. SPITERI, "Variational Approach for The Finite Element Method," AF503 V1, 2012.

Advances in Science, Technology and Engineering Systems Journal Vol. 5, No. 5, 630-636 (2020)

www.astesj.com

Special Issue on Innovative Research in Applied Science, Engineering and Technology

ASTESJ

ISSN: 2415-6698

Sustainable Development Practices in the Moroccan Small and Medium Enterprise: by What Means and for What Purpose?

Keltoum Rahali[*,1], Abdelaziz Chaouch[1], Elmahjoub Aouane[2], Sami Chbika[2], Abderrazzak Khohmimidi[3], Mustapha Kouzer[1], Abdellatif Elouali[3]

[1]*Department of Chemistry, IBN TOFAIL University, Kenitra, 14000, Morocco*

[2]*Department of Biology, IBN TOFAIL University, Kenitra, 14000, Morocco*

[3]*Sciences of Management, Mohamed V University, Rabat, 10090, Morocco*

ARTICLE INFO

Article history:
Received: 24 July, 2020
Accepted: 23 August, 2020
Online: 05 October, 2020

Keywords:
Management
SME
Sustainable development

ABSTRACT

The objective of this article is to highlight the relationship between the integration of sustainable development practices in Moroccan Small and Medium Enterprises (Smes) and the challenge sought by managers in order to ensure competitiveness and sustainability. Indeed, present-day Smes are operating in a world where economic, social, societal or environmental constraints are constantly evolving. The Sme has to face, on a daily basis, new challenges such as economic stability and sustainability alongside the major structures because the challenge of any company is to be able to differentiate itself by adding its own trace promoting a more stable positioning in a fairly hostile environment. The investigation is carried out on a sample 30 Smes in the city of Kénitra due to the importance that this city holds in terms of both geographical dimension and economic inputs on the regional scale, 13.6% of the jobs generated by the SME according to the report of the high Planning Commission (HCP 2017). The results obtained reveal that the major concern of the managers of the Moroccan Sme is a purely commercial concern and that the integration of the various practices related to sustainable development in their managerial vision is only a means and does not constitute an objective to ensure the expected survival and sustainability.

1. Introduction

Most of the researches on Sustainable Development (SD) were focused, for the majority of them and until recently only on large structures. That being said, we believe that our study on Smes will be very useful as it provides us with the opportunity to analyze the means deployed by managers and the objective sought through the integration of sustainable development practices. In fact, Ashton, Russell and Futch [1] find that the majority of Smes in the United States of America are driven primarily by cost and competitiveness concerns, rather than by the implementation of green practices in their managerial practice. It is, in this sense, the merits of this study that will allow us to touch the why of the Why the integration of sustainable development practices in Moroccan Small and Medium Enterprise and by what means?

In [2], the author found that Smes represent approximately 90% of international organizations, Bank Al Maghreb identified a percentage that is close to 95% [3] with a 50% contribution to job creation, a rate which is very significant at national level. It should be noted that these structures also play a significant role in negatively impacting their environment [4]-[6]

Indeed, all the literature research shows that Smes, by their rather particular features, translate differently the integration into their systems of management of Sustainable Development (SD) practices than large structures i.e. often working in a different way in terms of their involvement in this process. Although the term of sustainable development is differently defined by several authors, we have retained the Brundtland's report definition (1987) "Our Common Future" [7] which defines it as a development that must meet the needs of the present without compromising the ability to meet those of future generations. This is not about stopping economic growth, on the contrary."

It is with this in mind that our investigation focused on the concern behind the introduction of this concept of SD through all its facets (certification, social responsibility, societal responsibility, green projects, etc..) within the company as well as the means used by managers in terms of environmental management and training to establish and convey their SD culture in their managerial vision. A vision that positions

[*]Keltoum RAHALI, IBN TOFAIL University Kenitra, +212676975725, rahkel@hotmail.fr

commercial concern as a priority sought through these SD practices.

The aim is to present the results of an investigation that was carried out in the city of Kénitra, a city possessing considerable assets giving it a place and a promising situation in the new regionalization. Our approach will show a methodological approach with a presentation of the main results we have achieved.

2. Methodology

We opted to conduct this investigation for a quantitative study through the development of different headings that fed our questionnaire in order to approach the well-basis on the perception and adoption of the multiple practices of sustainable development in management that aims at corporate citizenship in order to clarify the why of the implementation of this model in Smes operating in the city of Kénitra. We pre-tested our questionnaire on a sample of 5 Managers operating within Smes and 4 university teachers-researchers in the field of sustainable development to check its fluidity, the flow of questions, the respondent's understanding of all the sections of the questionnaire as well as the veracity of the answers that will allow us to obtain an overview of the concept of sustainable development and the implementation of its tools within Smes through a kind of management that we can refer to as responsible [8].

The components of this study can be summarized in the following axes:

- Identification of the SME and the manager,
- The SME managers perception of the concept of sustainable development,
- The means employed by the company to ensure its environmental and/or social involvement,
- The place of training and communication of SD practices in the managerial vision and in the integration of a culture within the SME.

For each explored axis, we matched either closed questions with the possibility of a yes or no answer, or questions with a range of answers ranging from one to several checkboxes. For more suggestions from respondents such as directors, managers, or project managers, whose functional quality is interesting, we have suggested an open question that could be used to push them forward in order to collect more information that can help us to better develop our interpretation.

We have conducted our investigation on 30 Smes (This data gathering phase coincided with the confinement). The choice is often made depending on the number of employees and turnover [9] [10]; as far as our investigation is concerned, only the workforce criterion will be used, a permanent workforce between (10 and 200) employees according to the 2002 Charter classification1. This classification, which corresponds to the quantitative approach, integrates two other qualitative parameters, namely its location in the kénitra region and the type of activity that is part of the industrial sector.

It is important to note that our sample includes Smes in this region whose activity is in the secondary sector, which is considered as strategic because it provides engineering jobs and research and development work for service companies of the tertiary sector [11], while focusing on the most widespread fields where technical progress remains moderate [12].

The city of Kénitra covers, according to the HCP, a total area of 3,052 km², or 17.37% of the entire region of Rabat-Salé-Kénitra (RSK) which is one of the 12 regions of Morocco, created by the new territorial division of the regions of 2015 in application of the Decree No. 2-15-40 of the Official Bulletin of 05 March 2015.

Our choice has settled on this city because it benefits from an economic array that allows it to appropriate a fairly important place in terms of production and job creation in its region. Its environmental aspect allows it to own a special natural heritage that can be negatively impacted by the establishment of the Atlantic Free Zone and industrial districts (Bir Rami, ...) which are often accompanied by strong urbanization. Our sample size included 30 Smes with 10 to 200 employees who wanted to actively contribute in this survey while providing face-to-face interviews over a period of January 25 to March 30, 2020 which coincided with the confinement's end.

3. Results synthesis

The study population's target and the respondents' profiles: By referring to the first results we have obtained after the questionnaires' analysis, we confirm that the degree of interest of Smes in the theme of sustainable development and its perception as a concept are significant. Indeed, this observation allows us to confirm that the association of the concept with the trilogy (economy, environment, and social) represents a particular interest for Smes with 66.7% (Figure 2). This situation remains verified among all those who were interviewed, irrespective of their academic training, and the field of activity of the SME. At this level, we tackle the profile of respondents, whose specifications are inserted in Tables 2 and 3.

As for the field of activity of Smes that we have approached, it remains diversified within the economic activity spectrum of Kénitra city and we note thus the strong weight of the construction sector with 26.6% which is explained by the strong urban activity in this city.

The second parameter that we mobilized to clarify the profile of respondents is the function of the respondent within the SME. It was found that the distribution of the population remains fairly balanced with a dominance of the executives (Project Managers) who totalize a score equal to 33%; the second population is represented by the managers (of sites, factory or a management function) with 23.4% and managers operating in the quality field with a score of around 16.7%.

Table 1: Field of activity

Fields of Activity	Number	Weight
Construction and Public Works	8	26,6%
Plastics industry	6	20,0%
Agri-Food / Agribusiness	6	20,0%
Piping and annexed equipment	3	10,0%
Lumber and Wood industry	3	10,0%
Clothing industry	2	6,7%
Metalic and mechanical industries	2	6,7%
Total	**30**	**100,0%**

[1] SME/SMI 2002 Charter, Dahir n° 1-02-188 du 12 joumada I 1423 (23 july 2002) Official Bulletin n° 5036 of 15/09/2002

Table 2: The respondent's positions

Occupation	Number	Weight
Manager (Project supervisor)	10	33,4%
Director	7	23,4%
Quality manager	5	16,7%
Administrative manager	3	10,0%
Team leader	2	6,7%
Operations support agent	2	6,7%
Others	1	3,3%
Total	**30**	**100,0%**

Taking these results into account, we can advance that sustainable development is seen as the concern of all the company's staff since the focus on this issue is shared by the different functions that structure the companies we have visited. This situation confirms the integration of horizontal management led by top management and which must be at the initiative of the environmental policy and the implementation of responsible management with the aim of defining a citizenship and responsibility SME environment with the attribute of vertical management [13] which brings together the various hierarchical levels of the company. A second factor to take into account in the identification of the respondent's level of education.

As shown in Table 3, nearly 40% of the population we surveyed has an engineering level while the remaining respondents are dispatched between different levels of training ranging from Bachelor's to MBA which explains the strong adherence of this profile to the many facets of the sustainable development at a rate of 66,7% (Figure 2) concerning the definition of this concept while linking it with its three fundamental axes: economic, environmental and social.

Table 3: The education level

Education level	Number	Weight
Engineer	12	40,0%
Baccalaureate	10	33,3%
Bachelor	4	13,3%
Mba	3	10,0%
Others	1	3,3%
Total	**30**	**100,0%**

Based on the three dominant criteria of the Material Data Sheet (business sector, function, and level of training of the respondent), we end up with representativeness of each modality that is not null and that is ensured by a value exceeding 2%. Through the heading «Perception of the term sustainable development», we want to raise the level of knowledge of this concept among respondents in order to assign it the connotation that stands against the perceived image and this through the strategic orientation and internal communication that is mobilized by the «awakened SME» to be able to highlight the interest and usefulness of a sustainable development approach within the structure.

As shown in Figure 1, the results from flat sorting, the awareness of the concept of sustainable development remains positive to the extent of 77% of the people we interviewed are familiar with the concept of sustainable development; it is necessary to deal with this percentage with caution since we had not assigned a definition to this concept but rather we propelled the spontaneous notoriety that stipulates the terminological knowledge of the concept of sustainable development without insisting on its understanding, its definition or even its axes to be set up within the company.

This awareness of the notion of sustainable development that is sometimes associated with corporate social responsibility [14] through the application of responsible management [15] by developing a vision of citizenship [16] can be acquired through internal information within the structure or through the environment or through the various media that deal with the subject especially in this era of Information and Communication Technologies (ICT) dominance.

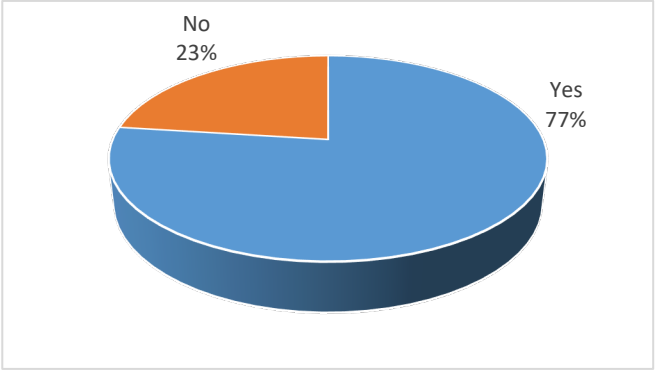

Figure 1: Sustainable development concept Notoriety

After identifying the awareness of the concept of sustainable development among the various companies that we were able to touch and whose score is of the order of 77%; we were interested in delimiting the definition of this concept in the image of each SME. At first glance, as shown in Figure 2, 66% of the population has recognized the concept of sustainable development associates it with the economic, social and environmental trilogy translated by T. Bansal [17] by the "3P" Profit, People and Planet.

Thus, SD can only be achieved through the three principles of economic efficiency, social equity and accountability; therefore, we can assume that the majority of people familiar with sustainable development have taken the time to document this concept either as a result of professional requirements or as a personal interest in the topic or in civic action since their definition falls under the common design adopted in 1987 at the Earth Summit and following the preparation of the first report of (G.H. Brundtland) which was carried out at the initiative of the United Nations and which identified the problem by associating it among other things with ecology, biodiversity and global warming...

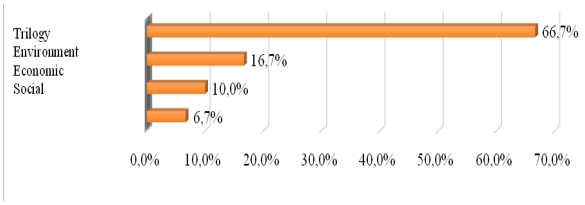

Figure 2: « Sustainable development » definition axes

Two parameters make it possible to justify the interest of the concept of sustainable development according to the perception of the respondents, namely the global necessity with 53,3% and that stipulates the preservation of natural resources with exploitation that will not alter that of future generations and this by the setting up of equipment aimed at the use of renewable energies and also promoting the optimization of the water

management (intelligent watering systems, featuring awareness regarding drinking water, etc.) and by adopting, each SME in its own way, responsible models to decrease the pollution that can arise during the exercise of their activities by putting in place an ecological vision within their operating method in terms of waste management, paper mining, moving more and more towards the concept of "zero paper" [18], without excluding, of course, the rationalization of their production systems.

Originating from the respondents, this vision shows their responsibility, regardless of their functions within the structure and activity they carry out. The second wave, represented by a total of 46,7%, is distributed with fairly close rates and emphasizes the competitiveness and the need for the implementation of sustainable development policies that will allow them to adjust into the new economic models as they are required by globalization.

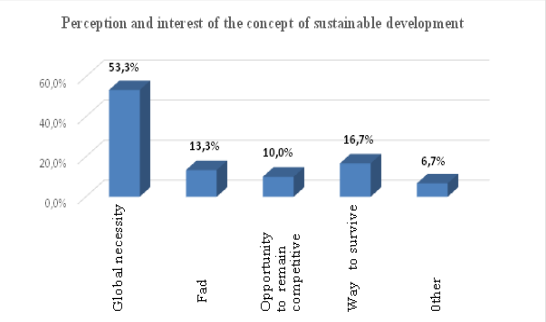

Figure 3: Perception and interest of the concept of sustainable development

3.1. *Interest and commitment of Smes in a sustainable development policy*

More than half of the Smes we interviewed, meaningly 56.7%, have an environmental policy as shown in Table 4. A policy initiated within the framework of sustainable development and characterized by the foundations of responsible management. Moreover, we note that European and Canadian Smes [19] increasingly integrate management practices in favour of Corporate Social Responsibility (CSR) and are more likely to opt for certifications that are closely related to the environment or sustainable development because several studies [20] point out that SME owners claim to have started integrating sustainable development into their management practices and that 20.8% of a population of future leaders declare that they intend to do so according to the survey conducted in 2010 by the Entrepreneurship Foundation (EF). This only shows the growing commitment and involvement of Moroccan SME managers in policies stemming from sustainable development with an awareness of this concept especially following the organization of the 22nd Conference of parties held in November 2017 at Marrakech, Morocco (COP22) in Morocco.

This environmental policy is quite often associated with certification, as shown in Figure 4. Indeed, the majority of Smes with 46,7% are certified in the quality management system, which is the result of the production system, that guarantees they conquer new markets, especially foreign markets, when they post a reference to a standardization label for their production process, which ranges from the purchase of the raw material, storage, production and supply chain management. Thus, we can observe that this initiative is more a commercial requirement than an environmental one. On the other hand, the company's affiliation to a Corporate Social Responsibility certification is only 6.7% which allows us to deduce that the Social responsibility is much more a state of mind and that environmental certification, which translates into 26.7% is more sought after by the Moroccan manager.

Table 4: Existence of environmental policy within the SME

Existence Of An A Environmental Policy In The Sme	Number	Weight
Yes	17	56,7%
No	13	43,3%
Total	**30**	**100,0%**

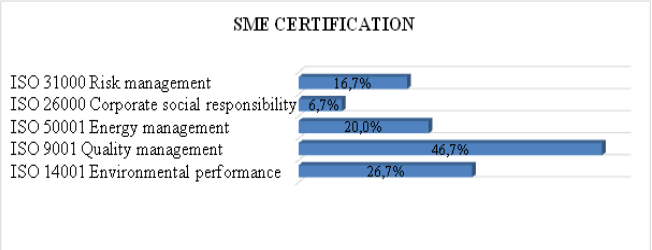

Figure 4: SME certification

Regarding the management and management methods within the SME, they must be able to lead, when implementing an environmental policy, a responsible act that aims to mobilize all staff around a collective vocation such as respect for the environment and the company's citizenship towards its stakeholders. We note in Figure 5, that the implementation of an environmental management plan is quite often the result of a 40% certification whereas the CSR approach is only 13,3%, a gap that remains significant due to the level of social involvement in Smes that remains relatively small compared to large enterprises.

Sharma, S [21] points out, financial constraints of an SME as opposed to a large enterprise that is more comfortable investing in a CSR business and has the ability to absorb fixed costs and ease of access to capital and other resources. It should also be stressed that when a certification project is set up, an accompanying system is put in place to standardize all production processes, the information system, the training of teams and all staff and the production platform which must meet in a manner that complies with a specification and a requirement of the chapters of the standard in relation to the (HSE) which refers to the safety and optimization of the quality system throughout the production process; therefore, the implementation of an environmental management plan is an indispensable act in the global certification chain (ISO 9001 version 2015).

At this level, the implementation of this plan by Smes is not necessarily voluntary but rather compulsory to obtain their certification that will allow them to open up to the foreign market. This is more of a purely commercial strategic act than an awareness of respect for and protection of the environment.

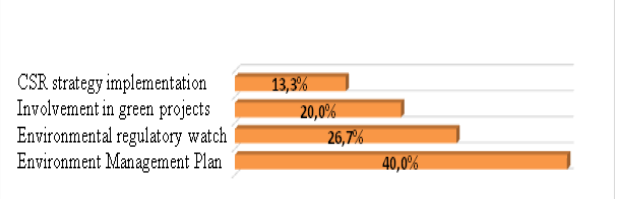

Figure 5: Management mode derived from sustainable development

3.2. Integration of sustainable development in the Smes managerial mode

The operational integration of sustainable development through the adoption of a management approach that takes into account the efficient use of natural resources (Figure 6), reveals that nearly 67% of the Smes we interviewed adopt a policy that optimizes their natural resources. This figure is quite encouraging and allows us to confirm the orientation of the SME of Kénitra city towards a green economy, thus promoting the setting up of a mindset that goes in a parallel way with respect for the environment while associating economic profit of the SME with its social and environmental dimensions.

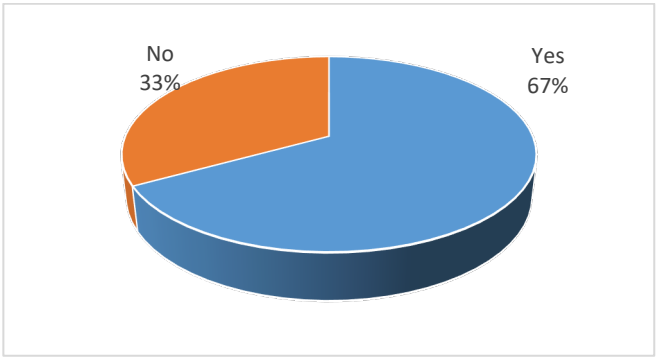

Figure 6: The efficient use of natural resources

It was necessary to stress this question, which concerns natural resources, by identifying the various means used by the SME to meet the challenge of sustainable development through the adoption of an environmental policy that must be based on the managers' actions and which represents their day-to-day activities as shown in Figure 7. It should be noted that all the answers must be stratified between the requirement of a certification process which has as its objective a commercial fact and the personal initiative which emerges more from the awareness of the mobilization and the individual commitment of everyone with regard to the environment.

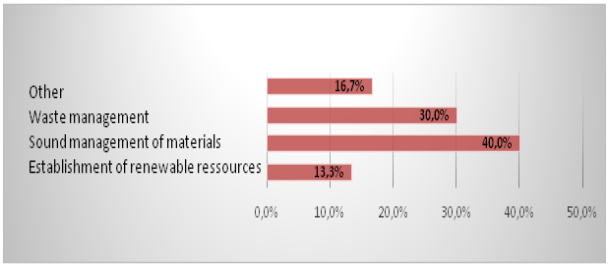

Figure 7: Means deployed to ensure efficient use of natural resources

The rational management of materials represents the largest part of the optimization of natural resources with a rate equal to 40 % and which often directly impacts the decrease of the expenses of the Smes monthly bill, followed by waste management which represents 30%. From this perspective, we can also deduce that the environmental policy adopted by Smes, which results in optimized management of natural resources, is more linked to the production process than to the specificity of the SME's activity. A production which, the more optimized it is, the more profit it will generate in the company's annual balance.

In addition, the implementation of renewable resources represents 13.3% although the latter allows to reduce costs considerably and to guarantee a low nuisance to the ecosystem. On the other hand, the investment cost of its implementation risks slowing down the environmental project of Smes and hinders the continuity of the sustainable development axes hoped by the manager. Through these results, we were able to highlight the importance of the implementation of environmental policy within Smes to ensure continuity, competitiveness indispensable in this era of globalization of markets especially with the outsourcing of activities from developed countries to emerging or developing countries through structures that demonstrate their support for sustainable development because the more the manager reveals its environmental involvement, the more he will gain responsible management and the more the market shares will increase. This brings us back to the fact that the implementation of this type of management requires a serious collective and individual awareness with the adoption of true corporate culture.

In the same line of thought and following the results inserted in figure 8, which represent the contribution of sustainable development to Smes, we point out that the overall trend in responses focused on seeking a competitive advantage and minimizing costs. While the reduction of the environmental impact and the production with the eco-label that allow to model own production come last; this trend of response allows us to confirm that Smes have more a commercial concern and consider, thus, sustainable development as an opportunity to label their production process (the process most targeted by the customer) in order to be able to integrate an international standardization that guarantees their acquisition of competitive advantage [22] and a referral to all their clients, subcontractors who are, quite often, already engaged in environmental policies.

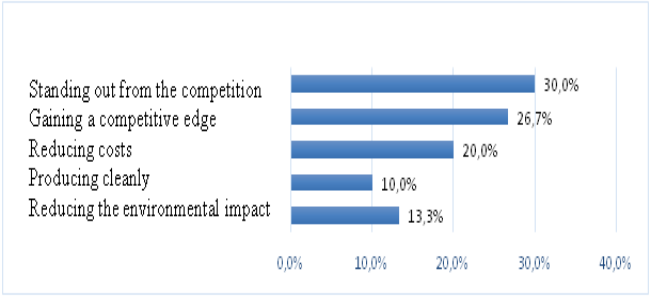

Figure 8: Contribution of sustainable development to Smes

3.3. The role of training and communication in the managerial perspective derived from sustainable development

In any management system qualified as performing, staff training constitutes a crucial axis in the implementation of either environmental or social policies. In fact, this is why we found that practically all the respondents were able to take a training course which is largely in the form of a conference with 40%, seminars 33.3% and internships in Morocco or abroad with respectively 10% and 16.7%.

Note, for example, that according to the survey that was conducted by the association for the sustainable Development practices (Apdd) [23], SME executives attended only 50% of conferences or seminars on sustainable development and wanted 33% more information on the various actions related to sustainable development. The observation that allows us to point out that the definition of this concept has undergone a marked evolution within the Moroccan SME which shows itself, aware of the impact of this type of training on the achievement of the goals of sustainable development as a whole.

Table 5: Kinds of contributions to sustainable development

Kinds of contributions to sustainable development	Number	Weight
Conferences	12	40,0%
Seminars	10	33,3%
Symposiums	5	16,7%
Internship Abroad	5	16,7%
Internship Inside Morocco	3	10,0%
Total	**30**	**100,0%**

Nearly 40% of the population took a training course focused on environmental management, followed by responsible management with a rate of 33.3%. The other topics are also related to environmental matters, such as sustainable development, the green economy and the management. The importance of these training actions is to demonstrate to what extent they enable participants to better perceive the concepts of implementing an environmental policy within the SME and to be able to customize their actions according to the sector and the process within which they operate.

It should be mentioned that our investigation has focused particularly on the themes that affect directly sustainable development while deliberately excluding the other themes that are oriented towards the Quality Management System, internal audit, communication, languages, etc. which are often planned either on the initiative of the manager or the staff.

Table 6: Sustainable development training topics

Sustainable Development Training Topics	Number	Weight
Environmental Management	12	40,0%
Sustainable Development	6	20,0%
Green Economy	7	23,3%
Eco-Management	5	16,7%
Responsible Management	10	33,3%
Total	**30**	**100,0%**

We conclude that the training of staff in the various topics related to the environment and Corporate Social Responsibility makes it possible to successfully integrate the practices of sustainable development within the company and therefore, increase awareness of the SME towards its social, social and environmental responsibility. This action mobilizes internal customers (the company's staff) and promotes the external SME's image towards all its stakeholders as well as its suppliers, which will enable it to evolve in terms of productivity and profitability, or its customers, which will ensure its successful positioning in an increasingly competitive market.

4. Discussion

The integration of sustainable development into the way of managing within Smes remains voluntary and expresses the company's commitment to its environment and stakeholders. With the emergence of this new concept that evolves in a framework marked by the economic demands that keep changing the world especially after the financial crisis of 2008, the political wave of 2011 (year of the new constitution in Morocco), the growing interest in environmental, social equity and human rights requirements; the adoption of more and more new management methods within companies and, particularly within Smes [24] who represent a significant share in the global economic weight, becomes a compulsory requirement in order to guarantee certain sustainability through the consecration of an economic asset which must be combined with environmental and social requirements. This new approach dictates that human capital is and will be for a long time to come to the cornerstone of any economy. Hence, its awareness, its training and support represents the optimal solution for Smes that want to go towards the acquisition of a sustainable competitive advantage.

Consequently, according to Torugsa, N.A [25], a social responsibility strategy can bring significant value to the market performance of an SME and can have a very significant impact on its financial performance. In addition, Lin, L et al, [26], consider that the corporate social responsibility (CSR) has presently become an essential aspect in a company's strategy and it is closely linked to its reputation because positive reputations generally lead to very positive financial results and performance.

During this survey, we were able to demonstrate that the concept of sustainable development through a few facets remains fairly well introduced within the Moroccan SME (77%); most often associated with the quality process or certification, it converges towards the same goal, namely, increasing competitiveness, resisting new changes in world trade and establishing an opportunity for referencing with all external stakeholders [27] that are very demanding and very committed in environmental policies.

References

[1] W. Ashton et al., "The Adoption of Green Business Practices Among Small US Midwestern Manufacturing Enterprises" J. Environ. Plan. Manag. 2017.

[2] C.M. Parker et al., "A review of interventions to encourage SMEs to make environmental improvements" Environmental and Planning C, 2009.

[3] Bank-Al-Maghreb, Rapport annuel, 285p, 2013.

[4] F. Labelle et al., "la responsabilité sociétale des petites et moyennes entreprises ou la RSPME" une analyse de la littérature des dix dernières années. 2010.

[5] L. Temri, "Partage des bonnes pratiques de développement durable" le cas des PME agroalimentaires du Languedoc-Roussillon, Innovations, **1**, 2009.

[6] H. Jenkins, "A critical of conventional CSR theory" An SME Perspective, journal of General Management, **29**, 2004.

[7] G.H. Brundtland, "Notre avenir à tous, Commission mondiale de l'environnement et du développement, Edition du Fleuve, 1987.

[8] J.C. Dupuis, "management responsable : vers un nouveau comportement des entreprises ? La Revue des Sciences de Gestion, n° 211-212, 2007. https://www.cairn.info/load_pdf.php article=rsg_247

[9] C. Blais, "Indicateur et tableau de bord de gestion : Mesure de la performance des PME en développement durable. Mémoire de maîtrise, Université de Sherbrooke, Sherbrooke, 2011.

[10] K. Delchet, "Développement durable, l'intégrer pour réussir, 2007.

[11] C. Clark, Les conditions du progrès économique, Paris, P.U.F., I960. https://www.universalis.fr/encyclopedie/colin-clark/

[12] J. Fourastié, préface de l'édition du Grand Espoir du XXe siècle, 1989.

[13] S. Ghoshal, "Changing the Role of Top Management : Beyond Structure to Processes", la Harvard Business Review, 1995

[14] E. Reynaud, "Impact de la protection de l'environnement sur la gestion des coûts, Responsabilité Sociale de l'Entreprise et Performance, éd. : d'organisation, Paris, 2004.

[15] R. Perez, "La revue des sciences de gestion, Direction et Gestion, n°211-212- RSE, Quelques réflexions sur le management responsable, le développement durable et la responsabilité sociale de l'entreprise, 2002

[16] Turcotte et al, Comprendre la responsabilité sociétale de l'entreprise et agir sur les bases de la norme ISO 26 000, 2011

[17] T. Bansal, "le développement durable en entreprise, Le développement durable en entreprise, c'est contribuer à la prospérité économique, à la santé des écosystèmes et au pouvoir des communautés, 2012.

[18] A. Bernillon, "Implanter et gérer la qualité totale, Les Éditions d'Organisation, 1988.

[19] M. Doucet, "le développement durable dans les PME au Québec : outil de diagnostic de facteurs d'influence et des pratiques mises en œuvre, 2012, https://www.usherbrooke.ca/environnement/fileadmin/sites/environnement/documents/Essais_2013/Doucet_M. 15-10-2012.pdf

[20] J. Rollin, Comment les entrepreneurs québécois jonglent-ils avec

l'intégration des principes de développement durable ? Site de la fondation de l'entrepreneurship, http://www.entrepreneurship.qc.ca/developpement_durable

[21] S. Sharma, Managerial Interpretations and Organizational Context as Predictors of Corporate Choice of Environmental Strategy. Acad. Manag. J.**43**, 681–697, 2000.

[22] C. Martinet, "Entreprise durable, finance et stratégie, 2004, https://www.cairn.info/revue-francaise-de-gestion-2004-5-page

[23] S. Lagarde-Dupraz, Questionnaire réalisé par l'Association pour les Pratiques du Développement Durable Apdd, 2000.

[24] D. Lebegue, l'ORSE – (Observatoire sur la Responsabilité Sociétale des Entreprises), 2003.

[25] N.A. Torugsa, O'Donohue,W.; Hecker, R. Capabilities, Proactive CSR and Financial Performance in SMEs:Empirical Evidence from an Australian Manufacturing Industry Sector. J. Bus. Ethics, **109**, 483–500, 2012.

[26] L. Lin et al., Financial performance and corporate social responsibility: Empirical evidence from Taiwan. Asia Pac. Manag. Rev, **24**, 61–71, 2019

[27] R. Freeman, Divergent Stakeholder Theory, Academy of Management Review, **4**, 1999.

ASTES

Advances in Science, Technology and Engineering Systems Journal Vol. 5, No. 4, 633-637 (2020)

www.astesj.com

Special Issue on Innovative Research in Applied Science, Engineering and Technology

ASTESJ

ISSN: 2415-6698

Earthquake Response of Multi-Storey Infilled Reinforced Concrete Buildings

Miloud Mouzzoun*, Abdelkader Cherrabi

Civil engineering department, Hassania School of Public Works, Casablanca, BP8108, Morocco

ARTICLE INFO

Article history:
Received: .22 June, 2020
Accepted: 20 July, 2020
Online: 25 August, 2020

Keywords:
Frame
Infill
Seismic
Time history
Pushover
Strut

ABSTRACT

The aim of this work is to study the effect of infill brick panels on the response of multi-storey buildings under seismic loading. An eight storey building is investigated. The building is analysed under gravity and seismic loads. Infill panel is replaced by two struts according to FEMA306. Time history and pushover analyses are performed to assess seismic strength of the building. Simulations are performed by SAP2000. Numerical results show that behavior of bare and infill frames under lateral loading are too distinct. There is a change in the manner in which the infill frame carries the lateral loads.

1. Introduction

Concrete frames infilled by bricks are generally used as structural system for multi-storey buildings to carry gravity and lateral seismic loads. Past earthquakes, have indicate that infill panels change the structural response of buildings under seismic loads. Figures 1 and 2 show collapses caused by soft storey and short column effects. Structural behavior of infilled frames was studied by many authors [1]-[7]. The studies were concentrated on the response of infilled frames by masonry under horizontal loading. Experimental results indicate that masonry infills modify the structural behavior of the frame. There is a modification in the manner in which the frame carries the lateral loads. In this article the seismic effect of infill on structural response of buildings is investigated. For this purpose, a multi-storey framed building is studied. Infill panel is modeled by two concentric diagonal struts according to FEMA306 [8]. Numerical simulations are performed using the software analysis SAP2000.

2. Material Nonlinearity

2.1. Concrete members

Beams and columns are idealized as frame elements with two concentrated plastic hinges at the extremities. For pushover analysis, P-M3 hinge is assigned to the columns and M3 hinge is assigned to the beams. The hinge parameters are calculated according to FEMA356 [10].

Figure 2: Short column mechanism [9]

*Corresponding Author: Miloud Mouzzoun, Hassania School of public works, Morocco, mouzzoun.mouloud@gmail.com

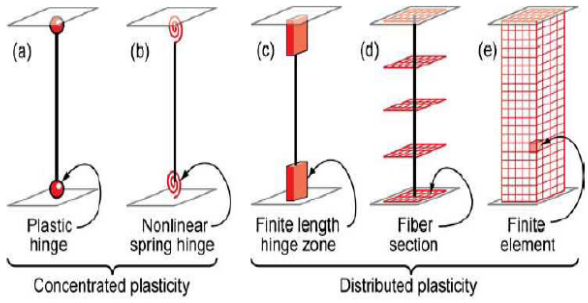

Figure 3: Introduction of material nonlinearity in concrete members [11]

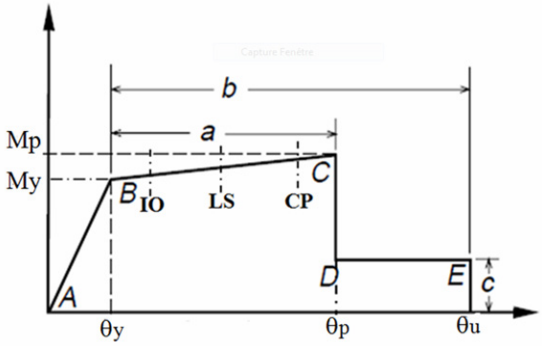

Figure 4: behavior of plastic hinge

2.2. Masonry infill wall

When lateral seismic forces are applied, infilled frame is replaced by two struts as shown in figure 5. The strut doesn't support any tension, it carries only compression loads. Strut width W is calculated by the equation (1).

$$w = 0.175d(\lambda H_c)^{-0.4} \quad (1)$$

$$\lambda = \sqrt[4]{\frac{E_m t \sin 2\theta}{4E_c I_c H_m}} \quad (2)$$

$$\theta = \tan^{-1}\frac{H_m}{L_m} \quad (3)$$

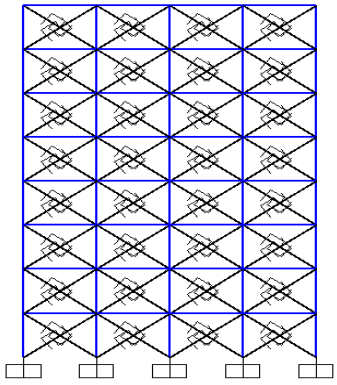

Figure 5: Frame with equivalent diagonal struts

3. Numerical investigations

The building studied here is an eight storey framed building, having 20 meters in the transversal direction and 25 meters in the longitudinal direction. Each storey height is 3m. The beams sections are 25cmx40cm; slabs thicknesses are 14cm. The columns sections vary from 30cmx30cm to 45cmx45cm. Building is analyzed under gravity and lateral seismic loads. Time history and Pushover analyses are performed by SAP2000 [12].

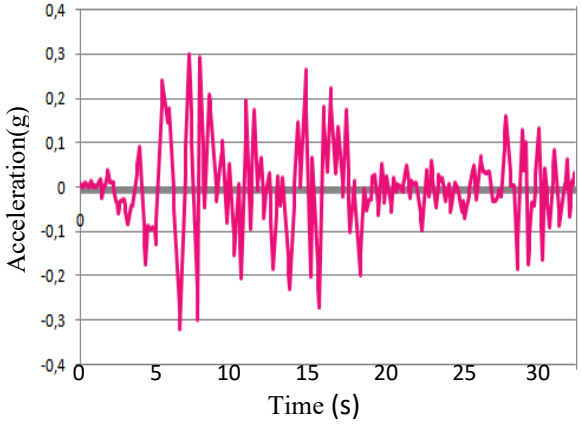

Figure 6: Elcentro Earthquake ground motion

4. Results and discussion

4.1. Periods of vibration

In the table 1, the periods of vibration of infill and bare frames are presented. It's found that introduction of infill walls reduces significantly the vibration periods.

Table 1: Natural periods of vibration

Mode Number	Infill frame	Bare frame
1	0.265	0.498
2	0.092	0.166
3	0.054	0.089
4	0.037	0.055
5	0.028	0.039
6	0.027	0.029

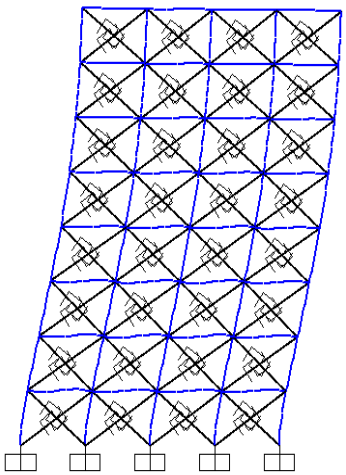

Figure 7: First mode of vibration of infill frame. T=0.265s

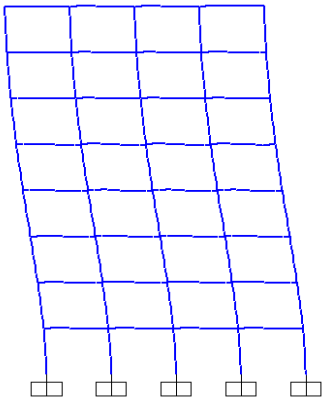

Figure 8: First mode of vibration of bare frame. T=0.498s

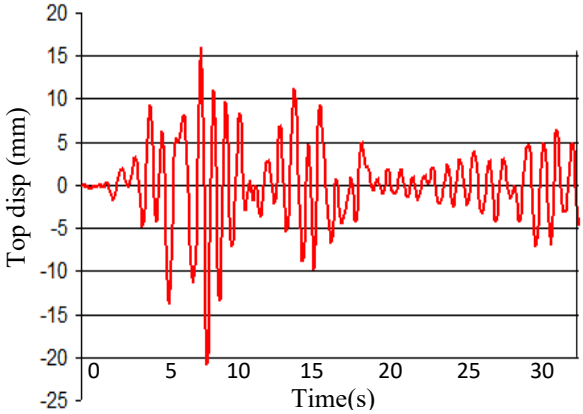

Figure 9: Top displacement time history. Infill frame

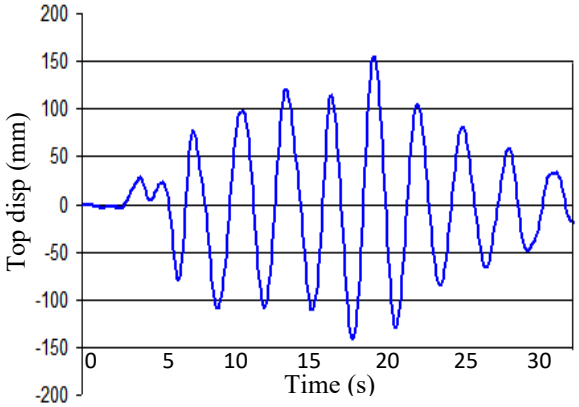

Figure 10: Top displacement time history. Bare frame

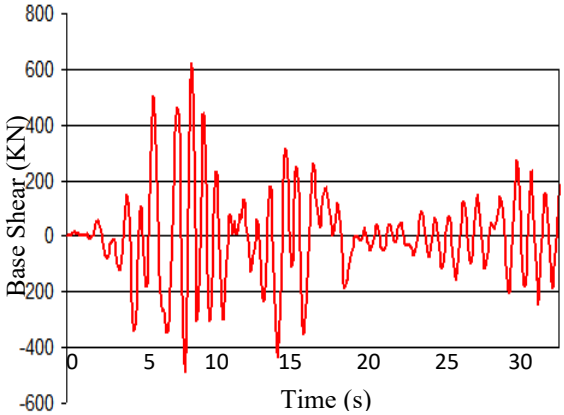

Figure 11: Base shear time history. Infill frame

4.2. Top displacement and base shear

Base shear and roof displacement time histories are shown in the figures 9, 10, 11 and 12. The results show that top displacement decreases and base shear increases when infill panels were introduced in the model by diagonal strut concept.

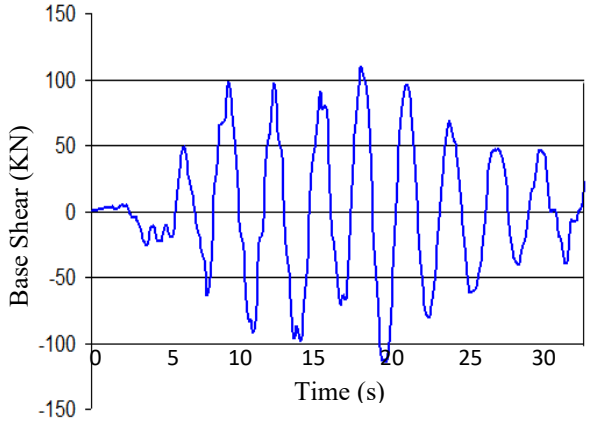

Figure 12: Base shear time history. Bare frame

4.3. Bending moments and shear forces

In the tables 2 to 5, we present the results of internal forces. The obtained results show that there is a great reduction in the values of bending moments and shear forces when infill wall is introduced in the structural model.

Table 2: Bending moments in the columns

Storey	Bare frame	Infill frame
	M(KN.m)	M(KN.m)
8°	68,02	23,81
7°	103,71	37,57
6°	153,61	63,17
5°	168,90	70,58
4°	171,49	75,95
3°	215,12	82,65
2°	298,60	132,40
1°	450,97	280,97

Table 3: Shear forces in the columns

Storey	Bare frame	Infill frame
	V(KN)	V(KN)
8°	33,15	11,42
7°	54,81	18,86
6°	81,87	32,33
5°	97,47	39,07
4°	109,03	43,81
3°	122,19	55,08
2°	122,45	62,65
1°	117,48	86,27

Table 4: Shear forces in the beams

Beam	Bare frame	Infill frame
	V (KN)	V (KN)
B1	104,71	60,50
B2	107,74	61,64
B3	104,68	61,59
B4	105,48	61,44

Table 5: Bending moments in the beams

Beam	Bare frame	Infill frame
	M (KN.m)	M (KN.m)
B1	166,02	78,63
B2	168,16	81,90
B3	168,04	81,86
B4	172,27	82,07

4.4. Seismic performance

Pushover analyses are carried out for infill and bare frames. The obtained pushover curves are superposed with the seismic demand curves to obtain the performance point. Two seismic demands are considered; moderate shaking with design acceleration A=0.16g and high shaking with design acceleration A=0.20g.

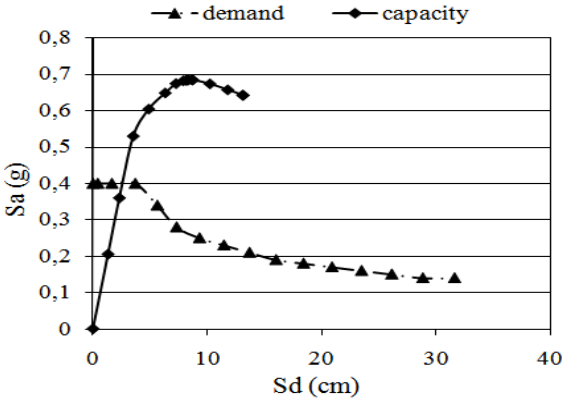

Figure 13: Seismic performance of infill frame under moderate shaking

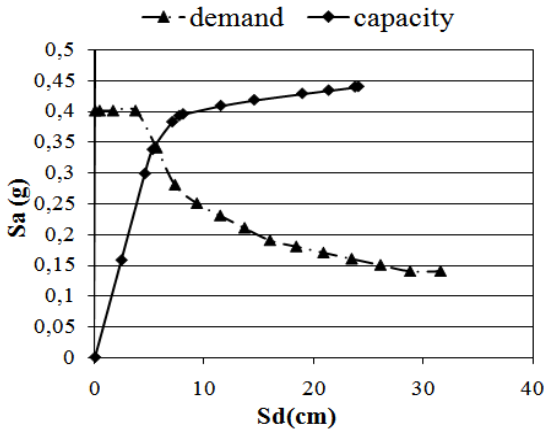

Figure 14: Seismic performance of bare frame under moderate shaking

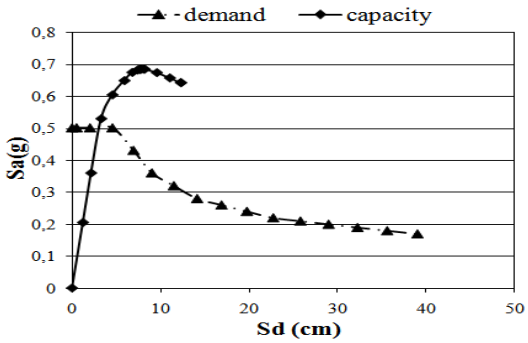

Figure 15: Seismic performance of infill frame under high shaking

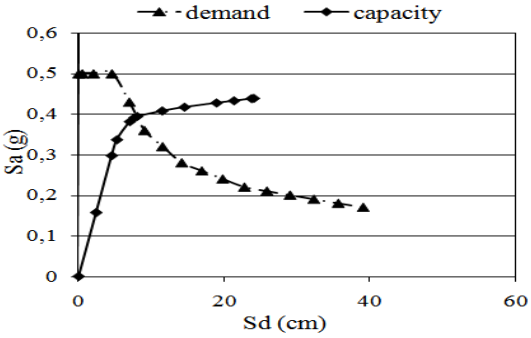

Figure 16: Seismic performance of bare frame under high shaking

4.5. Lateral storey displacements

The seismic demands for infill and bare frames under moderate and high shaking are presented in the figures 17 to 20. The results show that infill frame performs well compared with bare frame.

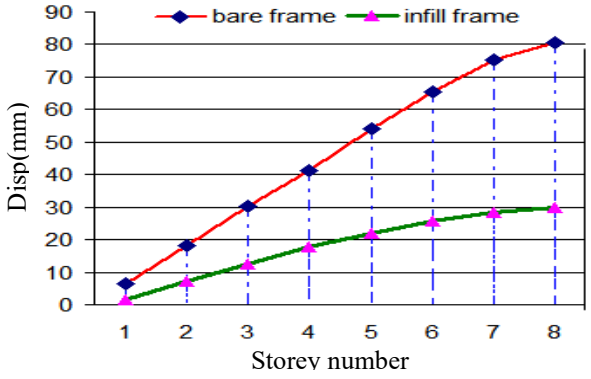

Figure 17: Lateral story displacements under moderate shaking

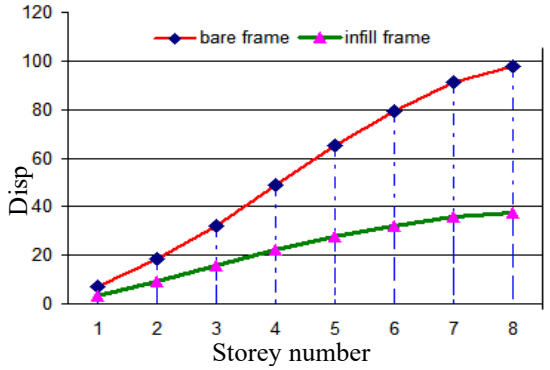

Figure 18: Lateral story displacements under high shaking

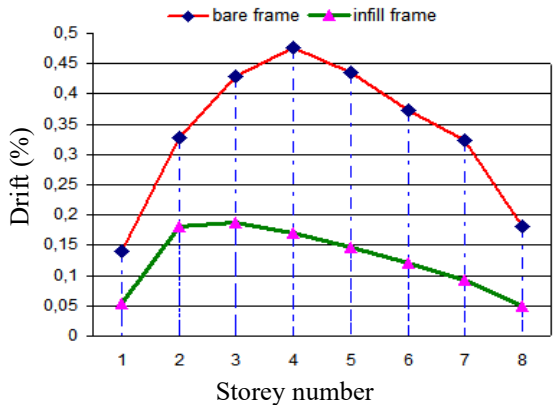

Figure 19: Inter-storey drifts under moderate shaking

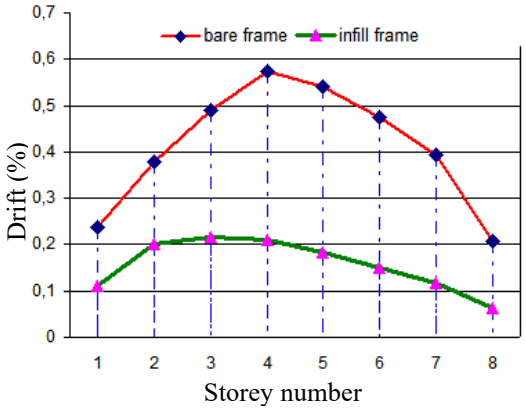

Figure 20: Inter-storey drifts under high shaking

5. Conclusion

The structural behavior of multi-storey buildings with infill panels under earthquake motion was investigated. The essential results are:

- Results show that natural periods of bare frame are greater than those of infill frame. Therefore, frame analysis without infill idealization underestimates the lateral shear design.
- Numerical simulations indicate that infill walls change considerably the internal forces. Maximum bending moments and shear forces of frame without infill are greater than those of infill frame.
- Pushover analysis shows that infill walls increase both lateral strength and stiffness of the building. Therefore, the seismic vulnerability of infilled building will be significantly reduced.
- Pushover analysis indicates that seismic performance of infill frame is largely superior to that of bare frame under different seismic intensities.
- Investigation results show that there is a change in the manner in which the infill frame carries the lateral loads. Diagonal strut concept of infill transforms the flexible frame into braced frame and then the values of internal forces will be changed.

Finally, this study has highlighted the influence of uniform infills on the earthquake response. Infill walls have a significant influence under seismic loads. Neglecting infills in the structural analysis is note a safe way. In perspective, it seems important to study the seismic effect of irregular configurations of infill panels, in order to prevent their unfavorable effects as in the case of soft storey and short column failures.

Conflict of Interest

The authors declare no conflict of interest.

References

[1] R.J. Mainstone, "on the stiffness and strength of lnfilled frames" Proceedings of the Institution of the Civil Engineers, **49**(2). 1971. https://doi.org/10.1680/iicep.1971.6267.

[2] D.V. Malick, RT Severn, "dynamic characteristics of infilled frames" Proceedings of the Institution of the Civil Engineers, **39**(2). 1968. https://doi.org/10.1680/iicep.1968.8091.

[3] B. Stafford, C. Carter, "A method for analysis for infilled frames" Proceedings of Institution of Civil Engineers, No. 7218, 31-48, 1969. https://doi.org/10.1680/iicep.1969.7290.

[4] A.B. Mehrabi, P.B.Shing, M.P.Schuller, J.L.Noland, "Experimental Evaluation of Masonry-Infilled RC Frames" ASCE Journal of Structural Engineering, **122**(3), 228-237, 1996. https://doi.org/10.1061/(ASCE)0733-9445(1997)123:5(604).

[5] P. Negro, A. Colombo, "Irregularities induced by non structural masonry panels in framed buildings" Engineering Structures. **19**(7), 576–585.1997. https://doi.org/10.1016/S0141-0296(96)00115-0.

[6] G. Al-Chaar, Evaluating strength and stiffness of unreinforced masonry structures. US Army Corps of Engineers. Construction Engineering Research Laboratories, 2002.

[7] A.Hashemi, K.M.Mosalam, "Shake-Table Experiment on Reinforced Concrete Structure Containing Masonry Infill Wall" Journal of Earthquake Engineering and Structural Dynamics. **14**(35), 1827-1852, 2006. https://doi.org/10.1002/eqe.612.

[8] FEMA306, Evaluation of Earthquake Damaged Concrete and Masonry Wall Buildings, Basic Procedures Manual, Federal Emergency Management Agency, 1999.

[9] M.Mouzzoun, "Seismic behaviour of reinforced concrete frame buildings with masonry infill", PhD thesis, Mohammadia School of engineers, Morocco, 2015.

[10] FEMA356, Federal Emergency Management Agency, NEHRP recommended Provisions for Seismic Regulations for New Buildings and Other Structures, 2000.

[11] ATC40, Applied Technology Council, Partnership for Response, and United States. Federal Emergency Management Agency. Evaluation of Earthquake Damaged Concrete and Masonry Wall Buildings: Basic Procedures Manual, 1999.

[12] CSI, Analysis Reference Manual for SAP2000, ETABS and SAFE, Computers and Structures, Inc. Berkeley, California, USA, 2005.

ASTES

Advances in Science, Technology and Engineering Systems Journal Vol. 5, No. 4, 638-644 (2020)

www.astesj.com

Special Issue on Innovative Research in Applied Science, Engineering and Technology

ASTESJ

ISSN: 2415-6698

Machine Learning for Network Intrusion Detection Based on SVM Binary Classification Model

Anouar Bachar[*,1,2], Noureddine El Makhfi[1], Omar EL Bannay[2]

[1]*FST, Abdelmalek Essaadi University, PMIC Lab, Al-Hoceima, 32003, Morocco*

[2]*ENSA, Sultan Moulay Slimane University, ASTI Lab, Khouribga, 25000, Morocco*

ARTICLE INFO

Article history:
Received: .23 June, 2020
Accepted: 20 July, 2020
Online: 25 August, 2020

Keywords:
IDS
Intrusions
Machine Learning
SVM classification model
UNSWNB-15 dataset

ABSTRACT

Recently, the number of connected machines around the worldwide has become very large, generating a huge amount of data either to be stored or to be communicated. Data protection is a concern for all institutions, it is difficult to manage the masses of data that are susceptible to multiple threats. In this work, we present a novel method of Intrusion Detection System (IDS) based on the detection of anomalies in computer networks. The aim is to use artificial intelligence techniques in the form of Machine Learning (ML) for intrusion detection. For this purpose, we have proposed a Support Vector Machine (SVM) classification model with two kernels, one Polynomial and the other Gaussian. This model is trained and tested with the recent UNSWNB-15 dataset. Regarding the results obtained, we have evaluated our model with six metrics capable of offering all potential threats. As a result, we have achieved a percentage of 94% for the detection rate (DR).

1. Introduction

The application of artificial intelligence in the field of computer network security has become an inescapable reality. In this context, we propose an extended version of an oral communication [1] which deals with network intrusion detection based on the SVM model.

The use of computer network services has become essential in several areas, particularly those related to daily life. The exchange of data can be very costly in the case of sometimes fatal threats, especially when it is a large-scale exchange at the level of governments or businesses [2]. These threats affect the integrity, confidentiality, and availability of these data. Possible solutions for the protection of computer networks are divided into two categories, those related to hardware or those related to software. We can cite firewalls, antivirus, cryptography, etc. as solutions. However, these solutions are insufficient to protect all networks [3]. In order to strengthen network security, another higher level of security such as IDSs is needed.

An IDS is a medium that allows us to protect our computer network from any unwanted activity as described in [4]. It filters incoming and outgoing network traffic to detect possible threats in the network. We distinguish between two types of IDS, the classical ones based on signatures as in the open-source software SNORT. They have a database of intrusion signatures. The signature of each incoming entity is compared with the signatures present in this database. Thus, the signature-based-IDS is very efficient for the detection of common threats and generates a very low FAR (False Alarm Rate). Despite this, it is unable to detect modern attacks. The second type of IDS is based on artificial intelligence techniques using ML for the detection of new attacks (0 Day attack) as described in the work [5]. However, the only problem is the very high false alarm rate generated by this type of IDS. This is the reason why several scientific research works are interested in this topic.

In this article, we present an IDS based on the technique of ML. We have chosen to use an SVM binary classification model associated with a UNSWNB-15 dataset for training and testing the proposed model. This article is structured into seven sections: In section 2, we present the related work. In the next section, we discuss the basic principle of an IDS. Then, section 4 concerns the existing data sources and the description of the UNSWNB-15 data set that we have used in this paper. In Section 5, we present our methods. In section 6, we show the performance of our proposed model with a comparison and interpretation of the results obtained. In the last section, we have a general conclusion and the perspectives of this work.

2. Related Work

In recent years, protecting computer networks against various threats is a priority for most companies. The evolution of

[*]Corresponding Author: Anouar Bachar, Email: anouar.bachar@gmail.com

cyberattacks requires the use of highly developed ways for the detection of these threats. Among the first works, we can cite the work of James Canady [6] who used the Artificial Neural Network (ANN) classification model in 1998. Netssan P, et al [7] obtained a detection rate of 85.87% with the KDD-CUP 99 dataset by combining two naive Bayesian models and decision trees. Other work using the same KDD-CUP 99 dataset has been proposed by O. Deepen et al [8]. They obtained a DR of 99.9% so the FAR is too low in the order of 1.25%. Also, Divyatmika et al [9] achieved a detection rate close to 99% with the Multilayer Perceptron (MLP) classification model algorithm using KDD-CUP 99 dataset. Finally, G-H Zhou [10] proposed a very efficient model (Detection rate = 99.54%) using a KDD-CUP 99 dataset for an IDS.

In parallel to the above, several works have used different ML algorithms for the detection of threats in computer networks. We cite the work of G. Meena et al [11] who recently published a paper using some Machine Learning algorithms associated with the two datasets NSL-KDD and KDD-CUP 99. Also, L. Dhanabal et al [12] published a study evaluating the efficiency of ML algorithms with the NSL-KDD dataset.

The two datasets KDD-CUP 99 and NSL-KDD are used in most of the previous work. They remain ineffective for the detection of recent attacks, even though the detection rate is very high for the different classification algorithms [13]. Therefore, it is necessary to use a newly updated dataset containing the behavior of modern network traffic. In Section 4, we will develop a study of the different existing datasets to show the effectiveness of a modern intrusion detection system.

3. Intrusion Detection System

An IDS allows us to protect our computer network infrastructure from any malicious activity. These activities are generally targeting the integrity, confidentiality, and availability of data in our network.

We classify IDS according to several criteria such as the type of IDS and the associated classification method. Regarding the type, we have the (N-IDS) and the (H-IDS) (Figure 1):

- N-IDS (Network Intrusion Detection System): It secures the entire network. Its location in the network affects the false alarm rate. For example, if the NIDS is located upstream of a Firewall (Figure 1), then it generates fewer false alarms. Since the traffic is already filtered by the Firewall. Otherwise, if it is placed downstream of a Firewall (location 2). It generates more false alarms.
- H-IDS (Host Intrusion Detection System): It allows the machine to be secured on its own without the use of other systems.

The IDSs are classified according to the detection method as in the work [14]. The first is signature-based-IDS. In this case, the IDS have a signature base compared with the signature of each incoming entity. This allows the IDS to be very favorable for the detection of already known intrusions. However, this first class of IDS only detects modern attacks (0 Day attack) i.e. threats with unknown signatures [15]. The second detection class is anomaly-based-IDS as in [16]. In this work, we have used this last class of threat detection. We have focused on new machine learning techniques. Knowing that an IDS builds a user profile based on the normal behavior of the system. It then monitors the network to identify any abnormal activity in the network. The anomaly-based-IDS can detect modern attacks, but it generates a high FAR in contrary to the signature-based-IDS.

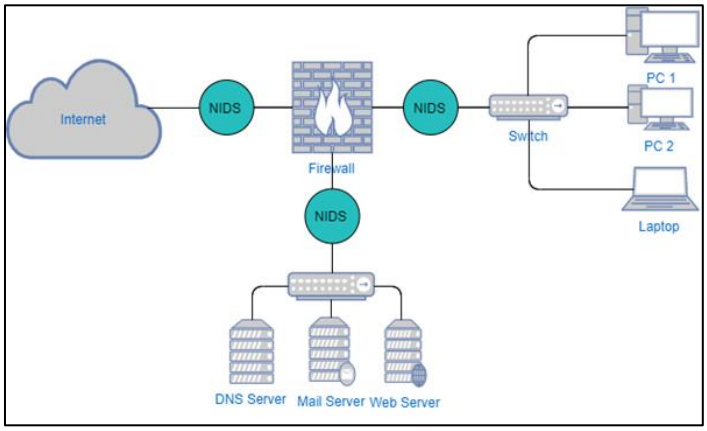

Figure1: Architecture of an IDS

4. Datasets

4.1. IDS-Dataset

Since the end of the 1990s, research work has been developing datasets for IDSs. These data sources are collected from network traffic simulators or by real systems, although the latter is very difficult to achieve because it may contain private data. One of the most widely used data sources is DRAPPA98 [17] published publicly in 1998 by MIT. Also, the dataset KDD-CUP 99 [18] published in 1999. This dataset contains the features of four categories of attacks (DOS, Probe, R2L, U2R). The major problem encountered is the considerable amount of redundant data which makes the use of this dataset difficult. We can also mention NSL-KDD dataset [19]. It is an updated version of the KDD-CUP 99. The NSL-KDD dataset is widely used for the network intrusion classification. Finally, we have other but less popular datasets such as CAIDA, DARPA, ISCX dataset, CICIDS.

4.2. Selecting-dataset

Previous researches are based on the two datasets KDD-CUP 99 and NSL-KDD for the classification of threats in computer networks. The authors of the works [13,20,21] have shown that these datasets encounter significant problems and their use is unreliable. These datasets suffer from a lack of diversity in traffic volumes. They contain duplicate data which does not cover real and recent attacks. To overcome these dataset issues, we have adopted the UNSWNB-15 [22] data source for training and testing our proposed model. Table 1 presents a comparison between the three datasets KDD-CUP 99, NSL-KDD, and UNSWNB-15.

Table 1: Comparison between the three datasets

Dataset	***RNC***	***RNT***	***LO***	***TIC***	***FPC***	***MMC***
KDD Cup 99	✓		✓	✓	✓	✓
NSL-KDD	✓		✓	✓	✓	✓
UNSW-NB15 (used in our method)	✓	✓	✓	✓	✓	✓

RNC: Realistic Network Configuration
RNT: Realistic Network Traffic
LO: Labelled Observations
TIC: Total Interaction Capture
FPC: Full Packet Capture
MMS: Many Malicious Scenarios

4.3. UNSWNB-15 dataset description

In this work, we have used a UNSWNB-15 dataset. This dataset was developed by ACCS (Australian Centre for Cyber Security) using IXIA Perfect storm tools. It is published in 2015 by authors Mustapha & Slay [23]. The UNSWNB-15 dataset contains 49 features categorized into six data associations (See Table 2 below).

Table 2: UNSWNB-15 dataset features

	N°	Features	Type
Flow features	1	srcip	N
	2	sport	I
	3	dstip	N
	4	dsport	I
	5	proto	N
Basic features	6	state	N
	7	dur	F
	8	sbytes	I
	9	dbytes	I
	10	sttl	I
	11	dttl	I
	12	sloss	I
	13	dloss	I
	14	service	N
	15	sload	F
	16	dload	F
	17	spkts	I
	18	dpkts	I
Content features	19	swin	I
	20	dwin	I
	21	stcpb	I
	22	dtcpb	I
	23	smeansz	I
	24	dmeansz	I
	25	Trans_depth	I
	26	Res_bdy_len	I
Time features	27	sjit	F
	28	djit	F
	29	stime	T
	30	ltime	T
	31	sintpkt	F
	32	dintpkt	F
	33	tcprtt	F
	34	synack	F
	35	ackdat	F
Additional features: general purpose	36	is_sm_ips_ports	B
	37	ct_state_ttl	I
	38	ct_flw_http_mthd	I
	39	is_ftp_login	B
	40	ct_ftp_cmd	I
Additional features: Connection features	41	ct_srv_src	I
	42	ct_srv_dst	I
	43	ct_dst_ltm	I
	44	ct_src_ ltm	I
	45	ct_src_dport_ltm	I
	46	ct_dst_sport_ltm	I
	47	ct_dst_src_ltm	I
Labelled features	48	attack_cat	N
	49	Label	B

Type:
N: Nominal, I: Integer, F: Float, T: Timestamp, B: Binary

The UNSW-NB15 dataset provides two label features: 'Attck_cat' represent the nine attack types (see table 3). It is used for a Multi-Class classification. The feature 'label' is used for binary classification (Normal and Attack). In this work, we choose to use a binary classification based on the second label feature.

Table 3: Types of attacks on UNSWNB-15

category	Sample
DOS	A DOS attack is a malicious activity in a computer network whose purpose is to prevent a network service from working for a given time.
Fuzzers	Is a method that randomly generates data to be injected into programs to detect possible vulnerabilities in a computer system.
Backdoors	A malicious program that provides access to a remote system for an unauthorized user.
Exploit	Consists of exploiting a software or hardware vulnerability in a computer network.
Analysis	This type of threat makes it possible to use vulnerabilities in a computer network to collect data useful for identifying future attacks.
Generic	This category opposes all block ciphers regardless of their structure. It concerns block cipher defined by given key sizes and blocks.
Recognition	This attack consists of discovering a computer system in order to detect vulnerabilities for future attacks.
Shellcode	A block of code to be injected into a computer program by a hacker. This makes it possible to exploit system deficiencies for malicious purposes.
Worms	A worm activates in a computer system by exploiting various vulnerabilities. It then spreads across the network by selecting other targets.

5. Proposed model

As we have previously shown, a signature-based-IDS is very efficient to detect the known attacks. However, it has a very low detection rate for recent attacks with unknown signatures. Figure 2 shows the Machine Learning steps followed in our model for the detection of attacks in a computer network. We used the SVM model to separate the two classes (Attack and No-Attack). Since in our case the data are non-linearly separable, we used the two functions with Polynomial and Gaussian kernel. These two functions are known by their good performances at the classification level in the SVM.

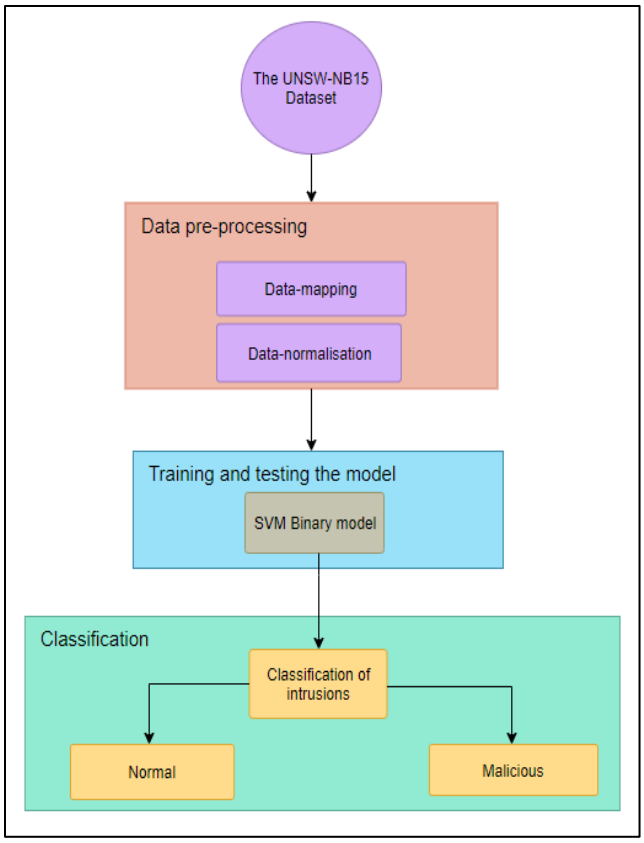

Figure 2: SVM binary classification proposed model

In our experience, the UNSWNB-15 dataset is composed of both CSV (Comma-separated values) files called UNSW_NB15_training_set.csv and UNSW_NB15_testing_set.csv. The first file contains 175 341 records for training the model (68%). However, the second contains 82 332 records for testing the model (32%). This dataset contains an integer, float, timestamp, and binary data type [23].

5.1. Data preprocessing

To train and test our model, a pre-processing step is necessary to select useful data ready for classification.

- Data-mapping: the first pre-processing step is data-mapping. It consists in transforming nominal data into numerical data (see figure 3). For example, the state field contains nominal data (INT, FIN, CON). In this phase, we converted these nominal values into numerical values (1,2,3).

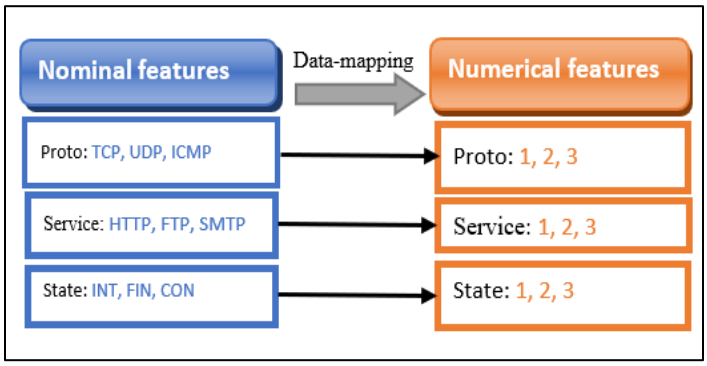

Figure 3: Data-mapping

- Data normalization: this step consists of increasing the speed of data processing. In this work, we applied the Min-Max method for data normalization. This consists in putting the numerical data in the margin [0-1] according to the following formula (1):

$$\text{X_normalised} = \frac{(X - \min(X))}{(\max(X) - \min(X))} \quad (1)$$

5.2. The SVM classifier

In this work, we have two observed classes (Attack and No-Attack). We used the SVM model for binary classification. This model is one of the algorithms of Machine Learning that have provided great performances either in classification or regression. It is a supervised learning model developed by Vapnik. In the case of classification, as in our case, the SVM model consists in finding a better boundary between the two observed classes (attack and No-Attack) (see figure 4). In this case, the data are non-linearly separable. For this purpose, we propose the kernel trick to have an optimal data separation as described in the work [24]. We assign two kernels one Gaussian and the other Polynomial because the data of the UNSWNB-15 dataset are also not linearly separable.

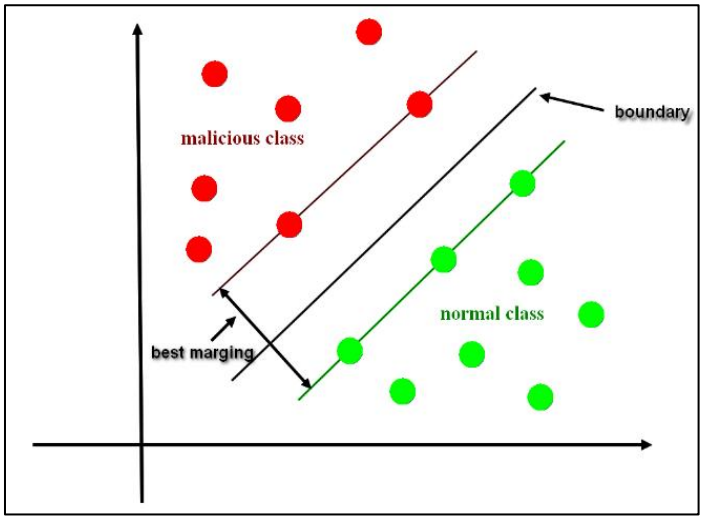

Figure 4: SVM Model hyperplane separation

6. Results and discussions

6.1. Criteria for Evaluating an IDS

The evaluation of an IDS is dependent on two main criteria:

- The Reliability of the IDS: The IDS must produce an alert for each incoming threat. An unreported intrusion is a system failure.
- The relevance of the IDS: Each alert must relate to a real threat. If we have a normal input event and it is classified as an intrusion also considered as well as a system failure. Table 4 presents the 4 possible cases.

Table 4: The confusion matrix

	Predicted Normal	Predicted Abnormal
Normal event	TN	FP
Abnormal event	FN	TP

TP (True Positive): Normal traffic is classified normal
FP (False positive): Normal traffic is classified abnormal.
FN (False Negative): abnormal traffic is classified normal
TN (True Negative): abnormal traffic is classified abnormal.

In our case, the confusion matrix gives the number of right and wrong predicted attacks, the same for the normal class (No-Attack).

6.2. Evaluation metrics of an IDS

To illustrate the effectiveness of our model, in this work we used six evaluation metrics.

We begin with the TPR (True Positive Rate) or Sensitivity. It describes the proportion of the positive class (Attack) correctly classified. The TPR calculates the quality of the IDS in terms of detection. To calculate the TPR, we use formula (2), note that the TPR must be close to 1 for a good IDS.

$$TPR = \frac{TP}{(TP+FN)} \quad (2)$$

On the opposite, the FPR (False Positive Rate) or Specificity. It describes the proportion of the negative class (No-Attack) correctly classified. To calculate the FPR, we use the formula (3), note that the FPR must be close to 0 for a good IDS.

$$FPR = \frac{FP}{(FP+TN)} \quad (3)$$

An effective IDS should provide a TPR close to 1 and a FPR close to 0.

The third evaluation metric is accuracy, which provides the true predictions for the entire test base. We calculate the accuracy according to the following formula (4):

$$\text{Accuracy} = \frac{(TP+TN)}{(TP+TN+FP+FN)} \quad (4)$$

Accuracy calculation (PR) provides the proportion of true positive predictions in the forecast class (Attack). The accuracy is shown by the following formula:

$$Precision = \frac{TP}{TP+FP} \quad (5)$$

The fifth metric is RECALL (RE). It returns the proportion of correct predictions in the attack class. It is calculated according to the formula (6):

$$RE = \frac{TP}{TP+FN} \quad (6)$$

The last metric that we have used is F1-Score. This is a calculation of the harmonic average between precision (PR) and recall (RE). It is calculated according to formula (7):

$$\text{F1} - \text{score} = \frac{2\times(PR\times RE)}{(PR+RE)} \quad (7)$$

6.3. The obtained results

Our model is tested with the UNSWNB-15 dataset. The SVM classifier is used with two kernel functions Polynomial and Gaussian for binary classification. With this model, we obtained good results in terms of DR for the classes normal and malicious.

The figures 5 and 6 show, respectively the confusion matrix for the two kernels SVM-Gaussian and SVM-Polynomial.

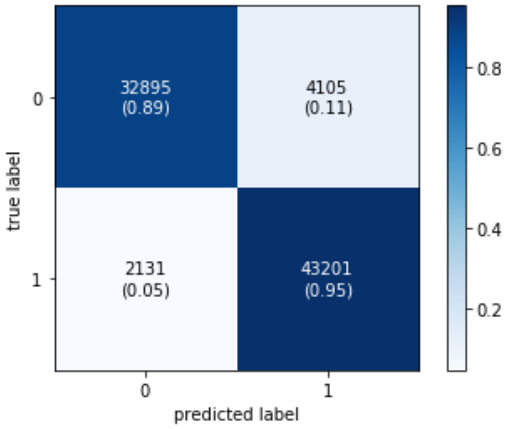

Figure 5: Confusion Matrix for the SVM- Gaussian model

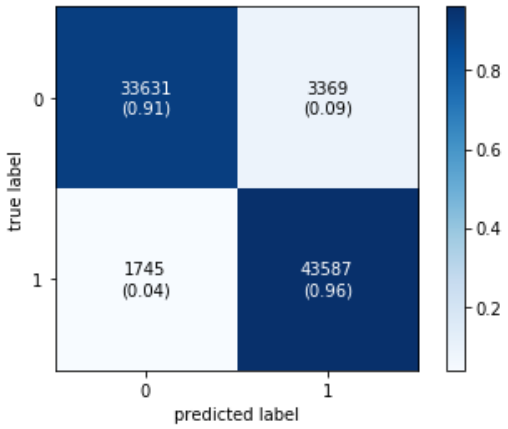

Figure 6: Confusion Matrix for the SVM-Polynomial model

To present our obtained results, we have plotted the ROC curves for the two kernels. These curves represent the TPR (Sensitivity) as a function of FPR (Specificity). They show that we have a very high rate of true positives (close to 1) against a low rate of false alarms (close to 0). This validates the performance of our model.

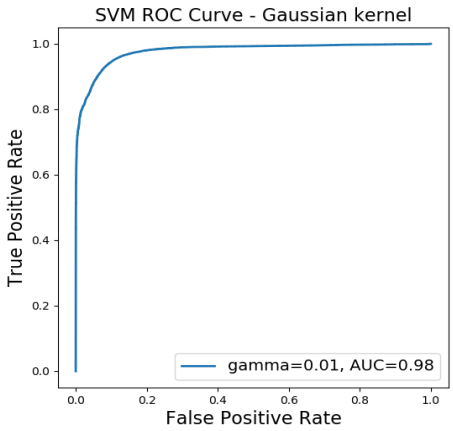

Figure 7: ROC curves correspond to Gaussian kernels

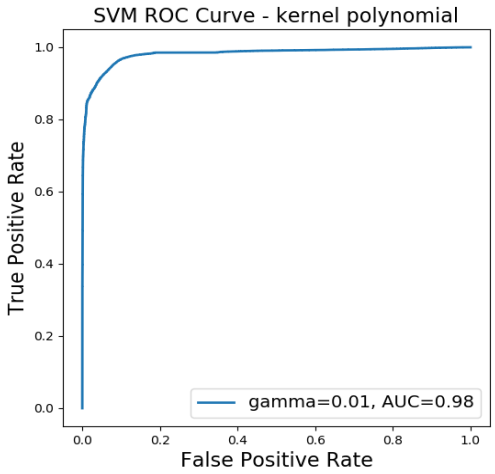

Figure 8: ROC curves correspond to Polynomial kernels

Tables 5 and 6 show the performance of the two kernels SVM-Gaussian and SVM-Polynomial:

- With the Gaussian kernel, we obtained a DR of 94% for the normal class and 91% for the malicious class.
- For the Polynomial kernel, we found slightly high results compared to the Gaussian function. We obtained a detection rate of 95% for the normal class and 93% for the abnormal class.

Table 5. SVM Gaussian kernel results

Class	Precision (5)	Recall (6)	F1-Score (7)
No-Attack	0.94	0.89	0.91
Attack	0.91	0.95	0.93
Accuracy (4)	0.93	0.92	0.92

Table 6. SVM Polynomial kernel results

Class	Precision (5)	Recall (6)	F1-Score (7)
No-Attack	0.95	0.91	0.93
Attack	0.93	0.96	0.94
Accuracy (4)	0.94	0.94	0.94

6.4. Performance evaluation of the proposed model

To evaluate the effectiveness of our model, we compared our obtained results with those of other work using the same UNSWNB-15 dataset (Table 7). The comparison results of our SVM model with other classification models are good. We obtained for the Polynomial kernel an accuracy equal to 94% as shown in the following table:

Table 7. Comparison with of other models

Reference	Model	Accuracy	F1-score
[25]	RepTree	88.95	-
[26]	RandomForest	90.3	92.4
[27]	MLP	86.7	89 .22
Proposed model	SVM Kernel-Gaussian	93	92
Proposed Model	SVM Kernel-Polynomial	94	94

7. Conclusions and perspective

In this work, we have developed a novel method for detecting attacks in computer networks. For this purpose, we presented a binary model for the classification of intrusions. We used the UNSWNB-15 data source. This source is widely used in the field of cybersecurity. We based on the SVM classifier with two kernel functions SVM-Polynomial and SVM-Gaussian. The evaluation results show high performance for both Gaussian (Accuracy = 93%) and Polynomial (Accuracy = 94%) kernels. In perspective, we will opt for a multi-class classification for the detection of each type of intrusion separately.

References

[1] A. BACHAR, N. E. MAKHFI and O. E. Bannay, "Towards a behavioral network intrusion detection system based on the SVM model", 1st International Conference on Innovative Research in Applied Science, Engineering and Technology (IRASET), Meknes, Morocco, pp. 1-7, 2020. doi: 10.1109/IRASET48871.2020.9092094.

[2] L.A. Maglaras et al., "Cyber security of critical infrastructures. ICT Express, 4(1), 42-45, 2018. doi:10.1016/j.icte.2018.02.001

[3] K. Choo, "The cyber threat landscape: Challenges and future research directions". Computers & Security 30:719–731, 2011. doi: 10.1016/j.cose.2011.08.004

[4] M. Aydın, M. Ali, A. Halim Zaim, and K. Gökhan Ceylan. "A hybrid intrusion detection system design for computer network security", Computers & Electrical Engineering, p 517-526, 2009. Doi: 10.1016/j.compeleceng.2008.12.005

[5] D.K. Bhattacharyya, J.K. Kalita, "Network Anomaly Detection: A Machine Learning Perspective" : CRC Press, 2013.

[6] J. Cannady, "Artificial Neural Networks for Misuse Detection," Proc eedings, National Information Systems Security Conference (NISSC '98), October, Arlington ,VA, 443 -456. 1998.

[7] P. Natesan, P. Balasubramanie, "Multi Stage Filter Using Enhanced Adaboost for Network Intrusion Detection. International Journal of Network Security & Its Applications", **4**(3), 121-135, 2012. doi:10.5121/ijnsa.2012.4308

[8] O. Depren et al., "An intelligent intrusion detection system (IDS) for anomaly and misuse detection in computer networks. Expert Systems with Applications", **29**(4), 713-722, 2005. doi:10.1016/j.eswa.2005.05.002

[9] Divyatmika, M. Sreekesh, "A two-tier network based intrusion detection system architecture using machine learning approach. International Conference on Electrical, Electronics, and Optimization Techniques (ICEEOT), 2016. doi:10.1109/iceeot.2016.7755404

[10] G. Zhou, "An Effective Distance-Computing Method for Network Anomaly Detection. Security Technology Communications in Computer and Information Science", 177-182, 2011. doi:10.1007/978-3-642-27189-2_19

[11] G. Meena et al., "A review paper on IDS classification using KDD 99 and NSL KDD dataset in WEKA". International Conference on Computer, Communications and Electronics (Comptelix), 2017. doi:10.1109/comptelix.2017.8004032

[12] L. Dhanabal and S. P. Shantharajah, "A study on NSL-KDD dataset for intrusion detection system based on classification algorithms,"International Journal of Advanced Research in Computer and Communication Engineering, **4**(6), 446–452, 2015. doi:10.17148/IJARCCE.2015.4696

[13] N. Moustafa, J. Slay, "The Significant Features of the UNSW-NB15 and the KDD99 Data Sets for Network Intrusion Detection Systems". 4th International Workshop on Building Analysis Datasets and Gathering Experience Returns for Security (BADGERS), 2015. doi:10.1109/badgers.2015.014

[14] W. Hu, S. Maybank, "AdaBoost-Based Algorithm for Network Intrusion Detection. IEEE Transactions on Systems, Man, and Cybernetics, Part B (Cybernetics), 38(2), 577-583, 2008. doi:10.1109/tsmcb.2007.914695

[15] A.L. Buczak, E. Guven, "A Survey of Data Mining and Machine Learning Methods for Cyber Security Intrusion Detection. IEEE Communications Surveys & Tutorials, **18**(2), 1153-1176, 2016. doi:10.1109/comst.2015.2494502

[16] P. Garc´ıa-Teodoro, J. D´ıaz-Verdejo, G. Maci´a-Fern´andez, E. V´azquez, "Anomalybased network intrusion detection: Techniques, systems and challenges. Comput. Secur. **28**(1-2), 18–28, Feb 2009. https://doi.org/10.1016/j.cose.2008.08.003

[17] L. Lincoln, "DARPA datasets. In: DARPA 1998 & 1999. Datasets. https://www.ll.mit.edu/r-d/datasets. Accessed June 23, 2020

[18] KDD Cup (1999) KDD Cup 1999 Data. In: KDD Cup 1999 Data. http://kdd.ics.uci.edu/databases/kddcup99/kddcup99.html. Accessed June 23, 2020

[19] NSL-KDD (2009) NSL-KDD | Datasets | Research | Canadian Insti- tute for Cybersecurity | UNB, https://www.unb.ca/cic/datasets/nsl.html Accessed June 23, 2020.

[20] M. Tavallaee, E. Bagheri, W. Lu, A.A. Ghorbani, "A detailed analysis of the KDD CUP 99 data set". 2009 IEEE Symposium on Computational Intelligence for Security and Defense Applications, 2009. doi:10.1109/cisda.2009.5356528

[21] N. Moustafa, J. Slay, "The evaluation of Network Anomaly Detection Systems: Statistical analysis of the UNSW-NB15 data set and the comparison with the KDD99 data set". Information Security Journal: A Global Perspective, **25**(1-3), 18-31, 2016. doi:10.1080/19393555.2015.1125974

[22] N. Moustafa, "UNSW_NB15 dataset", IEEE Dataport, 2019. Online Available: http://dx.doi.org/10.21227/8vf7-s525. Accessed June 23, 2020.

[23] N. Moustafa, J. Slay, UNSW-NB15: "A comprehensive data set for network intrusion detection systems (UNSW-NB15 network data set)". 2015 Military Communications and Information Systems Conference (MilCIS), 2015. doi:10.1109/milcis.2015.7348942

[24] B.M. Aslahi-Shahri et al., "A hybrid method consisting of GA and SVM for intrusion detection system. Neural Computing and Applications", **27**(6), 1669-1676, 2015. doi:10.1007/s00521-015-1964-2

[25] M. Belouch, S. El, M. Idhammad, "A Two-Stage Classifier Approach using RepTree Algorithm for Network Intrusion Detection". International Journal of Advanced Computer Science and Applications, **8**(6), 2017. doi:10.14569/ijacsa.2017.080651

[26] R. Vinayakumar et al., "Deep Learning Approach for Intelligent Intrusion Detection System". IEEE Access, 7, 41525-41550, 2019 doi:10.1109/access.2019.2895334

[27] J. Yan, D. Jin, C. Lee, P. Liu, "A Comparative Study of Off-Line Deep Learning Based Network Intrusion Detection". 2018 Tenth International Conference on Ubiquitous and Future Networks (ICUFN), 2018. doi:10.1109/icufn.2018.8436774

ASTES

Advances in Science, Technology and Engineering Systems Journal Vol. 5, No. 5, 652-659 (2020)

www.astesj.com

Special Issue on Innovative Research in Applied Science, Engineering and Technology

ASTESJ

ISSN: 2415-6698

Investment of Classic Deep CNNs and SVM for Classifying Remote Sensing Images

Khalid A. AlAfandy[*,1], Hicham Omara[2], Mohamed Lazaar[3], Mohammed Al Achhab[1]

[1]*ENSA, Abdelmalek Essaadi University, Tetouan, 93002, Morocco*

[2]*FS, Abdelmalek Essaadi University, Tetouan, 93002, Morocco*

[3]*ENSIAS, Mohammed V University in Rabat, 10000, Morocco*

ARTICLE INFO

Article history:
Received: 08 August, 2020
Accepted: 21 September, 2020
Online: 05 October, 2020

Keywords:
Remote Sensing Images
ResNet
VGG
DenseNet
CNN
SVM
Deep Learning
Machine Learning

ABSTRACT

Feature extraction is an important process in image classification for achieving an efficient accuracy for the classification learning models. One of these methods is using the convolution neural networks. The use of the trained classic deep convolution neural networks as features extraction gives a considerable results in the remote sensing images classification models. So, this paper proposes three classification approaches using the support vector machine where based on the use of the ImageNet pre-trained weights classic deep convolution neural networks as features extraction from the remote sensing images. There are three convolution models that used in this paper; the Densenet 169, the VGG 16, and the ResNet 50 models. A comparative study is done by extract features using the outputs of the mentioned ImageNet pre-trained weights convolution models after transfer learning, and then use these extracted features as input features for the support vector machine classifier. The used datasets in this paper are the UC Merced land use dataset and the SIRI-WHU dataset. The comparison is based on calculating the overall accuracy to assess the classification model performance.

1. Introduction

With the growth of communication especially using satellites and cameras, the remote sensing images was appeared with the importance of processing and dealing with this type of images (remote sensing images). One of these substantial image processing is classification which done using machine learning technology. Machine learning is one of the artificial intelligence branches that based on training computers using real data which result that computers will have good estimations as an expert human for the same type of data [1]. Deep learning is a branch of machine learning that counts on the Artificial Neural Networks (ANNs) which can be utilized in the remote sensing image classification [2]. In the recent years, which the latest satellites versions and its updated cameras with high spectral and spatial resolution are released, the very high resolution (VHR) remote sensing images are appeared. As logical results, the VHR remote sensing images have redundancy pixels that can cause an over-fitting problem through training process with using the ordinary machine learning or ordinary deep learning in classification. So it must optimize the ANNs and extract convenient features from remote sensing images as a preprocessing before training [3]. The convolution neural networks (CNNs) are derived from the ANNs who haven't fully connected layers as the ANNs layers; it have an excited rapid advance in computer vision [4]. It is based on some blocks can enforced on images as filters and then extracting a convolution object features from the input images which solving many of computer vision problems, one of these problems is classification [5]. The need of dealing with the huge data, that be contained in the VHR remote sensing images, produced the need of specific CNNs deep networks architectures that can generate an elevated accuracy in the classification problems. So, the classic networks are appeared. Many of classic networks are mentioned by researchers in their research papers. In this paper we use three widely used classic networks as features extraction in our proposed approaches. These classic networks are; the DenseNet 196, the VGG 16, and the ResNet 50 models. There are many researchers used these networks in their researches that related to the remote sensing images classification. In [6], authors proposed a new model to improve the classification accuracy using the DenseNet model. In [7], authors built dual channel CNNs for the remote sensing images using the DenseNet as features extraction. In [8],

[*]Corresponding Author: Khalid A. AlAfandy, +212635549566, khalid_yuosif@yahoo.com

authors built small number of convolutional kernels using dense connections to achieve large number of reusable feature maps. It was lead them to propose a convolutional network based on the DenseNet for the remote sensing images classification. In [9], authors used the VGG and the ResNet models to propose the RS-VGG classifier for classifying the remote sensing images. In [10], authors were built a combination between CNNs algorithms outputs, the VGG model is one of these algorithms, so a representation of the VHR remote sensing images understanding were established by their proposed method. In [11], authors used the remote sensing images classification to distinguish the airplanes by using the pre-trained VGG model. In [12], authors built a classifier model that classifying the high spatial resolution remote sensing images by using a fully convolution network that based on the VGG model. In [13], authors proposed the use of the ResNet model to extract the VHR remote sensing images features, then concatenated with low level features to generate a more accurate model using the SVM. In [14], authors used the ResNet to extract the 3-D features by transfer learning. They proposed a classification method for the hyper-spectral remote sensing images. In [15], authors proposed a method for classifying forest tree species using high resolution RGB color images that captured by a simple grade camera mounted on an unmanned aerial vehicle (UAV) platform. They used the ResNet in their proposed. In [16], authors proposed aircraft detection methods that based on the deep ResNet and super vector coding. In [17], authors combined edge and texture maps to propose a remote sensing image usability assessment method based on the ResNet. In [18], authors presented a comparative study that discussed the difference between the using of the SVM and the deep learning in classifying the remote sensing images. In [19], authors proposed a remote sensing image classification method that based on the SVM and sequential classifier. In [20], authors proposed a remote sensing images classifier using the genatic algorithm (GA) and the SVM.

The problem that attended by this paper is the difficulty of reaching a high accuracy assessment in the VHR remote sensing images classification models. Many researchers proposed solutions for this problem in their researches but they depend on the deep learning only or the machine learning only. Few of them are proposed hybrid classification techniques that consist of combination of the deep learning and the machine learning such as [13] and [20]. The deep learning and the machine learning combination can lead to considerable results.

The aim of this paper is to propose a combination of a classic network and the SVM to build a novel remote sensing images classifier. In this paper, the desired classic networks that combined with the SVM classifier are the DenseNet 169, The VGG16, and the ResNet 50 models. We used the ImageNet pre-trained weights with these mentioned models, transfer learning, and then extract features. These extracted features are considered as input features for the SVM classifier which trained to achieve the desired performance classification models. A comparative study is done for the use of the mentioned three convolution models as features extraction that combined with the SVM classifier, as proposed in this paper, to determine the performance of using each model. This comparison is based on calculating the overall accuracy (OA) to determine the performance of each model as a features extraction. There are two used datasets in this study; the UC Merced land use dataset and the SIRI-WHU dataset.

The rest of this paper is organized as follow. Section 2 gives the methods. The experimental results and setup are shown in section 3. Section 4 presents the conclusions followed by the most relevant references.

2. The Methods

In this section the proposed models will explained with its structures. The classic networks that used in these proposals and the SVM will illustrate in brief as a literature review, ending with how to measure the learning model performance.

2.1. The Proposed Models

The features extraction from the remote sensing images is provided an important basis in the remote sensing images analysis. So, in this paper the classic networks outputs can considered as the features that extracted from the remote sensing images. Where the train of a new model of the CNNs requires large amount of data, so in these three models, we used the ImageNet pre-trained weights, transfer learning, and then extract the desired features, then use these features as input features in training the SVM classifier. In the DenseNet 169 model, we transfer learning to the last hidden layer, before the output layer, that had 1664 neurons. Its outputs considered as the input features for the SVM classifier. In the VGG 16 model, we transfer learning to the last hidden layer, before the output layer, that had 4096 neurons. Its outputs considered as the input features for the SVM classifier. In the ResNet 50 model, we transfer learning to the last hidden layer, before the output layer, that had 2048 neurons. Its outputs considered as the input features for the SVM classifier.

2.2. The Convolution Neural Networks (CNNs)

The CNNs are possessed from the ANNs with exclusion that it is not fully connected layers [21]. The CNNs considered as the magic solution for much computer vision problems. The CNNs depend on some of filters that reduce the image height and width and increase the number of channels, then processing the output with full connected (FC) neural network layers [21, 22]. Figure 1 shows one of the CNNs model structures [22].

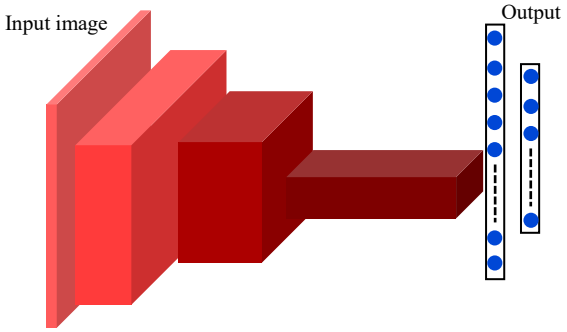

Figure 1: One of the CNNs model structures [23]

2.3. The DenseNet Model

In 2017, the DenseNets was proposed in the CVPR 2017 conference (Best Paper Award) [23]. The start point was from endeavored to construct a deeper convolution network that contains shorter connections between its layers close to the input and those close to the output, this deep convolution network can be more accurate and efficient to train. It is different from the

ResNet which has skip-connections that bypass the nonlinear transformation, the DenseNet add a direct connection from any layer to any subsequent layer. So the l^{th} layer receives the feature-maps of all former layers x_0 to x_{l-1} as (1) [23].

$$x_l = H_l([x_0, x_1, \dots, x_{l-1}]) \quad (1)$$

where $[x_0, x_1, \dots, x_{l-1}]$ refers to the spectrum of the feature-map produced in the layers $0, 1, 2, \dots, l-1$. Figure 2 shows the 5-layers dense block architecture. Table 1 shows the DenseNet 169 model architecture with the ImageNet pre-trained weights [23].

Table 1: the DenseNet 169 model architectures for ImageNet [23]

Layers	Output Size	DenseNet 169
Convolution	112×112	7×7 conv, stride 2
Pooling	56×56	3×3 max pool, stride 2
Dense Block (1)	56×56	$\begin{bmatrix} 1\times1 \text{ conv} \\ 3\times3 \text{ conv} \end{bmatrix} \times 6$
Transition Layer (1)	56×56	1×1 conv
	28×28	2×2 average pool, stride 2
Dense Block (2)	28×28	$\begin{bmatrix} 1\times1 \text{ conv} \\ 3\times3 \text{ conv} \end{bmatrix} \times 12$
Transition Layer (2)	28×28	1×1 conv
	14×14	2×2 average pool, stride 2
Dense Block (3)	14×14	$\begin{bmatrix} 1\times1 \text{ conv} \\ 3\times3 \text{ conv} \end{bmatrix} \times 32$
Transition Layer (3)	14×14	1×1 conv
	7×7	2×2 average pool, stride 2
Dense Block (4)	7×7	$\begin{bmatrix} 1\times1 \text{ conv} \\ 3\times3 \text{ conv} \end{bmatrix} \times 32$
Classification Layer	1×1	7×7 global average pool
	1000	1000D fully-connected, softmax

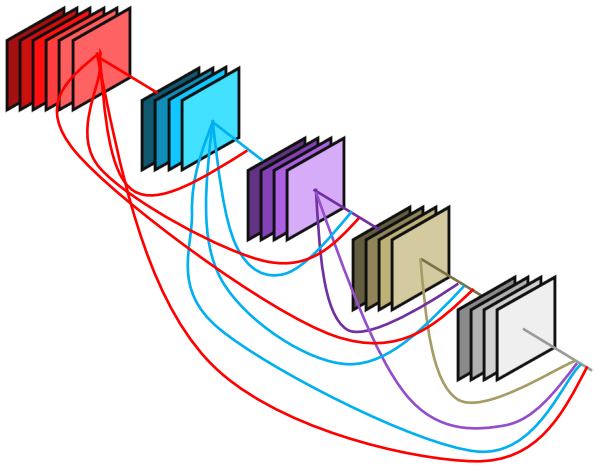

Figure 2: The 5 layers Dense block architecture [23]

2.4. The VGG Model

In 2015, the VGG network was proposed in the ICLR 2015 conference [24]. The start with inspected the effect of the convolution network depth on its accuracy with using the large-scale images. Through they rectified the deeper networks architecture using (3×3) convolution filters, they showed that an expressive growth on the prior-art configurations can be achieved by pushed the depth to 16-19 weight layers. The VGG model is a deeper convolution network that trained on the ImageNet dataset. Table 2 shows the VGG 16 model architecture with the ImageNet pre-trained weights [24].

Table 2: The VGG 16 model architectures for ImageNet [24]

Block	Layers	Output Size	VGG 16
Input		224×224×3	
Block 1	Convolution	224×224×64	3×3 conv 64, stride 1
	Convolution	224×224×64	3×3 conv 64, stride 1
	Pooling	112×112×64	2×2 max pool, stride 2
Block 2	Convolution	112×112×128	3×3 conv 128, stride 1
	Convolution	112×112×128	3×3 conv 128, stride 1
	Pooling	56×56×128	2×2 max pool, stride 2
Block 3	Convolution	56×56×256	3×3 conv 256, stride 1
	Convolution	56×56×256	3×3 conv 256, stride 1
	Convolution	56×56×256	3×3 conv 256, stride 1
	Pooling	28×28×256	2×2 max pool, stride 2
Block 4	Convolution	28×28×512	3×3 conv 512, stride 1
	Convolution	28×28×512	3×3 conv 512, stride 1
	Convolution	28×28×512	3×3 conv 512, stride 1
	Pooling	14×14×512	2×2 max pool, stride 2
Block 5	Convolution	14×14×512	3×3 conv 512, stride 1
	Convolution	14×14×512	3×3 conv 512, stride 1
	Convolution	14×14×512	3×3 conv 512, stride 1
	Pooling	7×7×512	2×2 max pool, stride 2
FC		4096	
FC		4096	
Output		1000, softmax	

The input images of this network is $(224 \times 244 \times 3)$. This network consists of five convolution blocks, each block containing convolution layers and pooling layer, then ending with two FC hidden layers (each layer has 4096 neurons), then ending with the output layer with softmax activation (1000 classes) [24].

2.5. The ResNet Model

In 2016, the ResNet was proposed in the CVPR 2016 conference [25]. They concerted the degradation problem by presenting a deep residual learning framework. Instead of intuiting, each few stacked layers directly fit a desired underlying mapping. The ResNet is based on skip connections between deep layers. These skip connections can skipping one or more non-linear transformation layers. The outputs of these connections are added to the outputs of the network stacked layers as (2) [25].

$$H(x) = F(x) + x \quad (2)$$

where H(x) is the final block output, x is the output of the connected layer, and F(x) is the output of the stacked networks layer in the same block. Figure 3 shows the ResNet one building block and tables 3 shows the ResNet 50 model architecture for the ImageNet [25].

Table 3: the ResNet 50 model architectures for ImageNet [25]

Layers	Output Size	ResNet 50
Conv 1	112×112	7×7 conv 64, stride 2
Conv 2_x	56×56	3×3 max pool, stride 2
		$\begin{bmatrix} 1\times1 \text{ Conv } 64 \\ 3\times3 \text{ Conve } 64 \\ 1\times1 \text{ Conv } 256 \end{bmatrix} \times 3$
Conv 3_x	28×28	$\begin{bmatrix} 1\times1 \text{ Conv } 128 \\ 3\times3 \text{ Conv } 128 \\ 1\times1 \text{ Conv } 512 \end{bmatrix} \times 4$
Conv 4_x	14×14	$\begin{bmatrix} 1\times1 \text{ Conv } 256 \\ 3\times3 \text{ Conve } 256 \\ 1\times1 \text{ Conv } 1024 \end{bmatrix} \times 6$
Conv 5_x	7×7	$\begin{bmatrix} 1\times1 \text{ Conv } 512 \\ 3\times3 \text{ Conve } 512 \\ 1\times1 \text{ Conv } 2048 \end{bmatrix} \times 3$
Classification Layer	1×1	7×7 global average pool
	1000	1000D fully-connected, softmax

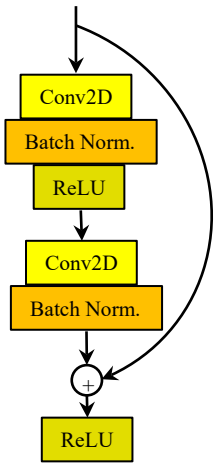

Figure 3: The ResNet building block[25]

2.6. The Support Vector Machine (SVM)

The SVM is a machine learning algorithm can act as a classifier or regression. It is based on small sample statistic theory that establishes optimal hyper-planes from the training data. These hyper-plans separate the different classes by building margins between classes. Maximizing these margins between classes, specially the nearest classes, on both sides of hyper-planes is the target for achieving the optimal SVM classifier [26, 27]. Figure 4 shows the possible and the optimal hyper-planes in the SVM model [26, 27].

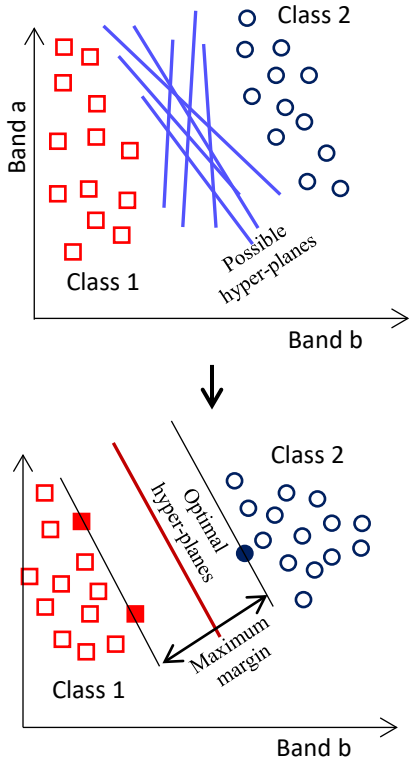

Figure 4: The possible and the optimal hyper-planes in the SVM model [26, 27]

2.7. The Performance Assessment

There are many matrices for gauge the performance of the learning models. One of them is the overall accuracy (OA). The OA is the main classification accuracy assessment [28]. It is measure the percentage ratio between the corrected estimation test data objects and all the test data objects in the used dataset. The OA is calculated using (3) [28, 29].

$$OA = \frac{Number\ of\ Correctly\ Estimations}{Total\ number\ of\ Test\ Data\ Objects} \times 100 \quad (3)$$

3. Experimental Results and Setup

This section will illustrate the experiments setup of the proposed algorithms, and then presents a comparative study for using each convolution model in our proposed. This comparison is based on calculating the OA for each model. The UC Merced land use dataset and the SIRI-WHU dataset are the used datasets. The details of these datasets will introduce in this section and then the experiments setup and results.

3.1. The UC Merced Land Use Dataset

The UC Merced Land use dataset is a collection of remote sensing images which has been prepared in 2010 by the University of California, Merced [30]. It is consists of 2100 remote sensing images divided into 21 classes with 100 images per each class. The

images were manually extracted from large images from the USGS National Map Urban Area Imagery collection for various urban areas around the USA. All images in this dataset are Geo-tiff RGB images with 256×256 pixels resolution and 1 square foot (0.0929 square meters) spatial resolution [30]. Figure 5 shows image examples from the 21 classes in the UC Merced land use dataset [30].

Figure 5: Image examples from the 21 classes in the UC Merced land use dataset [30]

3.2. The SIRI-WHU Dataset

The SIRI-WHU dataset is a collection of remote sensing images which the authors of [31] used this dataset in their classification problem research in 2016. This dataset consists of two versions that must complete each other. The total images in this dataset are 2400 remote sensing images divided into 12 classes with 200 images per each class. The images were extracted from Google Earth (Google inc.) and mainly cover urban areas in China. All images in this dataset are Geo-tiff RGB images with 200×200 pixels resolution and 2 square meters (21.53 square foot) spatial resolution [31]. Figure 6 shows image examples from the 12 classes in the SIRI-WHU dataset [31].

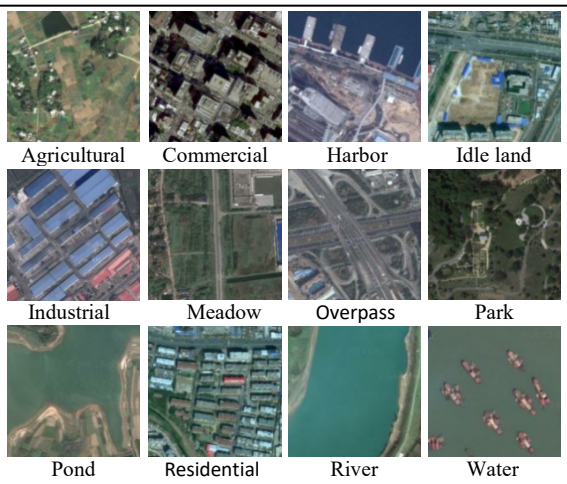

Figure 6: Image examples from the 12 classes in the SIRI-WHU dataset [31].

3.3. The Experimental Setup

All tests were performed using Google-Colab. The Google-Colab is a free cloud service hosted by Google inc. to encourage machine learning and artificial intelligence researches [32]. It is acts as a virtual machine (VM) that using 2-cores Xeon CPU with 2.3 GHz, GPU Tesla K80 with 12 GB GPU memory, 13 GB RAM, and 33GB HDD with Python 3.3.9. The maximum lifetime of this VM is 12 hours and it will be idled after 90 minutes time out [33]. Performing tests has been done by connecting to this VM online through ADSL internet line with 4Mbps communication speed. This connection was done using an Intel® coreTMi5 CPU M450 @2.4GHz with 6 GB RAM and running Windows 7 64-bit operating system. This work is limited by used the ImageNet pre-trained weights because the train of new convolution models needs a huge amount of data and more sophisticated hardware, this is unlike the lot of needed time consumed for this training process. The other limitation is that the input images shape is mustn't less than 200×200×3 and not greater than 300×300×3 because of the limitations of the pre-trained classic networks. The preprocessing step according to each network requirements is necessary to get efficient results; it must be as done on ImageNet dataset through these models were trained and produced the ImageNet pre-trained weights. The ImageNet pre-trained weights classic networks that used in this paper have input shape (224, 224, 3) and output layer with 1000 neurons according to the ImageNet classes (1000 classes) [34, 35]. So, it must perform transfer learning as stated in section 2.1. The used datasets were divided into 80% training set and 20% testing set before training the SVM model. It is must be notice that the SVM penalty value were determined by iterations and self-intuition. To extract the convolution features, the normalization preprocessing must done before extract features using the DenseNet 169 model, then using these features as input features to train the SVM model with penalty = 1.7. Where the BGR mode convertion is the desired preprocessing before extract features using the VGG 16 and the ResNet 50 models, then using its outputs as input features to train the SVM model with penalty = 2 for the VGG 16 extracted features and penalty =20 for the ResNet 50 extracted features. Figure 7 shows the flow charts of the proposed algorithms in this paper; figure 7.a. for using the DenseNet 169 model as features extraction, figure 7.b. for using the VGG 16 model as features extraction, and figure 7.c. for using the ResNet

50 model as features extraction, and then training the SVM classifier.

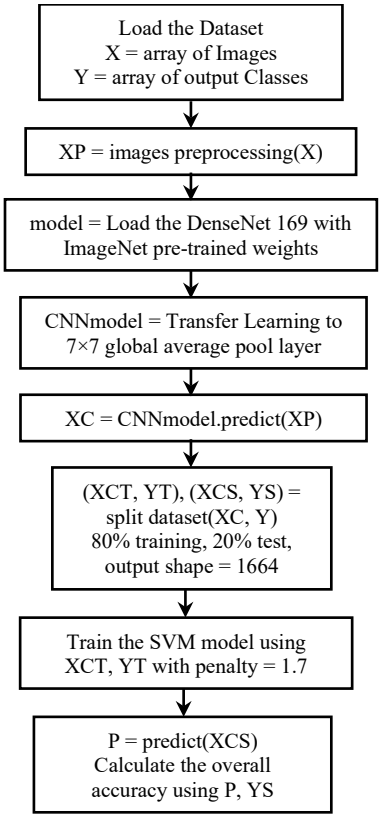

a: Using the DenseNet 169 model

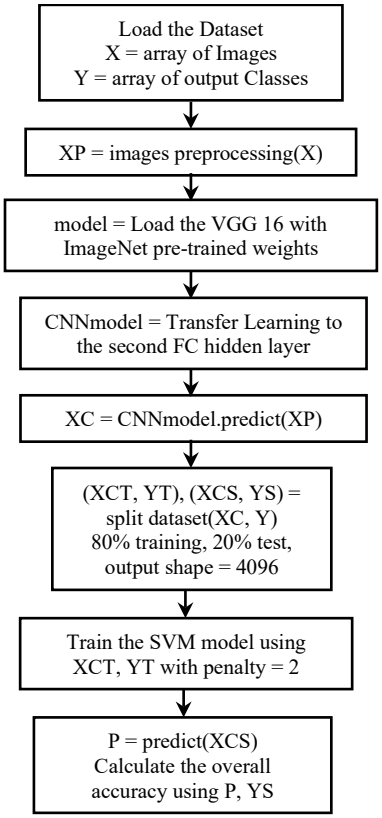

b: Using the VGG 16 model

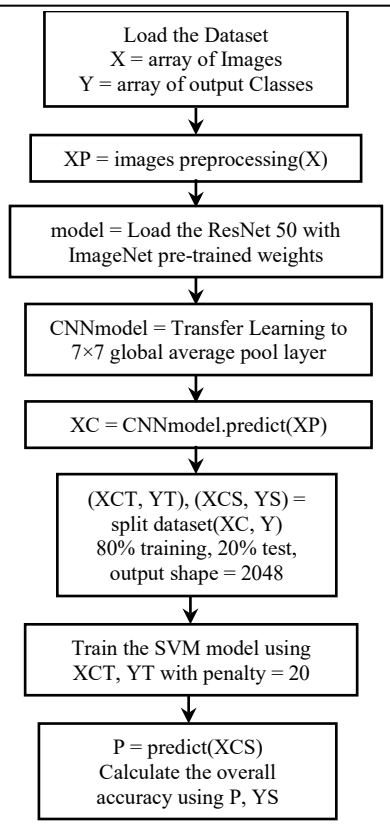

c: Using the ResNet 50 model

7: The flow charts of the proposed algorithms in this paper

3.4. The Experimental Results

This section presents the results of the proposed algorithms with the used datasets in this paper. Through the training process we used the training data (80% from the used dataset) and then calculate the OA using the predictions of the test data (20% from the used dataset) to assess the performance of each model. Table 4 and figure 8 show the OA for the using of each model to extract features that act as the input features to train the SVM classifier using the both datasets.

Table 4: The OA for the use of the convolution models with the SVM classifier using the both datasets

	The DenseNet-SVM	The VGG-SVM	The ResNet-SVM
The UC Merced land use Dataset	0.902	0.881	0.926
The SIRI-WHU Dataset	0.94	0.942	0.958

As shown from these results, the ResNet–SVM model had the higher OA in this study where the VGG–SVM model had the lowest OA. In the other hand the DenseNet–SVM model had higher OA than the VGG–SVM model when using the UC Merced land use dataset and had very little lower OA than the VGG–SVM when using the SIRI-WHU dataset. The use of the SIRI-WHU dataset had higher OA than the use of the UC Merced land use dataset. These results illustrated that the OA had an opposite relation with the dataset image resolution and the dataset number

of classes, so the use of the SIRI-WHU dataset which has 12 classes, image resolution 200×200 pixels, and spatial resolution 2 square meters gave higher OA than the use of the UC Merced land use dataset which has 21 classes, image resolution 256×256 pixels, and spatial resolution 0.0929 square meters (1 square feet). Extracting features using the deeper convolution networks gave considerable accuracy but the connections between layers may have another influence. The VGG–SVM model, that has deeper network without any layers connections, gave a good OA so it had an efficient result. In the other hand the ResNet–SVM model, that has skip layers connections, and the DenseNet–SVM, that has full layers connections, gave higher OA but still the ResNet–SVM gave the highest OA in this comparison. If keeping in mind the penalty values that used in training the SVM classifier using the three models as features extraction, we saw that the VGG–SVM and the DenseNet–SVM had normal penalty to give its OA in this comparison, where the ResNet–SVM had a high penalty value and given the highest OA in this comparison. The ResNets are based on the skip layers connections so the layer connections can raise the classification accuracy. The DenseNets may have more connections but still the use of the ResNets has the higher OA. As a total the deeper convolution networks may give better accuracy but the deeper networks that have layers connections may give the more better accuracy. The convolution models that have skip connections can give the better OA than the convolution models that have full layers connections. A high penalty value is needed for training the SVM models when using input features that extracted from the skip connection convolution models. For the SVM classifiers, extracting features from the high resolution remote sensing images are preferred with the use of deep convolution models that have layers connections where extracting features from the low resolution remote sensing images are preferred with the use of deep convolution models that haven't layers connections.

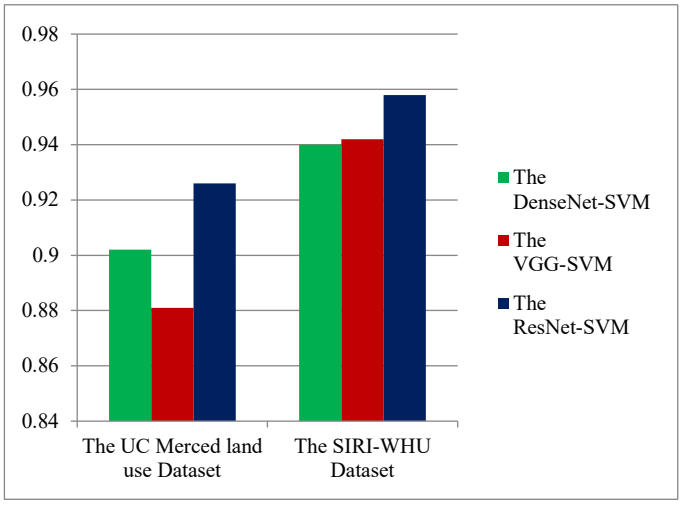

Figure 8: The OA for the use of the convolution models with the SVM classifier using the both datasets

4. Conclusions

This paper proposed remote sensing images classification approaches using the SVM classifier. The proposed approaches were based on using the deep convolution models classic networks as features extraction. The used classic networks in these approaches were the Densenet 169, the VGG 16, and the ResNet 50 models. The remote sensing images convolution features were extracted from these convolution models using the ImageNet pre-trained weights, which used as input features to train the SVM classifier. This paper also presented a comparison between the uses of the mentioned convolution models with the SVM classifier as proposed in this paper. This comparison was based on calculating the OA for using each model with the SVM classifier. There were two used datasets in this study; the UC Merced land use dataset and the SIRI-WHU dataset. This comparison illustrated that the ResNet–SVM model was more accurate than the other models that mentioned in this paper, which the OA of the DenseNet–SVM model was higher than the VGG–SVM model for using the UC Merced land use dataset and very little lower than the VGG–SVM using the SIRI-WHU dataset. The overall accuracy had an opposite relation with the remote sensing images resolution (pixel or spatial) and the number of dataset classes. For the SVM classifiers, it is preferred to use the deep networks without layers connections as features extraction with the low resolution remote sensing images where the deep networks that have layers connection are the preferred with the high resolution remote sensing images.

Conflict of Interest

The authors declare no conflict of interest.

References

[1] M. Bowling, J. Furnkranz, T. Graepel, and R. Musick, "Machine Learning and Games", Machine Learning, Springer, **63**(3), 211-215, 2006. http://doi.org/10.1007/s10994-006-8919-x

[2] K. Hwan Kim and S. June Kim, "Neural Spike Sorting Under Nearly 0-dB Signal-to-Noise Ratio Using Nonlinear Energy Operator and Artificial Neural-Network Classifier", IEEE Transactions on Medical Engineering, **47**(10), 1406-1411, 2000. http://doi.org/10.1109/10.871415

[3] M. Nair S., and Bindhu J.S., "Supervised Techniques and Approaches for Satellite Image Classification", International Journal of Computer Applications (IJCA), **134**(16), 1-6, 2016. http://doi.org/10.5120/ijca2016908202

[4] W. Rawat, and Z. Wang, "Deep Convolutional Neural Networks for Image Classification: A Comprehensive Review", Neural computation, **29**(9), 2352-2449, 2017. http://doi.org/10.1162/NECO_a_00990

[5] A. Khalid et al., "Artificial Neural Networks Optimization and Convolution Neural Networks to Classifying Images in Remote Sensing: A Review", in The 4th International Conference on Big Data and Internet of Things (BDIoT'19), 23-24 Oct, Rabat, Morocco, 2019. http://doi.org/10.1145/3372938.3372945

[6] Y. Tao, M. Xu, Z. Lu, and Y. Zhong, "DensNet-Based Depth-Width Double Reinforced Deep Learning Neural Network for High-Resolution Remote Sensing Images Per-Pixel Classification", Remote Sensing, **10**(5), 779-805, 2018. http://doi.org/10.3390/rs10050779

[7] G. Yang, B. Utsav, E. Ientilucci, Micheal Gartley, and Sildomar T. Monteiro, "Dual-Channel DenseNet for Hyperspectral Image Classification", in IGARSS 2018 - 2018 IEEE International Geoscience and Remote Sensing Symposium, 05 Nov, Valencia, Spain, 2595-2598, 2018. http://doi.org/10.1109/IGARSS.2018.8517520

[8] J. Zhang, C. Lu, X. Li, H. Kim, and J. Wang, "A Full Convolutional Network based on DenseNet for Remote Sensing Scene Classification", Mathematical Biosience and Engineering,, **6**(5), 3345-3367, 2019. http://doi.org/10.3934/mbe.2019167

[9] X. Liu, M. Chi, Y. Zhang, and Y. Qin, "Classifying High Resolution Remote Sensing Images by Fine-Tuned VGG Deep Networks", in IGARSS 2018 - 2018 IEEE International Geoscience and Remote Sensing Symposium, 22-27 Jul, Valencia, Spain, 7137-7140, 2018. http://doi.org/10.1109/IGARSS.2018.8518078

[10] S. Chaib, H. Liu, Y. Gu, and H. Yao, "Deep Feature Fusion for VHR Remote Sensing Scene Classification", IEEE Transactions on Geoscience and Remote Sensing, **55**(8), 4775-4784, 2017. http://doi.org/10.1109/TGRS.2017.2700322

[11] Z. Chen, T. Zhang, and C. Ouyang, "End-to-End Airplane Detection Using Tansfer Learning in Remote Sensing Images", Remote Sensing, **10**(1), 139-153, 2018. http://doi.org/10.3390/rs10010139
[12] G. Fu, C. Liu, R. Zhou, T. Sun, and Q. Zhang, "Classification for High Resolution Remote Sensing Imegery Using a Fully Convolution Network", Remote Sensing, **9**(5), 498-518, 2017. http://doi.org/10.3390/rs9050498
[13] M. Wang et al., "Scene Classification of High-Resolution Remotely Sensed Image Based on ResNet", Journal of Geovisualization and Spatial Analysis, Springer, **3**(2), 16-25, 2019. http://doi.org/10.1007/s41651-019-0039-9
[14] Y. Jiang et al., "Hyperspectral image classification based on 3-D separable ResNet and transfer learning", IEEE Geoscience and Remote Sensing Letters, **16**(12), 1949-1953, 2019. http://doi.org/10.1109/LGRS.2019.2913011
[15] S. Natesan, C. Armenakis, and U. Vepakomma, "ResNet-Based Tree Species Classification Using UAV Images", International Archives of the Photogrammetry, Remote Sensing & Spatial Information Sciences, **XLII**, 2019. http://doi.org/10.5194/isprs-archives-XLII-2-W13-475-2019
[16] J. Yang et al., "Aircraft Detection in Remote Sensing Images Based on a Deep Residual Network and Super-Vector Coding", Remote Sensing Letters, Taylor & Francis, **9**(3), 229-237, 2018. http://doi.org/10.1080/2150704X.2017.1415474
[17] L. Xu and Q. Chen, "Remote-Sensing Image Usability Assessment Based on ResNet by Combining Edge and Texture Maps", IEEE Journal of Selected Topics in Applied Earth Observations and Remote Sensing, **12**(6), 1825-1834, 2019. http://doi.org/10.1109/JSTARS.2019.2914715
[18] P. Liu et al., "SVM or Deep Learning? A Comparative Study on Remote Sensing Image Classification", Soft Computing, Springer, **21**(23), 7053–7065, 2016. http://doi.org/10.1007/s00500-016-2247-2
[19] Y. Guo et al., "Effective Sequential Classifier Training for SVM-Based Multitemporal Remote Sensing Image Classification", IEEE Transactions on Image Processing, **27**(6), 3036-3048, 2018. http://doi.org/10.1109/TIP.2018.2808767
[20] C. Sukawattanavijit et al., "GA-SVM Algorithm for Improving Land-Cover Classification Using SAR and Optical Remote Sensing Data", IEEE Geoscience and Remote Sensing Letters, **14**(3), 284-288, 2017. http://doi.org/10.1109/LGRS.2016.2628406
[21] Y. Chen et al., "Deep Feature Extraction and Classification of Hyperspectral Images Based on Convolutional Neural Networks", IEEE Transactions on Geoscience and Remote Sensing, **54**(10), 6232-6251, 2016. http://doi.org/10.1109/TGRS.2016.2584107
[22] E. Maggiori et al., "Convolutional Neural Networks for Large-Scale Remote-Sensing Image Classification", IEEE Transactions on Geoscience and Remote Sensing, **55**(2), 645-657, 2017. http://doi.org/10.1109/TGRS.2016.2612821
[23] G. Huang, Z. Liu, L. Maaten, and K. Q. Weinberger, "Densely Connected Convolutional Networks", in 2017 IEEE Conference on Computer Vision and Pattern Recognition (CVPR), 21-26 Jul, Honolulu, HI, USA, 2261-2269, 2017. http://doi.org/10.1109/CVPR.2017.243
[24] K. Simonyan and A. Zisserman, "Very deep convolutional networks for large-scale image recognition", in International Conference on Learning Representations (ICLR 2015), 7-9 May, San Diego, USA, 2015. https://arxiv.org/abs/1409.1556
[25] K. He, X. Zhang, S. Ren, and J. Sun, "Deep Residual Learning for Image Recognition", in 2016 IEEE Conference on Computer Vision and Pattern Recognition (CVPR), 27-30 Jun, Las Vegas, NV, USA, 770-778, 2016. http://doi.org/10.1109/CVPR.2016.90
[26] G. Mountrakis, J. Im, and C. Ogole, "Support vector machines in remote sensing: A review", ISPRS Journal of Photogrammetry and Remote Sensing, Elsevier, **66**(3), 247-259, 2011. http://doi.org/10.1016/j.isprsjprs.2010.11.001
[27] B.W. Heumann, "An Object-Based Classification of Mangroves Using a Hybrid Decision Tree-Support Vector Machine Approach", Remote Sensing, **3**(11), 2440-2460, 2011. http://doi.org/10.3390/rs3112440
[28] G. Banko, "A Review of Assessing the Accuracy of Classifications of Remotely Sensed Data and of Methods Including Remote Sensing Data in Forest Inventory", in International Institution for Applied Systems Analysis (IIASA), Laxenburg, Austria, IR-98-081, 1998. http://pure.iiasa.ac.at/id/eprint/5570/
[29] W. Li et al, "Deep Learning Based Oil Palm Tree Detection and Counting for High-Resolution Remote Sensing Images", Remote Sensing, **9**(1), 22-34, 2017. http://doi.org/10.3390/rs9010022
[30] Y. Yang and S. Newsam, "Bag-Of-Visual-Words and Spatial Extensions for Land-Use Classification", in the 18th ACM SIGSPATIAL international conference on advances in geographic information systems, 2-5 Nov, San Jose California, USA, 270-279, 2010. http://doi.org/10.1145/1869790.1869829
[31] B. Zhao et al., "Dirichlet-Derived Multiple Topic Scene Classification Model for High Spatial Resolution Remote Sensing Imagery", IEEE Transactions on Geoscience and Remote Sensing, **54**(4), 2108-2123, 2016. http://doi.org/10.1109/TGRS.2015.2496185
[32] E. Bisong, "Building Machine Learning and Deep Learning Models on Google Cloud Platform: A Comprehensive Guide for Beginners", Apress, Berkeley, CA, 2019.
[33] T. Carneiro et al., "Performance Analysis of Google Colaboratory as a Tool for Accelerating Deep Learning Applications", IEEE Access, **6**, 61677-61685, 2018. http://doi.org/10.1109/ACCESS.2018.2874767
[34] O. Russakovsky and L. Fei-Fei, "Attribute Learning in Large-Scale Datasets", in European Conference on Computer Vision, 6553, Springer, Berlin, Heidelberg, 10-11 Sep, Heraklion Crete, Greece, 1-14, 2010. http://doi.org/10.1007/978-3-642-35749-7
[35] J. Deng et al., "What Does Classifying More Than 10,000 Image Categories Tell Us? ", in The 11th European conference on computer vision, 6315, Springer, Berlin, Heidelberg, 5-11 Sep, Heraklion Crete, Greece, 71-84, 2010. http://doi.org/10.1007/978-3-642-15555-0

ASTES

Advances in Science, Technology and Engineering Systems Journal Vol. 5, No. 4, 783-794 (2020)

www.astesj.com

Special Issue on Innovative Research in Applied Science, Engineering and Technology

ASTESJ

ISSN: 2415-6698

The Effects of Transmission Power and Modulation Schemes on the Performance of WBANs in on-Body Medical Applications

Marwa Boumaiz[*,1], Mohammed El Ghazi[1], Mohammed Fattah[2], Anas Bouayad[1], Moulhime El bekkali[1]

[1]*LIASSE-ENSA, Sidi Mohammed Ben Abdellah University, Fes, 30050, Morocco*

[2]*EST, Moulay Ismail University, Meknes,50050, Morocco*

ARTICLE INFO

Article history:
Received:13 July, 2020
Accepted:02 August, 2020
Online: 28 August, 2020

Keywords:
Wireless Body Area Networks
IEEE 802.15.6
On-body medical applications
Packet Loss Rate
Throughput
Latency

ABSTRACT

Wireless Body Area Networks support the operation within multiple frequency bands. Thus, they can be integrated in several applications, one of which is on-body medical monitoring applications, as concerned in this paper. Therefore, the purpose of this study is to present the impact of transmission power and both of Differential Binary Phase Shift Keying and Differential Quadrature Phase Shift Keying modulation schemes, on the performance of a WBAN model based on the IEEE 802.15.6 2.4 GHz narrow-band, dedicated to on-body medical applications. This involves identifying the modulation scheme(s) and transmission power level(s) to be adopted for these applications, that can be classified into three types depending on their data rate (low, medium and high data rate medical applications), in order to meet Packet Loss Rate and latency requirements. The numerical study has confirmed that the adoption of DBPSK modulation and low transmission powers provides good performance for low data rate monitoring applications. At medium data rates, a relatively increased transmit power was required. However, at high data rates, DQPSK modulation with a 0 dBm transmission power seemed to be the right choice to be made in terms of the mentioned performance indicators.

1. Introduction

The actual improved life expectancy all over the world has led to an increased rate of population ageing [1], which may overburden conventional healthcare infrastructures and consequently increase healthcare costs. In addition, each year millions of people die due to late diagnosis of certain fatal diseases such as cancer, cardiovascular diseases, Parkinson's disease and many others [1]. These losses could have been largely avoided if those illnesses were detected in time.

The massive growth of electronic systems [2] resulted in the appearance of small biosensors operating at the human body scale as Wireless Body Area Networks. When used in healthcare systems, WBANs can simplify the monitoring of simple parameters such as body temperature, blood pressure, ECG, etc., or be integrated in more complicated processes like changing programs for implantable pacemakers and defibrillators [3], retrieving biokinetic information [4–6], or adjusting body limbs movements when damaged by car accidents, for example.

In medical applications [7], WBANs are considered to be the key solution to prevent a variety of cardiovascular diseases [8–9], such as myocardial infarction, which are often related to intermittent rather than permanent anomalies s[10]. In addition, as the number of diabetic people worldwide is expected to reach 380 million by 2025, WBANs can also be adopted in diabetes monitoring [11–12]. Therefore, it will be necessary to integrate medical monitoring systems based on WBANs in our day to day life, in order to correctly and timely dose medicines, and thus reduce the risk of many complications. Similarly, miniaturized sensors can further be used to detect cancer cells, allowing the doctor to first diagnose tumors without the need for a biopsy [10]. As for people suffering from asthma, WBANs may also ensure the detection of allergenic agents in the environment surrounding the patient. In [13] for example, The authors proposed an alert system triggered by the detection of an environment the patient is allergic

[*]Corresponding Author: Marwa Boumaiz, marwaboumaiz@gmail.com

to. Moreover, they can be integrated into the rehabilitation process to bring patients' functional capacity back to normal [5].

For all the above mentioned medical applications, data traffic can be classified into three categories [10]: on-demand, urgent and normal traffic. For diagnostic purposes, on-demand traffic is initiated by the coordinator in order to obtain information about the patient's state of health. As for urgent traffic, it is initiated by sensor nodes when the data collected exceeds a predefined threshold. This type of data is not time-dependent and is generated in an unpredictable manner. As for normal traffic, it generally concerns normal non-critical data, that include discrete and systematic health monitoring.

In non-medical applications, WBANs take place in fitness, performance and wellness monitoring, in cognitive biometry [14] for a secure authentication to information systems, in serious gaming [15] for educational purposes, and in sport.

Given this variety of applications , the actual wireless short range technologies do not fully comply with the specific requirements and technical challenges of WBANs [16]. For this reason, IEEE 802.15.6 was created in November 2007 to deliver an international standard for highly reliable, short-range, and bodywide communications, while providing a broad range of data rates going from 75.9 Kbps (narrowband) to 15.6 Mbps (ultra-broadband); to cover a variety of applications. The standard provides an advanced MAC layer that serves three physical layers: The Narrowband (NB), the Ultra Wide Band (UWB) and the Human Body Communication (HBC) physical layers. These are chosen according to the intended application. We are interested in the narrowband physical layer, which alone offers 7 different frequency bands, one of which is the 2.4 GHz band (2400-2483.5 MHz) and is often favored over the other ones for its worldwide availability [17]. It is also the most mature band [18] which offers a larger bandwidth. Furthermore, it uses familiar PHY modules, that are already extensively applied in WiFi and Bluetooth [19], and adopts smaller antennas, which makes it ideal for the majority of on body WBAN applications. All these features contribute to make the 2.4 GHz ISM band of IEEE 802.15.6, the most widely used band.

According to the specifications of the IEEE 802.15.6 standard [20–21], The 2.4 GHz narrowband provides two modulation schemes: DQPSK and DBPSK. In addition, the nodes in a WBAN must be able to transmit their data using a power level ranging from -10 dBm (0.1 mW) to 0 dBm (1 mW) [1], so as not to exceed the specific absorption rate fixed at 1.6 W / kg in 1g of body tissue. However, the choice of one of these two modulations and the appropriate level of node transmission power, may be related to the intended application and its technical requirements, such as data rate, duty cycle, sensitivity to data loss and latency, etc.

Therefore, the aim of this paper is to study the adequacy of DBPSK and DQPSK modulations, as well as different transmission power levels in the 2.4 GHz narrowband, for a realistic WBAN model based on the IEEE 802.15.6 standard, with the requirements of normal traffic on-body medical monitoring applications, such as electrocardiogram, pulse oximetry, body temperature measurement etc., in terms of PLR, throughput and latency.

The proposed contributions of the present paper are based on two detailed numerical studies dealing with the impact of transmission power on one hand, and the two modulation schemes DBPSK and DQPSK on the other, on the performances of a WBAN model based on the IEEE 802.15.6 standard. This evaluation is done by means of three parameters: PLR, throughput and latency.

The remainder of this paper is presented as follows:

Section 2 gives an overview of the IEEE 802.15.6 standard, addressing its technical requirements for the MAC layer, with a special highlight on the beacon mode with superframe boundaries, and for the Narrow Band physical layer. Section 3 presents the PHY and MAC layer configuration of the studied WBAN model. The emphasis in this section is put on the adopted on-body channel model and the settings of MAC and radio modules. Section 4 discusses the obtained results from the performed study. and Section 5 concludes the paper.

2. The IEEE 802.15.6 Standard

2.1. Technical requirements

To implement a WBAN compliant with the IEEE 802.15.6 standard, several requirements should be considered as listed below [1] :

- Bit rate: Inter-sensor communications within WBANs should be carried out at data rates ranging from 10 kbps to 10 Mbps.
- Packet Error Rate (PER): For the majority (~95%) of the best performing links, the PER must be below 10% for a reference payload of 256 bytes.
- Easy integration and removal of nodes: Adding, removing or replacing nodes in a WBAN, should be done easily and in less than 3 seconds approximately.
- Maximum number of nodes: the size of a WBAN must not exceed 256 nodes.
- Communication reliability in case of mobility: The performance of a WBAN network must not be degraded to the point of causing data loss if the patient is mobile. Furthermore, WBANs must not cause any discomfort to the patient while moving.
- Latency and jitter: Latency and jitter are two important metrics for evaluating the performance of a WBAN. Latency should not be greater than 125 ms in medical applications and 250 ms in non-medical applications. For the jitter, it should be lower than 50 ms.
- On-body and in-body WBANs should be able of coexisting.
- Coexistence between adjacent BANs: up to 10 WBANs should be able to coexist in a space of 6m3 approximately.
- Transmission power: All nodes in a WBAN must be capable of transmitting data in the range [-10 dBm, 0 dBm].
- Specific Absorption Rate (SAR): according to the Federal Communications Commissions (FCC) SAR is 1.6 W / kg in 1 g of body tissue.
- Cross-interference: WBANs must be able to provide acceptable functional performances in an environment of heterogeneous coexistence with other wireless network technologies (wifi, IEEE 802.15.14, etc.).

- Quality of Service (QoS) management must be able to provide security mechanisms, and priority features for services in a WBAN.

2.2. MAC layer of the standard

In order to control channel access in a WBAN, the IEEE 802.15.6 standard has defined a sophisticated MAC layer serving 3 physical layers that are designated according to the desired application.

To ensure time-referenced resources allocations in its WBAN, the coordinator (hub) must divide its transmission time axis (channel), into a series of superframes while having the choice of delimiting them or not with beacons (frames transmitted by the hub to simplify network management, such as coordination in the access to the media and power management for nodes, or to synchronize time in a WBAN, etc). However, in some cases, the coordinator may not need to time reference its allocations in the WBAN, so it can operate without using a time base, therefore, without having to transmit beacons. This means that a hub in a WBAN is able to function in one of the three access modes:

- The beacon mode with superframe boundaries.
- The non-beacon mode with superframe boundaries.
- The non-beacon mode without superframe boundaries

In this paper we only focus on Beacon mode with superframe boundaries, in which the hub sends a beacon (B) in the beginning of every active superframe to delimit it. unlike non-bacon modes, where the WBAN node can transmit its data to the coordinator using CSMA/CA or poll it to receive the data. In the beacon mode with superframe boundaries, the access phases that constitute each superframe are:

- Exclusive access phases (EAP1 and EAP2): These are time slots allocated by the hub to the rest of the WBAN nodes to transmit urgent and high-priority traffic.
- Random access phases (RAP 1 and RAP2): Dedicated to ensure random access to the medium, using CSMA/CA or Slotted ALOHA protocols (but not both at once).
- Managed Access Phases (MAP): During these access phases, the coordinator can guarantee different methods of access to the medium by the nodes of the WBAN, namely: improvised access, scheduled access and unscheduled access.
  - Improvised access: where polled (uplink allocation interval, adapted to unexpected or additional ordinary traffic service) or posted (downlink allocation interval, adapted to "unexpected" or "additional" traffic service on the downlink) allocations are generally assigned outside the planned uplink or downlink allocations.
  - Scheduled access: which is based on a pre-reservation and a validated scheduling, in such a way that nodes and the coordinator obtain scheduled recurrent time intervals to initiate frame transactions.
  - Unscheduled access: which is a combination of scheduled access and polling.
- Contention access phase (CAP): with this access phase, a time interval is defined by the coordinator and announced via a previous non-beacon frame (B2) for contention access.

2.3. Narrowband physical layer (NB)

As noted earlier in section I, due to the multitude of applications supported by WBANs, The IEEE 802.15.6 standard has defined three physical layers (NB, UWB and HBC). These are responsible for activating/deactivating the radio transceivers of sensor nodes, evaluating the RF channel by listening to the RF transmissions of the different sensor nodes (this mission is known as Clear Channel Assessment or CCA) and controlling the transmission/reception of data on the channel. In this work we are interested in the NarrowBand physical layer (NB), specific to medical applications like the capture of physiological signals such as temperature, blood pressure, ECG, EEG, etc.

2.3.1. Physical frame structure of NB-PHY

As shown in figure 1, the Physical Protocol Data Unit (PPDU) for the NB PHY layer includes:

- A PLCP (Physical Layer Convergence Procedure) preamble: 90-bit coded and used to help the receiver in time synchronization and carrier offset recovery.
- A PLCP header: it is a 31-bit coded sequence that must be inserted after the PLCP preamble to transmit information about the PHY parameters responsible for helping the receiver to decode the PSDU, essentially information about the data rate and length of the MAC frame body (data without a MAC or FCS header), and information about the following packet, whether it will be sent in BURST mode or not. These data will then be protected by a 4-bit header check sequence (HCS) (CRC-4 ITU). moreover, to improve the robustness of the PLCP header, a BCH code (31, 19, t = 2) will be applied.
- PSDU (Physical Service Data Unit): this is the last major component of the PPDU to be transmitted, it is constructed by combining the MAC header (7 bytes), the MAC frame body with a size ranging from 0 to 255 bytes, and a 2-bit Frame Check Sequence (FCS).

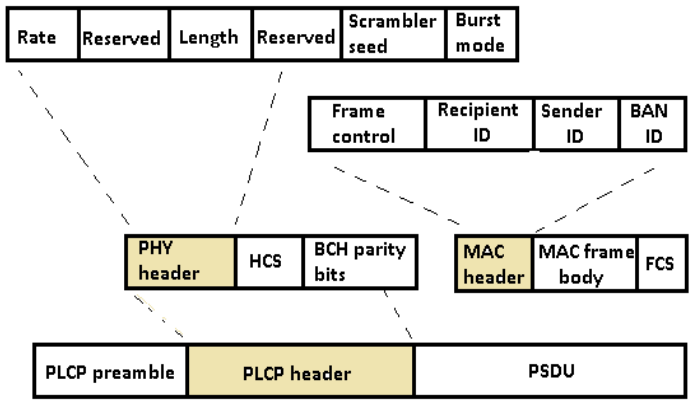

Figure1: NB PHY frame structure

2.3.2. NB physical layer Specifications

The IEEE 802.15.6 NB physical layer supports data transmission in a multiple frequency bands, summarized in Table 1, supporting different modulation schemes and data rates ranging from 75.9kbps to 971.4 kbps. one of the bands mentioned in the table is the 2.4 GHz band (2400-2483.5MHz) which is often the most preferred for the reasons mentioned earlier. However, several other technologies such as Wi-Fi (IEEE 802.11), Bluetooth (IEEE 802.15.1), IEEE 802.15.4 / ZigBee and others operate in this same band, and this is a real challenge due to the interference caused by the coexistence of these technologies with WBANs operating at 2.4 GHz (cross interference), and the mutual interference resulting from the coexistence of more than one WBAN in the same area [22] .

3. Description and Settings of the Studied WBAN Model

Nodes in a WBAN can be logically arranged in different topologies, star, tree or mesh. Therefore, choosing the most suitable topology is important because of its direct impact on WBAN performances in terms of power consumption, ability to handle heterogeneity and robustness against failures [10]. As a result, most researchers assume that a one-hop star topology, where nodes send data directly to the hub without the need for relays, is the best solution [10].

The WBAN model chosen for this study operates in the NB PHY layer, at 2.45 GHz more specifically. It is composed of eleven sensor nodes, including a coordinator, which is placed at the center of the patient's belly as shown in Figure 2 [22–24]. The eleven sensors are distributed over the patient's body in a single-hop (single coordinator) star topology, where communication frames are sent directly between the coordinator and each of the other ten sensors, with no need to additional relays. Choosing these node positions is driven by the desire to monitor most of the vital signs described in the on-body medical applications of WBANS, as those proposed for IEEE 802.15.6 [25–26]. This monitoring is carried out by means of regular and programmed sampling of a number of physiological parameters such as temperature, blood pressure, pulse oximetry, ECG, EEG, etc. We have classified these applications in Table 2 into three categories: low, medium and high data rate on-body medical applications. Their technical requirements are covered and described in the references [3, 27].

3.1. On-body channel model

Unlike in-body communications, where signal propagation occurs through body tissues, signals in on-body systems often propagate over body surface. Such propagation might bring up a mixture of surface, creeping, diffracted, scattered and free space waves, according to the position of the antenna [10, 28]. Furthermore, placing WBAN nodes on or around the human body, exposes them to antenna-body interaction effects, including near field coupling, distortion of the radiation pattern, and changes in the antenna impedance, which affects the functional performances of the nodes [29]. This has prompted many researchers to design on-body antennas [30–31] that take these constraints into account. In addition, patient mobility (caused by usual gestures or physiological processes such as breathing) as well as physical variations in the patient's local environment, make it difficult to model or select the appropriate on-body BAN channel, especially since it is sensitive to temporal variations of the received signal [29]. Thus, taking into account all these issues, a good characterization of the propagation channel is required before designing any WBAN solutions.

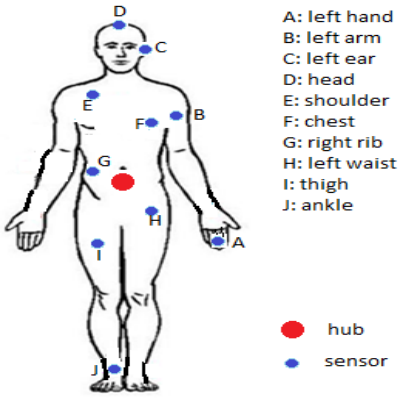

Figure 2: The proposed WBAN model

3.1.1. Path loss model

To approach a realistic on-body channel modeling in our WBAN model of study, we consider that signal propagation between nodes happens on the human body surface. This brings us to distinguish two possible kinds of on-body channels:

- **The Line Of Sight channel (LOS):** characterized by the absence obstacles between sensors and the hub.
- **The Non-line Of Sight channel (NLOS)** characterized by the presence of obstacles between sensors and the hub.

Thus, for the 2.4 GHz narrow band, IEEE 802.15.6 specified two path loss models, for propagation both with and without a line-of-sight, referred to as CM3A and CM3B, respectively [32]. In this paper, the CM3B trajectory loss model is adopted, where path loss is reduced in an exponential manner around the body circumference when BAN nodes are out of line of sight. It becomes flat over longer distances due to the introduction of multipath elements from indoor conditions [32].

In this model, path loss at a distance d is defined by equation (1):

$$PL(d)[dB] = -10log_{10}\left(P_0 e^{-m_0 d} + P_1\right) + \sigma_P n_P \qquad (1)$$

Where :

- PL (d) is the path loss at a distance d measured in dB
- P_0 represents a factor of average losses that occur close to the transmitter, and is related to the antenna design
- P_1 denotes the mean attenuation in indoor conditions of the elements irradiated from the body and reflected back to the receiver
- m_0 means the exponential mean rate of decay in dB / cm of the creeping wave diffracted around the body
- n_p is a random Gaussian variable of null unit and mean
- σ_p is the log-normal variance measured in dB

Table 1: Frequency bands and modulation parameters for the NB PHY layer

Frequency band (MHz)	Description	Modulation scheme		Information data rate (kbps)	Code rate (k/n)		Spreading factor		Symbol rate (Ksps)
		Preamble & PLCP header	PSDU		PLCP header	PSDU	PLCP header	PSDU	
402-405	Medical Implant Communication Service (MICS): Communications between implants	DBPSK	DBPSK	75.9	19/31	51/63	2	2 or 1	187.5
			DQPSK	151.8					
				303.6					
				455.4					
420-450	Wireless Medical Telemetry Services (WMTS) (Japan)	GMSK	GMSK	75.9	19/31	51/63	2	2 or 1	187.5
				151.8					
				187.5					
863-870	WMTS (Europe)	DBPSK	DBPSK	101.2	19/31	51/63	2	2 or 1	250
902-928	ISM (North America/ Australia/ New Zealand)		DQPSK	202.4					
950-958			D8PSK	404.8					
				607.2					
2360-2400	ISM worldwide	DBPSK	DBPSK	121.4	19/31	51/63	4	4/2/1	600
2400-2483.5			DQPSK	242.9					
				485.7					
				971.4					

Table 2: Targeted on-body medical applications

Application category	Sensor node	description	Data Rate	Duty Cycle (per device) % per time	Power Consumption	latency	Privacy
Low rate medical applications	Temperature sensor	Measures body temperature	120 bps	<1%	low	250 ms	high
	Glucose sensor (wearable)	Measures glucose level	1.6 kbps	<1%	low	250 ms	High
	Blood Pressure (BP)	The pressure of circulating blood on the walls of blood vessels.	<10 bps	< 1%	High	250 ms	Medium
Medium rate medical applications	SpO2	the oxygen saturation of hemoglobin at the blood capillaries.	32 Kbps	< 1%	Low	250 ms	High
	EEG	Electroencephalogram : an electrophysiological monitoring technique to record electrical activity of the brain.	12 leads: 43.2 kbps	< 10%	low	250 ms	high
High rate medical applications	ECG	Electrical activity of the heart.	-288 kbps (ECG-12 leads)	< 10%	Low	250 ms	High
			-71 kbps (ECG-6 leads)				

We have measured for each node the distance separating it from the hub, and by considering that our network is under the same ambient conditions as a normal hospital room, we have calculated the values of path loss for all the links of our WBAN. We present in Table 3, the values of CM3B model parameters, under the conditions of a hospital room [32].

3.1.2. Temporal variation

Temporal variation is also another important aspect in BAN channel modeling due to the rapid changes that can occur in this type of environment. In our WBAN model of study, the mobility of body limbs is captured by a temporal variation component. To the best of our knowledge, no unique model exists in the literature describing temporal variation, but rather a general modeling of this parameter is used [33]. The description of the approach used in the majority of simulators to describe temporal variation is as follows: it is considered that the actual propagation loss may differ from the average propagation loss over time. Therefore, a probability density function (pdf) is developed to cope with this issue. The pdf is determined from the previous observed value and the time elapsed since then. This function cannot be dynamically produced from real models but must rather be derived from experimental measurements.

The actual propagation loss is calculated as the sum of the pre-calculated average propagation loss and the temporal variation.

3.2. MAC module settings

In the studied WBAN model, the beacon mode with superframe boundaries is adopted, in which a beacon is transmitted at the beginning of every active superframe. This mode allows the coordinator to divide the communication channel into multiple access phases. As a result, the MAC module configuration adopted in this work, combines both of random access based on CSMA/CA and scheduled access based on TDMA as presented in detail in our previous work [23].

3.3. Radio module settings

In the 2.4 GHz narrowband, the preamble is always modulated using π/2-DBPSK, and the binary information is modulated with one of the following two differential modulations: π/2-DBPSK or π/4 DQPSK. For both of these, the bitstream b(n), n= 0,1,..,N-1 is transformed into a sequence of symbols s(k), k= 0,1,..,(N/Log2(M))-1 as follows :

$$s(k) = s(k-1)\exp(j\varphi_k) \quad (2)$$

M denotes the modulation order, and s(-1) = exp (jπ/2) is the reference for the first preamble symbol [20]. The transition values between the φ_k symbols are shown in Tables 4 and 5. for both π/2-DBPSK et π/4 DQPSK.To the best of our knowledge, there is still no radio chip available in the market that has been specifically designed to meet IEEE 802.15.6 standard requirements. Therefore, our work relies on a proposed radio chip by Alan Wong et al [34], compliant with the IEEE 802.15.6 standard recommendations for the 2.4 GHz NB PHY layer. The parameters for both modulation schemes of the proposed radio are defined in Table 6.

Table 3: Values of CM3B path loss model parameters in a hospital room

Parameter	Value
Frequency (GHz)	2.45
P_0[dB]	-25.8
m_0[dB/cm]	2.0
P_1[dB]	-71.3
σ_P[dB]	3.6

Table 4: Symbols transition values of π/2-DBPSK

B(K)	φ_k
0	+π/2
1	- π/2

Table 5. Symbols transition values of π/4 DQPSK

B(2K), B(2K+1)	φ_k
0 0	π/4
0 1	3π/4
1 0	7π/4
1 1	5π/4

4. Results and Discussion

4.1. Effects of transmission power and modulation schemes on the performance of the proposed WBAN model

To assess the impact of transmission power and modulation schemes on the studied WBAN performance, in terms of packet loss rate, throughput, and latency, we used Castalia sensor network simulator as a basis, which is based on OMNeT++ (4.6) platform and includes as standard the support of the IEEE 802.15.6 specifications, which justifies its choice in our numerical study.

In our simulations, BAN nodes send their packets at different data rates to the coordinator using a different transmission power ranging from -10 to 3 dBm, each time, and a different modulation scheme (DBPSK or DQPSK).

4.1.1. Packet Loss Rate (PLR)

Packet losses in a WBAN can be due to various possible causes such as the disconnection of a sensor from the network (no beacon reception is detected) or simply the inability to transmit data in the defined transmission tries. Therefore, The packet loss rate indicates the chance that a packet produced by a node cannot be received normally and as expected by the coordinator [35].

Nevertheless, this parameter can be impacted by different factors [36]:

- Environmental factors such as distance between sensors, activity and body posture.
- Technical factors such as transmission power, receiver

sensitivity, antenna gain or coding.

In this work, we are interested in the evaluation of two technical factors that can impact PLR in WBANs, which are modulation and transmission power. For this reason, we show in Figures 3, 4, 5, and 6, the PLR for DBPSK and DQPSK modulations as a function of different data rates when the transmission power is set to -10, -5, 0 and 3 dBm, respectively.

As expected, the analysis of the results obtained in Figures 3, 4, 5 and 6, clearly shows that packet loss rate decreases as the transmission power increases. In fact, CM3B channel model introduces relatively high path losses depending on the distance between the communicating nodes (71.3 dB for an inter-sensor distance d greater than 30cm). Therefore, to ensure a better received signal level at the coordinator (signal level higher than the minimum threshold of receiver sensitivity), corresponding to a better throughput, the transmission power of WBAN nodes must be sufficient enough. Moreover, as shown in the four figures (3, 4, 5 and 6), for low and medium data rates (below 60 kbps), DBPSK modulation shows a lower packet loss rate compared to that obtained with DQPSK. This can be explained by the difference in radio sensitivity due to the modulation scheme adopted. We can notice in table 6, that receiver sensitivity is significantly lower in DBPSK (-104 dBm) compared to DQPSK (-96.5 dBm). However, at high transmission data rates (from 60 kbps onwards), the packet reception rate appears to be better with DQPSK than with DBPSK.

We can relate the low performance of DBPSK in high data rates to the well-known problems of buffer saturation. Furthermore, DQPSK allows with 4 phases to encode two bits per symbol instead of only one in the case of DBPSK. Thus, at the same transmission data rate, DQPSK modulation allows the transmission of twice as many symbols (i.e. a multiplication of the data rate by a factor of 2) as DBPSK modulation. This explains the relatively fast saturation of the coordinator buffer at high data rate with DBPSK. This is further confirmed by the equation (3) below [10].

$$R_d = \left(\frac{R_s.N}{S} * \frac{k}{n}\right)(kbps) \qquad (3)$$

where Rd refers to the information dara rate, Rs means the symbol rate, S is the spreading factor, k/n is the code rate BCH, and N is a variable linked to the modulation order M by $M=2^N$.

4.1.2. Throughput

Throughput is an important metric in WBANs, it refers to the number of packets received successfully per second (p/s). However, this parameter can be weakened due to several causes including low duty cycles, or the transmission of control packets. As demonstrated in equation (4) [35], throughput (S, expressed in bytes/s) is much higher when packet loss rate is lower.

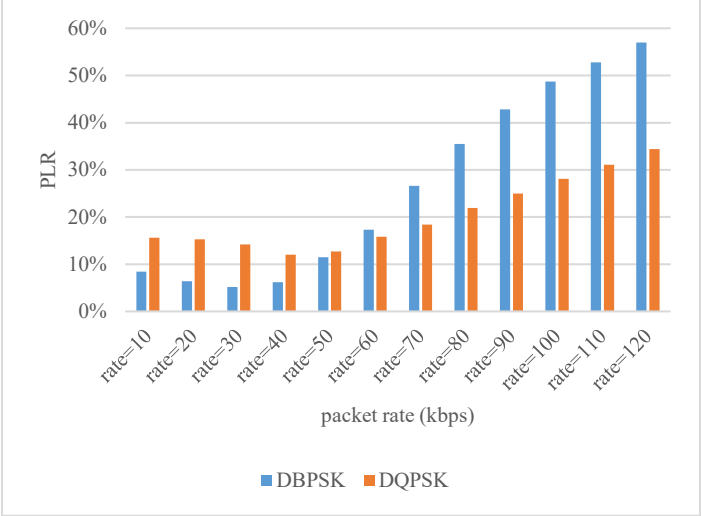

Figure 3: PLR at -10 dBm

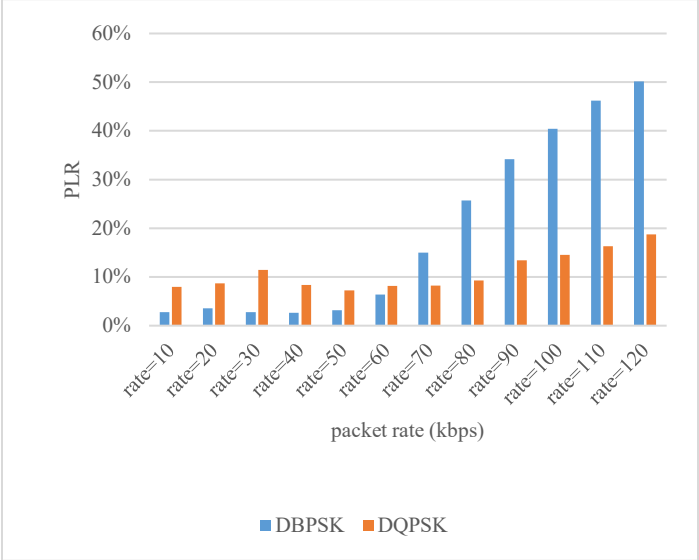

Figure 4: PLR at -5 dBm

Table 6: Settings of the modulation schemes used

Frequency band (Ghz)	Rx sensitivity (dBm)	Channel spacing (MHz)	Symbol rate (ksps)	Tx power (dBm)	Power consumption for Tx mode
2.4	-96.5(for DQPSK) -104 (for DBPSK)	1	600	-10 to 3	• 5.9 mW (for DPSK -10 dBm). • 9.5 mW (for DPSK 0 dBm). • 12.3 mW (for DPSK 3 dBm)

At constant PLR, S is proportional to the number M of nodes in the network and to the traffic payload (P) expressed in bytes, and is inversely proportional to the length of the beacon period Bp.

$$S = \frac{M.P}{B_P}(1 - PLR) \quad (4)$$

Figures 7, 8, 9 and 10 illustrate the throughput of the DBPSK and DQPSK modulations as a function of various data rates at -10, -5, 0 and 3dBm respectively.

These results show, once again, as in the earlier PLR study, that the higher the transmission power the better the throughput. Furthermore, as illustrated in the four figures, for low and medium data rates (below 60 kbps), DBPSK guarantees a better throughput compared to DQPSK modulation, as the receiver sensitivity in the case of DBPSK is lower. However, at high transmission data rates (60 kbps and more) DQPSK modulation seems to be more efficient, for the same reasons (and the same high data rate context) previously formulated with the results obtained for PLR.

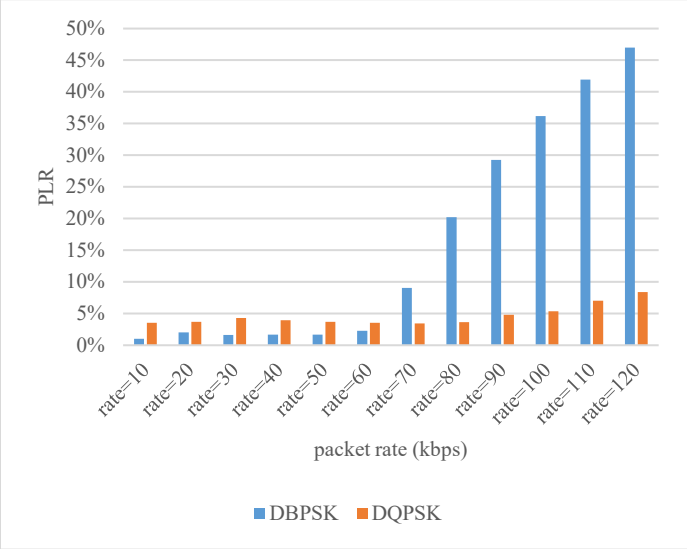

Figure 5: PLR at 0 dBm

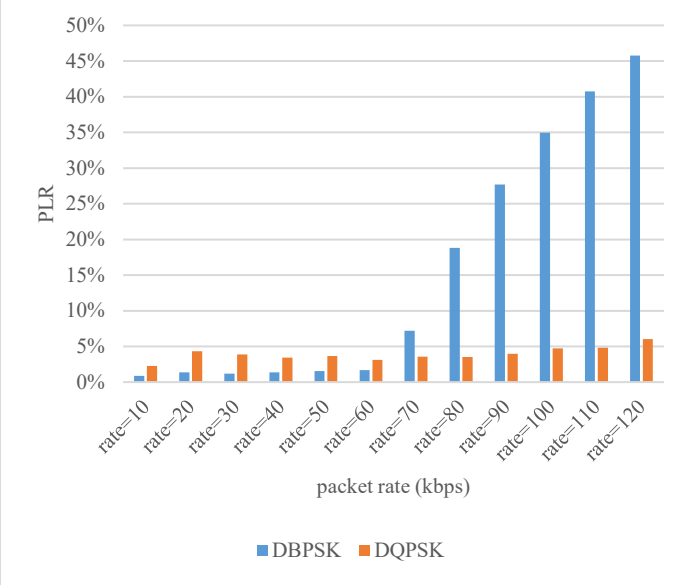

Figure 6: PLR at 3dBm

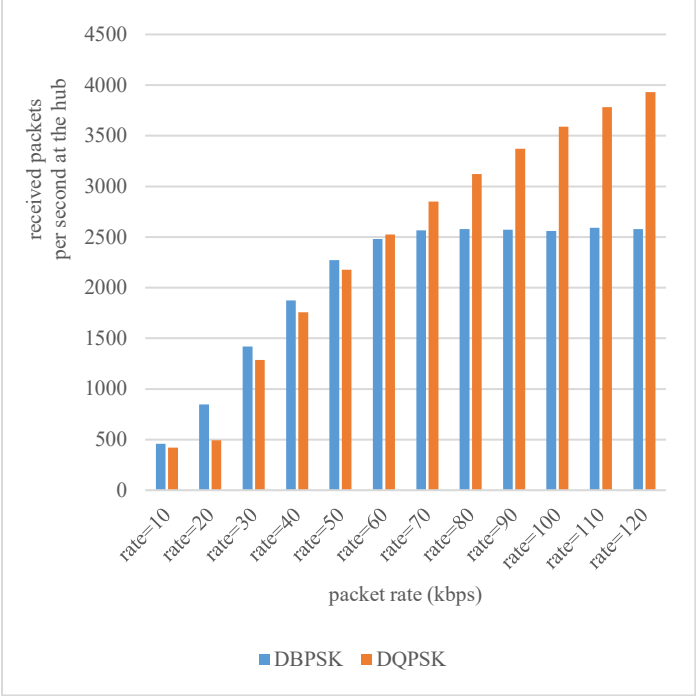

Figure 7: Throughput at -10dBm

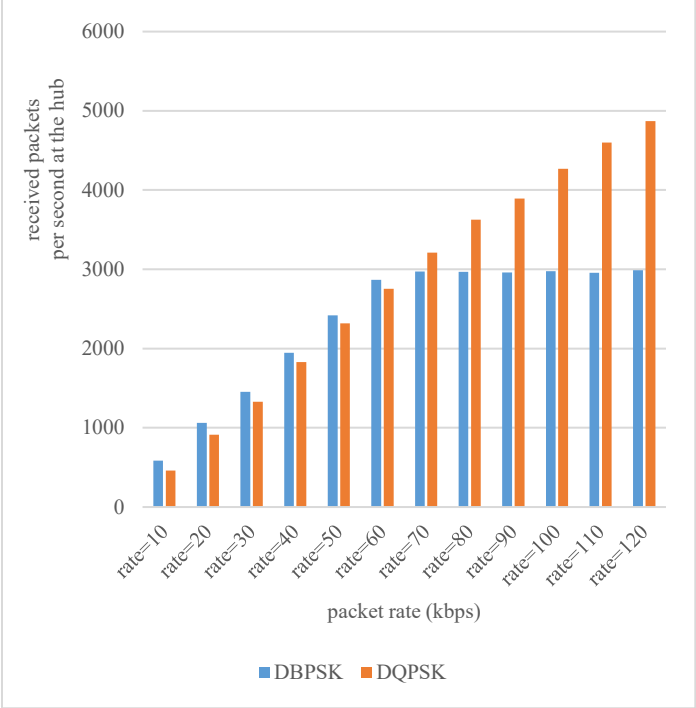

Figure 8: Throughput at -5 dBm

4.1.3. *Latency*

Latency is a metric defined, in the context of our work, as the time interval between the node receiving a beacon, and the coordinator correctly receiving the node's frame. We evaluate this metric in our WBAN model of study, at low, medium, and high data rates, for several transmission powers (-10dBm, -5dBm, 0dBm and 3dBm). For this purpose, we have considered the three following simulation scenarios:

- Transmission data rate less than 10 kbps with DBPSK modulation: to represent the case of low data rate on-body medical applications (according to the categorization in Table 2).

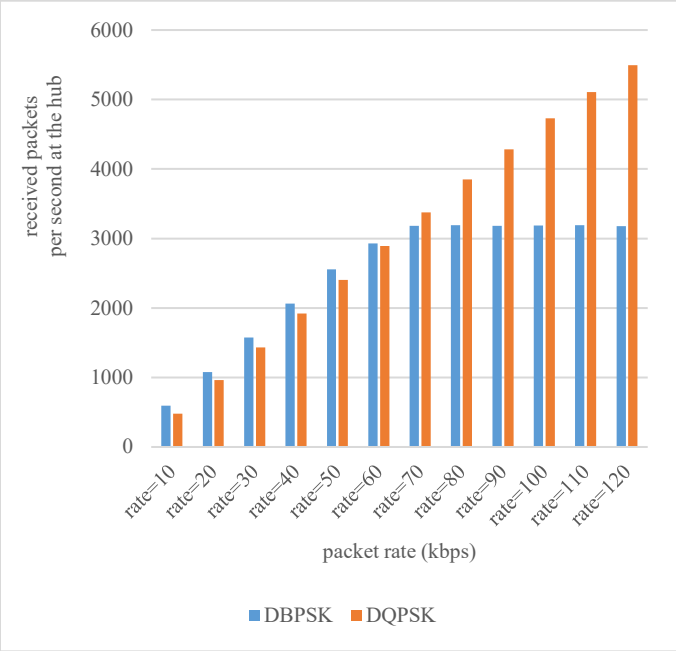

Figure 9: Throughput at 0 dBm

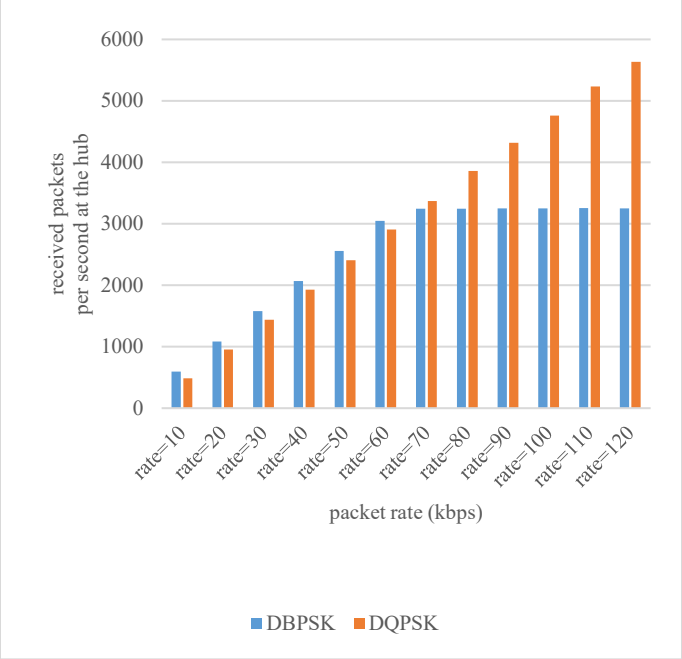

Figure 10: Throughput at 3 dBm

- Maximum transmission rate of 50 kbps with DBPSK modulation: to represent the case of medium rate on-body medical applications.
- Maximum transmission data rate of 71 kbps with DQPSK modulation: to represent the case of high data rate on-body medical applications (example of ECG monitoring with 6-electrode).

Thus, we show in Figures 11, 12, and 13 the distribution of received packets at different time intervals for the three cases respectively, when the transmission power varies from -10 to 3dBm.

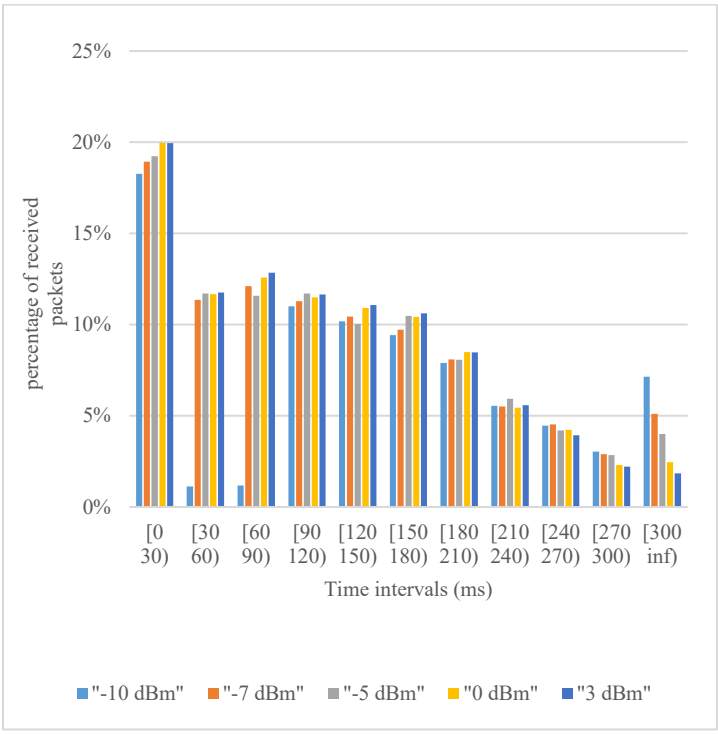

Figure 11: latency for low data rate medical applications (DBPSK)

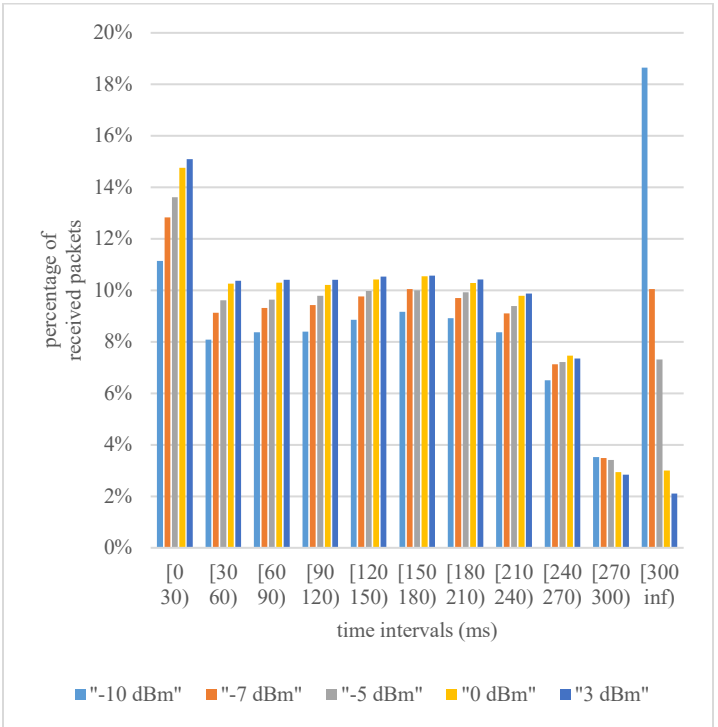

Figure 12: latency for medium data rate applications (between 32 and 43 kbps)

Table 7. Optimal modulation scheme and transmit power values for medical on-body applications

Medical applications	Optimal values of transmit power		Optimal modulation scheme
Medium data rate medical applications: EEG monitoring (12 leads) and SpO2	-10 dBm	PLR <10 % Throughput: 2270 p/s Latency: 52 % of packets received before 240 ms	DBPSK
	-5 dBm	PLR <10 % Throughput: 2418 p/s Latency: 69 % of packets received before 240 ms	
	0 dBm	PLR <10 % Throughput: 2555 p/s Latency: 81 % of packets received before 240 ms	
	3 dBm	PLR <1 % Throughput: 2559 p/s Latency: 84 % of packets received before 240 ms	
Low data rate medical applications: (<10 kbps)	-10 dBm	PLR <10 % Throughput: up to 456p/s Latency: 86 % of packets received before 240 ms	DBPSK
	-5 dBm	PLR <3 % Throughput: up to 585 p/s Latency: 90 % of packets received before 240 ms	
	0 dBm	PLR <2 % Throughput: up to 593p/s Latency: 92 % of packets received before 240 ms	
	3 dBm	PLR <1 % Throughput: up to 594 p/s Latency: 93 % of packets received before 240 ms	
ECG (6 leads)	-10 dBm	PLR =19 % Throughput: 2850 p/s Latency: 60 % of packets received before 240 ms	DQPSK
	-5 dBm	PLR = 8 % Throughput: 3208 p/s Latency: 70 % of packets received before 240 ms	
	0 dBm	PLR <10 % Throughput: 3377 p/s Latency: 79 % of packets received before 240 ms	
	3 dBm	PLR <10 % Throughput: 2380 p/s Latency: 84 % of packets received before 240 ms	

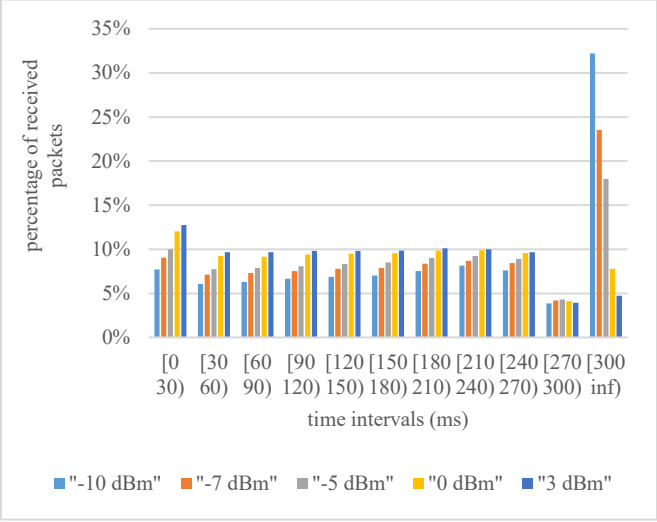

Figure 13: Latency for high data rate applications (72 kbps)

4.2. Discussion and synthesis

E-health applications can be classified into real-time and near real-time applications [37–38]. Nevertheless, the QoS requirements of each of these applications may differ depending on the context in which the service is invoked. This means that in emergency cases, for example, remote medical monitoring will require real-time data transmission, with no tolerance for data loss. Whereas in non-emergency situations, vital signs transmission does not require the same level of QOS (can tolerate delay). In addition, depending on the application demands, three basic data delivery models can be distinguished [39–40] : continuous model, query model and event model. The continuous model is the most basic data delivery model, which aims to periodically transmit the data collected by sensor nodes, which can either be real-time data such as voice or image that does not tolerate delay (but packet loss can be tolerated within threshold limits), or non-real-time continuous data where latency and packet loss can be permissible. However, In the query data delivery model, the coordinator requests the transmission of packets to sensors, this model requires

reliable and timely data transmission. As for event-delivery model, data transmission only takes place when an event of interest occurs. In this case, reliable and real-time data transmission is required. Moreover, the QOS requirements also depend on the needs of the patients, for some patients it may be enough to send their signals every few minutes, while others may need to transmit the collected data every few seconds [41].

The simulation results of our WBAN model have shown that in the case of low data rate medical applications (about 10 kbps), including blood pressure, glucose and body temperature measurement, we can note that DBPSK modulation can guarantee a PLR < 10% even when nodes transmit in the lowest power range. At -10 dBm for example, a PLR of about 8% is achieved with 86% of packets received under 250 ms, and a throughput of 456 packets/s. So if the target of these applications is non-emergency continuous real-time monitoring, the choice of DBPSK modulation with the lowest power level (-10 dBm) can guarantee the intended results.

5. Conclusion

In this paper we have studied a realistic WBAN model based on the 2.4 GHz narrowband of the IEEE 802.15.6 standard and dedicated to on-body medical applications. With this model, we have investigated the adequacy of the modulation schemes proposed by the standard in this frequency band as well as transmission power, while considering the requirements of these applications in terms of PLR, throughput and latency. Simulation results have shown that DBPSK modulation can be a good choice for low and medium data rate applications. However, DQPSK modulation would be more suitable for high data rate medical applications. Regarding the transmission power, low data rate medical applications can accept minimum transmission powers (-10 dBm for example). However, when the required application data rate increases, higher transmission powers, e.g. 0 dBm, must necessarily be used to ensure a reduced packet loss rate, acceptable latency, and higher throughput.

The 2.4 GHz frequency band is through a band adopted by several other technologies such as Wifi, Bluetooth etc. This is likely to influence the operation of the proposed WBAN model if it is located in an environment that includes these technologies or other WBANs. This is known as mutual interference, which must be taken into account in the physical layer configuration.

References

[1] S. Movassaghi, M. Abolhasan, J. Lipman, D. Smith and A. Jamalipour, "Wireless Body Area Networks: A Survey" IEEE Commun. Surv. Tut., **16**(3), 1658-1686, 2014. https://doi.org /10.1109/SURV.2013.121313.00064.

[2] A. Es-saqy, M. Abata, S. Mazer, M. Fattah, M. Mehdi, M. El bekkali and C. Algani, "Very Low Phase Noise Voltage Controlled Oscillator for 5G mm-wave Communication Systems" in 2020 1st International Conference on Innovative Research in Applied Science, Engineering and Technology (IRASET), Meknes, Morocco, 2020. https://doi.org /10.1109/IRASET48871.2020.9092005.

[3] S. Ullah, "A Review of Wireless Body Area Networks for Medical Applications" Int'l J. Commun. Netw. Syst. Sci., **02**(08), 797–803, 2009. https://doi.org /10.4236/ijcns.2009.28093.

[4] Boulemtafes A., Badache N. "Design of Wearable Health Monitoring Systems: An Overview of Techniques and Technologies" mHealth Ecosystems and Social Networks in Healthcare. Springer, Chamv, 2016.

[5] R. Negra, I. Jemili, and A. Belghith, "Wireless Body Area Networks: Applications and Technologies" Procedia Comput. Sci., **83**, 1274–1281, 2016. https://doi.org /10.1016/j.procs.2016.04.266.

[6] B. Antonescu and S. Basagni, "Wireless body area networks: Challenges, trends and emerging technologies" in BODYNETS 2013 - 8th Int. Conf. Body Area Networks, 2013. https://doi.org /10.4108/icst.bodynets.2013.253722.

[7] M. Boumaiz, M. El ghazi, S. Mazer, M. Fattah, A. Bouayad, M. El bekkali, and Y. Balboul, "Energy harvesting based WBANs: EH optimization methods" Procedia Comput. Sci., **151**, 1040–1045, 2019. https://doi.org /10.1016/j.procs.2019.04.147.

[8] Z. Jin, J. Oresko, S. Huang, and A. C. Cheng, "HeartToGo: A personalized medicine technology for cardiovascular disease prevention and detection" in 2009 IEEE/NIH Life Science Systems and Applications Workshop, Bethesda, MD, 2009. https://doi.org /10.1109/LISSA.2009.4906714.

[9] M. Hadjem, O. Salem and F. Naït-Abdesselam, "An ECG monitoring system for prediction of cardiac anomalies using WBAN" in 2014 IEEE 16th International Conference on e-Health Networking, Applications and Services (Healthcom), Natal, 2014. https://doi.org /10.1109/HealthCom.2014.7001883.

[10] Ullah, S., Higgins, H., Braem, B. Latre, B. Blondia, C. Moerman, I. Saleem, S. Rahman, Z. and Kwak, K, S. "A Comprehensive Survey of Wireless Body Area Networks". J Med Syst. **36**(3), 1065-1094. https://doi.org /10.1007/s10916-010-9571-3.

[11] Huzooree G., Khedo K.K., Joonas N. "Wireless Body Area Network System Architecture for Real-Time Diabetes Monitoring" In: Fleming P., Vyas N., Sanei S., Deb K. Emerging Trends in Electrical, Electronic and Communications Engineering. Springer, Cham, 2016.

[12] M. Udin Harun Al Rasyid, F. A. Saputra, and A. Christian, "Implementation of blood glucose levels monitoring system based on Wireless Body Area Network" in 2016 IEEE Int. Conf. Consum. Electron, 2016. https://doi.org /10.1109/ICCE-TW.2016.7521005.

[13] Hsueh-Ting Chu, Chir-Chang Huang, Zhi-Hui Lian and J. J. P. Tsai, "A ubiquitous warning system for asthma-inducement" in IEEE International Conference on Sensor Networks, Ubiquitous, and Trustworthy Computing (SUTC'06), Taichung, 2006. https://doi.org /10.1109/SUTC.2006.20.

[14] K. Revett and S. T. De Magalhães, Cognitive biometrics: Challenges for the future, Springer, Berlin, Heidelberg, 2010.

[15] T. M. Connolly, E. A. Boyle, E. Macarthur, T. Hainey, and J. M. Boyle, "Computers & Education A systematic literature review of empirical evidence on computer games and serious games" Comput. Educ., **59**(2), 661–686, 2012. https://doi.org /10.1016/j.compedu.2012.03.004.

[16] K. Hasan, K. Biswas, K. Ahmed, N. S. Nafi, and M. S. Islam, "A comprehensive review of wireless body area network" J. Netw. Comput. Appl., **143**, 178–198, 2019. https://doi.org /10.1016/j.jnca.2019.06.016.

[17] R. Cavallari, F. Martelli, R. Rosini, C. Buratti, and R. Verdone, "A survey on wireless body area networks: Technologies and design challenges" IEEE Commun. Surv. Tutorials, **16**(3), 1635–1657, 2014. https://doi.org / 10.1109/SURV.2014.012214.00007.

[18] P. Mathew, L. Augustine, D. Kushwaha, D. Vivian and D. Selvakumar, "Hardware implementation of NB PHY baseband transceiver for IEEE 802.15.6 WBAN" in 2014 International Conference on Medical Imaging, m-Health and Emerging Communication Systems (MedCom), Greater Noida, 2014. https://doi.org /10.1109/MedCom.2014.7005977.

[19] Wang, Y., & Wang, Q. "Evaluating the IEEE 802.15.6 2.4GHz WBAN Proposal on Medical Multi-Parameter Monitoring under WiFi/Bluetooth Interference" International Journal of E-Health and Medical Communications (IJEHMC), **2**(3), 48-62, 2020. https://doi.org /10.4018/jehmc.2011070103 103.

[20] IEEE Standard for Local and metropolitan area networks - Part 15.6: Wireless Body Area Networks," in IEEE Std 802.15.6-2012, 1-271, 2012. https://doi.org /10.1109/IEEESTD.2012.6161600.

[21] S. AhmadSalehi, , M.A Razzaque, I. Tomeo-Reyes and N. Hussain, "IEEE 802.15.6 standard in wireless body area networks from a healthcare point of view" in 2016 22nd Asia-Pacific Conference on Communications (APCC), 2016. https://doi.org /10.1109/APCC.2016.7581523.

[22] M. Boumaiz, M. E. Bekkali, A. Bouayad and M. Fattah, "The Impact of Distance between Neighboring WBANs on IEEE 802.15.6 Performances" in 2019 7th Mediterranean Congress of Telecommunications (CMT), Fès, Morocco, 2019. https://doi.org /10.1109/CMT.2019.8931341.

[23] M. Boumaiz, M. El Ghazi, M. Fattah, A. Bouayad, and M. El Bekkali, "Mutual coexistence in WBANs: Impact of modulation schemes of the IEEE 802.15.6 standard" Int. J. Adv. Comput. Sci. Appl., **11**(5), 294–302, 2020. https://doi.org /10.14569/IJACSA.2020.0110539.

[24] M. Boumaiz, M. El ghazi, A. Bouayad, M. Fattah, M. El bekkali and S. Mazer, "The impact of transmission power on the performance of a WBAN prone to mutual interference" in 2019 International Conference on Systems of Collaboration Big Data, Internet of Things & Security (SysCoBIoTS), Casablanca, Morocco, 2019. https://doi.org /10.1109/SysCoBIoTS48768.2019.9028035.

[25] F. Di Franco, C. Tachtatzis, R. C. Atkinson, I. Tinnirello and I. A. Glover, "Channel estimation and transmit power control in wireless body area

networks" in IET Wireless Sensor Systems, **5**(1), 11-19, 2015. https://doi.org /10.1049/iet-wss.2013.0070.

[26] K. Takizawa, A. Aoyagi, J. Takada, N. Katayama, K. Yekeh, Y. Takehiko and K. Kohno. "Channel models for wireless body area networks", in 2008 30th Annual International Conference of the IEEE Engineering in Medicine and Biology Society, Vancouver, BC, 2008. https://doi.org /10.1109/IEMBS.2008.4649465

[27] M. Shu, D. Yuan, C. Zhang, Y. Wang, and C. Chen, "A MAC protocol for medical monitoring applications of wireless body area networks," Sensors (Switzerland), **15**(6), 12906–12931, 2015. https://doi.org /10.3390/s150612906.

[28] P. S. Hall, "Antennas Challenges for Body Centric Communications" in 2007 International workshop on Antenna Technology: Small and Smart Antennas Metamaterials and Applications, Cambridge, 2007. https://doi.org /10.1109/IWAT.2007.370076.

[29] S. L. Cotton, R. D'Errico, and C. Oestges, "A review of radio channel models for body centric communications". Radio science, **49**(6), 371–388, 2014. https://doi.org/10.1002/2013RS005319

[30] B. Hazarika, B. Basu, and J. Kumar, "A Multi-Layered Dual-Band On-Body Conformal Integrated Antenna for WBAN Communication" Aeu-int J Electron C., **95**, 226-235, 2018. https://doi.org /10.1016/j.aeue.2018.08.021.

[31] I. Suriya and R. Anbazhagan, "Inverted-A based UWB MIMO antenna with triple-band notch and improved isolation for WBAN applications," Aeu-int J Electron C., **99**, 25–33, 2019. https://doi.org /10.1016/j.aeue.2018.11.030.

[32] K. Y. Yazdandoost, Channel Modeling Subcommittee Report. 2010.

[33] M. Boumaiz, M. El ghazi, S. Mazer, M. El bekkali, A. Bouayad and M. Fattah, "Performance analysis of DQPSK and DBPSK modulation schemes for a scheduled access phase based Wireless Body Area Network" in 2019 9th International Symposium on Signal, Image, Video and Communications (ISIVC), Rabat, Morocco, 2018. https://doi.org /10.1109/ISIVC.2018.8709232.

[34] A. Wong, M. Dawkins, G. Devita, N. Kasparidis, A. Katsiamis, O. King, F. Lauria, J. Schiff and A. Burdett., "A 1V 5mA multimode IEEE 802.15.6/bluetooth low-energy WBAN transceiver for biotelemetry applications" in IEEE International Solid-State Circuits Conference, San Francisco, CA, 2012. https://doi.org /10.1109/ISSCC.2012.6177022.

[35] F. Martelli, C. Buratti and R. Verdone, "On the performance of an IEEE 802.15.6 Wireless Body Area Network" in 17th European Wireless 2011 - Sustainable Wireless Technologies, Vienna, Austria, 2011.

[36] H. Zhang, F. Safaei, and L. C. Tran, "Joint transmission power control and relay cooperation for WBAN systems" Sensors (Switzerland), **18**(12), 1–26, 2018. https://doi.org /10.3390/s18124283.

[37] L. Skorin-Kapov and M. Matijasevic, "Analysis of QoS requirements for e-Health services and mapping to evolved packet system QoS classes" Int. J. Telemed. Appl., 2010. https://doi.org /10.1155/2010/628086.

[38] D. Vouyioukas, I. Maglogiannis, and D. Komnakos, "Emergency m-Health Services through High-Speed 3G Systems: Simulation and Performance Evaluation" Simulation, **83**(4), 329–345, 2007. https://doi.org /10.1177/0037549707083113.

[39] M. A. Yigitel, O. D. Incel, and C. Ersoy, "QoS-aware MAC protocols for wireless sensor networks: A survey," Comput. Networks, **55**(8), 1982–2004, 2011. https://doi.org /10.1016/j.comnet.2011.02.007.

[40] M. A. Razzaque, S. S. Javadi, Y. Coulibaly, and M. T. Hira, "Qos-aware error recovery in wireless body sensor networks using adaptive network coding," Sensors (Switzerland), **15**(1), 440–464, 2015. https://doi.org /10.3390/s150100440.

[41] A. Maroua and F. Mohammed, "Characterization of Ultra Wide Band indoor propagation". in 2019 7th Mediterranean Congress of Telecommunications (CMT), Fès, Morocco, 2019. https://doi.org /10.1109 / CMT.2019.8931367.

ASTES

Advances in Science, Technology and Engineering Systems Journal Vol. 5, No. 5, 799-807 (2020)

www.astesj.com

Special Issue on Innovative Research in Applied Science, Engineering and Technology

ASTESJ

ISSN: 2415-6698

A Study on Methodology of Improvement the Hydraulic System for Cometto Self-Propelled Trailer System

Hai Minh Nguyen-Tran, Quang Minh Pham, Hoa Binh Le-Nguyen, Cao Tri Nguyen, Tri Nhut Do*

Division of Electronics and Electrical Engineering, Faculty of Engineering, Van Lang University, HCMC, 700000, Vietnam

ARTICLE INFO

Article history:
Received: 19 August, 2020
Accepted: 21 September, 2020
Online: 12 October, 2020

Keywords:
Self-propelled trailers
Hydraulic system
MSPE
Heavy transport

ABSTRACT

In recent years, the transport of large packages with super weight from 100 tons to several thousand tons is no longer a difficult problem due to the continuous development of technology. Experienced transport companies, specializing in transporting heavy goods in Vietnam, have invested in very modern equipment and machinery such as self-propelled trailers of Cometto (Italy) in order to transport safely mentioned parcels of great economic value arrive at the requested location. This trailer can be self-propelled, does not need to use a tractor, and only needs to use a remote-control handheld device. Moreover, the trailer gear shaft can rotate 360 degrees. In particular, the hydraulic system supports trailers operating with high accuracy and absolute safety including functions such as 360-degree rotation, lifting, transmission, braking, etc. In order to improve the performance of trailers when actually used in large projects, an important detail in the trailer's hydraulic system has been inserted a throttle valve with to increase the safety of the hydraulic pump and the entire system as well as the safety of the goods that trailers are transporting. The trailer system has transported the rig with a capacity of up to 3,200 tons in Vietnam, the shipment of 15,000 tons in the world and beyond in the future.

1. Introduction

The operation of moving of oversized and overweight packages onboard is called load-out. The oversized and overweight packages such as: 1) topside, jackets for oil and gas industry; 2) Big equipments for power stations; 3) Super-weighted equipments for oil refineries and thermal power plants.

The load-out task is based on several techniques such as skidding, lifting, float-on, etc and is a high-risk task. In this paper, a self-propelled trailers system is utilized to do load-out task. Adverse events can occur such as trailer overloaded, broken trailer structure, damaged path due to temporary breakdown such as tire explosion, the frequent failure of the Electronic Load Sensing (ELS). Engineers should give priority to solving the problem of damage to the road surface during transportation by many options in many different places [1, 2]. Theoretically, the self-propelled trailer system is navigated by methods such as GPS-based, IMU-based [3], vision-based [4], and combined method of the single mentioned methods [5].

*Corresponding Author: Tri Nhut Do, Division of Electronics and Electrical Engineering, Van Lang University, 45 Nguyen Khac Nhu Street, District No. 1, Ho Chi Minh City 700000, Vietnam, Cell No. +84938113898, trinhutdo@gmail.com

However, this method has many limitations as follows:

- It is difficult to control the synchronous speed of tractors.
- It is difficult to adjust the center to lower the required position because each delegation is a different rotation center.
- It is unable to transport too heavy cargos.

The self-propelled trailers come with many special functions are manufactured by employed the modern technology in order to carry such overlength, overweight and oversized cargos as illustrated in Figure 1. This self-propelled trailer system greatly improves the limitations of the towing method as follows:

- The trailer speed is controlled very synchronously due to the control needs only one person to operate via a remote controller.
- Adjusting the lower center to the expected position is much simpler due to only one driving center is rotated.
- The trailer modules are connected to each others more or less depending on the size and load of packages: Very maneuverable in assembling.
- Distributes loads evenly on the trailer floor via the hydraulic suspension.

Figure 1: A project to load out the gantry using self-propelled trailers

Many leading companies in the world have approached to invest in self-propelled trailer systems. However, several companies in Vietnam also invest but are limited because of the high cost. In particular, Vietranstimex has invested a Cometto self-propelled trailer system that made in Italy [6] and is a Modular Self-Propelled Electric (MSPE) type. During operation, the Cometto system has shown many advanced features such as:

- Flexible assembly: modules are joined together by vertical or horizontal coupling depending on the size and load of packages.
- Mobile steering system: The ability to rotate the package 360 degrees when not moving and many driving modes: wheel steering, parallel steering, single-headed steering.
- The ability to shift the center of steering system in order to adjust the trailer to overcome difficult roads without interfering with the initial programming.

However, the Cometto self-propelled trailer system still presents many problems during operation, including the frequent failure of the ELS valve. Therefore, a new method was proposed in order to handle fastly the ELS valve damage. A throttle valve M is used in series with both tap J and ELS valve. Accordingly, when the ELS valve fails, no matter the status of tap J and without locking tap J, the hydraulic pump is adjusted by turning the throttle valve M only so that the system pressure, which is displayed on the driving pressure gauge, reaches to 200 bar or to 220 bar. The system works stably by those pressures. When more pressure is needed, the throttle valve M continues to be adjusted. After the throttle valve M is installed in the hydraulic system controlling the pump, the self-propelled trailer system works very stably and the proposed self-propelled trailer system has safely transported and launched a lot of oversized and overweight packages.

The remainder of the article is organized as follows: Section II describes in details the origin Cometto self-propelled trailer system and the method to enhance its performance; Section III describes in details the experimental results by applying the proposed method and summarizes the evaluation and Section IV concludes the article.

2. The Cometto self-propelled trailer system and the proposed method

Three problems discussed in this section is organized as follows: Subsection 2.1 introduces the overview of Cometto self-propelled trailer system including Power Pack Unit (PPU) and Modules; Subsection 2.2 specially describes about the main features of PPU hydraulic system; and Subsection 2.3 introduces the proposed method to enhance features of PPU hydraulic system.

2.1. The Cometto self-propelled trailer system

The system consists of main components as follows [7]:

- Power Pack Unit.
- The 4/4/3 electronic-hydraulic module (The module has 4 axes, 4 hydraulic motors, the module width is 3 meters).
- The 6/4/3 electronic-hydraulic module (The module has 6 axes, 4 hydraulic motors, the module width is 3 meters).

The PPU links one or more trailer modules together with either vertical or horizontal configurations as depicted in Figure 2.

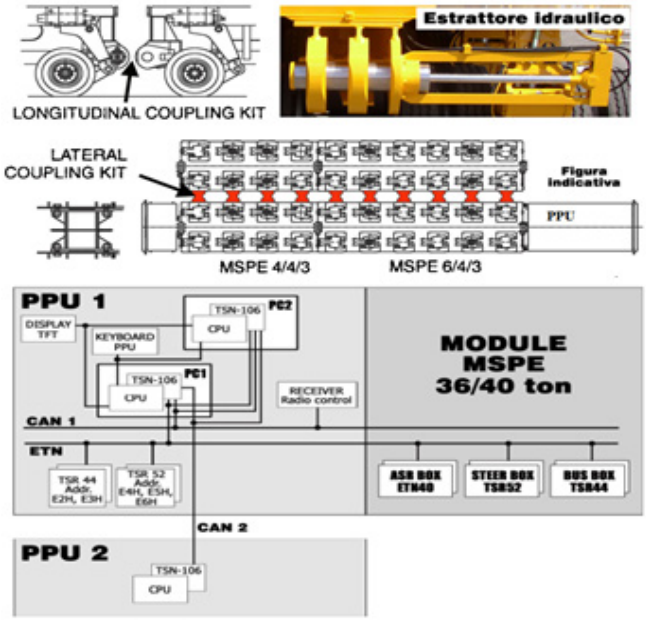

Figure 2: Main components of Cometto system

The number of PPUs and the number of modules is more or less depending on the package weight and package size. However, the system will be only controlled by one remote controller and operated by one person.

The system is operated by a Diesel engine that driving hydraulic pumps, generators and compressors. They provide hydraulic, electrical and steam power for the following main functions:

- Hydraulic drive function.
- Steering control function
- Lifting control function.
- Hydraulic brake function.
- Air brake function when connecting a self-propelled trailer and a non-self-propelled trailer.

2.1.1. The Power Pack Unit

The PPU is considered to be the brain of a self-propelled trailer system. The PPU consists of an electro-electronic control

system [8], a main hydraulic system that determines the functions of the trailer. The PPU can be adjusted in the angle range of 11.8 degrees as depicted in Figure 3.

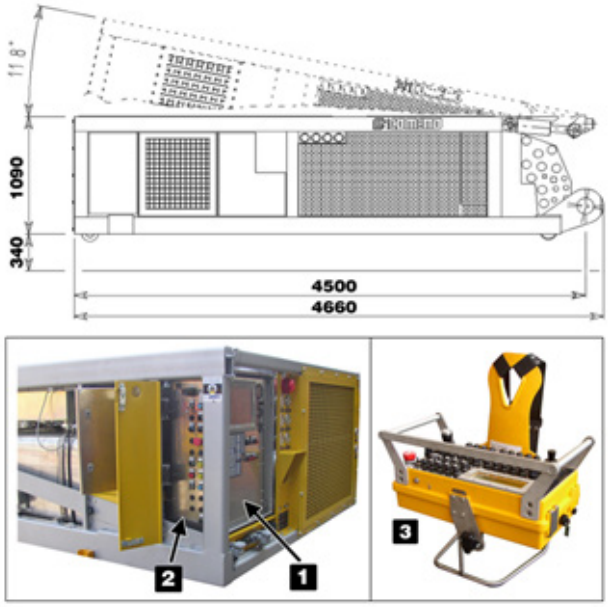

Figure 3: Power Pack and Radio Control

Between two mentioned systems, the hydraulic system, with the parameters listed in Table 1, is improved to make the trailer safer by adding a hydraulic system that controls the pump with a throttle valve. This adding valve replaces the main control valve ELS when this valve is damaged.

Table 1: The PPU hydraulic system parameters

Variable displacement pumps	
Lifting and steering	A11VLO190
Motorization (2 pumps)	A4VG180 + A4VG125
Gear pumps	
Oil cooling pump	SAUER SNP3/90
Pump for hydraulic oil supply to engine coolant radiators fan	SAUER SNP3/44
Pump for overfeeding planetary gearboxes.	SAUER SNP3/44
Pump for hydraulic oil supply to radiator fan	SAUER SNP2-17

Table 2: Module parameters

WEIGHTS	**MSPE 4/4/3 (4 axles)**			**MSPE 6/4/3 (6 axles)**		
Speed (km/h)	0.5	5	10	0.5	5	10
Axle load (2 suspensions), ton	34	34	31	34	34	31
Total gross weight, ton	136	136	124	204	204	186
Dead weight, ton	1.77			26		
Payload, ton	186.3	186.3	106.3	178	178	160
AXLES						
Number of axle lines	4 (8 suspensions)			6 (12 suspensions)		
Number of driven axles	2			4		
Number of braked axles with A.S.R.	2			2		
PLANETARY GEARBOX						
Wheel reducer (code 108.0204)	LOHMANN GFT 17 T3 9357					
Number of wheel reducer	8			8		
Variable displacement motor	A6VE 28HD1/63W					
Input speed	5960 rpm					
Reduction ratio	77.95					
Output speed	76,46 rpm					
Output torque	13881 Nm (10237 ft.lbs)					
Quantity of oil per wheel reducer	2 litres					
Oil type	SPARTAN EP 220~BP Energol GR-XF220					
SLEW GEAR						
Slew gear	IMO WD-HC 0300					
Motor	PARKER VOAC F12-060-MF-INF					

2.1.2. Modules

Modules with parameters such as in Table 2 include 6-axis type (6/4/3) and 4-axis type (4/4/3) with a maximum load for one axle of 3,4 tons. Modules are assembled by 3 types of connection such as mechanical connection, hydraulic connection and electronic connection. The connections are formed by serial configuration (back to back coupling) and parallel configuration (side by side coupling) as depicted in Figure 4.

2.2. The PPU hydraulic system.

The PPU hydraulic system [9] which is depicted in Figure5 consists of 5 pump assemblies as follows:

- One variable delivery pump A11VLO of 190cc (No. 22 in Figure 5) used for the steering and the lifting of the vehicle, and for the lifting cylinders of the Power Pack.
- Two variable delivery pumps: A4VG of 180cc and 125cc (No. **23** and No. **24 in** Figure 5); used for the motorization. Being a closed circuit, each of these two pumps is equipped with an overfeeding pump.
- One fixed delivery pump of 44cc (No. **25 in** Figure 5): this pump is used for overfeeding and piloting of the hydrostatic motors.
- One fixed delivery pump of 17cc (No. **26 in** Figure 5): this pump operates the hydraulic oil radiator fan.
- One further double-body fixed delivery pump of 90cc + 44cc (No.**27** and **27a in** Figure 5)
  - The 90cc pump (No. **27a in** Figure 5) is used for hydraulic oil recirculation in the radiator and in the return filter (No. **11 in** Figure 5).
  - The 44cc pump (No. **27 in** Figure 5) operates the Diesel engine coolant liquid/air radiator fans.

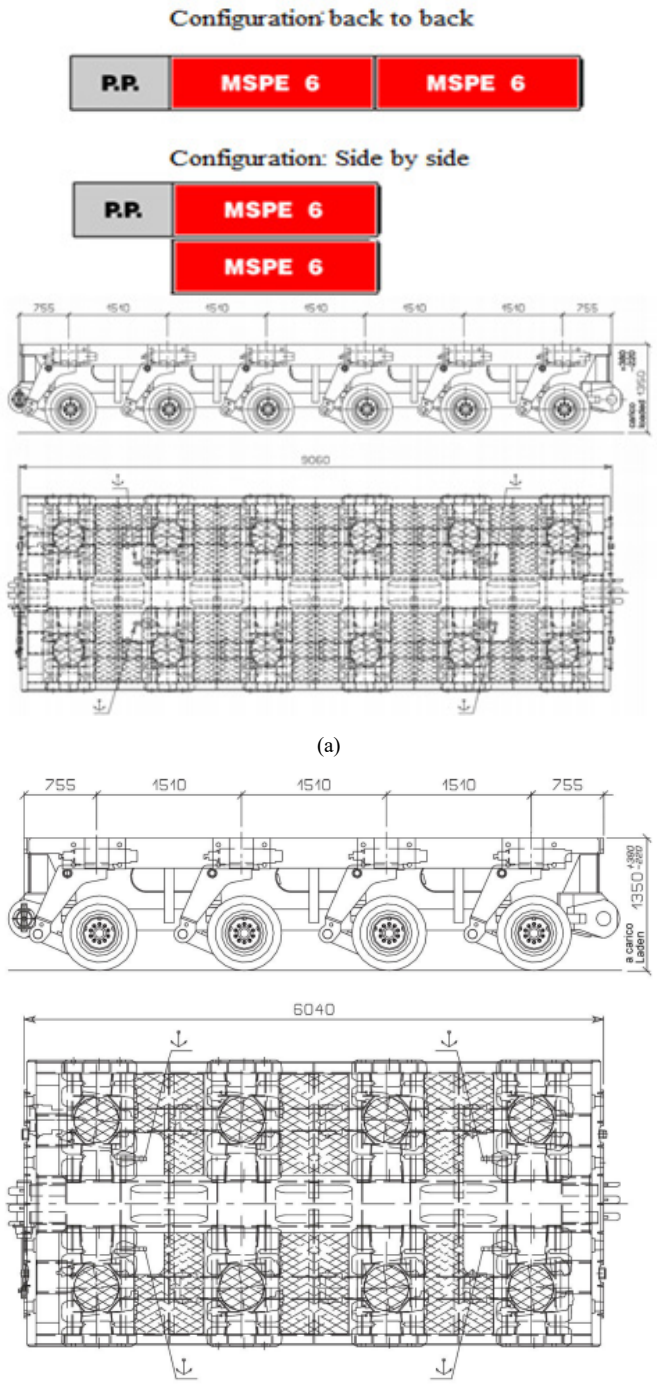

Figure 4: (a) Module Coupling and 6-axis type
(b) 4-axis type

The five pump assemblies are arranged as depicted in Figure 5 and are driven by a MERCEDES 335 KW Diesel engine. The pump assemblies are responsible for ensuring the operation of functions such as transmission, steering, lifting and braking. In particular, the hydraulic control valve ELS determines the operation of the braking, steering and lifting functions by adjusting the supply impeller A11VLO.

The hydraulic braking function: The braking function is to ensure the safety of the entire trailer system and packages. If the valve ELS is broken, the brake pressure cannot reach to 170 bar (as in Figure 6) and therefore the braking function will not work.

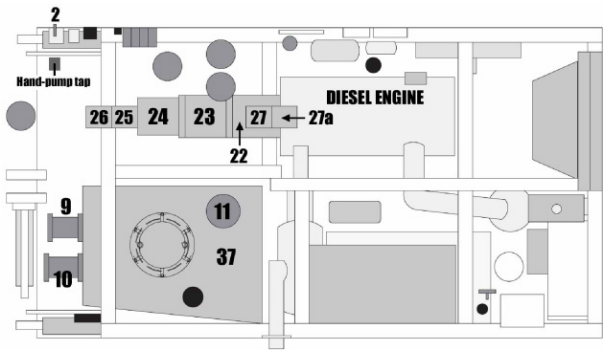

Figure 5: Pump Cluster Positions

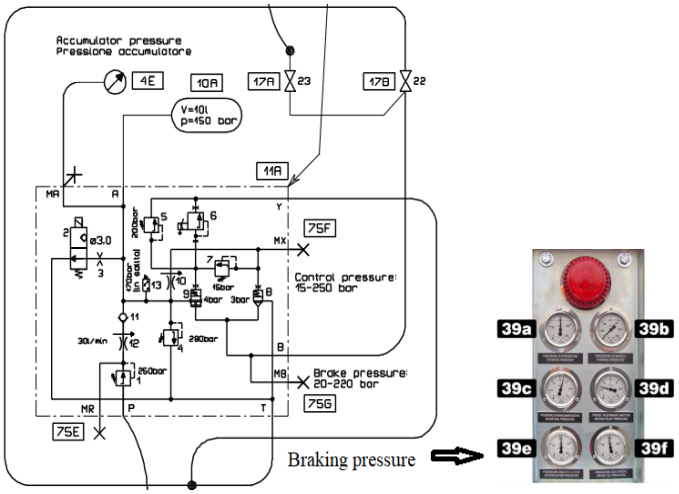

Figure 6: Diagram of the hydraulic braking system

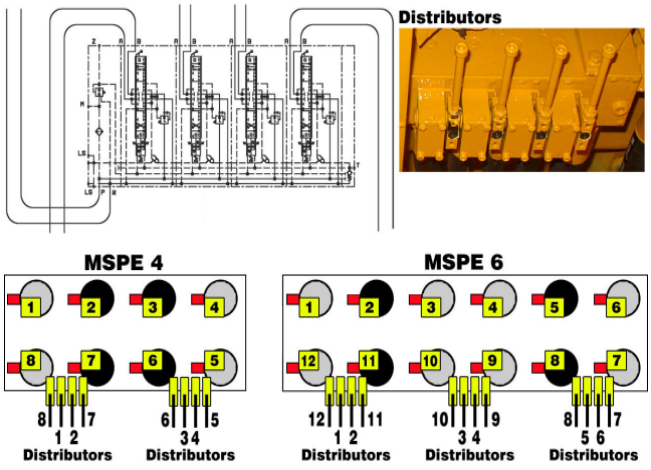

(a)

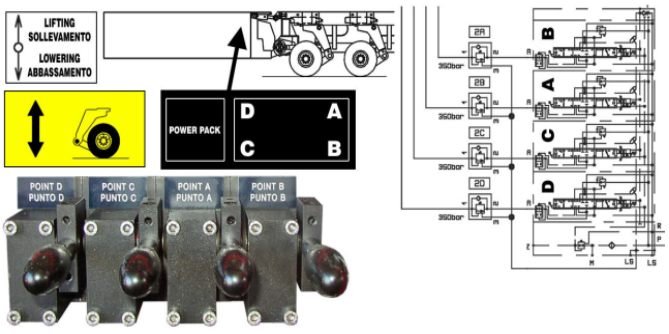

(b)

Figure 7: (a) The steering; and lifting/lowering function (b)

The hydraulic steering and lifting/lowering function: Diagram of hydraulic steering [9] and lifting/lowering function is shown in Figure 7. In addition, the hydraulic diagram for the pump A11V0 is depicted in Figure 8. The pump A11VO is used to open the steering and lifting/lowering function. This type of pump automatically changes the flow according to the load change. The working pressure of the steering and lifting/lowering function is adjusted by the proportional structure of the pressure reducing valve ELS.

If the load changes, the sensor detects and sends the signal to the central control system, then the controller processes and outputs the appropriate signal controlling the ELS regulating valve (No. **27A in** Figure 8). This valve ELS will regulate the amount of oil that back to the tank in order to control the impeller corresponding to the load.

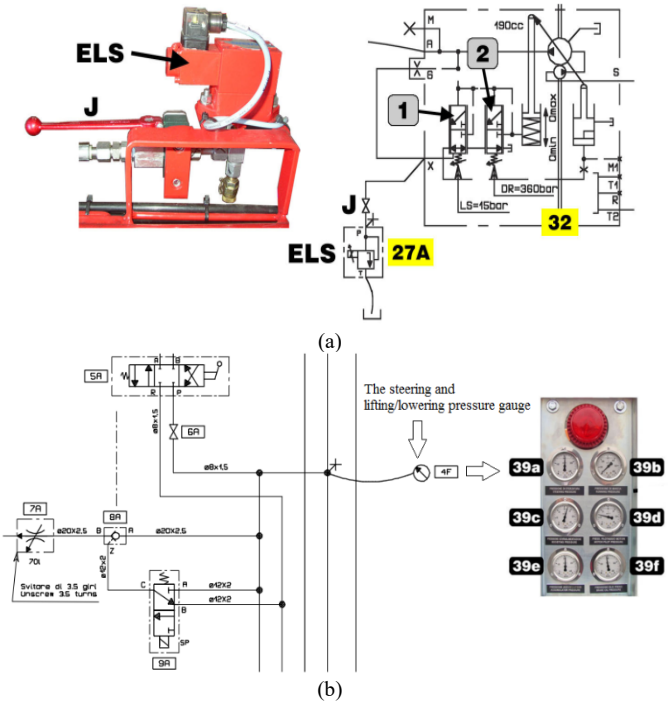

Figure 8: Valse ELS (a) and pressure gauge (b)

2.3. The proposed method

This section deals with the installation of a new throttle valve M [7] which is shown in Figure 9-b that is used to replace the hydraulic control valve ELS if it is unexpectedly damaged or failed.

The valve ELS is controlled by the electronic system with the following description:

- In the case of the diesel engine in starting and stand-by status: the system pressure approximately reaches to 15 bar during engine starting; after 5 seconds, the engine speed reaches to 900 rpm and therefore the system pressure will approximately reach to 220 bar.
- In the case of changing the direction of steering system and aligning it: the initial pressure is approximately 220 bar, the maximum pressure is 300 bar.
- In the case of lifting: The valve pressure is proportional to the load to be lifted. Working pressure is from 220 to 300 bar (approx.). Maximum pump pressure is 300 bar (approx.)
- In the case of lowering: Working pressure is from 220 to 300 bar (approx.)
- Maintain brake pressure from 170 bar to 220 bar.
- Pressure increase

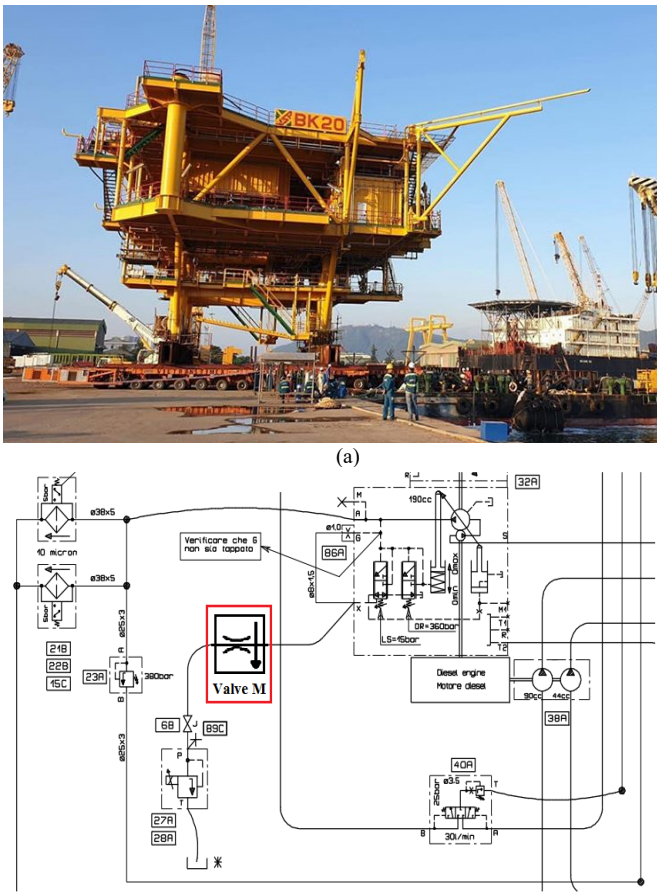

Figure 9: (a) The package is on the bridge leading to the barge (b) Install the throttle valve M into the system

In case of the valve ELS failure (pressure lack in the system), the tap J must be closed. This action allows to increase the pressure in the system to 360 bar again.

Failure of the valve ELS is an important issue because it determines all lifting, lowering, steering and braking functions when the Cometto self-propelled trailer is in operation. Therefore, the failure of this valve is very dangerous for all system because at that time the tap J needs to be closed in order to force the system to operate.

Closing the tap J will cause the pump A11VO to work at full capacity, considered to be high load, the working pressure of the pump and the piping system will be up to 360 bar (as shown in Figure 8, 39a). Diesel engine also works at high power and they often get drowned. Therefore, tap J can only be temporarily locked for a short time but not for long-term use.

Experience is learned during the actual use of self-propelled trailer system, the valve ELS often burns down when in operation because the suction coil of the valve is very hot when working due to the valve ELS is always soaked in electricity and the

environmental temperature in Vietnam is much higher than in Europe (Italy, where the system is made).

In an actual coincidence case, if tap J and valve ELS are damaged at the same time (called valve leakage), all lifting/lowering, steering, braking functions stop operating and cannot be controlled. Packages will overturn if there is a difference in load at any combination in the system that makes it impossible to adjust to the balance point.

Given the nature of transportation of oversized and overweight packages, such damages are very dangerous. Moreover, when the package is lying both on the wharf and on the barge (Figure 9-a) and the tide goes up/down quickly, the incident is absolutely impossible to happen because of much more dangerous. However, if this happens, there must be immediate remedies. And the fastest way to handle when the ELS valve is damaged is an essential issue.

Based on the operating principle of the system, the function of the ELS valve is to regulate the hydraulic oil flow that controls the A11VO impeller. Therefore, the amount of control oil will be at the maximum when this valve is broken. The pump will work as in no-load state, not enough pressure for the modes of steering, lifting/lowering and braking to operate. The proposed method is ultilizing the throttle valve M (as shown in Figure 10), which is located in the main connection between tap J and the ELS valve (as depicted in Figure 9b).

Figure 10: throttle valve M

The proposed method has improved the necessary requirements. Accordingly, when the ELS valve fails, no matter the status of tap J and without locking tap J, the hydraulic pump is adjusted by turning the throttle valve M only so that the system pressure, which is displayed on the steering pressure gauge, reaches to 200 bar or to 220 bar. The system works stably by those pressures. When more pressure is needed, the throttle valve M continues to be adjusted.

The throttle valve M theoretical basis is presented as follows:

2.3.1. Functions

The throttle valve M is responsible for regulating the flow rate in terms of the speed or running time of the actuator. The calculation method is presented in the next section.

2.3.2. Principles

The throttle works on the principle that the flow through the valve depends on the cross section (as shown in Figure 11). The oil flow qv through the gap is calculated using the Torricelli formula in (1) as follows:

$$q_v = \mathrm{C} \cdot A_j \sqrt{\frac{2 \cdot \Delta p}{\rho_j}} \quad (1)$$

where:

$\propto$: Flow coefficient.

A_j: Interstitial area of the gap, $A_j = \frac{\pi d^2}{4}$ [m^2].

$\Delta p = p_1 - p_2$: Pressure at previous and next positions of the gap [N/m^2].

p_j: Density of hydraulic oil [Kg/m^3].

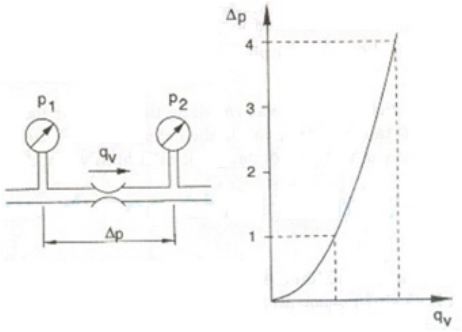

Figure 11: Difference in pressure and flow rate through the gap.

According to the flow control method, throttle can be classified into two main categories: the throttle adjusts axially (as shown in Figure 12-a) and the throttle adjusts around the shaft (as shown in Figure 12-b).

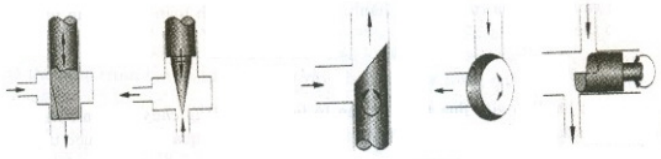

(a) (b)

Figure 12: Classification of throtle vale

Between them, the throttle adjusts axially as shown in Figure 12-a is selected for epxeriment in this article. The specifications requirement for the throttle valve M:

- System maximum working pressure p: 300-440 (Bar).
- Maximum working flow: 30 (l/ph).
- Threaded catch size: 1/2" (PT).
- Working Temperature: -25 ºC ÷ 80ºC.
- Valve Type): APT-04
- Standard size: DIN.

3. The Evaluation of Economic Efficiency

Since installing the throttle valve M into the hydraulic system controlling the pump, the self-propelled trailer system works very stable. The self-propelled trailer system safely and effectively transports a lot of petroleum packages. Some key projects had been applied the proposed method are as follows:

3.1. Hai Su Trang oil rig project in 2013:

Main task: Relocating and launching to barges the 1,700-ton upper block of Hai Su Trang rig at PTSC port, Vung Tau, Vietnam with following details:

- Relocation distance is 500 meters.
- Launching to barges.

While the trailers were moving through the bridge connecting the wharf and the barge, the ELS valve was damaged, the working pressure dropped to nearly 0 bar, the systems stopped working, unable to control the steering, lifting and braking functions. At this time, the technical worker adjusted the valve M so that the steering pressure and lifting/lowering pressure increased to 220 bar. Therfore, the system works again normally with this pressure. All actions only take 1 minute. If the valve M is not utilized, replacing the ELS valve will take 30 minutes or more, this will change the calculation parameters for the pump of bracing barges because the tide changes rapidly.

After the project is completed, our company is highly appreciated by the investors for quick action and mobility.

3.2. Su Tu Nau oil rig project in 2014:

Main task: Relocating and launching to barges the 2,200-ton upper block of Su Tu Nau rig at PTSC port, Vung Tau, Vietnam with following details:

- Relocation distance is 500 meters.
- Launching to barges.

When moving a site (site moving) from the installation location to the wharf, the ELS valve is damaged. At this time, it is very dangerous to stop and replace the ELS valve because the whole trailers and packages is lying in place for more than 30 minutes, that causes very large load impact on the road surface. Therefore, the valve M is adjusted to solve this problem within a minute and to bring the system back to normal operation.

In addition to the two typical projects just mentioned, all projects after Nov, 2014 (as listed in Table 3, 4, 5, 6) with application of the proposed method of improving the hydraulic system for Cometto self-propelled trailers have have made many investors trust our company and give the reputation of Vietranstimex is the leading company in Southeast Asia and the 34th rank in the world in the oversized and overweight transportation.

Table 3: Projects that applied the proposed method (2014-2016)

No.	**Project name; Weight (tons)**	**Port / Place; Time**
1	Load out BK4A Jacket; 1,080	Vietsovpetro Port – Vung Tau; Nov, 2014
2	Site moving DSF - HRD Project; 1,360	PTSC Port – Vung Tau; Nov, 2014
3	Transport gantry crane; 280	Hai Phong to Nha Trang; Mar, 2016
4	Load out Container crane; 560	Phu Huu Port – Ho Chi Minh; Jun, 2016
5	Load out ST-LQ Jacket; 1,279.72	PVC-MS Port – Vung Tau; Aug, 2016
6	Load out ThTC3 Jacket; 992.57	Vietsovpetro Port – Vung Tau; Aug, 2016
7	Load out ST-PIP Module 01 Topside; 1700.29	PTSC Port – Vung Tau; Aug, 2016
8	Load out ST-PIP Module 02 Topside; 2820.57	PTSC Port – Vung Tau; Aug, 2016
9	Load out ST-LQ Topside; 2429.17	PVC-MS Port – Vung Tau; Sep, 2016
10	Load out BKTNG Living Quarters; 823.79	Vietsovpetro Port – Vung Tau; Sep, 2016
11	Site Moving Sumitomo crane; 803	Tan Cang Port – Ho Chi Minh; Sep, 2016
12	Site Moving Container crane; 618.62	Tien Sa Port – Da Nang; Nov, 2016

Table 4: Projects that applied the proposed method (2017)

1	Site Moving Container crane; 560	ITC Phu Huu Port – HCM; Mar, 2017
2	Load out ThTC3 Topside; 1039.94	Vietsovpetro Port – Vung Tau; Mar, 2017
3	Load out DKI 16 Topside; 860	Vietsovpetro Port – Vung Tau; May, 2017
4	Load out DKI 16 Middle; 810	Vietsovpetro Port – Vung Tau; May, 2017
5	Load out DKI 17 Topside; 822.4	Vietsovpetro Port – Vung Tau; May, 2017
6	Load out DKI 17 Middle; 750	Vietsovpetro Port – Vung Tau; May, 2017

7	Load out DKI 18 Topside; 908.48	Vietsovpetro Port – Vung Tau; May, 2017
8	Load out DKI 18 Middle; 750	Vietsovpetro Port – Vung Tau; May, 2017
9	Load out DKI 19 Topside; 863.95	Vietsovpetro Port – Vung Tau; May, 2017
10	Load out DKI 19 Middle; 750	Vietsovpetro Port – Vung Tau; May, 2017
11	Site Moving Container crane; 650	Tan Vu Port – Hai Phong; Aug, 2017
12	Load out C24-P2 Topside; 1660	PTSC Port – Vung Tau; Dec, 2017
13	Load out C24-P2 Jacket; 1750	PTSC Port – Vung Tau; Dec, 2017
14	Load out B12-13 Topside; 1360	PTSC Port – Vung Tau; Dec, 2017
15	Load out B12-13 Jacket; 1679	PTSC Port – Vung Tau; Dec, 2017

Table 5: Projects that applied the proposed method (2018)

1	Load out B12-15 Topside; 1354.32	PTSC Port – Vung Tau; Jan, 2018
2	Load out B12-15 Jacket; 1530	PTSC Port – Vung Tau; Jan, 2018
3	Load out B12-11 Topside; 1781.88	PTSC Port – Vung Tau; Feb, 2018
4	Load out B12-11 Jacket; 1587	PTSC Port – Vung Tau; Feb, 2018
5	Load out B12-17 Topside; 1396	PTSC Port – Vung Tau; Feb, 2018
6	Load out B12-17 Jacket; 1762	PTSC Port – Vung Tau; Feb, 2018
7	Site Moving Container crane; 650	Tan Vu Port – Hai Phong; Mar, 2018
8	Load out CTC1 Jacket; 1025.23	Vietsovpetro Port – Vung Tau; May, 2018
9	Site Moving Container crane; 618.62	Tien Sa Port – Da Nang; Nov, 2018
10	Erection packages at Paper-mill; 150	SePon – Laos; Aug, 2018
11	Erection packages at Paper-mill; 90	SePon – Laos; Aug, 2018
12	Erection packages at Hoang Van Thu Bridge Project (2 packages); 140.3 &83.5	Hai Phong city – Vietnam; Aug, 2018
13	Erection the center arch span bridge from the barge grillage to final elevation by strand jack system; 440.3	Hai Phong city – Vietnam; Aug, 2018
14	Load out CTC1 Topside; 1047.3	Vietsovpetro Port – Vung Tau; Oct, 2018

Table 6: Projects that applied the proposed method (2019-2020)

1	Site moving for H387 & H388 Vessel; 788.5	Dong Xuyen Port – Vung Tau; Fed, 2019
2	Site moving for H765 Vessel; 1057.6	Dong Xuyen Port – Vung Tau; Fed, 2019
3	Load out BK20 Jacket; 721.2	Vietsovpetro Port – Vung Tau; Jul, 2019
4	Load out BK20 Topside; 800	Vietsovpetro Port – Vung Tau; Jul, 2019
5	Load out SVDN Pipes; 3x2000	PV Shipyard Port – Vung Tau; Jul, 2019
6	Site Moving Container crane; 2x700	Bason Port-Phu Mi; September, 2019

7	Site Moving SVDN Jacket; 1200	PTSC Port – Vung Tau; March, 2020
8	Site moving, Loadout,, Launching hight speed ferry	Dong Xuyen Port – Vung Tau; May, 2020

4. Conclusion

The article has proposed a new method of installing the throttle valve M into the hydraulic system for the Cometto self-propelled trailer system. The method has been raised by the practical difficulties arising during the operation of the Cometto self-propelled trailer system for transporting the oversized and overweight packages. The difficulties include suspending the Cometto system, unable to control the steering, lifting and braking functions and that caused by the damage of the hydraulic control valve ELS. The sudden stop of the system makes the packages also being abruptly stopped on the road, which will put high pressure on the road surface, affecting the structure of road and the balance of barges.

With the new installation of a part in the hydraulic system, it has brought a great effect to the business, creating peace of mind for investors, increasing mobility for transport equipment and great reducing troubleshooting time when trailers are under load as well.

However, it is necessary to note that the throttle valve M only replaces the ELS valve in an emergency when the incident occurs because the M valve only works with manual adjustment. This M valve cannot replace the ELS valve completely because the ELS valve opens and closes automatically via electronic card control in the PPU. When the load changes, the ELS valve automatically adjusts accordingly. Therefore, the ELS valve replacement should be performed when the system is maintained after the project.

Moreover, authors would like to introduce in this article a kind of world-specific trailers that have been approached for a long time in the word but it is still very new in Vietnam. Hopefully, much leading transportation companies in Vietnam will equip the system in the future and put them into use more, improve efficiency, increasingly develop oversized/overweight packages transportation industry in order to reach to the world standard. Besides Cometto, there are many companies producing Modular Self-Propelled Electric (MSPE) self-propelled trailer systems such as: Golghofer, Nicolas, Kamag ... Each company has different strengths but all of them enhance advanced operational features for the purpose of absolute safety for goods and people.

Conflict of Interest

The authors declare no conflict of interest.

Acknowledgment

This project is supported by Van Lang University (VLU) Electronics and Electrical Engineering Division, Ho Chi Minh City 700000, Vietnam.

References

[1] L. Černá, V. Zitrický*, and J. Daniš, “The Methodology of Selecting the Transport Mode for Companies on the Slovak Transport Market”, Open Engineering, **7**(1), 2006, doi: 10.1515/eng-2017-0002.

[2] S. Hameed, R. Chandra Prathap, “Study on Impact of Vehicle Overloading on National Highways in Varying Terrains”, International Journal of Engineering Research & Technology (IJERT), **7**(1), 2018, doi: 10.17577/IJERTV7IS010135.

[3] T.N. Do et al., “Personal dead reckoning using IMU mounted on upper torso and inverted pendulum model”, IEEE Sensors Journal, **16**(21), 7600–7608, 2016, doi: 10.1109/JSEN.2016.2601937.

[4] T. Nhut Do, S.Y. Soo, “Foot motion tracking using Vision”, IEEE 54th International Midwest Symposium on Circuits and Systems (MWSCAS), 1–4, 2011, doi: 10.1109/mwscas.2011.6026603.

[5] T.N. Do, S.Y. Soo, “Gait analysis using floor markers and inertial sensors”, International Journal of Sensors, **12**(2), 1594–1611, 2012, doi: 10.3390/s120201594.

[6] Self-Propelled Module Trailer - Use and Maintenance, Cometto, Via Cuneo, 2019.

[7] Self-Propelled Module Trailer - Electronic Manual, Cometto, Via Cuneo, 2019.

[8] Self-Propelled Module Trailer - Electric Electronic Diagrams, Cometto, Via Cuneo, 2019.

[9] Self-Propelled Module Trailer - Hydraulic Diagrams, Cometto, Via Cuneo, 2019.

ASTES

Advances in Science, Technology and Engineering Systems Journal Vol. 5, No. 6, 995-1000 (2020)

www.astesj.com

Special Issue on Innovative Research in Applied Science, Engineering and Technology

ASTESJ

ISSN: 2415-6698

Advanced Design of Current-mode Pass-band Filter using Ant Colony Optimization Technique

Kritele Loubna[1,*], Benhala Bachir[2], Zorkani Izeddine[1]

[1]*Faculty of Sciences Dhar el Mahraz, University of Sidi Mohamed Ben Abdllah, Fez, 30050, Morroco*

[2]*Faculty of Sciences, University of Moulay Ismail, Meknes, 50000, Morroco*

ARTICLE INFO

Article history:
Received: 02 September, 2020
Accepted: 02 November, 2020
Online: 08 December, 2020

Keywords:
Ant colony optimisation
Analog circuit design
Positive second-generation current conveyor

ABSTRACT

Ant Colony Optimization (ACO) algorithm, a well-known robust technique to solve easily both a simple and multiple objective optimization problems. This article presents an application of the ACO in order to achieve the optimal sizing of analog circuit. The proposed technique is employed to optimizing the sizing of a positive second-generation current conveyor (CCII+). Results show better objective functions than previously achieved by other optimization procedure. PSPICE simulations are used to confirm the validity of the reached optimal results and the accuracy of the proposed procedure.

1. Introduction

Current Conveyor (CC) represents the first construction block developed for current signal processing [1]. Two years later, in 1970, another variant of a CC, namely, Second Generation Current Conveyor (CCII) was published [2].

Recently, a Current Conveyor is seen as a good alternative for the voltage-mode. CC can be widely employed in different applications. The CCII is the most popular configuration [3].

Despite the number of positive proprieties ensured by the CCS [4], it seems that designing integrated CC circuits with high performance is in effect still open particularly in CMOS technology [5].

Currently, an important interest has been devoted to achieve the best sizing of the analog component efficiently and with high accuracy. Some (meta) heuristics were used in the scientific publications such as Genetic Algorithms (GA) [6, 7], Ant Colony Optimization (ACO) [8, 9], Particle Swarm Optimization (PSO) [10], Differential Evolution algorithm (DE) [11], Simulated Annealing (SA) [12] and Artificial Bee Colony Algorithm (ABC) [13, 14].

ACO algorithm is proposed in this work, with view to get an optimal design of positive second-generation current conveyor (CCII+). To this end, we applied three of the most important variants of ACO, specifically, the Ant System (AS), the Min-Max Ant System (MMAS) and the Ant Colony System (ACS). In fact, the ACO has already efficiently been used to treat real optimization problems, particularly in the analog circuit area.

A high performance CCII+ depends on the high-end cut-off frequency for the current waveform (F_{ci}) and the input impedance at port X. Hence, two objectives functions are taken into consideration: achieve a low input resistance R_X and a very high cut-off frequency F_{ci}. However, the suggested technique is a mono-objective one, to this end; the optimization process is treated using two distinct manners; firstly, each objective function is solved separately. In the second way, a mono-objective problem is considered by using a weighting technique.

This paper is organized in the following manner: The second section is about a detail description of the ACO technique. The third section proposes an example for the optimal sizing of CCII+. Then, a comparison with some similar works and simulation results are represented in the fourth section. Through the fifth section, the optimized CCII+ is exploited in order to form a current mode filter. Finally, the sixth section is the conclusion.

2. The ACO Technique Presentation

Ant Colony Optimization (ACO) is a nature-inspired algorithm, used to resolve various hard problems. The use of ACO has proved a capacity to deal with complex optimization problems successfully, for instance we can cite the traveling salesman

*Corresponding Author: Kritele Loubna, loubnakritele@gmail.com

problem (TSP) [15], vehicle routing problem [16], the quadratic assignment problem (QAP) [17].

The ACO takes inspiration from the real ant colonies behavior. The fundamental idea of this metaheuristic consists in simulating the social intelligence of ants in searching the shortest road from the nest and a source of food. In fact, real ants communicate indirectly through trails of chemical pheromone. Concretely, the agents of the colony deposit pheromone on the road to determine certain favorable route to be pursued by other ants [18].

2.1. Ant System

« Ant System » (AS) is the basic variant of the ACO. The modelling approach to resolve a given optimization problem is established as follows:

Ants choose the vertex to travel to by applying the state transition rule [19, 20]. Ant k in node a will move to vertex b according to the probability offered by (1):

$$P_{ab}^{k}=\begin{cases}\dfrac{(\tau_{ab})^{\alpha}\cdot(\eta_{ab})^{\beta}}{\sum_{l\in J_a^k}(\tau_{ab})^{\alpha}\cdot(\eta_{ab})^{\beta}} & \text{if } a\in J_a^k\\ 0 & \text{if } a\notin J_a^k\end{cases} \tag{1}$$

while J_a^k corresponds to the list of possible moves, which are possible for ants starting form vertex a, τ_{ab} represents the intensity of the trace associated to brink (a, b). α and β identify the relative impact of the trace intensity and the visibility value, η_{ab}.

where

$$\eta_{ab}=\frac{1}{d_{ab}} \tag{2}$$

The d_{ab} represents the distance between nodes a and b

The pheromone is updated by means of formula (3), when all agents of the colony construct their path:

$$\tau_{ab}=(1-\rho)\cdot\tau_{ab}+\sum_{k=1}^{m}\Delta\tau_{ab}^{k} \tag{3}$$

While ρ corresponds to the pheromone decay parameter, m represents the number of ants, and $\Delta\tau_{ab}^{k}$ is the amount of pheromone deposited by ant k on brink (a, b):

$$\Delta\tau_{ab}^{k}=\begin{cases}\dfrac{Q}{L_k} & \text{if } (a,b) \text{ belongs to tour done by k}\\ 0 & \text{otherwise}\end{cases} \tag{4}$$

Q is a constant; L_k represents the tour length built by ant k.

2.2. Min-Man Ant System

The Min-Max Ant System is an adjustment of the AS [21].

Min-Max Ant System (MMAS) is designed to attain the best result. To this end, only the optimal result is authorized to intensify the pheromone quantity. In fact, MMAS uses an instrument to border the trace intensity, and so that avoid the premature stagnation.

MMAS presents some new features and they are as follows:

- Only the ants that produced the best solution are allowed to update trails;
- To avoid stagnation, MMAS introduces upper and lower bounds so that the pheromone intensities lie inside the interval $[\tau_{min}, \tau_{max}]$;
- In each brink, the trail strength is initialized to τ_{max}.

2.3. Ant Colony System

The Ant Colony System (ACS) algorithm incorporates three main differences with respect to the AS algorithm:

- ACS algorithm uses a parameter q_0 ($0\le q_0\le 1$), which controls the tuning between exploitation and exploration. thus, the probability that ant moves to node b is given by this rule:

$$b=\begin{cases}\arg\max_{u\in B_a^k}\left[\left(\tau_{au}(t)*(\eta_{aB})^{\beta}\right)\right] & \text{if } q\le q_0\\ (1) & \text{if } q\succ q_0\end{cases} \tag{5}$$

where q is a random variable evenly distributed in [0, 1]

- The global pheromone update is applied only to edges that form part of the best solution, as in the following:

$$\tau_{ab}=(1-\rho)\cdot\tau_{ab}+\rho\cdot\Delta\tau_{ab} \tag{6}$$

where

$$\tau_{ab}=\begin{cases}1/L & \text{if } (a,b)\in best-global-tour\\ 0 & \text{otherwise}\end{cases} \tag{7}$$

- The updating of local pheromone is applied when each ant produce a solution:

$$\tau_{ab}=(1-\rho)\cdot\tau_{ab}+\rho\cdot\tau_{int} \tag{8}$$

The procedure of the ACO technique can be illustrated by means of the flowchart bellow:

3. Application of the ACO to the optimal sizing of CCII+

CCII is the most popular configuration of CCs; it replaces the conventional OPAMP in different applications as for example active filters, oscillators, and analog signal processing.

The CCII is three terminal devices; the current conveyor's response is illustrated by expression (9) [22]:

$$\begin{pmatrix}I_Y\\V_X\\I_Z\end{pmatrix}=\begin{pmatrix}0&0&0\\1&0&0\\0&\pm\beta&0\end{pmatrix}\begin{pmatrix}V_Y\\I_X\\V_Z\end{pmatrix} \tag{9}$$

The voltage at node X is duplicated from the voltage applied at node Y. Similarly, the current at Z port is copied from the current flowing through node X. A positive Z output current conveyor is considered when $\beta=+1$ and it is denoted CCII+. For optimal

circuit performance, it is desirable to have very high impedance on Y and Z nodes and small Rx, i.e. the resistance on X [22].

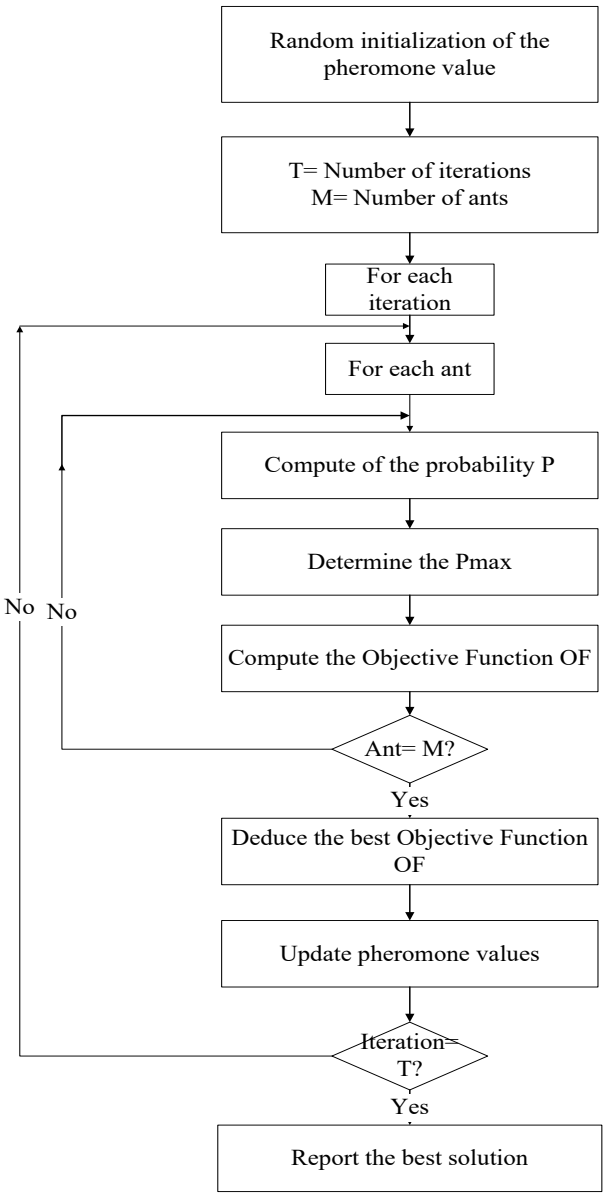

Figure 1: Flowchart of ACO

In this work, the ACO is used to optimize the performances of a positive second-generation CMOS current conveyor (CCII+) (figure2). Optimizing the most affecting parameters of the current conveyor is highlighted:

This optimization problem is resolved using two methods; in the first one, two mono objective function are considered. The objective functions are:

- Minimize the Rx, which represents the X-port input parasitic resistance

$$R_x \approx \frac{1}{gm_2 + gm_4} \tag{10}$$

- Maximize the Fci, which represents the current high cut off frequency

$$F_{ci} = \frac{1}{2\Pi}\sqrt{\frac{gm_5(gm_4 + go_4)}{Cgs_4(Cgs_5 + Cgs_6 + Cgd_4)}} \tag{11}$$

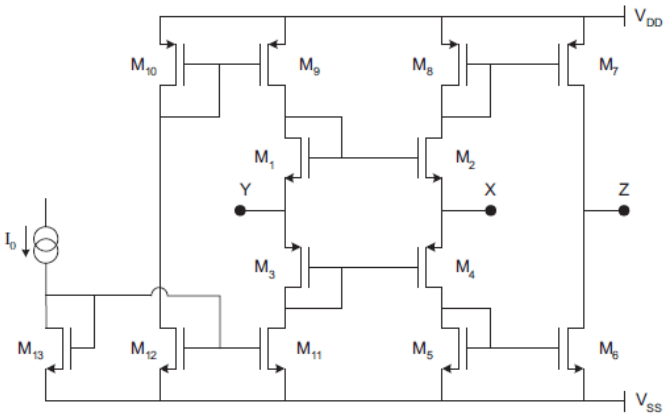

Figure 2: A positive second generation current conveyor

In the second method, the proposed objective function allows simultaneously minimizing Rx and maximizing Fci, and it is configured as:

$$f_{obj} = \frac{1}{F_{ci}} + R_X \tag{12}$$

The MOS transistors size represents the geometric variables that will be considered: the gates widths (WN and WP) and channels lengths (LN, and LP). The binding functioning conditions require that all the transistors of CCII+ must function in the saturation mode. So that, the main constrain of the optimization problem are presented by expressions (13) and (14):

$$\frac{V_{DD}}{2} + V_{TP} + \sqrt{\frac{2I_0}{\mu_N C_{ox}\frac{W_2}{L_2}}} \geq \sqrt{\frac{2I_0}{\mu_P C_{ox}\frac{W_8}{L_8}}} \tag{13}$$

$$\frac{V_{DD}}{2} - V_{TN} - \sqrt{\frac{2I_0}{\mu_N C_{ox}\frac{W_5}{L_5}}} \geq \sqrt{\frac{2I_0}{\mu_P C_{ox}\frac{W_4}{L_4}}} \tag{14}$$

where C_{ox}, μ_N, and μ_P are MOS technology parameters. V_{TN} and V_{TP} denote threshold voltages of NMOS and PMOS transistors respectively. The employed supply voltages are V_{SS}/V_{DD}= -2.5V/2.5 V and a bias current, Ibias=100 µA.

4. Results and Discussion

The proposed variants of the ACO technique were applied to deal with the optimal sizing of CCII+. The optimization technique works on C++ codes.

4.1. Optimization problem result using tow separated objective functions

The optimal values for the parameters of CCII+ achieved by the ACO algorithms and the circuit's performances linked with these values are indicated in tables 1 and 2.

Table 3 presents the performances provided by the AS, the MMAS and the ACS techniques versus to the ones ensured by Particle Swarm Optimization (PSO) and the Genetic Algorithm (GA) algorithms.

Table 1: the obtained results for RX

	LN (µm)	WN (µm)	LP (µm)	WP (µm)	$R_{X\text{-}min}$ (Ω)	
					Opt.	Sim.
AS	0.59	36.60	0.35	58.64	333.01	315.89
MMAS	0.60	36.34	0.35	59.00	335.63	318.69
ACS	0.59	36.68	0.35	59.00	**332.65**	**315.19**

Table 2: the obtained results for Fci

	LN (µm)	WN (µm)	LP (µm)	WP (µm)	Fci-max (GHz)	
					Opt.	Sim.
AS	0.55	5.48	0.35	9.52	1.795	1.739
MMAS	0.55	5.60	0.35	9.60	1.775	1.731
ACS	0.55	5.44	0.35	9.50	**1.801**	**1.754**

The results of the simulation under SPICE for Rx and Fci employing the optimal results acquired by the suggested techniques for CCII+ are exposed in figures 3 and 4. We can observe that simulation results are in good correspondence with theoretical values achieved by the ACO technique.

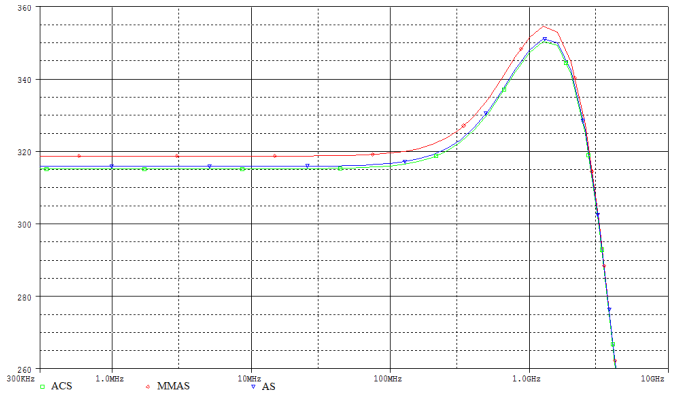

Figure 3: Variation of resistance (ohm) versus frequency (Hz) employing AS,MMAS and ACS

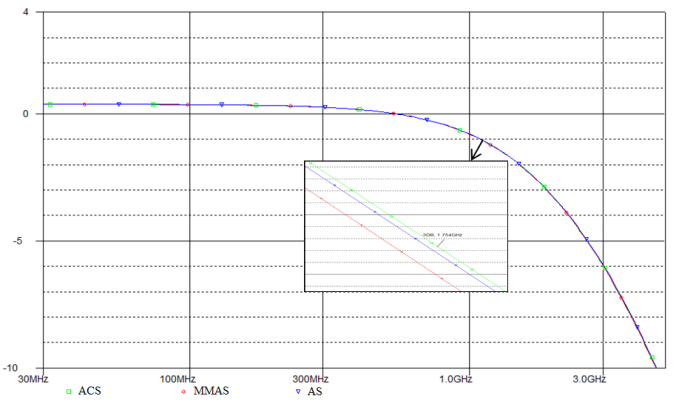

Figure 4: Current gain (dB) versus frequency (Hz) employing AS,MMAS and ACS

Table 3: Comparison results

	ACS	PSO[23]	GA[23]
R_{X}-min (Ω)	**332.65**	464	510
F_{ci}-max (GHZ)	**1.801**	1.751	1.541

It is shown that the three variants of the ACO algorithm offer similar results. The comparison with two techniques belonging to metaheuristics indicates that the ACS accomplished the greatest results with regard to objectives compared to Particle Swarm Optimization (PSO) and the Genetic Algorithm (GA) algorithms.

4.2. Optimization problem result using weighting approach:

The optimal physical parameters values of MOS transistors achieved employing the three variants of ACO algorithm are given in table 4. The comparison of the acquired results with those obtained by another metaheuristic namely, particle swarm optimization (PSO) algorithm, shows that ACS could reach a greatest F_{ci} value. However, PSO could achieve a smaller R_X value.

Table 4: Optimal parameter values and optimization results for R_X and Fci

	LN (µm)	WN (µm)	LP (µm)	WP (µm)	$F_{ci\text{-}max}$ (GHz)	$R_{X\text{-}min}$ (Ω)
AS	0.58	7.95	0.35	13.00	1.446	711.42
MMAS	0.59	8.08	0.35	13,00	1.420	708.75
ACS	0.55	7.53	0.35	12.97	**1.531**	721.08
PSO-2S [24]	0.52	14.30	0.35	23.62	1.358	**444**

The following table presents the simulation results:

Table 5: The optimal results for Rx and Fci

	F_{ci_max} (GHz)		R_{X_min} (Ω)	
	Opt.	Sim.	Opt.	Sim.
AS	1.446	1.495	711.417	825.896
MMAS	1.420	1.479	708.75	825.896
ACS	1.531	1.552	721.085	827.704

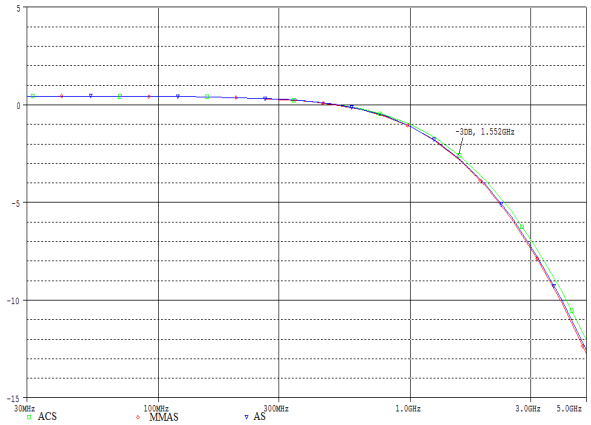

Figure 5: Current gain (dB) as a function of frequency (Hz) employing AS,MMAS and ACS

The figure 5 gives the SPICE simulation for current gain (in dB) as a function of frequency, and the figure 6 presents the SPICE simulation results for R_X (in ohm) as a function of frequency and this by employing the acquired optimal values by the three proposed variants of ACO algorithm for CCII+.

5. A Current Mode Filter based on the CCs

A second order filter can be implemented based on the use of simulated inductance [25]. In fact, Current conveyors present the basis of simulated inductance topology. Figure 7 shows a current mode active filter constituted of 4 current conveyors and two capacitors [26].

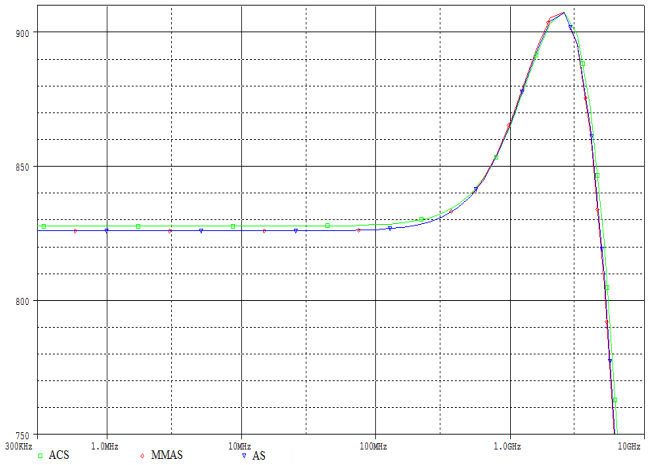

Figure 6: Variation of Rx (ohm) as a function of frequency (Hz) employing AS,MMAS and ACS

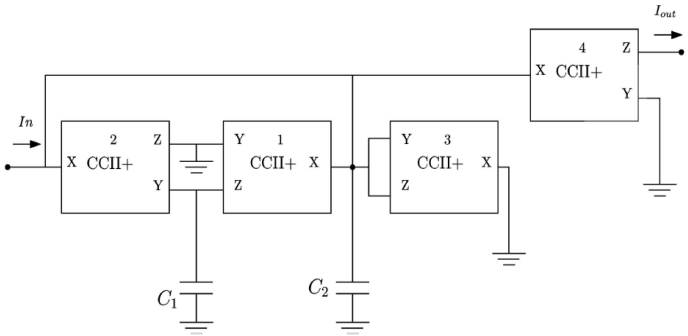

Figure 7: Current- mode pass-band filter

The quality factor and the resonance frequency of this filter are respectively presented by:

$$Q = \frac{R_G}{\sqrt{R_{X1}R_{X2}}}\sqrt{\frac{C_1}{C_2}} \quad (15)$$

$$f_0 = \frac{1}{2\pi}\frac{1}{\sqrt{R_{X1}R_{X2}C_1C_2}} \quad (16)$$

where:

$$\frac{1}{R_G} = \frac{1}{R_{X1}} + \frac{1}{R_{X2}} + \frac{1}{R_{X3}} + \frac{1}{R_{X4}} \quad (17)$$

R_{X1}, R_{X2}, R_{X3} and R_{X4} represent the parasitic resistances on port X of the considered CCII+.

The considered filter is simulated using SPICE, and it is designed based on the optimized CCII+ with optimal sizes determined by ACS for this cases:

a. Firstly, it is designed by employing the obtained CCII+ offering the maximum F_{ci}.
b. Secondly, it is designed by employing the obtained CCII+ offering the minimum R_X.
c. Finally, it is designed by employing the obtained CCII+ offering simultaneously maximum F_{ci} and minimum R_X.

The optimal parameters values of MOS transistors for the three cases are summarized in the table 6.

Table 6: Optimal physical parameters values of MOS transistors

	Minimum R_X	Maximum F_{ci}	Minimum R_X and Maximum F_{ci}
WN/ LN (µm)	36.68/0.59	05.44/0.55	7.53/0.55
WP/ LP (µm)	59.00/0.35	09.50/0.35	12.97/0.35

Figure 8 shows the SPICE simulation of the filter gain, where C1=C2=0.1pF.

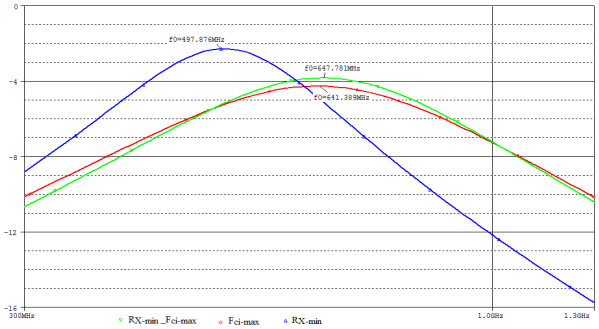

Figure 8: Resonance frequency of the second order current mode band-pass filter

The resonance frequencies reached by the ACS are presented in the following table; we can observe that the best resonance frequency of the current mode second order band pass filter is recorded in the third case.

Table 7: The obtained resonance frequencies

	$R_{X\text{-}min}$	$F_{ci\text{-}max}$	$R_{X\text{-}min}$ and $F_{ci\text{-}max}$
f_o (MHz)	497.896	641.389	647.781

6. Conclusion

In this work, the Ant System (AS), the Min-Max Ant System (MMAS) and the Ant Colony System (ACS), which are the most important variants of Ant Colony Optimization technique, are applied in order to optimize the sizing of conventional CMOS CCII circuit. The performances of a CCII+, especially the current high cut off frequency and the X-port parasitic resistance are optimized. The acquired results prove that the ACO algorithm offers a competitive optimizing capability for the design of CCII+. Then, the improved CCII+ structure was utilized as an elementary

block to build current mode band -pass filter. SPICE simulations and comparison with already published works were highlighted.

References

[1] K. C. Smith, A. Sedra. "The Current Conveyor-A new circuit building block" Proceedings of the IEEE, **56**(8), 1368-1369, 1968. DOI: 10.1109/PROC.1968.6591

[2] A. Sedra, K. C. Smith, "A Second-Generation Current Conveyor and Its Applications" IEEE Transactions on Circuits Theory, **17**(1), 132-134, 1970. DOI: 10.1109/TCT.1970.1083067

[3] D. Moro Frias, "Design and Applications of CMOS Current Conveyors," Master in electronics science, National Institute for Astrophysics, Optics and Electronics, 2008.

[4] P. Brandstetter, L. Klein, "novel wien bridge oscillator design using functional block structure with current conveyors", Advances in electrical and electronic engineering, **10**(1), 13-16, 2012. DOI: 10.15598/aeee.v10i1.556

[5] A. Chatterjee, M. Fakhfakh, P. Siarry, "Design of second-generation current conveyors employing bacterial foraging optimization", Microelectronics Journal, **41**(10), 616-626, 2010. doi:10.1016/j.mejo.2010.06.013

[6] J. B. Grimbleby, "Automatic analogue circuit synthesis using genetic algorithms", IEE Proceedings-Circuits, Devices and Systems, **147**(6), 319-323, 2000. DOI: 10.1049/ip-cds:20000770

[7] A. El Beqal, B. Benhala, and I. Zorkani, A Genetic algorithm for the optimal design of a multistage amplifier, Int. J. of Electrical and Computer Engineering (IJECE), **10**(1), 129-138, 2020. DOI: 10.11591/ijece.v10i1

[8] B. Benhala. Sizing of an inverted current conveyors by an enhanced ant colony optimization technique, Conference on Design of Circuits and Integrated Systems (DCIS), Granada, 1–5, 2016.

[9] L. Kritele, B. Benhala, and I. Zorkani. Ant Colony Optimization for Optimal Analog Filter Sizing, Chapter 10, Book: Focus on swarm intelligence research and applications, Eds., B. Benhala, P. Pereira and A. Sallem, NOVA Science Publishers, 193–220, 2017.

[10] F. T. S. Chan, M. K. Tiwari, Swarm Intelligence: focus on ant and particle swarm optimization, I-Tech Education and Publishing, 2007

[11] I. El hajjami, B. Benhala, and H. Bouyghf. Optimal Design of RF Integrated Inductors via Differential Evolution Algorithm, 1st International Conference on Innovative Research in Applied Science, Engineering and Technology (IRASET), Meknes, Morocco, 1-6, 2020.

[12] M. Fakhfakh, M. Boughariou, A Sallem and M Loulou, Design of Low Noise Amplifiers through Flow-Graphs and their Optimization by the Simulated Annealing Technique. Book: Advances in Monolithic Microwave Integrated Circuits for Wireless Systems: Modeling and Design Technologies, IGI global, 2012.

[13] B. Benhala, P. Pereira, A. Sallem, (Editors), Focus on swarm intelligence research and applications, NOVA Science Publishers, 2017.

[14] B. Benhala. Artificial bee colony technique for optimal design of folded cascode OTA, 2018 International Conference on Applied Mathematics and Computer Science, ICAMCS 2018, Paris, 59-64.

[15] Y. Jinhui, S. Xiaohu , M. Maurizio and L.Yanchun, "An ant colony optimization method for generalized TSP problem", Progress in Natural Science, **18**(11), 1417-1422, 2008. doi: 10.1016/j.pnsc.2008.03.028.

[16] Qi Chengming, "Vehicle Routing Optimization in Logistics Distribution Using Hybrid Ant Colony Algorithm", TELKOMNIKA Indonesian Journal of Electrical Engineering, **11**(9), 5308-5315, 2013. doi: 10.11591/telkomnika.v11i9.3284.

[17] L. M Gambardella, E. D Taillard, M. Dorigo. Ant colonies for the quadratic assignment problem. The Journal of the Operational Research Society, **50**(2), 167–176, 1999. doi:10.1057/palgrave.jors.2600676.

[18] M. Dorigo, M. Birattari, and T. Stützle, "Ant colony optimization: artificial ants as a computational intelligence technique", IEEE computational intelligence magazine, **1**(4), 28-39, 2006. doi:10.1109/CI-M.2006.248054.

[19] M. Dorigo and S. Krzysztof, An Introduction to Ant Colony Optimization, IRIDIA, 2006. doi: 10.1162/106454699568728.

[20] M. Dorigo, G. DiCaro and L. M. Gambardella, "Ant algorithms for discrete optimization", Artificial Life Journal, **5**(2), 137-172, 1999.

[21] T. Stützle, H. Hoos, "MAX-MIN Ant System", Future Generation Computer System, **16**(2000), 889-914.

[22] V.C. Gaudet, "Design of a CMOS current conveyor-based field-programmable analog array", Master of applied science, Department of electrical and cornputer engineering, University of Toronto, 1997.

[23] B. Benhala, "Metaheuristic Techniques for the Analog Circuits Performances Optimization-A comparison Issue", WSEAS Transactions on Circuits and Systems, **14**(20), 173-181, June 2015,

[24] A.El Dor, M. Fakhfakh, P. Siarry, "Performance optimization of CMOS second generation current conveyors using a multi-swarm algorithm", International Journal of Electronics and Communications (AEÜ), **8**(68), 496-503, 2014. DOI: 10.1016/j.aeue.2013.12.007

[25] A. Fabre, O. Saiid, F. Wiest, and C. Bouchern, "High frequency high-Q bICMOS current-mode bandpass filter and mobile communication application", IEEE Transactions on Circuits and Systems-I, **33**(4), 839–842, 1998. DOI: 10.1109/4.663567

[26] S.B. Salem, M.Fakhfakh, D.S.Masmoudi, M.Loulou, P.Loumeau and N.Masmoudi, "A High Performances CMOS CCII and High Frequency Applications", Journal of Analog Integrated Circuits and Signal Processing, Springer US, **49**(1), 2006. doi.org/10.1007/s10470-006-8694-4

ASTES

Advances in Science, Technology and Engineering Systems Journal Vol. 5, No. 5, 1013-1019 (2020)

www.astesj.com

Special Issue on Innovative Research in Applied Science, Engineering and Technology

ASTESJ

ISSN: 2415-6698

Fabrication and Properties of Hybrid Membranes Based on Poly (Vinyl Alcohol), Sulfosuccinic Acid and Salts of Heteropolyacid with or without Silica for Fuel Cells Applications

Said Maarouf [1,*], Zouhair Alouane[1,2], Bouchra Tazi[2], Farhate Guenoun[1], Khalil Fouad[3]

[1]*Laboratoire de Chimie Biologie Appliquée à l'Environnement, Faculté des Sciences, Université Moulay. Ismail, Zitoune Meknès, B.P. 11201, Maroc*

[2]*Laboratoire de Chimie, DSB, Ecole Nationale d'Agriculture. km. 10, Route Haj Kaddour,.B.P. S/40, Meknès, 50001, Maroc*

[3]*Laboratoire de Chimie Appliquée (LCA). Faculté des Sciences et Technique,– Route d'Imouzzer Fès, B.P. 2202, Maroc*

ARTICLE INFO

Article history:
Received: 24 June, 2020
Accepted: 21 September, 2020
Online: 20 October, 2020

Keywords:
Fuel cells
Polymer electrolyte membranes
Poly (vinylalcohol)
Silicotungstic acid
Sulfosuccinic acid

ABSTRACT

Novel ionic polymers were synthesized by crosslinking of poly (vinylalcohol) (PVA) with sulfosuccinic acid (SSA) and silicotungstic acid (SiWA) with or without silica. The polymer electrolyte membrane fuel cell (PEMFC) was developed using solution casting method. Infrared (IR) spectra revealed that the Keggin structure was insered in the PVA films. The thermal decomposition of the PVA/SSA/SiWA/SiO_2 membranes showed good thermal stability up to 200°C. Water uptake ranged between 31% and 88%. The maximum conductivity has been found to be 6,72.10^{-3} S.cm^{-1} at room temperature for PVA/SSA/SiWA containing 10% of silica weight. The ion exchange capacity of this membrane was 1,75 mmol.g^{-1}. The results showed that these membranes presented very promising performances for use in Proton Exchange Membrane Fuel Cells.

1. Introduction

Exhaustion of non-renewable fossil fuel invokes the development of environmentally friendly alternative energy sources. Fuel cells are being considered as interesting alternatives power sources for a wide range of applications, ranging from portable devices to electric vehicles [1, 2]. Fuel cells are of great interest in the recent research due to their attractive properties. They offer many advantages, such as environmentally benign, high energy efficiency and lower emission of pollutants [3, 4]. The principal component in PEMFCs is the proton exchange membrane (PEM) which is used as proton (or charge carriers) provider from anode to cathode. The membrane must be proton conductor with mechanical strength and chemical stability. The perfluorosulfonated membrane, Nafion produced by Dupont is the most used as a polymer in PEMFCs because of its combined chemical, electrochemical, and mechanical stabilities with high proton conductivity (~0.1 S.cm^{-1}) at ambient temperature [5].
However, it possesses some drawbacks, and especially its high cost; presents a high water swelling characteristic which reduces the lifespan of the membrane and decrease in conductivity at elevated temperature [6]. So, the utilization of Nafion membrane in fuel cell is limited. Therefore, "Hydrocarbon" proton conducting membranes have been designed as an alternative to perfluorinated membranes [7,8]. High performance polyarylenes are resistant to oxidation, thermo-stable and are mechanically strong with a relatively high glass transition temperature (Tg), sulfonated poly (ether ether) ketone [9], sulfonated polyimide [10], polybenzimidazole [11], sulfonated polyposphazene [12] and sulfonated poly(vinylalcohol) (PVA) [1,13], have been synthesized.
However, to enhance the proton conductivity of the polymers, a high acid content is needed. Unfortunately, this can decrease the mechanical strength of the composite membranes, or, even worse, degrade it, especially at higher temperatures [14].
Among the materials investigated, Poly (vinylalcohol) (PVA) has attracted great attention due to its good mechanical properties, chemical stability, low cost, film forming ability, and high hydrophilic behavior [15,16]. The PVA membranes are poor proton conductors and dissolve in water. Hence, to impart protonic conductivity as well as mechanical stability to PVA membranes, a crosslinking agent containing sulfonic acid group

*Corresponding Author: Said Maarouf, Email: saidmaarouf576@gmail.com

can be used, such as concentrated sulfuric acid, sulfosuccinic acid (SSA), acid sulfophthalic [13,17].

Many researchers have studied the properties of cross-linked PVA/SSA membranes as a function of SSA content. Recently, C.González, and A. Greus studied the proton-conducting membrane based on PVA/SSA/GO. Their experimental results showed the proton conductivity of the order of $2{,}06.10^{-3}$ S.cm^{-1} for the PVA/SSA humidified membrane [18]. Furthermore, Kim and al. demonstrated that the PVA/SSA/silica hybrid membranes prepared via a sol-gel process presents excellent proton conductivity [1].

In general, heteropolyacids (HPAs), and SiO_2 have served as an essential inorganic proton conductor for organic-inorganic hybrid membranes [19–22]. HPAs, a class of superionic conductor in their fully hydrated condition and thus it provides high proton conducting pathway [23,24]. For example, hydrated silicotungstic acid (H4 SiW12 O40 •28H2 O) has an ionic conductivity of 2.10^{-2} S.cm^{-1} at room temperature [25–27]. However, HPAs are generally water-soluble. Consequently, a major research objective is to fix the HPAs in stable structure by forming composites which can maintain or increase the proton conductivities of the membranes [22,28,29].

In our previous studies [30,31], we have synthesized the HPA and SiO_2 based hybrid membranes (PVA/PVP/SSA/HPAs/SiO_2). These membranes showed that proton conductivity increase significantly with the HPAs content. Silica was also added in the membranes preparation solution in order to improve thermal and mechanical stabilities of the PVA/PWA membranes.

The aim of this study was to prepare membranes for possible PEMFC. To do this, PVA/SiWA/SiO_2 hybrid membranes containing sulfonic acid groups were synthesized using solution casting method. Sulfonic acid groups were introduced into the PVA matrix by modifications of the chemical structure of the PVA through esterification with sulfosuccinic acid (SSA), which has sulfonic acid groups. In addition heteropolyacid and silica particles in the polymer matrix at varying concentrations, which were expected to achieve high proton conductivity, thermal stability and high water uptake. The effect of membrane thicknesses has also been studied. Ion exchange capacities have been studied for PVA/SSA/10wt.%SiWA/SiO_2 membranes. The prepared composite polymer electrolyte membranes have been characterized by various techniques TGA, and FTIR.

2. Experimental

2.1. Materials

Poly(vinylalcohol) with a molecular weight of 70.000 g.mol^{-1} was received from Sigma Aldrich. Sulfosuccinic acid 70wt.% from sigma Aldrich, Silicotungstic acid from Panreac, Silica 60A°,from sigma Aldrich.

2.2. Membrane preparation

10 wt% PVA solution was prepared by dissolving the pre-weighed amount of PVA in deionized water at 80°C for at least 4 h. The solution of PVA was mixed with SSA in mass ratio of 0,10g at 80°C for 3 hours. Then, Silicotungtic acid (0% - 40%) was added to the above solution and stirred for 2 hours at 80°C to produce PVA/SSA/SiWA membrane. Silica (1% - 15%) was subsequently added to the above solution and stirred at 70°C for about 4 hours to produce PVA/SSA/SiWA/SiO_2 membrane. The solvent was removed by evaporation at room temperature for 16 h, then the cast membranes were allowed to dry at 60°C for 24 h. and then in the oven at 140°C for 1 hour. Membranes thicknesses in the dray state are about 50 to 650 µm.

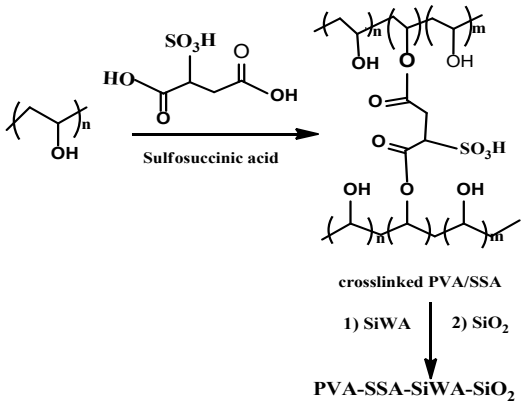

Figure 1: Molecular structure of PVA/SSA polymer matrix and silicotungstic acid with silica.

Figure 2: Homogeneous, transparent thin film of PVA-SSA-SiWA-SiO_2

2.3. Water Uptake

Membrane samples were dried at 60 °C for 24 h and weighed after (Wdry). Then immersed in boiling water during 24 h. The membranes were then removed, and the samples were finally weighed (Wwet). The water uptake of the membrane is deduced using the following equation:

$$WU = \frac{Wwet - Wdry}{Wdry} * 100 \quad (1)$$

2.4. Proton conductivity

Resistances were measured using a cell coupled with potentiostat-galvanostat–Amel instrument (70-50), the measurement cell is show in Figure 3 and has been described elsewhere (Table.1). It composed of two identical compartments linked with two platinum electrodes with the same surface as the membrane. In addition, in each compartment, Luggin capillaries are connected to two saturated calomel electrodes. The membrane is placed between the two compartments during measurements. The ionic conductivity of the membranes was determined by polarization. In 1M NaCl solution, the potential drop between the two references electrodes was measured, following application of a constant direct current (0.5 - 5 mA). The proton conductivity (σ) was obtained using the following equation:

$$\sigma = \frac{e}{RS} \quad (2)$$

where σ is the ionic conductivity in S.cm^{-1}, R is the Resistance of the membrane in Ω, e is the thickness of the membrane in cm, and S is the membrane surface in cm^2.

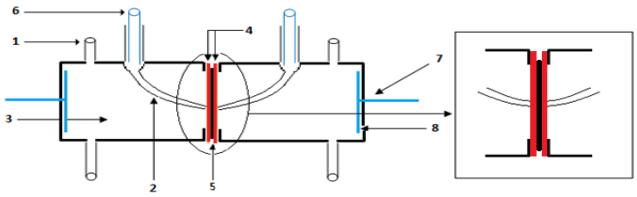

Figure 3: measurement cell of proton conductivity.

Table 1: Description of measurement cell of proton conductivity

1: Capillary (allow entry and exit of the solutions). 2: Capillary Luggin. 3: Electrolyte. 4: Teflon gaskets.	5: Membrane. 6: Reference electrodes. 7: Stem platinum. 8: Platinum electrodes.

2.5. FTIR spectroscopy

The spectrum of the membranes was recorded with a MVP 2 STAR ART DIAMANT (600-4000 cm^{-1}, resolution $4cm^{-1}$).

2.6. Thermal gravimetric analysis (TGA)

TGA was accomplished by thermogravimetric analyzer, TA 60 SHIMADZU TG-DTA. The samples were then heated from 25 °C to 600 °C at a heating rate of 20 °C.min^{-1}.

2.7. Ion exchange capacity (IEC) and fixed ion concentration

IEC has been determined by titration method. A sample membrane (0,375g to 0,765g) was immersed in a 250 ml of 1M HCl solution and stirring for 1h to change them into the H^+ form. The samples were then washed with deionized water to remove excess HCl, and then equilibrated with 230 ml of NaCl (0.1M) + 20 ml of NaOH (0.1M) solution for 24h at room temperature to permit the exchange between protons and sodium ions. Thereafter, 25 ml of the solution was titrated with HCl (0.1M) to evaluate the amount of H^+ generated from the exchange process. From the titration, the ion exchange capacity was determined from the following relation:

$$IEC = \frac{n(H^+)}{(W_{dry})} \quad (3)$$

where $n(H^+)$ is the number of moles of proton sites present in the membrane and Wdry is the weight of the dry membrane. Fixed ion concentration (FIC) can be determined from the following equation:

$$FIC = \frac{IEC}{WU} \quad (4)$$

where (WU) is the water uptake of the membrane sample.

3. Results & Discussions

3.1. Thermal gravimetric analysis (TGA)

The thermal degradation behavior of PVA/SSA, PVA/SSA/SiWA, and PVA/SSA/SiWA/SiO_2 composites membranes was illustrated in figure 4. Three major stages of the thermal decomposition can be considered. The first stage of the decomposition, which occurs between 25 and 200 °C, is the loss of absorbed water molecules formed after the esterification reaction of the membranes. Most of the absorbed water molecules in the membranes are supposed to exist in a bound state rather than in free molecules state. The water molecules seem to have been bound directly to the polymer chains and / or the $–SO_3H$ groups via hydrogen bonds [1]. The second decomposition stage between 200 and 400°C, is the degradation of the sulfonic acid groups ($–SO_3H$). The final major decomposition step comes about between 400 and 500 °C, which is ascribed to decomposition of salt of silicotungstic acid combined with silica. It is seen from TGA curves, that the thermal stability of the hybrid membranes is improved probably due to the additive effect of SiWA and SiO_2 fillers and the chemical cross-linked reaction between the PVA and SSA.

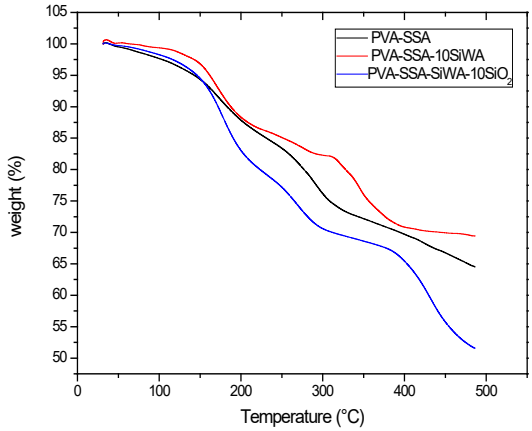

Figure 4: TGA curves for PVA/SSA, PVA/SSA/SiWA, and PVA/SSA/SiWA/SiO_2.

3.2. Fourier transform infrared spectroscopy

Figure 5 represents the F.T.I.R spectrum of the PVA/SSA, PVA/SSA/SiWA and PVA/SSA/SiWA/SiO_2 composite membranes. In the PVA/SSA/SiWA blend membranes, the characteristic ester absorption band (–COO) appeared around $1710cm^{-1}$ [32], and the band at $1030cm^{-1}$ is attributed to ($-SO_3H$) group [32]. These spectral data confirm the esterification between –OH in PVA and –COOH in SSA [1]. The peaks at $3300cm^{-1}$ (OH stretching), $2921cm^{-1}$ (symmetric CH_2–), and the band at $1420cm^{-1}$ is for (-CH3) bending which are characteristic of PVA. The peaks at 969.03; 914.16; 789.04 and $1141.89cm^{-1}$ which are respectively attributed to the W=Od, W-Ob-W and W-Oc-W and O-Si-O. The presence of these peaks in the spectra F.T.I.R confirms that silicotungstic acid is inserted into the blend membranes PVA/SSA/SiWA, the characteristic bands (Si-O-Si) appeared around 1082.14 and $1219.31cm^{-1}$ were observed in the spectra of the PVA/SSA/SiWA/SiO_2 hybrid membrane. This demonstrates that the esterification reaction was complete between the Poly (vinylalcohol) chains and the sulfosuccinic acid.

3.3. Water uptake and proton conductivity of the membrane PVA/SSA/SiWA

Figure 6 shows the water uptake and proton conductivity of the membranes PVA/SSA/xwt.%SiWA as function of the silicotungtic acid content. The water uptake varies from 47% to

60%. As shown in Figure 6, The water uptake increases with the increase of silicotungstic acid, and the maximum is obtained for 10wt.% of SiWA. After that, the addition of silicotungstic acid leads to a decrease in water uptake of the membrane. Invese behavior can be explained by the chemical structure of the PVA/SSA network. An increase in water uptake at low SiWA content maybe is due the restricted degree of their swelling as also of the hydrophilicity of silicotungstic acid to due presence of keggin cage in PVA/SSA/HPA bridged-matrix [33,34].

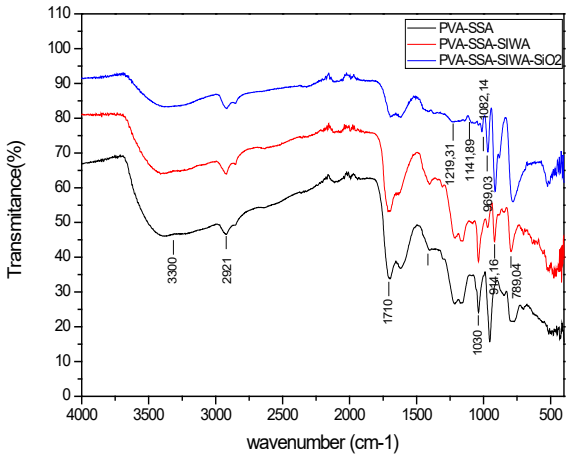

Figure 5: F.T.I.R spectra of PVA/SSA, PVA/SSA/SiWA, and PVA/SSA/SiWA/SiO_2 hybrid membranes.

The proton conductivity has been determined, as shown in this figure; the ionic conductivity of PVA/SSA/xwt.%SiWA membranes varies from 1,100.10^{-3} S.cm^{-1} to 3,015.10^{-3} S.cm^{-1}. The higher value is obtained for the composition PVA/SSA/10wt.%SiWA, which is much higher than that of the pure PVA films and pure 12-tungstogermanic heteropolyacid [35]. The results indicated that PVA film, composited with sulfosuccinic acid and silicoptungstic acid is a new kind of excellent high proton conductor.

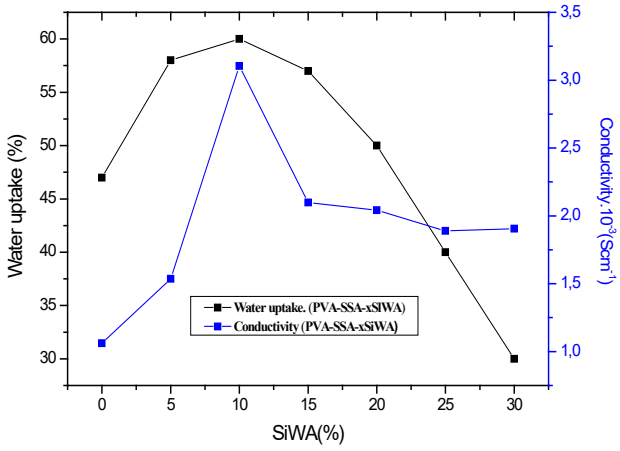

Figure 6: water uptake and proton conductivity of the hybrid membranes PVA/SSA/xwt.%SiWA with different amounts of SiWA.

Figure 7 shows a plot of water uptake of the membranes PVA/SSA/10wt.%SiWA as a function of the membrane thickness. The water absorption increases with the thickness of the membrane in the range 100 - 600 µm. It therefore goes from 28% for the PVA/SSA/10wt.%SiWA membrane of 110 µm thickness to 64% for the PVA/SSA/10wt.%SiWA membrane of 550 µm thickness.

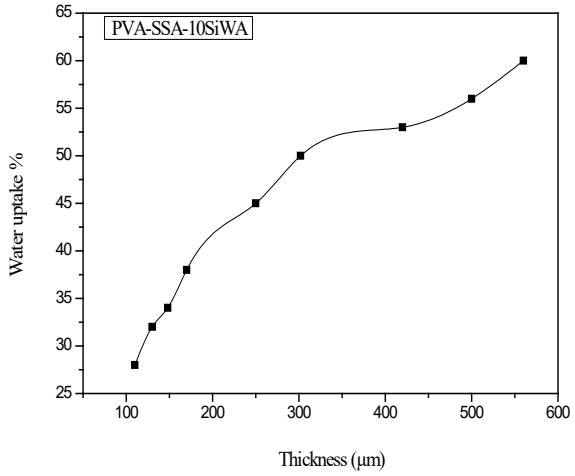

Figure 7: Water uptake of PVA/SSA/10wt.%SiWA membrane with thicknesses.

Figure 8 represents the ionic conductivity of the membrane PVA/SSA/10wt.%SiWA at saline media (NaCl 1M) as a function of the membranes thickness at room temperature. Ionic conductivity values increase from 0,567.10^{-3} to 3,668.10^{-3} S.cm^{-1} In line with thickness values from 100 to 650µm thick. This agrees well with the published results of B. Tazi and al. [22].

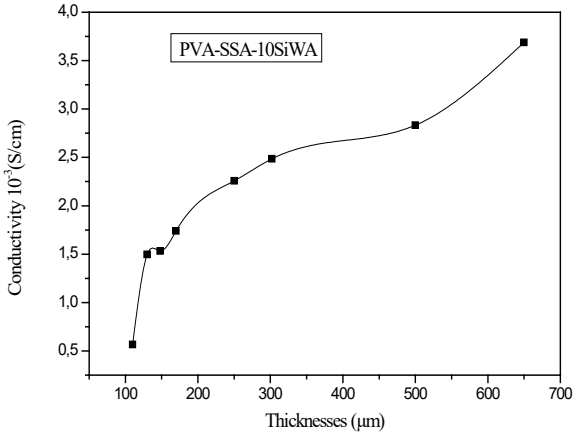

Figure 8: Proton Conductivity of PVA/SSA/10wt.%SiWA membrane with thicknesses.

3.4. Water uptake and proton conductivity of the membrane PVA/SSA/10wt.%SiWA/SiO_2

The water uptake of the membranes PVA/SSA/SiWA/ywt.%SiO_2 as function of SiO_2 content (0wt.%≤ y ≤16wt.%) varies from 60% to 88%. As shown in figure 9. We notice that the water uptake varies with the silica percentage. Hence, the maximum which is equal to 88% was obtained for the

membrane PVA/SSA/SiWA/10wt.%SiO_2. Thus, over 10 wt.% of silica, the water uptake of this membrane starts decreasing.

This figure shows that the ionic conductivities of PVA/SSA/SiWA/ywt.%SiO_2 membranes increase with the increase weight of SiO_2 percentage. The ionic conductivities go from 3,105.10^{-3} S.cm^{-1} for the membrane without SiO_2 to 6,720.10^{-3} S.cm^{-1} for the membrane containing SiO_2 (Table 2). The proton conductivity of the membrane based on PVA/SSA/SiWA/10wt.%SiO_2 reaches a maximum of 6,72.10^{-3} S.cm^{-1}, and decreases when the SiO_2 content exceeds 10 wt.%. The obtained value is higher than that of the Nafion®112 membrane (5,9.10^{-3} S.cm^{-1}) [36]. This is in agreement with the results which show that the latter membrane also has the best hydration rate. These membranes then experience a decrease in proton conductivity when the SiO_2 content exceeds 10 %. The inverse behaviors of the water uptake and ion exchange capacity (IEC) explain this behavior. As figure 12 shows. These results indicate that an inverse in water content can lead to higher proton conductivity at a low SiO_2 content. However, large adsorption of water in membranes does not simply improve proton conductivity, but also dilutes the charges carries [5], which causes a decrease in proton conductivity at high SiO_2 content in the membranes.

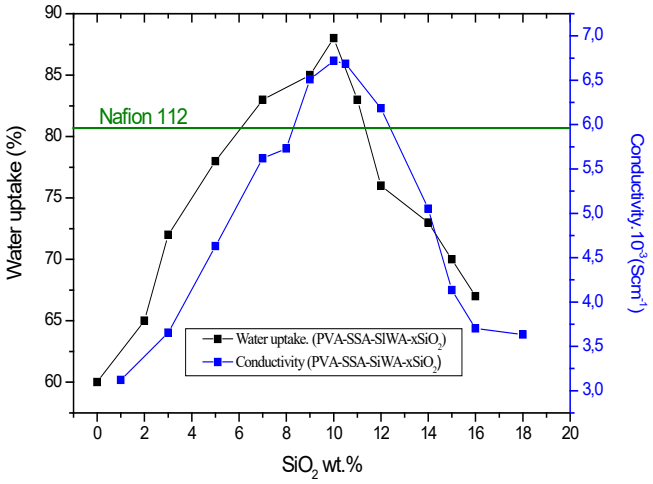

Figure 9: water uptake and proton conductivity of the membranes PVA/SSA/SiWA/ywt.%SiO_2 with different amounts of SiO_2

Table 2: Ionic conductivities (S.cm^{-1}) for Nafion®112, PVA-SSA-10wt.%SiWA and PVA-SSA-SiWA-10wt.%SiO_2 membranes

Membranes	Nafion®112	PVA/SSA/10wt. %SiWA	PVA/SSA/SiWA /10wt.%SiO_2
Ionic conductivity 10^{-3}S.cm^{-1}	5,900	3,105	6,720

Figure 10 shows the ionic conductivity of PVA/SSA/SiWA/10wt.%SiO_2 composite membrane as function thicknesses. The ionic conductivity of the composite membranes are in the order of 10^{-3} S.cm^{-1}. This figure shows that the ionic conductivity of the membrane increases when the membrane thickness increases. It goes from 0,672.10^{-3} S.cm^{-1} for the PVA/SSA/SiWA/10wt.%SiO_2 membrane 110 µm thick to 6,72.10^{-3} S.cm^{-1} for PVA/SSA/SiWA/10wt.%SiO_2 membrane 450 µm thick, for thicknesses greater than 450 µm the ionic conductivity remains close to 6,72.10^{-3} S.cm^{-1}.

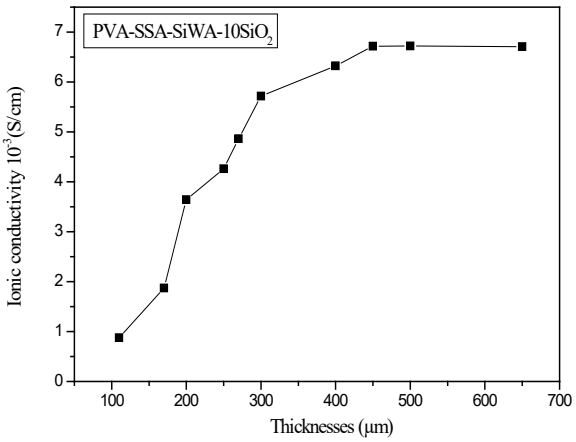

Figure 10: Proton Conductivity of PVA/SSA/SiWA/10wt.%SiO_2 membrane with thicknesses

3.5. Ion exchange capacity and fixed ion concentration

Figure 11(a,b) shows a plot of the ion exchange capacity (IEC) and fixed ion concentration as function of SiWA content. As shown in figure 11(a), the IEC of PVA/SSA/SiWA hybrid membrane varies from 0,90 to 2,20 mmol.g^{-1}, and increases with SiWA content up to a maximum value of 2,20 mmol.g^{-1} obtained with PVA/SSA/35wt.%SiWA hybrid membrane, the value obtained is higher than Nafion 115 (0,90 mmol.g^{-1}) [36]. This result indicates that an increase in silicotungstic acid content can lead to higher ion exchange capacity. At low HPA concentrations, the looser interaction between PVA and SiWA would provide less compact space for protons to be transported rather easily, resulting in higher ion exchange capacity. However, as the HPA concentration increased further, the interaction between PVA and SiWA would became stronger. The stronger interactions between not only PVA and SiWA but also PVA and SSA seem to inhibit the proton transport through the composite membranes, leading to lower ion exchange capacity.

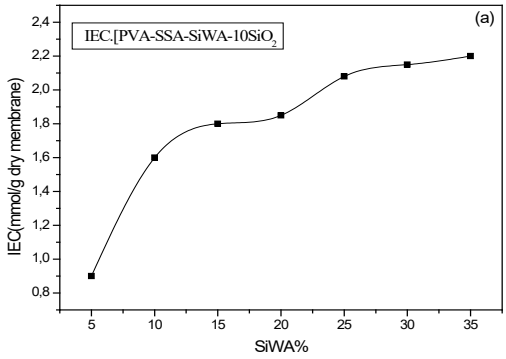

Figure 11(a): Effect of SiWA content on ion exchange capacity of PVA/SSA/SiWA membranes.

As shown in figure 11(b), the fixed ion concentration (FIC) of the PVA/SSA/SiWA hybrid membrane. The (FIC) values were observed to increase greatly from 5 to 35wt.% SiWA. The ion concentration sites increased with increasing the weight percent of silicotungstic acid. The ion concentration sites increased with the add of silicotungstic acid.

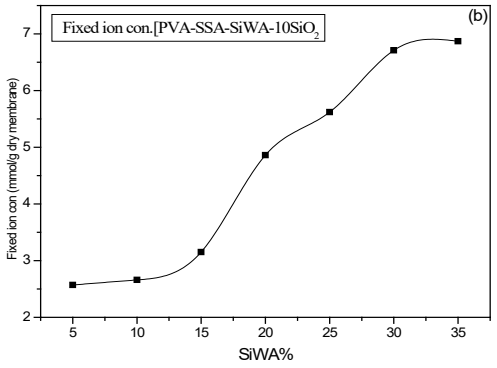

Figure 11(b): Effect of SiWA content on fixed ion concentration of PVA/SSA/SiWA membranes.

Figure 12 shows the IEC and water uptake of the membranes PVA/SSA/SiWA/ywt.%SiO_2 as function of SiO_2 content. As shown in this plot, the measured IEC value of the PVA/SSA/SiWA/ywt.%SiO_2 hybrid membranes decreases as the silica content increases from 2 to 10%.

in the other side, the water uptake of the PVA/SSA/SiWA/ywt.%SiO_2 membranes increases with the increase of SiO_2 content and reaches a maximum value of 88% for 10%.wt SiO_2 content membrane.

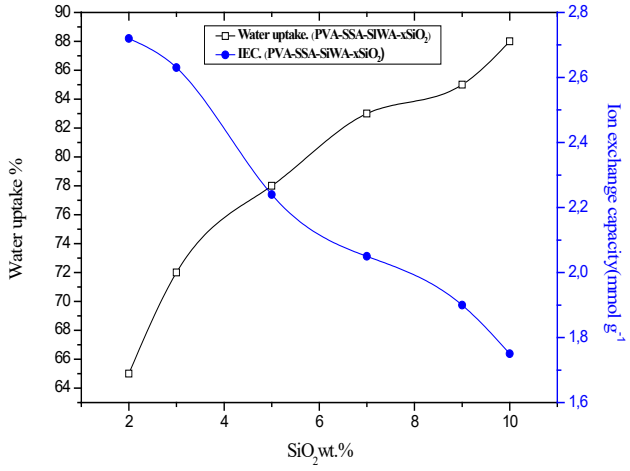

Figure 12: Water uptake and ion exchange capacity of the membranes based on PVA/SSA/10wt.%SiWA/ywt.%SiO_2

4. Conclusion

In the present work, we synthesized a new proton-conducting polymer membrane based on PVA/SSA/SiWA/SiO_2. The composite membranes were characterized by various techniques. The crosslinked networks and the formation of the intermolecular interactions between the hydroxyl groups on PVA and sulfosuccinic acid in membranes were proved with FTIR study. TGA showed that the membranes are thermally stable up to 200 °C. Moreover, high proton conductivity was obtained at room temperature for the membranes PVA/SSA/10wt.%SiWA and PVA/SSA/SiWA/10wt.%SiO_2, are about $3,105.10^{-3}$ and $6,72.10^{-3}$ $S.cm^{-1}$ respectively. The obtained ion exchange capacities values decreases as the SiO_2 content increases and reaches a maximum value of 1,75 $mmol.g^{-1}$ for the membrane PVA/SSA/SiWA/10wt.%SiO_2. This value is higher than that of the standard values of Nafion®112 and Nafion® 115 commercial membranes (use as reference membranes), which do not exceed 1 $mmol.g^{-1}$. Therefore, it can be concluded that the new composite polymer electrolyte membrane PVA/SSA/SiWA/10wt.%SiO_2 shows potential applications in PEMFC.

References

[1] D.S. Kim, H.B. Park, J.W. Rhim, Y.M. Lee, "Preparation and characterization of crosslinked PVA/SiO2 hybrid membranes containing sulfonic acid groups for direct methanol fuel cell applications," Journal of Membrane Science, **240**(1–2), 37–48, 2004. https://doi.org/10.1016/j.memsci.2004.04.010

[2] J. Qiao, T. Okada, H. Ono, "High molecular weight PVA-modified PVA/PAMPS proton-conducting membranes with increased stability and their application in DMFCs," Solid State Ionics, **180**(23–25), 1318–1323, 2009. https://doi.org/10.1016/j.ssi.2009.08.010

[3] M.M. Hasani-Sadrabadi, E. Dashtimoghadam, S.R. Ghaffarian, M.H.H. Sadrabadi, M. Heidari, H. Moaddel, "Novel high-performance nanocomposite proton exchange membranes based on poly (ether sulfone)," Renewable Energy, **35**(1), 226–231, 2010. https://doi.org/10.1016/j.renene.2009.05.026

[4] C.-C. Yang, "Synthesis and characterization of the cross-linked PVA/TiO2 composite polymer membrane for alkaline DMFC," Journal of Membrane Science, **288**(1–2), 51–60, 2007. https://doi.org/10.1016/j.memsci.2006.10.048

[5] J. Qiao, T. Hamaya, T. Okada, "New highly proton-conducting membrane poly (vinylpyrrolidone)(PVP) modified poly (vinyl alcohol)/2-acrylamido-2-methyl-1-propanesulfonic acid (PVA–PAMPS) for low temperature direct methanol fuel cells (DMFCs)," Polymer, **46**(24), 10809–10816, 2005. https://doi.org/10.1016/j.polymer.2005.09.007

[6] M.-C. Clochard, T. Berthelot, C. Baudin, N. Betz, E. Balanzat, G. Gébel, A. Morin, "Ion track grafting: A way of producing low-cost and highly proton conductive membranes for fuel cell applications," Journal of Power Sources, **195**(1), 223–231, 2010. https://doi.org/10.1016/j.jpowsour.2009.07.016

[7] C.H. Park, C.H. Lee, M.D. Guiver, Y.M. Lee, "Sulfonated hydrocarbon membranes for medium-temperature and low-humidity proton exchange membrane fuel cells (PEMFCs)," Progress in Polymer Science, **36**(11), 1443–1498, 2011. https://doi.org/10.1016/j.progpolymsci.2011.06.001

[8] W. Vielstich, A. Lamm, H.A. Gasteiger, Handbook of fuel cells: fundamentals technology and applications, Wiley New York, 2003.

[9] L. Li, J. Zhang, Y. Wang, "Sulfonated poly (ether ether ketone) membranes for direct methanol fuel cell," Journal of Membrane Science, **226**(1–2), 159–167, 2003. https://doi.org/10.1016/j.memsci.2003.08.018

[10] J. Fang, X. Guo, S. Harada, T. Watari, K. Tanaka, H. Kita, K. Okamoto, "Novel sulfonated polyimides as polyelectrolytes for fuel cell application. 1. Synthesis, proton conductivity, and water stability of polyimides from 4, 4 '-diaminodiphenyl ether-2, 2 '-disulfonic acid," Macromolecules, **35**(24), 9022–9028, 2002. https://doi.org/10.1021/ma020005b

[11] J. Lobato, P. Canizares, M.A. Rodrigo, J.J. Linares, "PBI-based polymer electrolyte membranes fuel cells: temperature effects on cell performance and catalyst stability," Electrochimica Acta, **52**(12), 3910–3920, 2007. https://doi.org/10.1016/j.electacta.2006.11.014

[12] Q. Guo, P.N. Pintauro, H. Tang, S. O'Connor, "Sulfonated and crosslinked polyphosphazene-based proton-exchange membranes," Journal of Membrane Science, **154**(2), 175–181, 1999. https://doi.org/10.1016/S0376-7388(98)00282-8

[13] J.-W. Rhim, H.B. Park, C.-S. Lee, J.-H. Jun, D.S. Kim, Y.M. Lee, "Crosslinked poly (vinyl alcohol) membranes containing sulfonic acid group: proton and methanol transport through membranes," Journal of Membrane Science, **238**(1–2), 143–151, 2004. https://doi.org/10.1016/j.memsci.2004.03.030

[14] H. Chen, S. Wang, F. Liu, D. Wang, J. Li, T. Mao, G. Liu, X. Wang, J. Xu, Z. Wang, "Base-acid doped polybenzimidazole with high phosphoric acid retention for HT-PEMFC applications," Journal of Membrane Science, **596**, 117722, 2020. https://doi.org/10.1016/j.memsci.2019.117722

[15] L. Lebrun, E. Da Silva, M. Metayer, "Elaboration of ion-exchange membranes with semi-interpenetrating polymer networks containing poly (vinyl alcohol) as polymer matrix," Journal of Applied Polymer Science, **84**(8), 1572–1580, 2002. https://doi.org/10.1002/app.10420

[16] G. Hirankumar, S. Selvasekarapandian, M.S. Bhuvaneswari, R. Baskaran, M. Vijayakumar, "AC impedance studies on proton conducting polymer electrolyte complexes (PVA+ CH 3 COONH 4)," Ionics, **10**(1–2), 135–138, 2004. DOI: 10.1007/BF02410322

[17] C. Chanthad, J. Wootthikanokkhan, "Effects of crosslinking time and amount of sulfophthalic acid on properties of the sulfonated poly (vinyl alcohol) membrane," Journal of Applied Polymer Science, **101**(3), 1931–1936, 2006. https://doi.org/10.1002/app.23660

[18] C. González-Guisasola, A. Ribes-Greus, "Dielectric relaxations and conductivity of cross-linked PVA/SSA/GO composite membranes for fuel cells," Polymer Testing, **67**, 55–67, 2018. https://doi.org/10.1016/j.polymertesting.2018.01.024

[19] P. Staiti, A.S. Arico, V. Baglio, F. Lufrano, E. Passalacqua, V. Antonucci, "Hybrid Nafion–silica membranes doped with heteropolyacids for application in direct methanol fuel cells," Solid State Ionics, **145**(1–4), 101–107, 2001. https://doi.org/10.1016/S0167-2738(01)00919-5

[20] S.P. Nunes, B. Ruffmann, E. Rikowski, S. Vetter, K. Richau, "Inorganic modification of proton conductive polymer membranes for direct methanol fuel cells," Journal of Membrane Science, **203**(1–2), 215–225, 2002. https://doi.org/10.1016/S0376-7388(02)00009-1

[21] B. Ruffmann, H. Silva, B. Schulte, S.P. Nunes, "Organic/inorganic composite membranes for application in DMFC," Solid State Ionics, 162, 269–275, 2003. https://doi.org/10.1016/S0167-2738(03)00240-6

[22] B. Tazi, O. Savadogo, "Effect of Various Heteropolyacids (HPAs) on the Characteristics of Nafion®-HPAS Membranes and their H~ 2/O~ 2 Polymer Electrolyte Fuel Cell Parameters," Journal of New Materials for Electrochemical Systems, **4**(3), 187–196, 2001.

[23] I. V Kozhevnikov, "Catalysis by heteropoly acids and multicomponent polyoxometalates in liquid-phase reactions," Chemical Reviews, **98**(1), 171–198, 1998. https://doi.org/10.1021/cr960400y

[24] M. Misono, "Heterogeneous catalysis by heteropoly compounds of molybdenum and tungsten," Catalysis Reviews Science and Engineering, **29**(2–3), 269–321, 1987. https://doi.org/10.1080/01614948708078072

[25] O. Nakamura, I. Ogino, T. Kodama, "Temperature and humidity ranges of some hydrates of high-proton-conductive dodecamolybdophosphoric acid and dodecatungstophosphoric acid crystals under an atmosphere of hydrogen or either oxygen or air," Solid State Ionics, **3**, 347–351, 1981. https://doi.org/10.1016/0167-2738(81)90111-9

[26] P. Staiti, "Proton conductive membranes constituted of silicotungstic acid anchored to silica-polybenzimidazole matrices," Journal of New Materials for Electrochemical Systems, 4(3), 181–186, 2001.

[27] O. Nakamura, T. Kodama, I. Ogino, Y. Miyake, "High-conductivity solid proton conductors: Dodecamolybdophosphoric acid and dodecatungstophosphoric acid crystals," Chemistry Letters, **8**(1), 17–18, 1979. https://doi.org/10.1246/cl.1979.17

[28] C.W. Lin, Y.F. Huang, A.M. Kannan, "Cross-linked poly (vinyl alcohol) and poly (styrene sulfonic acid-co-maleic anhydride)-based semi-interpenetrating network as proton-conducting membranes for direct methanol fuel cells," Journal of Power Sources, **171**(2), 340–347, 2007. https://doi.org/10.1016/j.jpowsour.2006.10.081

[29] S.M.J. Zaidi, S.D. Mikhailenko, G.P. Robertson, M.D. Guiver, S. Kaliaguine, "Proton conducting composite membranes from polyether ether ketone and heteropolyacids for fuel cell applications," Journal of Membrane Science, **173**(1), 17–34, 2000. https://doi.org/10.1016/S0376-7388(00)00345-8

[30] S. Maarouf, B. Tazi, F. Guenoun, "Synthesis and characterization of new composite membranes based on polyvinylpyrrolidone, polyvinyl alcohol, sulfosuccinic acid, phosphomolybdic acid and silica," J Chem Pharmaceut Res, **8**, 387–395, 2016.

[31] S. Maarouf, B. Tazi, F. Guenoun, "Preparation and Characterization of New Composite Membranes containing Polyvinylpyrrolidone, Polyvinyl alcohol, Sulfosuccinic acid, Silicotungstic acid and Silica for Direct Methanol Fuel Cell applications."," J. Mater. Environ. Sci., **8**, 2870–2876, 2017.

[32] J.E. Castanheiro, A.M. Ramos, I.M. Fonseca, J. Vital, "Esterification of acetic acid by isoamylic alcohol over catalytic membranes of poly (vinyl alcohol) containing sulfonic acid groups," Applied Catalysis A: General, **311**, 17–23, 2006. https://doi.org/10.1016/j.apcata.2006.05.039

[33] F. Lufrano, G. Squadrito, A. Patti, E. Passalacqua, "Sulfonated polysulfone as promising membranes for polymer electrolyte fuel cells," Journal of Applied Polymer Science, **77**(6), 1250–1256, 2000. https://doi.org/10.1002/1097-4628(20000808)77:6<1250::AID-APP9>3.0.CO;2-R

[34] S. Hietala, M. Koel, E. Skou, M. Elomaa, F. Sundholm, "Thermal stability of styrene grafted and sulfonated proton conducting membranes based on poly (vinylidene fluoride)," Journal of Materials Chemistry, **8**(5), 1127–1132, 1998. DOI: 10.1039/A708288F

[35] Q. Wu, S. Tao, H. Lin, G. Meng, "Preparation, characterization and proton-conductivity of silica gel containing 71 wt.% 12-tungstogermanic heteropoly acid," Materials Chemistry and Physics, **64**(1), 25–28, 2000. https://doi.org/10.1016/S0254-0584(99)00244-8

[36] S. Anisa, A. Utami, "Preparation of Sulfonated PVA-TMSP Membranes for Direct Methanol Fuel Cell," Makara Journal of Science, 95–100, 2013. https://doi/org/10.7454/mss.v16i2.1403

ASTES

Advances in Science, Technology and Engineering Systems Journal Vol. 5, No. 5, 1028-1035 (2020)

www.astesj.com

Special Issue on Multidisciplinary Innovation in Engineering Science & Technology

ASTESJ

ISSN: 2415-6698

Understanding Risk Assessment in the Context of Fractional Ownership using Ethereum Smart Contract

Mohamed Laarabi*, Abdelilah Maach

Mohammadia school of Engineers, Mohammed V University, Rabat, 10090, Morocco

ARTICLE INFO

Article history:
Received: 31 July, 2020
Accepted: 27 September, 2020
Online: 20 October, 2020

Keywords:
Smart contracts
Block chain
Non-fungible assets
Risk Assessment

ABSTRACT

Ethereum smart contract system has seen a steady adoption as it continues to support tens of thousands of contracts. This feature has evolved to give a practical shape to the ideas leading up to fractional ownership transfer, using advanced smart contracts such as ERC-981. However, alongside its numerous benefits, various risks arise with the actual implementation of the ERC-981. This paper documents high-level processes and risk factors involved in the transfer-system, building a theoretical risk model based on Electre Tri-framework belonging to MCDA classification/sorting models. This model deals with detecting problems that are pre-defined on a central reference. The approach is illustrated through several stages: following comparison between the methods of risk analysis towards a risk assessment model, proposing recommendations and solutions. The framework was able to detect 18 major risks and bugs assigned to 6 categories.

1. Introduction

In the past, the value of fractional ownership of assets (such as the right of publicity, trade secrets, copyrights, software, and real estates) have had little to no understanding as an asset, leading in some cases to a determination of having no value as assets. [1]. Fractional ownership of assets has been classified as "intangible" on corporate balance sheets regarding intellectual rights, such as products and technologies based in large portions upon such intellectual property [2]. They have also frequently been assigned little or no concrete value.

In large measures, placing a value on a co-ownership of the property has been difficult [1], and has led to some confusion over the valuation of the property at the time of selling, leading to the conventional diminution of value placed on the property.

Fractional ownership transfer is one of the most complex-prone operations. Many attempts have been made to develop dependable and accurate selling methods and evaluation for co-ownership of property assets, most unsuccessful because of the long process and the huge risk associated with the transaction.

However, selling a property for co-ownership is becoming a main target for the new era of decentralized ledger technologies using blockchain plate forms and as a base for developing larger multi-unit projects such as (tokenization, colored coins) [3]. Addressing multiple complications in the design of the contract, aiming to reduce unnecessary costs and time expenditure while enhancing transparency, by using this technology it becomes possible to tokenize existing financial assets - equities, debt instruments, the share of investment funds, or real estate by representing them in the form of tokens.

The decentralized ledger is a design pattern that underpins the Bitcoin cryptocurrency it can be described as a ledger of any transactions or contracts maintained in decentralized form across different levels [3]. However, its capacity to validate interaction amongst participant nodes is a vital key enabler for participants that require mutually distrusting peers to conduct their affairs. One such use is the smart contract, designed to encode rules to reflect any kind of multi-party interaction [4]. With the huge amount of investment in the decentralized ledger technologies, especially blockchain, and its rapid evolution as a trend towards being accepted as a new solution to record, share and synchronize transactions in their respective electronic ledgers [5]. Ethereum smart contracts are becoming the preferred mechanism to implement a wide range of applications, including financial instruments (e.g., Ether, mining, and saving wallets.).

A smart contract is a program that runs on the block chain and has its correct execution enforced by the consensus protocol. A contract can encode any set of rules represented in its programming language, offering new solutions such as [6]:

- ERC20: for fungible assets,
- ERC721: for non-fungible tokens, used for collectibles and games,

*Corresponding Author: Mohamed Laarabi, Mohammadia school of Engineers, Mohammed V University, Rabat, 10090, Morocco, Cell No. 00 212 6 61 95 42 22, laar.mohamedd@gmail.com

- ERC777: for fungible tokens, provide a new use and building on past learnings that match with ERC20,
- ERC1155: allowing for a single smart contract to represent multiple fungible and non-fungible tokens.

However, despite the expressiveness of the smart contracts, the present form of these technologies lacks transactional privacy. There are numerous risks that need to be identified and documented when going through the process of tokenizing an asset and selling it. The entire sequence of actions taken in a smart contract is propagated across the network and/or recorded on the blockchain and therefore are publicly visible [7]. Even though parties can create new pseudonymous public keys to increase their anonymity, the values of all transactions and balances for each (pseudonymous) public key are publicly visible [8].

The main purpose of this study is to document several new zones and factors of risks and bugs on the Ethereum's smart contracts as well as the whole tokenization process.

We formalize a theoretical decision framework alongside with a risk assessment model, proposing recommendations and solutions for the documented risks. We provide a new approach of handling co ownership of property, a frame work able to detect major risks and bugs.

The rest of the article is organized as follows: Section 2 provides a review of risks and deferent methods of risk assessment alongside with MCDA classification/ sorting techniques to handle fractional rights. Section 3 the contextual setting and the main risk factors. Section 4 presents applications of these techniques in a framework that can be used in a risk assessment model for real cases, as well as listing some multi-criteria decision that supports the transfer of fractional rights using smart contract which can be developed for classification and sorting model development in general. In Section 5, we will be discussing the results and provide a summary. Finally, section 6 concludes the paper and discusses some interesting future research extensions and directions.

2. Related work and Open Challenges

The concept of tokenization is not recent. In monetics, tokenization is the process of substituting bank data (card number) with disposable data called "tokens". This solution helps to reassure the wearer especially in payment on the Internet or in NFC. For the trader, this is a way to reduce the perimeter of PCI-DSS since no sensitive items will be stored in his information system. For the bearer's bank (issuer), it is simply a way to reduce fraud [3].

the author mainly explains that the process of tokenization is highly promising for illiquid assets: their valuation is now sanctioned by low rate of liquidity in important proportions (which he calculate at "25% to 35 %"). Tokenization will increase market depth by opening markets to more participants, resulting in more exchanges. Traditional assets will be tokenized because they will lose the liquidity premium if they do not (such as real estate, residential assets, or artistic works), therefore, individuals could collectively acquire a valuable painting for a local museum through a sale of tokens, even if none of them can afford to buy the painting individually [9].

Following the literature review, two major types of assets are more easily "tokenizable" than others: -Intangible assets (patents, carbon credits, copyrights.) because of their lack of physical existence, these assets can lend themselves more easily than others to this tokenization process, even though some laws barriers can make the transfer process more expensive and complex, these assets are easier to tokenize, they can often be divided into multiple units (such as bitcoins) and all tokens can be associated with a general set of interchangeable asset components (example: 10kg gold), conversely, non-fungible active ingredients are less suitable for tokenization. For example, when securitized, mortgages are often grouped with other loans with similar but not identical characteristics.

In this paper, we will only be focusing on the risks occurring the tokenization of non-fungible assets using smart contract that's runs on Ethereum's platform, as we assume that the risks presented are much more complex and require more documentation.

Many papers presented methods for risk measurement based on different criteria, from classification models to multi-criteria methods [8, 9]. In recent years, formal methods have been largely used to analyze tokenization using smart contracts with the aim of verifying the security protocols of potential risks with untrusted codes. One of the most cited problems has been the infamous DAO attack, taken millions of dollars during a crowdfunding service and caused a huge bug in the Ethereum's blockchain. Among methods of classification and sorting, the MCDA method is used to assign selected areas to one of the four collapse risk classes previously defined by a committee of experts. By convention, Class 1 is the class corresponding to the highest risk, and Class 4 is the least significant risk [10].

The classification or risk has been the subject of extensive archiving work leading to the development of a geographic information system (GIS) [11]. The choice of areas to be classified according to risk was the subject of a pre-assigned selection procedure presented in table 1. The data available for each area is either quantitative (probability rate, depth, tokens) or qualitative (presence of a fault, nature of the fraud). These data are used, first, to identify the so-called homogeneous areas (with constant characteristics in their perimeter) [9], and on the other hand, to select the so-called (at-risk areas), presenting a predisposition to the occurrence of a collapse off chain or smart contract infrastructure in other words (operational, strategic). We first present the procedure for selecting the areas studied and the criteria chosen for the prioritization of these areas, then we explain the principle of prioritization based on the Electre- tri method [9]. Finally, we illustrate the course of the method.

3. Contextual Setting and Methods

On the block chain, risks are a major concern. In addition to their ability to cause losses of money and time, they can also degrade the performance of these systems and render them incapable of achieving their objectives [11]. However, in order to consider tokenizing non-fungible assets using smart contracts, it is crucial to assess the feasibility of it. In this section, we are interested in presenting the main methods used to manage risks and their influencing factors.

Many works characterize risk using two distinct components of "probability" and "severity". The probability represents an average value of its eventuality over a period of time. As for severity, it is defined as the amount of damage [12], following the occurrence of a dreaded event. In a two-dimensional space, a risk can be presented by a point admitting an 'S' severity component

and a probability component 'P' (see figure 1). It is important to note that there are different types of risks that can reach a system. According to the author these "risks" can be internal (industrial, bugs, errors), external (legal framework, economical), or chronic [11]. In this work, we are interested in documenting all of those risks, specifically risks that can damage the platform of a transaction, degradation of the production tool as well as human errors, [13]. We will limit ourselves, in terms of causes of damage, to technical failures, human errors and organizational problems.

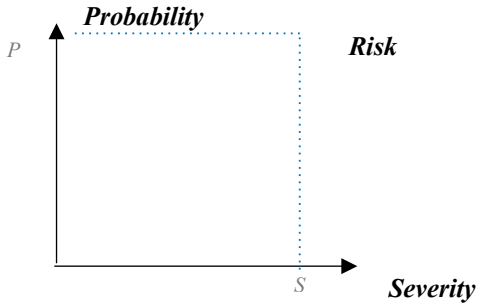

Figure 1: Representation of risk in a two-dimensional space, axis (Y) represent probability while axis (X) represent severity

The previous section illustrated the philosophy of conventional methods for risk analysis. These methods are based mainly on an iterative approach that allows, depending on the method, to identify and analyze a particular type of danger (dangerous phenomena, failures) [14]. The methods are based on the representation of results in different forms (such as diagrams, tables), however, and despite their proliferation, the methods that are dedicated to risk assessment, have certain limitations that can compromise the quality of their results, some of these methods present their results in different forms that can limit the risk detection in the system. In terms of quantifying the impact of risks, conventional methods are generally based on a qualitative risk assessment. For example, in the APR and AMDEC methods, a criticality index is given to each risk, this index is unreliable as it is calculated from qualitative indices of probability and severity. As for the fault tree method, it provides a quantification reliable probability of an adverse event, however, the assessment of the severity of the event remains unreliable [15]. Given the limitations of conventional risk analysis methods, other risk analysis methods have emerged. One of those methods is MCDA methods of classification and sorting, simply defined as an algorithm, which from the elements of a comparison matrix, can document the most likely risks [9]. During our analysis of the existing risk factors, we found various work aimed at integrating risk factors in different zones. Among them, some work has tried to identify only internal risks [5], others focused on integrating the inclusion of certain risk effects in the external environment [9] (see figure 2). In addition, another category of contribution was interested in the automatic conversion of multiple risk factors to one model [16]. We present in the following sections the frame work used in order to document all the risk factors [17].

4. Risk Assessment

Similar to the above definitions of risk, there are several definitions of risk management. Among these definitions, we will settle for the one given by NASA [18], which defines risk management as a process in which the program/project team is responsible for identifying, analyzing, planning, tracking, monitoring, and communicating risks effectively [19]. According to this definition, risk management is a practice of character methodical and ordered as an iterative process (see figure 3). It aims to reduce the impact of hazards to a level described as acceptable, given the efforts spent on its implementation [20].

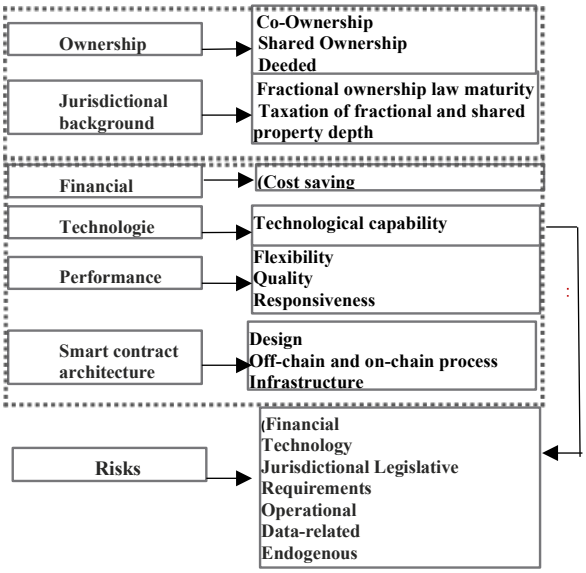

Figure 2: Factors influencing fractional ownership transfer

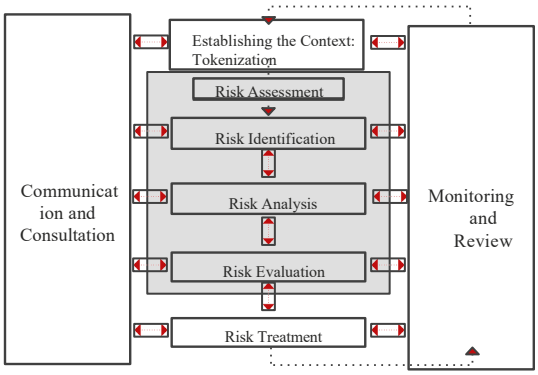

Figure 3: Risk assessment Process

4.1. Risk identification: Identifying risks that need to be assessed

It is important to note that, like any production system, tokenizing assets using Ethereum smart contract is subject to a multitude of risks [6], however, given the mission of tokenizing non-fungible assets, some risks can have a huge impact, as they affect in some cases the life savings of the users, causing in the process some dramatic damages [17]. Identifying risks aims to represent and describe the dysfunctions that can occur in a system (see table 1) [9]. A malfunction is characterized by an alteration that reaches the behavior of elements of a system already identified, in general, a function fails if it does not achieve the objective to which it is intended, with the desired quality [11].
These malfunctions represent events with different natures. Based on literature and available data, we are able to identify 6 major categories:

Table 1: Categories of risks in non-fungible tokenization

Category	Risk
Operational	R1- Lack of a standardized mode of operation, function and security deficiencies R2- Server/Infrastructure Breach R3- Poor service performance: failure in attaining an acceptable degree of responsiveness and flexibility R4- On and off chain information's disorder R5- lack of privacy
Financial	The transaction costs of the public block chain are high. R7- Lack of recipients and users
Technology	R8-Poor implementation of the smart contract to failure in the execution phase
Data Related	R9- Private keys information's leakage R10-Latent information asymmetry between sellers and buyers. (Wang and Regan 2002)
Legal Framework	R11-Insufficient basis for cooperation and information exchange R12- Absence of legal framework R13- Legal taxes basis inadequate or overly rigid
Endogenous	R14- Prior supervisory approval not required R15- No definition of significant ownership, nor qualitative criteria to determine ownership R16- Unrealistic or high expectations regarding the service provide performance R17- Inadequate response to week audits and control R18- Loss of control over the service provider

4.2. Risk Analysis

Risk analysis is the systematic use of information to identify risk factors and target entities and estimate risk [9]. The risk factor is a parameter that is thought to play a role in the accidental sequence without being proven to be a direct or indirect cause. Estimating risk is defined as a "process used to assign values to the probability and consequences of a risk" [8]. As for risk estimation, the stakeholder may consider cost, benefits, concerns, and other variables required for risk assessment.

Two major risk analysis approaches are used in risk analyses: "Deterministic approach" that consists of identifying events that could lead to an accident by looking for the worst possible case (the worst-case scenario) and assigning extreme gravity to its potential consequences [9], and the "probabilistic approach" that involves calculating probabilities for the occurrence of events that are part of the process of materializing a given accident-scenario [18].

Table 2: Deterministic risk assessments

Deterministic risk assessments	Description
Single scenario	Risks are defined and handled as static entities and outputs have fixed values [4]
Maximum-credible scenario'	The scenario selected may be a 'worst-case scenario' or 'most likely scenario' (i.e. based on a historical event) [8]
Stochastic Dominance	A partial order between random variables [11]
Consequence/probability matrix	Matrix with different layers of severity at the top and the levels of probability [12]

4.3. Deterministic Risk Analysis

In this paper, we will use the deterministic approach that has been generally adopted in high-risk areas such as nuclear, military, guided transport, where the slightest significant risk is tracked down and reduced at source [9]. It consists of identifying events that could lead to an accident scenario by looking for the worst possible case and assigning extreme gravity to its potential consequences, this means that deterministic risk analysis only has a single and specific outcome based on the scenario being assessed [18]. Using a scenario-based approach can be extremely useful for communicating risk assessment results to non-experts.

4.4. Risk evaluation

Evaluating a risk is a process used to assign values to the probability and consequences of a risk. It's a fundamental requirement for risk evaluation to identifier risk functions. As we are using Elctre-tri method, we categorize the parameters that we have mentioned earlier (such as fragility, vulnerability, likelihood and occurrence), into categories with the same nature in order to have a significant results. The natures of some parameters can vary significantly from one function to another [18, 19]. Using the MSDC tri method oblige us to choose categories with the same nature. Selecting appropriate functions is an essential aspect of risk evaluation as a mediocre selection can cause unsound decision making and unintentionally increase risk [9]. There is a significant challenge and a huge barrier to both the selection criteria and development of effective risk frame work as the parameters used are strongly limited by the availability of data:

- Financial impact
- Ethuriem Infrastructure impact
- Security impact
- Regulation impact
- Technological impact
- Likelihood of occurrence
- Risk mitigation effort

Once the severity, frequency of occurrence is estimated, the risk is assessed from a risk graph, of which here is a prototype (see figure 4).

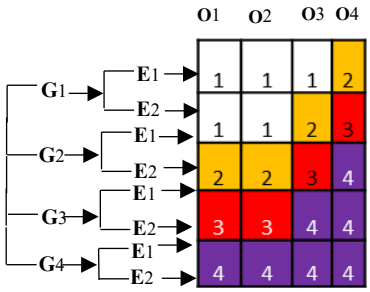

Figure 4: Prototype of a risk graph

As we pointed out in section 3, it is worth remembering that our ontological commitment is minimal, therefore, the user can either accept our risk graph (see figure 4), or define its own levels of severity [12], as well as the frequency of occurrence and/or exposure, they may also consider gravity if they chose to use the hazard analysis approach such as ODA (preliminary hazard analysis) [19]. In fact, many papers tried to provide a risk model based on ODA such as model-checking of smart contracts that contain three layers capturing respectively the behavior of Ethereum blockchain, the smart contracts themselves and the execution framework [20]. However, they don't consider external factors outside the platform as relevant, unlike our framework that work as a formal verification technique based on a description of

the variables. This technique consists in performing an efficient systematic inspection of all possible risk factors described by the risk assessment model in order to satisfy the conditions in our first step of building a risk model [21].

Table 3: Risk acceptability criteria

Area of criticality	Risk acceptability	
Negligible	Acceptable	Risks that do not require the approval of the guardianship authority.
Acceptable		Risks requiring proper control and agreement from the supervisory authority.
Undesirable		Risks that cannot be reduced or insufficient and require agreement from the guardianship authority.
Unacceptable		Risks to be reduced.

5. Method Proposed

By identifying 18 risks (see table 1), by applying the Electre-tri method, we were able to classify those risks into four zones (see table 2). The Four proposed zones are built-in after assigning each risk to a specific area. The outranking concept by building binary relationships among each alternative and the profiles that bound each category. This method proposes both procedures for assigning to the collapsing risk classes under the two scenarios pessimist and optimistic procedure [19]. The pseudo-disjunctive procedure of the Electre-tri method corresponds to the procedure optimized with the outranking relation [16].

5.1. Implementation of the ELECTRE-TRI method and Results

Each of the 18 risks must be assigned to qualified zones to take on the implementation of the risk management. Nevertheless, Ethereum platform face an organizational challenges in controlling risk [20], due to the clutter of the continuum of risk reduction measures. We will devote this part to build a theoretical model formulation using Electre-tri.

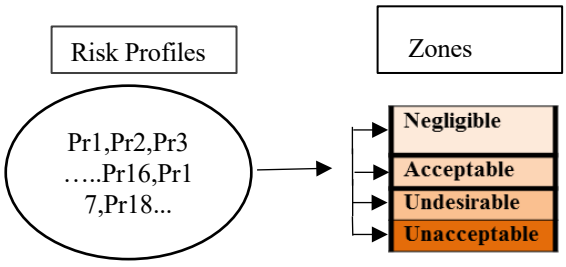

Figure 5: Risk level assignment

Zones are necessarily exclusive and orderly (with the Electre-tri method), zone 1 being the riskiest, the Pr_1 profile, is presented on each criterion, a risk at least as high as Pr_2, Pr_2, also presents, on each criterion, a risk at least as high as Pr_3, (see figure 7). The set of comparisons, on each criterion 9, between the evaluation of a Z_1 zone, and each Pr_n profile provides a partial response to the entry of an area into a risk class h (figure 6 and 7)

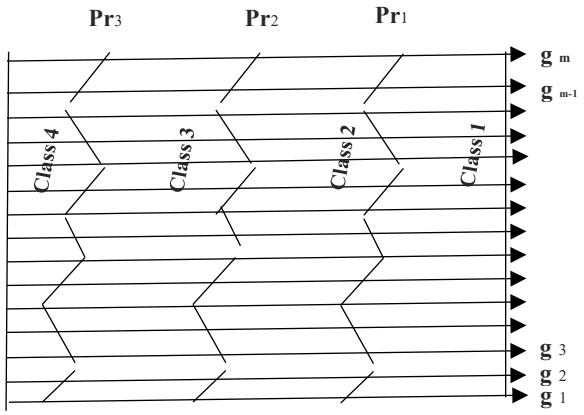

Figure 6: Position of principle of Pr_h class profiles on each criterion g_j.

The data available are tainted with uncertainties, Electre-tri allows it to be taken into account through the introduction of two thresholds [8, 9]. The threshold of indifference q_j and the threshold of preference P_j, they represent, respectively, the minimum and maximum margin of uncertainty related to the nature of the data and the calculations to be made and are defined as follows (see figure 7)

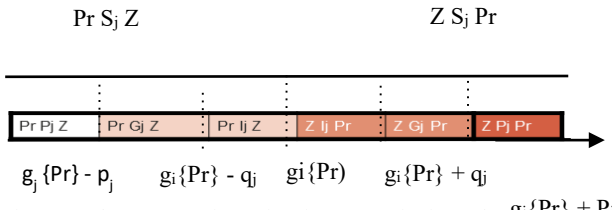

Figure 7: Three Comparison Situations, on Criterion J, between a Z zone and an Pr (S) profile at least as risky as, (I) indifference, (Q) low riskier and (P) strictly riskier.

- If $lg_j,(Z,) – g_j (Pr_j)l$ is less than q_j, it is considered that this difference is not significant and that $g_j(Z_j)$ and $g_j (Pr_h))$ are practically equivalent; it will be said then that zone Z, and the low profile of the h class, Pr_h, are indifferent (l_j) from the point of view of the g_j ($Z_j I_j Pr_h$) criterion;

- If $lg_j(Z_j) – g_j (Pr_h)l$ is greater than p_j, this difference is considered significant; in the event that $g_j (Z_j)$ is greater than $g_j (Pr_h)$, it will be said that zone Z, is strictly riskier than the low profile of the h class, Prh, for the gj criteria, (ZjPj Prh); Prh is strictly riskier (Pj) and that Z, in reverse (Prh PjZj)

-If the threshold of preference p_j is not equal to the threshold of indifference q_j, the interval between these two values represents a range of ambiguity in which the risk is presumed to be higher without the difference $lg_j(Z_j) - g_i (Pr_n)l$ can be considered truly significant. It will be said that zone Z, is weakly riskier (Q_i) than Pr_h, for the criterion g_j (Z Q, Pr_h); Pr_h is weakly p_j us risky than Z, in reverse (Pr_h Q, Z,)'. By convention, if an area is indifferent to a low profile of a class, the area is then assigned to that class: we can say that the risk class is closed from below [9]. Therefore, if a Z, presents a risk assessment on each criterion, between the risk assessment made for Pr_n and Pr_h, then Z_j is assigned to class h, however, this case is rarely encountered.

Two extreme logics of sorting to risk classes are then possible: either Z, is assigned in the class the lowest encounter on a criterion, Z, is assigned to the highest class met on a criterion. These two logics imply a principle of caution which is, in the first case, minimum and, in the second case, maximum. To mitigate these two logics, Electre- tri proposes two assignment procedures: a pseudo-conjunctive procedure and a pseudo-disjunctive procedure [9]. To achieve this, a credibility index σ is introduced. This index, which takes a value between 0 and 1, aggregates, taking into account importance of risk, partial comparisons, criterion by criterion, and expresses the credibility with which one can consider overall that a Z, is more risky than a Pr_h profile [22].

In this case, it will be said that the area outperforms (S) the profile. When this index is worth 1, it means that the assertion (Z, is riskier than Pr_h) is completely credible (100% credibility resulting from the adherence of all criteria to this assertion).When it is worth 0, it means that this assertion is not at all credible (credibility of 0% resulting from the rejection of the assertion by all the criteria or by one of the criteria that imposes its veto).When it takes a value between 0 and 1, it means that the (opinions - are divided (some criteria validate the assertion while others oppose it)[9]. The credibility index then expresses the force with which the favorable criteria are expressed, corrected by the opposite force of the adverse criteria. When it's above 0.5, this means that an absolute majority of criteria is in favor of the assertion. The credibility index that makes it possible to judge this upgrade relationship is rated o(Z,Pr_h).In Electre- tri, one must also calculate the credibility index of the inverse relationship, noted o (Pr_h, Z), because the calculation of this index is not commutative. [23]

To judge whether or not a Z zone enters a class h, f credibility index o(Z,Pr_h) is compared to a parameter λ (including enter 0,5 and 1) that expresses the desired level of requirement to validate that entry. For example, an λ=0,6 means that it is hoped that at least 60% of the criteria (including risk importance) will be favorable to entry into the class. Three situations are possible and only possible if:

-If the Z is indifferent to Pr_h when: $\sigma(Z, Pr_h) \geq \lambda$ and $\sigma(Pr_h, Z_j) \geq \lambda$ => Z_j I Pr_h ;
-If the Z is preferred to Pr_h when: $\sigma(Z, Pr_h) \geq \lambda$ and $\sigma(Pr_h, Z_j) < \lambda$=> Z_j I Pr_h ;

-Pr_h is preferred to the Z when: $\sigma(Z, Pr_h) < \lambda$ and $\sigma(bh, Z_j) \geq \lambda$=> Z_j I Pr_h ;

-Is incomparable to Pr_h when: $\sigma(Z, Pr_h) < \lambda$ and $\sigma(Pr_h, Z_j) < \lambda$=> Z_j I Pr_h ;
Out of the two sorting procedures offered by the Electre- tri method, pseudo-disjunctive is the most prudent. This procedure involves assigning a Z-zone, to an h-class, if:

- Z, has a strictly higher level of risk than the low profile Prn (Z,P Pr_h), Z_j and low profile Pr_n present the same level of risk (Z,I Pr_n), or Z_j and the low profile Pr_h presents incomplete levels of risk (Z_j ,R Pr_h);

- And if none of the previous situations is valid when comparing Z, and the Pr_h .profile, (low profile of class h-1).

From the moment the first condition is checked by a Pr_h profile, it is also verified by all the lower n profiles
($Pr_{k>h}$).

The assignment h class can therefore be characterized by the highest h value such as Prn_, violates the first condition. This corresponds to the lowest profile such as Pr_{hj1} presents a strictly higher risk level than Z.

It is important to note the λ parameter [21], which adjusts the allocations of areas to risk classes, is chosen by the user and raises the question of the degree of severity (or requirement) with which the allocations from the zones to the classes are to be dealt with [8], it must be greater than 0.5 to mean that, in order to validate an assignment from an area to a class, it is necessary that more than half of the criteria validate the assertion based on their respective weight or importance. Since importance of risks are different, it is important not to leave the decision to a single criterion, even if it is the most important [15].

Table 4: Comparative analysis between multi-criteria methods

Multi-criteria methods	Criteria	Benefits	Disadvantages
Weighted sum = WSM	Quantitative	Simple, known, no change to the underlying problem [28].	Drafting criteria, need for homogeneity of units and scales of criteria [28].
Goal-Programming GP	Quantitative	Suitable for initial internships in the decision-making process [29].	No qualitative criteria [29].
MAUT = Multiple Attribute Utility Theory	Quantitative and qualitative	Accommodates scales of units of different criteria.Mathematically represents the decision-making process [30].	Little intervention from the decision maker. Difficulty establishing utility functions [30].
AHP = Analytic Hierarchy Process	Quantitative and qualitative	Great flexibility, varied range of unstructured problems [31].	Decision-makers' comparisons of potentially tricky criteria and alternatives [31].
ELECTRE 1 = Elimination And Choices Translating Reality	Quantitative and qualitative	First method of upgrade. Suitable for the problems of choice between alternatives [23].	Effects of significant thresholds. (too) simple modeling of the decision-making process.Real criteria only [23].
ELECTRE 2 - Elimination And Choices Translating Reality	Quantitative and qualitative	Represents the decision-maker's preference, indifference and veto in front of two alternatives by fixed values [23].	Real criteria only [23].
ELECTRE 3 = Elimination And Choices Translating Reality	Quantitative and qualitative	Represents the decision-maker's preference, indifference and veto in front of two alternatives by an index between 0 and 1 (introduction of quasi-criterion and blur).Stable results [23].	Implementation of the full potential of this delicate method. No physical interpretation of certain parameters (discordance thresholds).Results can be difficult to interpret [23].
ELECTRE 4 - Elimination And Choices Translating Reality	Pseudo-criteria (fuzzy logic)	No weighting of the criteria but no criteria can be preponderant or negligible in relation to the others.Use fuzzy logic [32] .	Little flexibility in calculations [32].

The advantage of our model in the light of literature as we have said, is that the semantics of our model is given by a system of functions what can be more or less complex. Thus, the main challenge in our framework is the combinatory explosion of the framework. Nevertheless, this technique combined with Electre-tri has a huge potential to check most of risks in the design process

of the smart contract [24]. The Electre- tri method always come up with a solution, however, the downside is that the proposed solution may be far from returning to the original classification if there are inconsistencies in the decision making process. In addition, the complexity of the calculations means that the theoretical model only works in cases where neither the criteria nor the alternatives are too numerous. [25] The algorithms used often rely on linear programming algorithms, whose computational time increases rapidly with the number of input variables (criteria and/or instances). [26, 27]

For example, Kappalab's capacity calculation is limited to less than 10 criteria, which is more than enough in our case (it is common to consider that a problem with more than 6 or 7 criteria is a poorly defined problem) but not necessarily in machine learning .Taking into account the particular structure of machine learning problems may reduce computational time, particularly for "utility" or " Electre- tri" method, this is an important step in the decision-making process, to inform on the options for this choice, a summary of the main characteristics of the methods described in the papers presented in table 4. Implementation of these tools may require the expertise of someone who will serve decision-makers and stakeholders. [26] These tools must be implemented in a decision-making process that can, depending on the case, be relatively complex and time-consuming and involve experts and members of civil society. The use of a facilitator who is familiar with the tools and conditions of their implementation can then be useful, especially for knowledge and preference management aspects. This theoretical framework is improved if it has a structured approach, it is with this in mind, that the decision-making tools described in this paper were designed, helping stakeholders and top management to reach consensus [27].

6. Conclusion

In this paper, we have introduced a unified theoretical framework for handling fractional rights using Ethereum smart contracts, which runs on the blockchain. This study links jurisdictional studies to computer science which deserves further investigations. While this direction of research has been already pointed out in other contributions, our results are meant to serve as a model for top management in order to handle a situation where they are too many criteria that are not connected. As we pointed out in our paper, this is achieved by expressing the decision-making process as a formula and solving arithmetic constraints.
Risk analysis on the Ethereum requires effective methods and tools to respond to the urgency with which risk sometimes needs to be managed. This method makes it possible to formalize expert knowledge through criteria that all contribute to the explanation of risk even when the knowledge of the phenomena involved is partial or imprecise.

The conclusions provided by Electre- tri serve as consultation between experts and decision-makers, their robustness depends on several aspects, including the reliability of data. To this end, Electre- tri imposes sensitivity analyses on the various parameters. It exploits such as weights, thresholds, and the λ fuzzy index before providing robust conclusions.

We believe that there is still much work to be done. As regards our results, several questions must be considered. First of all, we will be working on providing a new template for smart contracts to handle fractional rights, also we will be providing a real case study using our new template studying the response behavior of these templates regarding their abilities to handle different variables and information's.

In conclusion, it is necessary to clarify that the method used does not intend to provide a forecast, but rather, a risk assessment, taking into account the availability of data, we will continue in our research aiming to provide a safer template to transfer non fungible assets using smart contracts.

Conflict of Interest

The authors declare no conflict of interest.

References

[1] M.D. Jones, system of fractional ownership of ntellectual.patent no.: us 7,720,740 b2.date of patent: may 18, 2010

[2] M. Zeilinger, "Digital Art as 'Monetised Graphics': Enforcing Intellectual Property on the Blockchain," Philosophy & Technology, **31**(1), 15–41, 2018, doi:10.1007/s13347-016-0243-1.

[3] M. Mohammadi, A. Al-Fuqaha, M. Guizani, J.-S. Oh, "Semisupervised Deep Reinforcement Learning in Support of IoT and Smart City Services," IEEE Internet of Things Journal, **5**(2), 624–635, 2018, doi:10.1109/JIOT.2017.2712560.

[4] Kalra, S. Goel, M. Dhawan, S. Sharma, "ZEUS: Analyzing Safety of Smart Contracts," in Proceedings 2018 Network and Distributed System Security Symposium, Internet Society, Reston, VA, 2018, doi:10.14722/ndss.2018.23082.

[5] R. Shinde, O. Nilakhe, P. Pondkule, D. Karche, P. Shendage, "Enhanced Road Construction Process with Machine Learning and Blockchain Technology," in 2020 International Conference on Industry 4.0 Technology (I4Tech), IEEE: 207–210, 2020, doi:10.1109/I4Tech48345.2020.9102669.

[6] M. Alharby, A. van Moorsel, "Blockchain Based Smart Contracts : A Systematic Mapping Study," Computer Science & Information Technology (CS & IT), 125–140, 2017, doi:10.5121/csit.2017.71011.

[7] BEN-ARI, Adi,A System and method for blockchain smart contract data privacyinternational search report (art. **21**(3)),62/259,090 24 november, 2015

[8] A. Kosba, A. Miller, E. Shi, Z. Wen, C. Papamanthou, "Hawk: The Blockchain Model of Cryptography and Privacy-Preserving Smart Contracts," in 2016 IEEE Symposium on Security and Privacy (SP), IEEE: 839–858, 2016, doi:10.1109/SP.2016.55.

[9] L. Luu, D.-H. Chu, H. Olickel, P. Saxena, A. Hobor, "Making Smart Contracts Smarter," in Proceedings of the 2016 ACM SIGSAC Conference on Computer and Communications Security, ACM, New York, NY, USA: 254–269, 2016, doi:10.1145/2976749.2978309.

[10] G.W. Peters, E. Panayi, Understanding Modern Banking Ledgers Through Blockchain Technologies: Future of Transaction Processing and Smart Contracts on the Internet of Money, 239–278, 2016, doi:10.1007/978-3-319-42448-4_13.

[11] N. Atzei, M. Bartoletti, T. Cimoli, A Survey of Attacks on Ethereum Smart Contracts (SoK), 164–186, 2017, doi:10.1007/978-3-662-54455-6_8.

[12] C.F. Torres, J. Schütte, R. State, "Osiris," in Proceedings of the 34th Annual Computer Security Applications Conference, ACM, New York, NY, USA: 664–676, 2018, doi:10.1145/3274694.3274737.

[13] B. Roy, D. Bouyssou, Comparison of a Multi-Attribute Utility and an Outranking Model Applied to a Nuclear Power Plant Siting Example, 482–494, 1985, doi:10.1007/978-3-642-46536-9_35.

[14] J. Figueira, B. Roy, "Determining the weights of criteria in the ELECTRE type methods with a revised Simos' procedure," European Journal of Operational Research, **139**(2), 317–326, 2002, doi:10.1016/S0377-2217(01)00370-8..

[15] C. Liu, H. Liu, Z. Cao, Z. Chen, B. Chen, B. Roscoe, "Finding Reentrancy Bugs in Smart Contracts," in 2018 IEEE/ACM 40th International Conference on Software Engineering: Companion (ICSE-Companion), IEEE, Gothenburg: 65–68, 2018..

[16] O. Deck, M. Al Heib, F. Homand, "Taking the soil–structure interaction into account in assessing the loading of a structure in a mining subsidence area," Engineering Structures, **25**(4), 435–448, 2003, doi:10.1016/S0141-0296(02)00184-0.

[17] J.R. Figueira, S. Greco, B. Roy, R. Słowiński, "An Overview of ELECTRE Methods and their Recent Extensions," Journal of Multi-Criteria Decision

Analysis, **20**(1–2), 61–85, 2013, doi:10.1002/mcda.1482.
[18] C. Harland, R. Brenchley, H. Walker, "Risk in supply networks," Journal of Purchasing and Supply Management, **9**(2), 51–62, 2003, doi:10.1016/S1478-4092(03)00004-9.
[19] S. Scheuer, D. Haase, V. Meyer, "Towards a flood risk assessment ontology – Knowledge integration into a multi-criteria risk assessment approach," Computers, Environment and Urban Systems, **37**, 82–94, 2013, doi:10.1016/j.compenvurbsys.2012.07.007.
[20] Z. Nehai, P.-Y. Piriou, F. Daumas, "Model-Checking of Smart Contracts," in 2018 IEEE International Conference on Internet of Things (iThings) and IEEE Green Computing and Communications (GreenCom) and IEEE Cyber, Physical and Social Computing (CPSCom) and IEEE Smart Data (SmartData), IEEE: 980–987, 2018, doi:10.1109/Cybermatics_2018.2018.00185.
[21] K. Govindan, M.B. Jepsen, "Supplier risk assessment based on trapezoidal intuitionistic fuzzy numbers and ELECTRE TRI-C: a case illustration involving service suppliers," Journal of the Operational Research Society, **67**(2), 339–376, 2016, doi:10.1057/jors.2015.51.
[22] A. Ahmed et al., "Modeling and Simulation of Office Desk Illumination Using ZEMAX," in 2019 International Conference on Electrical, Communication, and Computer Engineering (ICECCE), 1–6, 2019. DOI: 10.1109/ICECCE47252.2019.8940756
[23] U. Okoro, A. Kolios, L. Cui, "Multi-criteria risk assessment approach for components risk ranking – The case study of an offshore wave energy converter," International Journal of Marine Energy, **17**, 21–39, 2017, doi:10.1016/j.ijome.2016.12.001.
[24] E. Mengelkamp, J. Gärttner, K. Rock, S. Kessler, L. Orsini, C. Weinhardt, "Designing microgrid energy markets," Applied Energy, **210**, 870–880, 2018, doi:10.1016/j.apenergy.2017.06.054.
[25] N. Xiao, H.Z. Huang, Y. Li, L. He, T. Jin, "Multiple failure modes analysis and weighted risk priority number evaluation in FMEA," Engineering Failure Analysis, **18**(4), 1162–1170, 2011, doi: 10.1016/j.engfailanal.2011.02.004.
[26] S. Sterlacchini, S. Frigerio, P. Giacomelli, M. Brambilla, "Landslide risk analysis: a multi-disciplinary methodological approach," Natural Hazards and Earth System Sciences, **7**(6), 657–675, 2007, doi:10.5194/nhess-7-657-2007.
[27] K. Bhargavan, N. Swamy, S. Zanella-Béguelin, A. Delignat-Lavaud, C. Fournet, A. Gollamudi, G. Gonthier, N. Kobeissi, N. Kulatova, A. Rastogi, T. Sibut-Pinote, "Formal Verification of Smart Contracts," in Proceedings of the 2016 ACM Workshop on Programming Languages and Analysis for Security - PLAS'16, ACM Press, New York, New York, USA: 91–96, 2016, doi:10.1145/2993600.2993611.
[28] S. Kaddani, D. Vanderpooten, J.-M. Vanpeperstraete, H. Aissi, "Weighted sum model with partial preference information: Application to multi-objective optimization," European Journal of Operational Research, **260**(2), 665–679, 2017, doi:10.1016/j.ejor.2017.01.003.
[29] B. Bankian-Tabrizi, K. Shahanaghi, M. Saeed Jabalameli, "Fuzzy multi-choice goal programming," Applied Mathematical Modelling, **36**(4), 1415–1420, 2012, doi:10.1016/j.apm.2011.08.040.
[30] D. Von Winterfeldt, G.W. Fischer, Multi-Attribute Utility Theory: Models and Assessment Procedures, Springer Netherlands, Dordrecht: 47–85, 1975, doi:10.1007/978-94-010-1834-0_3.
[31] M. Younas, S.H.I. Jaffery, M. Khan, M.A. Khan, R. Ahmad, A. Mubashar, L. Ali, "Multi-objective optimization for sustainable turning Ti6Al4V alloy using grey relational analysis (GRA) based on analytic hierarchy process (AHP)," The International Journal of Advanced Manufacturing Technology, **105**(1–4), 1175–1188, 2019, doi:10.1007/s00170-019-04299-5.
[32] M.A. Alghamdi, N.O. Alshehri, M. Akram, "Multi-Criteria Decision-Making Methods in Bipolar Fuzzy Environment," International Journal of Fuzzy Systems, **20**(6), 2057–2064, 2018, doi:10.1007/s40815-018-0499-y.

ASTES

Advances in Science, Technology and Engineering Systems Journal Vol. 5, No. 5, 1064-1074 (2020)

www.astesj.com

Special Issue on Innovative Research in Applied Science, Engineering and Technology

ASTESJ

ISSN: 2415-6698

Comparison by Correlation Metric the TOPSIS and ELECTRE II Multi-Criteria Decision Aid Methods: Application to the Environmental Preservation in the European Union Countries

Mohammed Chaouki Abounaima*, Loubna Lamrini, Noureddine EL Makhfi, Mohamed Ouzarf

Laboratory of Intelligent Systems and Applications, Faculty of Sciences and Technologies, Sidi Mohammed Ben Abdellah University, Fez 35000, Morocco

ARTICLE INFO

Article history:
Received: 02 September, 2020
Accepted: 23 September, 2020
Online: 20 October, 2020

Keywords:
Multi-Criteria Decision Aid
Metric correlation
Ranking Quality
TOPSIS
ELECTRE
The Europe 2020 indicators
Environmental Preservation

ABSTRACT

This article is part of the field of Multi-Criteria Decision Aid (MCDA), where several criteria must be considered in decision making. All criteria are generally as varied as possible and express different dimensions, and aspects of the decision problem posed. For more than four decades, several MCDA methods have emerged and have been applied perfectly to solve a large number of multi-criteria decision problems. Several studies have tried to compare these methods directly with one another. Since each method has its disadvantages and advantages, a direct comparison between the two methods is normally far from common sense and becomes subjective. In this article, we propose a rational and objective approach that will be used to compare the methods between them. This approach consists of using the famous correlation measure to evaluate the quality of the results obtained by different MCDA approaches. To prove the effectiveness of the proposed approach, experimental examples, as well as a study of real cases, will be studied. Indeed, a set of indicators, known as The Europe 2020 indicators, are defined by the European Commission (EC) to control the smart, sustainable and inclusive growth performance of the European Union countries (EU). In this proposed real study, a subset of indicators is used to compare the performance of environmental preservation and protection of the EU states. For this, the two-renowned methods MCDA ELECTRE II and TOPSIS are used to classify from the best to the worst CE countries with regard to environmental preservation. The results of the experiment that the proposed ranking quality measure is significant. For the case study shows that the ELECTRE II method results in a better ranking than that obtained by the TOPSIS method.

1. Introduction

This present article is an extension of the paper published at the international conference IRASET'20 [1]. In this article, we have shown the importance of the correlation metric to evaluate the quality of the ranking results of the MCDA methods. In this paper, we will suggest an extension of the measurement of quality, this time considering the relative importance of the criteria selected. Indeed, in numerous multi-criteria decision problems, the decision-makers (DMs) do not have the same vision and the same levels of importance of the criteria, which is naturally given the priorities of the choices are not always equal and even sometimes conflicting.

For taking into consideration the criteria importance, the MCDA methods use a weighting system, represented by a set W, in which the highest weight is assigned to the most important criterion, and the lowest weight is assigned to the least important criterion. The difference between the MCDA methods lies in the approach used to aggregate the criteria with their weights to select the best choice with regard to the criteria considered.

Nowadays, the field of MCDA has known a remarkable abundance of methods which have emerged and applied to several areas [2], [3] such as Human Resources, Health, Industry and Logistic Management, Economy Management, Energy Management, Water Resources Management, the Environment Management, and recently some methods are used in applications on the fight against Covid19 [4]. Generally, an MCDA problem is defined by considering a finite set A of n alternatives, where each alternative is described by a family F of m criteria. In MCDA

*Corresponding Author: Mohammed Chaouki ABOUNAIMA, Laboratory of Intelligent Systems and Applications, Faculty of Sciences and Technologies, Sidi Mohammed Ben Abdellah University, Fez 35000, Morocco. medchaouki.abounaima@usmba.ac.ma

discipline, three obvious problematics are possible. The first allows ranking the set *A* from the best to the bad alternative, known as Ranking Problematic. The second consists in classifying the set *A* into predefined classes, called Sorting Problematic. Finally, in the third decision problem, we find to select the best alternative, known as Choice Problematic. In this article, we discuss the ranking problematic. Prospects are possible to apply the results of this paper to the other two problematics.

For the same ranking problematic, there are many MCDA methods are proposed in multi-criteria analysis literature, each with its resolution process as well as its advantages and disadvantages [5]. Thus, for a given multi-criteria ranking problem, the DM obtains several proposals for ranking solutions, and it becomes not obvious to opt objectively for a single solution.

The approach proposed in this work allows us to remedy this inconvenience of the choice embarrassment of ranking solutions. Indeed, a metric will be defined to evaluate the quality of each ranking solution obtained. The ranking which gives a better quality will, therefore, be retained. In the first version of the proposed metric [1] no reference was made to the importance of the criteria. It was supposed that all the criteria are treated with the same importance, i.e. each criterion is not considered more interesting than others. In this paper, we extend this metric for measuring the quality of a ranking to the general case where all the criteria do not necessarily have the same importance.

The proposed correlation metric not only can be used to distinguish the best ranking among several results of the MCDA methods, but it can also be used to guide and help the DM to perform the robustness analysis. The latter is a primordial activity and highly recommended in the multi-criteria analysis [6]. Indeed, the primary motivation for this activity is since the data provided by the DMs are often subject to uncertainty and imprecision, in particular at the level of the choice of the parameters required by specific MCDA methods is not sometimes obvious for DMs, as in the case of criteria weights [7]. The uncertain and imprecise choices of parameters will undoubtedly have repercussions on the quality of the final result. The robustness analysis then consists in verifying the stability of the results by testing a set of slightly different values of parameters. The metric thus proposed could help to compare objectively all the results obtained by the robustness analysis.

Intending to prove and illustrate the significance and importance of the ranking quality measure, we propose a real case study that aims to rank the European Union countries according to the level of preservation environmental. In fact, a set of indicators are defined and monitored by the European Commission, known as Europe 2020 indicators, to compare and control the smart sustainable and inclusive growth performance of all the EU countries (http://epp.eurostat.ec.europa.eu/portal/page/portal/europe_2020_indicators/headline_indicators). In the proposed case study, a subset of indicators is selected as criteria, and all relate to environmental performance. As for the example of these indicators: “Waste generated except main mineral waste”, “Recycling rate of e-waste”, “Exposure to PM10 pollution”, “Exposure of the urban population to air pollution by fine particles”, “Final energy consumption”, “Greenhouse gas emissions”, “Share of renewable energies”, and etc. A total of 11 indicators are selected. In first exploitation, these indicators are used by the two-popular methods MCDA ELECTRE II and TOPSIS to rank and evaluate the environmental performance of the EU countries. All results obtained are compared based on quality measurement.

The case study remains valid and open to all other MCDA ranking methods. The choice of methods used in this paper is only illustrative.

The rest of the article is structured as follows. In the second section, a brief reminder will be given on MCMA methods. In section III, a reminder of the ELECTRE II and TOPSIS methods will be presented. Section IV presents the case study to rank the EU countries according to the environmental preservation performance. In section V, we will present the extension of the ranking quality measurement approach. In section VI, all the numerical experiments for the test example and the case study will be detailed. Lastly, the paper will be concluded with new and possible research axes.

2. Overview of MCDA methods

2.1. *Background*

Certainly, the decision-making is often multi-criteria, where several criteria are considered to find a solution, such as a better choice, a ranking or a sorting, according to the problematics mentioned above. The criteria adopted are often contradictory insofar as a better choice in relation to one criterion is not necessarily so for another criterion, as price and quality are two contradictory criteria. In addition, the criteria are not always expressed on the same measurement scale and can represent from different points of view [8]: such as political, military, economic, comfort, social, education, investment cost, environmental impact, etc.

In some MCDA methods, such as the Weighted Sum method [9] and TOPSIS method [3] all criteria are normalized and aggregated into a single criterion, called synthesis criterion, on the basis of which the final decision will be made. Note that any transformation of the criteria by normalization will not be innocent and will have an influence on the final solution. Indeed, the final solution may depend on the normalization operation used, so these methods are to be used with recklessness [10].

Nowadays, the MCDA field has experienced great progress both in theory and in application [11]. Many methods have emerged, each has its own approach to aggregate criteria, and each has its advantages and disadvantages. There are currently two main resolution processes [12].

The first process is known as the Synthesis Criteria Approach. The principle of the methods of this approach is to transform the multi-criteria problem into a simple mono-criterion problem, by the first normalization of all the criteria, and then an aggregation of all the normalized criteria into a single decision criterion. As an example of these methods, we find the method of the weighted sum (WSM) [7], [9], the method of programming by objective [13], TOPSIS method [3] and many other methods. In this paper, the TOPSIS method will be used. The second resolution process takes the name of outranking approach. Whose main idea is to develop a relationship, by comparing the alternatives two by two, named

outranking relation and denoted by S. This relation S will be used in a second step of the process to find the compromise solution according to the problem to be solved: problematic choice, classification or sorting. There are numerous methods which are based on the principle of this approach, of which we cite the two popular methods: the methods family PROMETHEE (Preference Ranking Organization METHod for Enrichment of Evaluations) [14], and the methods family ELECTRE (Elimination And Choice Translating Reality) [15], [16]. In this paper, the ELECTRE method will be used and compared to the method TOPSIS.

The principal objective of the presented paper is to propose a rational tool to compare MCDA methods objectively. Several authors have tackled this question, but for the majority of them, they have tried to compare the methods directly according to their resolution processes. For example, we cite the works [17], [18]. The direct comparison between methods, for example, based on their own characteristics and the approach to which they belong, will undoubtedly be a devoid comparison of objectivity, as each method has its limitations and advantages. We propose to use the correlation metric as a tool to compare the results obtained by the ranking methods instead of a direct comparison.

2.2. *The data necessary for an MCDA method*

The data hypotheses of an MCDA problem are at least the set of n alternatives *A*, which contains all the possible solutions, and a set of m criteria *F*, which are the dimensions along which the alternatives will be evaluated.

The following Table 1, called the performance matrix *M* [16], summarizes all the data which we need in a decision problem.

Table 1: Sample Table

Criteria						
Weights		*g1*	...	*gj*	...	*gm*
		w1	...	*wj*	...	*wm*
		Min/Max	...	*Min/Max*	...	*Min/Max*
Alternatives	*X1*	*g1(X1)*	...	*gj(X1)*	...	*gm(X1)*
	...	...	...	...	...	...
	Xi	*g1(Xi)*	...	*gj(Xi)*	...	*gm(Xi)*
	...	...	...	...	...	...
	Xn	*g1(Xn)*	...	*gj(Xn)*	...	*gm(Xn)*

In this paper, the following notations will be deployed:

- $A = \{X_1, ..., X_i, ..., X_n\}$ are the n alternatives.
- $F = \{g_1, ..., g_j, ..., g_m\}$ are the m criteria, $m \geq 2$.
- Min means that the criterion to be minimized
- Max means that the criterion to be maximized
- $W = \{w_1, ..., w_j, ..., w_m\}$ are the weights of criteria.
- $g_j(X_i)$ is the evaluation of the alternative Xi on the criterion g_j.

3. The remainder of the MCDA ELECTRE II and TOPSIS methods

The ELECTRE II and TOPSIS methods are considered among the most widely used methods in the MCDA field. Several research works and real applications have successfully deployed these two methods [8], [19]. However, the two methods proceed differently. The ELECTRE II method is a method which is the basis of the outranking approach, while the TOPSIS method is a method which is part of the approach of the unique synthesis criterion. The common point between the two methods is that both are able to rank the alternatives of set A from the best alternative(s) to the bad alternative(s); moreover, they take as starting data the decision matrix M and a set W of criteria weights.

In this section, we present the algorithms of the two methods, which we will need for the case study.

3.1. *The TOPSIS method*

The TOPSIS method (Technique for Order Preference by Similarity to Ideal Solution) [3] is developed to rank all the alternatives of the set A from the best alternative(s) to the bad alternative(s). As shown in Figure 1, the TOPSIS method starts with a normalization of the decision matrix M, then it calculates a Euclidean distance between all the alternatives and two reference solutions Ab, and Aw, respectively called Ideal Solution and Anti-Ideal Solution. Then the similarity Swi, called the relative closeness, is calculated between each alternative Xi and the tow solutions Ab and Aw. Lastly, the alternatives are ranked according to the similarities Sw, thus calculated.

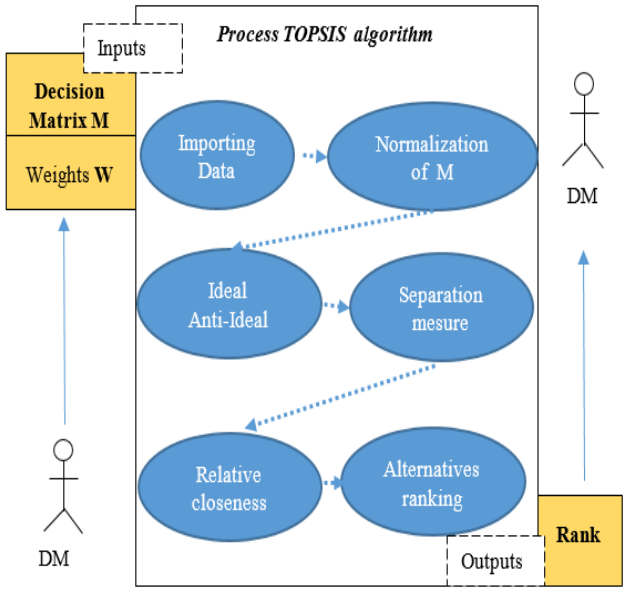

Figure 1: Process TOPSIS algorithm

TOPSIS algorithm proceeds in the following seven steps:

- Step 1: Establishment of the performance matrix

In the first step, we build the decision matrix *M* which is composed of *m* criteria and *n* alternatives, as shown in Table 1.

- Step 2: Normalization of the performance matrix

To compare the performances of the alternatives by the Euclidean distance, one of the conditions imposed by the TOPSIS method is that all the performances must be expressed on the same measurement scale. In this step, a normalization is then calculated. This normalization consists of replacing each performance *gj(Xi)* by an equivalent normalized performance calculated by the following equation 1.

$$r_{ij} = \frac{g_j(X_i)}{\sqrt{\sum_{k=1}^{n} g_j(X_k)}} \quad (1)$$

For the rest of the decision process, the decision matrix M is therefore replaced by the new normalized matrix $R = (r_{ij})_{n\times m}$.

- Step 3: Construction of weighted normalized decision matrix T.

For taking into account the importance wj of criteria in the decision-making process, the matrix R is again replaced by a new matrix $T = (t_{ij})_{n\times m}$ which is obtained by the following equation 2:

$$t_{ij} = \frac{w_j \times r_{ij}}{\sum_{j=1}^{m} w_j} \quad (2)$$

In equation 2, the performance of alternative Xi on criterion gj is reinforced by the weight of criterion gj. The performance will, therefore, be multiple depending on the importance of the criterion.

- Step 4: Calculation of the Ideal solution Ab and the anti-ideal solution Aw

In step 4, we determinate the worst solution Aw and the best solution Ab. For each criterion gj, we calculate the performances Abj and Awj by the following equations 3 and 4.

$$A_{bj} = \begin{cases} \max\limits_{i=1\ to\ n} t_{ij} \ \ if\ g_j\ is\ a\ criterion\ to\ be\ maximized \\ \min\limits_{i=1\ to\ n} t_{ij}\ if\ g_j\ is\ a\ criterion\ to\ be\ minimized \end{cases} \quad (3)$$

The worst solution Aw is calculated in an opposite way to the best solution Ab, it is obtained by the following formula 4.

$$A_{wj} = \begin{cases} \min\limits_{i=1\ to\ n} t_{ij} \quad if\ g_j\ is\ a\ criterion\ to\ be\ maximized \\ \max\limits_{i=1\ to\ n} t_{ij} \quad if\ g_j\ is\ a\ criterion\ to\ be\ minimized \end{cases} \quad (4)$$

- Step 5: Calculation of the Euclidian distance between each action Xi and the Ab and Aw

We calculate by equations (5) and (6) the Euclidean distance between all the alternatives Xi and the solutions Aw and Ab.

$$d_i^+ = \sqrt{\sum_{j=1}^{m} (t_{ij} - A_{wj})^2} \quad (5)$$

And

$$d_i^- = \sqrt{\sum_{j=1}^{m} (t_{ij} - A_{bj})^2} \quad (6)$$

- Step 6: Calculation the similitude coefficient Sw to Aw and Ab

For each action Xi, the similarity S_{wi}, called the relative closeness, is calculated, by equation 7, between each action Xi and the Ideal Ab solution and the Anti-Ideal solution Aw. This similarity is the Euclidean distance between the action Xi and the Anti-Ideal Aw attenuated by the sum of the two distances from Xi to the solutions Aw and Ab. An alternative obtains so the best ranking when its similarity is better.

$$s_{wi} = \frac{d_i^-}{d_i^+ + d_i^-} \quad (7)$$

- Step 7: Rank the actions in descending order by similitude coefficient

Lastly, the actions are ranked from the best action to the bad action according to similarities s_{wi} $(i=1, \ldots, n)$ calculated.

In summary, the main idea of the TOPSIS method is an alternative will be better when it is closer to the Ideal Ab solution and further from the Anti-Ideal Aw solution.

2.3. *ELECTRE II method*

The ELECTRE family of methods currently has 6 different methods ELECTRE I, IS, II, III, VI, and ELECTRE TRI [8][10]. The six versions have the same principle of constructing an outranking relation in the first step of the method, and then its exploitation in the second step. However, the six ELECTRE methods are distinguished by the problem posed (choice, sorting or ranking), and whether the DM hesitates to prefer an alternative x to another alternative y, in the case where the alternatives have very similar performances.

In this article, we will compare the ELECTRE II method and the TOPSIS method on the basis of the real case study on environment preservation and the quality measurement of ranking.

The ELECTRE II method [10][12], like all the other versions, proceeds in two phases. In the first phase, two outranking relations S^1 and S^2 are developed. In the second phase, the relations S^1 and S^2 are exploited to rank the alternatives.

In the approach to developing the outranking relation, pairwise comparisons between pairs of alternatives (x, y) are performed. For all ELECTRE versions, the outranking relation S is developed as follows:

xSy, if two conditions are satisfied:

• x is better than y for most criteria (majority principle)

• without there being a criterion for which y has a preference much greater than that of x (principle of minority).

The two conditions of majority and minority are known as the concordance condition and the non-discordance condition.

- Step 1: Construction of relations S^1 and S^2

In ELECTRE II method, we construct two relations S^1 and S^2, such that S^1 is included in S^2, i.e.: if xS^1y then xS^2y. To do this we require two thresholds of concordance c1 and c2, and two thresholds of discordance, which all verify: c1>c2 and d1<d2.

The relation S^1 is, therefore, more stringent than the relation S^2, because the majority of criteria required to satisfy the condition of concordance in relation S^1 is much larger than that required for the relation S^2: c1>c2. In addition, the maximum acceptable difference to reject the discordance effect is too small in S^1 and larger in S^2: d1<d2.

The S^1 and S^2 outranking relations are called respectively the "strong outranking" relation and the "weak outranking" relation: $x\ S^1y \Longrightarrow x\ S^2y$.

The concordance threshold defines the minimum majority required of the criteria that match the assertion of the outranking relation. As an example, a concordance threshold of 0.6 requires a

majority of more than 60% of criteria to accept the concordance test.

However, the discordance threshold defines the maximum difference supported between the performance of two alternatives on a given criterion to accept the second discordance test.

The construction of the two outranking relations S^1 and S^2 is formulated by the following equation 8.

$$xS^i y \Leftrightarrow \begin{cases} \text{Concordance condition :} \\ c(x,y) = \dfrac{\sum wj}{\sum wj} \geq ci \\ 1 \leq j \leq m \\ \text{Non - discordance condition :} \\ \forall\, gj \in F / gj(x) > gj(y) : \; gj(x)\text{-}gj(y) \leq dji \end{cases} \quad (8)$$

For $i \in \{1,2\}$

- Step 2: Exploitation of relations S^1 and S^2

After the construction in the first step of the two relations S^1 and S^2, we calculate two reverse pre-orders, the first, named *P1*, is obtained by exploring the graph, corresponding to the relation S^1, from the root to the leaves. A second pre-order, named *P2*, is obtained by exploring the graph in the reverse direction, this time starting from the leaves towards the root. Then the two pre-orders *P1* and *P2* are combined to give a final median pre-order *P* of the form $P = \frac{P1+P2}{2}$.

Lastly, the alternatives having obtained the same rank in the ranking median *P*, will be separated according to the second relation S^2.

4. A real case application

The Europe 2020 indicators (http://epp.eurostat.ec.europa.eu/portal/page/portal/europe_2020_indicators/headline_indicators) are set up and deployed by the European Commission (EC) in order to control the objectives of the strategy set out for smart, sustainable and inclusive growth in the member states of the European Union (EU). The objectives of sustainable growth aim for a more resource-efficient, greener, and more competitive economy. It is decided to achieve a 20% reduction in greenhouse gas emissions from 1990 levels, in addition, an increase in the share of renewable energy sources in energy consumption. All of the above objectives must be measurable and comparable. This is why the main indicators have been defined by the EC to facilitate the monitoring of the progress of the indicators in each member state, of which we cite:

- Greenhouse gas emissions;
- Share of renewable energies in gross final energy consumption;
- Contributions to eco-innovation;
- Waste management and recycling;
- Water management and production;
- Energy intensity of the economy;
- Employment rate by sex;
- Early leavers from education and training;
- The population at risk of poverty or exclusion;
- Integration rate of emigrants;
- Etc.

The different indicators can reflect the diversity of performance in each country. Also, they measure the level of progress of the goals over time and can, therefore, be used for comparison purposes at the European and international level.

In the case study presented in this paper, the study focuses on the level of ecological conservation performance and environmental preservation in the EU. For this, a subset of the Europe 2020 indicators is used. More precisely, all the indicators having a direct and indirect relationship with the environmental dimension are retained. The list of indicators selected is not exhaustive and remains the first exploitation of the institutional database developed and put online by Eurostat (https://ec.europa.eu/eurostat/).

The annual values recorded on the indicators cover several years from the years 1990 to the year 2018. For the indicators selected for the evaluation of environmental performance, we have deployed the latest data available on each indicator and each country. Some countries are excluded from the study because they lack information on certain indicators, such as Switzerland.

As shown below, there are a multitude and varied of conflicting indicators and not necessarily reducible into a single indicator. The multi-criteria approach is, therefore, essential to compare and classify European countries according to the different indicators. The European countries represent the set *A* of the alternatives, and the indicators constitute the set *F* of the criteria. The proposed problematic consists of ranking the EU member states, according to environmental performance. The decision matrix *M* is shown in Table 2, and a brief description of the criteria is given below.

Table 2: Performance matrix for selected indicators

Country	Indicators	Criterion g1	Criterion g2	Criterion g3	Criterion g4	Criterion g5	Criterion g6	Criterion g7	Criterion g8	Criterion g9	Criterion g10	Criterion g11
		MIN	MAX	MIN	MIN	MAX	MIN	MIN	MIN	MIN	MAX	MAX
	Weights	1	1	1	1	1	1	1	1	1	1	1
X1	Germany	1897	38.7	0.06	12.7	7.34	215.37	291.75	441.22	70.44	16.481	137
X2	Austria	1886	50.1	3.77	13.8	24.08	27.91	31.8	50.65	102.66	33.426	119
X3	Belgium	3383	38.6	0	12.9	6.56	36.33	46.84	71.37	82.67	9.423	83
X4	Bulgaria	2527	68.8	77.59	23.8	2.56	9.91	18.36	26.76	57.16	20.528	50
X5	Croatia	828	81.3	99.08	19	6.94	6.85	8.18	17.21	75.23	28.024	88
X6	Denmark	1657	38.5	0	9.2	9.75	14.96	17.96	32.44	70.69	35.708	115
X7	Spain	1480	41	1.32	12.1	9.28	86.84	124.63	202.66	119.74	17.453	105

Country	Indicators	Criterion g1	Criterion g2	Criterion g3	Criterion g4	Criterion g5	Criterion g6	Criterion g7	Criterion g8	Criterion g9	Criterion g10	Criterion g11
		MIN	MAX	MIN	MIN	MAX	MIN	MIN	MIN	MIN	MAX	MAX
	Weights	1	1	1	1	1	1	1	1	1	1	1
X8	Estonia	8965	69.8	0	5.3	20.57	2.96	6.17	6.34	49.98	29.996	81
X9	Finland	2595	48.2	0	4.9	13.09	25.84	32.99	30.04	81.41	41.162	121
X10	France	1455	36.6	0.39	12	7.01	146.61	238.91	343.07	83.1	16.593	112
X11	Greece	1328	32.9	28.64	14.7	9.32	15.95	22.42	44.88	90.84	18.002	83
X12	Hungary	1119	51.1	58.88	20.9	3.92	18.54	24.49	43.33	67.82	12.489	73
X13	Ireland	1765	47.7	0	7.7	2.63	12.27	14.54	45.37	113.6	11.061	94
X14	Italy	1799	32.1	49.28	19.4	15.17	116.47	147.24	274.75	84.41	17.775	112
X15	Latvia	1065	40.6	3.78	13.6	14.47	4.18	4.69	9.18	45.95	40.292	82
X16	Luxembourg	2697	45.5	0	11.2	4.39	4.35	4.46	9.09	94.16	9.059	138
X17	Netherlands	2539	42.1	0	11.3	3.18	50.27	64.71	101.8	88.58	7.385	92
X18	Poland	2090	36.1	70.09	23.8	3.33	71.93	101.06	217.98	87.42	11.284	59
X19	Portugal	1148	43.5	0.89	12	5.93	16.91	22.64	40.75	118.9	30.322	101
X20	Romania	1084	25	21.55	20.4	2.43	23.53	32.48	74.27	46.84	23.875	66
X21	United-Kingdom	1813	42.2	0	10	2.64	134.67	176.27	329.4	61.59	11.017	110
X22	Slovakia	1459	46.5	40.2	17.5	9.85	11.11	15.79	21.92	59.16	11.896	68
X23	Slovenia	1457	33.4	4.81	19.7	10.01	4.98	6.67	10.98	94.35	21.149	107
X24	Sweden	2136	47	0.16	5.4	20.29	32	46.78	32.69	75.28	54.645	132
X25	Czechia	1214	46.5	31.12	18.4	14.76	25.32	40.39	64.11	64.82	15.15	100

* Source: The institutional sources of data are European Commission - Directorate-General for Environment (DG ENV)- Eco-innovation Observatory.

In this first analysis of the indicators, we consider that no criterion is privileged over the others. In other words, all the criteria have a weight equal to 1.

- Criterion 1: Waste generated except main mineral waste

This indicator is defined as all hazardous and non-hazardous waste produced in a country per year and per capita. The total annual number of kilograms of waste produced per person measures the indicator.

- Criterion 2: Recycling of electronic waste (e-waste)

This criterion e-waste is a rate which is estimated by multiplying the “collection rate” by the “reuse and recycling rate”.

The indicator is expressed as a percentage (%).

- Criterion 3: Exposure to PM10 pollution

This criterion expresses the percentage of citizens living in urban areas exposed to concentrations of particles <10 µm (PM10) exceeding the daily limit value (50 µg / m3).

The European Environment Agency collects air quality data on an annual basis.

- Criterion 4: Exposure of urban citizens to atmospheric pollution by fine particles

This criterion expresses the concentration of suspended particles PM10 and PM2.5 weighted according to the urban population potentially exposed to air pollution.

The particles PM10 and PM2.5 are harmful, and they can cause serious lung inflammation.

- Criterion 5: Agricultural area covered by organic farming

The criterion is expressed in terms of the share of the agricultural area using only organic farming. It is a criterion that we choose to maximize in the ranking.

- Criterion 6: Final energy consumption

By "final energy consumption" we mean the sum of the energy consumption of the transport industry in the residential sector, services, and agriculture. This quantity is relevant for measuring energy consumption in the last resort of energy use and for comparing it with the objectives of the Europe 2020 strategy. More information can be found on the statistics of energy savings on Statistics Explained.

This indicator is measured in millions of tons of oil equivalent (TOE)

- Criterion 7: Primary energy consumption

By "primary energy consumption" is meant gross domestic consumption with the exception of any non-energy use of energy products (e.g. natural gas used not for combustion but for the production of chemicals). This quantity is relevant for measuring actual energy consumption and for comparing it with the Europe 2020 targets.

This indicator is measured in millions of tons of oil equivalent (TOE)

- Criterion 8: Greenhouse gas emissions in the sectors included in the effort distribution decision

The calculation of the indicator is based on the emissions covered by the decision on shared effort 406/2009 / EC. The decision on the shared effort provides for annual quantified commitments for emissions not covered by the emissions trading system (ETS). The emissions governed by the decision are calculated by deducting the verified emissions relating to the ETS from the CO2 emissions associated with domestic flights and the NH3 emissions from the total national emissions.

- Criterion 9: Greenhouse gas emissions to the base year 1990

This indicator shows trends in total anthropogenic greenhouse gas emissions contained in the “Kyoto basket”. It

presents the total annual emissions compared to 1990 emissions. The "Kyoto basket" includes the following greenhouse gases: carbon dioxide (CO2), methane (CH4), nitrous oxide (N2O), and so-called fluorinated gases (hydrofluorocarbons, per-fluorinated hydrocarbons, nitrogen trifluoride (NF3) and sulfur hexafluoride - SF6). These gases are grouped into a single unit according to specific factors corresponding to their global warming potential (GWP). Aggregate greenhouse gas emissions are expressed in CO2 equivalent units.

The EU as a whole is committed to reducing its greenhouse gas emissions by at least 20% by 2020 compared to 1990.

- Criterion 10: Use of renewable energies

This criterion expresses the level of use of renewable energies.

This indicator is then to be maximized in the ranking.

- Criterion 11: The eco-innovation index

The criterion is calculated on the basis of 16 sub-indicators from 8 data sources in 5 thematic areas: contributions to eco-innovation, eco-innovation activities, consequences of eco-innovation, results in terms of 'efficient use of resources and socio-economic results.

The overall index of an EU country is evaluated by the average of these 16 sub-indicators. It shows how each country practices eco-innovation compared to the EU average.

This indicator is then to be maximized in the ranking.

5. The proposed approach to measure the quality of rankings

5.1. Process of the extension approach

For the extension of the quality measure of any ranking P, we propose to compare this ranking P to all the rankings induced by the criteria. Indeed, it is so easy to rank the alternatives on each criterion gk, and we baptize this rank by P^k. The quality measurement then makes it possible to measure the correlations between the P ranking and the various P^k rankings.

In practice, the rankings P^k and P are replaced by the comparison matrices R^k and R given by the equations 9 and 10. In order to consider the differences between the importance of the criteria, the final result of the comparisons is aggregated by a weighted average of the correlations between the R and R^k.

The approach proceeds in three steps: In the first step, the comparison matrices R^k induced by the different criteria gk are evaluated. In the second step, the comparison matrix R induced by the ranking P result of the MCDA method is evaluated. In the last step, all the matrices R^k are compared to the matrix R. The results of the comparison are then aggregated with the weighted average. The approach is presented as follows.

- Step 1: Compute the comparisons matrix R^k induced by the criterion gk

Let $(R_{ij}^K)_{i.j\in\{1.....n\}}$ be the comparison matrix R^k induced by the criterion gk. This matrix is calculated by the formula 9.

$$R_{ij}^k = \begin{cases} 1 \; if \; gk(i) > gk(j) \\ 0 \qquad otherwise \end{cases} \tag{9}$$

The matrix R^K contains only the numbers 0 and 1. The value 1 means that the alternative i is preferred to the alternative j according to the criterion gk.

- Step 2: Compute the comparisons matrix R induced to the ranking P

The matrix R is calculated by formula 10.

$$R_{ij} = \begin{cases} 1 \; if \; "i" \; is \; better \; ranked \; than \; j \; in \; the \; ranking \;\; P \\ 0 \qquad\qquad\qquad\qquad\qquad\qquad\qquad\qquad otherwise \end{cases} \tag{10}$$

The value 1 indicates that the action i is ranked before the action j for the MCDA method used.

- Step 3: Evaluate the quality for the ranking P

As the example E1 of the experiment section proves, a P ranking will be better if it follows the same direction of all the P^k rankings of the gk criteria. This amounts to measuring the dependence between the matrix R and each matrix R^k. The dependence between the matrices is measured mathematically by the correlation coefficient [1]. To take into account all the correlations calculated as well as the relative importance of the criteria W, the quality measure $Q(P)$ is then calculated by a weighted average, which is given by the following formula (11).

$$Q(P) = \frac{\sum_{k=1}^{m} w_k \times \text{correlation}(R^k, R)}{\sum_{k=1}^{m} w_k} \tag{11}$$

With:

$$\text{correlation}(X,Y) = \frac{\sum_{i=1}^{n}\sum_{i,\,j=1}^{n}(X_{ij}-\bar{X})\times(Y_{ij}-\bar{Y})}{\sqrt{\sum_{i=1}^{n}\sum_{i,\,j=1}^{n}(X_{ij}-\bar{X})^2} \times \sqrt{\sum_{i=1}^{n}\sum_{i,\,j=1}^{n}(Y_{ij}-\bar{Y})^2}} \tag{12}$$

- X and Y are two square matrices of order n.

$$\bar{X} = \frac{1}{n(n-1)} \times \sum_{\substack{i,\,j=1 \\ i\neq j}}^{n} X_{ij}$$

- is the empirical average a square matrix X of order n.

5.2. Propriety: Equivalence between P and R

Let P be a ranking and R the comparison matrix deduced from P. The matrix is given by the equations (1) or (2) and let Xi be any alternative of A.

The rank of Xi in P can be deduced from the matrix R and conversely. In other words, the vector P and the matrix R are equivalent. Indeed, by definition, from ranking P we can build the

matrix R. Now, we suppose that we only have the matrix *R*. If for the alternative *Xi* we calculate the sum of all the values 1 on its line of the matrix *R*. Let *L* be this value, so we have $L(Xi)=\sum_{j=1}^{n} R_{ij}$.

The value *L(Xi)* gives the number of alternatives that are classified behind *Xi*. The ranking *P* is obtained by sorting the alternatives *Xi* in decreasing order of the values *L(Xi)*.

As an essential result of this propriety, it is that the comparison between two any comparison matrices *R1* and *R2* gives the same result as the direct comparison of the rankings *P1* and *P2* associated because as we have just demonstrated, the comparison matrices of and rankings are equivalent.

We will show in the discussion paragraph this equivalence at the base of the numerical results obtained by the case study.

6. Numerical experimentation and discussion

6.1. Numerical results of the experimentation example

To show that the metric of correlation proposed gives a significant result for the measurement of the quality of the rankings, we propose a sample of 15 varied rankings. In this example, we consider an MCDA problem of 3 criteria: *F={g1, g2, g3}*, and a set of four alternatives *A={A1, A2, A3, A4}*. For the simplification of the example, we propose that the three criteria give the same ranking: *A1> A2> A3> A4*, as shown in Table 2 below. This ranking expresses that the alternatives *A1*, *A2*, *A3* and *A4* are respectively in rank 1, 2, 3 and 4.

Moreover, we choose the three criteria with the same weighting *w1=w2=w3=1*.

Table 3: The criteria rankings *P1*, *P2*, and *P3*

Alternatives/Rankings	P1(g1)	P2(g2)	P3(g3)
X1	1	1	1
X2	2	2	2
X3	3	3	3
X4	4	4	4

The matrices R^1, R^2 and R^3 induced by the three criteria *g1*, *g2* and *g3* are given by Table 4.

Table 4: Matrices induced by the criteria R^1, R^2, and R^3

	X1	X2	X3	X4
X1	0	1	1	1
X2	0	0	1	1
X3	0	0	0	1
X4	0	0	0	0

The 15 rankings are chosen as an experiment to determine the significance of the proposed correlation metric. We have carefully chosen these rankings in order to cover almost all possible cases. Moreover, to show how the quality can vary according to these classifications choices. Table 4 gives all the rankings selected for the test.

In total, we propose two borderline cases of rankings with other intermediate cases. The first limit ranking is the ranking E1: X1>X2>X3>X4 which is the same as all the rankings given by the criteria g1, g2 and g3. The second limit ranking is the E15 ranking: X4> X3> X2> X1, which is the opposite of the three classifications given by the three criteria. The 13 other cases are the rankings intermediate where the alternatives permute their ranks between cases E1 and E15.

In this experiment, we also consider the case where the rankings can contain alternatives obtained from the same ranks. It is the case of the rankings E11, E12, E13 and E14.

Table 5 summarizes the calculated quality results for the 15 selected rankings. An interpretation of the results will be given in the following discussion section.

Table 5: Quality measurement for the 15 rankings

Example number	Ranking *P*	*Q(P)*
E1	X1>X2>X3>X4	1.0000
E2	X1>X3>X4>X2	0.4667
E3	X2>X1>X3>X4	0.7333
E4	X2>X3>X1>X4	0.4667
E5	X2>X3>X4>X1	0.2000
E6	X3>X1>X2>X4	0.4667
E7	X3>X2>X4>X1	-0.0667
E8	X3>X4>X2>X1	-0.3333
E9	X4>X1>X3>X2	-0.0667
E10	X4>X2>X1>X3	-0.0667
E11	X1>X2>X3=X4	0.8704
E12	X1>X2=X3=X4	0.6202
E13	X1=X2>X3>X4	0.8704
E14	X1=X2>X3=X4	0.7454
E15	X4>X3>X2>X1	-0.6000

The graph illustrated by Figure 2 below represents the variation in the quality *Q(P)* of the 15 selected test rankings.

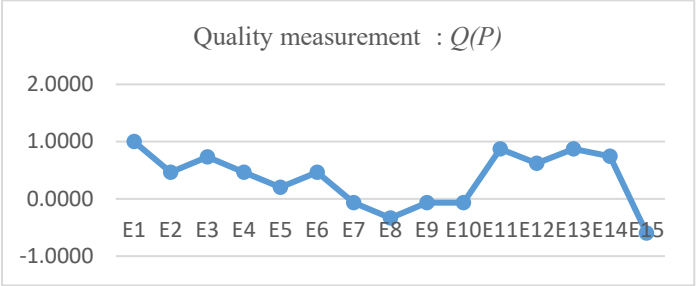

Figure 2: Graphical representation of variations of the quality measurement of rankings

The graph undoubtedly proves that the quality measure *Q(P)* is significant. Indeed, for the ideal-ranking, *E1: X1>X2>X3>X4*, which coincides with the three rankings induced by the three supposed criteria *g1*, *g2* and *g3*, gives a maximum quality, which is worth *Q(E1)=1*. From more, the ranking *E15: X4>X3>X2>X1*, which is opposed to the three rankings induced by the three criteria *g1*, *g2* and *g3*, gives the most inferior quality which is worth *Q(E15)=-0.63*. For all other cases of rankings, even for rankings with equal rank, the quality varies between 1 and -0.63. In addition, that depends on the ranks of the alternatives.

In summary, the quality remains close to the maximum value when the alternatives keep almost the same ranks of the rankings induced by the criteria. And, the quality becomes poorer when the alternatives score far from the ranks of the rankings induced by the criteria.

6.2. Numerical results of the study case

For the comparison and ranking of European countries according to performance and environmental preservation, we use the two methods TOPSIS and ELECTRE II at the base of the decision matrix *M* illustrated by Table 2. The rankings obtained by the two methods are given in Table 8.

Ranking of countries by the TOPSIS method

We calculate the *swi* similarities, given by equation 7, for each country. Then we rank the countries in descending order according to the *swi* scores thus calculated. The result of the ranking obtained by the TOPSIS method is given in Table 8.

Ranking of countries by the ELECTRE II method

The first step of the ELECTRE II method consists of calculating the matrix of concordance indices *C(Xi, Xk),* given by equation 8, for all pairs *(Xi, Xk)* of countries. Then, in the second step of the method, we build the two outranking relations *S1* and *S2*, as indicated previously in the method remainder paragraph. For the concordance thresholds to be provided, we choose c1=0.8 and c2= 0.6. These values are the standard choices of several MCDA software. Moreover, for the discordance thresholds, we choose d1=60% of the extent of each criterion. Furthermore, d2=80% of the extent for each criterion, see Table 6.

The extent of a criterion *gj* is given by *extent(gj)=Max(gj(a))-Min (gj (a)))* for any *a* of *A*.

In MCDA, for the case of the ELECTRE method, it is strongly recommended to make a robustness analysis [6], which shows the stability of results. This analysis involves testing multiple values for the parameters required by the method, such as concordance and discordance thresholds, and seeing how the results obtained by the method may change depending on the parameter values used. For this reason, we choose the second test of discordance values. However, we keep the same concordance thresholds, because we obtained almost the same rankings for different values of concordance thresholds. The values used are the best thresholds which disperses the ranking of countries as much as possible.

Table 7 below summarizes all the parameters used for the ELECTRE II method. Furthermore, it gives two versions of results according to the parameters provided: ELECTRE II V1 and ELECTRE II V2.

Table 6: The discordance thresholds for d_2 =80% for extent and d_1 = 60% for extent

	Criterion 1	Criterion 2	Criterion 3	Criterion 4	Criterion 5	Criterion 6	Criterion 7	Criterion 8	Criterion 9	Criterion 10	Criterion 11
Extent	8137.000	56.300	99.080	18.900	21.650	212.410	287.290	434.880	73.790	47.260	88.000
d1	4882.20	33.78	59.45	11.34	12.99	127.45	172.37	260.93	44.27	28.36	52.80
d2	6509.60	45.04	79.26	15.12	17.32	169.93	229.83	347.90	59.03	37.81	70.40

Table 7: Discordance and concordance thresholds

Thresholds	ELECTRE II V1	ELECTRE II V2
d1	80%	90%
d2	60%	80%
c1	0.60	0.60
c2	0.80	0.80

Table 8: Rankings obtained by the ELECTRE II and TOPSIS methods

Code	County	Rank TOPSIS	Rank ELECTRE II V1	Rank ELECTRE II V2
X24	Sweden	1	2	4
X15	Latvia	2	1	2
X2	Austria	3	6	6
X9	Finland	4	2	3
X6	Denmark	5	3	5
X23	Slovenia	6	5	7
X19	Portugal	7	5	5
X16	Luxembourg	8	3	5
X13	Ireland	9	8	9

Code	County	Rank TOPSIS	Rank ELECTRE II V1	Rank ELECTRE II V2
X25	Czechia	10	8	13
X11	Greece	11	7	12
X22	Slovakia	12	7	10
X20	Romania	13	13	17
X3	Belgium	14	12	15
X8	Estonia	15	4	1
X17	Netherlands	16	13	16
X12	Hungary	17	9	14
X7	Spain	18	13	18
X4	Bulgaria	19	10	11
X5	Croatia	20	3	8
X21	United-Kingdom	21	11	17
X18	Poland	22	16	22
X14	Italy	23	14	19
X10	France	24	14	21
X1	Germany	25	15	20

Table 9: Comparison of ELECTRE II method to TOPSIS method

	Correlation between R and R^K											
	R1	*R2*	*R3*	*R4*	*R5*	*R6*	*R7*	*R8*	*R9*	*R10*	*R11*	*Q(P)*
ELECTRE II V1	0.10	0.35	0.18	0.33	0.32	0.54	0.57	0.68	0.10	0.48	0.17	0.35
ELECTRE II V2	-0.03	0.39	0.23	0.34	0.35	0.60	0.62	0.72	0.09	0.46	0.13	0.36
TOPSIS	0.04	0.14	0.22	0.28	0.32	0.37	0.43	0.48	-0.04	0.38	0.21	0.26

Comparison of ELECTRE II method to TOPSIS method

All this work aims to show how quality measurement can be used as a rational tool to compare the results obtained by several methods objectively. This same tool can be used to compare the results of the robustness analysis, as is the case of the ELECTRE II V1 and ELECTRE II V2 versions. To choose the best ranking, we use the quality measure of rankings *Q(P)* given by equation 11. Table 9 gives the results of the comparison between the ELECTRE methods, for versions V1 and V2, and the TOPSIS method.

Where R is the comparison matrix of the ranking P result of the method. R^k is the comparison matrix induced by the criterion gk, with $1 \leq k \leq 11$.

According to this Table 9, we can confirm that the ranking obtained by the ELECTRE II V2 method is the best ranking to be prescribed and recommended to the decision-maker.

According to the rankings results of the three methods ELECTRE II V1, ELECTRE II V2 and TOPSIS, almost all the most industrialized countries, such as Germany, France, and Italy, are placed at the end of the rankings, but more or less not with the same ranks in the three rankings. This result is well justified by the fact that most industrial and developed countries consume much energy and have high rates of carbon dioxide emissions CO2. Except for Sweden, Denmark and Austria, which are industrial countries, but according to the three rankings, they are considered among the top five most environmentally conservative countries in Europe.

According to the numerical results, the robustness analysis is very useful in the MCDA context, where the parameters are sometimes very vague and uncertain concerning the decision-maker. For example, the countries having obtained equal ranks, in the ELECTRE II V1 version, were separated into countries with different ranks in the ELECTRE II version, which gave the best ranking in terms of the measurement of quality *Q(P)*.

7. Conclusions

In summary, this article has addressed the following contributions.

On the one hand, a quality measure at the base of the correlation metric of the matrices, which takes into account the relative importance is proposed. This proposed quality measurement is a rational tool for the decision-maker to compare the rankings results of several MCDA methods adopted for its decision problem to be solved.

On the other hand, in order to prove the significance of the proposed quality measure, an experimental test was tested. This example clearly showed the relevance of the proposed measure. In addition, a real application on the preservation of the environment in the countries of the European community was studied. This case study has been proposed to practically illustrate the meaning and

relevance of quality measurement to compare MCDA methods. Two popular methods ELECTRE II and TOPSIS were used and compared on the basis of quality measurement. It turns out that the ELECTRE II method gives a better ranking.

Besides, it was shown that the quality measurement *Q(P)* could be very useful to support the decision-maker in the operation of the robustness analysis. An illustrated example of the robustness analysis has been done on the ELECTRE II method.

The results obtained in this article apply to the case of ranking methods. In our future works, we intend to use the metric for evaluating the quality of the rankings for the case of sorting and choosing problematics.

References

[1] M.C. Abounaima, F.Z. El Mazouri, L. Lamrini, N. Nfissi, N. El Makhfi, M. Ouzarf, "The Pearson Correlation Coefficient Applied to Compare Multi-Criteria Methods: Case the Ranking Problematic," in 2020 1st International Conference on Innovative Research in Applied Science, Engineering and Technology, IRASET 2020, 2020, doi:10.1109/IRASET48871.2020.9092242.

[2] M. Aruldoss, "A Survey on Multi Criteria Decision Making Methods and Its Applications," American Journal of Information Systems, **1**(1), 31–43, 2013, doi:10.12691/ajis-1-1-5.

[3] M. Behzadian, S. Khanmohammadi Otaghsara, M. Yazdani, J. Ignatius, "A state-of the-art survey of TOPSIS applications," Expert Systems with Applications, **39**(17), 13051–13069, 2012, doi:10.1016/j.eswa.2012.05.056.

[4] O.S. Albahri, J.R. Al-Obaidi, A.A. Zaidan, A.S. Albahri, B.B. Zaidan, M.M. Salih, A. Qays, K.A. Dawood, R.T. Mohammed, K.H. Abdulkareem, A.M. Aleesa, A.H. Alamoodi, M.A. Chyad, C.Z. Zulkifli, "Helping doctors hasten COVID-19 treatment: Towards a rescue framework for the transfusion of best convalescent plasma to the most critical patients based on biological requirements via ml and novel MCDM methods," Computer Methods and Programs in Biomedicine, **196**, 105617, 2020, doi:10.1016/j.cmpb.2020.105617.

[5] S. Greco, M. Ehrgott, J.R. Figueira, Multiple Criteria Decision Analysis: State of the Art Surveys, Springer, 2016.

[6] H. Aissi, B. Roy, "Robustness in Multi-criteria Decision Aiding," Trends in Multiple Criteria Decision Analysis, 87–121, 2010, doi:10.1007/978-1-4419-5904-1_4.

[7] G. Kumar, N. Parimala, "A Sensitivity Analysis on Weight Sum Method MCDM Approach for Product Recommendation," in Distributed Computing and Internet Technology, Springer, Cham: 185–193, 2019, doi:10.1007/978-3-030-05366-6_15.

[8] K. Govindan, M.B. Jepsen, "ELECTRE: A comprehensive literature review on methodologies and applications," European Journal of Operational Research, **250**(1), 1–29, 2016, doi:10.1016/j.ejor.2015.07.019.

[9] J.R.S.C. Mateo, "Weighted Sum Method and Weighted Product Method," Multi Criteria Analysis in the Renewable Energy Industry, 19–22, 2012, doi:10.1007/978-1-4471-2346-0_4.

[10] Bernard Roy, Denis Bouyssou, Aide multicritère méthodes et cas, Economica, Paris, 1993.

[11] E.K. Zavadskas, Z. Turskis, S. Kildienė, "State of art surveys of overviews on MCDM/MADM methods," Technological and Economic Development of Economy, **20**(1), 165–179, 2014, doi:10.3846/20294913.2014.892037.

[12] F.Z. El Mazouri, M.C. Abounaima, K. Zenkouar, "Data mining combined to the multicriteria decision analysis for the improvement of road safety: case of France," Journal of Big Data, **6**(1), 2019, doi:10.1186/s40537-018-0165-0.

[13] N. Vivekanandan, K. Viswanathan, S. Gupta, "Errata to: Optimization of cropping pattern using goal programming approach," OPSEARCH, **47**(1), 104, 2010, doi:10.1007/s12597-010-0007-0.

[14] M. Behzadian, R.B. Kazemzadeh, A. Albadvi, M. Aghdasi, "PROMETHEE: A comprehensive literature review on methodologies and applications," European Journal of Operational Research, **200**(1), 198–215, 2010, doi:10.1016/j.ejor.2009.01.021.

[15] I. Emovon, O.S. Oghenenyerovwho, "Application of MCDM method in material selection for optimal design: A review," Results in Materials, **7**, 100115, 2020, doi:10.1016/j.rinma.2020.100115.

[16] F.Z. El Mazouri, M.C. Abounaima, K. Zenkouar, A.E.H. Alaoui, "Application of the ELECTRE III Method at the Moroccan Rural Electrification Program," International Journal of Electrical and Computer Engineering (IJECE), **8**(5), 3285–3295, 2018, doi:10.11591/ijece.v8i5.pp3285-3295.

[17] M. Wang, S.-J. Lin, Y.-C. Lo, "The comparison between MAUT and PROMETHEE," in 2010 IEEE International Conference on Industrial Engineering and Engineering Management, 753–757, 2010, doi:10.1109/IEEM.2010.5675608.

[18] J.M. Sánchez-Lozano, M.S. García-Cascales, M.T. Lamata, "Comparative TOPSIS-ELECTRE TRI methods for optimal sites for photovoltaic solar farms. Case study in Spain," Journal of Cleaner Production, **127**, 387–398, 2016, doi:10.1016/j.jclepro.2016.04.005.

[19] Y. Çelikbilek, F. Tüysüz, "An in-depth review of theory of the TOPSIS method: An experimental analysis," Journal of Management Analytics, **7**(2), 281–300, 2020, doi:10.1080/23270012.2020.1748528.